Child health in South Africa, a generation after apartheid p. 820

Conformal transfer printing using sugar pp. 826 & 894

Transcriptome recordings win *Science* & SciLife Lab Prize p. 844

Science

$15
25 NOVEMBER 2022
science.org

AAAS

SPECIAL ISSUE

CELL ENGINEERING

Putting modified cells to work in basic science and medicine p. 846

SCIENCE FOR HUMANITY

AAAS | ANNUAL MEETING

The hybrid 2023 AAAS Annual Meeting will be held in Washington, DC, and online, March 2–5. Registration and program are now available!

Visit our website for the list of the 2023 Plenary and Topical Sessions by renowned speakers and topical experts, who will discuss the latest interdisciplinary research.

aaas.org/meetings | #AAASmtg

Optimizing an ADCC assay with cryopreserved immune cells

Antibody-dependent cellular cytotoxicity (ADCC) assays are commonly used in immunology research, drug discovery, and therapeutic antibody development. These assays involve effector cell recognition of antibody-bound surface antigens on target cells, triggering cell death. The use of cryopreserved, or "frozen," cells in ADCC assays offers many advantages including the ability to plan experiments ahead of time with ready-to-use cells that do not require culturing and can be stored in the freezer until needed.

One concern with the use of cryopreserved cells is the potential loss of viability, phenotype, or function resulting from the cryopreservation process. However, with proper validation, frozen immune cells can be used in place of freshly isolated immune cells for ADCC and other immune cell-based applications. Viability can be measured post-thaw using techniques such as propidium iodide or trypan blue staining. To assess phenotype, fluorescent antibodies against specific cell surface markers including CD14 (a monocyte marker), CD56 [a natural killer (NK) cell marker], CD4 and CD8 (T cell markers), and CD19 (B cell marker) can be used in combination with flow cytometry or fluorescence microscopy. These data can also be used to determine the composition of frozen peripheral blood mononuclear cell (PMBC) populations. Assays that measure response—such as T cell activation—are used to help confirm functionality.

While in many cases cryopreserved immune cells can behave and perform in the same manner of freshly isolated cells, assays using frozen cells should always be optimized as suitability and performance depend on the supplier or manufacturer, cryopreservation process, or even specific lot or donor. With the right optimizations, you can achieve the performance required from cryopreserved cells.

The optimizations include:

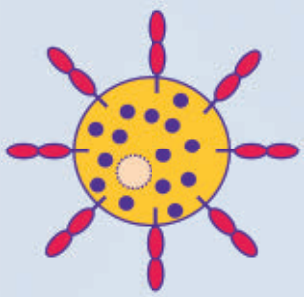

1. Effector cell preparation

The use of fresh effector cells in ADCC assays often requires precise timing of target cell preparation and effector cell collection. Variable activity may be observed between collections, even from the same donor. In contrast, cryopreserved effector cells can be purchased at appropriate cell numbers, stored in a freezer until needed, and thawed for immediate use following overnight recovery—supporting a more flexible workflow and greater consistency in results across experiments.

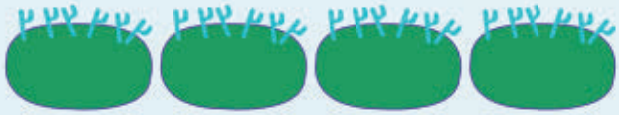

2. Target cell seeding density

Target cell seeding density should be optimized based on assay signal and uniformity of plating. A two-fold serial dilution ranging from 10,000 cells per well to 156 cells per well in a 96-well format can be used as a starting point for optimization. Allowing plated target cells to rest in the tissue culture hood for 1 hour before moving to a 37°C incubator for overnight incubation can result in more even cell distribution and better assay reproducibility for adherent cell lines.

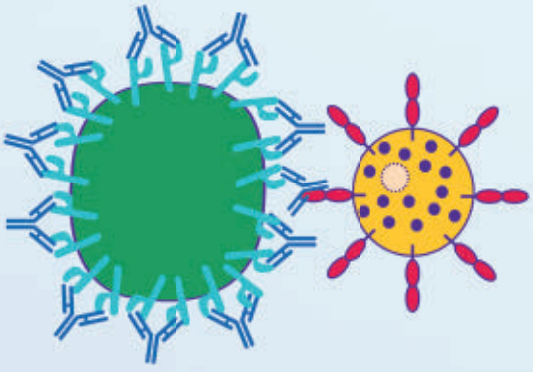

3. E:T ratio

In general, higher effector (E)-to-target (T) cell ratios give more robust results in ADCC assays. However, the availability of effector cells should be considered, as increasing the E:T ratio will require more effector cells. E:T ratios ranging between 2:1 and 20:1 should be tested. Culture media can also impact cell killing, so media appropriate for either the target or effector cells can be assessed for optimal performance.

4. Antibody concentration

A serial dilution of antibody, ideally centered around the expected half maximal effective concentration (EC_{50}), should be used to evaluate the dynamic range of the assay. In general, antibody concentrations ranging from 1 pg/mL to 1 µg/mL are used as a starting point when optimizing ADCC assays.

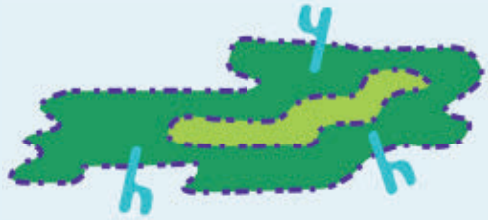

5. Killing time

Killing requires physical contact between target and effector cells. In ADCC assays, antibody-dependent cell killing can occur in as little as 30 minutes or require as long as 24 hours or more to achieve robust results (>50% cell killing). Time course experiments should be used to evaluate optimal killing time. In some cases, the use of cryopreserved NK effector cells was shown to require longer killing times when compared to optimized assays using freshly isolated NK cells.

6. Pretreatment of effector cells

Pretreatment with cytokines has been found to increase the activity of NK cells. For some assays, pre-treatment can yield a more robust ADCC assay. For assays that require longer incubation periods, overactivation of effector cells may result in robust nonspecific killing. In such cases, pretreatment should be optimized or omitted.

7. Data analysis

ADCC data are typically plotted in one of three ways:

1. Raw signal vs. antibody concentration.
2. Percent cytotoxicity vs. antibody concentration. Percent cytotoxicity is defined using the following equation:

   Cytotoxicity % = [(Max-BG) - (Expt-BG)] / (Max-BG) * 100

   where Max represents the average signal from target cells only, BG represents the average background signal from wells with no target cells, and Expt denotes signal from experimental samples.
3. Percent ADCC vs. antibody concentration. This essentially corrects for inherent NK cell killing (without antibody) using the following equation: ADCC % = Cytotoxicity % (with antibody) – Avg [Cytotoxicity % (without antibody)]

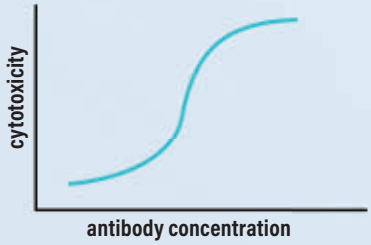

Summary

Cryopreserved immune cells can offer a practical alternative to freshly isolated immune cells for highly reproducible results in applications including ADCC, immunogenicity, screening, drug toxicity, immune regulation, and immunotherapy development. For more information on fully characterized, cryopreserved PBMCs, NK cells, and other immune cell subsets, visit **www.sigmaaldrich.com/bioivt.**

Contributors: Yue Li, Spencer Keilich, Victor Koong, Jun Park (MilliporeSigma)

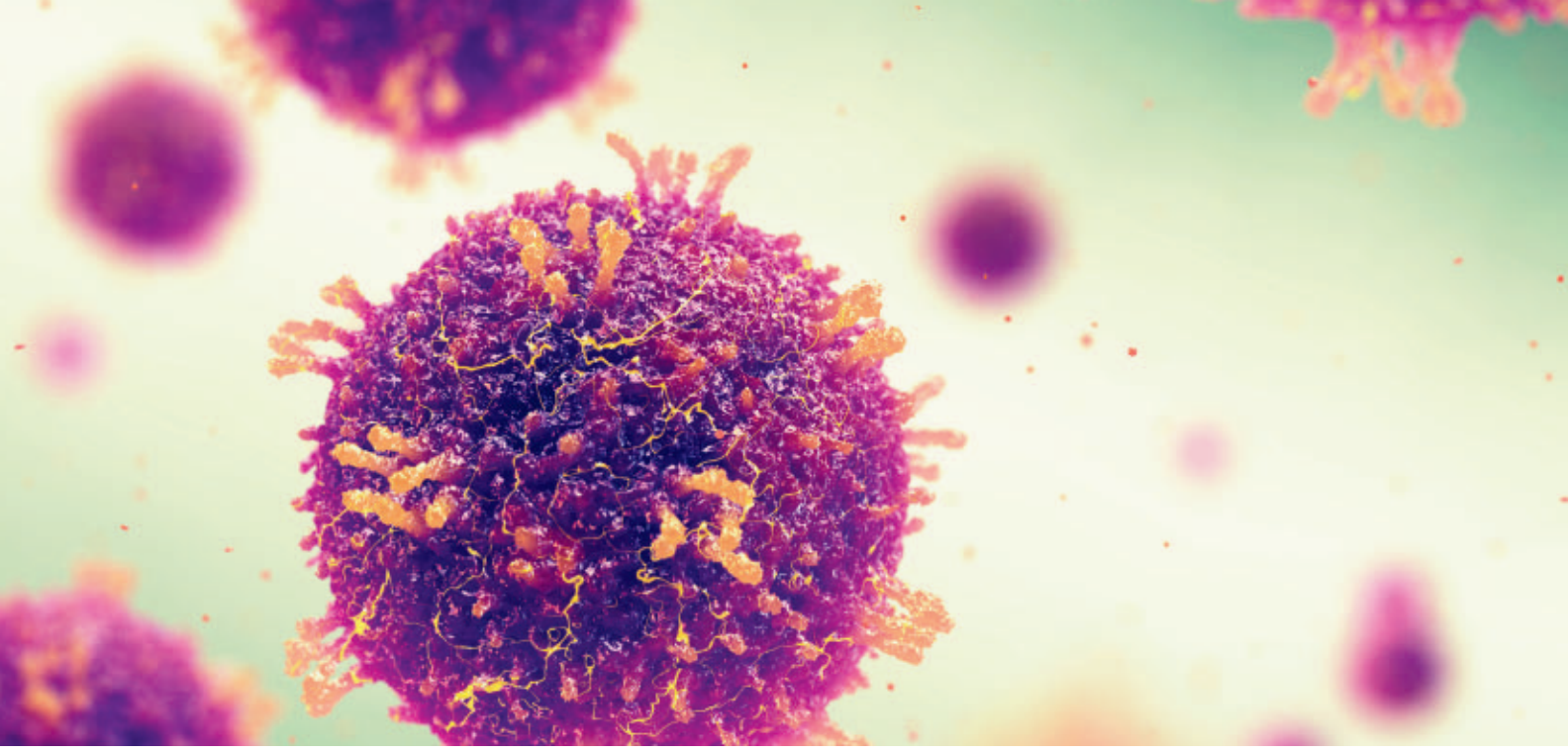

It's time to think differently.

Find out how NEB can support your infectious disease research and development.

Gaining a better understanding of infectious diseases, including their characterization, evolution and transmission, continues to be a priority, both from an R&D standpoint and as a public health issue. The COVID-19 pandemic has demonstrated the need for a wide range of tools to research infectious diseases, and has highlighted the importance of speed and the ability to pivot as new problems arise. This has emphasized the need for innovation and thinking differently about where to access those critical materials, including genomics reagents.

Many scientists know NEB as a trusted reagent supplier to the life science community, but what you may not know is that we also offer a portfolio of products that can be used in infectious disease research, development of diagnostics and therapies, and in epidemiological studies and disease surveillance. In fact, many of our products have supported the development of COVID-19 diagnostics and vaccines, and can also be utilized with other infectious diseases, such as influenza and malaria.

- Benefit from almost 50 years of experience in molecular biology & enzymology
- Partner with our OEM & Customized Solutions team to find the best solution for your needs
- Take advantage of our expanded manufacturing capabilities
- Access product formats, such as GMP-grade*, lyophilized, lyo-ready and glycerol-free
- Be confident in your product performance with our expanded quality and regulatory systems

Ready to get started? Learn more at
www.neb.com/InfectiousDiseases

"GMP-grade" is a branding term NEB uses to describe reagents manufactured at our Rowley, MA facility, where we utilize procedures and process controls to manufacture reagents in compliance with ISO 9001 and ISO 13485 quality management system standards. NEB does not manufacture or sell products known as Active Pharmaceutical Ingredients (APIs), nor do we manufacture products in compliance with all of the Current Good Manufacturing Practice regulations.

NEW ENGLAND BioLabs® Inc.

be INSPIRED
drive DISCOVERY
stay GENUINE

CONTENTS

25 NOVEMBER 2022 • VOLUME 378 • ISSUE 6622

SPECIAL SECTION

Cell engineering

INTRODUCTION

REVIEWS

ON THE COVER

The drawing evokes the powerful and momentous potential of cell engineering. The ability to alter cellular regulatory circuitry enables researchers to design modified cells to advance basic science and improve therapies. Investigators can now modify various cell types or groups of cells to operate as smart agents that facilitate experimentation or execute diagnostic or therapeutic functions. See the special section beginning on page 846. *Illustration: Jason Lyon*

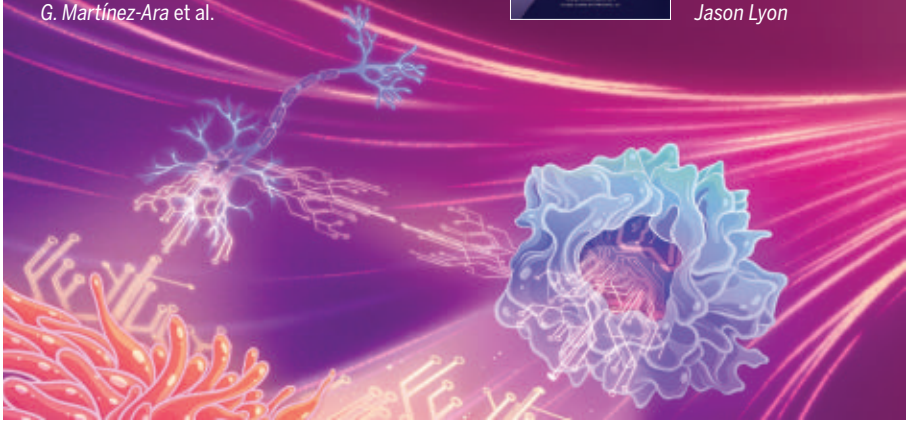

ILLUSTRATION: JASON LYON

NEWS

IN BRIEF

IN DEPTH

FEATURES

INSIGHTS

PERSPECTIVES

POLICY FORUM

BOOKS *ET AL.*

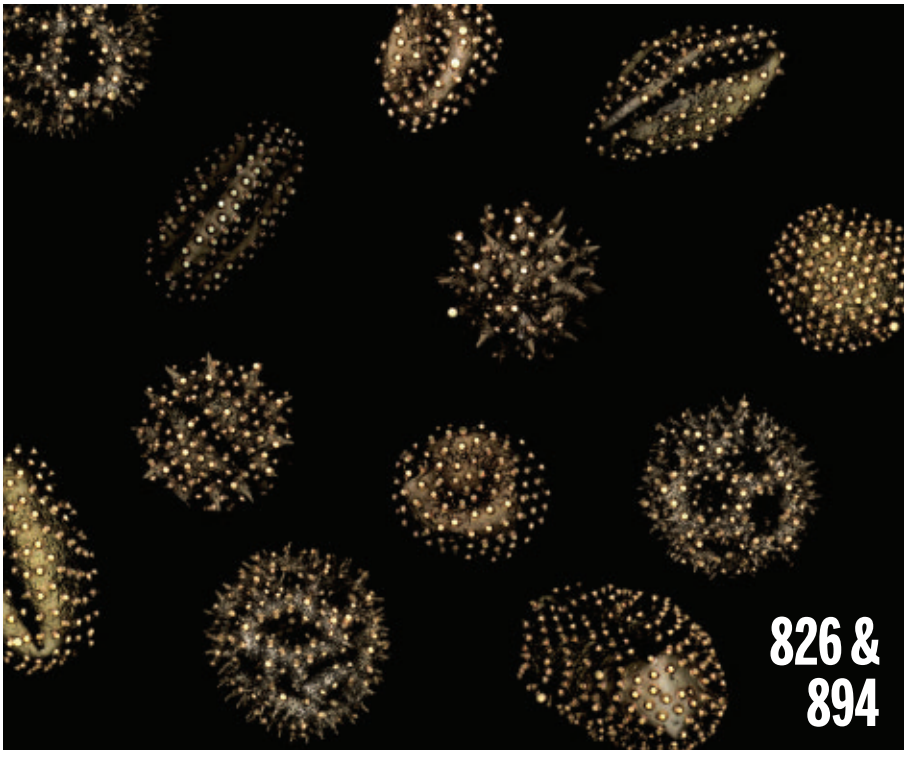

SCIENCE (ISSN 0036-8075) is published weekly on Friday, except last week in December, by the American Association for the Advancement of Science, 1200 New York Avenue, NW, Washington, DC 20005. Periodicals mail postage (publication No. 484460) paid at Washington, DC, and additional mailing offices. The title SCIENCE is a registered trademark of the AAAS. Domestic individual membership, including subscription (12 months): $165 ($74 allocated to subscription). Domestic institutional subscription (51 issues): $2212; Foreign postage extra: Air assist delivery: $98. First class, airmail, student, and emeritus rates on request. Canadian rates with GST available upon request, GST #125488122. Publications Mail Agreement Number 1069624. **Printed in the U.S.A.**
Change of address: Allow 4 weeks, giving old and new addresses and 8-digit account number. **Postmaster:** Send change of address to AAAS, P.O. Box 96178, Washington, DC 20090–6178. **Single-copy sales:** $15 each plus shipping and handling available from backissues.science.org; bulk rate on request. **Authorization to reproduce** material for internal or personal use under circumstances not falling within the fair use provisions of the Copyright Act can be obtained through the Copyright Clearance Center (CCC), www.copyright.com. The identification code for *Science* is 0036-8075. *Science* is indexed in the *Reader's Guide to Periodical Literature* and in several specialized indexes.

CREDITS: (IMAGE) GARY ZABOW; (ILLUSTRATION) ROBERT NEUBECKER

EDITORIAL

Rethinking premedical education

John A. Gladysz is a distinguished professor in the Department of Chemistry, Texas A&M University, College Station, Texas, USA. gladysz@chem.tamu.edu

The world needs more physicians. Increasing their numbers alone won't solve the many problems associated with improving health care. But it doesn't help to have a dearth of doctors, who were generally in short supply before COVID-19 struck. The pandemic has only exacerbated doctor shortages everywhere. This doesn't bode well for a world that must prepare for future pandemics and for populations that are both growing and aging. Better health outcomes require more physicians. So, where are the bottlenecks?

Physician training takes different tracks in different countries. The United States has the longest and most expensive medical education system in the developed world. Many facets of this system have been criticized, from the financial burden to the requisite 12 years of education and training, not to mention the intense competition to enter this career track. A US medical education requires 4 years of undergraduate studies and 4 years of medical school, whereas in most European countries, students can accomplish this in 6 years. Recently on this page, it was argued that the US pre–medical school (premed) curriculum should be reconsidered by medical schools and medical regulatory bodies. One question addressed the degree to which all undergraduates who pursue science and medicine require science courses of the same breadth and depth. For example, the content in the customary introductory four-semester chemistry sequence is highly relevant for future practicing chemists. But which units are essential for future medical professionals? Of course, some premed students major in chemistry, but does one chemistry track optimally serve all? Reconfiguring the science requirements for premed students might go a long way in attracting—and keeping—students in the physician pipeline.

> **"...which units are essential for future medical professionals?"**

When analyzing curriculum and policy issues in US academia, there can be a tendency to overlook practices in other countries. I've taught organic chemistry at all levels in the United States and Germany (Universität Erlangen–Nürnberg). The German premed students directly matriculate into medical schools on the basis of a post–secondary school exam. Unlike their US counterparts, they do not declare subject "majors." Rather, they take the same standardized 2-year preclinical curriculum. This culminates with a comprehensive "state exam" that lasts 2 or more days, which must be passed to advance to clinical training. In stark contrast to US practices, the premed students in Germany are only required to take one semester of a combined general and organic chemistry course, a single laboratory course, and (at Erlangen) one final exam that is graded as pass/fail (typically 85 ± 5% passing). Thus, what would take four semesters in the United States is condensed to a single semester in Germany (further biochemistry is required in subsequent preclinical semesters). Other European countries have different practices, but none require the depth and breadth of chemistry that is customary in the United States.

Given the successful operation of streamlined science tracks outside the United States, and an absence of data suggesting that less qualified physicians are produced as a result, what factors anchor the US status quo? The medical school at Texas A&M University, for example, requires two semesters of both general and organic chemistry (all including a laboratory) as well as biochemistry. There have been experiments with shortened versions of the four-semester sequence at several US universities, but this wouldn't suffice for admission into Texas A&M's medical school. Compounding this gridlock, the lines of communication to medical schools and examination boards regarding optimal "learning outcomes" for future generations of doctors are broken. To cut this Gordian knot and help increase the number of doctors and much needed clinics and hospitals, a high-profile forum is urgently needed in which all the constituents of the doctor-producing pipeline rethink premedical education. Otherwise, substantive modernization and the rational development of widely accepted alternative tracks will never be possible.

One overarching issue remains: Around the globe, students in premedical curricula face intense pressure both inside and outside the classroom and are often highly stressed. This leads to mental health difficulties and student attrition, consequences that could be ameliorated with renewed attention to program and pedagogy. To disregard this is collective malpractice that further constricts the bottleneck for producing the medical professionals that the world so desperately needs.

– John A. Gladysz

PHOTO: JANET BLUMEL

10.1126/science.adf8727

eppendorf & Science PRIZE FOR NEURO BIOLOGY

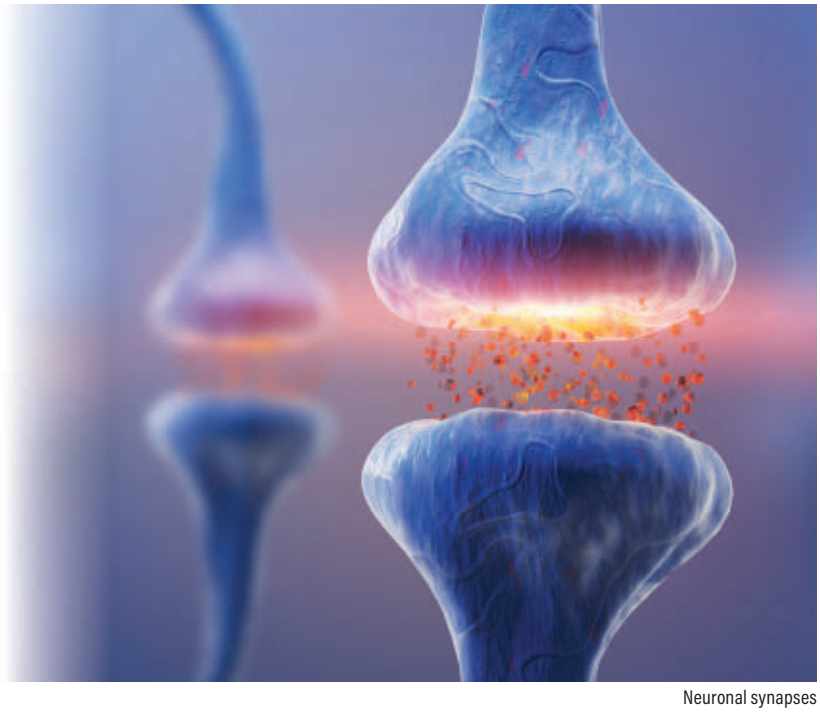

Neuronal synapses

Key insights in behavior, metabolism, and neuronal death honored with the Eppendorf & Science Prize for Neurobiology

Ann Kennedy grew up coding, enjoying the dance of deploying zeros and ones to solve problems from the mundane to the magnificent. And the more she learned about computing, the more she hankered to comprehend the ultimate computing machine: the human brain. "It drew me in—learning how the brain is wired and is able to recognize objects and play tennis and write novels," she recalls. Kennedy majored in biomedical engineering and got her Ph.D. in neuroscience at Columbia in New York City, and expected to go into industry or consulting. But it wasn't until her defense that "I figured I'd stick around," she says with a laugh, and went all in on a computational neuroscience research career aimed at unlocking the mysteries of the mind.

And now in a victorious confirmation of her stick-to-itiveness, the assistant professor at Northwestern University Feinberg School of Medicine, Chicago, Illinois has been awarded the Eppendorf & Science Prize for Neurobiology, a prestigious honor that comes with a USD 25,000 check, full support to attend the prize ceremony held in conjunction with the Annual Meeting of the Society for Neuroscience in the USA, complimentary products worth USD 1,000 from Eppendorf, an invitation to visit Eppendorf in Hamburg, Germany, and an essay on her research published in *Science*. The award acknowledges the increasingly active and important role of neurobiology in advancing our understanding of the functioning of the brain and the nervous system—a quest that seems destined for dramatic expansion in the coming decades. This annual international prize, established in 2002, encourages the work of promising young neurobiologists by providing support in the early stages of their careers. Winners of this award (a grand prize winner and up to three finalists) are determined from a 1,000-word essay that describes the research they have performed during the past 3 years.

Exploring the frontiers of neuroscience

Kennedy's project, in which she collaborated with experimentalists to characterize neural activity of the hypothalamic circuits that govern social and fear behaviors, and developed machine learning tools for animal behavior analysis, is an exciting endeavor. "We think we found a region responsible for keeping tabs on [the brain's] level of motivation to take action," she explains. Brains are not simple input–output machines, she notes. "We respond differently to the world we encounter depending on our internal motivational state, such as our levels of hunger, alertness, or anxiety. But how does the brain keep track of these signals, and how do they alter our decisions?" Kennedy and her student demonstrated how the complex responses of individual neurons gave rise at the population level to a low-dimensional signal that escalated in intensity with animals' level of aggressive motivation.

In addition to a grand prize winner, Kevin Guttenplan, a postdoctoral fellow at Oregon Health & Science University, Portland, and Filipa Cardoso, a scientist who did her research at the Champalimaud Foundation in Lisbon, Portugal, were selected as finalists. Guttenplan, whose background is in mathematics and neuroscience and who received his doctorate from Stanford University, California, studies the role of astrocytes in diseases and injuries of the nervous system. These types of brain cells are understudied, he says, and therefore poorly misunderstood. His work aims to clarify whether astrocytes contribute to neuronal death. "Because so little is known

and so few tools are developed, there's not a preestablished way of answering these questions. Each time you ask a question, you have to develop new tools. But that's appealing to me," he says. "It is the Wild West of neuroscience." Guttenplan's exploration yielded new tools to track astrocyte reactivity and demonstrated that neurotoxic astrocytes are found in a broad range of diseases and injuries, such as Alzheimer's disease and optic nerve injury. Additionally, his work identified one specific mechanism, the release of a toxic lipid, by which astrocytes can kill neurons, providing potential new therapeutic targets for neurodegenerative disease, such as amyotrophic lateral sclerosis (ALS).

Cardoso is an expert in how the nervous and immune systems interact to control metabolism. With a Bachelor's and Master's in health sciences from the University of Minho, Braga, Portugal, and her Ph.D. in immunology from the University of Lisbon, Portugal, Cardoso conducted her research as a doctoral student at the Champalimaud Foundation, Portugal. Her project showcased how adipose tissue and the nervous system communicate to regulate key metabolic responses and how this impacts immune cell function as well. "Adipose tissue has been viewed as a fat storage site, but it is actually able to coordinate with the whole body to affect bodily functions," she shares. "The functions rely on the connection between the adipose tissue and nervous system. Our question was how does this happen on the molecular level?" She discovered an intermediary cell type that enables the communication, almost like a translator, between the adipose and nervous system cells. "We showed that activating this axis—this three party response—leads to the control of fat storage and to improved metabolic control in mice."

Left: Kevin Guttenplan, **Center:** Ann Kennedy, **Right:** Filipa Cardoso

All of the prize-winning projects have the possibility of improving health outcomes for patients with serious concerns. Given that Kennedy's work centers around understanding behavior, she is enthusiastic that her contributions can serve as the groundwork for better support and interventions for mental health concerns such as depression or social isolation stress. "Understanding how these regions are operating and encoding these signals gives us a sense of what goes on in our brains when we experience these things that change our emotional state, so there is potential clinical relevance," she says. Cardoso's findings can springboard novel interventions for obesity and metabolic syndrome, which typically have been treated through diet or high risk surgery and pharmacological approaches, she says, none of which provide optimum outcomes. But with her discovery, "once we get this mechanism studied and [learn] how it regulates metabolism at the cellular level, there will be more targets and more therapies and less side effects," she says.

Additional powers of the prize

While the award is a triumph in itself, it's the promise of the prize's exposure that especially energizes these scientists. "It's a nice validation of my work," says Kennedy, "and it's nice to be able to explain what I do to a more general audience who might not hear of it otherwise." Guttenplan welcomes the attention the prize provides to the still burgeoning discipline of glial cells, the types of cells in the brain that preserve homeostasis and protect neurons. "The field of glial biology has been a lot slower to develop than neuroscience." he shares. For a long time, "people thought glial cells didn't do anything... [or that] they were [just] the 'glue' that held the neurons together. So having projects associated with studying glia considered valuable enough to be recognized by this prize is a good sign for the field that it is respected."

Kennedy encourages other young scientists to consider applying for the Eppendorf & Science Prize for Neurobiology, because it is a great reinforcement of why scientists do science: As her advisor told her, this is supposed to be fun. "There's a lot of reasons to be frustrated by the state of science, but it should be joyous and not a thorn in your side," she says, noting how much she liked both the research and writing experience.

For more information on the Eppendorf & Science Prize for Neurobiology go to www.eppendorf.com/prize.

PHOTOS: PROVIDED BY EPPENDORF

NEWS

> “We can’t say science is for everyone without providing resources for everyone to have a science career.”
>
> **Stephanie Wankowicz,** a Ph.D. student in biophysics, tweeting about a strike by University of California students and postdocs for better wages and benefits. It is one of the largest of its kind.

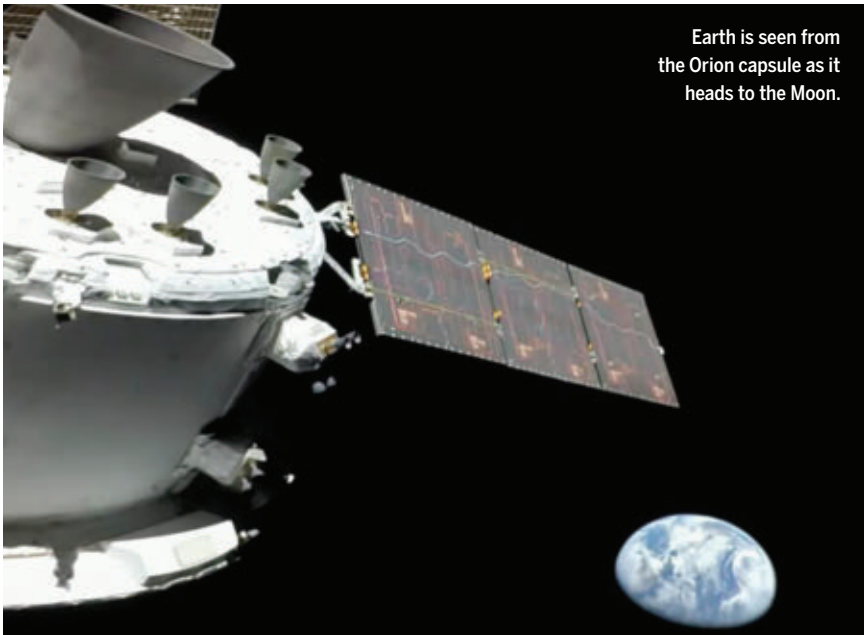

Earth is seen from the Orion capsule as it heads to the Moon.

IN BRIEF

Edited by **Jeffrey Brainard**

LUNAR SCIENCE

Science probes head for Moon orbit

After years of delay, NASA’s Space Launch System (SLS) rocketed toward the Moon last week, and data indicate its scientific payloads are working as planned. The rocket is the agency’s most powerful since the Apollo-era Saturn V, and the launch marks the first orbital flight on a NASA rocket since the retirement of the Space Shuttle in 2011. The uncrewed mission, which will take the Orion capsule on a 26-day journey past the Moon and back, is the first in Artemis, NASA’s plan to return astronauts to the surface of the Moon by 2025. At an estimated $4 billion per flight, critics say the SLS is not sustainable. But on its first flight, it did carry some relatively inexpensive science: 10 small CubeSats. As *Science* went to press, many of the small satellites were functioning normally after deployment. These included two, Lunar IceCube and the Lunar Polar Hydrogen Mapper, whose batteries were draining, and could not be recharged, as they sat aboard the rocket for more than a year before it launched. The two missions will orbit the Moon, seeking to understand the presence of water ice near its poles. Other CubeSats are headed for solar orbits to study asteroids and radiation.

NASA: Webb didn’t target staff

DIVERSITY | NASA said a search of government archives supports its decision not to remove the name of its former administrator, James Webb, from its flagship space telescope. Many astronomers had urged NASA to rename the telescope, following accusations Webb participated in discrimination and firing of LGBTQ+ staff from the U.S. federal workforce in the 1950s and ’60s. In an 89-page report last week, NASA’s chief historian, Brian Odom, describes a survey of more than 50,000 archived documents for evidence that Webb was involved in what was known as the Lavender Scare. No evidence “directly links Webb to any actions or follow-up related to the firing of individuals for their sexual orientation,” the report says. The report found no evidence he knew of the 1963 firing of NASA budget analyst Clifford Norton after he was arrested and accused of making a homosexual advance. Some astronomers said they were unpersuaded and will continue pressing for the James Webb Space Telescope to be renamed. “It is highly likely that [Webb] knew exactly what was happening with security at his own agency during the height of the Cold War,” cosmologist Chanda Prescod-Weinstein and colleagues wrote in a blog post. They added, “We are deeply concerned by the implication that managers are not responsible for homophobia or other forms of discrimination that happens on their watch.”

Protesters cleared of defamation

#METOO | A Finnish court last week dismissed criminal charges against two astronomers who had protested the hiring of a U.S. scientist found to have committed gender-based harassment in a previous academic job. The University of Helsinki’s Syksy Räsänen and Till Sawala had been charged with defaming and violating the privacy of Christian Ott, a former faculty member at the California Institute of Technology (Caltech). In 2015, that university’s finding that he had harassed two graduate students received extensive media coverage. Ott resigned from Caltech in August 2017 and in January 2018 signed a 2-year contract to work as a postdoctoral researcher at the

PHOTO: NASA TV

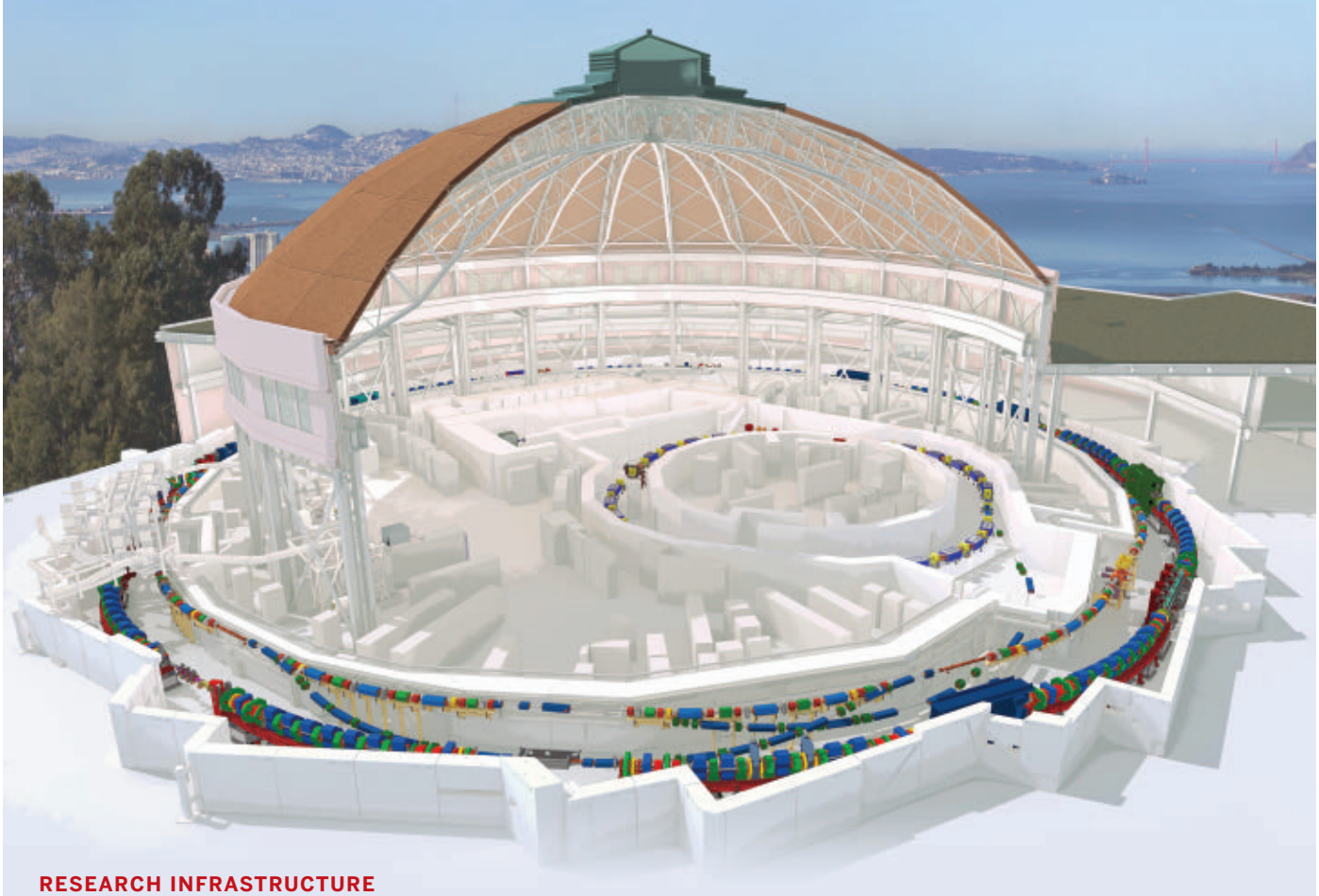

IMAGE: BERKELEY LAB

RESEARCH INFRASTRUCTURE

Berkeley x-ray source will soon pack a bigger punch

The future looks bright for scientists working with the Advanced Light Source (ALS), a 29-year-old x-ray synchrotron at Lawrence Berkeley National Laboratory that serves 1600 users annually. Last week, the U.S. Department of Energy gave the go-ahead to a $590 million rebuild of the 200-meter-long, ring-shaped accelerator, in which circulating electrons radiate x-rays with relatively long wavelengths that are well-suited for studying biological structures, polymers, and nanomaterials. The 4-year project should intensify the ALS's x-ray beams by a factor of 100. It will require replacing the existing synchrotron (largest ring, above) and adding a new, smaller one (intermediate ring) to help accumulate the electrons. An advance of $97 million from the Inflation Reduction Act, enacted in April, should help accelerate the project. Developers will have to wedge the new machines into the lab's iconic domed building, designed in 1940 by famed San Francisco architect Arthur Brown.

University of Turku's Tuorla Observatory. News of his appointment triggered protests in Finland and beyond, including a letter to Turku administrators organized by Räsänen and Sawala. A week later, Turku canceled the agreement. "No one should have to fear fines or a prison sentence for simply speaking out against harassment based on widely and reliably reported facts," Räsänen says about the 17 November ruling by a court in Turku.

CRISPR for blindness disappoints

CLINICAL TRIALS | The biotech company Editas Medicine is suspending its pioneering effort to treat a rare inherited blindness disorder with the CRISPR gene-editing tool, after a trial showed unsatisfactory results. Only three of 14 patients with Leber congenital amaurosis 10 (LCA10) who received an injection of the gene editor into their retina had "clinically meaningful" vision improvements. In two of the three, both copies of the *CEP290* gene targeted were defective. The finding shrank the potential market for the treatment, because only about 300 U.S. patients with LCA10 have two copies of the mutation. The company has paused enrollment and is now seeking a partner to help continue the program. The trial was the first to directly inject a CRISPR-derived treatment into the body. Two trials that are using CRISPR to treat genetic diseases by editing liver cells have been more successful.

Future pandemic fund kicks off

PUBLIC HEALTH | The World Bank has a new funding mechanism to help low- and middle-income countries beef up their abilities to prevent, prepare for, and respond to future pandemics. Launched last week at the Group of 20 (G-20) summit, a forum convened by the world's major developed and emerging economies, the Pandemic Fund already has more than $1.4 billion in seed money pledged from 24 countries. It aims to help countries improve surveillance of pathogens in animals that might trigger human pandemics, strengthen laboratories and health workforces, and fortify delivery of drugs and vaccines. An independent panel advised the G-20 that international financing for these efforts ideally should increase by $75 billion over the next 5 years. A variety of funders have separately provided money to financially strapped countries to help with their responses to the COVID-19 pandemic, but several expert groups had called for long-term, reliable, and well-coordinated funding mechanisms to handle future ones more effectively. The fund's secretariat, guided by an advisory panel that the World Health Organization chairs, will soon issue its first call for proposals.

IN DEPTH

SARS-CoV-2 hospitalized this child in January, but this winter the coronavirus may have to compete for hosts with influenza and respiratory syncytial virus.

BIOMEDICINE

Will viral interference hold off the tripledemic?

As multiple respiratory viruses surge, some researchers predict they will block one another

By **Jon Cohen**

Triple threat. Tripledemic. A viral perfect storm. These frightening phrases have dominated recent headlines as some health officials, clinicians, and scientists forecast that SARS-CoV-2, influenza, and respiratory syncytial virus (RSV) could surge at the same time in Northern Hemisphere locales that have relaxed masking, social distancing, and other COVID-19 precautions.

But a growing body of epidemiological and laboratory evidence offers some reassurance: SARS-CoV-2 and other respiratory viruses often "interfere" with each other. Although waves of each virus may stress emergency rooms and intensive care units, the small clique of researchers who study these viral collisions say there is little chance the trio will peak together and collectively crash hospital systems the way COVID-19 did at the pandemic's start.

"Flu and other respiratory viruses and SARS-CoV-2 just don't get along very well together," says virologist Richard Webby, an influenza researcher at St. Jude Children's Research Hospital. "It's unlikely that they will circulate widely at the same time."

"One virus tends to bully the others," adds epidemiologist Ben Cowling at the University of Hong Kong School of Public Health. During the surge of the highly transmissible Omicron variant of SARS-CoV-2 in Hong Kong in March, Cowling found that other respiratory viruses "disappeared … and they came back again in April."

Untangling such interference hasn't been easy given the number of respiratory viruses—coronaviruses, rhinoviruses, adenoviruses, RSV, and influenza are just among the best known—and the many infections that escape notice. Recent advances in technology, however, make it easier to detect infections in people and study how multiple viruses behave in the lab, in cell cultures or stem cell–derived tissues known as organoids. Increasingly, researchers are fingering a cause: chemical messengers that infected people produce called, fittingly, interferons.

When a respiratory virus sweeps through a community, interferons can broadly raise the body's defenses and temporarily erect a populationwide immune barrier against subsequent viruses that target the respiratory system. "Basically, every virus triggers the interferon response to some extent, and every virus is susceptible to it," says immunologist Ellen Foxman at Yale University, who has been exploring interference between SARS-CoV-2 and other viruses in a laboratory model of the human airway.

Rhinoviruses, which cause common colds, can trip up influenza A (the most prevalent flu virus). RSV can bump rhinoviruses and human metapneumoviruses. Influenza A can thwart its distant cousin influenza B. "There are a lot of major health implications from viral interference," says Guy Boivin, a virologist at Laval University who co-authored a review on viral interference earlier this year.

Still, interference isn't a sure thing when multiple viruses are circulating. A household survey of 2117 people in Nicaragua, for example, found both flu and COVID-19 cases peaked at the same time in February, suggesting "limited viral interference," the researchers concluded in a preprint. "I think of interference as a small push," says Aubree Gordon, the University of Michigan, Ann Arbor, researcher who led the study with colleagues from Nicaragua's Ministry of Health. "It depends on population immunity and when that virus last circulated and flu and COVID vaccination rates."

CLUES FROM EGGS

As early as 1957, two virologists at the National Institute for Medical Research in London reported a convincing mecha-

PHOTO: SCOTT OLSON/GETTY IMAGES

nism by which one animal virus might bump aside another. Alick Isaacs and Jean Lindemann probed a well-known mystery in virology circles: Membranes from chicken eggs inoculated with inactivated influenza virus cannot then be infected with a live version. Isaacs and Lindemann found that the chicken embryo secreted a chemical, which they dubbed interferon, that accounted for the interference. Unlike other immune responses—antibodies, for example—that target specific pathogens an animal has seen in the past, this nonspecific, rapid response is part of what's known as the immune system's innate arm.

A decade passed before interference between different viruses in humans received serious attention. Soviet virologist Marina Voroshilova at the Academy of Medical Sciences wondered why live but weakened versions of poliovirus used in vaccines sometimes didn't grow in the guts of people who received them, failing to trigger protective immune responses. She found that harmless enteroviruses in the intestinal tract appeared to interfere with the polioviruses. Voroshilova then ran large field trials of vaccines composed of attenuated enteroviruses. They worked against those gut pathogens and also, surprisingly, warded off multiple respiratory viruses. Her team pegged the protection against the respiratory viruses to increased levels of interferons.

But few studies followed up on the early findings. "If you look at the virology literature, over 95% of studies are based on the study of a single virus," says Pablo Murcia, a virologist at the University of Glasgow.

Sporadic epidemiologic reports have documented how waves of influenza seemed to crowd out RSV, parainfluenza, and other respiratory viruses. But confounding variables riddled the data. What if, for example, sick children who stayed home from school dodged the other viruses? And confirming which virus had sickened a person required culturing samples, which, until recently, was cumbersome and often inconclusive.

The influenza pandemic in 2009, driven by a novel flu virus dubbed pH1N1 that had recently emerged in pigs, put the study of viral interference on more solid footing. When populations have scant immunity to a novel flu strain, it can circulate widely outside of the winter season, as happened with pH1N1 worldwide. But groups from Sweden and France, who used the highly sensitive polymerase chain reaction (PCR) assays to detect viral genetic sequences, showed that in those countries, spikes of rhinovirus infections in late summer delayed the peaks of influenza until late fall, the normal start of flu season.

More recently, in one of the largest, longest, and most comprehensive studies of respiratory virus infections in humans, Murcia and colleagues used a PCR assay that can identify members of 11 viral families to probe nasal and throat samples from more than 36,000 individuals who sought care from the National Health Service in Glasgow over 9 years. Among other examples of viral interference, their data clearly showed rhinovirus and influenza A peaked at different times (see graph, below), demonstrating a "negative interaction" between the two viruses, the group concluded in the 26 December 2019 issue of the *Proceedings of the National Academy of Sciences*.

The next year, Foxman and colleagues reported finding interference after PCR testing for 10 different viruses in 13,000 respiratory samples from adults who sought care at the Yale New Haven hospital system. Between 2016 and 2019, about 7% of people tested positive for rhinovirus or influenza A virus, but of these 1911 samples, only 12 had both viruses, significantly fewer than expected, they reported in *The Lancet Microbe*. "It was great to see Ellen Foxman's paper," Murcia says. "She essentially showed similar results to ours, and they are completely independent studies."

In the same report, Foxman pinned down the causal role of interferons. Like normal airways, the organoids her team makes from bronchial epithelial cells mount immune responses, including secreting interferons. Infecting organoids with rhinovirus nearly halted the growth of influenza A viruses added later. The rhinovirus infections led to the expression of a flood of interferon-related genes, the study showed. And when her team treated the organoids with drugs that blocked their cells from mounting an interferon response, the influenza viruses thrived.

Colliding viruses

Testing of people in Scotland who had respiratory problems and sought medical care reveals peaks and troughs of influenza A and rhinovirus prevalence that indicate the two viruses likely interfere with each other.

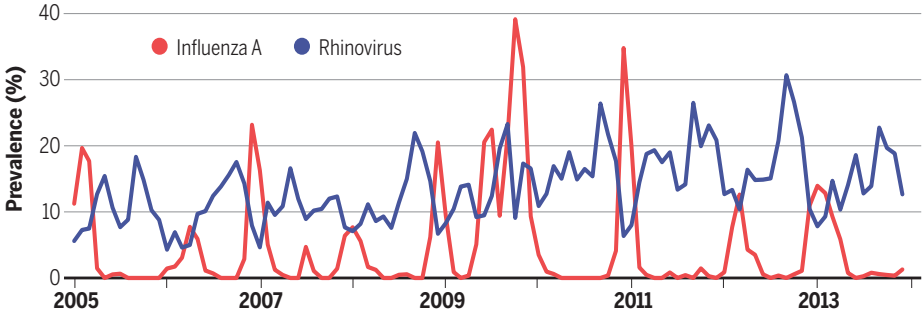

GRAPHIC: C. BICKEL/*SCIENCE*

WATCHFUL WAITING

Now, viral interference researchers are closely watching the newest respiratory virus to circle the globe. "What interactions could SARS-CoV-2 have with other viruses?" Murcia asks. "To this day, there are no robust epidemiological data." For one thing, the widespread social distancing and mask wearing in many countries meant there was little chance to see interference in action. "There was almost no circulation of other respiratory viruses during the first 3 years of the pandemic," Boivin says. Also, SARS-CoV-2 has many defenses against interferons, including preventing their production (*Science*, 14 October, p. 128), which might affect its interactions with other viruses.

Still, Foxman has published evidence that, in her organoid model, rhinovirus can interfere with SARS-CoV-2. And Boivin's team has reported that influenza A and SARS-CoV-2 each can block the other in cell studies.

Learning how SARS-CoV-2 and other viruses interfere with each other outside the lab will take prospective studies that closely monitor the same populations for several seasons. Cowling now has several, relatively small studies underway in Hong Kong, where people are repeatedly giving blood and respiratory samples, regardless of whether they have disease symptoms. It's slow going, he says. "At the moment we don't have many respiratory infections in Hong Kong," Cowling adds, noting that masking is still common.

Cowling, Murcia, and Foxman all say a dearth of funding has limited their abilities to do large population studies. Still, they and others remain optimistic that we will soon have the best data yet about the tussle between SARS-CoV-2 and other respiratory viruses. "This will be the first real winter where we have a normal mixing pattern of people, and we hopefully will start to see some signals," Murcia says. With multiple viruses running into each other for the first time in 3 years, he hopes to learn that interference remains alive and well, and able to blunt this winter's triple threat. ■

A forest has regrown all by itself in a former pasture in northern Costa Rica over the past 3 decades.

PHOTO: ROBIN CHAZDON

ECOLOGY

How to regrow a forest? Scientists aren't sure

Reforestation has become a global priority but evidence on what works is still scant

By **Elizabeth Pennisi**

The world is set to get a lot greener over the next 10 years. The United Nations has designated 2021–30 the Decade on Ecosystem Restoration, and many countries, with help from donors, have launched ambitious programs to restore forests in places where they were chopped down or degraded. At the U.N. Climate Change Conference in Egypt last week, the European Union and 26 nations pledged $16 billion in support of forests, banking on trees' ability to slow climate change by storing carbon. A significant chunk will be spent on reforestation.

"It's a really exciting time," says Susan Cook-Patton, a restoration researcher at the Nature Conservancy. "We've got an opportunity to really restore forests at scale, and that's really encouraging." But little is known about how best to achieve that.

Between 2000 and 2020, the amount of forest increased by 1.3 million square kilometers, an area larger than Peru, according to the World Resources Institute, with China and India leading the way. But about 45% of those new forests are plantations, dense aggregations dominated by a single species that are less beneficial for biodiversity and long-term carbon storage than natural forests.

Many reforestation projects focus on the number of trees planted, with less attention to how well they survive, how diverse the resulting forests are, or how much carbon they store. "We still know relatively little about what is working well or not, where, and why," says Laura Duncanson of the University of Maryland, College Park, who studies carbon storage in forests.

A theme issue of the *Philosophical Transactions of the Royal Society* published last week offers guidance, in the form of 20 articles—both original research and reviews. One in-depth look at reforestation projects in South and Southeast Asia details the challenge. Co-editor Lindsay Banin, a forest ecologist at the UK Centre for Ecology & Hydrology, and her colleagues examined data on how well newly planted trees survived at 176 reforested sites that differed in soil and environmental conditions as well as in what was planted. In some places, fewer than one in five saplings survived, and on average only 44% lasted more than 5 years.

> **"You can have a trillion dollars, but there's no simple answer that fits all."**
>
> **Bill Laurance**, James Cook University, Cairns

The study did offer one encouraging hint: When seedlings were planted near mature trees, an average of 64% survived, possibly because those spots were not as degraded. Other research has shown that measures such as fencing out cattle and improving soil conditions can boost saplings' chances of survival as well, but they can be costly.

Planting a couple of species that establish themselves easily can also help. These vanguard species pave the way for others to settle in on their own—an approach "sort of halfway between natural forest regeneration and intensive tree planting," Duncanson says. A study by plant ecologists Stephen Elliott and Pimonrat Tiansawat of Chiang Mai University concluded that the early species should be native to the area, thrive in exposed areas, grow fast, inhibit the growth of weeds, and attract seed-dispersing animals. One effective kick-starter used in Australia is a rainforest shrub named bleeding heart (*Homalanthus novoguineensis*). Its roots loosen the soil and its leaves add nutrients, allowing other species to take hold, while its fleshy green fruits attract animals that can spread seeds.

Picking the right place to plant is important as well. Ecologists Louis König and Catarina Jakovac of Wageningen University & Research examined reforestation efforts in the wastelands left behind by closed tin mines in Brazil the past 25 years. Trees have a hard time growing on piles of tailings, where the soil layers are disrupted and toxic, they report; the planted seedlings do better in mining pits and close to remnant forests.

A possible cost-saving measure is not to replant an entire site, but to set out discrete bunches of seedlings, creating "islands of re-

generation" around which a new forest will grow by itself. A comparison of 13 experimental sites in Costa Rica by Andy Kulikowski and Karen Holl of the University of California, Santa Cruz, showed this approach, called "applied nucleation," can be as good or better at promoting the regrowth of a diverse forest than densely planting an entire area with one or just a few species. Nucleation allows more space for the trees as well as light, says forest ecologist Robin Chazdon of the University of the Sunshine Coast (USC), a co-editor of the special issue: "Trees like that!" But forests can even recover all on their own. Since 1997, Chazdon has monitored a former pasture in northern Costa Rica where not a single tree was planted. A healthy natural forest has sprung up.

How reforestation affects local people—and vice versa—is an important factor in planning a project. Reforestation can reduce the land available for farming, but local communities can be compensated—and the new forest can provide timber, wildlife hunting opportunities, and other sources of income. "We need to make sure restoration is beneficial and wanted by local communities," Banin says.

University of York conservation scientists Robin Loveridge and Andrew Marshall, also at USC, studied the well-being of people involved in reforestation projects in eastern Tanzania. They compared the satisfaction of people who sell timber certified as sustainable with that of communities that did not have a sustainability program. The better a forest was managed, the happier those doing the managing were, the team found. "It's not just about getting the ecological dynamics right, but also the social and economic dynamics," Cook-Patton says.

Many other issues need attention as well, says Marshall, also a co-editor of the theme issue. They range from the role of lianas and vines—which can both hamper reforestation by hindering light and help it by offering protection from storms—to how to measure success and manage the projects. The answers will depend on local conditions. "You can have a trillion dollars," says Bill Laurance, a forest ecologist at James Cook University, Cairns, "but there's no simple answer that fits all."

Forest ecologist Simon Lewis of University College London is excited about the momentum behind reforestation but worries about the quality of the new forests. "There is a risk that as countries try to meet tough targets on curbing deforestation, old-growth forests are still cut but are replaced elsewhere," Lewis says. That means no net deforestation, "but a high-carbon, high-biodiversity forest is replaced by lower carbon and lower diversity forest." ■

GENE EDITING

'Ancestry problem' sends CRISPR astray in some people

Reference genomes used to direct the gene editor fail to account for human diversity in those of African descent

By **Jocelyn Kaiser**

The 10-year-old gene-editing tool known as CRISPR is indispensable for engineering plants, tailoring lab animals, and probing basic biology. But there's a caveat when it is used to tweak human genes: Unlike lab mice, which are usually inbred and genetically identical, people's genomes differ individually and by ancestry.

These ancestry differences mean CRISPR doesn't always edit some genomes as intended, particularly in people of African descent, whose genomes are most likely to differ from those used to steer CRISPR to a specific gene. A new analysis finds that failing to account for ancestry slightly skewed a massive sweep for cancer genes, causing it to miss genes important as drug targets in those of recent African descent.

The study, posted online, "shows a clear example of this [ancestry] problem," says computational biologist Luca Pinello of the Harvard University–affiliated Massachusetts General Hospital, who has also studied the issue. He and the scientists behind the new work propose tools to avoid it.

To edit a human gene, scientists first design a short strand of RNA to match part of the gene's DNA sequence. This guide RNA then leads CRISPR's DNA-snipping enzyme to the right spot. If the guide RNA doesn't closely match the genome being edited, CRISPR may not make the desired cut.

The guide RNAs are usually based on a reference genome compiled from just a few people's DNA that doesn't fully capture human diversity. And people with African ancestry are more genetically diverse than Europeans or Asians, whose ancestors left Africa and spread across the globe only relatively recently.

Ancestry issues with CRISPR were first reported 5 years ago, but Sean Misek, a postdoc at the Broad Institute of MIT and Harvard and lead author of the new preprint, wanted to explore them in cancer biology. His team turned to the Cancer Dependency Map, a collaboration that used CRISPR to systematically knock out roughly 18,000 genes in 1000 lines of cancer cells grown from individual human tumors. The project looked for genes involved in cancer growth or survival that could be targeted with drugs.

The team, which included senior authors Jesse Boehm at the Massachusetts Institute of Technology and Broad and Rameen Beroukhim of Broad and the Dana Farber Cancer Institute, found CRISPR failed to knock out 2% to 5% of the 18,000 genes in an individual cell line. These errors were about 20% more common in the 41 cell lines from people with recent African ancestry than in other groups, the team reports. As a result, "We're missing [cancer drug] targets in individuals of African descent," Misek says.

Similarly, Pinello's lab and others have shown how ancestry mismatches can cause CRISPR to cut the genome in the wrong spot when it is used to treat diseases such as sickle cell disorder, which mainly affects people of African ancestry. Such off-target cuts could lead to cancer. The CRISPR ancestry problem is an example of how excluding diverse populations in genomics studies "may inevitably contribute to cancer health inequity," says translational cancer biologist Olorunseun Ogunwobi of Hunter College of the City University of New York.

Both teams have built free web tools that compare a proposed guide RNA with tens of thousands of genomes procured from diverse populations. Ancestrygarden.org from the Boehm and Beroukhim labs lets users assess the impact of ancestral diversity on standard CRISPR guide RNAs. And CRISPRme from Pinello's team checks for off-target matches. "The hope here is that we push people to rethink how they're using CRISPR in the laboratory," Misek says.

"This is an important issue," and the web tools should help, says Melissa Davis, a genomicist who studies disparities in breast cancer at Weill Cornell Medicine. Adam Phillippy of the National Human Genome Research Institute agrees. "It is exactly tools like this—tools that make human genomic variation easy to explore and understand—that can help alleviate the bias in the first place." ■

Diplomacy players negotiate to build (and betray) alliances as they seek to control Europe.

PHOTO: NICK MOORE

MACHINE LEARNING

AI learns the art of Diplomacy

Meta's algorithm tackles both language and strategy in a classic board game that involves negotiation

By **Matthew Hutson**

Diplomacy, many a statesperson has argued, is an art: one that requires not just strategy, but also intuition, persuasion, and even subterfuge—human skills that have long been off-limits to even the most powerful artificial intelligence (AI) approaches. Now, an AI algorithm from the company Meta has shown it can beat many humans in the board game Diplomacy, which requires both strategic planning and verbal negotiations with other players. The work, researchers say, could point the way toward virtual exercise coaches and dispute mediators. International chatbot diplomacy may not be far behind.

"These are spectacular new results," says Yoram Bachrach, a computer scientist at DeepMind who has worked on the game Diplomacy but was not involved in the new research. "I'm particularly excited about Diplomacy because it's an exceptional environment for studying cooperative AI," in which machines don't just compete, but collaborate.

AI has already bested humans in games of strategy such as chess, Go, poker, and the video game Dota 2. It is also proving powerful at natural-language processing, in which it can generate humanlike text and carry on conversations. The game of Diplomacy requires both. It involves seven players vying for control of Europe. On each turn, players issue orders regarding the movement of army and naval units, following discussion with other players, whom they can attack or support. Success typically requires building trust—and occasionally abusing it. Both former President John F. Kennedy and former Secretary of State Henry Kissinger were fans of the game.

Previous AI research has focused on a version of the game called no-press Diplomacy, in which players do not communicate. That itself is a challenge for computers because the game's combination of cooperation and competition requires pursuing conflicting goals. The new work, published this week in *Science*, is the first to achieve respectable results in the full game. Noam Brown, a computer scientist at Meta who co-authored the paper, says when he started on the project, in 2019, he thought success would require a decade. "The idea that you can have an AI that's talking strategy with another person and planning things out and negotiating and building trust seemed like science fiction."

Meta's AI agent, CICERO, welds together a strategic reasoning module and a dialogue module. As in other machine learning AIs, the modules were trained on large data sets, in this case 125,261 games that humans had played online—both the game plays and transcripts of player negotiations.

The researchers trained the strategic reasoning module by having the agent play against copies of itself. It learned to choose actions based on the state of the game, any previous dialogue, and the predicted actions of other players, looking several moves ahead. During training, the researchers also rewarded it for humanlike play so that its actions wouldn't confound other players. In any domain, whether dinner-table manners or driving, conventions tend to ease interactions.

The dialogue module also required tuning. It was trained not only to imitate the kinds of things people say in games, but to do so within the context of the state of the game, previous dialogue, and what the strategic planning module intended to do. On its own, the agent learned to balance deception and honesty. In an average game, it sent and received 292 messages that mimicked typical game slang. For example, one message read, "How are you thinking Germany is gonna open? I may have a shot at Belgium, but I'd need your help into Den[mark] next year."

Jonathan Gratch, a computer scientist at the University of Southern California who studies negotiation agents—and provided early guidance for a Defense Advanced Research Projects Agency program that is also trying to master Diplomacy—notes two technical innovations. First, CICERO grounds its communication in multistep planning, and second, it keeps its remarks and game play within the realm of human convention.

To test its skill, the researchers had CICERO play 40 online games against humans (who mostly assumed it was a human). It placed in the top 10% of players who'd played at least two games. "In a game that involves language and negotiation, that agents can reach human parity is very exciting," says Zhou Yu, a computer scientist at Columbia University who studies dialogue systems.

Gratch says the work is "impressive" and "important." But he questions how much CICERO's dialogue, as opposed to its strategic planning, contributed to its success. According to the paper, Diplomacy experts rated about 10% of CICERO's messages as inconsistent with its plan or game state. "That suggests it's saying a lot of crap," Gratch says. Yu agrees, noting that CICERO sometimes utters non sequiturs.

Brown says the work could lead to practical applications in niches that now require a human touch. One concrete example: Virtual personal assistants might help consumers negotiate for better prices on plane tickets. Gratch and Yu both see opportunities for agents that persuade people to make healthy choices or open up during therapy. Gratch says negotiation agents could help resolve disputes between political opponents.

Researchers also see risks. Similar agents could manipulate political views, execute financial scams, or extract sensitive information. "The idea of manipulation is not necessarily bad," Gratch says. "You just have to have guardrails," including letting people know they are interacting with an AI and that it will not lie to them. "Ideally people are consenting, and there's no deception." ■

Matthew Hutson is a journalist in New York City.

EARTH OBSERVATION

NASA mulls end for long-lived climate sentinels

Drifting satellites could still yield insights into wildfires and storms, researchers argue

By **Paul Voosen**

Since NASA's Terra satellite launched in 1999, it has seen a world utterly transformed. Surface temperatures have risen half a degree. Sea levels have climbed 80 millimeters higher. Plants have expanded across an area as big as the Amazon rainforest. Through it all, Terra and two other satellites—Aqua, launched in 2002, and Aura, in 2004—served as the foremost sentinels of a changing planet, running far past their expected 6-year missions.

Now, all three satellites are approaching their end. They must save their remaining fuel to dodge space junk and slow down for a final plunge into Earth's atmosphere. Too little is left to maintain the precise pole-crossing orbits that allow them to swoop past lower latitudes at exactly the same time every day. In the next month, NASA is expected to decide whether to terminate the missions, which cost $85 million a year to run, and invest that money in its next-generation Earth System Observatory satellite program, which will replace some of the trio's capabilities by the late 2020s (*Science*, 7 May 2021, p. 554).

But killing them off now would be a mistake, the missions' scientists argue. The satellites are healthy enough to survive until the middle of this decade and provide measurements no other spacecraft can match. Their drifting orbits, far from hampering them, will allow them to see Earth from new vantages, at other times of day. "These are almost like new missions," says Norman Loeb, a physical scientist at NASA's Langley Research Center and principal investigator of Ceres, an instrument on Terra and Aqua that measures Earth's energy imbalance.

NASA is worried about the cost. If all three missions are extended, "it would require delays in the Earth System Observatory," NASA said in a statement to *Science*. But the scientists are now lobbying NASA to let them make their case next year at a "senior review," a meeting convened every 3 years to decide the fate of ongoing missions.

First conceived in the 1980s, the bus-size Terra and Aqua were each outfitted with an array of instruments, including the pioneering Moderate Resolution Imaging Spectroradiometer (MODIS), capable of parsing reflected light from vegetation, clouds, and sea ice in 36 different frequency channels. Other instruments, such as the infrared sounder on Aqua, capture temperature, water vapor, and dozens more variables globally each day. Aura, meanwhile, makes a close study of atmospheric chemistry. Because the instruments were mounted on the same spacecraft and tightly calibrated, they caught trends that otherwise would have been invisible. "These will be sorely missed observations," said Waleed Abdalati, a remote sensing scientist at the University of Colorado, Boulder, and former NASA chief scientist.

Before Aqua, for example, clouds were thought to cover half the planet at any time; now it's known to be nearly 70%. Terra has shown that plants cover 5% more of the planet than 20 years ago, a "greening" aided by rising carbon dioxide levels and warming. Aura has captured the intrusion of water vapor into the stratosphere from volcanic eruptions, where it adds to global warming and damages protective ozone. And the Ceres instruments have helped researchers discover that the deficit of energy escaping Earth has doubled since 2005, because of rising greenhouse gases and a decline in Sun-reflecting pollution hazes. "We're the only ones in the world doing this," Loeb says. "We're it."

A mission extension for NASA's Aqua satellite could enable observations of afternoon storms and fires.

New polar-orbiting weather satellites from the National Oceanic and Atmospheric Administration (NOAA) carry similar instruments, but they only have two-thirds as many channels as MODIS, says Miguel Román, chief climate scientist at Leidos, a large Washington, D.C.–based technology contractor, and principal investigator of MODIS. "At a fundamental level, you're trading a Swiss Army knife with 36 features down to 22," he says. The NOAA instruments are also designed to prioritize weather forecasting, not climate science, which few satellites are tailored for. "The public in general assumes that everyone is monitoring the climate," says João Teixeira, an atmospheric scientist at NASA's Jet Propulsion Laboratory and principal investigator of Aqua's infrared sounder.

Keeping the satellites alive would also ensure overlap with observations that will begin in early 2024 on the International Space Station. A new instrument on the station, the Climate Absolute Radiance and Refractivity Observatory (CLARREO) Pathfinder, will measure Earth's reflected light 10 times more precisely than past sensors. If the Ceres and MODIS measurements are calibrated with CLARREO Pathfinder's, long-term trends in Earth's energy balance will be easier to identify, says Kurtis Thome, Terra's project scientist at NASA's Goddard Space Flight Center (GSFC). "We'll have a long enough record to start and feel confident that if we see a trend, it's a real trend."

If the Aqua mission is continued, it will drift out of its current orbit, which crosses the equator more than a dozen times a day at 1:30 p.m. local time, and end up in one that crosses at 3:50 p.m. local time, says Claire Parkinson, Aqua project scientist at GSFC, who has led the mission for 29 years. Terra will drift to an earlier morning pass, from 10:30 a.m. to 9 a.m., and Aura will drift 50 minutes later, from 1:45 p.m. to 2:35 p.m.

The time changes will enable critical new investigations, researchers say. By observing earlier in the morning or later in the afternoon, the satellites will capture long shadows, which can reveal the 3D structure of surface features or clouds. Crossing the Arctic Ocean earlier and later in the day will reveal how it exchanges heat with the atmosphere at previously unobserved times. And Aqua will be primed to explore the severe storms and wildfires that tend to peak in late afternoon. "We're getting a new fire satellite by maintaining orbital drift," Román says. "They will get so much bang for their buck."

Even if NASA decides to end the missions, they have already secured their legacy. The researchers who conceived them originally wanted three sets of satellites, each lasting 6 years, to capture 18 years of change. Only one set was launched, but their longevity ensured the wish was fulfilled, Thome says. "We got it. We got the data we wanted to get." ■

PHOTO: NASA

SMALL VICTORIES

Nearly 30 years after apartheid's demise, a reporter revisits children's health in South Africa

By **Meredith Wadman**, *in KwaZulu-Natal, South Africa; Photography by* **Gulshan Khan**

By her country's standards at the time, there was nothing too unusual about how Nosipho Mshengu arrived in the world. She was born on the side of the road on 20 September 1993, as her mother tried to get from Mafakatini, a rural village in South Africa where there was then no health facility, to a Roman Catholic clinic an hour away. The bus she awaited was nowhere in sight when time ran out, and Mshengu made her entry then and there.

A little more than 14 years later, Mshengu was pregnant herself. Her labor story was different. Because teen pregnancies are high-risk, an ambulance drove her from the government health clinic that opened in Mafakatini in 1999 to Greys Hospital in Pietermaritzburg, the capital of the province of KwaZulu-Natal. The 41-kilometer trip paid off with a smooth delivery and a healthy baby boy, Esihle, now a teenager.

Unlike her mother, "I had access," Mshengu said through a translator. "They took me to experts to give birth in a safe, controlled environment. So my child didn't have any complications. Neither did I."

This story was supported by the Pulitzer Center.

It has been nearly 30 years since the demise of apartheid, the system of forced racial segregation and institutionalized discrimination that white South Africans created in 1948 and fought to defend until the early 1990s. Apartheid disenfranchised people who were not white, denied them job opportunities, and forced many black men to live in blighted townships beside whites-only cities, while their families languished in distant rural "homelands." Among the many devastating effects of apartheid on black South Africans, its harm to children's health stood out.

In 1994, as apartheid ended, 60 of every 1000 babies born in South Africa died be-

Nosipho Mshengu was born on the side of the road in her village the year before apartheid crumbled. In 2008, she gave birth to her son at a major hospital.

fore their fifth birthday. (In the United States at the time, the number was 10.) The death rate was so concerning that after Nelson Mandela's African National Congress handily won the country's first multiracial election that year, the new president immediately announced health care would be free for pregnant women and young children. It remains that way today in the nation of more than 60 million, of whom 81% are black and 36% are younger than 20.

In 1986, when the apartheid regime was still ruthlessly quelling dissent, I spent 2 months in South Africa as a visiting medical student studying pediatrics. I worked on the pediatric wards at the King Edward VIII Hospital, a huge, decrepit Durban hospital where black people were obligated to seek care and, briefly, in a small rural hospital far from the city. I saw toddlers suffer and die from vaccine-preventable diseases such as measles, a "typhoid isolation" unit that consisted of a crib placed in a corner of an open ward, and newborns crammed four to a bassinet. I also saw white children receive high-end care at a segregated beachfront hospital across town. The experience altered my career trajectory, sending me toward journalism and away from clinical medicine, which was so clearly outgunned in the face of a brutal political system.

I have often wondered, since the great democratic changes of the early 1990s, how pediatric health care has fared in the new South Africa. In July, I went back to find out.

THE DURBAN where my plane lands is different from the one I remember. The Indian Ocean seaport of more than 3 million then showcased a beachfront of glamorous hotels and restaurants, exclusively for white people. Now, the city's core has deteriorated markedly, blighted by riots last year. They were sparked by political divisions and fanned by a yawning economic divide between rich and poor, the largest in the world when last measured in 2014. Corruption has hobbled public services, resulting in daily electricity outages and perennial water shortages. Crime is rampant. And although democracy has elevated a substantial black middle class, the face of South African poverty remains overwhelmingly black. This shows up in the health care system, where there's high-end private care for those who can afford it and largely free but beleaguered public facilities for those who cannot.

Yet apartheid's collapse also ushered in transformative changes in health care that went well beyond free services for pregnant women and young children. Within a few years, Mandela's government launched a national immunization program to replace one that required "homelands," where black people lived, to have separate vaccination schemes. It built 1345 community health clinics and refurbished another 263—today there are more than twice as many—while making primary health care free to all. The government launched programs and passed laws aimed at making clean water and sanitation universal. The proportion of the population with access to a flush toilet, a ventilated pit latrine, or a composting toilet rose from 73% to 93% between 2000 and 2021, according to estimates from UNICEF.

All of this has fueled major gains in child health 30 years later. The under-5 mortality rate fell by nearly half, to 32 deaths per 1000 live births, by 2020. (In the United States today, the figure is 6.3.)

But a nuanced picture emerges when I visit the medical campus of the University of KwaZulu-Natal (UKZN), in Durban. It sits next to the sprawling 17-hectare site of King Edward. (The hospital is soon to be renamed for Victoria Mxenge, a nurse, midwife, lawyer, and antiapartheid activist murdered by

agents of the regime in 1985.) Moherndran Archary, a pediatric infectious disease specialist, has worked at the hospital and the Nelson R. Mandela School of Medicine almost continuously for 3 decades, and has seen the easing of some of the misery I remember.

I think back to a 5-year-old boy I saw in 1986 with a raging case of measles that had invaded his lungs. The doctor supervising me, speaking Zulu, asked the boy's mother whether the child had been vaccinated. "She says it's a long wait at the immunization clinic," he translated for me, shaking his head. At the time, just 64% of South African 1-year-olds had received a first dose of measles vaccine.

Today, Archary tells me, such children rarely turn up on the pediatric wards. Last year, 87% of babies received a first shot for measles, according to estimates from UNICEF—an all-time high. South Africa has also been a continental leader in introducing vaccines against bacteria that cause meningitis and pneumonia, and against rotavirus, which can cause fatal diarrhea in young children.

Sanitation improvements begun under Mandela also helped children stay healthy. When Archary began as a medical student at King Edward in 1991, "we had an entire ward of gastroenteritis," life-threatening diarrhea caused by various microbes in unclean water. That ward no longer exists, and although gastroenteritis remains a leading cause of hospital admission for young kids, the numbers are far lower than they were. "Cholera is a rarity," Archary adds, and in the past year he estimates he's seen one child with typhoid fever, another dangerous water-borne disease that was once commonplace.

But Refiloe Masekela, a specialist in pediatric lung disease who heads the medical school's pediatrics department, is troubled by other conditions that land children in her hospital. Vaccination coverage isn't as good as it appears at first blush, she says, because it falls off in kids more than a few months old. By age 2, she tells me, only about 70% of kids in KwaZulu-Natal are up to date with their vaccines.

Chronic malnutrition, meanwhile, is widespread. Twenty-seven percent of children under age 5 were growth-stunted in 2016, the same fraction as in 2003. And the COVID-19 pandemic—a "catastrophe" for kids, Masekela says—worsened malnutrition because schools, where many children get daily meals, were closed and parents lost their jobs. At King Edward and outlying provincial hospitals, pediatricians like her are again starting to see patients with acute malnutrition—their ribs in stark relief, their eyes gigantic in sunken faces.

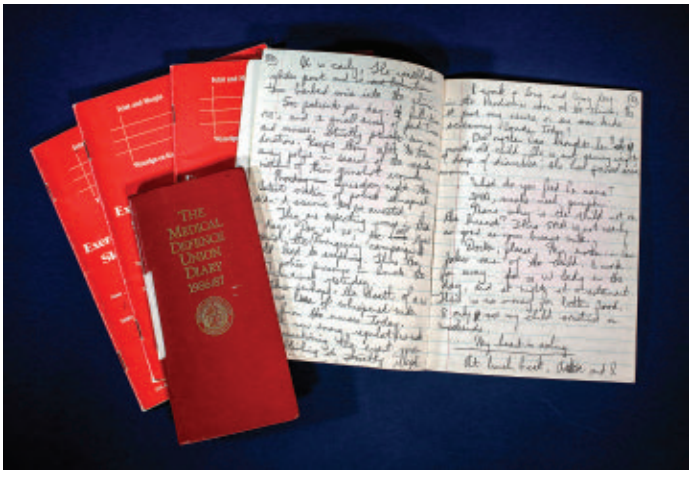

Overcrowding in the newborn nursery at Durban's King Edward VIII Hospital in 1986 (top). Journals the author kept as a medical student in South Africa that fall (bottom).

For Masekela and Archary, statistics like these underscore a painful reality: The end of apartheid didn't help black people as they had imagined it would. "South Africa has such an ingrained system of racial disparity, it has now translated into economic disparity," Archary says. "The economic disparity is still along racial lines."

MAFAKATINI, where Mshengu was born at the side of the road, nestles in the hills of rural KwaZulu-Natal, the province with the leading HIV burden in a country with one of the highest HIV burdens in the world. I travel there in a van belonging to the Centre for the AIDS Programme of Research in South Africa, which everyone calls CAPRISA. It's based at the UKZN medical campus in Durban but has research clinics elsewhere, including one in this village of 8000, where some people work as cashiers, drivers of taxi minivans called combis, and domestic workers although most are unemployed.

The deeply rutted dirt road disappears before we reach the edge of the village. There, I find 14-year-old Sandiswa Zondi outside her family's windowless wooden hut. It lacks electricity and running water and looks out on a parched valley; somewhere on the far side, her grandmother is searching for firewood. Sandiswa isn't at school on this winter Wednesday because her parents, who work on a flower farm 45 kilometers away, couldn't spare 10 rand—58 cents—for her and her 9-year-old brother to take a combi to get there. Sandiswa likes school and wants to become an airline pilot. She also yearns for her family to have a proper three-room house and intends to "stay away from boys," she says through a translator.

Her resolve is well placed. At Sandiswa's age, HIV prevalence in South African girls is about the same as it is in boys; by the time young women reach their early 20s, it's nearly 16%, three times what it is in young men. And by the time they get pregnant, 41% of girls and women at prenatal clinics in KwaZulu-Natal test positive for the virus. Nationwide, the figure is 30%. It hasn't budged in at least 15 years.

For girls like Sandiswa, who are almost always powerless to negotiate the use of condoms, it's crucial to have a means of protection that they themselves control, such as preventive antiretroviral pills, says Quarraisha Abdool Karim, an infectious disease epidemiologist at CAPRISA. Karim was a senior author on a landmark study in KwaZulu-Natal showing the cycle of HIV transmission is maintained by older men infecting younger women.

For decades, Karim has borne witness to South Africa's handling of the AIDS epidemic and its impact on teen girls. Mandela's administration largely ignored the virus in the 1990s; he became outspoken about fighting HIV only after leaving office. And in 1999, Thabo Mbeki, an AIDS

PHOTOS: (TOP TO BOTTOM) M. WADMAN/*SCIENCE*; E. PETERSEN/*SCIENCE*

Fourteen-year-old Sandiswa Zondi in the yard of her family's hut in Mafakatini, South Africa. She dreams of becoming an airline pilot.

PHOTO: GULSHAN KHAN

denialist, became president. Mbeki for several years refused to provide antiretroviral drugs to pregnant women and other infected people. The result: In the late 1990s and the early 2000s, about one in three infected pregnancies resulted in a baby with HIV, and child mortality rates skyrocketed (see graph, p. 824). "Just as we were reaping the benefits of democracy, HIV swoops in and robs us of it," recalls epidemiologist Salim Abdool Karim, CAPRISA's director and Quarraisha Abdool Karim's husband. "And it wasn't pharmaceutical companies charging too much. It was your own government." (Mbeki was forced out of office in 2008.)

Today, children in South Africa are faring far better when it comes to HIV, says Daya Moodley, a research scientist with CAPRISA and UKZN, who has spent decades seeking to prevent mother-to-child transmission. Thanks to an aggressive program that tests pregnant women at prenatal clinics and treats those infected with HIV, mother-to-child transmission is rare, occurring in less than 3% of infected pregnancies. On the horizon are long-acting, injected antiretroviral drugs such as one called cabotegravir, which was recently recommended by the World Health Organization after protecting women from infection in an African clinical trial. If such drugs can be deployed in at-risk girls and young women, Moodley says, they "will have a huge impact," reducing maternal infections and the resulting risk to babies. But she notes that high hurdles remain to distributing the drugs, and in sub-Saharan Africa, "we're always at the end of the stick to receive any effective and cost-effective treatment."

EVEN AS PREVENTABLE causes of death including AIDS, measles, and gastroenteritis have declined in young children, their early days are still perilous. Perinatal mortality—death late in pregnancy or in the first week of life—remains stubbornly persistent. As other preventable deaths have declined, data from Statistics South Africa indicate that perinatal mortality has become the leading cause of under-5 mortality. Prematurity, high maternal blood pressure, infections, and trauma during birth are all causes.

As a medical student I witnessed one such death in a small hospital in remote KwaZulu-Natal. A young woman labored and her baby's feet emerged first, soon followed by the legs, torso, and arms. The doctor tried in vain to deliver the baby's head. I watched with mounting horror as the little body hung limply while pulsations in the trapped umbilical cord slowed and then stopped.

In the awful silence, the doctor moved to stand beside the woman's shoulders. Without looking her in the eye he told her what had happened, and what needed to happen now to save her life. He used local anesthetic and cut the cartilage that binds the pubic bone together at the midline, widening the birth canal to deliver the head. When it at last emerged, it was clear the baby had hydrocephalus, a buildup of fluid on the brain, which caused an enlarged head. Hydrocephalus is common in spina bifida, in which the neural tube fails to close in early development. This infant had that condition, too. (Rates of spina bifida began to fall soon after South Africa began fortifying food staples with folic acid in 2003.)

"The mother was inconsolable," I wrote in my journal that night.

Since 1986, South Africa's neonatal mortality rate—death in the first month of life—has fallen by more than half. But those gains have stalled in the past decade, as has the rate of stillbirths. That's in spite of the country's strides in prenatal care. Seventy-six percent of pregnant women and girls completed at least four prenatal visits in 2016, and about 96% delivered their babies in health facilities. Still, numbers are uneven across the country; in KwaZulu-Natal, too few visits at prenatal clinics are a problem, Masekela says. And a large 2015 study of perinatal deaths in the province of Mpumalanga suggested subpar care during labor and delivery was also a factor.

Halting progress

Mortality in South African children younger than 5 years old shot up after apartheid ended in the early 1990s, as a devastating epidemic of HIV/AIDS took hold. Treatment of infected pregnant women, along with improvements in sanitation and vaccination, has improved the outlook over time.

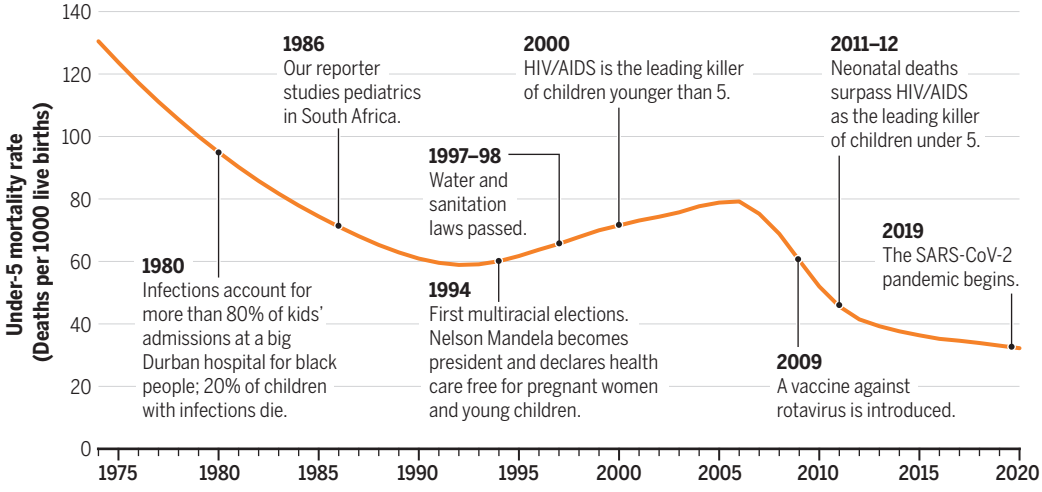

IN MALUKAZI, a squalid settlement of shacks with corrugated iron roofs on the southern fringe of Durban, a charity clinic copes with fallout from the conditions that babies face at home. The clinic, run by the Islamic Medical Association (IMA), sees a parade of crying toddlers with vomiting, diarrhea, and fever. Nurses take weights and temperatures and dispense acetaminophen, antibiotics, and oral rehydration therapy for diarrhea. On the day I visit, none of the small patients is in need of hospital admission: Their eyes are moist and their skin snaps elastically back into place when pinched, rather than tenting, as happens in cases of severe dehydration.

Sister Honey Allee, IMA's nursing director, is 76, with a mischievous smile, a white hijab, and a white suit with purple epaulets. She makes no effort to hide her disgust with the democratic government's failure, after nearly 30 years, to provide basic infrastructure for the inhabitants of Malukazi and other squatter settlements. This, she is sure, ensures that diarrhea remains a killer of small children in South Africa. It also means the clinic's nurses see an endless stream of children with scabies and skin abscesses from playing in the garbage-strewn landscape and urinary tract infections because they wipe their bottoms with newspaper fished out of refuse piles.

For the poorest of the poor, little has changed in the new South Africa, Allee says. "I feel—excuse me—the square root of bugger all is provided" by the government. "We don't have a place that's really fit for human habitation," she adds. Her charity has, among other things, dug boreholes and installed water taps in the shantytown, which lacks reliable running water.

Several of the women who have brought their charges here today share her lack of faith in the system. Nokwanda Mkhize took a 45-minute combi trip with a vomiting 8-month-old daughter and feverish 9-year-old niece, rather than using a free government health clinic a little closer to home. At IMA, she is charged a nominal fee that's well worth it, she says. "I prefer their service and they have medication to help the baby."

Nokwanda Mkhize with her baby daughter and niece at an Islamic charity clinic in Durban. She prefers it to a government clinic where medications often run out.

Her sentiments are echoed by Samkelisiwe Ndlovu, who has borrowed taxi fare from a relative in order to bring her daughter to the clinic from the four-room house that she shares with 11 people. The baby girl screams, perhaps from the rash that covers her groin and armpits. Yesterday, Ndlovu tried a government clinic and was told to go buy her own paracetamol, the generic form of Tylenol.

I'VE WAITED IMPATIENTLY for days to cross the threshold of the hospital that so influenced my life's trajectory: King Edward. When I think of the place, I remember the pediatric ward with its peeling paint, rats scurrying between dilapidated buildings, and a toddler with measles we found dead one morning under her oxygen tent. Her chart read: "Respiratory distress. Needs artificial ventilation. No beds available in intensive care unit."

Now, the hospital includes a gleaming pediatric center, with a sophisticated neonatal intensive care unit (ICU), a resuscitation room, and a pediatric emergency department, built with charitable donations. But permission to access King Edward and see for myself how conditions have changed doesn't come. So early one morning I stand outside, approaching patients in line to hear their stories.

Twenty-four-year-old Anele Macanhe is looking exasperated. She has forgotten the appointment card that would grant her access to the gated grounds of the 852-bed public hospital. Her phone to her ear, she is asking her partner to text her a photo of the card.

Macanhe's 4-year-old daughter, Sbahle Thunzi, who is standing by with her pink backpack, has eczema, which has turned her knees several shades darker than the rest of her skin and also afflicts her elbows, hands, fingers, and face. Her mother brings her regularly to the hospital, where a doctor examines Sbahle and refills her medications at no cost.

This Macanhe appreciates. She earns $250 each month working at a call center and cutting hair on the side. She also has an infant son to support. Today's trip will cost her $2.86 for round-trip bus fare—plus a day's wages, because visits to the hospital inevitably take hours.

CREDITS: (GRAPHIC) K. FRANKLIN/*SCIENCE*; (DATA) UNICEF DATA WAREHOUSE; UNITED NATIONS INTER-AGENCY GROUP FOR CHILD MORTALITY ESTIMATION; (PHOTO) GULSHAN KHAN

Four-year-old Sbahle Thunzi waits to enter the King Edward VIII Hospital, where she gets regular treatment for eczema free of charge. "Our government is looking out for us," says her mother, Anele Macanhe.

PHOTO: GULSHAN KHAN

"They help us without paying if you don't have money," she says. "Our government is looking out for us." (Patients at King Edward, as at other public hospitals, are charged on a sliding scale and many pay nothing.)

On the other hand, Macanhe concedes, she would take Sbahle to a private hospital if she could afford it. The crowding at King Edward is bad, the waiting times long, and medications often out of stock. "The doctor prescribes 10 things and you get five," she says.

Inside and out, the hospital is a study in contrasts. Despite the high-end pediatric facility, government and press accounts report broken CAT scanners and raw sewage running in the gutter beside the hospital. According to a 2017 report, when a government team visited King Edward, patients were being carried up to the fifth-floor surgical ward because an elevator was broken. "The food is bad. The cleaning is bad. The bedding, linen service is nonexistent," says Allee, who sometimes accompanies patients there.

King Edward is not alone. The government team in 2017 visited three other Durban-area public hospitals and reported similar problems at all of them. And this past spring, a physician at a children's hospital in Johannesburg wrote in an open letter to administrators: "Come to our unit and see doctors trying to intubate children and administer [CPR] by their mobile phone's torch, as the power has failed … again. … Come and see how hospital-acquired infections spread like wildfire through the neonatal ward because the taps are dry. … Children are dying and the horrendous conditions in our public hospitals are contributing to their deaths."

"Our health care services are on a path to ruin," Salim Abdool Karim says. He was assistant superintendent of King Edward in 1990, an era when "white managers barked orders at black staff," he recalls. Apartheid's end thankfully made that model of management a thing of the past, he says. But he contends that it's been replaced by a system with its own deep troubles. "Corruption has thrived, because of ineptitude and ineffectiveness in management. So across the board, the provision of services and the quality of care has been compromised."

The head of the province's health department, Sandile Tshabalala, did not respond to repeated requests for permission to visit the hospital or to emailed questions. But King Edward's CEO, Thami Mayise, wrote in an email: "My team is doing the best they can, given the circumstances they operate under."

It's also worth noting that children with serious ailments can receive high-end care in the public system. Still, Masekela notes, there are just 23 ICU beds for more than 3 million children in KwaZulu-Natal province.

Macanhe and her daughter leave King Edward that day around noon with a neighbor they bumped into, saving Macanhe from spending precious rands on taxi fare. It was a good visit: On her lap is a plastic bag stuffed, for once, with 10 out of 10 eczema medications.

That evening, as my plane lifts off from the tarmac, my heart is heavy. I think of Mshengu and her risky roadside birth in apartheid's twilight, and her own son's safer entry into the world years later. The numbers make clear that black children are doing better than they were in the 1980s and early '90s, when the apartheid regime compounded their suffering. But hunger, disease, and death still shadow many of them.

Today, "The primary problem is a socioeconomic problem," Masekela told me. "When you don't have access to clean water or electricity; when you're living in a crowded space and you have no food—that cannot be fixed by the health system." Meanwhile, children like would-be airline pilot Sandiswa, earthbound in her dusty village, are still waiting for a better day. ■

Science capitalizes Black to acknowledge the ethnic and cultural identity of Black Americans. Many South Africans use "black people" to refer to people of African descent, a style we follow here.

INSIGHTS

PERSPECTIVES

MATERIALS SCIENCE

A sweet solution to complex microprinting

A simple sugar mixture transfers functional components to surfaces with intricate geometry

By **Blake N. Johnson**

Design and manufacturing processes that modify surfaces have seen rapid development in recent years (*1*–*4*). Besides aesthetics, these modifications can add new functionalities to an object. For example, the regular arrangement of modifications on a surface (periodic structuring) is used to create chemical sensors, cloaking devices, and optical fibers, among other tools (*5*). Despite the versatility of surface modification techniques, such as direct transfer, three-dimensional (3D) printing, and "wrapping," there are limitations associated with properties of the functional components and target objects, as well as from the desired deposition patterns. On page 894 of this issue, Zabow (*6*) presents a relatively simple approach for transferring arrays of diverse functional components onto objects with complex 3D geometries. The method uses a familiar material—table sugar—in a "reflow" process that leverages sugar's melting and dissolving properties to create a flowable "stamp."

Surface modification is an umbrella term that covers a wide range of processes, from the 3D printing of complex circuits onto an object to the wrapping of a guitar body with graphics using water transfer. Additive-based surface modification can be achieved by printing (using a nozzle), pick-and-place (using a tweezer), or transfer (using a wrapper) processes, with each technique offering different advantages. Transfer processes use a liquid or solid "carrier" to deposit a functional component onto an object. The carrier must be capable of capturing the component from an initial surface (such as stiff wafer) and releasing it onto the surface of the target. Stretchable and flexible solid carriers (such as silicone stamps) can be used to integrate an array of components, typically one type, on a range of elaborate 3D objects. However,

IMAGE: GARY ZABOW

Laser confocal micrographs show pollen grains bearing complex surface topologies that have been micropatterned with a flowable "stamp."

objects bearing discontinuities in surface slope and protruding features (peaks) of high height-to-width ratio that hang over the surface present challenges. Alternatively, liquid carriers (such as a transfer film floating in water onto which an object is dipped) can be used to integrate functional components onto objects of complex geometry. However, it is difficult to deposit arrays of small components that are not first formed on a thin transferrable film with precision on complex geometry, because the movement of each array element is relatively restricted on a film compared with a liquid carrier. By comparison, printing and pick-and-place processes are more versatile regarding an object's geometry, but require the component material to be printable or graspable. This also requires the object to be digitally mapped in 3D, adding even more time and cost to manufacturing.

To overcome some of the constraints in additive-based surface modification processes associated with use of only solid or liquid carriers, Zabow describes a transfer technique for an array of functional components that are arranged in a complex geometry on the target (such as a periodic pattern of components, conforming to a curved surface). The method uses a sugar mixture as a pourable and dissolvable carrier and a process similar to that used in making hard candy. A heated sugar and corn syrup mixture is allowed to cool, but before it solidifies, it is poured over the components to be integrated onto the surface, forming a meltable "stamp." Zabow starts with a pouring and solidification step (casting) in which the sugar-based carrier is poured at low temperature over the functional components (including microscale metal, polymer, and glass elements) that have been prearranged in a desired pattern on an initial surface. The components—now embedded in a hardened sugar mixture "stamp"—are then transferred by slowly melting the stamp over the target object (hence, reflowing). After the deformed sugar mixture cools and resolidifies, the sugar mixture is washed away using water. Because the process uses a carrier that undergoes a phase change, it provides the control of solid carriers with the geometry matching of liquid carriers. Thus, the technique removes some constraints of solid, fluid, and contact mechanics associated with water and solid stamp-based transfer methods.

Zabow demonstrated the technique on a wide range of objects, including those with protruding features that overhang the surface, as well as on component and object materials such as metal disks, ellipses, and rings; polymer and glass microspheres; and hydrogels. The precision of the method was also demonstrated by attaching an array of thousands of 1-μm disks onto a pin head, which surpasses the boundaries of current transfer techniques.

The author also transferred desired functionality onto multiple biological surfaces including individual hair fibers, plant seeds, and animal cells. The ability to deposit conformal arrays across a range of micro- to macroscale objects that bear complex geometry using a biocompatible, water-based, low-temperature process may be transformative to various disciplines, including tissue engineering, as well as technologies such as biomedical devices, metamaterials, and sensors. For example, functionality integration with commonly used biomedical components (needles, fibers, tubings) could enable the design and manufacture of diagnostic and therapeutic tools, such as bioelectronic therapeutics (*7*–*9*).

There are many different directions to further develop the reflow-transfer technique of Zabow by considering fundamental principles in rheology (deformation of flowing films) and phase equilibria (optically or chemically driven phase transition). The process also opens the door to questions about quality and reproducibility. How the placement precision of the integrated functional components can be optimized and determining the limits on functional components that can be transferred are also questions to be explored. ■

Grado Department of Industrial and Systems Engineering, Department of Materials Science and Engineering, Department of Chemical Engineering, School of Neuroscience, Virginia Tech, Blacksburg, VA, USA. Email: bnj@vt.edu

REFERENCES AND NOTES

1. K. Sim *et al.*, *Nat. Electron.* **2**, 471 (2019).
2. B. Le Borgne *et al.*, *Adv. Mater. Technol.* **4**, 1800600 (2019).
3. E. Kucukdeger *et al.*, *Flex. Print. Electron.* **6**, 044002 (2021).
4. Y.-K. Lee *et al.*, *Sci. Adv.* **6**, eaax6212 (2020).
5. J. Hu *et al.*, *Front. Phys.* (Lausanne) **8**, 586087 (2021).
6. G. Zabow, *Science* **378**, 894 (2022).
7. A. Canales *et al.*, *Nat. Biotechnol.* **33**, 277 (2015).
8. A. Branner, R. B. Stein, E. Fernandez, Y. Aoyagi, R. A. Normann, *IEEE Trans. Biomed. Eng.* **51**, 146 (2004).
9. D. Qi *et al.*, *Adv. Mater.* **29**, 1702800 (2017).

ACKNOWLEDGMENTS

B.N.J. acknowledges the support of GlycoMIP, a National Science Foundation Materials Innovation Platform funded through Cooperative Agreement DMR-1933525. B.N.J. also acknowledges the support of the National Science Foundation through CBET-2144310.

10.1126/science.ade6722

MEDICINE

The influenza universe in an mRNA vaccine

An mRNA–lipid nanoparticle vaccine protects animals from 20 influenza lineages

By **Alyson A. Kelvin**[1,2] *and* **Darryl Falzarano**[1,3]

The greatest challenge to preventing the next influenza pandemic is the extensive diversity within the influenza virus family (*1*). At present, 20 lineages of influenza A and B viruses have been identified, each containing numerous strains (*2*, *3*). Current influenza vaccines, composed of four influenza viral antigens, provide little protection beyond the viral strains targeted by the vaccines. Universal influenza vaccines that can protect against all 20 lineages could help to prevent the next pandemic (*4*). Designing and manufacturing a vaccine that can provide such broad protection has been challenging, but the demonstration of the feasibility of mRNA–lipid nanoparticle COVID-19 vaccines offers a possible strategy (*5*). On page 899 of this issue, Arevalo *et al.* (*6*) report an influenza vaccine, using mRNA–lipid nanoparticle technology incorporating representatives of all 20 influenza virus lineages, that protected mice and ferrets from diverse influenza viruses. This provides a pathway to a universal influenza vaccine.

Influenza viruses are an ever-constant public health threat because circulating viruses continue to evolve, and new viruses spill over from animal reservoirs. The 20 influenza virus lineages over both A and B viruses are defined by 20 different hemagglutinin (HA) proteins. Current approved seasonal vaccines focus immune responses on the surface HA protein of circulating influenza viruses. The HA protein is responsible for host cell receptor binding, thus facilitating infection (*7*). Neutralizing antibodies, directed toward the HA receptor binding domain can block influ-

[1]Vaccine and Infectious Disease Organization (VIDO), University of Saskatchewan, Saskatoon, Saskatchewan, Canada. [2]Department of Biochemistry, Microbiology, and Immunology, University of Saskatchewan, Saskatoon, Saskatchewan, Canada. [3]Department of Veterinary Microbiology, Western College of Veterinary Medicine, University of Saskatchewan, Saskatoon, Saskatchewan, Canada. Email: alyson.kelvin@usask.ca

enza viruses from binding host cells, thereby providing protection from infection.

The most commonly used influenza vaccine is the split virion protein vaccine. These vaccines are produced in chicken eggs to grow selected viruses, which are subsequently inactivated with detergent to break up the viral particle. For seasonal vaccines, a maximum of four viral antigens are prepared in this manner. However, this platform has a limited ability to induce broadly protective responses. Recognizing the challenge of targeting 20 lineages at once, previous universal vaccine strategies have largely focused on exploiting conserved regions of viral proteins and manipulating the host immune responses to focus on these regions (*3*). Universal vaccine targets have included the internal nucleoprotein (NP) and the less accessible yet conserved regions of surface proteins, such as the matrix 2 (M2) protein and the stalk region of HA (*3*, *4*). Although more highly conserved, these proteins or protein domains are often difficult to produce, are poorly immunogenic, and elicit immune responses without blocking infection.

Arevalo *et al.* took an alternate approach to universal vaccine design by leveraging the mRNA–lipid nanoparticle platform to include mRNAs that encode HA proteins representing each influenza virus lineage in a single formulation. Although a good seasonal vaccine target, HA has so far been suboptimal as a single-antigen universal vaccine candidate (*7*). Using a brute-force approach, representative HA molecules of each of the 20 lineages were chosen for the mRNA vaccine. Selection was based on phylogenetic analysis and the likelihood that a particular HA would be a threat to humans. In mice and ferrets, vaccination elicited specific antibodies toward each of the 20 different HA targets in the vaccine. These findings highlight the flexibility of the mRNA vaccine platform to encompass a high number of vaccine antigens without interference among the various mRNAs.

Immunization of ferrets and mice also provided protection from both a virus that matched the vaccine components as well as mismatched (or heterologous) influenza viruses. Notably, lung infection of vaccinated ferrets with a matching virus strain was completely blocked, outperforming previous egg-based split virion vaccines (*8*, *9*). Additionally, the universal mRNA vaccine candidate elicited antibodies to the conserved HA stalk region, which is associated with broadly reactive antibodies and cross-protection. Because the HA antibodies elicited by the mRNA vaccine were against both conserved regions and the receptor binding domain, each antibody is hypothesized to cover other strains within each lineage. This was demonstrated by a heterologous influenza virus challenge whereby mice and ferrets vaccinated with the 20-lineage mRNA vaccine were protected from severe disease and mortality despite having evidence of viral infection in the lungs. Nonneutralizing antibodies and antibody-dependent cellular cytotoxicity (ADCC) were identified as mechanisms of protection. Conversely, T cell depletion studies suggested little involvement of cell-mediated immunity.

These results indicate that people vaccinated with a universal mRNA vaccine would also be protected from severe disease through B cell–dependent mechanisms if a completely new influenza virus strain were to emerge. Moreover, because most people above the age of 6 months have previously been infected with influenza viruses or are vaccinated, it is essential to determine whether a previous exposure could influence the outcome of immunization with a universal mRNA vaccine (*10*–*12*). To this end, Arevalo *et al.* showed that a previous infection with influenza H1N1 virus in mice did not alter vaccine-associated immunogenicity or protection.

"Using a brute-force approach, representative hemagglutinin molecules of each of the 20 lineages were chosen for the mRNA vaccine."

The strengths of the mRNA platform for pandemic vaccine production include flexibility of antigen design, increased numbers of potential viral targets, speed of production, and inexpensive and scalable manufacturing (*13*). These strengths are important when designing and producing vaccines for a highly diverse, unpredictable family of viruses that can easily spread globally in a matter of weeks (*3*, *14*). The current production timeline of the standard egg-based influenza split virion protein vaccines is 6 months, which is not sufficient to stop the next potential pandemic virus in the targeted time frame of 100 days, as recommended by the Coalition for Epidemic Preparedness Innovations (*3*, *15*). Formulating and manufacturing 20-valent vaccines on the current split virion vaccine platform would be nearly impossible. The high amount of protein needed for each component would potentially be unfavorable to the vaccinee and, as Arevalo *et al.* demonstrated, would not induce a balanced immune response to each of the 20 proteins. Currently, it is not clear why immunogenicity after mRNA vaccination remained stable as the number of targets increased. The authors hypothesized that this lack of immunodominance may be the result of the induction of long-lived germinal center reactions that regulate B cell clonal expansion, B cell maturation, and antibody focusing. It is also possible that the initial events after immunization may provide equal opportunity for antigen presentation. mRNA vaccines can be taken up by both muscle cells and antigen-presenting cells (APCs), whereas protein vaccines rely specifically on APCs for uptake. This may result in less opportunity for all antigens to initiate robust immune responses.

Although the 20-lineage universal mRNA vaccine or another mRNA influenza vaccine can quickly be scaled up to prevent the next pandemic, questions remain regarding the regulatory and approval pathway of such a vaccine that targets viruses of pandemic potential but that are not currently in human circulation. Hence, estimating vaccine effectiveness and developing a target product profile for a vaccine against viruses not yet identified is not straightforward. Clearly, discussions of this nature should not wait until the next pandemic virus emerges. Additionally, it is unknown how far this high-valency vaccine model can be extended and whether additional antigens from each lineage can be included to further increase protection or decrease the need to update the vaccine. Critics may argue that increasing the number of vaccine targets will increase influenza virus evolution to circumvent vaccine immunity. But this scenario seems unlikely because the multivalent vaccine from this study was associated with preventing viral infection and replication in vivo. These results suggest that this vaccine will most likely decrease the potential of new viral strains to emerge. Addressing both the limits of mRNA components and clarifying a pathway to approval are essential to the optimization and use of truly universal vaccines. ■

REFERENCES AND NOTES

1. H. Kim, R. G. Webster, R. J. Webby, *Viral Immunol.* **31**, 174 (2018).
2. J. S. Long, B. Mistry, S. M. Haslam, W. S. Barclay, *Nat. Rev. Microbiol.* **17**, 67 (2019).
3. W. N. Harrington, C. M. Kackos, R. J. Webby, *Exp. Mol. Med.* **53**, 737 (2021).
4. F. Krammer, P. Palese, *Nat. Rev. Drug Discov.* **14**, 167 (2015).
5. M. J. Hogan, N. Pardi, *Annu. Rev. Med.* **73**, 17 (2022).
6. C. P. Arevalo *et al.*, *Science* **378**, 899 (2022).
7. N. C. Wu, I. A. Wilson, *Cold Spring Harb. Perspect. Med.* **10**, a038778 (2020).
8. Y.-C. Tseng *et al.*, *Proc. Natl. Acad. Sci. U.S.A.* **116**, 4200 (2019).
9. N. Pardi *et al.*, *Nat. Commun.* **9**, 3361 (2018).
10. A. A. Kelvin, M. Zambon, *Euro Surveill.* **24**, 1900720 (2019).
11. D. M. Skowronski *et al.*, *Euro Surveill.* **24**, 1900585 (2019).
12. M. E. Francis, M. L. King, A. A. Kelvin, *Viruses* **11**, 122 (2019).
13. N. Pardi, M. J. Hogan, D. Weissman, *Curr. Opin. Immunol.* **65**, 14 (2020).
14. Centers for Disease Control, 2009 H1N1 Pandemic Timeline (2019); www.cdc.gov/flu/pandemic-resources/2009-pandemic-timeline.html.
15. M. Saville *et al.*, *N. Engl. J. Med.* **387**, e3 (2022).

10.1126/science.adf0900

ATMOSPHERIC CHEMISTRY

Australian wildfires depleted the ozone layer

Various mechanisms initiated by wildfires thinned the stratospheric ozone layer

By **Ross J. Salawitch**[1,2,3] *and* **Laura A. McBride**[1,2,4]

The Australian wildfires of late 2019 and early 2020 claimed the lives of 33 people and more than 1 billion animals (*1*). The fires blanketed southeastern Australia with thick smoke that may have caused the loss of an additional 417 people from hospitalizations associated with elevated levels of fine particulate matter in the air (*2*). The smoke layer led to a series of atmospheric phenomena that reduced the thickness of Earth's protective ozone layer in the stratosphere, which lies between ~15- and 50-km altitude above the surface. The reduction of total column ozone (TCO), a measure of ozone layer thickness, was particularly strong at mid-latitudes of the Southern Hemisphere during late 2020. Various explanations linking smoke from these wildfires to this observed decline in TCO have been proposed. This debate highlights the shortcomings in our understanding of how wildfires, which are increasingly common because of climate change, affect stratospheric chemistry and Earth's protective ozone layer.

Massive wildfires can initiate or intensify thunderstorms, leading to pyrocumulonimbus (pyroCB) clouds, which are dense, towering structures that often rise to the upper troposphere (12 to 17 km) or lower stratosphere (13 to 22 km) (*3*). In early 2020, a series of pyroCB clouds connected to the Australian wildfires injected smoke-laden, tropospheric air deep into the stratosphere, reaching an altitude as high as 35 km (*4*–*6*). These wildfire-induced convective events are the largest pyroCB clouds ever observed—in terms of both the amount of smoke injected into the stratosphere and the height of the plume—since modern satellite data became available in 1978 (*6*). The largest smoke-laden plume generated a vortex-like circulation system with a diameter of ~1000 km that persisted for several months and rose to 35-km altitude because of heating driven by the absorption of sunlight by smoke (*4*–*6*). As this vortex moved between 30°S and 55°S, roughly the latitude region of the wildfires, pockets of very low TCO persisted (TCO is the vertical integral of the concentration of ozone from the ground to the top of the atmosphere and is an established measure of ozone layer thickness). The largest reduction in TCO was ~100 Dobson units (DU), meaning that the thickness of the ozone layer was ~60% of the unperturbed value, which is a large decline in the thickness of the ozone layer (*5*). These reductions in TCO, which existed in ~1000-km-wide structures that traversed the globe every 10 weeks (*5*), were caused by the injection of ozone-poor tropospheric air into the stratosphere, as confirmed by the associated simultaneous increase of nitrous oxide (N_2O) and several chemical markers of combustion (*4*, *6*).

As the smoke-laden vortices dispersed, greatly increased concentrations of suspended particulate matter (aerosols) were observed throughout the stratosphere in the Southern Hemisphere (*7*). The principal method of detecting the aerosols in the stratosphere is to measure the transmission of solar radiation through the stratosphere to the ground, called stratospheric aerosol optical depth (SAOD). Satellite observations show a substantial increase of SAOD, spanning 30°S to 60°S, that started in mid-January of 2020. The aerosols responsible for the elevated SAOD exhibit a spectral signature characteristic of oxygenated organics (*8*). The maximum increase of SAOD at Southern Hemisphere mid-latitudes because of the Australian wildfires was larger than the perturbation caused by the April 2015 eruption of the Calbuco volcano in southern Chile yet well below the increase that followed the June 1991 eruption of Mount Pinatubo (*9*). Both of these eruptions resulted in considerable depletion of stratospheric ozone owing to chemical transformations that were initiated by reactions on the surface of volcanic aerosols, which predominately have a chemical composition of sulfate (H_2SO_4). The increase of stratospheric aerosols after the Australian wildfires had a number of important consequences for the thickness of the ozone layer: warming of ~1° to 2°C in the mid-latitude lower stratosphere of the Southern Hemisphere (*7*), the near-immediate alteration of stratospheric winds as a result of this warming (*4*), and changes in the abundance of reactive chemical species that drive photochemical loss of ozone (*7*, *10*–*13*) (see the figure).

Response of stratospheric ozone to wildfire aerosols

The thickness of the stratospheric ozone layer in 2020 at Southern Hemisphere mid-latitudes could have been reduced because of changes in wind patterns and by chemical loss reactions involving chlorine monoxide (ClO). The cross section of atmospheric ozone (left) shows changes in stratospheric winds that may have been initiated by the absorption of sunlight by aerosols injected into the lower stratosphere by the Australian wildfires. The chemical process responsible for the observed changes in hydrochloric acid (HCl), chlorine nitrate ($ClONO_2$), and ClO (right) in the lower stratosphere after exposure of air to wildfire aerosols is important for ozone and is not currently understood.

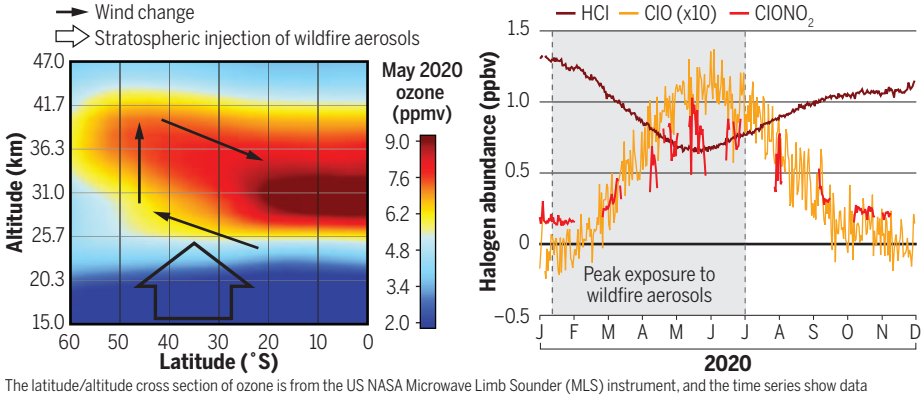

The latitude/altitude cross section of ozone is from the US NASA Microwave Limb Sounder (MLS) instrument, and the time series show data acquired by the MLS (HCl and daytime minus nighttime ClO) and by the Canadian Space Agency's Atmospheric Chemistry Experiment–Fourier Transform Spectrometer instrument ($ClONO_2$) (*12*). ppbv, parts per billion by volume; ppmv, parts per million by volume.

GRAPHIC: K. FRANKLIN/*SCIENCE*

[1]Department of Atmospheric and Oceanic Science, University of Maryland College Park, College Park, MD, USA. [2]Department of Chemistry and Biochemistry, University of Maryland College Park, College Park, MD, USA. [3]Earth System Science Interdisciplinary Center, University of Maryland College Park, College Park, MD, USA. [4]Department of Chemistry and Biochemistry, Albright College, Reading, PA, USA. Email: rsalawit@umd.edu; lmcbride@albright.edu

Quantification of the effect of wildfire aerosols on ozone is challenging because the concentration of ozone responds to numerous radiative, chemical, and dynamical factors. Furthermore, the nature of surface-mediated reactions occurring on the resulting oxygenated aerosols is uncertain. Soon after the stratospheric injection of smoke by the Australian wildfires had been documented, one study predicted that decreases in TCO of 10 to 20 DU could occur throughout southern middle to high latitudes (40°S to 70°S) owing to changes in stratospheric circulation and chemistry (*10*). Observations show a substantial reduction in the abundance of ozone in the lower stratosphere between 30°S and 60°S that maximized during May to August 2020 at ~6 to 7 DU below the 2012 to 2019 mean value (*7*). A different study showed that TCO over much of Southern Hemisphere mid-latitudes during July to November 2020 was ~8 to 15 DU lower than normal, coincident with a substantial reduction in stratospheric nitrogen oxides (NO_x) that are characteristic of the heterogeneous hydrolysis of nitrogen pentoxide (N_2O_5) that occurs on the surface of sulfate aerosols (*11*). Both studies (*7*, *11*) suggested anomalously low ozone was caused by chemical transformations occurring within the stratosphere, although one study (*11*) emphasized that wildfire-induced changes in stratospheric wind patterns could also play a role in the reduced TCO observed in 2020.

Some background on stratospheric chemistry helps elucidate the effect of smoke from the Australian wildfires on the ozone layer. The Antarctic ozone hole is caused by transformation of stratospheric inorganic chlorine compounds, most of which originate from anthropogenic activity, owing to heterogeneous (surface-mediated) chemical reactions that occur at appreciable rates only under extremely cold conditions. These heterogeneous reactions cause nearly complete removal of hydrochloric acid (HCl) and chlorine nitrate ($ClONO_2$), resulting in highly elevated abundances of chlorine monoxide (ClO) that lead to near-complete photochemical loss of ozone. Another heterogeneous chemical reaction, the hydrolysis of N_2O_5, occurs on the surface of sulfate aerosols for a wide range of temperatures (*14*). This second heterogeneous reaction converts nitrogen oxides (NO and NO_2) to nitric acid (HNO_3), suppressing the abundance of NO_2 and increasing ClO. The net effect of heterogeneous chemical reactions on the surface of sulfate aerosols injected into the stratosphere after recent major volcanic eruptions has been a reduction in the thickness of the ozone layer at mid-latitudes, with little or no variation in the stratospheric concentrations of HCl and $ClONO_2$ (*9*).

Chemical processes occurring on the surface of oxygenated organic aerosols injected into the stratosphere after the Australian wildfires led to unusual changes in the chemical composition of the mid-latitude Southern Hemisphere stratosphere that bear some relation to the transformations responsible for the ozone hole (*8*, *12*, *13*). In addition to the suppression of NO_2 (*11*), several studies document a large increase in the concentration of $ClONO_2$ coincident with a substantial reduction in HCl (*8*, *12*, *13*). Satellite observations reveal large increases in the concentration of ClO in the lower stratosphere, with a peak in June 2020 that is far above the 2005 to 2019 range of prior observations (*12*). This increased ClO led to a ratio of reactive chlorine to reservoir chlorine [i.e., ClO/(HCl+$ClONO_2$)] of ~7/100, which is close to that observed after the eruption of Mount Pinatubo (*14*). However, the SAOD increase after the Australian wildfires was much less than that observed after this eruption. Consequently, the observation of elevated ClO at a level comparable to that of the Mount Pinatubo eruption suggests that the composition of wildfire aerosols is the major determining factor in the observed chemical transformations.

The magnitude of elevated ClO in the mid-latitude Southern Hemisphere lower stratosphere after the Australian wildfires should result in appreciable chemical loss of ozone (*9*). Nonetheless, several studies attribute the observed reductions in TCO resulting from Australian wildfires to changes in stratospheric wind patterns (*12*, *13*) rather than to chemistry. The evidence for a change in the dynamical state (i.e., wind patterns) of the mid-latitude lower stratosphere of the Southern Hemisphere is strong. Ground-based observations show a rise in the total column (vertical integral) of N_2O, coincident with a decline in total column hydrogen fluoride (HF) starting in May 2020 that is a hallmark of air masses over the vast regions of the Southern Hemisphere becoming less photochemically aged than normal. This meteorological change leads to reductions in TCO because ozone accumulates as air photochemically ages. However, how much of this change in the dynamical state of the Southern Hemisphere stratosphere was caused by atmospheric heating caused by Australian wildfire aerosols is unclear. Before these fires, the direction of winds in the tropical stratosphere had transitioned from a westerly to easterly phase, a phenomenon typically associated with the transport of younger tropical air to mid-latitudes along with an associated reduction in TCO (*13*).

Understanding the effect of wildfires on stratospheric chemistry is at an early stage. Observations of reduced concentrations of NO_2 and HCl coincident with increased ClO and $ClONO_2$ are not reproduced by computational models that include known surface-mediated chemical reactions on stratospheric aerosols, assuming that these aerosols have acquired a sulfate coating (*12*, *13*). There is a need for laboratory studies to elucidate the heterogeneous reaction rates that occur on the oxidized organic particles responsible for increased stratospheric aerosol concentrations in 2020 (*11*). Until such models can accurately simulate observations of ClO after the stratospheric injection of Australian wildfire smoke, it will be difficult to properly assess the degree to which stratospheric photochemistry reduced the thickness of the ozone layer. Increased stratospheric aerosol loading caused by the Australian wildfires may be the driving factor in the severely depleted Antarctic ozone holes of 2020 and 2021 (*7*, *15*) as well as changes in the large-scale circulation of the Southern Hemisphere that extend to the surface (*15*). The radiative effect of Australian wildfire aerosols on the dynamical state of the Southern Hemisphere should be assessed on the basis of analyses of simulations of stratospheric transport with and without wildfire aerosols, similar to those conducted after the 1991 eruption of Mount Pinatubo (*9*). Better understanding of the effect of wildfire aerosols on both the chemical and dynamical properties of the stratosphere is needed before consensus is achieved regarding the magnitude of ozone layer depletion attributable to the Australian wildfires. Improved understanding of the threat to the ozone layer posed by massive wildfires is needed because climate change is expected to increase both the frequency and intensity of wildfires (*3*, *5*, *11*, *15*). ■

REFERENCES AND NOTES

1. A. I. Filkov *et al.*, *J. Saf. Sci. Resil.* **1**, 44 (2020).
2. N. Borchers Arriagada *et al.*, *Med. J. Aust.* **213**, 282 (2020).
3. M. Fromm, R. Servranckx, B. J. Stocks, D. A. Peterson, *Commun. Earth. Environ.* **3**, 243 (2022).
4. G. P. Kablick III, D. R. Allen, M. D. Fromm, G. E. Nedoluha, *Geophys. Res. Lett.* **47**, e2020GL088101 (2020).
5. S. Khaykin *et al.*, *Commun. Earth Environ.* **1**, 22 (2020).
6. M. J. Schwartz *et al.*, *Geophys. Res. Lett.* **47**, e2020GL090831 (2020).
7. L. A. Rieger, W. J. Randel, A. E. Bourassa, S. Solomon, *Geophys. Res. Lett.* **48**, e2021GL095898 (2021).
8. P. Bernath, C. Boone, J. Crouse, *Science* **375**, 1292 (2022).
9. D. E. Kinnison *et al.*, *J. Geophys. Res.* **99**, 25705 (1994).
10. P. Yu *et al.*, *Geophys. Res. Lett.* **48**, e2021GL092609 (2021).
11. S. Solomon *et al.*, *Proc. Natl. Acad. Sci. U.S.A.* **119**, e2117325119 (2022).
12. M. L. Santee *et al.*, *Geophys. Res. Lett.* **49**, e2021GL096270 (2022).
13. S. E. Strahan *et al.*, *Geophys. Res. Lett.* **49**, e2022GL098290 (2022).
14. D. W. Fahey *et al.*, *Nature* **363**, 509 (1993).
15. S. Yook, D. W. J. Thompson, S. Solomon, *Geophys. Res. Lett.* **49**, e2022GL098064 (2022).

ACKNOWLEDGMENTS

R. J. S. and L. A. M. received financial support from NASA (grant 80NSSC19K0983). R. J. S. and L. A. M. thank S. Varga and B. F. Bennett for helpful input and suggestions and M. Santee and N. Livesey for help with the figure.

10.1126/science.add2056

EVOLUTION

Putting heads together

Cambrian fossils reveal ancestry of the segmented brain in arthropods

By **Derek E. G. Briggs**[1,2] *and* **Luke A. Parry**[3]

The most species-rich group of animals today and during the Cambrian [539 million to 485 million years (Ma) ago] is the arthropods, which include shrimps, horseshoe crabs, scorpions, centipedes, and insects. These animals are characterized by their exoskeleton, jointed limbs, and repeated body segments. A notable feature of arthropods is their head appendages, which have adapted to a diversity of functions, from sensing the environment to capturing prey. Difficulties in interpreting the homology of head appendages in living and fossil arthropod groups [the arthropod head problem (*1*, *2*)] have complicated attempts to resolve their interrelationships. Understanding how these appendages are innervated by the brain, information rarely preserved in fossils, is crucial for identifying their evolutionary origins. On page 905 of this issue, Strausfeld *et al*. (*3*) report new details in the head of the lobopodian *Cardiodictyon catenulum*, preserved in 518 million-year-old Cambrian rocks near Kunming, China, that reveal the ancestry of the arthropod segmented brain.

The origin of animal groups is a major research question that requires multiple lines of evidence to resolve. Genomic data have revealed the shape of the tree of life, and studies of development (evo-devo) indicate the genetic modifications that may explain rapid evolutionary change. The fossil record, however, is the only direct source of evidence of what transpired in deep time. Almost all major groups of animals, including arthropods, first appeared in the oceans more than 500 Ma ago during or before a relatively brief interval known as the Cambrian "explosion" (*4*). This event was first identified by the sudden appearance of shelly remains (hard parts) in the fossil record. By contrast, soft tissues are prone to decay and rarely fossilized.

However, the preservation of traces of muscles, gut, and sometimes even the nervous system (*5*) was favored during the Cambrian in sediments with a particular clay-rich composition that inhibited decay. Some of the best-known examples are arthropods from the Burgess Shale of British Columbia, Canada (~508 Ma ago), and the Chengjiang deposits of Yunnan Province, China (~518 Ma ago) (*4*, *6*). At the base of the arthropod evolutionary tree are lobopodians, worm-like fossils with lobe-like limbs similar to those of living tardigrades (water bears) and onychophorans (velvet worms). Lobopodians were diverse during the Cambrian and hold the potential to reveal the ancestral stages that preceded the segmented arthropod brain.

The arthropod head comprises distinct units, or segments. The first is the protocerebrum, which houses the labrum (a lobe in front of the mouth) and lateral eyes in true arthropods, the piercing stylets of tardigrades, and the antennae of onychophorans. The second is the deutocerebrum, which is typically associated with a specialized appendage in front of the mouth—the chelicerae of spiders, scorpions, and horseshoe crabs (chelicerates) and the first antenna of crustaceans, insects, and their relatives (mandibulates). The origins of such distinctive appendages in living and fossil arthropods have been a source of ongoing controversy (*1*, *7*, *8*). Investigations of homeobox (*hox*) gene expression during the early development of living arthropods show that the anterior-most portion of the head includes a third cryptic component called the prosocerebrum. The prosocerebrum, which is not a segment, is demarcated by the expression of the *hox* gene *six3*, which occurs in the anterior-most region of embryos across the diversity of bilaterian animals (*9*).

Recent studies of remarkably preserved fossils have revealed persistent patterns that are diagnostic of the brain and even nerve connections to eyes and appendages (*10*). Factors that are still imperfectly understood inhibited decay and promoted preservation of nervous tissue. The first example of the prosocerebrum in a Cambrian fossil arthropod was demonstrated recently in the great appendage arthropod *Leanchoilia* (*10*). Specimens from the Cambrian Kaili Formation of China (~508 Ma ago) show that nerve ganglia associated with a pair of median eyes connect to the labrum and form an asegmental domain situated forward of the familiar components of the arthropod head. This prosocerebrum is combined with the first cephalic segment, the protocerebrum, in all living and most fossil arthropods (*10*).

C. catenulum from the Chengjiang biota of China was a lobopodian that was ~12 mm long and had ~22 pairs of long lobe-

Evolutionary scenario for the panarthropod brain and head

There are three domains in the arthropod brain: the prosocerebrum (ce1), protocerebrum (ce2), and deutocerebrum (ce3). These can be traced across the diversity of all arthropods. The caudal nervous system of *Cardiodictyon catenulum* combines attributes of tardigrades and onychophorans, and it is the only taxon with an appendage associated with ce2, suggesting that it represents an early ancestor in the arthropod tree of life.

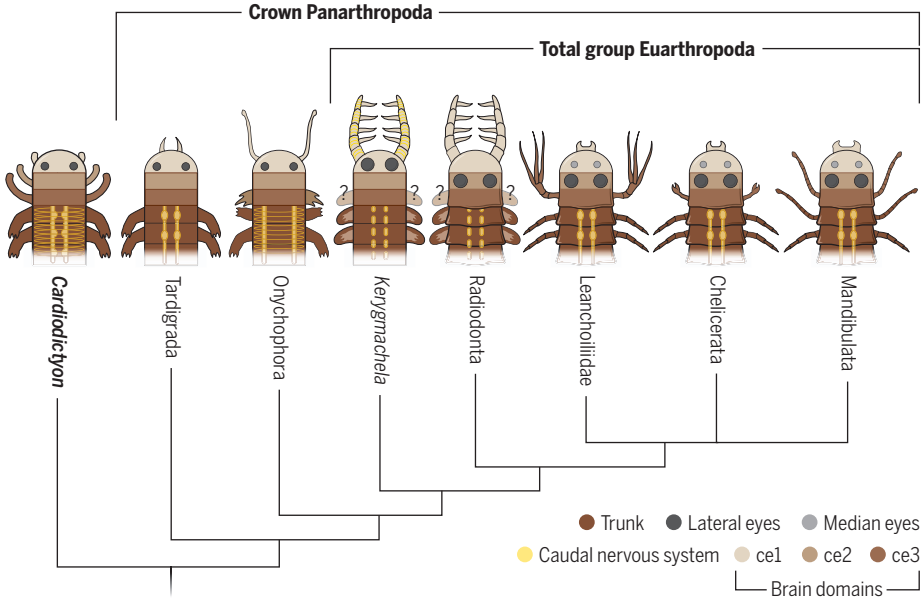

GRAPHIC: A. FISHER/*SCIENCE*

like limbs. Strausfeld *et al.* used chromatic filtering of digital images of the fossil to reveal details of the head, which was ~1 mm long and too small to be analyzed with energy dispersive x-ray spectroscopy, the method widely used to determine the composition of anatomical features within fossils and, crucially, to identify nervous tissues. The brain of *C. catenulum* comprises three cerebral domains that differ from the segments of the trunk and are not identical morphologically. Strausfeld *et al.* interpret this region as asegmental (i.e., distinct from the repeated units of the rest of the body) and representative of the condition that was ancestral to the brain of higher arthropods (euarthropods). The domains correspond to the prosocerebrum, protocerebum, and deutocerebrum in euarthropods and align with the cephalic segments of onychophorans and tardigrades based on *hox* gene expression and the position of the boundary between the foregut and hindgut in the digestive system (see the figure). Elements of these three domains can be identified in living panarthropods (the larger group, including tardigrades, onychophorans, and euarthropods), but *C. catenulum* is distinct in possessing a leg-like appendage corresponding to each of the three domains.

Although some phylogenetic analyses show that *C. catenulum* belongs to the onychophorans, the presence of limbs on each of the three asegmental domains that now comprise the arthropod brain may indicate that lobopodians occupy a very early branch in the panarthropod tree of life, a result found previously (*11*). Consequently, Strausfeld *et al.* propose that the nervous system of *C. catenulum* is a potential analog for the ancestral panarthropod brain, which has been extensively modified through condensation as well as evolution and loss of head appendages.

Nervous tissue has now been reported in fossils from multiple Cambrian localities, representing an unanticipated source of information on the origin and early evolution of the major arthropod groups. Strausfeld *et al.* offer compelling evidence for the origins of the arthropod brain. Since examples of fossilized arthropod brains were first described in 2012 (*12*), however, different studies have interpreted the evidence in different ways. The heads of onychophorans and tardigrades, for example, have been recently argued to contain a single neural region that lacks equivalents of the posterior components of the euarthropod brain (*7*). In this scenario, the tripartite euarthropod brain resulted from the subdivision of an ancestral single-segment head and the onychophoran deutocerebrum arose convergently with that of euarthropods (*7*).

Strausfeld *et al.*, like others (*13*, *14*), interpret the large head appendage of radiodonts, which include giant Cambrian predators such as *Anomalocaris*, as having belonged to the anterior part of the brain (prosocerebrum or protocerebrum). A recent study, however, argues that the radiodont limb is homologous with the chelicera of living horseshoe crabs and the first antenna of crustaceans and is therefore deutocerebral (*8*). Thus, the long-running debates regarding the homology of the head appendages of living and extinct arthropods are far from settled. Some lobopodians have as many as six pairs of differentiated anterior limbs (*15*) in contrast to the three clawless limbs in *Cardiodictyon*. Could all these legs belong to an asegmental head? Given the diversity of Cambrian arthropods, future discoveries of nervous tissue in these animals will provide more evidence of their nature. Interpreting such ancient fossils is challenging, but they provide the only direct data to address major questions in the early evolutionary history of this richly diverse group. ■

"Nervous tissue has now been reported in fossils from multiple Cambrian localities..."

REFERENCES AND NOTES

1. G. Scholtz, G. D. Edgecombe, *Dev. Genes Evol.* **216**, 395 (2006).
2. G. E. Budd, *Arthropod Struct. Dev.* **62**, 101048 (2021).
3. N. J. Strausfeld, X. Hou, M. E. Sayre, F. Hirth, *Science* **368**, 905 (2022).
4. D. E. G. Briggs, *Curr. Biol.* **25**, R864 (2015).
5. L. A. Parry *et al.*, *BioEssays* **40**, 1700167 (2018).
6. X.-G. Hou *et al.*, *The Cambrian Fossils of Chengjiang, China: The Flowering of Early Animal Life* (Wiley, ed. 2, 2017).
7. O. Lev, G. D. Edgecombe, A. D. Chipman, *Integ. Org. Biol.* **4**, obac015 (2022).
8. J. Moysiuk, J.-B. Caron, *Curr. Biol.* **32**, 3302 (2022).
9. P. R. Steinmetz *et al.*, *Evodevo* **1**, 14 (2010).
10. T. Lan *et al.*, *Curr. Biol.* **31**, 4397 (2021).
11. D. J. Siveter, D. E. G. Briggs, D. J. Siveter, M. D. Sutton, D. Legg, *R. Soc. Open Sci.* **5**, 172101 (2018).
12. X. Ma, X. Hou, G. D. Edgecombe, N. J. Strausfeld, *Nature* **490**, 258 (2012).
13. T. S. Park *et al.*, *Nat. Commun.* **9**, 1019 (2018).
14. P. Cong, X. Ma, X. Hou, G. D. Edgecombe, N. J. Strausfeld, *Nature* **513**, 538 (2014).
15. J. B. Caron, C. Aria, *Palaeontology* **63**, 979 (2020).

10.1126/science.add7372

[1]Department of Earth and Planetary Sciences, Yale University, New Haven, CT, USA. [2]Yale Peabody Museum of Natural History, Yale University, New Haven, CT, USA. [3]Department of Earth Sciences, University of Oxford, Oxford, UK. Email: derek.briggs@yale.edu; luke.parry@seh.ox.ac.uk

THERMOELECTRICS

Moving fast makes for better cooling

Optimizing carrier mobility with composition and processing is key for thermoelectric coolers

By **Bingchao Qin** *and* **Li-Dong Zhao**

Thermoelectric technology enables direct and reversible conversion between thermal and electrical energies, which includes waste heat recovery and solid-state cooling (*1*). Compared with power generation, because of the Peltier effect, thermoelectric cooling has application advantages in precise temperature control, fast response, and size controllability. Because it is mainly used around ambient temperature with a small temperature difference, the issue of device failure under large temperature differences is no longer a problem (*2*). In addition to use in civil and industrial areas, thermoelectric cooling has an important role for precise temperature control in key areas such as 5G communications and electronic devices. The development of highly integrated and miniaturized communication technologies and circuit systems and the urgent demand for lower power dissipations have put forward higher requirements for the development of thermoelectric cooling.

From a materials perspective, thermoelectric cooling technology requires highly effective performance near room temperature. The thermoelectric efficiency can be expressed by the dimensionless figure-of-merit ZT value, which is defined as $ZT = S^2\sigma T/(\kappa_{ele} + \kappa_{lat})$, in which S, σ, T, κ_{ele}, and κ_{lat} are the Seebeck coefficient (thermopower), electrical conductivity, absolute temperature, and electronic and lattice thermal conductivity, respectively (*3*). The crucial parameters for thermoelectric cooling, including the maximum temperature difference (ΔT_{max}) and coefficient of performance (COP), are strongly determined by ZT value. Following the selection rule of $E_g = 6 \sim 10\ k_B T$ (where E_g is the bandgap and k_B is the Boltzmann constant) and after decades of effort (*4*), bismuth tel-

School of Materials Science and Engineering, Beihang University, Beijing 100191, China. Email: zhaolidong@buaa.edu.cn

luride (Bi_2Te_3)–based alloys have been developed as the only commercialized thermoelectric cooler. However, the stagnant cooling performance for Bi_2Te_3, low processing yields owing to poor mechanical properties, and resource depletion issues caused by low Te reserves are becoming increasingly problematic, motivating the discovery of potential alternatives for Bi_2Te_3. Therefore, exploring more and better thermoelectric coolers is of vital importance to emerging global requirements for high-performance electronic device development.

Discovering different thermoelectric coolers is mainly focusing on improving electrical transport properties in the materials with intrinsically low thermal conductivity, with features such as strong anharmonicity and off-centering atoms. Apart from Bi_2Te_3-based materials, thermoelectric coolers—including cadmium (Cd)–doped $AgSbTe_2$ (*5*), $Mg_3(Bi,Sb)_2$ semimetals (*6*, *7*), and wide-bandgap ($E_g \approx 33\ k_BT$) tin selenide (SnSe) crystals (*8*)—have been developed. These advancements have important scientific merit, but practical application of them requires performance optimization and reliability verification. The key and first premise for developing a better cooler is to improve the thermoelectric performance near room temperature (see the figure). Around this critical temperature area, the thermoelectric transport is more dominated by charge carrier scattering instead of phonon scattering. Therefore, focusing on optimizing carrier mobility (μ) is crucial to enhance electrical transport properties [power factor (PF) = $S^2\sigma$] and thus high thermoelectric cooling performance. Weakening the carrier's scattering through strategies including bands-synglisis (*8*), growing crystals (*9*, *10*), controlling grain sizes (*11*), and manipulating atomic order-disorder (*5*) have all proven to be effective ways to improve μ. The strategies have been implemented in SnSe (*8*, *9*) and $Mg_3(Bi,Sb)_2$ systems (*10*). Taking SnSe as an example, compared with the polycrystal, single-crystal SnSe demonstrates metallic conduction behavior with ultrahigh electrical conductivity and PF especially near room temperature, at similar levels of carrier concentration and Seebeck coefficient, showing great potential for better thermoelectric cooling ability near room temperature.

Apart from exploring thermoelectric cooling performance on entirely new systems, we believe that it is rather critical to promote the cooling capabilities in more traditional thermoelectric materials with a basic strategy focused on boosting carrier mobility. In most traditional systems, at the optimized carrier concentration range of ~10^{19} to 10^{21} cm^{-3}, the electrical transport is also strongly affected by carrier-carrier scattering (*12*). Fewer carriers usually correspond to higher carrier mobility, and lower carrier concentrations are often accompanied by larger Seebeck coefficients, which are expected to promote better thermoelectric performance (*12*). To avoid additional defects scattering while reducing the carrier concentration by inducing extra point defects from atomic substitutions, we suggest using a composition control strategy. Taking the simple A^+B^- compound as an example, such as cubic lead chalcogenides PbQ [Q = tellurium (Te), selenium (Se), or sulfur (S)] with desirable mechanical performance, excess A provides electrons and leads to *n*-type transport, whereas less A leads to *p*-type conduction. This composition control can be regarded as an artificial and precise regulation of intrinsic defects within a material system. On this basis, the other approach to modulate intrinsic defects is adjusting the preparation and synthesis procedure, which we called the process control. Essentially, both the maximum synthesis temperature and annealing process for polycrystals and cooling rate for crystals have substantial impacts on the number and the type of intrinsic defects, and these defects could be activated as donors for *n*-type or acceptors for *p*-type (*13*). Therefore, combining the composition with process control, our proposal of this grid-design strategy will hopefully reduce carrier concentration by modulating intrinsic defects, thus achieving ultrahigh carrier mobility and thermoelectric performance, especially near room temperature. Thereby, we expect to achieve both *p*-type and *n*-type optimal performance with similar compositions, which will lay a solid foundation for developing better thermoelectric coolers, especially owing to perfect compatibility with contacting materials during thermoelectric device setup.

Following this grid-design strategy of composition-process control to improve carrier mobility, we believe that better cooling performance can be expected in more thermoelectric systems. For example, enhancing carrier mobility to ~2400 $cm^2\ V^{-1}\ s^{-1}$ in PbTe (*14*) and ~6000 $cm^2\ V^{-1}\ s^{-1}$ in PbSe (*15*) through defect modification confirms our outlook. Moreover, revisiting more traditional thermoelectric materials such as PbTe or PbSe may have greater strategic importance as we rethink and open a different era for the development of thermoelectric cooling. Further, carrier mobility optimization is accompanied by electrical conductivity improvement, thus achieving the lower power dissipation that is crucial for the practical applications of thermoelectric cooling devices, especially in the field of 5G communications. ■

Improving thermoelectric cooling

The Peltier effect works as the current causes heat absorption and active cooling at the junction of *p*-type and *n*-type semiconductors. High carrier mobility (μ) is critical for cooling and correlated electrical conductivity (σ), Seebeck coefficient (*S*), and power factor (*PF*). Systematically varying composition and processing improves the search for better cooling materials.

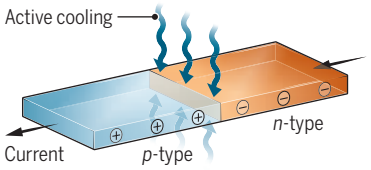

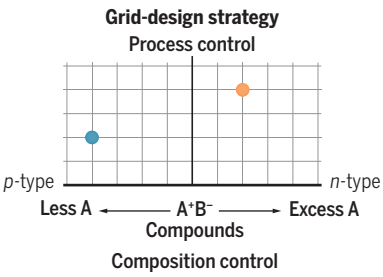

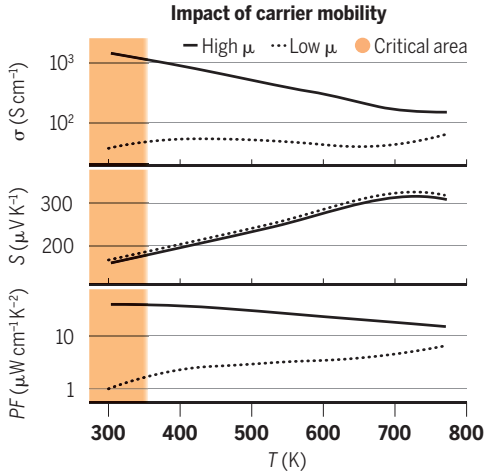

REFERENCES AND NOTES

1. J. Peltier, *Ann. Chim. Phys.* **56**, 371 (1834).
2. J. Mao, G. Chen, Z. Ren, *Nat. Mater.* **20**, 454 (2021).
3. Y. Xiao, L.-D. Zhao, *Science* **367**, 1196 (2020).
4. H. J. Goldsmid, *Thermoelectric Refrigeration*. (Springer, 1964).
5. S. Roychowdhury *et al.*, *Science* **371**, 722 (2021).
6. J. Mao *et al.*, *Science* **365**, 495 (2019).
7. J. Yang *et al.*, *Joule* **6**, 193 (2022).
8. B. Qin *et al.*, *Science* **373**, 556 (2021).
9. L.-D. Zhao *et al.*, *Nature* **508**, 373 (2014).
10. K. Imasato *et al.*, *Adv. Mater.* **32**, 1908218 (2020).
11. T. J. Slade *et al.*, *Energy Environ. Sci.* **13**, 1509 (2020).
12. B. Qin, L.-D. Zhao, *Mater. Lab* **1**, 220004 (2022).
13. V. Q. Nguyen *et al.*, *NPG Asia Mater.* **14**, 42 (2022).
14. Y. Xiao *et al.*, *Adv. Energy Mater.* **12**, 2200204 (2022).
15. Y. Xiao *et al.*, *Energy Environ. Sci.* **15**, 346 (2022).

ACKNOWLEDGMENTS

We acknowledge support from the Basic Science Center Project of the National Natural Science Foundation of China (51788104), the National Key Research and Development Program of China (2018YFA0702100), the National Natural Science Foundation of China (51571007 and 51772012), the Beijing Natural Science Foundation (JQ18004), the 111 Project (B17002), and the National Science Fund for Distinguished Young Scholars (51925101).

10.1126/science.ade9645

GRAPHIC: A. MASTIN/*SCIENCE*

ECOLOGY

How vulnerable are rangelands to grazing?

Assessing multiple site conditions and climate reveals the impacts of livestock pressure

By **Amy C. Ganguli** and **Megan E. O'Rourke**

The effect of livestock grazing on ecosystem services is a hotly debated challenge facing rangelands globally. Most studies do not recognize the complexity of these vast systems, which is fuelling the debate. Grazing is often assessed without acknowledging the confounding effects of rangeland properties such as soil, climate, and biodiversity. As the consequences of climate change become clear and agriculture is intensified to meet societal needs, it is paramount to consider land suitability for livestock, especially where the potential for land degradation is high. On page 915 of this issue, Maestre *et al.* (*1*) present a global synthesis of multiple variables in drylands to determine the impact of livestock grazing. The authors identify site characteristics of rangelands that are vulnerable to degradation when grazed more heavily than the land can support (*2*).

Across 98 sites and six continents, Maestre *et al.* applied consistent methodology to examine the effects of livestock grazing pressure (low to high) on the benefits that humans indirectly or directly receive from nature, otherwise known as ecosystem services. They further evaluated those relationships across site parameters that included climate (temperature, rainfall), soil properties (sand content, soil fertility), and biodiversity (plant and herbivore species richness). In most cases, grazing pressure did not affect the relationships between site parameters and the services measured. However, in some instances, the relationships between site parameters and services completely flipped direction under high versus low grazing pressures. For example, as mean annual temperatures increased, soil carbon storage, organic matter decomposition, and erosion control increased under low grazing pressure but decreased under high grazing pressure. Similarly, as seasonal rainfall increased, soil carbon storage increased under low grazing pressure but decreased under high grazing pressure. The findings provide critical insights into the consequences of omitting important site parameters when assessing grazing effects on ecosystem services.

Grazing pressure had mostly negative effects on drylands when conditions were warmer (soil carbon storage, organic matter decomposition, and erosion control were lower), rainfall was higher (soil carbon storage was lower), and plant species richness decreased (wood quantity and plant biomass and stability were lower). Conversely, grazing pressure had mostly positive effects under cooler conditions and high plant species richness. Climate parameters (mean annual temperature and rainfall seasonality) and plant species richness were the site factors that most often altered the impacts of grazing on ecosystem services.

Undoubtedly, the knowledge provided by Maestre *et al.* adds to the understanding of livestock grazing effects, but this information requires "translation" to be useful for communities facing climate change challenges. This study and similar meta-analyses that identify large-scale patterns and trends for agriculture and climate change are often top-down—that is, focused on quantitative research divorced from decision-makers. They also focus on biophysical factors (such as temperature, precipitation, and green leaf area) without considering social aspects (such as culture and livelihood) that underlie practical implementation of solutions (*3*, *4*). Although these studies are an important step toward informing decision-making, they rarely address stakeholder priorities, culture, or capacity. For example, the suggestion by Maestre *et al.* to increase the species richness of grazing herbivores as a climate adaptation strategy in dryland grazing systems may not be feasible for many communities.

"The hazards that climate change poses...require... research that transcends disciplines."

The hazards that climate change poses to the environment, productivity of ecosystems, and livelihoods are complex and require stakeholder participation and research that transcends disciplines. Going beyond interdisciplinary approaches, in which researchers from diverse fields work together, transdisciplinary approaches include stakeholders from project inception to implementation of results to assessment of effects. The use of transdisciplinary approaches are still limited, presumably because of a lack of dedicated resources to support partnerships between researchers and stakeholders, and systemic research paradigms that favor short-duration, narrowly focused approaches (*5*–*7*).

Despite these impediments, there are examples of successful transdisciplinary projects. The Collaborative Adaptive Rangeland Management project that was established in 2012 in the US central plains (*8*) has brought together ecologists, biologists, climate scientists, sociologists, and economists alongside a diverse stakeholder group of ranchers, conservationists, and state and federal agencies to codevelop project goals, objectives, monitoring indicators, and management strategies. This collaboration has provided insights into conceptual understanding, decision-making, and determining the efficacy of adaptive grazing management strategies to achieve multiple objectives, including wildlife habitat provision, ranch profitability, and economic sustainability, among others (*8*–*10*). This project can serve as a model of transdisciplinary science to be adapted for other scientist-practitioner partnerships.

The data of Maestre *et al.* can be used to identify drylands most susceptible to degradation under climate change and heavy grazing pressure. However, the study reflects limitations of interdisciplinary approaches to problems related to climate change. Transdisciplinary institutes that address sustainability can provide guidance for moving in this direction (*5*–*7*). Moreover, US land-grant institutions have stakeholder-driven missions and cooperative extension programs that connect with community stakeholders. These could be leveraged to implement usable science to combat climate change (*11*). ■

National Institute of Food and Agriculture, US Department of Agriculture, Kansas City, MO 64105, USA.
Email: amy.ganguli@usda.gov; megan.orourke@usda.gov

REFERENCES AND NOTES

1. F. T. Maestre *et al.*, *Science* **378**, 915 (2022).
2. J. E. Herrick *et al.*, *Environ. Sci. Policy* **96**, 52 (2019).
3. H.-P. Schmidt *et al.*, *Glob. Change Biol. Bioenergy* **13**, 1708 (2021).
4. S. Knapp, M. G. A. van der Heijden, *Nat. Commun.* **9**, 3632 (2018).
5. E. G. Irwin *et al.*, *Nat. Sustain.* **1**, 324 (2021).
6. M. G. Lawrence *et al.*, *One Earth* **5**, 44 (2022).
7. J. N. Hernandez-Aguilera *et al.*, *Nat. Sustain.* **4**, 374 (2021).
8. H. Wilmer *et al.*, *Rangeland Ecol. Manag.* **71**, 646 (2018).
9. M. E. Fernández-Giménez *et al.*, *Ecol. Soc.* **24**, 29 (2019).
10. J. D. Derner *et al.*, *Rangeland Ecol. Manag.* **75**, 1 (2021).
11. R. E. Kopp, *Clim. Change* **165**, 28 (2021).

ACKNOWLEDGMENTS

The views expressed do not necessarily represent those of the US Department of Agriculture or the US government.

10.1126/science.add4278

POLICY FORUM

PHOTO: JOSEP LAGO/AFP/GETTY IMAGES

BIOETHICS

Ethics guidelines for human enhancement R&D

Technologies to improve human performance raise ethical concerns

By **Yasemin J. Erden** *and* **Philip A. E. Brey**

The term "human enhancement" refers to a broad range of interventions and technologies that aim at improving human beings beyond what is considered typical or normal. Examples include prosthetic limbs that outperform biological limbs, or drugs that boost cognitive capacities beyond typical human range. Human enhancement is widely discussed as an area of serious ethical concern (*1*, *2*), but there has been no systematic means for implementing ethical oversight of research and development (R&D) that could be directed at human enhancement. In 2021, however, the European Commission (EC) endorsed a set of ethics guidelines for human enhancement that is now included in the ethics review guidance for its Horizon Europe funding program (*3*). This is the first time that extensive guidelines for human enhancement have been proposed and set for research. Though developed within a European context, the guidelines, whose development and limitations are discussed below, aim to be international in scope.

Department of Philosophy, University of Twente, Enschede, Netherlands. Email: y.j.erden@utwente.nl

HUMAN ENHANCEMENT AND ETHICS

In the guidelines and below (*4*), human enhancement is defined as a modification aimed at improving human performance—as opposed to restoring it—that is brought about by science-based and/or technology-based interventions in or on the human body. Enhancement is often contrasted with therapeutic and medical interventions intended to make someone well, that is, to restore their condition (e.g. from injury), or to return them to good or better health through the diagnosis, prognosis, treatment, and prevention of disease, as well as through the promotion of health. Enhancement seems to fall outside such scope, especially when developed in nonmedical settings. Yet, it is sometimes difficult to separate therapeutic treatment from enhancement. Much depends on how terms such as "healthy," "normal," and "average" are defined, within social and political contexts. The guidelines do not provide definitions for these terms, whose meanings will need to be negotiated for different types of interventions.

Cyborg artist and activist Neil Harbisson has had an antenna implanted and osseointegrated in his skull since 2004. The antenna, which qualifies as a human enhancement, is used for regular audio functions but can also transpose colors and images into audible vibrations, including colors invisible to the human eye such as infrareds and ultraviolets.

Currently, many envisioned types and techniques of human enhancement are technologically unfeasible, and few self-identified scientists, research programs, and companies in human enhancement exist. However, rapid developments in many areas of biomedical engineering, including prosthetics, tissue engineering, genome editing, neurotechnology, and nanomedicine, are bringing the possibility of human enhancement ever closer. Even when R&D takes place for therapeutic purposes, results may also prove applicable for human enhancement purposes—for example, a bionic eye that restores vision but also allows one to focus without squinting, or to increase resolution and brightness. If proven to be safe and effective, therapeutic enhancements could also be used for subsequent nontherapeutic enhancements. Moreover, because the boundary between

therapy and enhancement is blurred to begin with, it will likely be crossed easily.

A distinction can be made between different types of enhancements (see the box). Human enhancements can be classified and defined in several ways, including by relation to therapy, or in terms of area, application, and function. Classification can accord with the scientific field from which an enhancement stems, or a technique that is used (e.g., genetic enhancement, neural enhancement, and prosthetic enhancement). Enhancements can be distinguished according to their relation to the body—for instance, as removable or permanent and irreversible, or as internal to the body or external. Some technologies and techniques defy clear distinction.

Human enhancement is morally controversial and often polarizing. Strongly proenhancement advocates, sometimes called transhumanists, prioritize individual choice and emphasize benefits for individuals as well as society. Enhancement critics, sometimes called bioconservatives, tend to emphasize risks, especially to health, equality, or well-being. Some reject efforts to "play God" or subvert human nature, whereas others judge enhancements on a case-by-case basis in terms of beneficence, and/or non-maleficence (*2, 5*).

The will to improve human ability is not new, and prostheses, cosmetics, and performance-enhancing drugs have been common for a long time. Yet developments in tools and techniques have greatly extended the scope and success of enhancement technologies, leaving certain practices and applications in gray zones: professionally, institutionally, legally, and morally. Human enhancement research that does not also have a medical purpose (therapeutic or preventive) will usually not be covered by existing medical regulations and protocols, qualify for clinical trials, or be assessed by most medical research ethics committees (*6*).

DEVELOPMENT OF THE GUIDELINES

Given rapid developments in fields such as genomics, bioengineering, and artificial intelligence, and considering that R&D that is or can be used for human enhancement is already taking place and will likely grow, the EC tasked the European Union (EU)–funded SIENNA (stakeholder-informed ethics for new technologies with high socioeconomic and human rights impact) project to perform an ethical and legal study of human enhancement, and to develop ethics guidance for this technology (*7, 8*). SIENNA was a research project carried out by an international consortium of 12 partners and involved consultations with hundreds of experts and stakeholders (see supplementary materials for project details). These guidelines apply to human clinical, preclinical, and nonmedical applied R&D for which human enhancement is its central aim or one of its aims, or where that research can foreseeably lead to applications for human enhancement. The guidelines are intended for civilian research and do not cover military applications. Nor do they consider research with nonhuman animals, or ethical considerations for downstream regulation of products or services.

Existing ethics guidelines for medical research and practice were considered, including the Declaration of Helsinki, the World Health Organization Standards and Operational Guidance for Ethics Review of Health-Related Research with Human Participants, and the Oviedo Convention (*3*). However, because human enhancement is not done for therapeutic, diagnostic, or preventive purposes, medical ethics frameworks were not assumed to automatically apply to human enhancement. This is a broader issue: Because human enhancement is not clearly part of medicine, it is uncertain whether the laws, institutional requirements, conventions, and ethics guidelines that apply to medicine also apply to enhancement.

The ethics guidelines are based on six key values with largely universal appeal: well-being, autonomy, informed consent, equality, justice, and (moral and social) responsibility. These values have been proposed based on a combination of considerations: their recognition in philosophical ethics and international declarations and treaties such as the *Universal Declaration of Human Rights* (*9*) and the *Charter of Fundamental Rights of the European Union* (*10*), their relevance to ethical assessments of human enhancement, and their support for inclusion in these guidelines during consultation with stakeholders.

Most of these values have a strong basis in human rights law in many countries, including informed consent, equality, justice, and, to a lesser extent, autonomy. Well-being, or welfare, is not explicitly referenced in human rights law, but its promotion is a central policy objective in many countries. Other moral values that are sometimes proposed in relation to human enhancement, such as liberty, bodily integrity, and human dignity, are not explicitly referenced in these guidelines, because stakeholders held that the key ethical issues in human enhancement did not revolve around these values; some are referenced indirectly—e.g., liberty is indirectly referenced in autonomy and informed consent.

Individual well-being

The well-being of the recipient of an enhancement should be paramount. Enhancements, especially irreversible ones, should provide a clear benefit to the individual's life, both in the short and long term. This includes clarifying whether a treatment is irreversible and why, and what potential there is for an alternative, reversible enhancement with an identical or similar purpose. It also requires carefully weighing the potential benefits and harms to the recipient over the long term, considering their particular characteristics, circumstances, perspectives, and wishes, and any potential changes in their circumstances and life choices over time.

Assessments of the risks and benefits of human enhancement for the recipient should take into account the recipient's individual characteristics and circumstances pertaining to potential membership of a vulnerable group, including physical and psychological features, cultural background, health, social network, and occupation. Assessments should be thorough; based on empirical studies, especially when human enhancement is internal to the body and irreversible; and should cover consideration of side effects beyond the medical domain, including psychological and social consequences, such as potential loss of identity and self-esteem, addiction, and social stigmatization.

Where the enhancement is directly or indirectly related to, or affects, children, future risks must be considered—e.g., loss of future privacy owing to the need for long-term monitoring of an enhancement. Ensuring well-being may need to include considering any

Types of enhancements

Categories [based on summaries from (*7*)] may not be mutually exclusive, and some may necessitate others. For instance, a medication could result in both affective and moral enhancement.

Physical enhancements
Interventions that improve physical abilities or introduce new ones, including for performance or endurance

Cognitive enhancements
Interventions that enhance cognitive function, such as intelligence or memory

Moral enhancements
Interventions that modulate or foster attitudes and behaviors that are considered morally or socially acceptable

Cosmetic enhancements
Interventions that improve the appearance or traits of a human being

Longevity enhancements
Interventions that improve durability and that extend life span

required support systems—e.g., as technology develops—and how support may be offered over the lifetime of the enhancement. Such foresight is essential for responsible innovation. For enhancements that require continued support services, there should be clarity regarding the availability of those services.

A high ethical benchmark must be set whenever an enhancement (i) causes, or risks causing, the loss of necessary biological human function; (ii) has a risk of causing substantial or serious side effects, such as harm to health and chronic pain, especially if the enhancement is irreversible; or (iii) affects emotions and affect, cognition, and other mental capacities. It needs to be considered that these capacities are interrelated and that they are related to a person's values, beliefs, judgements, and personality, so that changing one element will also affect some or all of the others.

Informed consent

Human enhancement requires informed consent. Recipients should make a free and unconstrained choice after being informed about the nature, importance, implications, benefits, and risks of the enhancement. Ideally, intended recipients (groups and individuals) of an enhancement should be involved early in the decision and planning processes for the design and development of technologies and procedures.

To guarantee proper conditions for informed consent, human enhancements should only be administered by organizations and individuals with the appropriate background, knowledge, and training to evaluate and communicate risks and benefits, and verify that decisions by recipients are taken freely.

A very high threshold must be applied to the enhancement of children (pediatric enhancement) and individuals unable to give informed consent, all of which must conform with national law. Enhancements for these groups should only be considered if the enhancements have already proven to have clear benefits and minimal risks for adults capable of informed consent and have become widely accepted for them, and if empirical studies confirm that a similar benefit-risk ratio would apply to recipients unable to give informed consent. Pediatric enhancement must consider the United Nations Convention on the Rights of the Child; it must observe the principle of a child's best interests, as well as a child's needs and rights more generally.

Autonomy

Technologies and treatments aiming at human enhancement must not limit a person's ability and freedom to make their own choices and have the full range of cognitive, affective, and conative states that underlie human autonomy. This includes (i) considering contemporary or future legal implications regarding the ownership of human enhancement technologies (e.g., software licensing, or hardware that could become indivisible from the user); and (ii) considering and minimizing the risk from unwarranted interference by external parties, and ensuring informed consent for all remote access to an enhancement, especially where these could affect the enhanced individual's mental processes, emotional state, or behavior, among other outcomes.

Impermissible interventions are those that (i) impair the potential and capacity for human rationality and independent thought—for instance, by limiting a person's ability to imaginatively, critically, and autonomously engage with arguments and ideas, and reflect on and amend their position; (ii) deprive a person of their scope for broad and complex human desires and emotions—for instance, by inhibiting all but singular desires that fit the needs of governments or market forces, or by restricting empathy and conscience for dispassionate law enforcement or military applications; or (iii) change the personality of an individual in a way that either distorts or limits their potential to maintain existing control over their identity. This includes, for instance, where an enhancement affects an integrated conception of self [i.e., as a self that persists in time (past and present), and as located in one person], or a person's potential to live authentically, so that their actions are congruent with their beliefs, desires, and memories. Ordinary changes to personality and identity, as occur through a person's life, happen within a framework of decisions and actions, interpersonally and through introspection, and human enhancement should not disrupt this.

Justice and equality

Although human enhancement could diminish existing inequalities, it may also (i) cause new inequalities, by providing individuals and groups with superior abilities not possessed by others; (ii) exacerbate existing social inequalities and engender new ones, by creating new social identities and challenging or reifying existing conceptions of identity, including what is considered "normal" or typical, unusual or deviant; or (iii) put pressure on unenhanced persons to enhance themselves.

Human enhancement therefore should (i) avoid perpetuating or exacerbating existing inequities or inequalities between groups and communities. Whether enhancements are likely to do so can be established through social or ethical impact assessments. Human enhancement should also (ii) avoid promoting or perpetuating discrimination of (non)enhanced persons by anticipating and mitigating such outcomes where possible; (iii) not exacerbate harmful stereotypes, or propagate new ones, of average versus disabled bodies, or standards of beauty or presentability based on prejudicial stereotypes, such as gendered, racialized, or ethnic identities, or other protected characteristics; or (iv) consider where the abilities bestowed by the enhancement are considered crucial for having success in life, such as intelligence, memory, self-confidence, strength, dexterity, and endurance. Such enhancements should be equally available to all people who desire them.

Clinical trials and safety and efficacy studies

Any new human enhancement application aimed at interventions internal to the body should be subjected to clinical trials or safety and efficacy studies. New regulations and guidelines may be needed for such trials or studies. In many countries, clinical trials are highly regulated (*11*) and may not easily allow for studies of enhancement interventions without a medical (therapeutic or preventive) purpose. Clinical trials could then only be performed for therapeutic enhancement research. Nontherapeutic enhancement could only proceed with changed regulations. In countries that do not require clinical trials to have a strictly medical purpose, it is usually demanded that the societal benefits of the trial and benefits to participants outweigh the risks to participants. In this case, criteria may be required for assessing when human enhancements meet that threshold.

Social responsibility

Human enhancement could have serious implications for recipients, the institution of medicine and other social institutions, families, communities, and other social groups, and society at large. Therefore, social responsibility should be paramount in R&D and deployment of human enhancement.

Human enhancement R&D should be preceded and accompanied by social and ethical impact assessments considering both benefits and risks to individuals and implications for other stakeholders and society as a whole. These assessments should include the possibilities of misuse and dual use, involve relevant stakeholders (both directly and indirectly affected), and ensure that there is enough support from stakeholders for R&D to proceed. Developers should not promote their products in such a way that consumers believe that certain enhancements are necessary for their well-being and success or to fit into society, or that not acquiring the enhancement causes them to be deficient.

Public funding bodies should decide whether to fund enhancement research at all, and only after consulting with transparently selected stakeholders who have sufficient expertise. Public funding, specifically research aimed at interventions in the body, should only be provided if it can be shown in advance that the research will likely adhere to the SIENNA ethics guidelines, and that a risk-benefit assessment for recipients, and a social and ethical impact assessment for society, have a positive outcome.

Human enhancements that are internal to the body or are irreversible should not be specifically developed for workplace or education applications. This includes normalizing human enhancement for employment prospects, career progression and development, or education, and thus creating undesirable social pressure for it to be used. There should not be work or educational requirements that (in)directly refer to, or rely on, the presence of human enhancement.

Genetic enhancement

Although genetic changes frequently occur naturally, genetic enhancement is an artificial process involving the introduction of changes into the (epi)genome to modify and improve nonpathological human traits (see the box). It can take place in three ways: germline modification (germline genetic enhancement), embryo selection, and somatic genetic modification.

Both germline genetic enhancement and embryo selection for enhancement are controversial and outlawed in many countries because they could be done for eugenic purposes (i.e., for apparently improving the genetic quality of a human population by excluding people and groups judged to be inferior and promoting those judged to be superior). Further issues include the risk of creating a lack of diversity among humans, and the risk of creating designer babies that are shaped to accommodate the desires and preferences of parents and society. There are therefore important moral reasons to be cautious and to respect the equal dignity of all humans.

Specifically, germline genetic enhancement is controversial because it does not allow for informed consent by descendants and because there may be unforeseen risks to modification of the germline, and it is often prohibited as part of a more general prohibition of germline genetic modification. Embryo selection is allowed in most countries, but only to avoid implantation of embryos with serious defects that could result in serious disease or mortality, and selection on the basis of other characteristics is more rarely allowed (*12*).

Somatic genetic enhancement is also morally controversial, although less so than germline enhancement, because it involves medically unnecessary, yet permanent, alterations to healthy human tissues and organs, and because it could be used to biologically reengineer human beings to make them have desired traits, which could be understood as a type of eugenics. Somatic genetic engineering for therapeutic and preventive purposes is much more widely accepted, unlike germline genetic engineering for these same purposes. The unclear boundary between enhancement, therapy, and prevention will likely lead to scenarios where somatic gene editing undertaken for therapeutic or preventive purposes will be considered human enhancement.

These objections to genetic enhancement justify stringent ethics guidelines. Germline genetic enhancement, genetic enhancement for nonmedical reasons through embryo selection, and somatic genetic enhancement should not be undertaken, nor should clinical research be undertaken with the aim of facilitating these kinds of procedures (*13*). Precautions should be taken so that somatic genomic editing techniques used for therapy and prevention are not used for enhancement. It is important to note, however, that because both genetic engineering and our moral attitudes concerning it are still evolving, it is possible that a more permissive approach will be taken in the future.

CONCLUSION

These are the first extensive, stakeholder-supported and institutionalized set of guidelines for human enhancement and human enhancement-enabling R&D. The guidelines are currently being applied to research bids to the Horizon Europe funding program through 2027. Research that is considered to have potential for human enhancement will be screened by an independent ethics panel using these guidelines. It is hoped that these will inspire utilization beyond the EU research funding framework and stimulate discussion on providing better ethical guidance for research with possible application toward human enhancement. Already having mechanisms in place to guide and regulate R&D will help to move it forward in a way that is beneficial and that steers clear from unethical practices and outcomes.

Guidelines by themselves are not sufficient, however, so they should be incorporated into new regulations, policies, protocols, and procedures for human enhancement research, development, funding, and application that may be developed in the future. ■

REFERENCES AND NOTES

1. C. Coenen *et al.*, *Human Enhancement* (EU Parliament, STOA, 2009); https://www.europarl.europa.eu/stoa/en/document/IPOL-JOIN_ET(2009)417483.
2. S. Clarke, J. Savulescu, C. A. J. Coady, A. Giubilini, S. Sanyal, Eds., *The Ethics of Human Enhancement: Understanding the Debate* (Oxford Univ. Press, 2016).
3. Y. J. Erden, P. Brey, "Ethical guidance for research with a potential for human enhancement (Version V1)" in "Identifying serious and complex ethics issues in EU-funded research" (European Commission, Directorate-General for Research and Innovation, 2021); https://ec.europa.eu/info/funding-tenders/opportunities/docs/2021-2027/horizon/guidance/ethical-guidance-for-research-with-a-potential-for-human-enhancement-sienna_he_en.pdf.
4. S. R. Jensen *et al.*, SIENNA D3.1: State-of-the-art review: Human enhancement, V1.1 (2018); https://doi.org/10.5281/zenodo.4066557.
5. F. Allhoff, P. Lin, J. Moor, J. Weckert, *Stud. Ethics Law Technol.* **4**, 20121004 (2010).
6. For legal issues, international, EU and regional laws and human rights standards, including human rights challenges related to human enhancement, see (*14*).
7. S. R. Jensen, SIENNA D3.4: Ethical analysis of human enhancement technologies, V1.1, Zenodo (2020); https://doi.org/10.5281/zenodo.4068071.
8. M. Kühler, N.-F. Wagner, P. A. E. Brey, SIENNA D3.7: Proposal for an ethical framework for human enhancement, V10, Zenodo (2020); https://doi.org/10.5281/zenodo.4275579.
9. United Nations, *Universal Declaration of Human Rights* (1948); https://www.ohchr.org/EN/UDHR/Documents/UDHR_Translations/eng.pdf.
10. European Parliament, Council, and Commission, *Charter of Fundamental Rights of the European Union* (2012/C 326/02) (2012); https://www.refworld.org/docid/3ae6b3b70.html.
11. Regulation 536/2014, *Clinical trials* (European Parliament, Council of the European Union, 2014); https://ec.europa.eu/health/medicinal-products/clinical-trials/clinical-trials-regulation-eu-no-5362014_en).
12. M. J. Bayefsky, *Reprod. Biomed. Soc. Online* **3**, 41 (2016).
13. Germline genetic engineering, whether therapeutic, preventive, or enhancing, is currently prohibited in many countries. The European Oviedo Convention, art. 13, states: "An intervention seeking to modify the human genome may only be undertaken for preventive, diagnostic or therapeutic purposes and only if its aim is not to introduce any modification in the genome of any descendants" (*15*). The EU Charter has a clause that specifies "the prohibition of eugenic practices, in particular those aiming at the selection of persons," which appears to rule out germline modification (*10*).
14. Z. Warso, S. Gaskell, "SIENNA D3.2. Analysis of the legal and human rights requirements for human enhancement technologies in and outside the EU" (SIENNA Project, 2019); https://ec.europa.eu/research/participants/documents/downloadPublic?documentIds=080166e5c2e15872&appId=PPGMS.
15. Council of Europe, *Convention for the protection of Human Rights and Dignity of the Human Being with regard to the Application of Biology and Medicine: Convention on Human Rights and Biomedicine* (ETS No. 164, 1999); http://www.coe.int/en/web/conventions/full-list/-/conventions/treaty/164.

ACKNOWLEDGMENTS

Y.J.E. and P.A.E.B. were principal authors of the SIENNA guidelines (*3*) discussed in this paper. This article and its contents reflect only the work of SIENNA and do not intend to reflect views of the European Commission. SIENNA was funded under the European Union's Horizon 2020 research and innovation program (grant agreement no. 741716). The European Commission is not responsible for any use that may be made of the information it contains.

SUPPLEMENTARY MATERIALS

science.org/doi/10.1126/science.add9079

10.1126/science.add9079

BOOKS *et al.*

The ziggurat at Ur, shown here soon after its excavation in the 1920s and '30s, remains a mystery.

PHOTO: COURTESY OF THE PENN MUSEUM

ARCHAEOLOGY

Ancient Mesopotamian histories

A historian explores the remarkable early civilizations of the Near East, from Uruk to Babylon

By **Andrew Robinson**

The civilizations of ancient Egypt, Greece, and Rome are relatively familiar to most people today. We know of these societies through buildings such as the Pyramids of Giza and the Parthenon of Athens, the art of pharaohs such as Ramses II and Tutankhamun, and the works of Homer and Plato. Many modern words are also derived from Greek and Latin, including "science," borrowed from the ancient Roman *scientia*, meaning "knowledge, awareness, understanding."

However, this familiarity does not extend to the civilizations of the ancient Near East, despite extensive and intriguing evidence from stone inscriptions such as King Hammurabi of Babylon's code of laws and clay tablets such as the epic of Gilgamesh, excavated in this region. Written in the cuneiform script, these inscriptions began to be deciphered during the mid-19th century. However, the vast majority of cuneiform writing turned out to be related to government and commerce rather than ideas and literature, and it lacked the aesthetic appeal of the Egyptian hieroglyphic script. Even the fact that our measurement of time and angle uses a sexagesimal system derived from the Sumerians of ancient Mesopotamia is not a widely familiar fact.

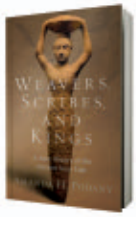

Weavers, Scribes, and Kings
Amanda H. Podany
Oxford University Press, 2022. 672 pp.

"It is astonishing just how much we know about some people of the ancient Near East and how deeply we can dive into their world, but it is also striking how little this knowledge has penetrated into the wider consciousness of educated people today," remarks academic historian Amanda Podany in her new book, *Weavers, Scribes, and Kings*. Thus Podany, who specializes in this civilization, introduces her remarkably lively, if inevitably lengthy, chronicle aimed at nonexperts, which ranges from the Uruk period of 3500 BCE to Alexander the Great's conquest of Babylon, where he subsequently died in the fourth century BCE.

Consider the celebrated stone statue of King Enmetena of Lagash, who ruled around 2450 BCE. Discovered at excavations in Ur a century ago, it was stolen from Iraq after the 2003 invasion, rediscovered in New York in 2010, and subsequently returned to the National Museum of Iraq in Baghdad. Although its head is missing, the statue's cuneiform inscription informs us that Enmetena erected the self-portrait before the god Enlil in his temple and named it "Enmetena (is the) Beloved of the god Enlil." He added that his personal god, Shul-utul, should "forever pray" to Enlil on behalf of Enmetena. Did the king intend to avoid the bother of making his own prayers to Enlil? No, argues Podany: Ancient Mesopotamians would have believed the statue contained part of Enmetena's "very being," which was perpetually praying to Enlil.

Amazingly, Uruk—the world's first city, located east of modern Samawah, Al-Muthanna, Iraq—was the same size in 3500 BCE as Athens was in 500 BCE. Its organizational requirements led to the development of proto-cuneiform script, which probably predated the earliest writing of Egypt. As Podany remarks, "it must have been magical to the Early Dynastic kings to realize that words, which had previously been as ephemeral as the wind in the trees, could be pinned down and preserved on stone." Now the kings, like the gods, might live forever, so to speak.

Advanced writing systems notwithstanding, the cities of ancient Mesopotamia lacked many truly striking buildings. The ziggurat at Ur, for example, was—on its longest side—only a quarter of the length of the side of the Great Pyramid of Egypt, built half a millennium earlier. It lacked the pyramid's smooth sides, rising instead in several giant steps. And unlike the pyramid, which enclosed three burial chambers, the ziggurat was a solid pile of bricks inscribed in cuneiform. It had crumbled into ruins by the sixth century BCE, when it was restored by the last king of the Neo-Babylonian Empire, Nabonidus. One is forced to wonder about the structure's purpose. "Honestly, scholars wonder too," admits Podany.

Yet Babylonian culture was much admired by the Persians under Cyrus the Great, who conquered Nabonidus's empire in 539 BCE, and also by the Macedonian Greeks under Alexander, who conquered the Persian rulers in 331 BCE. Both invaders sought to preserve the ancient city, and cuneiform continued to be written as late as 74 or 75 CE in Babylon and 79 or 80 CE in Uruk. However, with the rise of the Roman Empire in the second century CE, the region's cultural history was finally eclipsed. For the Romans, "ancient" literature was Greek, and their alphabetic script in Latin was derived from the Greek alphabet. With this development, the living culture of Mesopotamia vanished after more than three millennia. ■

10.1126/science.adf5457

The reviewer is the author of *Writing and Script: A Very Short Introduction* (Oxford Univ. Press, 2009).
Email: andrew@andrew-robinson.org

ANIMAL BEHAVIOR

Our entangled lives

A writer probes humanity's often fraught and paradoxical relationships with other creatures

Between Light and Storm: How We Live with Other Species
Esther Woolfson
Pegasus Books, 2022.
368 pp.

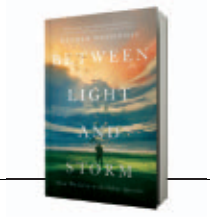

By **Barbara J. King**

Inside her house in Scotland, Esther Woolfson notices a spider walking across "the desert expanse of floor." She asks the tiny animal: "What are we doing here together? How, in the light of the hundreds of millions of years of our shared past should I behave towards you and others?" In response to that second question, Woolfson allows the spider to resume her perambulation, and she disappears behind the refrigerator; Woolfson has not so much rescued her as allowed her to carry out her own choices.

In choosing this anecdote to open *Between Light and Storm: How We Live with Other Species*, Woolfson telegraphs that we readers are about to take a journey, reflective as much as scholarly, through the past and present of humans relating with other animals. "We live in a world of sentience and consciousness," Woolfson maintains, one made manifest through looking open-heartedly at the behaviors of other animals. Too often, humans' stubborn belief that we alone in the animal kingdom are special and set apart harms other animals, leading to "the continuing ruination of the natural world."

Through 10 chapters, Woolfson takes up philosophical topics—Do animals have souls? What is the nature of our love for animals?—and ethical ones, including hunting and the fur trade. The chapter on medical research is especially relevant to readers of this magazine, where results of invasive experiments on animals are often reported. Despite supposed ethical oversight, "terrible cruelty still takes place," notes Woolfson, including with laboratory monkeys.

In a fascinating chapter titled "Tradition," Woolfson describes practices meant to be immune from criticism because they are considered traditional and key to cultural continuity. One example is whaling, as carried out by people in Iceland, Norway, Japan, and the Faroe Islands. In the Faroes, she notes, long-lived and sociable pilot whales are butchered "en masse, *en famille*" with spinal lances and hooks. Another is *kapparot*, carried out before Yom Kippur, the Day of Atonement, in some ultraorthodox Jewish communities. It involves "seizing an unfortunate chicken who is then swung three times around the head in symbolic transference of sin," at which point the chicken is killed and donated to charity.

Both game birds and hunting dogs may experience harsh treatment from humans.

Frequently, Woolfson writes with arresting grace, including when asking (as she did with the spider) provocative questions: "Is it worse to kill and eat something we deem to be clever, capable of love and fear? It stalks the mind, wakes the habitual worrier in the night. How can anyone do this?"

She often opens and closes a chapter with a vignette from her own life, then packs the middle with a dense examination of historical personages' views. Compared with these occasionally tedious review sections, there is a sense of vibrant immediacy in the personal ones.

Early on, Woolfson describes living with a rook called Chicken (in the acknowledgments, she says that her "greatest debt" is to Chicken, who stayed beside her throughout the book's writing), a crow called Ziki, and a blue-white dove. Her connection to birds imbues her exposure of their at-times-awful treatment with extra power. Although attuned to issues of animal welfare, I had no idea that processes surrounding the shooting of game birds such as pheasant and partridge for food are so repellant: Millions of young birds are imported from factory farms, then kept in overcrowded conditions "often with extreme cruelty before being released in order to be shot," she reveals.

Some wobbles appear in the book. Why does Woolfson write—15 times by my count—of "birds and animals," separating birds from the rest of the animal kingdom? Meanwhile, her summary of primate and hominid evolution is so stunted as to raise more questions than answers.

Sometimes, the lyricism in Woolfson's writing leads to mild bewilderment. Explaining how hard it is to put into words the clever nature of her magpie, Spike, she concludes, "I can say only that in observing everything he did and was, I knew him my equal and more likely not less than me but more." What does that mean? "More," how? Is putting a magpie above a human any more justified than putting a human above a magpie? I wonder why she is willing to say this, and to note that parrots can be jealous and bloody-minded, but puts animal "mourning" in quotation marks and tiptoes around "apparent grief" in animals, given the multispecies evidence for the expression of animal grief (*1*).

Overall, however, the book is a necessary and beautiful plea for us humans to do better by our fellow creatures. *Between Light and Storm* would make a wonderful contribution to classrooms of animal behavior, anthropology, philosophy, science, medicine, and public policy, among others. ■

The reviewer is professor emerita of anthropology at William & Mary, Williamsburg, VA 23185, USA.
Email: bjking@wm.edu

REFERENCES AND NOTES

1. B. J. King, *How Animals Grieve* (Univ. of Chicago Press, 2013).

10.1126/science.ade7859

PHOTO: MITCH KEZAR/DESIGN PICS/GETTY IMAGES

The problem with plastics is not only one of waste management but also of production, an idea evoked in this installation by artist Benjamin von Wong.

PHOTO: JAMES WAKIBIA/SOPA IMAGES/LIGHTROCKET/GETTY IMAGES

LETTERS

Edited by **Jennifer Sills**

Global plastic treaty should address chemicals

In March, the global community agreed to establish a legally binding treaty to end plastic pollution. To deliver on this goal, the treaty needs to cover all issues of plastics chemicals as an inseparable part of the problem.

Plastics are complex materials consisting of chemical mixtures, including polymers, additives, residual monomers and processing aids, and non-intentionally added substances. Such mixtures release across the plastics life cycle, from feedstock extraction, production, and use, to reuse, recycling, and disposal; they also recombine along complex, unplanned pathways (*1*). As a result, humans and environments are ubiquitously exposed to plastics chemicals, often with serious consequences.

Out of more than 10,000 known plastics chemicals, at least 2400 are classified as toxic, such as many phthalates and brominated flame retardants (*2*–*4*). Documented health effects span generations and include premature births, low birth weight, obesity, diabetes, cardiovascular disease, endometriosis, infertility, and cancers (*5*). In the United States alone, associated costs of endocrine-disrupting chemicals amount to USD$300 billion/year (*6*, *7*). The total burden on community, ecosystem health, and biodiversity is far greater (*8*, *9*).

Even with material recycling, plastics chemicals ultimately proliferate in the ecosystem, whether as emissions or by entering new products, exposing waste-laborers, consumers, and frontline communities to new chemical cocktails (*10*). An effective, fair, and safe circular economy can only be achieved by phasing out toxic chemicals from plastic production (*11*).

As negotiations for a global treaty begin, plastics chemicals need to be front and center. However, preparatory meeting documents focus on downstream plastic waste and work from a narrow definition of chemicals as hazardous additives (*12*). To enable the treaty to fully address plastics' ecological, health, and environmental justice problems, it is essential to redefine plastics as complex chemical mixtures and to integrate chemical issues across the life cycle within the scope and core obligations of the legal instrument.

Tridibesh Dey[1]*, Leonardo Trasande[2], Rebecca Altman[3], Zhanyun Wang[4], Anja Krieger[5], Melanie Bergmann[6], Deonie Allen[7,8], Steve Allen[9], Tony R. Walker[10], Martin Wagner[11], Kristian Syberg[12], Susanne M. Brander[13], Bethanie Carney Almroth[14]

[1]Department of Global Studies, Aarhus University, 8000 Aarhus C, Denmark. [2]Departments of Pediatrics, Environmental Medicine, and Population Health, New York University Grossman School of Medicine, New York, NY 10016, USA. [3]Independent scholar, Providence, RI, USA. [4]Swiss Federal Laboratories for Materials Science and Technology (EMPA), Technology and Society Laboratory, 9014 St. Gallen, Switzerland. [5]Freelance writer, Berlin, Germany. [6]Deep-Sea Ecology and Technology, Alfred-Wegener-Institut Helmholtz-Zentrum für Polar-und Meeresforschung, 27570 Bremerhaven, Germany. [7]School of Physical and Chemical Sciences, University of Canterbury, Christchurch 8041, New Zealand. [8]School of Geography, Earth, and Environmental Sciences, University of Birmingham Edgbaston, Birmingham B15 2TT, UK. [9]Ocean Frontier Institute, Dalhousie University, Halifax, NS B3H 4R2, Canada. [10]School for Resource and Environmental Studies, Dalhousie University, Halifax, NS B3H 4R2, Canada. [11]Department of Biology, Norwegian University of Science and Technology, 7491 Trondheim, Norway. [12]Department of Science and Environment, Roskilde University, 4000 Roskilde, Denmark. [13]Department of Fisheries, Wildlife, and Conservation Sciences, Coastal Oregon Marine Experiment Station, Oregon State University, OR 97333, USA. [14]Department of Biological and Environmental Science, University of Gothenburg, 40530 Gothenburg, Sweden.
*Corresponding author. Email: tdey@cas.au.dk

REFERENCES AND NOTES

1. J. Tickner, K. Geiser, S. Baima, *Environ. Sci. Pol. Sustain. Dev.* **63**, 6 (2021).
2. H. Wiesinger, Z. Wang, S. Hellweg, *Environ. Sci. Technol.* **55**, 13 (2021).
3. Y. Wang, H. Zhu, K. Kannan, *Toxics* **7**, 2 (2019).
4. L. Vandenberg *et al.*, *Environ. Health Perspect.* **118**, 8 (2010).
5. L. G. Kahn, C. Philippat, S. F. Nakayama, R. Slama, L. Trasande, *Lancet Diabetes Endocrinol.* **8**, 8 (2020).
6. T. M. Attina *et al.*, *Lancet Diabetes Endocrinol.* **4**, 12 (2016).
7. V. Obsekov, L. G. Kahn, L. Trasande, *Exposure Health* 10.1007/s12403-022-00496-y (2022).
8. L. Persson *et al.*, *Environ. Sci. Technol.* **56**, 3 (2022).
9. A. Barrick *et al.*, *PeerJ.* **9**, e11300 (2021).
10. S. Gerassimidou *et al.*, *J. Haz. Mat.* **430**, 128410 (2022).
11. N. Simon *et al.*, *Science* **373**, 6550 (2021).
12. United Nations Environment Programme, International Negotiating Committee to Develop an International Legally Binding Instrument on Plastics Pollution, Including in the Marine Environment (2022); https://www.unep.org/events/conference/inter-governmental-negotiating-committee-meeting-inc-1. Under the "Meeting documents" tab, see UNEP/PP/INC.1/5, UNEP/PP/INC.1/6, UNEP/PP/INC.1/7, and UNEP/PP/INC.1/11.

COMPETING INTERESTS
L.T. acknowledges scientific advisory board activities for Beautycounter, Ahimsa, and Footprint. R.A. is on the Board of Directors for the Science and Environmental Health Network. A.K. does journalistic reporting on plastics and hosts the podcast Plastisphere.

10.1126/science.adf5410

Assess and reduce toxic chemicals in bioplastics

To promote a circular economy and mitigate pollution, the bioplastics industry has begun to phase out polymers derived from petrochemicals (*1*–*3*). This action is a positive step, but it doesn't affect the many bioplastics on the market, which also contain potentially harmful additives. Given that bioplastics will likely replace polymers, it is crucial to determine which bioplastics cause the least harm.

Components of bioplastics can leak into the environment. After disposal, weathering and ultraviolet degradation lead to additional release of chemicals (*4*). When determining the safety of plastic materials, it is important to consider that such leakage could have adverse effects on ecosystems, wildlife, and humans (*5*–*8*).

Discarded plastics often end up in the ocean, where chemicals leaking into the aqueous environment are toxic to marine life. Additives such as phthalates from starch- and cellulose-based bioplastics can also leak into marine environments through wastewater and runoff from landfills. The chemicals affect bioluminescent bacteria and the development of sea urchin larvae (*5*–*7*). Bio-cups, bio-polyethylene bottles, and bioplastic supermarket bags are produced with polylactide (PLA), a polyester derived from renewable biomass. PLA contains chemicals of emerging concern (CECs), such as bisphenol A, that cause dose-dependent increases of malformed mussel larvae (*8*).

More information about the CECs in bioplastics is urgently needed. No protocols are available to characterize either the chemicals or the leachate of chemicals from conventional and bio-based plastics (*9*), making evidence-based, environmentally responsible management impossible. Manufacturers of plastic items and their consultants should be required to test for molecular, organismal, and population-level effects and make public the risks of each type of both conventional plastic and bioplastic (*10*). Integrated chemical and biological approaches should be used to assess the risks associated with low-level exposures to CECs released by bioplastics as well as their possible combined effects in mixtures. Assessing the toxicity of CECs that migrate from bioplastics into the surrounding environment could help determine how to prevent unexpected adverse health outcomes (*11*).

Instead of replacing one harmful material with another, the bioplastic industry and researchers should work together to identify the safest and most sustainable plastic alternatives (*6*). Creating and prioritizing the production of nontoxic materials with a low carbon footprint could lead to a reduced need for landfills and less ocean plastic waste.

Changlei Xia[1], Su Shiung Lam[1,2,3], Huan Zhong[4], Elena Fabbri[5], Christian Sonne[1,2,6]*
[1]Jiangsu Co-Innovation Center of Efficient Processing and Utilization of Forest Resources, International Innovation Center for Forest Chemicals and Materials, College of Materials Science and Engineering, Nanjing Forestry University, Nanjing, China. [2]University of Petroleum & Energy Studies, Uttarakhand, India. [3]Universiti Malaysia Terengganu, Terengganu, Malaysia. [4]School of Environment, Nanjing University, Nanjing, China. [5]University of Bologna and Interdepartment Center for Environmental Sciences Research, Ravenna, Italy. [6]Aarhus University, Roskilde, Denmark.
*Corresponding author. Email: cs@bios.au.dk

REFERENCES AND NOTES

1. J. G. Rosenboom *et al.*, *Nat. Rev.* **7**, 117 (2022).
2. W. W. Y. Lau *et al.*, *Science* **369**, 1455 (2020).
3. R. Geyer, J. R. Jambeckand, K. L. Law, *Sci. Adv.* **3**, e1700782 (2017).
4. O. O. Oluwasina, O. P. Akinyele, S. J. Olusegun, O. O. Oluwasina, N. D. S. Mohallem, *SN Appl. Sci.* **3**, 421 (2021)
5. L. Zimmermann, A. Dombrowski, C. Völker, M. Wagner, *Environ. Int.* **145**, 106066 (2020).
6. G. Anderson, N. Shenkar, *Environ. Pollut.* **268**, 115364 (2021).
7. T. Uribe-Echeverría, R. Beiras, *Mar. Environ. Res.* **176**, 105605 (2022).
8. E. Fabbri, "Chemical characterization and toxicity evaluation of bioplastics leachates in early larval stages and adult mussels, *Mytilus galloprovincialis*" (2022); https://easychair.org/smart-program/ESCPB2022/2022-08-31.html#talk:201967.
9. K. Gunaalan, E. Fabbri, M. Capolupo, *Wat. Res.* **184**, 116170 (2020).
10. M. Nazareth, M. R. C. Marques, M. C. A. Leite, Í. B. Castro, *J. Hazard Mater.* **366**, 714 (2019).
11. N. Caporale *et al.*, *Science* **375**, 735 (2022).

10.1126/science.ade9069

Rethink farm animal production: The 3Rs

Any scientist working with animals is familiar with the "3Rs"—replacement, reduction, and refinement (*1*). Replacement refers to using alternative methods instead of live animals. Reduction requires using the minimum number of animals. Refinement demands the optimization of experimental techniques, housing, and care to safeguard animal welfare. The 3Rs led to a paradigm shift in guiding the use of animals in research, through legislation or institutional review committees worldwide. The model could be similarly effective if applied to farm animal production.

Humans use animals predominantly to produce animal protein: 70 billion terrestrial animals (*2*) and between 59 and 129 billion aquatic animals (*3*) are used annually, compared with 192 million research animals (*4*). However, animal farming is not scrutinized through the lens of the 3Rs and instead remains focused on increasing production to feed the world. The justification for this ethical discrepancy is unclear.

The use of animals for food production should be reassessed according to each of the 3Rs. Replacement could be achieved by plant-based protein or in vitro meat (*5*), which would benefit the environment (*6*) and alleviate world hunger (*7*). Reduction could mean retaining only farm animals that exploit food sources that humans cannot use directly, such as ruminants on nonarable land. Massive reductions could also be attained by decreasing food waste (*8*) and overconsumption of meat and other animal products, which is typical for high-income countries and linked to diseases such as diabetes and cardiovascular disease (*9*). Refinement should not merely prevent animal suffering but guarantee husbandry conditions delivering animals a good life (*10*).

Most efforts to date, primarily through animal welfare science, have focused on refinement (*11*). Applying the 3Rs—especially replacement and reduction—to animal agriculture would reframe the focus on the sustainability of food production, limit its environmental and health impact, and support animal welfare.

Jean-Loup Rault[1]*, Regina Binder[1], Herwig Grimm[2]
[1]Institute of Animal Welfare Science, University of Veterinary Medicine Vienna, Vienna, Austria. [2]Messerli Research Institute, University of Veterinary Medicine Vienna, Medical University Vienna, University of Vienna, Vienna, Austria.
*Corresponding author.
Email: jean-loup.rault@vetmeduni.ac.at

REFERENCES AND NOTES

1. W. Russel, R. Burch, *The Principles of Humane Experimental Technique* (Methuen & Co. Limited, London, 1959).
2. Food and Agriculture Organization of the United Nations, "Crops and livestock products" (2021); www.fao.org/faostat/en/#data/QCL.
3. B. Franks *et al.*, *Sci. Adv.* **7**, eabg0677 (2021).
4. K. Taylor, L. Alvarez, *Altern. Lab. Anim.* **47**, 196 (2020).
5. J.-F. Hocquette, *Meat Sci.* **120**, 167 (2016).
6. M. Schlatzer, *Tierproduktion und Klimawandel* (LIT Verlag, Vienna, 2010) [in German].
7. S. Pyett *et al.*, "Chickpeas, crickets, and chlorella: Our future proteins" (Wageningen University & Research, 2019); http://edepot.wur.nl/496402.
8. Food and Agricultural Organization of the United Nations, "Food loss and food waste" (2022); www.fao.org/policy-support/policy-themes/food-loss-food-waste/.
9. S. Friel *et al.*, *Lancet* **374**, 2016 (2009).
10. Farm Animal Welfare Council (FAWC), "Farm animal welfare in Great Britain: Past, present, and future" (FAWC, London, 2009).
11. D. Fraser, *Understanding Animal Welfare: The Science in Its Ethical Context* (Wiley-Blackwell, Ames, IA, 2008).

10.1126/science.adf3351

TRILLIONS OF MICROBES ONE ESSAY

The NOSTER *Science* Microbiome Prize is an international prize that rewards innovative research by investigators who have completed their terminal degree in the last 10 years and are working on the functional attributes of microbiota. The research can include any organism with the potential to contribute to our understanding of human or veterinary health and disease, or to guide therapeutic interventions. The winner and finalists will be chosen by a committee of independent "scientists" chaired by a senior editor of *Science*. The top prize includes a complimentary membership to AAAS, an online subscription to *Science*, and USD 25,000. Submit your research essay today.

Jennifer Hill, Ph.D.
2022 Winner

NOSTER | Science
MICROBIOME
PRIZE

Apply by 24 January 2023 at www.science.org/noster

Sponsored by Noster Inc

PRIZE ESSAY

GRAND PRIZE WINNER
Florian Schmidt

Florian Schmidt received undergraduate degrees from the University of Heidelberg and a PhD from ETH Zürich. His research focuses on the development of technologies in the fields of genome engineering, transcriptional recording, and gene therapy. **www.science.org/doi/10.1126/science.adf4442**

Science & SciLifeLab PRIZE For Young Scientists

GENOMICS, PROTEOMICS, AND SYSTEMS BIOLOGY

Autobiography of a gut bacterium

Recordings of transient transcriptional events shed light on the gut microbiome

By **Florian Schmidt**

A picture paints a thousand words. And yet, it is a snapshot that captures only a split second in time, while it misses anything that happened before or after. Can you imagine how to describe the stunning complexity of life if you were only handed a single snapshot?

This scenario might sound profoundly impossible, yet many research tools today rely on snapshot-like measurements. Researchers describe complex cellular processes by performing time-point experiments. They break open cells to measure their intracellular contents such as metabolites and RNA. RNA-sequencing (RNA-seq) allows scientists to quantify the entirety of intracellular RNAs—the transcriptome—to paint a rich picture of cellular processes (*1*). This method allows researchers to investigate the cellular state at one moment in time at unprecedented depth. However, RNA molecules are short-lived and usually rapidly degraded (*2*). Because of this constant turnover of transcriptional signatures, RNA-seq only yields a short glimpse of highly dynamic processes (*3*). Unfortunately, this dynamism renders some biological systems exceptionally difficult to capture.

The human gut microbiome is one such example. The microbes that inhabit our gastrointestinal tract respond to environmental changes, such as alterations in our diet, or pathological states, such as inflammation, by rapidly adapting their gene expression (*4*). Understanding these adaptations can yield insights into nutrition, inflammation, cancer, and even psychiatric disease (*5*). Thus,

The hidden lives of microbiota

Transcriptional recording sentinel cells noninvasively report interactions with diet, host, other microbes, and pathological environments. Sentinel cells capture mRNA into CRISPR arrays through the action of a reverse transcriptase–Cas1–Cas2. This information is retrieved through fecal sampling and deep sequencing.

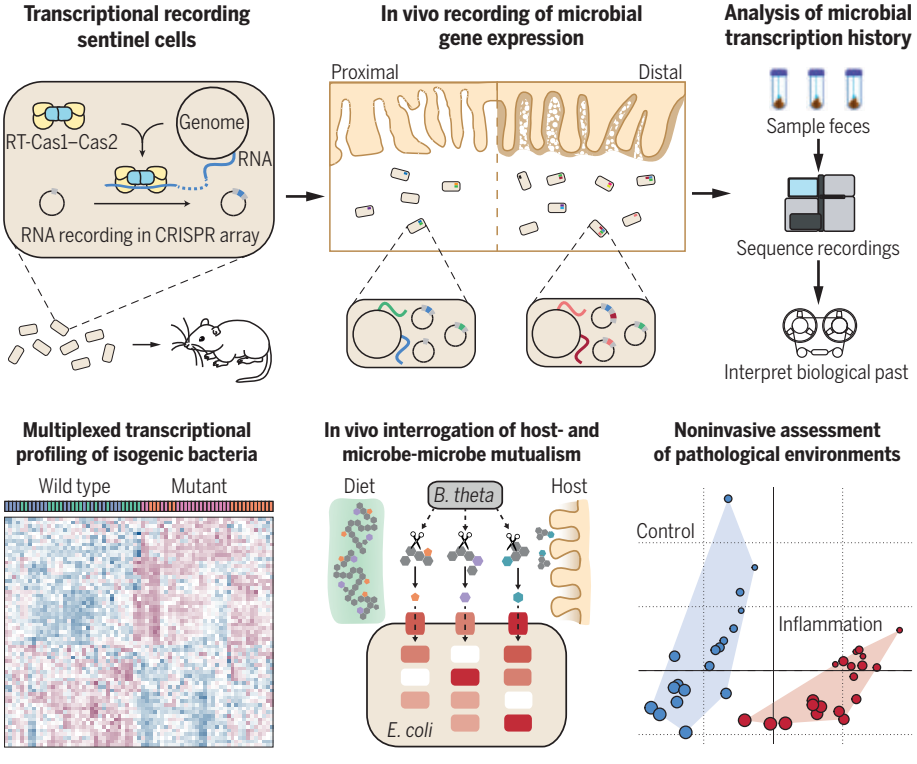

RT, reverse transcriptase; *B. theta*, *Bacteroides thetaiotaomicron*; *E. coli*, *Escherichia coli*

CREDITS: (PHOTO) COURTESY OF FLORIAN SCHMIDT; (GRAPHIC) F. SCHMIDT *ET AL.* (*10*)

the capacity to measure these adaptations is pivotal to understand human health and to develop diagnostics.

Our ability to investigate the gut microbiome with RNA-seq is limited: We can noninvasively sample the feces. However, the microbes take hours to traverse from proximal sections of the gastrointestinal tract, where many physiologically relevant processes occur, to the feces (*6*). Fecal samples are therefore poorly reflective of the state of the gut microbiome (*7*). Conversely, performing RNA-seq on microbiota directly inside their niches requires surgical procedures that are highly invasive, risky, and disruptive.

To address this long-standing challenge, we developed Record-seq—a sentinel cell system—that allows us to investigate the transcriptome of bacteria inside the gut (*8, 9*). We used principles of biological engineering to equip cells of the human commensal bacterium *Escherichia coli* with a molecular recorder that can convert RNA into DNA sequences. This conversion enables our *E. coli* sentinel cells to record their own rapidly changing transcriptome into DNA as a permanent storage form and preserve transcriptional information. As the sentinel cells pass through the gut and react to their environment (for example, the diet eaten by the host or inflammation of the intestine), they record their own transcriptional response to these events by means of our molecular recorder. We are then able to noninvasively collect the feces and sequence the DNA of our sentinel cells to retrieve the information that these bacteria collected inside the gut (*10*). Thereby, Record-seq allows us to gain new insights into the hidden life of *E. coli* inside our gastrointestinal tract as we obtain transcriptional records noninvasively and recover information from proximal sections of the gut that are "lost" in fecal RNA-seq.

We developed Record-seq by repurposing the adaptive microbial immune system CRISPR. CRISPR evolved to create molecular memories of invading genetic elements as a complex of the proteins Cas1 and Cas2 integrates short snippets of DNA (spacers) into the CRISPR array encoded in the bacterial genome (*11–12*). The vast majority of Cas1-Cas2 systems acquire spacers exclusively from DNA. However, in some bacteria a reverse transcriptase (RT) is naturally fused to Cas1 to form an RT-Cas1–Cas2 complex (*13*), where the RT can use RNA as a template to generate a complementary strand of DNA. It has been demonstrated that an RT-Cas1–Cas2 complex from the marine bacterium *Marinomonas mediterranea* (MMB-1) could acquire RNA-derived spacers into the CRISPR array and reverse transcribe them into DNA (*14*).

However, the MMB-1 RT-Cas1–Cas2 was only functional in its natural host and did not maintain RNA spacer acquisition when expressed heterologously in *E. coli* (the human commensal bacterium we wanted to use as a sentinel cell to monitor gut function). We tested a collection of evolutionarily distant RT-Cas1 orthologs from different bacteria and discovered one from *Fusicatenibacter saccharivorans* (*Fs*RT-Cas1–Cas2) that was functional in *E. coli*. We found that *Fs*RT-Cas1–Cas2 could indeed create transcriptional histories as it sampled cellular RNAs, acquired new spacers, and retained transcriptional responses of *E. coli* over time (*8*).

Thus, our Record-seq technology was born, and we were eager to apply it to the environment of the mammalian gut. As a multidisciplinary team of researchers, we began our investigation of the gut microbiome and fed our sentinel cells to mice. We were amazed to discover that our sentinels recorded transcriptional information inside the gut and that we could recover this information when we DNA-sequenced cells from the feces. We then started to alter the diet of our mice and revealed that Record-seq could reveal distinct adaptations of *E. coli* to different diets in proximal sections of the gut that RNA-seq did not capture. This approach allowed us to shed light on yet undiscovered adaptations of *E. coli* inside the intestine, which could in the future help to guide nutrition.

We went on to apply Record-seq as both a diagnostic and research tool for the gut microbiome. Much to our surprise, we could deploy Record-seq in a plethora of situations—for example, to detect inflammation in the intestine and the interaction of our *E. coli* sentinel cells with other commensal bacteria when gavaged into mice with a complex microbiota (*10*). This method allows us to eavesdrop on the chatter between different microbiota and their host and to uncover new interactions and implications for human health and disease.

The hidden lives of microbiota inside the intestine are fascinatingly complex. Record-seq opens a new window into understanding how nutrition, inflammation, and microbial interactions inside the gastrointestinal tract shape health and disease.

Department of Biosystems Science and Engineering, ETH Zürich, Zürich, Switzerland.
Email: florian.schmidt@bsse.ethz.ch

CATEGORY WINNER: ECOLOGY & ENVIRONMENT

Stefany Moreno-Gámez

Stefany Moreno-Gámez received an undergraduate degree from Universidad de los Andes and a PhD from the University of Groningen and ETH Zürich. She is currently a postdoctoral fellow at the Massachusetts Institute of Technology. Her research focuses on how dietary and host-derived glycans shape ecological and evolutionary dynamics in the gut microbiome. **www.science.org/doi/10.1126/science.adf4444**

CATEGORY WINNER: CELL & MOLECULAR BIOLOGY

James Daly

James Daly received undergraduate and PhD degrees from the University of Bristol. After completing his studies, he received a Wellcome Early Career Award fellowship and moved to the Department of Infectious Diseases, King's College London. His current research continues to explore the molecular interface between neuropilin receptors and viruses and the potential for antiviral inhibition of this process. **www.science.org/doi/10.1126/science.adf4469**

CATEGORY WINNER: MOLECULAR MEDICINE

Daniele Simoneschi

Daniele Simoneschi received an undergraduate degree from Manhattanville College and MPhil and PhD degrees from the Vilcek Institute at New York University (NYU). He is a research assistant professor in the Department of Biochemistry and Molecular Pharmacology at NYU, where he explores molecular and cellular mechanisms by which cullin-RING ubiquitin ligases regulate cell cycle execution. **www.science.org/doi/10.1126/science.adf4868**

PHOTOS: (TOP TO BOTTOM) DEYANIRA GAMEZ; COURTESY OF JAMES DALY; COURTESY OF DANIELE SIMONESCHI

REFERENCES AND NOTES

1. R. Stark, M. Grzelak, J. Hadfield, *Nat. Rev. Genet.* **20**, 631 (2019).
2. D. A. Vargas-Blanco, S. S. Shell, *Front. Microbiol.* **11**, 2111 (2020).
3. V. Bergen *et al.*, *Mol. Syst. Biol.* **17**, e10282 (2021).
4. G. P. Donaldson *et al.*, *Nat. Rev. Microbiol.* **14**, 20 (2016).
5. Y. Fan, O. Pedersen, *Nat. Rev. Microbiol.* **19**, 55 (2021).
6. D. Kumral, A. M. Zfass, *Dig. Dis. Sci.* **63**, 2500 (2018).
7. S. Sun *et al.*, *Sci. Rep.* **11**, 14828 (2021).
8. F. Schmidt *et al.*, *Nature* **562**, 380 (2018).
9. T. Tanna *et al.*, *Nat. Protoc.* **15**, 513 (2020).
10. F. Schmidt *et al.*, *Science* **376**, eabm6038 (2022).
11. P. M. Nussenzweig, L. A. Marraffini, *Annu. Rev. Genet.* **54**, 93 (2020).
12. S. A. Jackson *et al.*, *Science* **356**, PP (2017).
13. K. S. Makarova, N. V. Grishin, S. A. Shabalina, Y. I. Wolf, E. V. Koonin, *Biol. Direct* **1**, 7 (2006).
14. G. Mohr *et al.*, *Mol. Cell* **72**, 700 (2018).

10.1126/science.adf4442

PRIZE ESSAY

CATEGORY WINNER:
ECOLOGY & ENVIRONMENT

Stefany Moreno-Gámez

Stefany Moreno-Gámez received an undergraduate degree from Universidad de los Andes and a PhD from the University of Groningen and ETH Zürich. She is currently a postdoctoral fellow at the Massachusetts Institute of Technology. Her research focuses on how dietary and host-derived glycans shape ecological and evolutionary dynamics in the gut microbiome. **www.science.org/doi/10.1126/science.adf4444**

ECOLOGY & ENVIRONMENT

How bacteria navigate varying environments

Collective sensing and phenotypic diversification aid response to environmental fluctuations

By **Stefany Moreno-Gámez**

A key to the impressive success of bacteria in nature is their ability to adapt to new environments. Owing to their short generation times, these adaptations often result from genetic evolution. For instance, bacteria can rapidly evolve to acquire drug resistance or to specialize in the consumption of a resource (*1, 2*). Environmental fluctuations, however, can also happen at much shorter time scales that preclude adaptation by genetic mutation. How do bacteria cope with these situations?

Bacteria have sophisticated programs of gene regulation that control decisions involving hundreds of genes and lead to major physiological changes (e.g., the ability to become a dormant spore in unfavorable conditions). Bacteria rely on their ability to sense the environment to make these decisions, yet the information that one individual bacterium can gather is often incomplete or noisy. I found that bacteria can solve this problem when they sense the environment as a collective by quorum sensing (QS)—a process in which they secrete and respond to small molecules in the extracellular environment known as autoinducers (*3*).

The established view of QS is that bacteria use autoinducers to measure population density to control the expression of traits that require coordination and are only beneficial when expressed by many cells (e.g., bioluminescence) (*4, 5*). However, we found that beyond coordination of group behavior, QS could be used by bacteria to collectively sense their environment. The seed of this idea came from studying *Streptococcus pneumoniae*, a species that inhabits the nasopharynx and is a leading cause of pneumonia. *S. pneumoniae* uses QS to control the entry into competence: a state in which it up-regulates the expression of stress response genes together with machinery to take up and integrate extracellular DNA into its own genetic material (*6, 7*).

Parsons Laboratory for Environmental Science and Engineering, Department of Civil and Environmental Engineering, Massachusetts Institute of Technology, Cambridge, MA, USA. Email: stefany@mit.edu

I used a combination of experiments and mathematical modeling to find that although competence is regulated by population density, it simultaneously responds to various environmental factors including pH and antibiotics (*8*). This joint regulation occurs because bacteria do not secrete autoinducers at a constant rate but instead modulate this rate dependent on the environment they encounter (see the figure). For instance, upon exposure to a DNA-damaging agent, *S. pneumoniae* strongly up-regulates the secretion of autoinducers, and competence develops even when the quorum is low. This process helps bacteria fight off DNA damage through the uptake of extracellular genetic material in the competent state.

I built upon these findings and observations from other systems and developed a computational model of QS in which bacteria modulate the rate of autoinducer secretion dependent on their perception of the environmental state. As I studied how populations in this model adapt to environmental fluctuations, I found that bacteria profit from QS because autoinducer secretion allows them to pool their imperfect estimates of the environment and average out individual noise (*3*). Then, as they monitor the extracellular concentration of autoinducers, bacteria improve their estimation accuracy and make better-informed decisions about how to respond to the environment. In other words, bacteria exploit a well-known principle in decision theory: the wisdom of crowds.

This process of sensing and responding to external cues is just one of the strategies that bacteria use to cope with frequent environmental changes, as was revealed when I investigated how bacteria navigate through periods of feast and famine. Bacteria are often studied in the laboratory when they are actively growing, yet most bacteria in nature are in starved states where they eagerly await their next meal. To immediately resume growth when resources become available may seem like the best strategy for a bacterium because it maximizes its number of descendants. However, rapid resumption of growth makes bacteria vulnerable to several

PHOTO: DEYANIRA GAMEZ

Coping with environmental fluctuations as a bacterium

In nature, bacteria constantly navigate dynamic environments. To cope with fluctuations, bacteria have evolved different strategies. Some bacterial populations adapt by sensing the environment as a collective through the secretion of autoinducers that accumulate extracellularly and average out the noise inherent to individual sensing. Alternatively, bacteria rely on stochastic variation in their phenotypes to guarantee that some individuals in the population will always be adapted even if change is unpredictable.

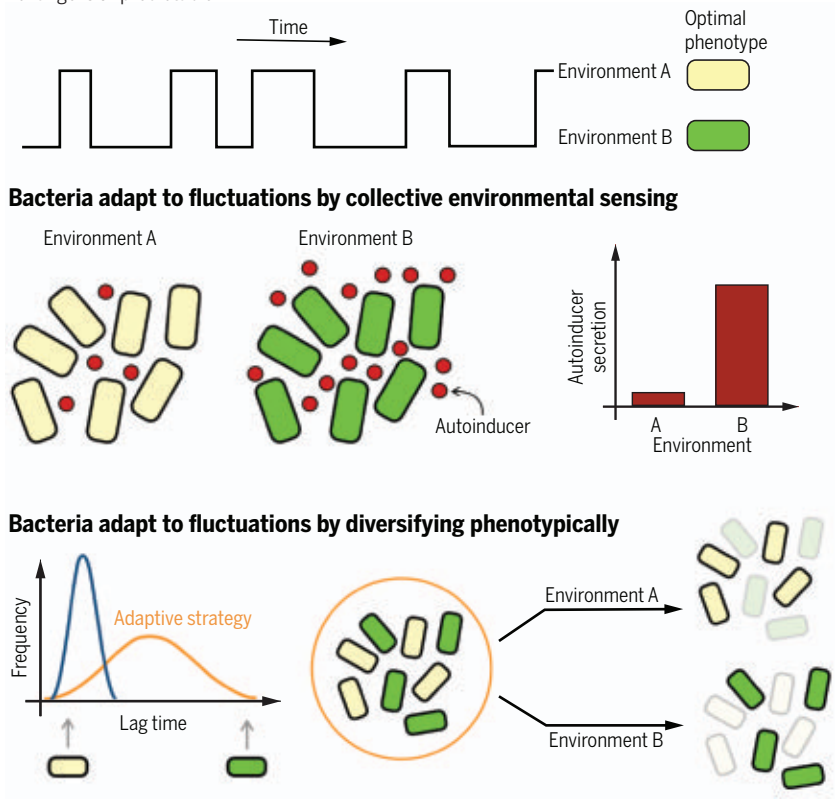

stressors that act primarily on dividing cells. Without any cues to anticipate whether stress is on the horizon, how can bacteria resolve this trade-off between growth and survival?

To study this question, I developed a device to follow the behavior of populations of *Escherichia coli* as they resume growth from starvation (*9*). Microscopy was used to observe hundreds of cells while they undergo this transition, and I found that there is large variation in lag time between populations of genetically identical bacteria. Whereas some individuals resumed growth right away, others of their clonemates took over 20 generations more to start reproducing (*10*).

This variation is not optimal for growth. Indeed, bacteria selected to resume rapid growth in stress-free conditions evolved shorter and less varied lag times than wild-type *E. coli*. However, this variation might be beneficial in times of stress. To study this possibility, as bacterial populations resumed growth from starvation, I exposed them to a sudden pulse of antibiotics. After the pulse was over, I observed that individuals that had not yet resumed growth had a much higher chance of survival and perpetuation of the population than individuals that were already growing. As a result, populations of mutants that evolved narrow lag time distributions—in which all bacteria began growing immediately—were fully eliminated by antibiotics, whereas wild-type populations with a mix of dormant and growing bacteria could survive (see the figure).

With mathematical modeling, I showed that intermittent exposure to antibiotics during feast-to-famine cycles can lead to the evolution of genotypes that have wide lag time distributions. In this way, bacteria can survive lethal antibiotic exposure without being resistant to antibiotics and without severely compromising their ability to rapidly proliferate when resources are available. Remarkably, not only can lag time variation contribute to antibiotic failure in the clinics (*11*), but increasing evidence indicates that it can facilitate the subsequent evolution of antibiotic resistance (*12, 13*).

Bacteria are one of the simplest forms of life on Earth. Despite their apparent simplicity, they deploy a variety of strategies to thrive in fluctuating environments. From relying on a hive mind, to hedging their bets like seasoned investors, or rapidly adapting by genetic mutation, bacteria seem to have figured out that the best way to cope with change is to play every possible trick in the book. ■

GRAPHIC: N. CARY/*SCIENCE* BASED ON STEFANY MORENO-GÁMEZ

REFERENCES AND NOTES

1. S. Moreno-Gámez *et al.*, *Proc. Natl. Acad. Sci. U.S.A.* **112**, E2874 (2015).
2. D. M. Ekkers *et al.*, *Mol. Biol. Evol.* **39**, msac124 (2022).
3. S. Moreno-Gámez, M. E. Hochberg, G. S. van Doorn, *bioRxiv* 10.1101/2022.03.16.481998 (2022).
4. C. Fuqua, M. R. Parsek, E. P. Greenberg, *Annu. Rev. Genet.* **35**, 439 (2001).
5. K. Papenfort, B. L. Bassler, *Nat. Rev. Microbiol.* **14**, 576 (2016).
6. L. S. Håvarstein, G. Coomaraswamy, D. A. Morrison, *Proc. Natl. Acad. Sci. U.S.A.* **92**, 11140 (1995).
7. S. N. Peterson *et al.*, *Mol. Microbiol.* **51**, 1051 (2004).
8. S. Moreno-Gámez *et al.*, *Nat. Commun.* **8**, 854 (2017).
9. S. Moreno-Gámez, A. Dal Co, S. van Vliet, M. Ackermann, *Methods Mol. Biol.* **2357**, 107 (2021).
10. S. Moreno-Gámez *et al.*, *Proc. Natl. Acad. Sci. U.S.A.* **117**, 18729 (2020).
11. C. Vulin, N. Leimer, M. Huemer, M. Ackermann, A. S. Zinkernagel, *Nat. Commun.* **9**, 4074 (2018).
12. I. Levin-Reisman *et al.*, *Science* **355**, 826 (2017).
13. I. Santi, P. Manfredi, E. Maffei, A. Egli, U. Jenal, *mBio* **12**, e03482 (2021).

10.1126/science.adf4444

PRIZE ESSAY

CATEGORY WINNER:
CELL & MOLECULAR BIOLOGY

James Daly

James Daly received undergraduate and PhD degrees from the University of Bristol. After completing his studies, he received a Wellcome Early Career Award fellowship and moved to the Department of Infectious Diseases, King's College London. His current research continues to explore the molecular interface between neuropilin receptors and viruses and the potential for antiviral inhibition of this process.

www.science.org/doi/10.1126/science.adf4469

CELL & MOLECULAR BIOLOGY

Endosomes, receptors, and viruses

Mechanisms of infection are deciphered at the host-pathogen interface

By **James L. Daly**

Viral infection is facilitated by the molecular recognition of specific receptors and host factors at the plasma membrane, which provides a gateway into host cells (*1*). These factors act as "locks" that control access to the intracellular environment, to which viruses have evolved cognate molecular "keys" to gain entry and replicate. In the evolutionary arms race between viruses and their hosts, the development of effective antiviral therapeutic strategies to inhibit this process poses a crucial public health challenge, recently emphasized by the COVID-19 pandemic.

The surface of our cells is not a static environment. A complex milieu of lipids, proteins, and carbohydrates incessantly jostle with each other and partition into discrete domains that interact with the surrounding environment. Components of the cell surface are routinely internalized by endocytosis, a dynamic process through which the extracellular environment is sampled by the cell, forming a conduit for viral entry (*1*). Once internalized, this material is delivered to a series of membranous organelles conserved within eukaryotes—the endosomal network.

I began my PhD research with Pete Cullen, with the aim to investigate the role of the endosomal network in the regulation of homeostasis in human cells. Endosomes are equipped with a range of protein machineries that perform a sorting role as they sift through a complex range of thousands of incoming proteins (collectively known as cargoes) and decide whether individual proteins should be degraded or recycled for reuse (*2*). Recycling is an increasingly appreciated strategy in our everyday lives: It conserves energy, reduces demand for raw materials, and limits the accumulation of toxic products within the environment. At the cellular level, endosomal cargo recycling is essential for the same fundamental reasons, and increasing evidence implicates endosomal dysfunction as an underlying hallmark of a range of age-related neurodegenerative pathologies, including Parkinson's and Alzheimer's diseases (*3*).

My colleagues and I recently developed a methodology to acutely inactivate endosomal sorting, which induced the rapid emergence of profound trafficking defects followed by chronic dysfunction that correlates with phenotypes observed in neurodegenerative diseases, emphasizing the central importance of this process to cellular health (*4*, *5*). Similarly, viruses have also evolved to intricately perturb and navigate the complexity of the cell surface and endosomal network to hide from host defenses, evade degradation, and gain access to the intracellular environment for replication (*6*).

I developed a proximity proteomics methodology to understand sorting between endosomes and the trans-Golgi network (TGN), an essential recycling pathway that has proved challenging to study historically. This approach enabled the molecular fingerprinting of the TGN proteome by mass spectrometry. When I compared the fingerprint of wild-type cells with those in which the endosomal SNX-BAR sorting complex promoting exit 1 (ESCPE-1) had been suppressed, I identified a cohort of cargoes that failed to be recycled from endosomes to the TGN. I coupled this technique with orthogonal biochemical and imaging approaches to characterize a particular transmembrane protein, neuropilin-1 (NRP1), as a cargo that undergoes endosome-to-TGN sorting (*7*).

NRP1 is a multifunctional co-receptor that regulates access of ligands to the intracellular environment to perform key roles in cell and developmental biology. NRP1 ligands harbor a particular amino acid motif to achieve NRP1 binding. This motif, comprising a C-terminal sequence of positively charged residues, was called the C-end rule (CendR—pronounced "sender") (*8*). CendR motifs specifically bind a conserved electrostatic pocket on the extracellular face of NRP1 and subsequently induce internalization into cells (*9*). Notably, viruses like the human T cell lymphotropic virus type 1 and Epstein-Barr virus can mimic this process by using a CendR motif located within their external glycoproteins, thereby hijacking NRP1 binding for infection (*10*, *11*).

Department of Infectious Diseases, School of Immunology and Microbial Sciences, King's College London, London, UK. Email: james.l.daly@kcl.ac.uk

PHOTO: COURTESY OF JAMES L. DALY

Molecular insights into the mechanisms of SARS-CoV-2 infection

(**A**) Schematic of severe acute respiratory syndrome coronavirus 2 (SARS-CoV-2) internalization into a host cell endosome via NRP1 followed by escape and intracellular replication. Direct fusion with the plasma membrane is not depicted for simplicity but can also occur. (**B** and **C**) Schematic (B) and crystal structure (C) of the host-pathogen interface, where the S1 CendR sequence is bound by the extracellular b1 domain of NRP1 (Protein Data Bank ID: 7JJC). (**D**) NRP1 knockout (KO) reduces SARS-CoV-2 infection in culture. (**E** and **F**) Schematic (E) and molecular model (F) of sequence-dependent recognition of the NRP1 cytosolic tail by ESCPE-1. (**G**) ESCPE-1 KO also reduces SARS-CoV-2 infection levels in cell culture.

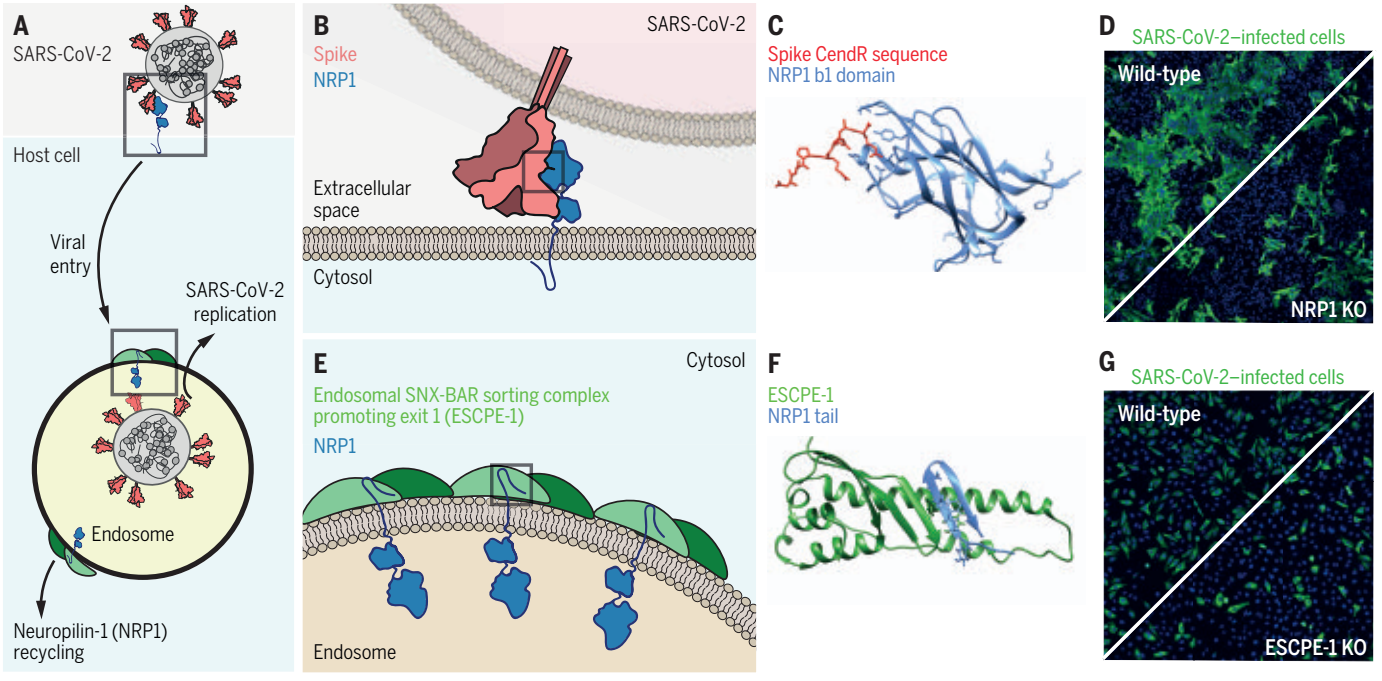

CendR, C-end rule; ESCPE-1, endosomal SNX-BAR sorting complex promoting exit 1; NRP1, neuropilin-1; S, spike.

Our discovery that NRP1 undergoes endosomal sorting to the TGN led us to become interested in how this pathway might influence the internalization and trafficking of NRP1-binding ligands and viruses.

In 2019, severe acute respiratory syndrome coronavirus 2 (SARS-CoV-2) emerged and instigated the COVID-19 pandemic. This unprecedented period in modern history has led to a remarkable interdisciplinary scientific response from across the globe. As seminal studies that characterized the virus emerged, it was discovered that SARS-CoV-2 harbored a polybasic cleavage site within the spike (S) glycoprotein that decorates the surface of virions. This cleavage is central to how S processes itself into two subunits: the receptor-binding S1 subunit and the fusogenic S2 subunit (*12*). I collaborated with an interdisciplinary network of scientists during this time, and we collectively noticed that cleavage at this site would liberate a sequence of amino acids at the C terminus of S1 that conforms to the NRP1-binding CendR consensus. This prompted us to ask whether this virus had acquired the ability to hijack NRP1 during infection.

We switched disciplines and used a variety of techniques to demonstrate that the CendR motif in S1 indeed directly binds to NRP1. Suppression of NRP1 rendered cells less susceptible to live SARS-CoV-2 infection, which identified this receptor as a key host factor implicated in COVID-19 (*13*). Furthermore, perturbation of the endosomal sorting process that regulates NRP1 trafficking also limits SARS-CoV-2 infection (*7*), which further emphasizes the complex interplay between cellular and viral biology during NRP1-dependent infection (see the figure).

Inhibitory compounds have been developed that specifically antagonize NRP1 to perturb CendR ligand binding (*14*). We demonstrated that a particular compound, EG00229, binds to NRP1 with higher affinity than the S1 CendR sequence and outcompetes it for NRP1 binding. Treatment of cells with EG00229 limits live SARS-CoV-2 infection (*13*) and highlights the future potential of NRP1 antagonist development for antiviral use. Through this approach, it may be possible to arm ourselves with additional weapons in the ongoing battle against viruses that hijack NRP1, such as SARS-CoV-2, and prepare for the emergence of future zoonotic viruses that harbor similar CendR sequences. Cell biology and virology are inextricably linked in my research, and more than 40 years since studies of Semliki Forest virus entry led to the characterization of endosomes, cells and viruses clearly still have more to reveal about each other (*15*). ■

GRAPHIC: N. CARY/*SCIENCE* BASED ON B. SIMONETTI *ET AL.* (*7*) AND J. L. DALY *ET AL.* (*13*)

REFERENCES AND NOTES

1. J. Mercer, M. Schelhaas, A. Helenius, *Annu. Rev. Biochem.* **79**, 803 (2010).
2. P. J. Cullen, F. Steinberg, *Nat. Rev. Mol. Cell Biol.* **19**, 679 (2018).
3. R. A. Nixon, D.-S. Yang, J.-H. Lee, *Autophagy* **4**, 590 (2008).
4. A. J. Evans, J. L. Daly, A. N. K. Anuar, B. Simonetti, P. J. Cullen, *J. Cell Sci.* **133**, jcs246033 (2020).
5. J. L. Daly *et al.*, bioRxiv 10.1101/2022.09.13.507260 (2022).
6. P. Cossart, A. Helenius, *Cold Spring Harb. Perspect. Biol.* **6**, a016972 (2014).
7. B. Simonetti *et al.*, *Proc. Natl. Acad. Sci. U.S.A.* **119**, e2201980119 (2022).
8. T. Teesalu, K. N. Sugahara, V. R. Kotamraju, E. Ruoslahti, *Proc. Natl. Acad. Sci. U.S.A.* **106**, 16157 (2009).
9. H.-B. Pang *et al.*, *Nat. Commun.* **5**, 4904 (2014).
10. S. Lambert *et al.*, *Blood* **113**, 5176 (2009).
11. H.-B. Wang *et al.*, *Nat. Commun.* **6**, 6240 (2015).
12. A. C. Walls *et al.*, *Cell* **181**, 281 (2020).
13. J. L. Daly *et al.*, *Science* **370**, 861 (2020).
14. A. Jarvis *et al.*, *J. Med. Chem.* **53**, 2215 (2010).
15. A. Helenius, M. Marsh, J. White, *Trends Biochem. Sci.* **5**, 104 (1980).

ACKNOWLEDGMENTS

I thank my supervisor P. Cullen for his mentorship, B. Simonetti for our collaborations, and my colleagues in the laboratory for their support throughout my PhD. I acknowledge and thank all those involved in our collaborative SARS-CoV-2 work, particularly K. Klein and Y. Yamauchi, without whom the research described in this essay would not have been possible. My PhD was supported by the Wellcome Trust Dynamic Molecular Cell Biology program (203959/Z/16/Z).

10.1126/science.adf4469

PRIZE ESSAY

CATEGORY WINNER: MOLECULAR MEDICINE

Daniele Simoneschi

Daniele Simoneschi received an undergraduate degree from Manhattanville College and MPhil and PhD degrees from the Vilcek Institute at New York University (NYU). He is a research assistant professor in the Department of Biochemistry and Molecular Pharmacology at NYU, where he explores molecular and cellular mechanisms by which cullin-RING ubiquitin ligases regulate cell cycle execution. **www.science.org/doi/10.1126/science.adf4868**

Science & SciLifeLab PRIZE For Young Scientists

MOLECULAR MEDICINE

Uncovering the degrader of D-type cyclins

AMBRA1 is identified as the long-sought, major controller of D-type cyclins

By **Daniele Simoneschi**

Throughout my PhD studies, in front of curious family members and friends, I often found myself faced with the question, "How close are we to finding a cure for cancer?" However, contrary to their expectations, I have always been at a loss for words, because the answer to this question is much more intricate than it first seems. To understand the complexity of this question, one must appreciate that cancer is not a single malady but rather myriad different diseases, each with its own molecular drivers and genetic vulnerabilities. The discovery of a panacea for all malignancies is utopian.

At the core of cancer development, one commonality does stand out among all others: the ability of tumor cells to bypass the normal restraints on cell division, which leads to uncontrollable proliferation. Healthy cells possess an arsenal of safeguard mechanisms that ensure the regulated progression through different cell cycle phases [i.e., gap 1 (G_1), synthesis, G_2, and mitosis]. The activation of cell cycle checkpoints by cyclin-dependent kinases (CDKs) in complex with their cyclin partners is one such regulatory mechanism that underlies proper cell cycle progression, and its deregulation in disease has been extensively reported (*1*, *2*).

When I first joined New York University as a PhD student, my mentor Michele Pagano was adamant in his decision to start me on a quest that would eventually take nearly 7 years to complete: the identification of the ubiquitin ligase of D-type cyclins—a family of well-established proto-oncoproteins (*3*). In the early 1990s, Pagano studied the three D-type cyclins (i.e., cyclin D1/2/3) as activators of CDK4/6 (*4*–*7*). He discovered that D-type cyclins are highly labile proteins, whose cell cycle oscillations, which are dependent on the ubiquitin-proteasome system, are crucial for progression through G_1. A plethora of research groups later reported several substrate receptors of CUL1-RING ubiquitin ligases (CRL1) and the anaphase-promoting complex/cyclosome (APC/C) as regulators of the degradation of D-type cyclins (*8*). However, a study published in 2012 by the laboratory of Keiichi Nakayama found that the stability of cyclin D1 was not affected by CRL1 or APC/C activities, which suggested that another ubiquitin ligase for D-type cyclins must exist to explain their rapid turnover (*9*). Puzzled and intrigued by these observations, I set out to rectify some of the previous controversies about the degradation of D-type cyclins.

My search for the missing degrader jump-started with three orthogonal approaches that resulted in the identification of $CRL4^{AMBRA1}$ as the long-sought ubiquitin ligase of all D-type cyclins (*10*, *11*). I combined biochemical and genetic approaches with the auxin-inducible degron system and found that autophagy and beclin 1 regulator 1 (AMBRA1), a substrate receptor for CUL4-RING ubiquitin ligases (CRL4), promotes the polyubiquitylation and proteasomal-mediated degradation of D-type cyclins to regulate cell cycle progression and G_1 checkpoint activation (see the figure). At that time, CRISPR-Cas9 had just begun to emerge as a new gene-editing tool. Eager to test this approach, I used CRISPR to engineer multiple cell lines and found that AMBRA1 regulated the levels of D-type cyclins in all systems tested (*11*, *12*).

Altered expression of D-type cyclins has been associated with neurological abnormalities (*13*), which indicates that tight regulation of their protein levels is required for embryogenesis. I decided to evaluate the effect of *Ambra1* deletion in mice and found that regulation of D-type cyclins by $CRL4^{Ambra1}$ ensures proper embryonic development. Importantly, treatment of pregnant mice with the CDK4/6 inhibitor abemaciclib rescued the morphological abnormalities of *Ambra1*-null embryos (*10*, *11*). Despite the successful clinical development of CDK4/6 inhibitors in oncology, such inhibitors have never been reported in the field of developmental biology. Our data showed that abemaciclib can enter the amniotic sac and correct the *Ambra1*

Department of Biochemistry and Molecular Pharmacology, Grossman School of Medicine, New York University, New York, NY, USA. Email: daniele.simoneschi@nyulangone.org

PHOTO: COURTESY OF DANIELE SIMONESCHI

Proteasomal-mediated degradation of D-type cyclins by CRL4^{AMBRA1}

In healthy cells, the modulation of D-type cyclins by CRL4^{AMBRA1} (A) controls the activation of the G_1 checkpoint, thus ensuring proper embryonic development and tumor suppression. Mutations in the genes encoding the three D-type cyclins or down-regulation of *AMBRA1* (B) impair the CRL4^{AMBRA1}-mediated degradation of D-type cyclins, thus accelerating cell cycle progression. This results in embryonic lethality, increased tumorigenic potential, and reduced sensitivity to CDK4/6 inhibitors. The formation of cyclin D–CDK2 complexes in DLBCL cells with defects in *AMBRA1* provides a cancer vulnerability that can be exploited using a CDK2/4/6 inhibitor (*10*–*12*).

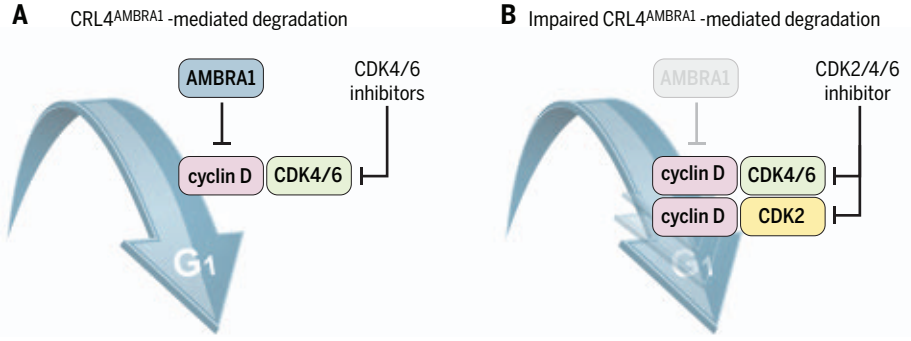

AMBRA1, autophagy and beclin 1 regulator 1; CDK,cyclin-dependent kinase; CRL4, CUL4-RING ubiquitin ligase; DLBCL, diffuse large B-cell lymphoma; G_1, gap 1 phase

phenotype, providing a rationale to target aberrant expression of D-type cyclins in patients who bear actionable mutations in this pathway.

Deregulation of key factors that control embryonic development depends on the meticulous regulation of cell cycle checkpoints and often contributes to tumorigenesis. I integrated bioinformatics analyses with two mouse models of cancer development and discovered that AMBRA1 also acts as a tumor suppressor in vivo (*10*, *11*). Consistent with this function, I identified low *AMBRA1* mRNA levels as a prognostic indicator of poor survival in cancer patients. Further, I found that mutations in D-type cyclins, or down-regulation of *AMBRA1*, contribute to the development of diffuse large B cell lymphoma (DLBCL), the most common type of non-Hodgkin lymphoma worldwide.

I had previously performed a whole-genome CRISPR/Cas9 screen that revealed *AMBRA1* as a regulator of the response to CDK4/6 inhibitors. Spurred by these observations, I dove deeper into the mechanism and found that DLBCL cells with defects in AMBRA1 can bypass CDK4/6 inhibitors by promotion of the formation of cyclin D–CDK2 complexes. These observations support AMBRA1 as a predictive biomarker for the stratification of DLBCL patients and highlight the need for the development of selective CDK2/4/6 inhibitors (see the figure). The translational relevance of my findings was corroborated in the following months by two studies that identified the first CDK2/4/6 inhibitor (*14*, *15*). I anticipate that this compound will finally offer a therapeutic strategy to patients who report low sensitivity to CDK4/6 inhibitors alone.

Although my quest has now reached its end, one lesson clearly resonates: The translation of cancer data into actionable information for patient therapy still requires a comprehensive understanding of the fundamental molecular processes that drive disease. Although the National Cancer Act of 1971 marked the beginning of the "war on cancer," we should learn from Chinese general Sun Tzu who, nearly 25 centuries ago, wrote the following in *The Art of War*: "If you do not know your enemies..., you will be imperiled in every single battle." I remain hopeful that the concerted efforts of our current army of scientists will eventually dissect the molecular mechanisms of individual cancer types to produce results worth translation into clinical practice. Only then will we be closer to finding cures for cancer. ■

REFERENCES AND NOTES

1. M. Malumbres, *Genome Biol.* **15**, 122 (2014).
2. A. Fassl, Y. Geng, P. Sicinski, *Science* **375**, eabc1495 (2022).
3. E. A. Musgrove, C. E. Caldon, J. Barraclough, A. Stone, R. L. Sutherland, *Nat. Rev. Cancer* **11**, 558 (2011).
4. V. Baldin, J. Lukas, M. J. Marcote, M. Pagano, G. Draetta, *Genes Dev.* **7**, 812 (1993).
5. S. W. Tam, A. M. Theodoras, J. W. Shay, G. F. Draetta, M. Pagano, *Oncogene* **9**, 2663 (1994).
6. J. Lukas, M. Pagano, Z. Staskova, G. Draetta, J. Bartek, *Oncogene* **9**, 707 (1994).
7. M. Pagano, A. M. Theodoras, S. W. Tam, G. F. Draetta, *Genes Dev.* **8**, 1627 (1994).
8. S. Qie, J. A. Diehl, *Semin. Cancer Biol.* **67**, 159 (2020).
9. T. Kanie *et al.*, *Mol. Cell. Biol.* **32**, 590 (2012).
10. A. C. Chaikovsky, J. Sage, M. Pagano, D. Simoneschi, *DNA Cell Biol.* **40**, 1457 (2021).
11. D. Simoneschi *et al.*, *Nature* **592**, 789 (2021).
12. E. Maiani *et al.*, *Nature* **592**, 799 (2021).
13. A. Satyanarayana, P. Kaldis, *Oncogene* **28**, 2925 (2009).
14. K. Freeman-Cook *et al.*, *Cancer Cell* **39**, 1404 e1411 (2021).
15. K. D. Freeman-Cook *et al.*, *J. Med. Chem.* **64**, 9056 (2021).

10.1126/science.adf4868

GRAPHIC: N. CARY/*SCIENCE* BASED ON DANIELE SIMONESCHI

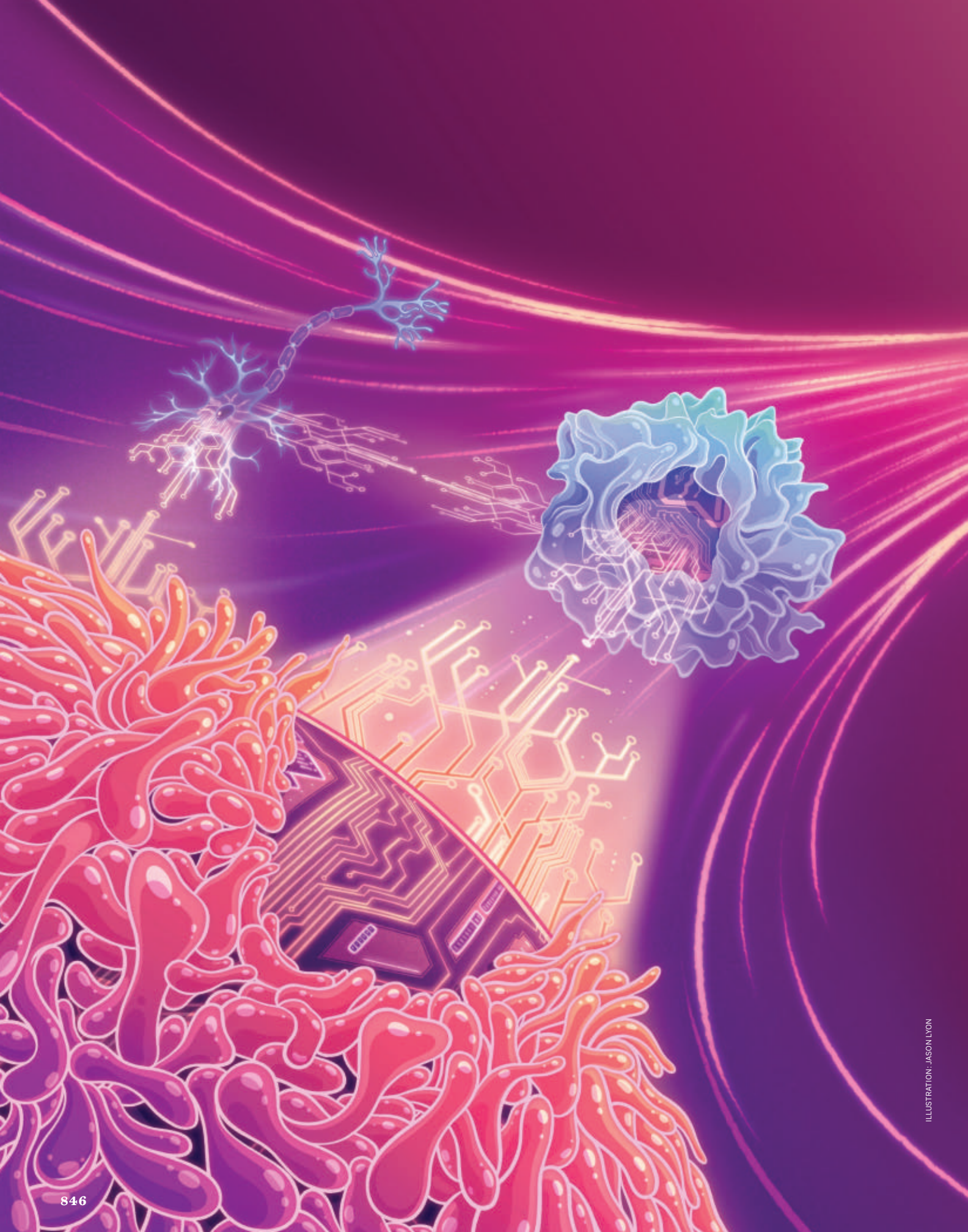

ILLUSTRATION: JASON LYON

CELL ENGINEERING

By **L. Bryan Ray** *and* **Priscilla N. Kelly**

The successful use of engineered white blood cells (cells that are removed from the human body, modified with receptors that allow them to recognize cancer cells, and then returned to the body) to fight and eliminate tumor cells has frequently been called revolutionary and has even allowed researchers the rare opportunity to refer to a cure for certain cancers.

Remarkably, this so-called CAR T cell technology is but one example from a burgeoning area of investigation in which cells can be customized to perform functions that bring us closer to realizing long-imagined medical and basic science applications. These efforts in cell engineering are the focus of this special issue. Decades of fundamental research on biological regulatory mechanisms have revealed basic principles and the characteristic modularity of cellular signaling systems that now allow researchers to endow cells with new or modified sensors that evoke desired cellular responses. Internally, cells can be programmed with logic circuits that respond appropriately to specified cues. In this way, cells or groups of cells can be turned into an arsenal of diagnostic and therapeutic agents capable of seeking out their targets and initiating actions that closely resemble those of natural biological regulatory systems.

The seemingly unlimited potential of cell engineering includes creating alternatives to common drug or gene-based therapeutics; devising improved strategies against cancer, inflammatory diseases, and other maladies; designing tissue regeneration and repair options; exploring the intricate dimensions of human development; and enhancing our fundamental understanding of how complex biological systems are controlled.

REVIEW

The emerging era of cell engineering: Harnessing the modularity of cells to program complex biological function

Wendell A. Lim

A new era of biological engineering is emerging in which living cells are used as building blocks to address therapeutic challenges. These efforts are distinct from traditional molecular engineering—their focus is not on optimizing individual genes and proteins as therapeutics, but rather on using molecular components as modules to reprogram how cells make decisions and communicate to achieve higher-order physiological functions in vivo. This cell-centric approach is enabled by a growing tool kit of components that can synthetically control core cell-level functional outputs, such as where in the body a cell should go, what other cells it should interact with, and what messages it should transmit or receive. The power of cell engineering has been clinically validated by the development of immune cells designed to kill cancer. This same tool kit for rewiring cell connectivity is beginning to be used to engineer cell therapies for a host of other diseases and to program the self-organization of tissues and organs. By forcing the conceptual distillation of complex biological functions into a finite set of instructions that operate at the cell level, these efforts also shed light on the fundamental hierarchical logic that links molecular components to higher-order physiological function.

As we explore ways to harness our knowledge of biology to solve diverse problems in medicine, one of the most innovative emerging concepts is that living cells can be engineered to execute therapeutic functions (*1*). Such efforts have been inspired by the successful use of engineered immune cells to treat hematological cancers (*2*–*4*). We now also have powerful suites of technologies to rewrite genomes and to transfect DNA. But what biological code should we write with these methods? How can we learn to program cells so that they carry out useful functions with the same degree of precision and reliability as naturally evolved cells? How can we expand the range of therapeutic problems to which cell engineering can be applied, beyond cancer or immunity? Perhaps there is a set of more universal principles, components, and approaches that can be used to functionally program cells, whether the goal is designing an immune cell to eliminate an evasive tumor or designing a set of cells that can regrow into a new organ.

Programming new biological function: Connecting cellular building blocks

Evolution has generated an inspiring array of organismal functions through gradual genetic changes. So how do we rationally alter biological behavior? One of the great barriers to understanding the relationship between genetic information and physiological function is the complex multiscale nature of biological systems (Fig. 1). Although all function is ultimately encoded in genes and their control elements, the expression of higher-level function depends on a diversity of contexts. For example, the simple expression of a receptor gene in a cell is not sufficient to generate "function" unless: (i) that cell has the necessary downstream components to mediate receptor response and (ii) that cell is localized, by history or migration, to a site where it can access signals from a partner cell expressing the cognate ligand. Thus, genetic components that contribute to any one physiological function often act at different spatial and temporal scales and in different cells. Given this multiscale complexity, where does one pragmatically focus when trying to create new function?

Although all scales of biology are important, there are many reasons to believe that the intermediate scale of cellular function and connectivity may prove to be the most pragmatic scale at which to intervene to create new biological functions (Fig. 1). Cells, after all, are compartmentalized agents that function as the fundamental units of life, providing a strong argument for viewing cells as the key "building blocks" for complex function. Much of complex biological function is ultimately determined by how cells interact and communicate with one another within multicellular systems, and thus, logically, many substantially new functions likely result from changes in the interactions between cells rather than the development of new cell-intrinsic functions. Notably, there are also a finite number of channels through which cells communicate with one another (send and receive systems) and finite types of core state changes that cells can undergo as a response (grow, die, secrete, express, migrate, adhere, etc.) (Fig. 2). Thus, focusing on reconnecting the external input and output properties of cells, whether in evolution or engineering, provides a conceptually simpler framework in which to link molecular-scale parts with physiological function.

Focusing on cells in terms of their external input and output properties provides a way to abstract the high molecular complexity of a cell but still productively manipulate how it works within a multicellular context. This abstraction is analogous to focusing on valance electrons in chemistry to understand

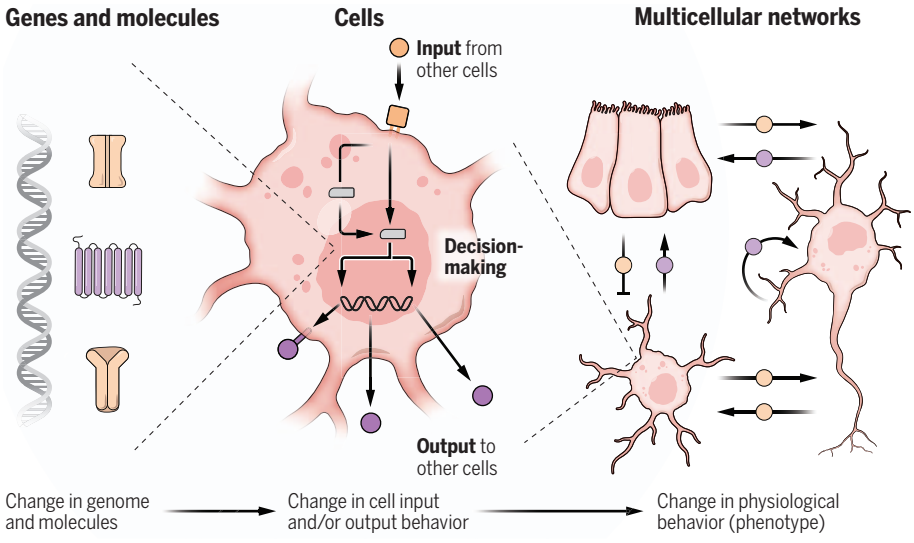

ILLUSTRATION: A. FISHER/*SCIENCE*

Fig. 1. Cell-centric perspective of programming complex biological function. Biological systems are encoded as genetic or molecular components, but their higher-scale functions ultimately manifest through the way the resulting cells interact with one another. Thus, focusing on how to rewire cell inputs and outputs may provide a particularly useful perspective from which to strategically guide engineering of biological function.

Cell Design Institute and Department of Cellular and Molecular Pharmacology, University of California, San Francisco, CA, USA.
Email: wendell.lim@ucsf.edu

the functional potential of an atom (*5*). Although atoms have complex nuclear components and structures, from the perspective of understanding bonding and reactivity with other atoms, one can largely focus on only those electrons in the outermost shell, as these are the ones that can interact to form chemical bonds. This is a substantial abstraction, yet it is sufficient to rationally guide the understanding and synthesis of a universe of larger chemical structures. An analogous concept of "cellular reactivity"—how individual genes, molecules, pathways, and organelles contribute to shaping the potential external interactions of a cell—could be similarly useful in understanding and synthesizing larger-scale biological systems.

Toward a universal tool kit for cell engineering: Learning to push a cell's buttons

Most cell–cell interactions are highly complex, but they can still be broken down into a core set of common primitive cell-state changes. For example, when a chimeric antigen receptor (CAR) T cell recognizes a cognate antigen on a cancer cell, a combinatorial response is triggered: The T cells secrete payload molecules that cause target cell death (from granules), they secrete cytokines that promote their autocrine T cell proliferation, and they undergo changes in adhesion, migration, and cell state. Although this composite response may be specific to T cells, each of the individual component responses can be found in many other cell types. For example, an analogous combination of core responses are observed in neurons, which respond to signals by changing their axon shape, precisely adhering to their target cells to form synapses, and expressing transmission or receiving signaling molecules localized to these termini (neurotransmitters and receptors). Even though T cells and neurons are very different cell types, their behaviors consist of similar core elemental cellular responses.

From this perspective, another way to frame a major goal of cell engineering is to be able to controllably "push a cell's buttons" to trigger the appropriate suite of core regulatory changes (Fig. 2). A chimeric receptor, such as that used in T cells, provides an orthogonal way to link detection of a user-specified surface antigen to induction of the endogenous T cell killing response. Optogenetically or chemogenetically controlled receptors provide a way to use orthogonal light or small-molecule inputs to trigger downstream responses.

Over the past several years, a growing set of orthogonal cell–cell linkage components have been developed, and more are in the pipeline. These include orthogonal cytokine-receptor systems that can controllably induce T cell proliferation without significant cross-interference with native cells (*6*). Other orthogonal cell–cell signaling ligand and receptor systems have also been developed (*7*, *8*). Synthetic Notch (synNotch) receptors and other related binding-triggered transcriptional receptors provide a particular flexible way to rewire cell–cell regulation (*9*). These receptors can be programmed with extracellular single-chain antibody domains to recognize a user-defined input ligand. When engaged, the receptors undergo transmembrane cleavage, releasing an intracellular transcriptional domain that then enters the nucleus to induce expression of a user-defined gene. The system can be used to induce expression of diverse payloads, including receptors, ligands, adhesion molecules, proliferative cytokines, master regulators, or apoptotic inducers. In short, the system can be used to rapidly create a host of completely new regulatory linkages, yielding engineered cells that respond to user-specified inputs by generating desired outputs.

So far, many endogenous cell–cell communication systems, such as those described above, have proven to be surprisingly engineerable platforms in which relationships between extracellular inputs and intracellular

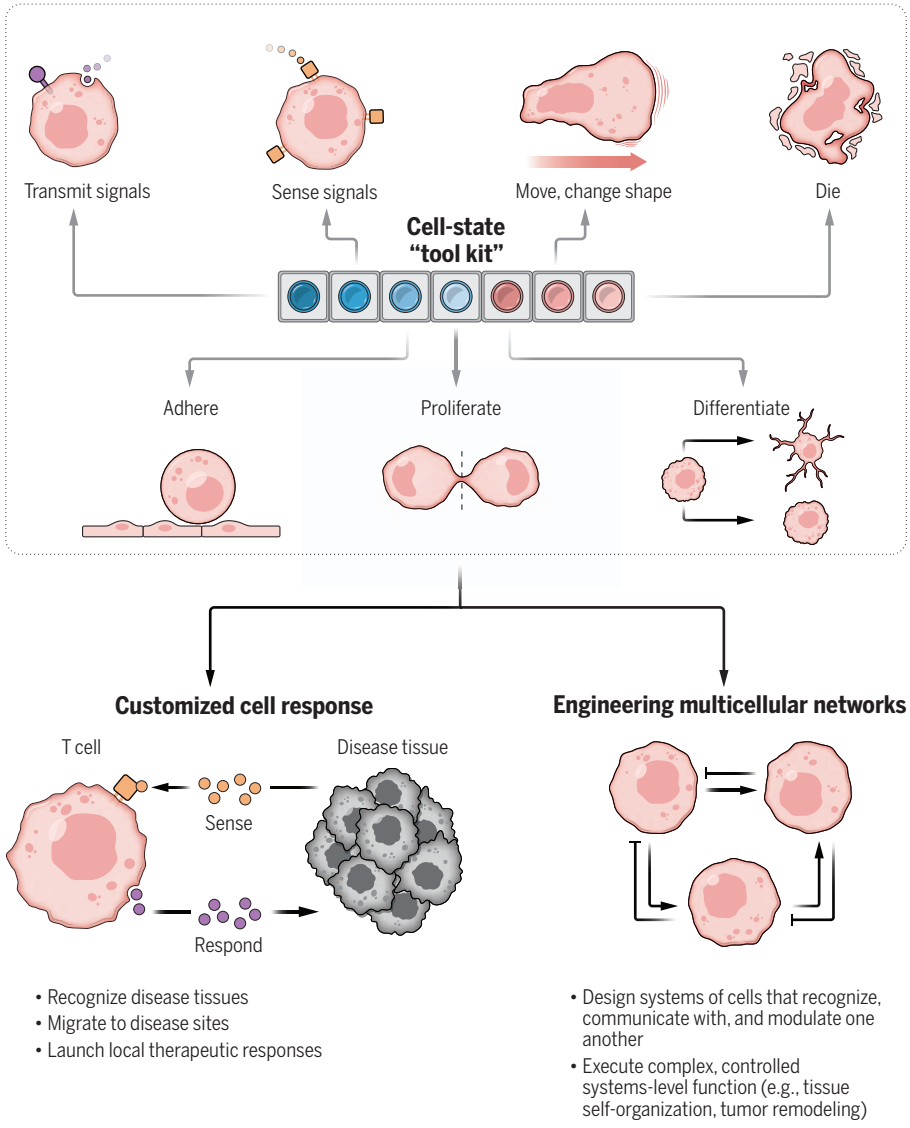

Fig. 2. Learning to push a cell's buttons: Fundamental tool kit for cell engineering. (Top) Nearly all cells can undergo a finite set of core types of state changes, a few of which are illustrated here. Many advances in cell engineering are based on developing new molecular tools that allow connecting new extracellular input to these core cellular outputs. (Bottom left) These types of tools for reconnecting cells with their environment can be used to engineer a T cell to recognize and kill a tumor. (Bottom right) The same tools can also be used to engineer more complex multicellular networks, which can involve both engineered and endogenous cell communication. Engineering tissue self-organization or remodeling of a tumor microenvironment likely requires thinking about cell engineering from a multicell-network perspective.

ILLUSTRATION: A. FISHER/*SCIENCE*

responses can be flexibly altered (*10*). In addition, these engineered receptors can function equally well in diverse cell types, as the downstream intracellular response machinery is often nearly universal. These findings speak to the highly modular structure and function of cell–cell communication molecules, many of which have undergone extensive modular recombination during the course of evolution (*11*).

Immune engineering and cancer: Lead applications

This growing tool kit of cell engineering components can be deployed in different contexts to engineer therapeutically useful behaviors, as summarized in Fig. 3. By far the most advanced and well-studied systems are those in which immune cells are engineered to treat cancer (*2–4*). The advent of the CAR first demonstrated that it was possible for a user to rationally redirect a powerful cellular immune response.

Although a primary focus of immune engineering in cancer remains on identifying antigens to target with a CAR, there is growing appreciation that this is a multifaceted problem (*12–14*). Not only must an antigen that is present at sufficiently high levels in the tumor be targeted, but it must also be homogeneous enough to avoid tumor escape. Furthermore, the antigen, or related cross-reactive antigens, must not be present in any critical normal tissues, lest it lead to toxic off-tumor killing. It is also critical to consider how the CAR T cells interact, not only with cancer cells but also with other cells in the tumor microenvironment. Especially in solid cancers, which have suppressive environments, regulatory T cells (T_{regs}), myeloid cells, and cancer-associated fibroblasts can have powerful suppressive functions that need to be overcome. Thus, to effectively treat solid tumors in the long term, it is likely necessary to view CAR T cell engineering more as a multicell interaction network problem than one focused solely on simple cellular retargeting.

To overcome this set of challenges, anticancer immune cells will likely require a combinatorial approach, in which multiple components in the cell engineering tool kit are used together to simultaneously address specificity, tumor heterogeneity, and tumor immune suppression. For example, with current tools, it is, in principle, possible to target a brain cancer such as glioblastoma with a multistep genetic program: T cells could be programmed to recognize that they are in the brain (via a synNotch receptor) and then induce the expression of a killing molecule, such as a CAR or a secreted bispecific engager (*15*, *16*). The specificity of these killing molecules need not be perfect, as long as their target antigens are not expressed in the brain. Moreover, these cells could be induced by tumor recognition to locally deliver proinflammatory payloads. A more in-depth perspective on immune engineering is given in the accompanying Review by Irvine *et al.* (*17*).

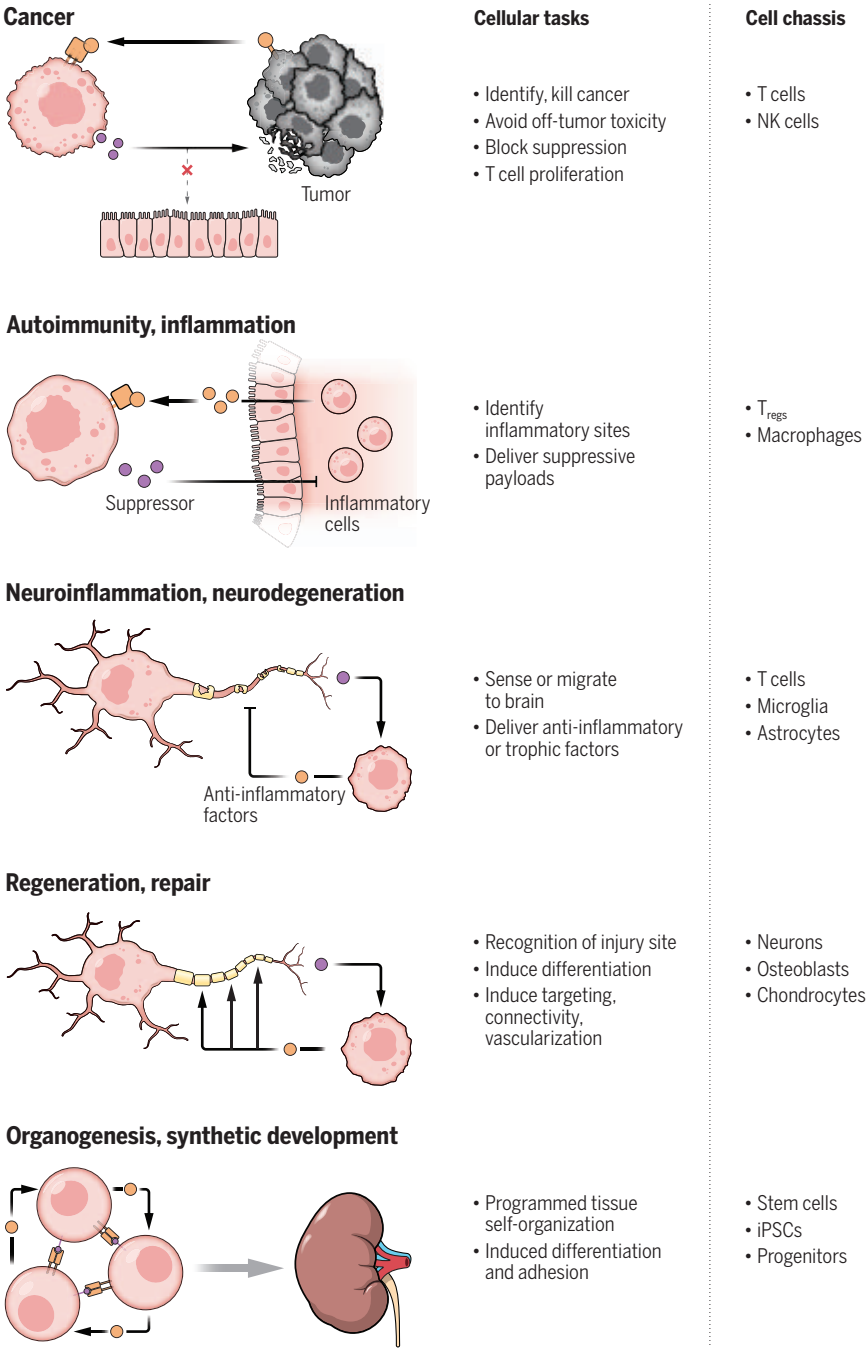

Fig. 3. An expanding set of potential therapeutic areas of application for cell engineering. Examples of fundamental cellular tasks that could be useful in each area, as well as cell types that could be useful chassis for these functions. NK cells, natural killer cells. Many of these examples are forward-looking, but see the following: cancer (*2–4*, *12–17*); autoimmunity and inflammation (*18–20*); regeneration, repair, and synthetic development (*23–28*).

Expanding the therapeutic scope of cell engineering

As the engineering of immune cells for cancer turns toward more-combinatorial solutions, an obvious question is how the cell engineering tool kit can be applied to other classes of diseases (*18–22*). In Fig. 3, we summarize a host of potential and emerging areas of application and the types of modular therapeutic cell programs that could be useful. Engineering cells to treat autoimmunity and inflammation is already a growing area and involves

ILLUSTRATION: A. FISHER/*SCIENCE*

strategies ranging from killing the attacking immune cells to redirecting the action of suppressor cells, such as T_{regs}, to the targeted delivery of suppressive payloads (*18*–*20*). Other tissue-based diseases, such as fibrosis, could benefit from cells designed to sense fibrosis and to produce responses that disrupt fibroblast activation. Neurological diseases, including neuroinflammation (e.g., multiple sclerosis) and neurodegeneration, are also potential targets. In this case, it might be possible to harness brain-sensing cells to migrate to the brain and locally deliver anti-inflammatory or trophic factors. Engineered immune cells might provide previously unexplored strategies to overcome the challenges faced by molecular agents in crossing the blood-brain barrier, if their active mechanisms of transmigration can be redirected.

Another growing focus in cell engineering is synthetic development, where the spotlight is on learning to program the self-organization of functional multicellular structures, a topic reviewed in this issue by Martínez-Ara *et al.* (*23*). The tools and approaches of cell engineering are being used to explore the logic of self-organizational circuits and to potentially guide and improve organoid growth or regeneration (*24*–*28*). Combining engineered morphogen and juxtacrine signaling with control over differentiation and cell adhesion can provide the basis for complex spatiotemporal organization.

Neuroengineering is an intriguing future area in which one might apply the same approaches and tools to wire, self-organize, or repair brain circuits. Advances will require learning how to trigger the localized differentiation of neural stem cells into specific cell types, such as neurons and oligodendrocytes, as well as how to synthetically control the connectivity of these cells (Box 1).

Another frontier is the engineering of bacteria as agents programmed to interact with mammalian cells and disease tissues. Changes in the microbiome have been linked to many diseases, and thus systematically engineering the microbiome might provide powerful therapeutic avenues. Such engineered bacterial/mammalian systems are also very relevant to treatment of cancer and inflammation, a topic reviewed in this issue by Gurbatri *et al.* (*29*).

Advantages of engineered cells over molecular-scale interventions

The realization that many different diseases and different areas of biology could be affected by these general cell engineering tools and approaches speaks to the fact that so many biological challenges (including therapeutic ones) require solving the same types of spatiotemporal problems that cells are uniquely well suited for. Say, for example, that a secreted factor that plays a role in a disease state is identified and proven to block a key disease mechanism in vitro. In most cases, the problem of how to precisely deliver this molecular factor to the right place at the right time will still need to be solved. Because this factor likely also functions in other normal processes throughout the body, it cannot simply be administered systemically, given the potential danger of inducing toxicity. Cells—which can move, send out processes, and conditionally secrete factors—provide an ideal platform for precision local delivery of factors (Fig. 4). It is the fact that cells can act in such a localized manner that allows multicellular organisms to repeatedly reuse the same molecular systems to control different aspects of biology (consider, for instance, how many distinct biological systems in a single organism use Wnt or transforming growth factor–β). Cells also have the power to act more as organizers, orchestrating decision-making and calling in other endogenous cell types to carry out their functions in a coordinated and spatially localized fashion (*30*).

"...engineering higher-order functions forces us to grapple with the underlying logic and hierarchy of biology."

Another potential advantage of engineered cells as therapies is that they have the potential to respond to a disease in a homeostatic manner. For example, when a molecular therapeutic such as an anti-inflammatory drug is given, the system is pushed in one direction and does not necessarily reestablish a stable state. A hallmark of living systems is their ability to achieve homeostatic, self-adjusting, and balanced responses. In nearly all cases, cellular systems are used to achieve these behaviors (Box 1), relying on a network of opposing positive and negative regulation (e.g., inflammatory versus anti-inflammatory responses), coordinated through feedback control (*31*). Similarly, regenerative processes must achieve a balance between proliferation and cell death, so that new tissue can emerge, without resulting in cancer. How to engineer robust homeostatic cellular circuits remains a great future challenge and opportunity.

Cell engineering also provides an opportunity to invent novel workarounds to roadblocks inherent to biology. There are cases in which therapeutic problems might be better solved by replacing, rather than repairing, a function (akin to surgical replacement or reconstruction). For example, consider a disease in which a gene involved in the early development of a tissue is disrupted. In the context of a mature organism, replacing this gene in a stem cell or pharmacologically interfacing with it would likely be useless, given that the critical developmental period has past, that is, the context of morphogens that guide development is likely long gone. In this case, it may be more effective to try to reinvent development—for example, to design a stem cell that can recognize specific signals present on the defective tissue and to use these as a trigger for establishing new synthetic morphogen fields that can guide regeneration. In such cases of creating new functions, it must be known how to apply the principles and modules of cellular networks, but in novel, nonnatural combinations.

Outlook

Although the broader field of cell engineering is still in its infancy, several clear lessons have emerged. First, it is certainly possible to engineer novel complex biological functions: Cells can be programmed to carry out highly precise synthetic multistep and precisely localized functions in vivo, especially as demonstrated in engineered cell systems developed to treat

Box 1. Examples of potential future challenges in therapeutic cell engineering.

Homeostatic therapeutic responses: Can we engineer therapeutic cellular systems that use feedback and counteracting positive versus negative control to achieve balanced, self-correcting therapeutic responses?

Neuro- and endocrine-engineering: Can we program neural connectivity to construct self-assembling neural circuits? Can we create new diffusible regulatory systems to exert homeostatic control over diverse diseases and/or organs?

In situ regeneration: Can endogenous signals of injury or damage be leveraged to prime synthetic developmental programs?

Bidirectional integration of extracellular matrix (ECM) into cell engineering: Can we artificially induce synthesis of ECM to drive formation of physically rigid tissues (e.g., epithelia)? Can we create orthogonal ECMs that are still genetically encoded, such that the ECM can serve as both input signal and output signal?

Cell modification and manufacturing: How do we upload larger genetic programs into cells? How do we reduce costs of manufacturing? How can we make allogeneic or induced pluripotent stem cells (iPSCs) that alleviate problems of immunogenicity and/or rejection?

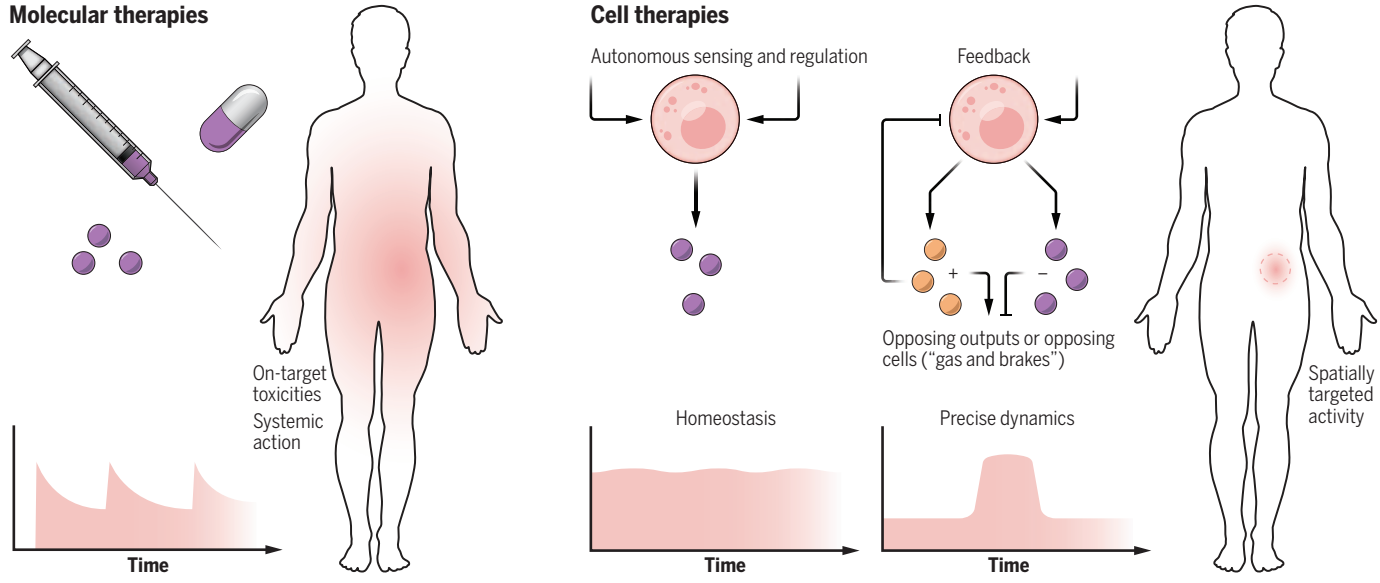

Fig. 4. Advantages of cell therapies over conventional molecular therapies. Molecular therapies (left), including small molecules and biologics, are given systemically, leading to toxicities that arise from multiple normal functions of most target molecules. Such therapies have limited dynamic and amplitude dosage control (see graphs). In contrast, cellular machines (right) can be engineered to execute a function or deliver a molecular payload in response to very specific sets of inputs, allowing for much more spatially targeted therapeutic action (with reduced toxicities). Additionally, cells can, in principle, coordinate multiple opposing outputs. This type of "gas and brakes" control is observed in most examples of natural homeostatic regulation. Feedback and cross-regulation in such systems could thus yield engineered therapeutic actions that are far more precise, robust, and autonomously controlled.

cancer. Cellular systems are generally far more flexible to rewiring than had been previously thought. Second, many of these new functions have been enabled by engineering new cell–cell connectivities. Extracellular signaling systems are, by nature, highly modular, and we can exploit this modularity to create user-specified orthogonal cell–cell communication systems. Third, there is growing appreciation that a key to accelerating advances in cell engineering is the development of a more comprehensive and robust tool kit of parts for rewiring fundamental cell behaviors. These cell–cell communication and interaction components are highly universal in their function, such that many of them are likely to prove useful in diverse future areas of application, well beyond oncology and inflammation. Regeneration and development represent such an area in which there is a growing interest in using these types of cell engineering tools to reprogram self-organization. Fourth is the recognition that rather than simply fixing or redirecting natural cellular programs, cell engineering offers the possibility of deploying new combinations of modular cellular responses to construct complex nonnatural cellular systems that can solve challenging medical problems.

Perhaps most importantly, trying to solve these problems in engineering higher-order functions forces us to grapple with the underlying logic and hierarchy of biology (*32*). The approaches of the molecular biology era have tended to focus on identifying and studying the genes or genetic elements involved in a process or disease. But while such information is critical to know, it alone does not necessarily give a holistic multiscale understanding of how a system works or a concrete and actionable path to treating a disease. Genes can only exert their functions in the context of living cells, and what may be most relevant is ultimately how those genes alter the interactions that a cell participates in. Thinking about parsing biological function through the lens of a more cell-centric perspective may help unleash the ability to better interface with and to modulate complex biological systems.

REFERENCES AND NOTES

1. M. A. Fischbach, J. A. Bluestone, W. A. Lim, *Sci. Transl. Med.* **5**, 179ps7 (2013).
2. C. H. June, M. Sadelain, *N. Engl. J. Med.* **379**, 64–73 (2018).
3. E. W. Weber, M. V. Maus, C. L. Mackall, *Cell* **181**, 46–62 (2020).
4. M. Hong, J. D. Clubb, Y. Y. Chen, *Cancer Cell* **38**, 473–488 (2020).
5. G. N. Lewis, *Valence and the Structure of Atoms and Molecules* (The Chemical Catalog Company, Inc., 1923).
6. J. T. Sockolosky *et al.*, *Science* **359**, 1037–1042 (2018).
7. K. S. Stapornwongkul, M. de Gennes, L. Cocconi, G. Salbreux, J.-P. Vincent, *Science* **370**, 321–327 (2020).
8. S. Toda *et al.*, *Science* **370**, 327–331 (2020).
9. L. Morsut *et al.*, *Cell* **164**, 780–791 (2016).
10. J. Manhas, H. I. Edelstein, J. N. Leonard, L. Morsut, *Nat. Chem. Biol.* **18**, 244–255 (2022).
11. R. P. Bhattacharyya, A. Reményi, B. J. Yeh, W. A. Lim, *Annu. Rev. Biochem.* **75**, 655–680 (2006).
12. G. M. Allen, W. A. Lim, *Nat. Rev. Cancer* 10.1038/s41568-022-00505-x (2022).
13. S. Simon, G. Bugos, A. I. Salter, S. R. Riddell, *Curr. Opin. Immunol.* **74**, 9–17 (2022).
14. Z. L. Chang *et al.*, *Nat. Chem. Biol.* **14**, 317–324 (2018).
15. J. H. Choe *et al.*, *Sci. Transl. Med.* **13**, eabe7378 (2021).
16. B. D. Choi *et al.*, *Nat. Biotechnol.* **37**, 1049–1058 (2019).
17. D. J. Irvine, M. V. Maus, D. J. Mooney, W. W. Wong, *Science* **378**, 853–858 (2022).
18. C. Raffin, L. T. Vo, J. A. Bluestone, *Nat. Rev. Immunol.* **20**, 158–172 (2020).
19. I. Rosado-Sánchez, M. K. Levings, *Cell. Immunol.* **358**, 104220 (2020).
20. A. Mackensen *et al.*, *Nat. Med.* **28**, 2124–2132 (2022).
21. C. Amor *et al.*, *Nature* **583**, 127–132 (2020).
22. J. G. Rurik *et al.*, *Science* **375**, 91–96 (2022).
23. G. Martínez-Ara, K. S. Stapornwongkul, M. Ebisuya, *Science* **378**, 864–868 (2022).
24. S. E. Harrison, B. Sozen, N. Christodoulou, C. Kyprianou, M. Zernicka-Goetz, *Science* **356**, eaal1810 (2017).
25. M. N. Shahbazi, M. Zernicka-Goetz, *Nat. Cell Biol.* **20**, 878–887 (2018).
26. M. Matsuda *et al.*, *Nature* **580**, 124–129 (2020).
27. J. Davies, *Development* **144**, 1146–1158 (2017).
28. S. Toda, L. R. Blauch, S. K. Y. Tang, L. Morsut, W. A. Lim, *Science* **361**, 156–162 (2018).
29. C. R. Gurbatri, N. Arpaia, T. Danino, *Science* **378**, 858–864 (2022).
30. M. L. Meizlish, R. A. Franklin, X. Zhou, R. Medzhitov, *Annu. Rev. Immunol.* **39**, 557–581 (2021).
31. J. E. Ferrell, *Systems Biology of Cell Signaling: Recurring Themes and Quantitative Models* (Garland Science, ed. 1, 2021).
32. M. Elowitz, W. A. Lim, *Nature* **468**, 889–890 (2010).

ACKNOWLEDGMENTS

I thank the following colleagues for discussions and assistance E. Lim, O. Troyanskaya, D. Fletcher, B. Mayer, T. Pawson, M. Fischbach, J. Bluestone, M. Elowitz, U. Alon, R. Medzhitov, J. Ferrell, C. Garcia, D. Baker, A. Khalil, D. Chen, C. June, C. Tang, C. Voigt, J. Hasty, R. Weiss, G. Altan-Bonnet, M. Ebisuya, J. Sharpe, and A. Martinez-Arias. I also thank H. El-Samad, H. Okada, O. Klein, M. Hebrok, Q. Tang, A. Parent, T. Desai, K. Roybal, F. Fattahi, V. Weaver, D. Mullins, A. Mangalik, Z. Gartner, W. Marshall, S. Hauser, M. Wilson, S. Zamvil, N. Blizzard, R. Almeida, and past and present members and collaborators of the Lim lab and the UCSF Cell Design Institute. **Funding:** This work was supported by NIH grants U54CA244438, U01CA265697, R01CA249018, and R01CA258789 and by NSF grant NSF 14-600. **Competing interests:** W.A.L. is on the scientific advisory board of Allogene Therapeutics and is a shareholder of Gilead Sciences and Intellia Therapeutics.

Submitted 27 September 2022; accepted 18 October 2022
10.1126/science.add9665

ILLUSTRATION: A. FISHER/*SCIENCE*

REVIEW

The future of engineered immune cell therapies

Darrell J. Irvine[1,2,3,4,5]*, Marcela V. Maus[2,6,7]*, David J. Mooney[8,9]*, Wilson W. Wong[10]*

Immune cells are being engineered to recognize and respond to disease states, acting as a "living drug" when transferred into patients. Therapies based on engineered immune cells are now a clinical reality, with multiple engineered T cell therapies approved for treatment of hematologic malignancies. Ongoing preclinical and clinical studies are testing diverse strategies to modify the fate and function of immune cells for applications in cancer, infectious disease, and beyond. Here, we discuss current progress in treating human disease with immune cell therapeutics, emerging strategies for immune cell engineering, and challenges facing the field, with a particular emphasis on the treatment of cancer, where the most effort has been applied to date.

The first uses of living immune cells as a therapy were demonstrated in the late 1980s, when tumor-infiltrating T cells isolated from cancer patients were used to treat metastatic melanoma. The early promise of these clinical trials fueled efforts exploring immune cell therapy (ICT) using diverse immune cell types and applying ICT to additional cancers and pathologies ranging from infectious disease to autoimmunity (*1*). However, taking the case of T cells as an example, a number of challenges quickly become evident: Isolation and preparation of large numbers of functional tumor-specific T cells are difficult in many types of cancer, natural T cells can lose function over time in the face of high tumor antigen burden (termed exhaustion), and tumors evolve diverse means to suppress attack by native lymphocytes (*1*). Such issues motivated the field early on to explore engineering of immune cells (*2*–*4*). Approaches to immune cell engineering include pharmacologic manipulation and genetic modification, which can be performed either ex vivo prior to infusion of the cell therapy or directly in the body. Genetic engineering has played a critical role in the development of clinically effective ICTs, with several important categories of modifications (Fig. 1A): (i) engineering of antigen receptors, including transgenic T cell receptors (TCRs) and synthetic antigen receptors termed chimeric antigen receptors (CARs); (ii) genetic modification of intracellular pathways that modulate natural properties such as metabolism, survival, and proliferation; and (iii) introduction of accessory genes that provide new functions to immune cells. ICTs are being developed based on T cells, macrophages, natural killer (NK) cells, and dendritic cells, derived from autologous patient-derived cells or "off the shelf" sources such as engineered cell lines or induced pluripotent stem cell (iPSC)–derived products (*1*, *5*). In parallel, important advances in immunobiology over the past 30 years have enabled this field, such as the discovery of key pathways mediating immune cell killing and dysfunction, definition of mechanisms underlying immunosuppression, and determination of factors that control successful immune cell engraftment (*3*). The first US Food and Drug Administration (FDA)–approved immune cell therapy product, a cell-based cancer vaccine (Provenge), was licensed in the US in 2010. Over the past 5 years, six CAR T cell therapies for hematologic malignancies and an engineered thymus tissue therapy for treatment of congenital athymia immunodeficiency have been approved in the US, and ICTs with tumor-infiltrating lymphocytes, as well as T cells engineered to express defined T cell receptors, are on the verge of approval. Furthermore, thousands of clinical trials of immune cell therapies in diverse diseases are currently underway, and the pace of discovery preclinically and in humans continues to accelerate.

[1]Koch Institute for Integrative Cancer Research, MIT, Cambridge, MA, USA. [2]Ragon Institute of Massachusetts General Hospital, Massachusetts Institute of Technology and Harvard University, Cambridge, MA, USA. [3]Department of Biological Engineering, Massachusetts Institute of Technology, Cambridge, MA, USA. [4]Department of Materials Science and Engineering, Massachusetts Institute of Technology, Cambridge, MA, USA. [5]Howard Hughes Medical Institute, Cambridge, MA, USA. [6]Cellular Immunotherapy Program, Massachusetts General Hospital Cancer Center, Boston, MA, USA. [7]Harvard Medical School, Boston MA, USA. [8]John A. Paulson School of Engineering and Applied Sciences, Harvard University, Cambridge, MA, USA. [9]Wyss Institute for Biologically Inspired Engineering at Harvard University, Boston, MA, USA. [10]Department of Biomedical Engineering and Biological Design Center, Boston University, Boston, MA, USA.
***Corresponding author. Email: djirvine@mit.edu (D.J.I.); mvmaus@mgh.harvard.edu (M.V.M.); mooneyd@seas.harvard.edu (D.J.M.); wilwong@bu.edu (W.W.W.)**

Clinical progress with engineered immune cell therapies

The first approved "gene therapy" in the US was a form of CAR T cell therapy (Kymriah, a CD19-targeting CAR T cell, approved in 2017). CARs are synthetic receptors composed of an antibody-like extracellular domain fused to a transmembrane domain and T cell activation and costimulatory domains. CAR expression endows T cells with specificity to a target antigen in a major histocompatibility complex (MHC)–unrestricted fashion, effectively initiating cytotoxicity, cytokine production, proliferation, and, in some cases, long-term memory formation (*2*). First-generation CARs had a single intracellular domain, composed of the CD3ζ chain or other signaling domains such as Fcγ; however, early trials showed that such CAR T cells had limited clinical impact (*6*), attributed to relatively short persistence or engraftment of the modified cells. Second-generation CARs included a costimulatory signaling domain derived from either CD28 or 4-1BB, and these CAR T cells directed to the CD19 antigen were shown to be effective in early trials in patients with B cell lymphomas and leukemias (*7*).

Over the ensuing decade, the clinical development of CAR T cells targeting CD19 progressed rapidly, with FDA approvals based on single-arm phase 2 clinical trials in different types of B cell malignancies using four different CD19-directed CAR T cell products (*7*). Tantalizingly, all these CD19-directed CAR T cell products result in durable remissions ("cures") in ~40% of patients with refractory or relapsed disease (*1*), and recent studies evaluating them in earlier lines of therapy have shown promise compared to standard high-dose chemotherapy. In addition, two CAR T cell products targeting the B cell maturation antigen (BCMA) have been tested and approved in multiple myeloma (*8*, *9*). Both of these BCMA-directed CAR T cell therapies resulted in high response rates in patients who progressed after multiple prior lines of therapy, though unlike in lymphoma, long-term "cures" have remained elusive.

In parallel to the development of CAR T cells, ICTs based on T cells transduced with transgenic T cell receptors (TCR T cells) have been pursued. TCR-T are generated by the identification of native or engineered TCRs that recognize peptides presented in the cleft of MHC molecules. Thus, in contrast to CAR T cells, TCR T cells can recognize peptides derived from mutated or overexpressed intracellular proteins, widening the space of potential antigen targets. TCR-T trials are at an early stage, but promising objective response rates have been seen with TCRs targeting tumor-associated antigens in melanoma and HPV antigens in HPV^+ epithelial cancers (*10*, *11*). CAR– and TCR–T cell therapies have complementary strengths and weaknesses—TCR T cells appear to have a lower prevalence of systemic toxicity (e.g., cytokine release syndrome) (*12*), and TCRs have high sensitivity, with the capacity to recognize a single ligand on a target cell (*13*). However, TCRs are restricted by requiring a specific MHC molecule that must be matched with the patient's MHC repertoire, limiting the number of patients that can be treated with any individual TCR product. Whether CAR– or TCR–T cell approaches will be more effective in addressing solid tumors remains to be determined.

T cell therapies have also entered clinical testing for diseases beyond cancer, though many of these studies are in very early stages. Preclinical studies indicated that the B cell

A

APPROACHES	EXAMPLE FUNCTIONS	MAJOR ATTRIBUTES
Receptor engineering	Logic Switch	Safety Specificity
Genome engineering	Knockout Knockin	Efficacy Consistency
Payload coengineering	Deliver therapeutic proteins	Efficacy

B

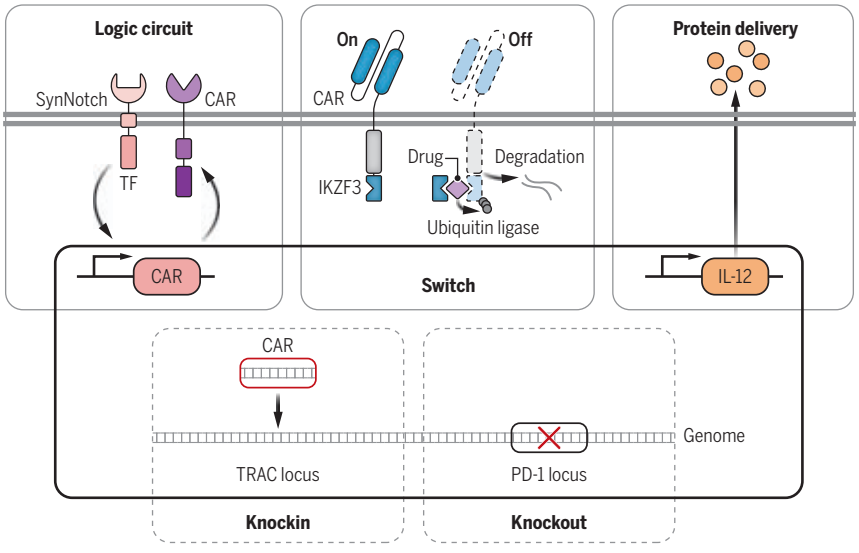

Fig. 1. Ex vivo immune cell engineering. (**A**) Major ex vivo immune cell engineering approaches and their key attributes. (**B**) Example systems of various engineering approaches. Logic circuit: Synthetic notch (SynNotch) receptor is composed of an extracellular binding domain, a notch core transmembrane domain, and a transcription factor (TF). The binding of the extracellular binding domain to a target antigen on another cell leads to the cleavage of the TF, which subsequently induces the expression of a CAR. The CAR is designed to bind to another antigen on the same target cell, forming an IF-THEN AND logic. Switch: A lenalidomide regulatable CAR is composed of a conventional CAR fused to a degron IKZF3. The binding of IKZF3 to lenalidomide recruits the endogenous ubiquitin ligase, leading to CAR degradation. Therapeutic protein delivery: Immune cells can be engineered to locally produce and secrete therapeutic proteins. Knockin: The specific integration of the CAR sequence into the T cell receptor α constant (TRAC) locus enables more uniformed CAR expression and better CAR T cell efficacy. Knockout: PD-1 is an inhibitory receptor that can limit immune cell therapy efficacy. PD-1 knockout can potentially lead to more potent immune cell therapy.

aplasia induced by CD19-targeting CARs could effectively treat murine models of B cell–mediated autoimmune disease (*14*), and an exploratory study that treated a patient with treatment-refractory lupus with a CD19 CAR T cell product led to a rapid drop in systemic autoantibody levels and disease remission (*15*). As an alternative approach to addressing autoimmunity, CARs created by replacing the antibody domain with an autoantigen enabled engineered T cells to eliminate autoreactive B cells in models of the skin disease pemphigus vulgaris (*16*); a phase 1 trial of this concept in patients is currently underway. Engineered regulatory T cells (T_{regs}) are also being developed for treatment of autoimmunity, transplant tolerance, and graft-versus-host disease (*3*). Examples include ongoing clinical trials of T_{regs} expressing a CAR in which the antibody domain is replaced by the class I MHC molecule human leukocyte antigen HLA-A2, with the goal of suppressing rejection of HLA-A2$^+$ kidney and liver transplants (*17*). Further cell engineering to stabilize the T_{reg} phenotype may be important for these approaches. In infectious disease, CARs generated with an HIV-1 broadly neutralizing antibody as the binding domain were recently tested in HIV$^+$ subjects and were shown to be safe, delayed viral rebound up to 10 weeks following temporary suspension of antiretroviral therapy, and temporarily reduced the viral reservoir (*18*). Further refinements of this therapy may provide an approach toward a functional cure of HIV.

Therapies based on other immune cells are also now entering clinical testing. In a first phase 1 trial, MHC-mismatched NK cells transduced with an anti-CD19 CAR, interleukin-15 (IL-15; a key cytokine to maintain NK cell survival in vivo), and a suicide gene (enabling deletion of the cells by a small-molecule drug in case of safety issues) were administered to 11 lymphoma and leukemia patients, leading to eight objective responses and seven complete remissions (*19*). Because these cells were prepared from third-party cord blood, these findings are a promising step toward an "off the shelf" ICT. Macrophages transduced with a CAR were recently demonstrated to phagocytose tumor cells and remodel the tumor microenvironment, polarizing bystander macrophages to an antitumor phenotype and recruiting T cells to treated tumors (*20*). A first-in-humans clinical trial of this concept is currently underway.

At the macro level, the field has grown substantially: There are now hundreds of companies developing new types of engineered T cells, using CARs, TCRs, and various new synthetic antigen receptors, and additional functionalities to enhance T cell functions. Currently, there are over 1000 clinical trials of just "CAR T cells" listed on clinicaltrials.gov. However, important biologic challenges have also been identified. Fundamentally, discovery and testing of tumor-specific targetable antigens remains a notable barrier, which may not be completely overcome by engineering strategies. Even in leukemias and lymphomas initially susceptible to CAR T cell treatment, loss or down-regulation of antigens targeted by the CAR T cells can lead to relapse. Beyond hematologic malignancies, small clinical studies have reported complete responses in patients with carcinomas (*11*) or brain cancers (*21*) treated with TCR- or CAR-engineered T cells, but, in general, responses to ICT in common solid tumors have been poor. Several barriers have been identified (Fig. 2), including inefficient tumor infiltration, heterogeneity of antigen expression, poor functional persistence or exhaustion of cells, and diverse mechanisms of immunosuppression including metabolic inhibitors (adenosine), checkpoint molecules (PD-L1), suppressive cytokines such as transforming growth factor–β (TGF-β) or IL-10, and various suppressive cell types (cancer-associated fibroblasts, myeloid-derived suppressor cells, and regulatory T cells) (*4*, *5*). Toxicity of immune cell therapies is a particular concern, especially with efforts to engineer amplified immune cell effector functions (*22*). Finally, although autologous T cells have a clear biological advantage in terms of safety and potential for long-term engraftment, there is considerable interest in developing a more "drug-like" model, using off-the-shelf, allogeneic immune cells to enable greater control of the input cell product, faster delivery to patients, and reduced cost of manufacturing. Ongoing efforts in ex vivo and in vivo cell engineering are underway to address each of

ILLUSTRATION: A. MASTIN/*SCIENCE*

these challenges. Here we highlight key examples of progress and challenges in the field.

Ex vivo cell engineering

Inspired by the complexity of biological networks, sophisticated engineered immune cells capable of sensing and logically responding to diverse stimuli with enhanced efficacy have been developed. From the clinical perspective, therapeutic immune cells are primarily designed with three main objectives: to improve (i) target specificity, (ii) efficacy, and (iii) safety. Regulatory, manufacturing, and commercial (e.g., cost) challenges are also beginning to influence cell therapies. From the ex vivo engineering standpoint, the clinical cell design objectives are typically achieved through three genetic and molecular engineering approaches, such as (i) receptor engineering, (ii) host cell genome engineering, and (iii) therapeutic payload coengineering (Fig. 1, A and B). These design objectives, which typically lead to a larger DNA footprint (more than the DNA size limit of a lentiviral vector, ~6 to 7 kilo–base pairs), demand innovation in gene delivery and manufacturing to ensure their successful clinical translation.

Antigen receptor engineering

Immune cell surface receptors are tolerant to many types of modifications and protein engineering, which has enabled design of receptor circuits with new sense-and-respond phenotypes to improve targeting specificity and safety or address antigen escape (*23*). One of the most-studied receptors in immune cell therapy is the CAR, which has been engineered to fine-tune signaling, introduce remote controls, and implement logic computation circuits. CARs incorporate both TCR and costimulatory receptor signaling domains that control T cell proliferation, effector function, and metabolic fitness (*24*, *25*); genetic screens are being pursued to identify optimal signaling domains for these synthetic receptors (*26*). Logic CAR circuits, in particular, underscore the engineering potential of CARs: The identity of target cells (e.g., cancer cells) is best classified by multiple antigens, and T cell therapies targeting a single marker have resulted in fatalities when the targeted antigen is also expressed by healthy tissues (*27*). Receptors that can sense multiple antigens and perform combinatorial logic operations can effectively discriminate between healthy and cancer cells, thus minimizing "on-target/off-tumor" effects (*28*). Such logic circuits can also be combined with receptors that sense factors in the tissue microenvironment rather than cell surface antigens, to aid in "decoding" tissue location of the engineered cell (*29*). Currently, three receptor platforms have demonstrated up to three input logic operations (*23*). These complex logic operations are very difficult, if not impossible, to achieve with other therapeutic modalities, such as small molecules or engineered proteins, thus highlighting the potential that cell therapy has to offer.

As stated above, an advantage of CARs over TCRs is their ability to target any surface antigen independent of patients' MHC haplotype. However, compared to TCRs, CARs tend to have a lower antigen sensitivity. In an effort to marry the strengths of CARs and TCRs, recently hybrid receptor designs have been described. TruCs (T cell receptor fusion constructs) link antibody domains to different components of the TCR complex and showed a similar antigen sensitivity to that of CARs while lowering inflammatory cytokine production (*30*). STARs [synthetic TCR and antigen receptors (*31*)] and HITs [HLA-independent TCRs (*32*)] are synthetic receptors with antibody binding domains fused to the native TCR receptor constant regions. These new receptors have shown pronounced in vivo activity and antigen sensitivity.

Although many new antigen receptor and advanced logic receptors are still undergoing preclinical testing, CARs designed to mitigate relapse owing to antigen escape have already been evaluated in initial clinical trials. These studies showed that OR gate CARs (CARs that can be triggered by binding to one of two different target antigens) were safe, but relapses were still observed in a proportion of patients owing to poor CAR T cell persistence or unequal potency of the two CARs employed (*33*–*35*). Some AND-gate CAR systems (CARs that are only activated when two different target antigens are engaged simultaneously) have demonstrated high specificity in multiple preclinical tumor models (*36*), and these systems are primed for testing in clinical trials. Several companies have also demonstrated promising preclinical results with NIMPLY CAR circuits (CARs activated by the presence of one or more antigens in the absence of a third antigen) and are preparing for trials against solid and blood tumors.

Therapeutic payload coengineering

In addition to expressing an antigen-specific receptor, engineering immune cells to express therapeutic payloads provides an additional dimension for modulating cell function. When combined with CAR expression, they are sometimes referred to as "armored" CARs or TRUCKs (T cells redirected toward universal cytokine killing) (*37*). Some of the most promising therapeutic payloads are secreted factors such as cytokines (e.g., IL-12, IL-15), therapeutic antibodies (e.g., anti-PD-L1), or enzymes that can remodel the tumor microenvironment or activate prodrugs (*37*, *38*). As such, ICTs can also serve as a living drug delivery device. Examples include NK cells engineered to express IL-15, a critical cytokine for NK cell survival (*19*), and myeloid cells transduced to express IL-12, which can counter the immunosuppressive gene signature found in solid tumors (*39*). Though potent, many of these factors have substantial side effects that require careful regulation for safe deployment. One approach

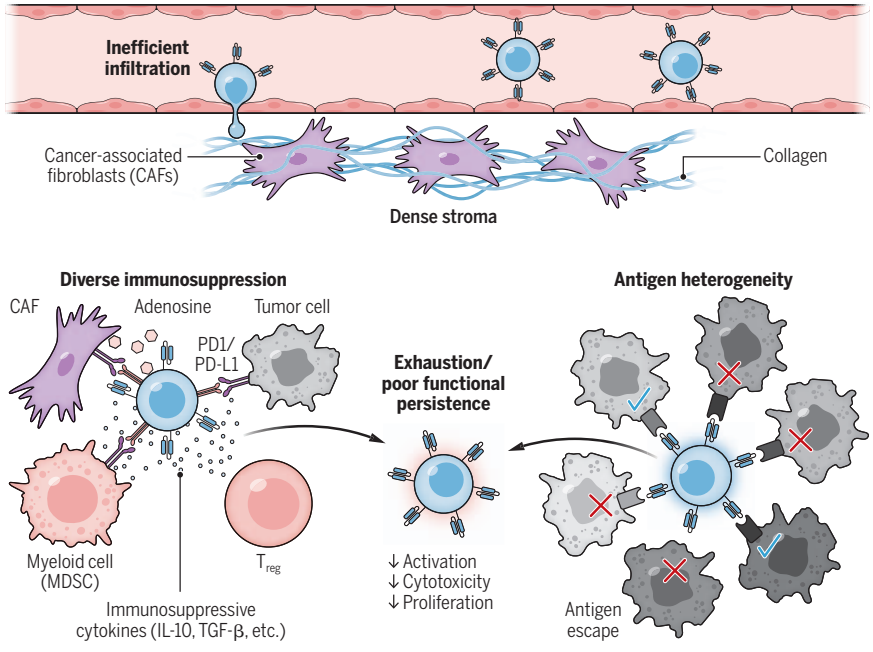

Fig. 2. Barriers to the effectiveness of engineered T cells in solid tumors. Several barriers to eradication of solid tumors by immune cell therapies have been identified, including inefficient migration of T cells from the blood to reach viable tumor cells (limited in some cases by dense tumor extracellular matrix), many mechanisms of tumor-induced immune suppression, loss of T cell function due to persistent engagement with antigen (exhaustion), and tumor escape due to antigenic heterogeneity.

ILLUSTRATION: A. MASTIN/*SCIENCE*

is to engineer soluble factors such as cytokines to be expressed on the plasma membrane, to restrict their dissemination and focus signaling on the donor cell (*40*). Another strategy is to design inducible gene switches to tune the strength and timing of accessory payload production. Many mammalian gene switches have been developed, but most are incompatible with ICTs because they either are derived from nonhuman origins, have a large DNA footprint, or use inducers that are not clinically approved or have poor or undefined pharmacokinetic properties; a promising exception is a lenalidomide-based switch (*41*). A flexible platform, such as those based on human zinc-finger proteins (*42*) and using clinically approved drug inducers, could help to optimize immune cell therapy.

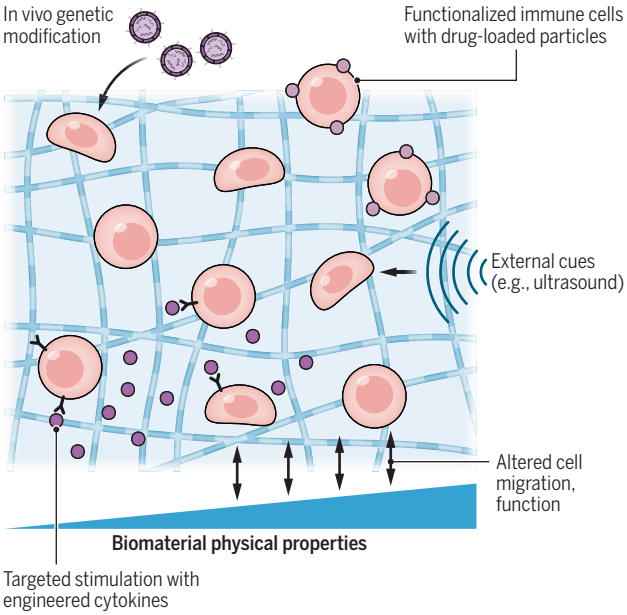

Fig. 3. In vivo immune cell engineering approaches. Cell transfer can be aided by biomaterial delivery vehicles that localize immune cells to specific anatomic sites and provide biochemical cues (e.g., cytokines) or mechanical properties that promote desirable cell phenotypes. Transferred cells can also be manipulated through externally applied signals such as ultrasound or magnetic fields. Alternatively, host or transferred immune cells may be genetically altered in situ, through viral or nonviral strategies, bypassing ex vivo cell manipulation and transfer.

Genome engineering

Beyond expression of tumor-specific receptors and immunomodulatory factors, recent work has demonstrated the potential of engineering the immune cell genome to enhance cell therapy safety and efficacy. Several genes, such as checkpoint receptors (e.g., PD-1), are known to inhibit ICTs. Furthermore, the TCR and MHC from donor cells can cause graft-versus-host disease or rejection if the immune cell source is allogenic. Genetic disruption of these genes in immune cells has enhanced their ability to combat tumors and prevent immunogenicity related to the use of allogeneic cell sources in preclinical models. Moreover, many knockout screens have been performed on immune cells to identify genes (*43*), such as RASA2 RAS guanosine triphosphatase–activating protein (*44*), or RNA helicase Dhx37 (*45*), which, when deleted, promote T cell persistence and activity against cancer. We are now waiting to see which of these genetic perturbations have the most impact in the clinic.

Currently, genetic modification of immune cells for clinical application utilizes engineered viruses, which randomly integrate payload DNA into the genome of donor cells, presenting the possibility of causing unregulated cell growth and cancer. Targeted integration at defined genomic locations is an attractive alternative approach to ensure the generation of safe and consistent ICTs. Furthermore, genome editing enzymes such as CRISPR-Cas can be introduced by electroporation as a ribonucleoprotein (RNP) complex with high efficiency, removing the possibility that the genome editing enzyme will persist for a long duration. Moreover, integrating CARs directly into the native genetic locus of the TCR complex can improve CAR T cells' efficacy, probably because of the more favorable expression dynamics afforded by the TCR promoter (*46*). In a recent clinical trial with eight patients, T cells with a CD19 CAR integrated into the PD-1 locus using CRISPR-Cas have demonstrated an 87% complete remission rate with mild CRS in some patients and no immune effector cell–associated neurotoxicity syndrome (*47*). This result underscores the potential of using CRISPR-Cas to manufacture CAR T cell products with precise genome placement of the cargo DNA.

One of the major limitations in targeted integration is the need to deliver a sequence template prescribing the insertion site. The most efficient approach to deliver such DNA is by using adeno-associated virus (AAV). However, AAV is expensive and complicated to manufacture. Codelivery of double-stranded DNA templates with the CRISPR-Cas RNP is toxic to primary cells. Recently, a method using single-stranded DNA achieved 62% knock-in efficiency with a high yield (more than a billion cells) (*48*). Although these new genome editing technologies can provide precise manipulation of the immune cell genome, they can have off-target effects or exhibit errors in genome rearrangement; more research is needed to precisely determine the risk of these editing errors.

Immune cell manufacturing

Challenges in immune cell therapy manufacturing are well documented (*49*), which has hampered their clinical and commercial potential. Beyond the logistics around implementation, such as maintenance of chain of custody, one of the biggest challenges in ICT production is the use of viral transduction to deliver DNA payloads, a complex process with a high failure rate. To overcome this challenge, nonviral approaches to gene delivery in primary human immune cells, such as mRNA transfection or transposon-based genome engineering tools, are being developed (*47*, *50*). Cell source variability is another challenge, especially when using patient-derived cells. The medical history or the stage of the patient's disease can result in T cell dysfunction and alter immune cell composition, leading to suboptimal T cell products during the manufacturing process (*51*). Many resources have been devoted to developing allogeneic "off-the-shelf" cell products, either through alternative cell types (e.g., NK cells, iPSC–derived immune cells) or via genome editing tools to disrupt proteins that lead to allogeneic rejection (e.g., β_2 microglobulin) and graft-versus-host disease (e.g., endogenous TCRs) (*37*). However, these approaches have their own particular sets of challenges. For instance, NK cells are less amenable to viral transduction than T cells, and the regulatory issues related to genome editing specificity have yet to be resolved.

In vivo cell engineering

Upon adoptive transfer, engineered immune cells face a number of challenges in finding and destroying their target, including surviving for a sufficient time frame, homing to the appropriate anatomic site and engaging the target cell, and maintaining an appropriate phenotype to allow cancer clearance. Both passive and active barriers in the host are responsible for these challenges, and a variety of technologies are under development to overcome and enable efficient and safe immune cell therapy. These technologies include materials used to place transferred immune cells at the desired site, targeting of transferred cells by externally controlled cues, and direct genetic manipulation in the body (Fig. 3).

Targeted stimulation of transferred cells

Achieving an appropriate balance of therapeutic efficacy and safety is increasingly being pursued with strategies providing targeted, in vivo stimulation of the transferred cells. These approaches often involve pharmacologic manipulation to allow remote, temporal control over transcriptional activity, or alterations of

ILLUSTRATION: A. MASTIN/*SCIENCE*

the cells' microenvironment to achieve greater spatial control over the activity of transferred and host immune cells. For example, the favorable bioavailability and pharmacokinetics of FDA-approved small-molecule drugs are being exploited to control genetic on/off switches with rapid, reversible dynamics to tune the functionality of engineered T cells. This allows (for example) tight control over the activity of CAR T cell therapy while reducing exhaustion in preclinical studies and also provides a safety switch allowing cell activity to be turned off at toxicity onset (*52*). Activating factors such as cytokines and costimulatory ligands play a critical role in the function of immune cells, but systemic delivery of these potent, pleiotropic molecules often results in side effects, which has motivated several strategies to deliver these cues in a controlled manner to ICTs. For example, cytokines are being packaged into nanoparticles and microparticles that can be adhered to immune cells before transfer, or targeted to immune cells in vivo by metabolic labeling, to enable cytokine activity to be localized to the desired therapeutic site with minimal systemic exposure (*53*, *54*). Cytokine receptors have also been engineered to allow donor T cells (but not native endogenous cells) to respond specifically to engineered cytokine drugs administered in tandem, or to engineer distinctive intracellular signals in response to cytokine stimulation (*55*). Engineered T cells can also be stimulated specifically with vaccines that activate their synthetic antigen receptor, promoting cell expansion, survival, and effector functions (*56*, *57*). Extracellular vesicles, lipid bilayer–enclosed particles derived from cells, provide a potent intracellular communication pathway and are also being engineered to elicit specific immune responses (*58*). The physical microenvironment of transferred cells is also being manipulated to alter their activity: For example, CAR T cells engineered to be heat sensitive can be stimulated with local temperature increases mediated by external cues applied to the tumor (*59*, *60*). It is also becoming increasingly clear that the mechanical properties of tumors (e.g., stiffness) can be a barrier to immune cell and therapeutic transport and function; thus, modulation of mechanosensing provides a means to alter immune cell activity in vivo (*61*).

Engineered systems to modulate immune cells

Biomaterial strategies provide another opportunity to enhance ICT efficacy, manipulate immune cells directly in the body, and/or synergize host immunity and adoptive cell therapy. Biomaterials can protect molecular and cellular cargoes in harsh environments, localize therapies to a desired anatomic location, and control the trafficking and activation of host cells. The poor solid tumor localization of transferred T cells and exhaustion of tumor-resident T cells have motivated the fabrication of biomaterial carriers that provide continuous stimulation (e.g., TCR stimulation, cytokines) to cargo T cells after transplantation, allowing their direct placement in the vicinity of tumors and maintaining desirable phenotypes (*62*). Antigen-presenting cells (APCs) have also been engineered, using biomaterial scaffolds designed to accumulate large numbers of APCs in situ, load them with sustainably released antigen, and stimulate their migration to draining lymph nodes by activation with codelivered adjuvants (*63*). A wide array of nanoparticles have also been developed to traffic antigen and adjuvant directly to lymph nodes, demonstrating robust, specific immune responses (*64*).

Direct gene modification in vivo

Engineering cells in culture before transfer is expensive, is complex, and requires considerable time, motivating approaches to genetically modify host cells in situ to bypass ex vivo manipulation (*65*). CAR-encoding retroviral particles have been incorporated into implantable scaffolds used to transfer human immune cells, leading to CAR T cell generation in vivo (*66*). Bypassing any ex vivo cell manipulation, lentiviruses and polymer nanoparticles are being developed to specifically target T cells, and single infusions have demonstrated the ability to transduce sufficient host cell numbers to generate effective CAR T cell responses in humanized mouse cancer models (*65*). In vivo transduction of T cells and other immune cells is now an intensive area of research and may be critical for the long-term success of cell therapy.

Conclusions and future outlook

The science and technology of engineering immune cells for therapeutic purposes has made great progress, but there remains an enormous space for exploration to find safer and more effective immune cell–based treatments. In addition, new ways of applying ICTs to treat disease are being discovered, such as the use of CAR T cells to block fibrosis during heart failure (*67*). Notably, human trials of immune cell therapies are providing important insights into the function of the immune system in health and disease, leading to discoveries such as the identification of genes that regulate lymphocyte survival and function (*68*).

Two critical challenges facing the long-term utility of immune cell therapies in medicine include their cost and complexity of manufacture. In some settings, successful development of injectable drug alternatives [e.g., use of bispecific T cell engager proteins for treatment of hematologic malignancies (*69*)] may eventually supplant the use of ICTs if shown to be equivalently effective. However, the ability of immune cells to be chemically and/or genetically engineered with multiple environment-responsive, controllable functions not present in native cells gives ICTs the potential to enact changes in the disease microenvironment that cannot be achieved by traditional therapeutics. There are ongoing clinical and regulatory efforts to explore decentralized, faster, and automated manufacturing to increase efficiency and reduce costs (*70*). In addition, intensive efforts focused on engineering ICTs directly in vivo or to use engineered "off the shelf" third-party cell sources may eliminate some or all of the practical issues surrounding cell therapy.

To enable engineered immune cell therapies to reach their full potential, a diverse scientific effort is needed. Exciting progress is currently being made through collaborative efforts cutting across immunology, oncology, synthetic biology, and molecular biology. Combination therapies employing the expertise of protein, chemical, materials, and biological engineers may open new ways to enhance immune cell therapies that cannot be achieved by genetic engineering alone. As data from human trials continues to expand, there is also scope for a substantial impact of computational modeling to make predictions of key parameters to be optimized in cell therapy and machine learning–based data analysis. Finally, the intersection of ICTs with the larger systems biology of the immune system must be accounted for—interactions of cell therapies with the endogenous immune system, the nervous system (*71*), and the role of the microbiome (*72*) in cell therapy outcomes are areas that may hold important new discoveries.

REFERENCES AND NOTES

1. E. W. Weber, M. V. Maus, C. L. Mackall, *Cell* **181**, 46–62 (2020).
2. M. V. Maus, C. H. June, *Clin. Cancer Res.* **22**, 1875–1884 (2016).
3. C. Raffin, L. T. Vo, J. A. Bluestone, *Nat. Rev. Immunol.* **20**, 158–172 (2020).
4. M. Sadelain, I. Rivière, S. Riddell, *Nature* **545**, 423–431 (2017).
5. A. V. Finck, T. Blanchard, C. P. Roselle, G. Golinelli, C. H. June, *Nat. Med.* **28**, 678–689 (2022).
6. M. H. Kershaw *et al.*, *Clin. Cancer Res.* **12**, 6106–6115 (2006).
7. C. H. June, M. Sadelain, *N. Engl. J. Med.* **379**, 64–73 (2018).
8. N. C. Munshi *et al.*, *N. Engl. J. Med.* **384**, 705–716 (2021).
9. J. G. Berdeja *et al.*, *Lancet* **398**, 314–324 (2021).
10. Y.-C. Lu *et al.*, *J. Clin. Oncol.* **35**, 3322–3329 (2017).
11. N. B. Nagarsheth *et al.*, *Nat. Med.* **27**, 419–425 (2021).
12. E. A. Stadtmauer *et al.*, *Blood Adv.* **3**, 2022–2034 (2019).
13. D. J. Irvine, M. A. Purbhoo, M. Krogsgaard, M. M. Davis, *Nature* **419**, 845–849 (2002).
14. R. Kansal *et al.*, *Sci. Transl. Med.* **11**, eaav1648 (2019).
15. D. Mougiakakos *et al.*, *N. Engl. J. Med.* **385**, 567–569 (2021).
16. C. T. Ellebrecht *et al.*, *Science* **353**, 179–184 (2016).
17. K. Schreeb *et al.*, *Kidney Int. Rep.* **7**, 1258–1267 (2022).
18. B. Liu *et al.*, *J. Clin. Invest.* **131**, (2021).
19. E. Liu *et al.*, *N. Engl. J. Med.* **382**, 545–553 (2020).
20. M. Klichinsky *et al.*, *Nat. Biotechnol.* **38**, 947–953 (2020).
21. C. E. Brown *et al.*, *N. Engl. J. Med.* **375**, 2561–2569 (2016).
22. E. C. Morris, S. S. Neelapu, T. Giavridis, M. Sadelain, *Nat. Rev. Immunol.* **22**, 85–96 (2021).
23. J. Manhas, H. I. Edelstein, J. N. Leonard, L. Morsut, *Nat. Chem. Biol.* **18**, 244–255 (2022).
24. K. Hirabayashi *et al.*, *Nat. Cancer* **2**, 904–918 (2021).
25. O. U. Kawalekar *et al.*, *Immunity* **44**, 380–390 (2016).
26. K. S. Gordon *et al.*, *Nat. Biomed. Eng.* **6**, 855–866 (2022).
27. R. A. Morgan *et al.*, *Mol. Ther.* **18**, 843–851 (2010).
28. R. Dannenfelser *et al.*, *Cell Syst.* **11**, 215–228.e5 (2020).
29. Z. L. Chang *et al.*, *Nat. Chem. Biol.* **14**, 317–324 (2018).
30. P. A. Baeuerle *et al.*, *Nat. Commun.* **10**, 2087 (2019).
31. Y. Liu *et al.*, *Sci. Transl. Med.* **13**, eabb5191 (2021).
32. J. Mansilla-Soto *et al.*, *Nat. Med.* **28**, 345–352 (2022).
33. J. Y. Spiegel *et al.*, *Nat. Med.* **27**, 1419–1431 (2021).
34. S. Cordoba *et al.*, *Nat. Med.* **27**, 1797–1805 (2021).
35. N. N. Shah *et al.*, *Nat. Med.* **26**, 1569–1575 (2020).
36. A. Hyrenius-Wittsten *et al.*, *Sci. Transl. Med.* **13**, eabd8836 (2021).

37. S. Rafiq, C. S. Hackett, R. J. Brentjens, *Nat. Rev. Clin. Oncol.* **17**, 147–167 (2020).
38. T. J. Gardner *et al.*, *Nat. Chem. Biol.* **18**, 216–225 (2022).
39. S. Kaczanowska *et al.*, *Cell* **184**, 2033–2052.e21 (2021).
40. L. V. Hurton *et al.*, *Proc. Natl. Acad. Sci. U.S.A.* **113**, E7788–E7797 (2016).
41. M. Jan *et al.*, *Sci. Transl. Med.* **13**, eabb6295 (2021).
42. M. L. Maeder *et al.*, *Mol. Cell* **31**, 294–301 (2008).
43. M. W. LaFleur, A. H. Sharpe, *Annu. Rev. Cancer Biol.* **6**, 103–122 (2022).
44. J. Carnevale *et al.*, *Nature* **609**, 174–182 (2022).
45. M. B. Dong *et al.*, *Cell* **178**, 1189–1204.e23 (2019).
46. J. Eyquem *et al.*, *Nature* **543**, 113–117 (2017).
47. J. Zhang *et al.*, *Nature* **609**, 369–374 (2022).
48. B. R. Shy *et al.*, *Nat. Biotechnol.*, 10.1038/s41587-022-01418-8 (2022).
49. P. Vormittag, R. Gunn, S. Ghorashian, F. S. Veraitch, *Curr. Opin. Biotechnol.* **53**, 164–181 (2018).
50. A. Moretti *et al.*, *Front. Immunol.* **13**, 867013 (2022).
51. J. A. Fraietta *et al.*, *Nat. Med.* **24**, 563–571 (2018).
52. L. Labanieh *et al.*, *Cell* **185**, 1745–1763.e22 (2022).
53. C. W. Shields 4th, L. L. Wang, M. A. Evans, S. Mitragotri, *Adv. Mater.* **32**, e1901633 (2020).
54. H. Wang *et al.*, *Nat. Mater.* **19**, 1244–1252 (2020).
55. A. Kalbasi *et al.*, *Nature* **607**, 360–365 (2022).
56. K. Reinhard *et al.*, *Science* **367**, 446–453 (2020).
57. L. Ma *et al.*, *Science* **365**, 162–168 (2019).
58. E. I. Buzas, *Nat. Rev. Immunol.* 10.1038/s41577-022-00763-8 (2022).
59. Y. Wu *et al.*, *Nat. Biomed. Eng.* **5**, 1336–1347 (2021).
60. I. C. Miller *et al.*, *Nat. Biomed. Eng.* **5**, 1348–1359 (2021).
61. H. Du *et al.*, *Nat. Rev. Immunol.*, 10.1038/s41577-022-00761-w (2022).
62. M. E. Coon, S. B. Stephan, V. Gupta, C. P. Kealey, M. T. Stephan, *Nat. Biomed. Eng.* **4**, 195–206 (2020).
63. H. Wang, D. J. Mooney, *Nat. Mater.* **17**, 761–772 (2018).
64. D. J. Irvine, E. L. Dane, *Nat. Rev. Immunol.* **20**, 321–334 (2020).
65. N. N. Parayath, M. T. Stephan, *Annu. Rev. Biomed. Eng.* **23**, 385–405 (2021).
66. P. Agarwalla *et al.*, *Nat. Biotechnol.* **40**, 1250–1258 (2022).
67. J. G. Rurik *et al.*, *Science* **375**, 91–96 (2022).
68. J. A. Fraietta *et al.*, *Nature* **558**, 307–312 (2018).
69. M.-E. Goebeler, R. C. Bargou, *Nat. Rev. Clin. Oncol.* **17**, 418–434 (2020).
70. P. Marks, S. Gottlieb, *N. Engl. J. Med.* **378**, 954–959 (2018).
71. M. Schiller, T. L. Ben-Shaanan, A. Rolls, *Nat. Rev. Immunol.* **21**, 20–36 (2021).
72. D. A. Schupack, R. A. T. Mars, D. H. Voelker, J. P. Abeykoon, P. C. Kashyap, *Nat. Rev. Gastroenterol. Hepatol.* **19**, 7–25 (2022).

ACKNOWLEDGMENTS

Funding: This work was supported by the NIH (awards CA247632 and CA235375 to D.J.I.; 5U54CA244726 and 5R01CA223255 to D.J.M.; U01CA265713, R01EB029483, R01DK132576, and R01EB031904 to W.W.W.), the Marble Center for Nanomedicine (to D.J.I.), the Mark Foundation (to D.J.I.), the Wyss Institute of Harvard (to D.J.M.), and the Ragon Institute of MGH, MIT, and Harvard (to D.J.I.). D.J.I. is an investigator of the Howard Hughes Medical Institute. **Competing interests:** D.J.I. is a consultant and holds equity in Elicio Therapeutics, Repertoire Immune Medicines, Ankyra Therapeutics, Strand Therapeutics, Window Therapeutics, Venn Therapeutics, Alloy Therapeutics, SQZ Biotechnologies, Jupiter Therapeutics, Surge Therapeutics, and Gensaic Therapeutics. D.J.I. is a consultant for Third Rock Ventures and Senda Biosciences. D.J.I. is an inventor on patents licensed to Elicio Therapeutics, Strand Therapeutics, Ankyra Therapeutics, and Repertoire Immune Medicines. M.V.M. is an inventor on patents related to adoptive cell therapies, held by Massachusetts General Hospital (some licensed to Promab) and University of Pennsylvania (some licensed to Novartis). M.V.M. has grant and research support front Kite Pharma and Novartis. M.V.M. serves on the board of directors of 2Seventy Bio and holds equity in 2SeventyBio, Century Therapeutics, Neximmune, Oncternal, and TCR2 and has served as a consultant for multiple companies involved in cell therapies. D.J.M. holds equity in Lyell, Attivare, IVIVA Medical, Limax, and Lightning Bio and consults for Johnson & Johnson, IVIVA medical, Medicenna, and Boston Scientific. D.J.M. is an inventor on patents licensed to Novartis, Lyell, Attivare, Limax, Epoulosis, Amend Surgical, and Sirenex. W.W.W. holds equity and consults for Senti Biosciences and 4Immune. W.W.W. is an inventor on patents licensed to Senti Biosciences and 4Immune.

Submitted 2 August 2022; accepted 10 October 2022
10.1126/science.abq6990

REVIEW

Engineering bacteria as interactive cancer therapies

Candice R. Gurbatri[1], Nicholas Arpaia[2,3], Tal Danino[1,3,4]*

With increasing evidence that microbes colonize tumors, synthetic biology tools are being leveraged to repurpose bacteria as tumor-specific delivery systems. These engineered systems can modulate the tumor microenvironment using a combination of their inherent immunogenicity and local payload production. Here, we review genetic circuits that enhance spatial and temporal control of therapeutic bacteria to improve their safety and efficacy. We describe the engineering of interactions among bacteria, tumor cells, and immune cells, and the progression from bacteria as single agents toward their rational combination with other modalities. Together, these efforts are building toward an emerging concept of engineering interactions between programmable medicines using synthetic biology.

Bacteria were first identified as potential cancer treatments in the 19th century, with evidence of tumor regressions observed in patients injected with *Streptococcus pyogenes* and *Serratia marcescens* (*1*). Although it was not known at the time, bacteria are immunostimulatory, directing an immune response toward tumors, and can also preferentially grow in hypoxic and immunosuppressive tumor microenvironments (TMEs). Several genera, such as *Salmonella*, *Escherichia*, *Clostridium*, *Bifidobacterium*, *Proteus*, and *Lactobacillus*, have demonstrated these characteristics, suggesting their utility as tumor-targeting vehicles (*2*, *3*).

Bacteria can be genetically engineered to encode and locally deliver several classes of payloads that might otherwise be toxic if administered systemically, including small molecules, toxins, immunomodulators, pro-drug–converting enzymes, small interfering RNAs, and nanobodies (*3*). These released agents provide a way for bacteria to influence tumor, immune, stromal, microbial, and other cell types within the TME. Furthermore, bacteria and their payloads can interface with external imaging modalities such as magnetic resonance imaging (MRI) and focused ultrasound (FUS) to enable bacterial detection and actuation.

Synthetic biology enables the precise tuning of these bacterial interactions with other cells and technologies to enhance the therapeutic efficacy and safety of bacteria cancer therapy. The development of sense-and-respond genetic circuitry can autonomously control bacterial behavior to regulate where and when they grow and release their payloads (*4*). In this Review, we highlight the progress in engineering *Salmonella typhimurium* and *Escherichia coli* model systems and explore how synthetic gene circuits enable bacteria to more effectively interact with other living and nonliving modalities.

[1]Department of Biomedical Engineering, Columbia University, New York, NY 10027, USA. [2]Department of Microbiology & Immunology, Vagelos College of Physicians and Surgeons of Columbia University, New York, NY 10032, USA. [3]Herbert Irving Comprehensive Cancer Center, Columbia University, New York, NY 10027, USA. [4]Data Science Institute, Columbia University, New York, NY 10027, USA.
*Corresponding author. Email: tal.danino@columbia.edu

Engineering the bacteria-tumor interface

Tumor localization

Because of tumor characteristics such as hypoxia and low immune surveillance, administered bacteria can accumulate ~10,000-fold in tumors relative to other tissues. However, some strains can survive or grow in healthy organs, prompting the need for genetic attenuations to reduce inherent virulence and endotoxicity. A notable example is the attenuated *S. typhimurium* VNP20009 strain, which includes chromosomal deletions of *purI* and *msbB*, creating a purine auxotrophic strain and modified lipopolysaccharide (LPS), respectively. Together, these attenuations reduced systemic inflammation, as measured by tumor necrosis factor (TNF-α), in mice (*6*). When clinically evaluated in metastatic melanoma patients, intravenously administered VNP20009 was generally well tolerated, but did not efficiently colonize tumors and provided no therapeutic benefit, demonstrating the challenge of achieving both safety and therapeutic efficacy (*7*).

Strategies to improve the tumor specificity of bacteria include mutagenesis and directed evolution, which select for auxotrophic bacteria that have increased relative growth within tumors or strain variants with increased adherence to cancer cells, respectively (*8*, *9*). Alternatively, bacteria can be engineered to display tumor-targeting moieties such as adhesion peptides and tumor-associated antigens on their membranes (*10*). For example, an attenuated *Salmonella* strain was engineered to display a tumor-homing arginine-glycine-aspartate (RGD) peptide by fusing the peptide to the bacterial outer membrane protein A (OmpA) (*11*). This peptide then bound to $\alpha_v\beta_3$ integrins, which are widely overexpressed on tumor cells, thus increasing the adherence of bacteria to tumor cells compared with healthy cells.

An alternative approach for improved tumor tropism is to leverage genetic circuits that couple bacterial growth to tumor hallmarks such as high concentrations of lactate, low

amounts of oxygen, and low pH. In these sensing circuits, the transcription of the essential gene(s) for bacterial growth is controlled by bacterial promoters responding to these environmental cues, thereby limiting bacterial growth to tumors (*12*). Because other tissues may contain one of these signals, combining the sensing circuits through "AND" logic gates further improves tumor specificity and reduces instances of bacterial mutational escape, enabling longer-term biocontainment (*13*).

Once inside the tumor, bacteria can locally deliver high concentrations of a multitude of payloads to specific locations appropriate for the therapeutic targets and type of molecules generated by the bacteria. For example, some small molecules reach their targets by passive diffusion or transport through microbial and mammalian membranes. Other payloads, such as nucleic acids, need to be delivered intracellularly into the cytoplasm or nucleus, and some proteins act on extracellular receptors and require localization to the extracellular space (Fig. 1, A to D).

Targeting the intracellular space

Intracellular delivery has been a long-standing challenge with many orthogonal methods such as virus and nanoparticle delivery platforms developed to access intracellular targets (*14*). As a living medicine, bacteria can demonstrate autonomous control, sensing and responding to the internalization process, and subsequently releasing cargo. Moreover, intracellular delivery is beneficial because it allows for the targeting of proteins and pathways that have been traditionally challenging to pursue.

Bacteria with intracellular life cycles, such as *S. typhimurium*, have been used to secrete an array of cargos, into tumor cells, using a type 3 secretion system (T3SS). T3SS is one of multiple secretion systems found in Gram-negative bacteria in which a needle-like complex enables the direct injection of effector proteins from external bacteria into the cytoplasm of host cells. Studies have improved the efficiency of T3SS-based cytosolic delivery of macromolecules, including synthetic binding proteins such as Designed Ankyrin Repeat Proteins (DARPins) and monobodies (*15*). A generalizable secretion system used for these larger protein families is a pCASP-hyperinvasive

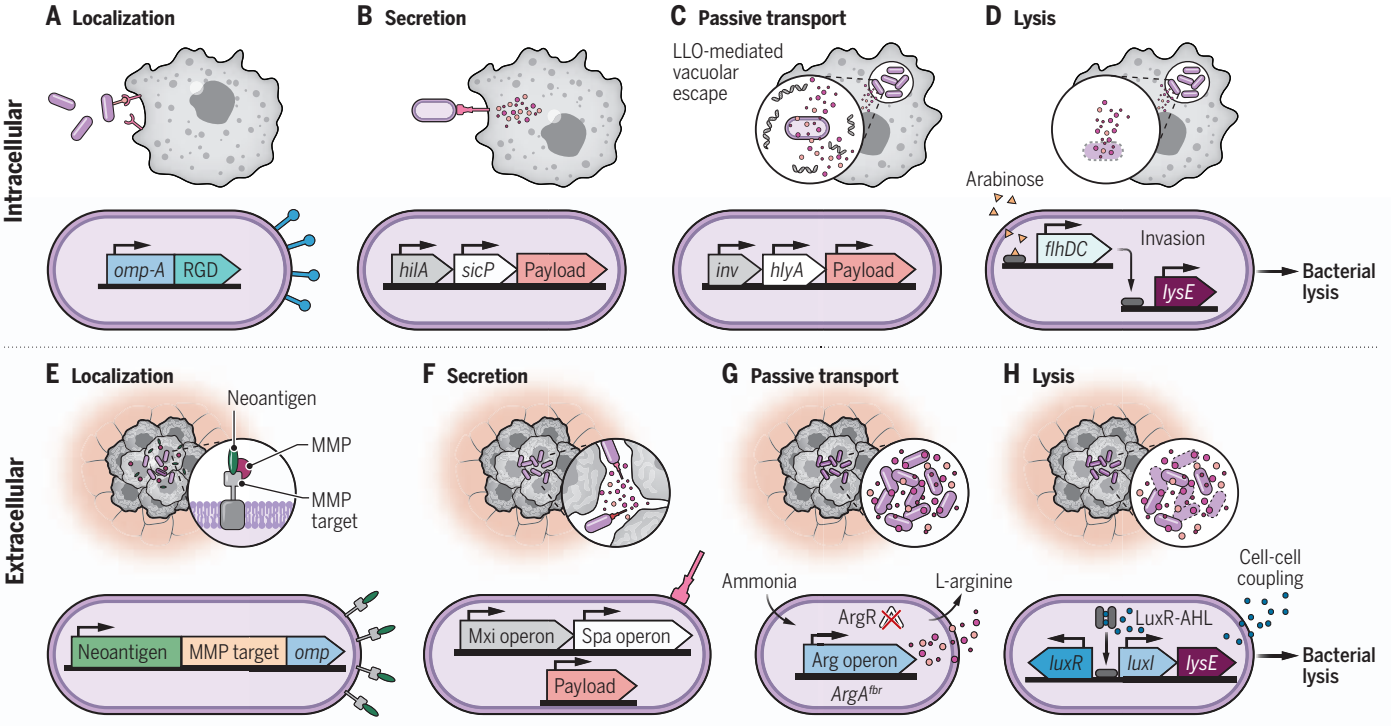

Fig. 1. Engineering the bacteria-tumor interface. Engineered bacteria localize their payloads intracellularly [(A) to (D)] or extracellularly [(E) to (H)] and release them by secretion, diffusion, or lysis mechanisms. (**A**) Bacteria have been engineered to more specifically bind to tumor cells by displaying targeting moieties such as RGD on the external loop of outer membrane proteins such as Omp-A (*11*). (**B**) Modified T3SS secretion using the pCASP-HilA vector enables bacterial delivery of macromolecules. *hilA* and *sicP* are expressed to improve secretion efficiency and the payload is tagged with a type III secretion signal sequence and chaperone binding domain for cytosolic delivery (*15*). (**C**) Expression of invasin, encoded by *inv*, promotes bacterial uptake into phagosomes and increases invasion efficiency of otherwise extracellular bacteria such as noninvasive *E. coli* strains, allowing for protected intravacuolar replication. The addition of LLO, encoded by *hlyA*, increases transfer efficiency of payloads such as plasmids into target cells by forming pores within the vacuolar membrane (*17*). (**D**) Bacteria have also been encoded with lysis circuits to enhance the passage of drugs through the bacterial membrane. An arabinose-inducible circuit regulates expression of the *flhDC* operon, which mediates *Salmonella* motility and invasion. In turn, bacterial lysis, achieved through the expression of by the bacteriophage-derived lysis gene *lysE*, is activated upon invasion (*23*). (**E**) Neoantigens with an MMP target sequence can be expressed with outer membrane proteins (omp) of *S. typhimurium*. Tumor-enriched MMPs can then cleave the MMP target sequence, releasing neoantigens locally within the extracellular tumor space (*41*). (**F**) Extracellular bacteria such as *E. coli* have also been encoded with modified T3SS components, whereby expression of the *mxi* and *spa* operons are necessary for the expression of T3SS structural components. This construct allows the secretion of therapeutic payloads modified with an N-terminal type III secretion signal sequence to be released outside of the tumor cell (*28*). (**G**) Acting as intratumoral bioreactors, *E. coli* have been engineered to metabolize ammonia, a waste product generated by tumors, into L-arginine. Genomic modifications were made to prevent the negative regulation or inhibition of genes in the biosynthesis pathway by deleting ArgR and integrating $ArgA^{fbr}$ (*42*). (**H**) Bacteria have also been engineered with *LuxR*-based QS systems that rely on the diffusion of the autoinducer AHL between cells. In this system, *luxI* produces AHL, which binds to LuxR, engaging the *plux* promoter for positive feedback regulation. Because AHL is also able to diffuse freely between cells, bacteria can sense when they are at a critical density and drive expression of *lysE*, inducing quorum-based lysis and repeated intratumoral drug delivery (*30*).

CREDIT: K. HOLOSKI/*SCIENCE*

locus A (HilA) vector in which expression of the recombinant protein is co-regulated with the *Salmonella* pathogenicity island-1 (SPI-1) operons and tagged with a type III secretion signal sequence and chaperone-binding domain (*15*, *16*). These modifications resulted in the recognition of the heterologous proteins as type III secreted proteins. A regulator of the SPI-1 genes, *hilA*, was also cloned under an arabinose-inducible promoter, allowing for the induction of high levels of protein secretion into target cells. To validate this secretion approach, multiple DARPins and monobodies inhibiting the largely undruggable RAS signaling pathway were delivered to the cytosol of human colon cancer cells using this bacterial system, and functional inhibition of RAS signaling was confirmed in vitro.

S. typhimurium can also be phagocytosed and replicate in a *Salmonella*-containing vacuole (SCV) within the host cell. Indeed, the T3SS needle complexes of *Salmonella* can penetrate through the SCV membrane, enabling payload protein secretion into the host cytosol. However, this barrier limits the transport of additional bacterial contents through the SCV once bacteria are internalized by the host tumor cell, prompting investigation into strategies to actively lyse bacteria and break down the SCV. Escape strategies from intracellular species such as *Listeria monocytogenes* and *Shigella flexneri* have been adapted to make *S. typhimurium* more effective at vacuolar escape (*17*). Specifically, the *hlyA* gene encodes for listeriolysin-O (LLO), a pore-forming cytolysin natively found in *L. monocytogenes*, that enables escape of bacterial plasmids and contents. Attenuated *S. typhimurium* engineered to express LLO can deliver plasmids into specific target cells, but the transfer efficiency is low (*18*). For otherwise extracellular bacteria such as *E. coli*, the expression of invasin (encoded by the *inv* gene from *Yersinia pseudotuberculosis*) can enable binding to β1-integrins present on many cell lines and promote bacterial uptake into phagosomes (*19*, *20*). Engineering diaminopimelate auxotrophic *E. coli* strains allows for additional bacterial cell lysis upon entry into mammalian cells because the auxotrophic bacteria are unable to synthesize a cell wall, in turn enabling plasmid DNA delivery to the host cell (*20*). Similar to *S. typhimurium* strains, *E. coli* strains can additionally encode LLO, which, when combined with auxotrophy and invasin expression, enhances the efficiency of nucleic acid transfer to host cells (*18*, *20*, *21*).

Synthetic biology approaches have enabled the integration of spatial and temporal controls to tune bacterial release from the vacuole. For example, inducible circuits have been used to temporally control the transcription of phage-derived lysis genes encoded by internalized *S. typhimurium*, resulting in bacteria cell lysis within the SCV. To enhance the passage of drugs through the SCV membrane, mutations in the *sifA* gene were made to compromise the integrity of the vacuole, allowing for release of bacterial payload into the host cell cytosol hours after internalization (*22*). In another example, an attenuated *S. typhimurium* strain (Δ*asd* VNP20009) was engineered to self-destruct upon sensing invasion into tumor cells (*23*). Bacterial motility and invasion were tuned by placing the operon, *flhDC*, under an arabinose-inducible circuit. Additionally, bacterial lysis genes were placed under the control of a SPI-2 promoter, which was activated after host cell invasion, further regulating lysis behavior. This "intracellular delivery (ID) *Salmonella*" platform was used to deliver drugs that effectively inhibited intracellular protein phosophatase 1 holoenzymes and mitigated tumor burden in vivo (*23*).

Targeting the extracellular space

Many therapeutic targets, such as tumor cell receptors, necessitate extracellular delivery methods. Generally, targeting extracellular molecules is somewhat simpler in that these delivery strategies depend less on the physical proximity of bacteria to tumor cells. Furthermore, the extracellular space enables bacteria to grow to high densities. As more bacteria grow, more of their payload can be produced and diffuse throughout the tumor space to act upon their intended targets (Fig. 1, E to H).

Extracellular delivery strategies also provide an opportunity to leverage non-invasive bacteria, such as the probiotic strain *E. coli* Nissle 1917 (EcN) (*24*). Because EcN and other inherently extracellular bacteria do not readily secrete most proteins, efforts to translocate recombinant proteins from the cytoplasm have relied on signal peptides and secretion tags (*25*, *26*). For direct delivery of cargo into mammalian cells, *E. coli* can also be engineered to encode a *Shigella*-derived type 3 secretion apparatus (*27*). A modified version of this system, named $PROT_3$EcT (probiotic type 3 secretion *E. coli* therapeutic) was expressed in EcN and allowed for secretion only within the extracellular space. Specifically, to constrain protein release to outside of the cell, the therapeutic proteins was fused to a sequence lacking the *Ipa* operon necessary for host cell invasion. When evaluated in a preclinical mouse model of colitis, $PROT_3$EcT-secreted anti-TNF-α nanobodies had comparable efficacy to systemically delivered antibodies to TNF-α in reducing inflammation (*28*).

Genetic circuits that use quorum sensing (QS) can enable coordinated bacterial behaviors in the extracellular tumor environment. Because bacteria only reach high densities in the TME, QS effectively acts a tumor-specific signature that can trigger recombinant protein expression (*29*). Additionally, these systems can offer temporal control, where QS parameters control a predetermined bacterial density for when therapeutic expression is activated. Similar to methods for lysing bacteria intracellularly, bacteriophage-derived lysis genes can be cloned under QS control, enabling intratumoral bacterial proliferation, lysis, and therapeutic release of payloads into the extracellular space. For example, a synchronized lysis circuit was designed such that bacteria grow and produce the QS molecule acyl homoserine lactone (AHL). Over time, AHL accumulates to a threshold concentration, triggering a lysis event and releasing bacterial contents upon reaching a critical density. After lysis, a small number of remaining bacteria begin to produce AHL anew, and the process continues in a cyclical fashion, allowing for repeated drug delivery within tumors (*30*). Such circuits have been used to release various toxins and immunotherapeutics, including hemoylysin E (hlyE), cell death domain–RGD integrin peptide (CDD-iRGD), C-C chemokine ligand-21 (CCL-21), and nanobodies targeting Cluster of Differentiation 47 (CD47), Cytotoxic T-lymphocyte associated protein 4 (CTLA-4), and Programmed death-ligand 1 (PD-L1), from both *S. typhimurium* and *E. coli* strains. Furthermore, therapeutic efficacy has been demonstrated in mice bearing colorectal, melanoma, breast, and lymphoma subcutaneous tumors, suggesting its versatility as a release mechanism (*30*–*32*).

QS approaches provide autonomous spatial and temporal control that can confine bacteria to tumors and allow for continuous and sustained therapeutic delivery. Furthermore, these circuits can be tuned such that multiple payloads can be delivered sequentially in accordance with a predetermined dosing regimen. Although this has not been achieved in bacteria, examples of similar recombinase-based circuits resulting in sequential gene expression have been explored in mammalian cells (*33*). Some limitations of QS-based strategies include their reliance on reaching a critical bacteria density, which may not be achieved across all tumor sizes, and the use of bacteriophage-derived lysis genes, which can induce a strong evolutionary pressure for mutation.

Reprogramming the immune system

The introduction of engineered bacteria into a host can prompt a predictable immune response, thereby establishing a bacteria-immune cell interface and an exploitable response timeline. Bacteria are inherently immunogenic by virtue of their overall foreignness through expression of surface and intracellular biomolecules that activate innate immune receptors, secretion of immunostimulatory metabolites, and the ability of certain species to inject effector proteins that permit them to invade tumor and local immune cells (*34*). Immune stimulation by bacteria increases when bacterial lysis products

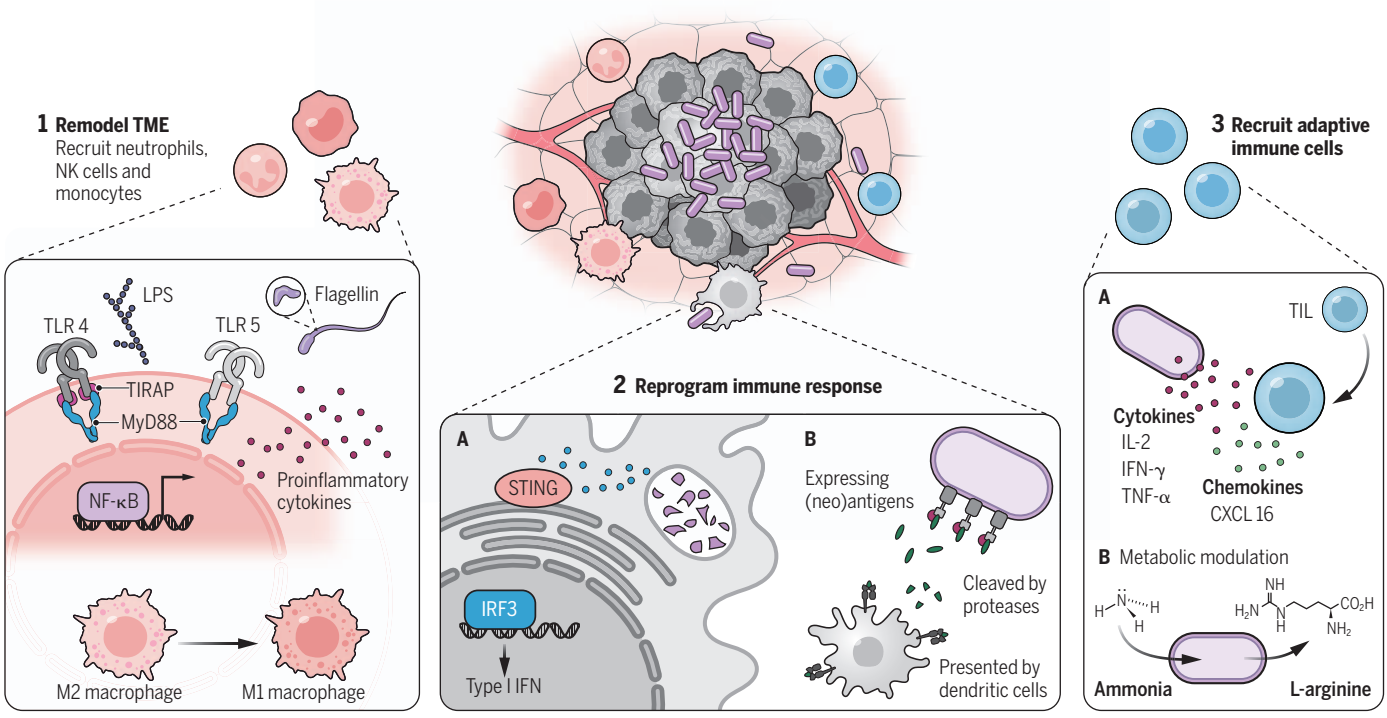

Fig. 2. Engineering the bacteria-immune interface. As single agents, bacteria are immunogenic and can remodel the TME through engagement of TLR-4 and TLR-5, which are stimulated by bacterial LPS and flagella, respectively. Their presence can also lead to an influx of innate immune cells such as neutrophils, natural killer (NK) cells, and monocytes into the tumor and change the phenotype of resident macrophages. As immune cells infiltrate into the tumor, bacteria are phagocytosed, presenting an opportunity to deliver immune cell–specific cargo intracellularly. For example, *E. coli* have been engineered to deliver STING agonists to intratumoral APCs, thereby inducing an IFN-I response (*36*). *S. typhimurium* have also been encoded to express neoantigens on their outer membrane so that once inside the tumor, they can be cleaved, taken up, and presented by surrounding dendritic cells (*41*). Bacteria can also engage the adaptive immune system through the production of immunomodulators such as cytokines and chemokines to recruit TILs into the tumor space. In addition to directly producing immunomodulatory cargo, they have also been engineered to convert tumor metabolic waste products such as ammonia into metabolites such as L-arginine, which has been correlated with increased frequency of TILs, thereby remodeling the TME (*42*).

are released within the necrotic tumor core or upon killing and phagocytosis of bacteria by cellular and humoral immune components. Beyond these intrinsic immunostimulatory features, synthetic biology techniques can be used to engineer bacteria that deliver cargo capable of targeting discrete steps in the development of an antitumor immune response, potentially synergizing with the inherent innate immune activation elicited by bacteria to enhance the overall therapeutic efficacy of bacterial cancer therapies across multiple tumor types (Fig. 2).

Programming innate immunity

At the earliest stages of colonization and intratumoral proliferation, the presence of bacterial ligands can act as immune adjuvants to stimulate the recruitment and activation of monocytes, macrophages, and neutrophils. These innate immune cells participate in the lysis and clearance (through phagocytosis) of tumor-colonizing bacteria and produce inflammatory cytokines in response to the detection of liberated surface bacterial components by their expressed repertories of Toll-like receptors (TLRs). An attenuated *S. typhimurium* was engineered to produce and secrete heterologous flagellin, FlaB, which was derived from another bacterial species, *Vibrio vulnificus*, and was more potent than flagellin native to *Salmonella* (*35*). This modified strain of *S. typhimurium* expressing *flaB* stimulates an innate immune response through the cooperative activation of TLR4 and TLR5, where TLR4 recognizes *S. typhimurium* LPS and TLR5 recognizes the secreted FlaB. Recognition of *S. typhimurium* LPS induced the infiltration of monocytes, macrophages, and neutrophils into the TME, which, in conjunction with their recognition of LPS through TLR4, may detect FlaB through TLR5 and support an observed M2 macrophage (protumor) to M1 macrophage (antitumor) shift and increased secretion of the antitumor cytokines interleukin-1β (IL-1β) and TNF-α. Testing of the system in murine and human colon cancer models demonstrated delayed primary tumor growth and inhibition of metastases only when bacteria were engineered to secrete FlaB. The necessity of both components suggests that bacteria can encode payloads to uniquely and effectively alter immune functions (*35*).

As an innate immune response continues, antigen-presenting cells (APCs) will enter the tumor and likely engulf dead tumor cells and intratumoral bacteria, thereby providing further interactions that can be precisely modulated for an enhanced antitumor response. For example, EcN can be engineered to deliver STING agonists such as a cyclic di-AMP (CDA)–producing enzyme and passively release their payload within intratumoral phagocytic APCs (*36*). This strain, SYNB1891, relies on its phagocytic uptake to deliver CDA directly to APCs and induce a type I interferon (IFN-I) response. Combined with the benefit of bacteria-mediated proinflammatory cytokine production, delivery of STING agonists resulted in durable antitumor immunity and tumor regression in multiple murine tumor models. Currently, SYNB1891 is being evaluated in a phase 1 clinical trial of patients with advanced solid tumors and lymphomas (NCT04167137). Similarly, STACT (*S. typhimurium*–attenuated cancer therapy), another strain in clinical development, was engineered to encode a Three Prime Repair Exonuclease 1 (TREX-1) inhibitor, and leverages a similar mechanism, ultimately activating the STING pathway upon uptake by tumor-resident APCs (*37*).

Programming adaptive immunity

As APCs engulf cells, they can present new antigens and stimulate an adaptive immune

response. Antigens derived from native intracellular bacteria within the tumor microbiome, specifically patient-derived melanoma tumors, can be presented by melanoma cells and infiltrating APCs, thus activating adaptive immunity (*38*). Additionally, *Listeria*-based approaches have been commonly used to deliver intracellular payloads, including tumor antigens (*39*, *40*). Although *L. monocytogenes* is common for antigen delivery because of its preference for APC invasion, attenuated *S. typhimurium* have been used as an alternative chassis for neoantigen peptide delivery. In one study, multiple neoantigen peptides were tethered to the outer *S. typhimurium* membrane with a matrix metalloproteinase (MMP) target sequence (*41*). Once engineered bacteria home to tumors, neoantigens can be cleaved from bacteria by proteases abundantly found in the tumor and released into the TME for site-specific recruitment and activation of lymphocytes. Treatment of murine colorectal tumors with the engineered neoantigen-producing strain led to an increase in proinflammatory cytokines such as IL-2, TNF-α, and INF-γ, and increased the accumulation of tumor-infiltrating lymphocytes (TILs).

In addition to presenting immunomodulators, intratumoral bacteria can also remodel the TME and indirectly potentiate an adaptive immune response through metabolic modulation. For example, EcN was engineered to convert ammonia, a metabolic waste product in tumors, into L-arginine (*42*). Further modifications were made to the EcN genome to increase L-arginine production, including deleting the arginine repressor (ArgR), thereby preventing the negative regulation of genes in the biosynthesis pathway. Additionally, a feedback-resistant dominant mutant version of ArgA ($ArgA^{fbr}$) was integrated into the bacterial genome to prevent inhibition of the pathway by high levels of L-arginine. When combined with checkpoint blockade, intratumoral injections of this L-arginine–producing strain resulted in increased accumulation of TILs and enhanced overall therapeutic efficacy (*42*).

Bacteria can also be encoded with a multitude of payloads to further program the adaptive antitumor immune response by the activation and recruitment of immune cells through the production of immune checkpoint blockade nanobodies, cytokines, and chemokines (*2*). Tumors lacking infiltrating cytotoxic T cells can become more responsive to immune-based therapies through the production of intratumoral cytokines and chemokines. Examples of cytokines recombined into the bacterial genome include, but are not limited to, IL-2, IL-18, and CCL-21, all of which work to ultimately stimulate immune effector functions against cancer cells. IL-2 has been the most extensively investigated, with examples of IL-2 producing *S. typhimurium* strains demonstrating anticancer and prophylactic properties (*2*). EcN can also be encoded to produce C-X-C chemokine ligand 16 (CXCL16) and promote chemotaxis of cytotoxic T cells into tumors (*43*), subsequently supporting tumor regression. Collectively, these studies demonstrate an opportunity to exploit the inherent temporal structure of an immune response to tune bacteria-immune cell interactions. At each stage of the response, bacteria can produce payloads to communicate with specific immune cells, reprogramming a more effective antitumor response.

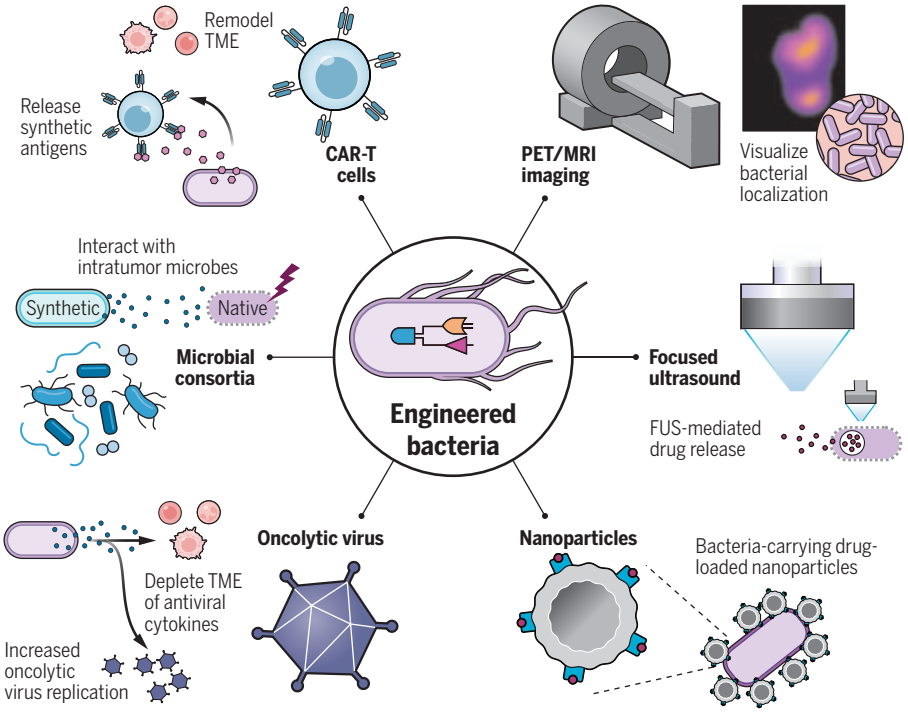

Fig. 3. Engineering bacterial interactions with other modalities. Bacteria can be used together with both living and nonliving technologies for improved diagnostic and therapeutic outcomes. Combinations with imaging techniques such as MRI, PET, and FUS enable tracking and visualization of systemically delivered bacteria. When bacteria are encoded with acoustic reporter genes or thermal switches, FUS can be used to activate therapeutic release. Drug-loaded nanoparticles can be physically bound to bacteria, which can traffic them to tumor depths that they otherwise would be unable to reach. Shifting from nonliving modalities, efforts have focused on engineering interactions between replicating or living modalities. For example, bacteria can remodel the TME, making it more favorable for oncolytic virus therapy. Synthetic consortia of bacteria can also work together to prompt predictable immune responses or limit populations of tumor-promoting bacteria. Finally, CAR-T cells can be activated by bacterial adjuvants and programmed to respond to bacterially released synthetic antigens.

CREDIT: K. HOLOSKI/*SCIENCE*

Engineering microbial interfaces

In addition to interfacing with tumor and immune cells within the TME, bacteria can also work in combination with materials and technologies outside of the tumor. External technologies such as ultrasound and magnetic-based approaches can further manipulate bacterial behavior, allowing for tumor visualization and remote control to precisely tune bacterial location and timing of therapeutic release within the tumor. Moreover, nanoparticles, their cargo, and radiation therapy can remodel the TME and modulate bacterial interaction with the immune system. When combined, these technologies create systems of living and nonliving modalities in which each singular therapy can supplement the limitations of the other, resulting in an overall improved outcome (Fig. 3).

Interfacing with nonliving technologies

Imaging modalities such as positron emission tomography (PET) and MRI have long been used to assist in cancer detection and visualization. These imaging techniques can also be used in combination with native or engineered bacteria enhancing visualization of tumor and bacterial localization in situ (*44*). In addition to imaging-based detection, bacteria can produce molecules recoverable in urine, blood, and stool for additional noninvasive diagnoses (*45*–*47*). Once inside the tumor, engineered bacteria can report on tumor presence, burden, and possibly on microenvironmental conditions when coupled to bacteria-based sensors and circuits.

Moreover, external actuation can be used to interface with microbes in vivo. FUS is one

such approach with the ability to penetrate deeply into tissue with high spatial resolution, allowing engineered bacteria to be visualized and manipulated within precise locations. To facilitate bacterial visualization, *E. coli* and *S. typhimurium* can be encoded with acoustic reporter genes derived from intracellular, protein-enclosed gas vesicles native to other microorganisms. Expression of these gene clusters enabled bacterial detection by FUS and, more specifically, visual mapping of their locations in the gastrointestinal tract and TME (*48*). Such bacteria can also be engineered with temperature-actuated genetic switches to release immune checkpoint inhibitors (*49*) or cytokines (*50*) intratumorally in response to applied FUS hyperthermia. Finally, FUS can be used in combination with bacteria as a mechanotherapy in which bacteria encode micrometer-scale cavitating bubbles that unleash strong local mechanical effects to disrupt and kill tissue and cells, further lysing bacteria and releasing therapeutic cargo (*51*).

In parallel, multiple efforts have coupled microbes with magnetic guidance to enhance the penetrance of engineered bacteria strains into hypoxic tumor cores. Several studies have leveraged the magneto-aerotactic property of *Magnetococcus marinus*, demonstrating that external magnetic torque-driven actuation can wirelessly control bacteria bearing liposomal cargo and enhance bacterial accumulation deep within the TME (*52*, *53*). Coating the surface of *E. coli* with both magnetic nanoparticles and chemotherapeutic-encapsulating nanoliposomes allowed the magnetic guidance of bacteria through three-dimensional materials, where they homed to the externally placed magnetic field and released payloads in vitro (*54*).

External therapeutic modalities such as radiation can also combine favorably with bacteria and nanoparticle therapies by promoting bacteria-immune cell interactions. Attenuated *S. typhimurium* (VNP20009) coated with positively charged polyamidoamine dendrimer nanoparticles can bind negatively charged antigens through electrostatic interactions. When immunosuppressive tumors are irradiated, tumor antigens are released and engineered bacteria can then transport the antigens to functional dendritic cells at the tumor periphery, eliciting a strong systemic immune response against the tumor (*55*).

Engineering communities of programmable medicines

In addition to combinations with external technologies and nonliving materials, it is also possible to engineer interactions between bacteria and other living cellular modalities. In the simplest case, bacteria can remodel the TME to be more favorable to other microbial and cellular therapies. For example, nonpathogenic *E. coli* encoded with an IFN-I antagonist, B18R, enhanced the intratumoral replication of vesicular somatitus virus (VSV) by effectively protecting it from immune-mediated clearance (*56*). When used as a monotherapy, neither microbe had any notable antitumor efficacy, but combining the two provided an improved antitumor response and survival outcome in murine cancer models. Underlying this response is the engineering of both microbes such that bacteria depleted the TME of antiviral cytokines, making the environment hospitable to sequentially delivered VSV. In this study, bacteria were repurposed to limit, not provoke, an immune response, and specific bacterial species and immune-effector payloads can be chosen purposefully to complement oncolytic virus therapy. Similarly, bacteria can be favorably combined with chimeric antigen receptor (CAR)–T cell therapies. An attenuated bacterial strain, *Brucella melitenis*, promoted proinflammatory M1 polarization of tumor macrophages and increased the frequency of $CD8^+$ T cells within tumors (*57*). When it was delivered with CAR-T cells to treat a murine model of colon cancer, mice displayed lower tumor burden and their survival significantly improved.

Establishing direct communication between engineered bacteria and cellular therapies, such as CAR T cells, is another strategy to enhance therapeutic outcomes. Probiotic-guided CAR-T cells (ProCARs) were engineered such that bacteria encode a synthetic antigen that can be recognized by the CAR T cells (*58*). In this study, the synthetic antigen served as communication between the engineered bacteria and the ProCARs, allowing for spatiotemporal control of CAR activation within the tumor space after tumor-colonizing bacteria released a synthetic antigen. When evaluated in mice bearing xenografts of human tumors, the ProCAR system significantly delayed tumor growth in multiple models, with an enhanced benefit over a bacteria vehicle and CAR-T cell combination control. Further analysis of the therapeutic response showed increased ProCAR activation from both synthetic antigen presence and stimulation of TLRs by bacteria, demonstrating the potential of engineering communities of programmable medicines (*58*).

In addition to cellular therapies, the human body, and particularly tumors, contains a plethora of microbes that can be manipulated for therapeutic purposes (*59*). Intratumoral bacteria have been linked to chemotherapeutic resistance by metabolizing gemcitabine into an inactive form and other studies have demonstrated that *Fusobacteria* may be associated with cancer progression (*60*). In these cases, engineered bacteria could be designed to sense tumor-promoting microbes and eliminate them by producing antimicrobial payloads. Alternatively, innocuous tumor-resident bacteria could be converted to microbes that assist with antitumor immunity. Another approach is to leverage small microbial consortia as therapeutics. An 11-strain commensal consortium of bacteria was identified within the gut microbiome and shown to mediate cytotoxic T cell immunity and induce $IFN\gamma^+$ $CD8^+$ T cells, potentiating the efficacy of immune checkpoint blockade in inhibiting tumor growth (*61*). Using a synthetic biology approach, designing robust synthetic communities with cooperative or antagonistic symbiosis could be engineered to improve therapeutic outcome (*62*–*64*).

Summary and future outlook

Bacteria are a versatile platform that can be engineered as single agents or in combination with other modalities to improve tumor detection and treatment. Alone, bacteria are immunostimulatory and capable of directing an immune response toward the tumor. They can be further engineered to produce various payloads both extracellularly and intracellularly. By nature of favorable bacterial accumulation within tumor cores, the spatial and temporal drug release profiles differ from conventional systemic therapies, thereby mitigating off-target toxicities and accessing otherwise difficult to reach therapeutic targets (*5*).

Although substantial advances have been made in the progression of bacteria cancer therapies, biocontainment and safety concerns need to be evaluated during clinical translation. Bacillus Calmette-Guerin (BCG), an attenuated *Mycobacterium bovis* strain that is used clinically for bladder cancer treatment, provides a benchmark for a US Food & Drug Administration–approved bacteria cancer therapy. In addition to BCG, attenuated bacterial strains alone or engineered with a payload are also being evaluated in patients (*2*). As systems of bacteria for cancer therapy continue to enter clinical trials, these results will guide future engineering approaches to enhance their effectiveness. Beyond their use as single agents, we envision the use of bacteria therapies in combination with other cellular therapies or external modalities, whereby their interactions with the technologies can be engineered in rationally designed bidirectional systems.

REFERENCES AND NOTES

1. E. F. McCarthy, *Iowa Orthop. J.* **26**, 154–158 (2006).
2. M. T.-Q. Duong, Y. Qin, S.-H. You, J.-J. Min, *Exp. Mol. Med.* **51**, 1–15 (2019).
3. S. Zhou, C. Gravekamp, D. Bermudes, K. Liu, *Nat. Rev. Cancer* **18**, 727–743 (2018).
4. M. P. McNerney, K. E. Doiron, T. L. Ng, T. Z. Chang, P. A. Silver, *Nat. Rev. Genet.* **22**, 730–746 (2021).
5. N. S. Forbes, *Nat. Rev. Cancer* **10**, 785–794 (2010).
6. K. B. Low *et al.*, *Nat. Biotechnol.* **17**, 37–41 (1999).
7. J. F. Toso *et al.*, *J. Clin. Oncol.* **20**, 142–152 (2002).
8. R. M. Hoffman, *Amino Acids* **37**, 509–521 (2009).
9. M. Zhao *et al.*, *Cancer Res.* **66**, 7647–7652 (2006).
10. B. F.-L. Sieow, K. S. Wun, W. P. Yong, I. Y. Hwang, M. W. Chang, *Trends Cancer* **7**, 447–464 (2021).
11. S.-H. Park *et al.*, *Theranostics* **6**, 1672–1682 (2016).
12. B. Yu *et al.*, *Sci. Rep.* **2**, 436 (2012).
13. T. Chien *et al.*, *Nat. Biomed. Eng.* **6**, 94–104 (2022).

14. M. P. Stewart *et al.*, *Nature* **538**, 183–192 (2016).
15. A. Chabloz *et al.*, *Commun. Biol.* **3**, 342 (2020).
16. D. M. Widmaier *et al.*, *Mol. Syst. Biol.* **5**, 309 (2009).
17. S. Weiss, S. Krusch, *Biol. Chem.* **382**, 533–541 (2001).
18. C. Grillot-Courvalin, S. Goussard, P. Courvalin, *Cell. Microbiol.* **4**, 177–186 (2002).
19. J. C. Anderson, E. J. Clarke, A. P. Arkin, C. A. Voigt, *J. Mol. Biol.* **355**, 619–627 (2006).
20. C. Grillot-Courvalin, S. Goussard, F. Huetz, D. M. Ojcius, P. Courvalin, *Nat. Biotechnol.* **16**, 862–866 (1998).
21. O. D'Cruz *et al.*, *Gastroenterology* **112**, S162–S163 (2017).
22. E. M. Camacho, B. Mesa-Pereira, C. Medina, A. Flores, E. Santero, *Sci. Rep.* **6**, 30591 (2016).
23. V. Raman *et al.*, *Nat. Commun.* **12**, 6116 (2021).
24. J. P. Lynch, L. Goers, C. F. Lesser, *Trends Pharmacol. Sci.* **43**, 772–786 (2022).
25. C. L. Ho *et al.*, *Nat. Biomed. Eng.* **2**, 27–37 (2018).
26. J. H. Choi, S. Y. Lee, *Appl. Microbiol. Biotechnol.* **64**, 625–635 (2004).
27. A. Z. Reeves *et al.*, *ACS Synth. Biol.* **4**, 644–654 (2015).
28. J. P. Lynch *et al.*, *Cell Host Microbe* 10.2139/ssrn.4133893 (2022).
29. C. A. Swofford, N. Van Dessel, N. S. Forbes, *Proc. Natl. Acad. Sci. U.S.A.* **112**, 3457–3462 (2015).
30. M. O. Din *et al.*, *Nature* **536**, 81–85 (2016).
31. S. Chowdhury *et al.*, *Nat. Med.* **25**, 1057–1063 (2019).
32. C. R. Gurbatri *et al.*, *Sci. Transl. Med.* **12**, eaax0876 (2020).
33. T. Kim, B. Weinberg, W. Wong, T. K. Lu, *Nat. Commun.* **12**, 2711 (2021).
34. T. Harimoto *et al.*, *Nat. Biotechnol.* **40**, 1259–1269 (2022).
35. J. H. Zheng *et al.*, *Sci. Transl. Med.* **9**, eaak9537 (2017).
36. D. S. Leventhal *et al.*, *Nat. Commun.* **11**, 2739 (2020).
37. H. Kehoe *et al.*, *J. Immunother. Cancer* **9** (Suppl 2), A894–A894 (2021).
38. S. Kalaora *et al.*, *Nature* **592**, 138–143 (2021).
39. V. Shahabi *et al.*, *Cancer Immunol. Immunother.* **57**, 1301–1313 (2008).
40. B. C. Selvanesan *et al.*, *Sci. Transl. Med.* **14**, eabc1600 (2022).
41. J. Hyun *et al.*, *ACS Synth. Biol.* **10**, 2478–2487 (2021).
42. F. P. Canale *et al.*, *Nature* **598**, 662–666 (2021).
43. T. M. Savage *et al.*, Engineered bacteria recruit and orchestrate anti-tumor immunity. bioRxiv 496462 [Preprint] (2022); https://doi.org/10.1101/2022.06.16.496462.
44. S.-R. Kang, J.-J. Min, *Nucl. Med. Mol. Imaging* **55**, 7–14 (2021).
45. T. Danino *et al.*, *Sci. Transl. Med.* **7**, 289ra84 (2015).
46. R. M. Cooper *et al.*, Engineered bacteria detect tumor DNA. bioRxiv 459858 [Preprint] (2022); https://doi.org/10.1101/2021.09.10.459858.
47. J. T. Panteli, N. Van Dessel, N. S. Forbes, *Int. J. Cancer* **146**, 137–149 (2020).
48. R. W. Bourdeau *et al.*, *Nature* **553**, 86–90 (2018).
49. M. H. Abedi *et al.*, *Nat. Commun.* **13**, 1585 (2022).
50. Y. Chen, M. Du, Z. Yuan, Z. Chen, F. Yan, *Nat. Commun.* **13**, 4468 (2022).
51. A. Bar-Zion *et al.*, *Nat. Nanotechnol.* **16**, 1403–1412 (2021).
52. O. Felfoul *et al.*, *Nat. Nanotechnol.* **11**, 941–947 (2016).
53. T. Gwisai *et al.*, Magnetic torque-driven living microrobots for enhanced tumor infiltration. bioRxiv 473989 [Preprint] (2022); https://doi.org/10.1101/2022.01.03.473989.
54. M. B. Akolpoglu *et al.*, *Sci. Adv.* **8**, eabo6163 (2022).
55. W. Wang *et al.*, *Nat. Biomed. Eng.* **6**, 44–53 (2022).
56. M. Cronin *et al.*, *Mol. Ther.* **22**, 1188–1197 (2014).
57. F. Guo *et al.*, *J. Immunother. Cancer* **10**, 10 (2022).
58. R. L. Vincent *et al.*, Probiotic-guided CAR-T cells for universal solid tumor targeting. bioRxiv 463366 [Preprint] (2021); https://doi.org/10.1101/2021.10.10.463366.
59. D. Nejman *et al.*, *Science* **368**, 973–980 (2020).
60. G. D. Sepich-Poore *et al.*, *Science* **371**, eabc4552 (2021).
61. T. Tanoue *et al.*, *Nature* **565**, 600–605 (2019).
62. M. J. Liao, M. O. Din, L. Tsimring, J. Hasty, *Science* **365**, 1045–1049 (2019).
63. B. D. Karkaria, A. J. H. Fedorec, C. P. Barnes, *Nat. Commun.* **12**, 672 (2021).
64. W. Kong, D. R. Meldgin, J. J. Collins, T. Lu, *Nat. Chem. Biol.* **14**, 821–829 (2018).

ACKNOWLEDGMENTS

We thank members of the Danino and Arpaia labs for their critical review of the manuscript. **Funding:** This work was supported by the National Institutes of Health (grants U01CA247573, R01CA249160, and R01EB029750), the Pershing Square Foundation (PSF grant PSSCRA CU20-0730), and the Cancer Research Institute (CRI grant 3446). **Competing interests:** All authors have financial interests in GenCirq Inc.

10.1126/science.add9667

REVIEW

Scaling up complexity in synthetic developmental biology

Guillermo Martínez-Ara, Kristina S. Stapornwongkul, Miki Ebisuya*

The application of synthetic biology approaches to study development opens the possibility to build and manipulate developmental processes to understand them better. Researchers have reconstituted fundamental developmental processes, such as cell patterning and sorting, by engineering gene circuits in vitro. Moreover, new tools have been created that allow for the control of developmental processes in more complex organoids and embryos. Synthetic approaches allow testing of which components are sufficient to reproduce a developmental process and under which conditions as well as what effect perturbations have on other processes. We envision that the future of synthetic developmental biology requires an increase in the diversity of available tools and further efforts to combine multiple developmental processes into one system.

One of the most noteworthy features of biological systems is their inherent complexity. During development, numerous highly coordinated processes unfold to generate an entire organism from a single cell. Cells execute precise gene expression patterns, form complex tissue structures, and specialize into different cell types. Traditionally, biologists have observed and perturbed embryonic development through mutagenesis screens and targeted manipulation of gene expression (*1*–*4*). These approaches have led to the association of specific genes with different developmental processes, but they do not provide knowledge about which components are sufficient to reproduce the process and the conditions under which they interact appropriately. These aspects can be addressed through synthetic biology, which allows for the study of development through the control and reconstitution of such developmental processes. This recently emerging field is known as synthetic developmental biology (*5*–*12*). Combined with in vitro culture technologies, such as organoids (*13*, *14*), it allows researchers to acquire a new level of understanding through control and creation.

"...control over each component in the system enables not only the fine-tuning of their properties but also rigorous modeling, which can help explore system capabilities."

Reconstitution in cell culture

Using model systems more controllable than embryos, researchers have started to engineer developmental processes in two-dimensional (2D) mammalian cell culture systems to gain a deeper understanding of the mechanisms involved. One outstanding approach has been the introduction of synthetic gene circuits to reconstitute cell communication and tissue patterning. For example, a minimal symmetry-breaking system was engineered to reconstitute lateral inhibition based on cell-cell contact through the membrane-bound ligand-receptor pair Delta and Notch (Fig. 1A) (*15*). As they do during the formation of hair cells in the inner ear (*16*), adjacent daughter cells adopted distinct transcriptional programs. Further studies developed the engineering of cell state bifurcation by creating multiple stable states of gene expression (*17*). Moreover, the development of synthetic Notch (synNotch) receptors that allow modulation of both signal input and transcriptional output permitted the reconstitution of gene expression patterns (*18*). The expression of different cadherins was sufficient to reconstitute synthetic cell sorting mechanisms, reminiscent of the cell sorting in the inner cell mass of the mammalian embryo (Fig. 1B) (*19*, *20*). Likewise, long-range communication mechanisms have been explored to achieve in vitro patterning. One example is morphogen-like systems, where cells respond in a concentration-dependent manner to diffusible signaling molecules (*21*, *22*). Reaction-diffusion systems have also been reconstituted, leading to a better understanding of conditions under which a short-range activator and long-range inhibitor can generate complex patterns (Fig. 1C) (*23*). In these examples, full gene circuits were engineered into cells, showing that the components used were sufficient to mimic biological patterning processes.

For the control of processes that alter tissue structure, optogenetics has proven to be a

European Molecular Biology Laboratory (EMBL) Barcelona, 08003 Barcelona, Spain.
***Corresponding author. Email: miki.ebisuya@embl.es**

valuable approach. By making biological processes light sensitive, researchers gain high spatiotemporal control over the manipulation of engineered cells or tissues (*24*). For example, optogenetic control of cell migration was achieved through the design of a photoactivatable version of the guanosine triphosphatase Rac1 (PA-Rac1). This engineered PA-Rac1 was not only used to test how different localized pulses of RAC activation inhibited RhoA activity and induced lamellipodial protrusions, but also to demonstrate that these pulses could be used to direct cell migration (Fig. 1D) (*25*). This tool, which has proven valuable to understand and control single-cell migration, can potentially be used to study cell migration in developmental contexts (*26*). Optogenetic tools capable of inducing cell death (*27*) also have a great potential to be used to study the effect of cell death on developing tissues (Fig. 1E). Finally, optogenetic control of apical constriction permitted cell shape changes and resulting tissue folding in simple epithelial monolayers in vitro (Fig. 1F) (*28*).

A main advantage of in vitro reconstitution is that the sufficiency of the components to reproduce the process can be tested outside of the developmental context. Moreover, these experiments can also drive the development of orthogonal components to replace biological ones or to create new synthetic tissues with novel functions. Such in vitro systems—normally 2D cell cultures—are more amenable to perturbations to study the parameters under which these mechanisms function. We highlighted two ways to control and evaluate developmental processes. First, gene circuits have been used to reconstitute patterning using either components already involved in development (such as Nodal and Lefty) or through the development of new tools to make orthogonal circuits (e.g., synNotch). Second, morphogenetic processes, such as migration, apoptosis, or folding, can be controlled through optogenetic tools, which provide spatiotemporal control; however, not all of them have been applied to study developmental processes yet.

Synthetic control in complex systems

Developmental processes can also be controlled in more complex systems, such as organoids or embryos. By making use of tools to direct developmental processes or by engineering circuits partially substituting the original components, researchers can interact with developing tissues to study the process in situ, discover new interactions, or perturb the process in a fine-tuned way.

OptoShroom3, an optogenetic tool to control apical constriction in mammalian tissues, was used to modify the shape of optic vesicles and neuroectodermal organoids (Fig. 2A) (*28*). The lumen of optic vesicles was reduced upon stimulation, and neuroectodermal organoids with outer apical polarity were flattened upon illumination. This is an example of how a tool designed to engineer the control of a morphogenetic process (apical constriction) can be applied to modify tissue shape with spatiotemporal control. Similarly, *Drosophila* embryos could be triggered to invaginate through optogenetic control of apical constriction (*29*). These

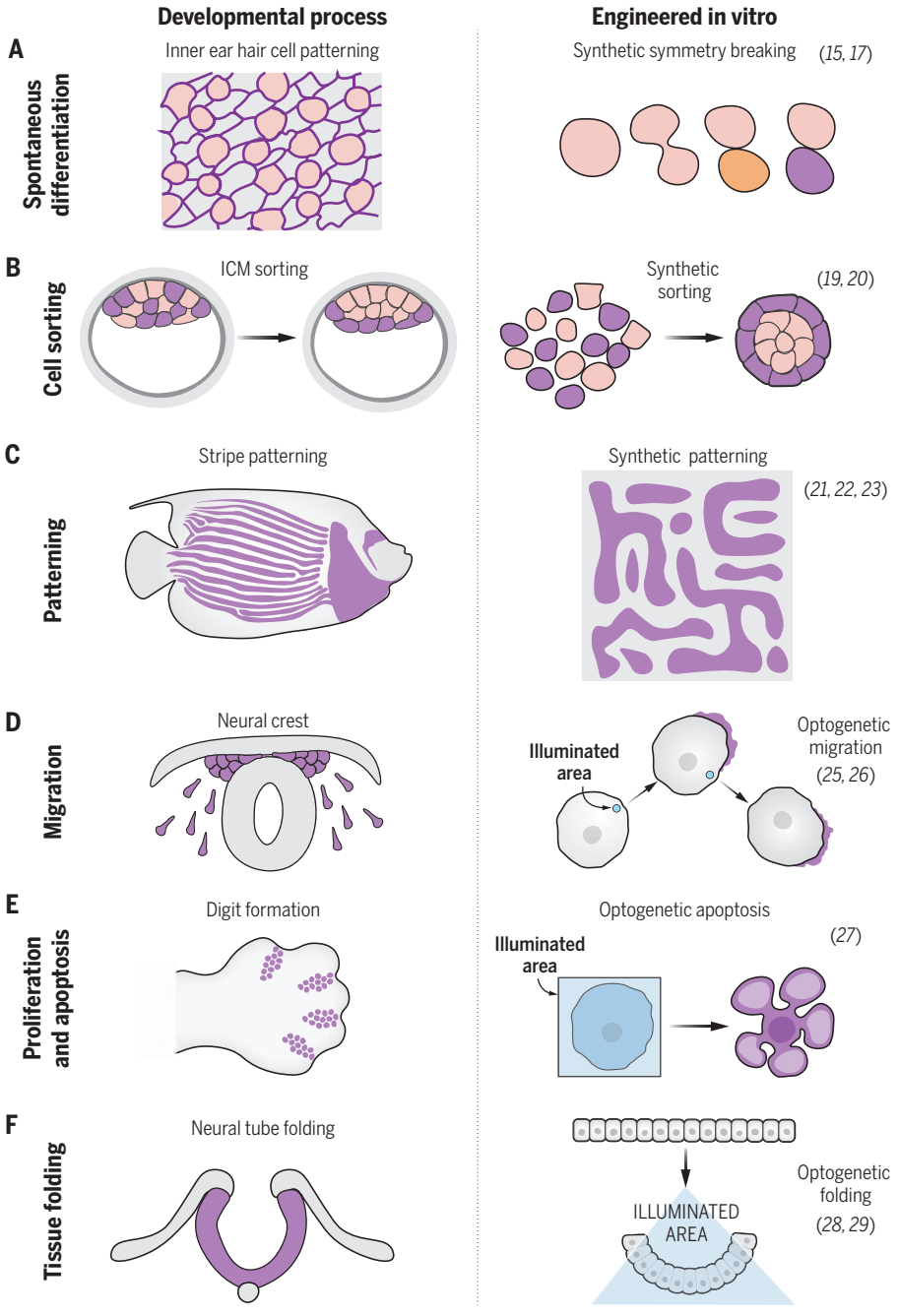

Fig. 1. Reconstitution of developmental processes in 2D cell culture. (**A**) Lateral inhibition, a symmetry-breaking mechanism observed in inner ear patterning, was recapitulated with a synthetic circuit. (**B**) Cell sorting, as observed in the inner cell mass (ICM), was reconstituted through a circuit combining cell-cell communication and cadherin expression. (**C**) Reaction-diffusion systems can generate complex patterns. Using a circuit based on the interaction of two secreted signaling molecules, such patterns were recapitulated in mammalian tissue culture. (**D**) Cell migration, a process crucial for many developmental events, was controlled through the optogenetic activation of RAC1. (**E**) Apoptosis, a key process during limb digit formation, was optogenetically controlled in cells in tissue culture. (**F**) Epithelial tissue folding, as observed in the formation of the neural tube, was recapitulated through the optogenetic control of apical constriction. Cited references also include related examples.

ILLUSTRATION: N. CARY/*SCIENCE*

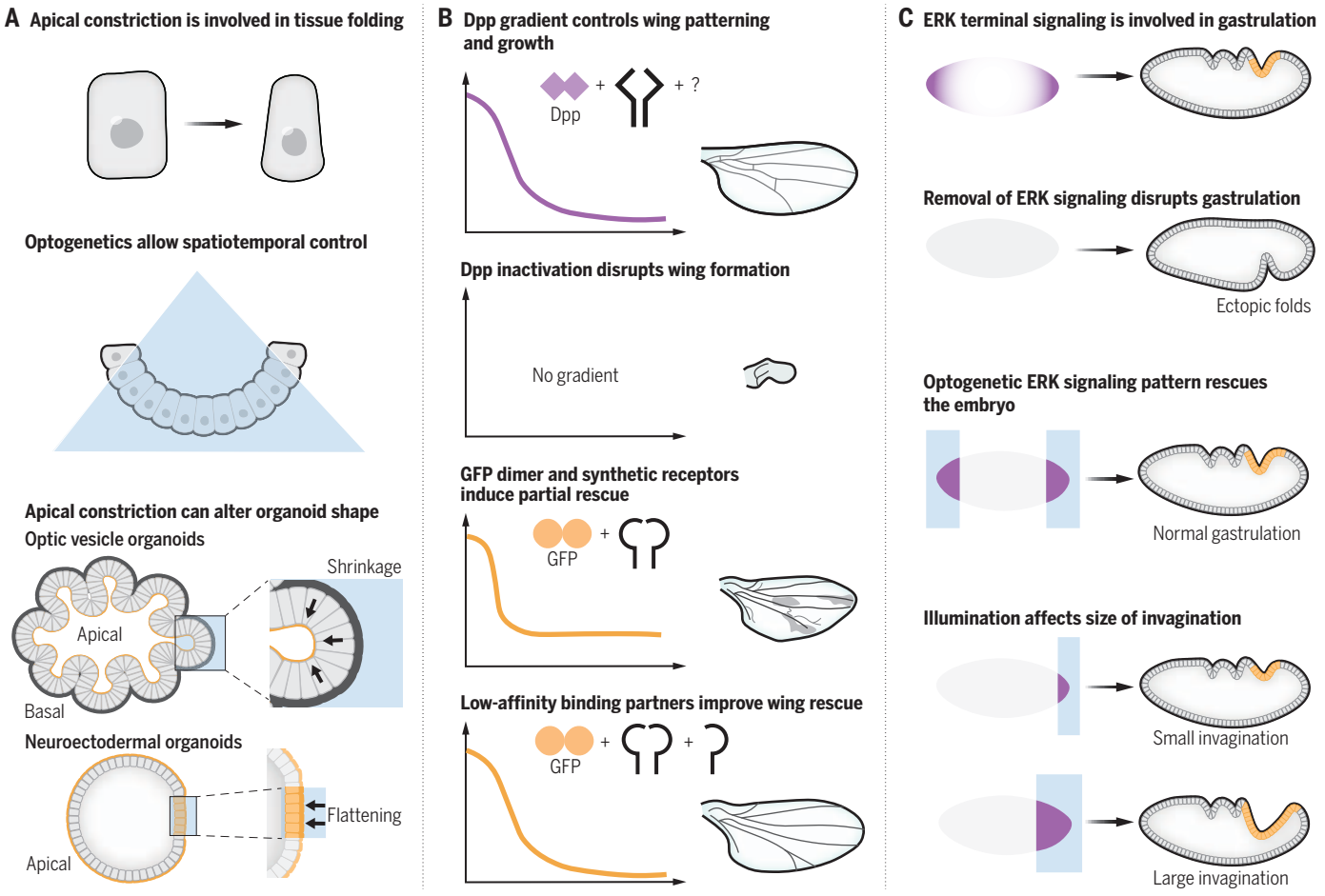

Fig. 2. Engineering of developmental processes in organoids and embryos. (**A**) Optogenetic control of apical constriction in neural organoids. (**B**) Construction of synthetic morphogen gradient to rescue wing patterning. (**C**) Optogenetic control of ERK signaling rescues embryonic development.

applications demonstrated that apical constriction can, in these contexts, modify tissue structure. It is expected that such dynamic control over biological forces will open the way to new studies about how such forces affect other developmental processes.

Synthetic biology techniques can also be applied to reconstitute processes in vivo, such as patterning or morphogenesis. In the *Drosophila* wing imaginal disc, the graded extracellular distribution of the Decapentaplegic (Dpp) morphogen [a homolog of bone morphogenetic protein (BMP)] induces a concentration-dependent signaling response in the underlying epithelium to organize vein patterning. To test the minimal requirements for morphogen gradient formation, Stapornwongkul *et al.* deleted the *dpp* allele and replaced it with green fluorescent protein (GFP) (Fig. 2B) (*30*). Anti-GFP nanobodies were used to engineer Dpp receptors to be responsive to extracellular GFP. Thus, the authors could restrict their observations to the extracellular part of the patterning system. An advantage of such experimental design is the knowledge of key components and their properties in the system. In combination with mathematical modeling, the authors suggested that both high-affinity signaling receptors and low-affinity glycosylphosphatidylinositol-anchored binding partners are needed to form a long-range, diffusion-based GFP gradient that could rescue wing patterning.

Similarly, optogenetic techniques were used to explore the spatiotemporal requirements of extracellular signal–regulated kinase (ERK) signaling in *Drosophila* embryonic development (Fig. 2C) (*31*). By deleting the tyrosine-kinase ligand *trk* and implementing optogenetic control of ERK signaling, the authors gained external control of signaling events. This allowed the rescue of gastrulation to be used as a functional readout to dissect ERK signaling requirements and evaluate robustness to ectopic signaling. The spatiotemporal precision of the optogenetic tool enabled study of how parameters, such as the duration of the pattern and its width, affect the formation of other structures later in development. These examples highlight how the substitution of natural components with synthetic ones can help to elucidate mechanisms of fundamental developmental processes.

Synthetic biology methods have proven useful to reconstitute developmental processes in simple in vitro systems. A minimalistic approach allows for the study of the sufficiency of the components to reconstitute the process. By contrast, engineering control over such processes in complex tissues opens opportunities to explore the parameters required for that specific tissue as well as to study the interactions with other developmental events. These two approaches can complement each other, creating a rich blend of experimental systems.

Engineering input, processing, and output in development

Despite such notable advances, the diversity of developmental processes that have been engineered is still limited. New tools must be developed for the synthetic developmental biology field to mature, and researchers will need to examine processes that are still underexplored. When engineering cells for synthetic

ILLUSTRATION: N. CARY/*SCIENCE*

biology purposes, it can be helpful to apply an input-processing-output work frame (Fig. 3). Inputs are perturbations that influence tissues with cells that have been engineered to perceive such perturbations. Processing encompasses all the changes that these perceptions cause inside the cells. Outputs are made up of all the interactions that cells might have in response to inputs and processing. Here, we summarize those processes that input, process, and output information in multicellular systems as well as point to those types of processes that remain mostly unexplored.

We can alter biological processes by adding drugs, hormones, ligands, or peptides. Through the design of synthetic receptors, cells can be made sensitive to specific compounds and proteins (*18*). For instance, initiation of transcription and induction of the formation of protein complexes can be triggered by ligands that are widely used by biologists (*32*, *33*). Moreover, tissue engineering technologies allow for the alteration of the structure and composition of the extracellular matrix by prepatterning gels with different ligands or modifying the physical properties of the gel (*34*, *35*). Optogenetics has made it possible to engineer light-sensitive biological processes through the use of protein pairs that will bind to each other upon illumination (*24*, *36*, *37*). These inputs (ligands, matrix, and light) have been heavily deployed in synthetic developmental biology.

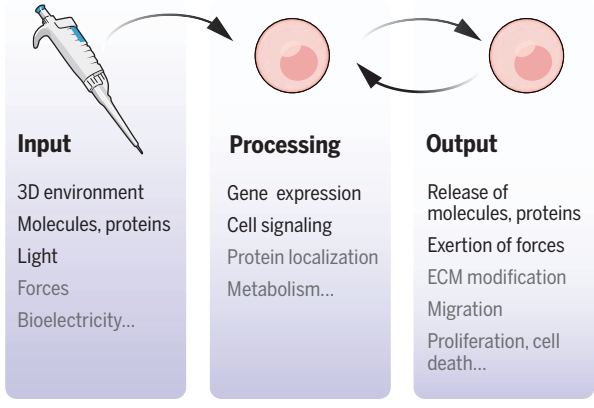

Fig. 3. Input-processing-output framework. Those processes that remain mostly unexplored are marked in gray. ECM, extracellular matrix.

However, there are still some aspects of input recognition whose engineering has remained mostly unexplored. Cells can perceive the forces that they are subjected to, and these forces can be translated to changes in the gene expression profile and protein distribution (*38*, *39*). Varied devices can be used to exert forces like stress or tension on tissues in vitro (*40*). We can engineer the perception of mechanical forces through reengineering of synNotch receptors to activate genes of interest in response to mechanical forces (*41*). New tools could be developed to engineer the recognition of stiffness and mechanical properties of the matrix. Another potential input to direct cellular systems is electricity. Electrical fields can affect development and regeneration (*42*). Efforts to use bioelectricity to direct development point out the possible applications of electrical fields to control collective migration (*43*). However, it remains to be studied how bioelectrical sensors can be repurposed to control other processes.

We define processing as all those changes that can be induced inside the cell, without necessarily affecting its environment. Complex networks can be introduced in the cell to further process signals and integrate them for decision making. The most commonly used layer of information processing is gene expression control. Inputs can be engineered to control the activation of a transcription activator or repressor or to lead to epigenetic modifications. We also include in this category the regulation of mRNA abundance, for instance through targeted mRNA degradation or stabilization (*44*). Similarly, protein concentrations can be manipulated by degron systems (*45*). Most efforts in engineering signal processing have focused on gene regulatory circuits with examples in bacteria and mammalian cells (*17*, *46*–*48*).

However, we expect that other levels of cell organization can also be used to store and process information. There are few works on how to engineer protein-protein interactions to store or process information (*49*). One possible way in which an input can alter the inner state of a cell is by reorganizing protein distribution. A protein of interest can be shuttled into a vesicle or an organelle, where it may provoke new interactions. Another possible yet underexplored way to process a signal inside the cell is by altering the metabolic state. Metabolic pathway activity can promote epigenetic and transcriptional changes through intermediate metabolites—such as acetyl–coenzyme A (acetyl-CoA), α-ketoglutarate, and oxidized nicotinamide adenine dinucleotide (NAD^+)—that function as substrates, cofactors, and allosteric regulators of posttranslational modification, such as methylation, acetylation, and glycosylation (*50*, *51*). A new layer of engineering could be created by targeting the metabolic state of the cells, which would then require more processing tools to read out this state into an output. Theoretically, a cell could be instructed to change the proportions in which each metabolic pathway is being used, altering the by-products generated and its available energy to be consumed in other processes.

After receiving inputs, processing, and storing information, cells can be programmed to exert changes on their environment in response to these inputs. At the same time, the outputs can be interpreted as new inputs for other cells. The same types of proteins, hormones, molecules, or peptides that can be read as inputs can be secreted as outputs by cells. Alternatively, proteins can be displayed on the plasma membrane. Expression of diffusible or membrane-bound ligands can propagate input signals along tissues, such as synNotch or the GFP morphogen mentioned above (*21*, *30*). Cells could also be programmed to alter the extracellular matrix through the expression of polymers, adhesion components, or enzymes for their degradation. Moreover, the expression of genes that will induce force-exerting processes will also affect the surrounding tissues and extracellular matrix. These forces can alter the shape or location of surrounding cells, which will also be sensed as an input. Light-induced apical constriction has been achieved (*28*, *29*), but tools for many other processes are lacking, including for the control of osmolarity and hydraulics. Local myosin relaxation can be achieved through the recruitment of a protein phosphatase binding domain to the plasma membrane (*52*). From a different perspective, cells might be triggered to change location toward or away from a biochemical or physical signal. The displacement could allow the cell to sense a new set of inputs in the new location and also to exert outputs (cell-cell contacts, forces, etc.) to the other cells in the newly occupied area. Work on the control of cell migration indicates that this output could be ready to be integrated into a synthetic circuit (*25*, *43*). Another possible output is the initiation of cell division or death. Both provoke forces on the surrounding tissue. Cell proliferation increases cell packing, whereas cell death lowers cell density and may additionally trigger the liberation of factors, phagocytosis, and regeneration. Although there are already optogenetic tools available for the induction of cell death (*27*), applications of these tools to study developmental processes remain to be explored. Finally, the specialization of cells can lead to more complex and fine-tuned functions. Some examples are hormone segregation, fluid pumping, synaptic connections, or muscle contraction. Further study is needed to understand in which contexts the induction of differentiation can provoke functional tissue structures. As with inputs and processing, there are still many output processes left to be explored.

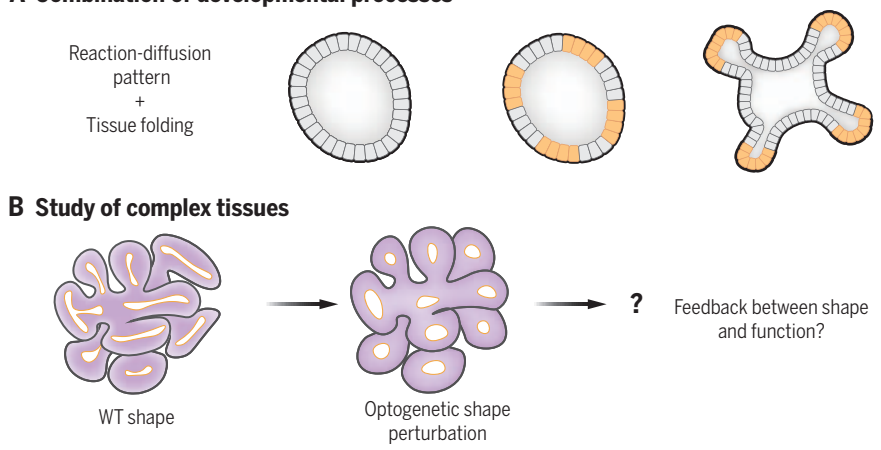

Fig. 4. Future perspectives for synthetic developmental biology. (**A**) The combination of developmental processes, such as reaction-diffusion patterning and tissue folding, can generate more complex in vitro models. (**B**) The application of synthetic biology approaches to organoids and embryos, such as the use of optogenetic tools to control tissue structure, will open new ways to study the interactions between different developmental processes. WT, wild-type.

Promising approaches for synthetic developmental biology

The design of tools to engineer input, process, and output mechanisms into cells will broaden the range of developmental processes that can be studied. Nevertheless, the future of synthetic developmental biology will not only be restricted to the creation of new tools. Combinations of different components to control two different developmental processes (e.g., cell communication and sorting) can be used to create complex reconstitutions in vitro (*19*). We foresee that the combination of new tools for controlling input, processing, and output will allow researchers to develop more elaborate models that implement more than one developmental process. For instance, combining patterning circuits with the expression of genes that direct morphogenesis or differentiation will result in synthetic tissues of higher complexity (Fig. 4A). The application of these approaches to study organoids and embryos should be further extended. With more available tools, researchers will be able to ask new questions about the interplay of developmental processes in complex systems. For example, the use of optogenetic tools to manipulate tissue shape presents the opportunity to alter organoid shape and study the feedback of shape change on other aspects of development (Fig. 4B).

Techniques of synthetic biology are increasingly used to address fundamental developmental biology questions from a new perspective. Advances in genome editing have allowed sophisticated cell engineering to reconstitute developmental processes, such as tissue folding, patterning, and cell sorting. Experiments with engineered cells and control systems have led to the identification of key components and mechanisms that are sufficient to drive processes in early development. Notably, the control over each component in the system enables not only the fine-tuning of their properties but also rigorous modeling, which can help explore system capabilities. Although such approaches have the ability to address the fundamental mechanisms that underlie complex processes, they also provide versatile tools that can be used to manipulate tissues. Particularly in the context of more complex in vitro systems, such as organoids, ex utero embryos, or synthetic embryos (*53*–*55*), these tools can be used to provoke informative feedback responses. So far, several input, processing, and output mechanisms have been engineered into different circuits, but there are still many types of processes left to be engineered. Making components interchangeable should facilitate the progress of the field. The combination of components to develop more complex reconstitution models and the application of synthetic biology tools to embryos and organoids are two valuable approaches that we expect will lead to further discoveries in synthetic developmental biology.

REFERENCES AND NOTES

1. D. St Johnston, *Nat. Rev. Genet.* **3**, 176–188 (2002).
2. C. Nüsslein-Volhard, E. Wieschaus, *Nature* **287**, 795–801 (1980).
3. A. Nasevicius, S. C. Ekker, *Nat. Genet.* **26**, 216–220 (2000).
4. M. R. Capecchi, *Science* **244**, 1288–1292 (1989).
5. J. A. Davies, *J. Anat.* **212**, 707–719 (2008).
6. M. B. Johnson, A. R. March, L. Morsut, *Curr. Opin. Biomed. Eng.* **4**, 163–173 (2017).
7. J. J. Velazquez, E. Su, P. Cahan, M. R. Ebrahimkhani, *Trends Biotechnol.* **36**, 415–429 (2018).
8. M. R. Ebrahimkhani, M. Ebisuya, *Curr. Opin. Chem. Biol.* **52**, 9–15 (2019).
9. M. Santorelli, C. Lam, L. Morsut, *Curr. Opin. Biotechnol.* **59**, 130–140 (2019).
10. S. Toda, J. M. Brunger, W. A. Lim, *Curr. Opin. Syst. Biol.* **14**, 41–49 (2019).
11. I. Zarkesh *et al.*, *Stem Cell Reports* **17**, 715–733 (2022).
12. H. M. McNamara, B. Ramm, J. E. Toettcher, *Semin. Cell Dev. Biol.* 10.1016/j.semcdb.2022.04.013 (2022).
13. M. A. Lancaster, J. A. Knoblich, *Science* **345**, 1247125 (2014).
14. H. Clevers, *Cell* **165**, 1586–1597 (2016).
15. M. Matsuda, M. Koga, K. Woltjen, E. Nishida, M. Ebisuya, *Nat. Commun.* **6**, 6195 (2015).
16. R. Goodyear, G. Richardson, *J. Neurosci.* **17**, 6289–6301 (1997).
17. R. Zhu, J. M. Del Rio-Salgado, J. Garcia-Ojalvo, M. B. Elowitz, *Science* **375**, eabg9765 (2022).
18. L. Morsut *et al.*, *Cell* **164**, 780–791 (2016).
19. S. Toda, L. R. Blauch, S. K. Y. Tang, L. Morsut, W. A. Lim, *Science* **361**, 156–162 (2018).
20. E. Cachat *et al.*, *Sci. Rep.* **6**, 20664 (2016).
21. S. Toda *et al.*, *Science* **370**, 327–331 (2020).
22. D. Greber, M. Fussenegger, *Nucleic Acids Res.* **38**, e174 (2010).
23. R. Sekine, T. Shibata, M. Ebisuya, *Nat. Commun.* **9**, 5456 (2018).
24. D. Krueger *et al.*, *Development* **146**, dev175067 (2019).
25. Y. I. Wu *et al.*, *Nature* **461**, 104–108 (2009).
26. X. Wang, L. He, Y. I. Wu, K. M. Hahn, D. J. Montell, *Nat. Cell Biol.* **12**, 591–597 (2010).
27. K. Shkarina *et al.*, *J. Cell Biol.* **221**, e202109038 (2022).
28. G. Martínez-Ara *et al.*, *Nat. Commun.* **13**, 5400 (2022).
29. E. Izquierdo, T. Quinkler, S. De Renzis, *Nat. Commun.* **9**, 2366 (2018).
30. K. S. Stapornwongkul, M. de Gennes, L. Cocconi, G. Salbreux, J.-P. Vincent, *Science* **370**, 321–327 (2020).
31. H. E. Johnson, N. J. V. Djabrayan, S. Y. Shvartsman, J. E. Toettcher, *Curr. Biol.* **30**, 3414–3424.e3 (2020).
32. A. T. Das, L. Tenenbaum, B. Berkhout, *Curr. Gene Ther.* **16**, 156–167 (2016).
33. J. H. Bayle *et al.*, *Chem. Biol.* **13**, 99–107 (2006).
34. G. A. Primo, A. Mata, *Adv. Funct. Mater.* **31**, 2009574 (2021).
35. A. J. Hughes *et al.*, *Dev. Cell* **44**, 165–178.e6 (2018).
36. T. R. Mumford, L. Roth, L. J. Bugaj, *Curr. Opin. Biomed. Eng.* **16**, 61–71 (2020).
37. J. Hartmann, D. Krueger, S. De Renzis, *Curr. Opin. Cell Biol.* **66**, 19–27 (2020).
38. F. Martino, A. R. Perestrelo, V. Vinarský, S. Pagliari, G. Forte, *Front. Physiol.* **9**, 824 (2018).
39. J. H.-C. Wang, B. P. Thampatty, *Biomech. Model. Mechanobiol.* **5**, 1–16 (2006).
40. A. R. Harris *et al.*, *Proc. Natl. Acad. Sci. U.S.A.* **109**, 16449–16454 (2012).
41. D. C. Sloas, J. C. Tran, A. M. Marzilli, J. T. Ngo, bioRxiv 2022.05.01.490205 [Preprint] (2022). https://doi.org/10.1101/2022.05.01.490205.
42. A. Pietak, M. Levin, *Prog. Biophys. Mol. Biol.* **137**, 52–68 (2018).
43. T. J. Zajdel, G. Shim, L. Wang, A. Rossello-Martinez, D. J. Cohen, *Cell Syst.* **10**, 506–514.e3 (2020).
44. B. DiAndreth, N. Wauford, E. Hu, S. Palacios, R. Weiss, *Nat. Commun.* **13**, 2582 (2022).
45. Y. Prozzillo *et al.*, *Biology* **9**, 421 (2020).
46. A. Becskei, L. Serrano, *Nature* **405**, 590–593 (2000).
47. M. B. Elowitz, S. Leibler, *Nature* **403**, 335–338 (2000).
48. T. S. Gardner, C. R. Cantor, J. J. Collins, *Nature* **403**, 339–342 (2000).
49. Z. Chen, J. M. Linton, R. Zhu, M. B. Elowitz, bioRxiv 2022.07.10.499405 [Preprint] (2022). https://doi.org/10.1101/2022.05.01.490205.
50. H. Miyazawa, A. Aulehla, *Development* **145**, dev131110 (2018).
51. O. A. Tarazona, O. Pourquié, *Dev. Cell* **54**, 282–292 (2020).
52. K. Yamamoto *et al.*, *Nat. Commun.* **12**, 7145 (2021).
53. S. Tarazi *et al.*, *Cell* **185**, 3290–3306.e25 (2022).
54. G. Amadei *et al.*, *Nature* **610**, 143–153 (2022).
55. A. Aguilera-Castrejon *et al.*, *Nature* **593**, 119–124 (2021).

ACKNOWLEDGMENTS

We apologize for all the relevant works that were left out because of the size limitation of the manuscript. **Funding:** This work was supported by EMBL. K.S.S. was supported by an EMBL interdisciplinary postdoctoral (EIPOD4) fellowship under H2020 Marie Skłodowska-Curie Actions COFUND 4 (grant agreement no. 847543) and a Human Frontier Science Program long-term postdoctoral fellowship (LT000685/2021). **Competing interests:** The authors declare no competing interests.

Submitted 26 August 2022; accepted 17 October 2022
10.1126/science.add9666

ILLUSTRATION: N. CARY/*SCIENCE*

RESEARCH

IN *SCIENCE* JOURNALS

Edited by **Michael Funk**

Dry grasslands, such as Patagonian rangeland, provide important ecosystem services.

PHOTO: JUAN J. GAITÁN

DRYLAND ECOLOGY

Complex effects of livestock

Livestock grazing provides food and livelihoods for billions of people but at the cost of ecosystem degradation in many places. Maestre *et al.* investigated how grazing by livestock and native herbivores affects ecosystem functions and services and how these effects vary with climate, soil properties, and biodiversity (see the Perspective by Ganguli and O'Rourke). Using a replicated survey at 98 dryland sites spanning six continents, the authors found that grazing effects on ecosystem services often depend on other factors. Interactions between grazing and climate were especially important; warmer sites had lower rates of carbon storage, organic matter deposition, and erosion control under high (but not low) grazing pressure. —BEL

Science, abq4062, this issue p. 915; see also add4278, p. 834

CRISPR

RNA-activated protein cleavage

CRISPR-Cas systems typically function as RNA-guided nucleases to protect bacteria against foreign genetic material; however, diverse associated genes have been identified within CRISPR-Cas systems, raising the possibility that new RNA-guided enzymatic functions exist in nature. One example is a CHAT family protease found next to the RNA-targeting CRISPR effector gRAMP. Strecker *et al*. found that this CRISPR-associated protease performs RNA-activated protein cleavage of a sigma factor inhibitor to activate a transcriptional response after infection. Characterization and engineering of this natural system allows for new possibilities in biology, including RNA-sensing applications in human cells. —DJ

Science, add7450, this issue p. 874

PHOTOCATALYSIS

Harnessing iron for photocatalysis

Good catalysts bind substrates at intermediate strengths so that neither reactant binding nor product desorption limits the reaction. Platinum group metals often meet this criterion for many reactions and cannot be replaced with cheaper metals such as iron, which often oxidize under reaction conditions. Yuan *et al*. demonstrate ammonia decomposition to liberate hydrogen with a copper-iron photocatalyst in which plasmons excited in copper generate hot electrons that react with ammonia bound to iron. Iron is not a good thermal catalyst for this reaction, but photoinduced oxygen desorption makes it competitive with a similar copper–ruthenium photocatalyst and with ruthenium thermal catalysts. This reaction, which is driven with light-emitting diodes, may be competitive with thermal catalysts used in this hydrogen carrier system. —PDS

Science, abn5636, this issue p. 889

CRISPR

Two enzymes in one

Apart from their RNA-guided nuclease activity, CRISPR systems encompass multiple accessory proteins that enhance or modulate immune functions. Kato *et al*. found that type III-E CRISPR systems include the caspase-like protease Csx29, which cleaves another accessory protein, Csx30, when activated upon target RNA recognition by Cas7-11. This cleavage yields toxic

Csx30 fragments that presumably inhibit the specialized sigma factor RpoE, modulate bacterial response to infection, and cause bacterial growth arrest, thereby abrogating phage infection. These findings expand the known complexity of CRISPR immune responses and enable the engineering of protease-based programmable RNA sensing in mammalian cells. —DJ

Science, add7347, this issue p. 882

PHYSIOLOGY

Human water requirements

Water requirements for human consumption may become more difficult to manage as changes occur in the Earth's climate and in human populations. Yamada *et al*. used an isotope-labeling technique to follow water intake and loss in individuals in a broad range of environments and living conditions. Total water input and output varied according to many factors, including body size, physical activity, air temperature, humidity, and altitude. The authors derived an equation to predict water usage according to such parameters. —LBR

Science, abm8668, this issue p. 909

CELL MIGRATION

Squeezing nuclei in neutrophils to fit

Neutrophils are among the first responders to infection and are recruited from the circulation by chemoattractant molecules called chemokines. Nuclei are the main source of friction as neutrophils squeeze through the confines of the interstitial space. Calì *et al*. found that the chemokine CXCL12, which was previously implicated in stimulating neutrophil migration, increased the deformability of nuclei in primary mouse neutrophils. CXCL12 activated the receptor ACKR3 to induce chromatin compaction, thereby facilitating neutrophil movement through restricted microenvironments in vitro. —JFF

Sci. Signal. **15**, eabk2552 (2022).

VACCINES

Sublingual vaccine for UTIs

Urinary tract infections (UTIs) affect a large percentage of the population. Many UTIs recur and some become chronic, resulting in a lower quality of life. Long-term antibiotic prophylaxis to manage UTIs alters the patient's microbiota, and this disturbance may give rise to antibiotic-resistant microbes. Kelly *et al.* designed mucus-penetrating, peptide-polymer nanofibers to enable sublingual (under the tongue) delivery of a vaccine against UTI-causing bacteria. Using a mouse model, they showed that this vaccine design is capable of eliciting antibody responses against uropathogenic *Escherichia coli* both systemically and in the urogenital tract. —ETP

Sci. Adv. 10.1126/sciadv.abq4120 (2022).

INNATE IMMUNITY

Another brick in the wall against herpes

A wide variety of host immune defenses are mobilized to contain human infection with the HSV-1 herpesvirus. Herpes simplex encephalitis (HSE) is a devastating outcome of HSV-1 infection that can indicate an underlying host immunodeficiency. Using whole-exome sequencing to search for a genetic etiology of HSE in a young boy, Naesens *et al.* discovered hypofunctional mutations in the *GTF3A* gene encoding the transcription factor IIIA (TFIIIA), which is a cofactor of RNA polymerase III, and found this to be the cause of impaired innate immunity to HSV-1. TFIIIA-mediated transcription of a host-derived noncoding ribosomal RNA pseudogene promoted the activation of the RIG-I cytoplasmic RNA sensor and a type I interferon response that contributes to HSV-1 control. These findings reveal another critical layer of innate defense that human cells use to control HSV-1 herpesvirus infections. —IRW

Sci. Immunol. **7**, eabq4531 (2022).

IN OTHER JOURNALS

Edited by **Caroline Ash** *and* **Jesse Smith**

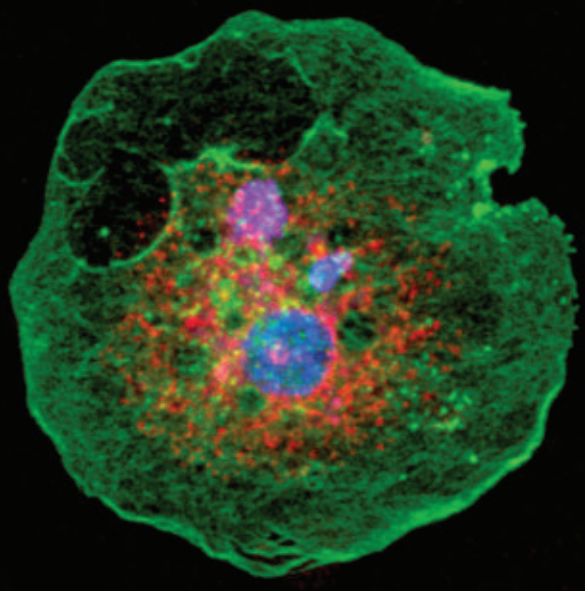

MALARIA

Mosquitoes mega fight back

Malaria parasites are transmitted by blood-feeding female *Anopheles* spp. mosquitoes. However, mosquitoes are not passive vectors: There are substantial physiological costs to carrying replicating malaria parasites. Barletta *et al.* investigated the role of the mosquito's Toll immune signaling responses by manipulating its suppressor, *Cactus*. Malaria parasites carried in the insect's blood meal attempted to burrow through the insect's midgut wall to reach a protected site for replication. By silencing *Cactus*, the authors found that plasmodium invasion triggered Toll signaling to stimulate immune cells called granulocytes to differentiate into super-large active and plastic megacytes. These cells surrounded the parasites and released mitochondria-like structures and microvesicles carrying an effector of the mosquito's complement-like system, which lysed the invaders. —CA *eLife* 10.7554/eLife.81116 (2022).

Transmission electron micrograph of a megacyte, a type of immune cell found in mosquitoes infected with malaria parasites.

IMAGE: BARLETTA *ET AL.*

NEURODEVELOPMENT

Stress overwhelms the hippocampus

Newborn mice exposed to at least one stressful event show reduced hippocampal synaptic pruning, which occurs during early normal development to remove redundant synapses in the brain. Dayananda *et al.* exposed newborn mice to a range of stressors and reported increased hippocampal synaptic density later in life compared with nonstressed animals. Reduced pruning was caused by impaired activity of phagocytic microglia and became more evident after a single stress compared with multiple adverse events. The authors suggest that reduced synaptic pruning might contribute to the

structural, behavioral, and cognitive changes seen in animals exposed to stressors in the early postnatal period. —MM

Brain Behav. Immun. **107**, 16 (2022).

EVOLUTION

Surviving on the roof of the world

The High Himalaya frog, *Nanorana parkeri*, is found only in the Tibetan Plateau at more than 4500 meters above sea level. Such altitudes present multiple challenges to species living there, one of which is high ultraviolet (UV) radiation. Excessive UV radiation can induce DNA damage, which can lead to cancer. However, species living at extreme altitudes have a variety of adaptations to cope with the dangers of UV exposure. In a comparison of the High Himalaya frog with its lower-elevation relatives, Fu *et al.* found a role for microRNAs in regulating the expression of genes in the frog's UV defense systems, including those involved in the regulation of cell cycle genes and skin antioxidant activity. —DJ

Proc. Natl. Acad. Sci. U.S.A. **119**, e2212406119 (2022).

CANCER

Signals to help clear tumors

Senescence is a cellular stress response associated with the release of specific proteins and the activation of signaling pathways that can trigger inflammation. Tumors are typically exposed to a variety of stressors such as hypoxia and nutrient shortages, and they are also stressed by anticancer treatments, so they usually contain senescent cells. Marin *et al*. and Chen *et al*. investigated the effects of senescence signals in the tumor microenvironment, showing that the presence of senescent cells stimulates innate and adaptive immune responses against the tumors. The authors looked at both cancer cells and senescent fibroblasts, and used different methods of inducing senescence to identify a range of approaches that might induce effective antitumor immune responses. —YN

Cancer Discov. 10.1158/2159-8290.CD-22-0523; 10.1158/2159-8290.CD-22-0528 (2022).

FRAMEWORK MATERIALS

A CO_2-induced shift

Two-dimensional covalent organic frameworks (2D-COFs) form as layers held together by van der Waals forces, and often stack with the atoms in registry, as seen in graphite. Kang *et al*. found that the 2D COF TAPB-OMeTA, formed by Schiff base condensation of 1,3,5-tris(4-aminophenyl)benzene and 2,5-dimethoxyterephthaldehyde, underwent slight lateral layer shifting during the adsorption of CO_2. Although the initial interaction of CO_2 with the layers was weak, after sufficient adsorption, the interaction became strong enough to shift the layers. This structural change accommodated more CO_2 and led to a sharp increase in adsorption. —PDS

J. Am. Chem. Soc. **144**, 20363 (2022).

APPLIED CHEMISTRY

A concentrated effort is detected

When present at levels approaching the critical micelle concentration, amphiphilic molecules change the bulk wetting properties of a solution. However, in many scenarios, detection at much lower concentrations is required. Yao *et al.* patterned silicon wafers with a square array of pillars, which were then functionalized with a self-assembled monolayer (SAM) lubricant and coated with silicone oil. This caused the amphiphiles inside a water droplet to concentrate and pin at the disordered, loosely packed SAM regions, and these largely overlapped with the droplet's contact line. The pinning forces affected the mobility of analyte-containing droplets, enabling measurement by visual inspection of the sliding angle, even when the concentration of amphiphiles was as low as five orders of magnitude below the amphiphile's critical micelle concentration. —MSL

Proc. Nat. Acad. Sci. U.S.A. **119**, e2211042119 (2022).

SCIENCE EDUCATION

Reframing the teaching of sex and orientation

Diversity is central in biology, the study of life. This includes diversity in sex and gender and in sexual, romantic, and related orientations. However, undergraduate biology courses tend to focus on a narrow representation of this diversity (e.g., binary sexes and heterosexual orientations). Casper *et al.* interviewed students with queer genders to better understand the narratives that these students encounter about sex and gender in undergraduate biology courses. Students described narratives that made biology implicitly exclusionary and explained how these narratives affect their sense of belonging, career preparation, and interest in biology content. Students also provided specific examples of unrealized potential for biology and biology courses to validate queer identities by representing the diversity in sex and orientation in biology. Suggestions for reframing the teaching of sex and orientation, derived from student interview data, are provided. —MMc

CBE Life Sci. Educ. 10.1187/cbe.21-12-0343 (2022).

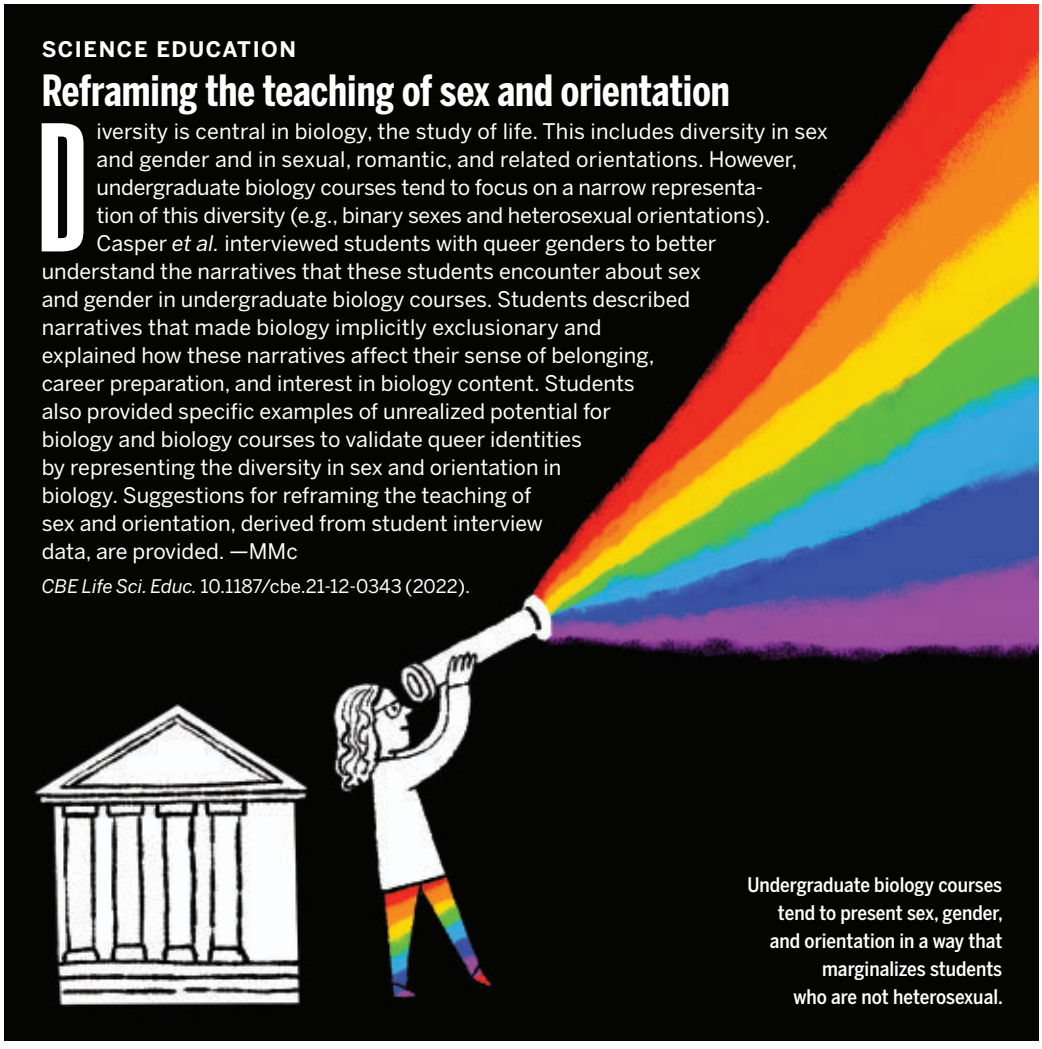

Undergraduate biology courses tend to present sex, gender, and orientation in a way that marginalizes students who are not heterosexual.

ILLUSTRATION: ROBERT NEUBECKER

ALSO IN *SCIENCE* JOURNALS

Edited by **Michael Funk**

MICROFABRICATION

Sweetening the transfer printing process

Micropatterning is the fabrication of specifically textured or patterned surfaces through either lithographic methods or the transfer of a prefabricated pattern using a sacrificial layer onto the substrate surface. However, the various methods generally only work for flat or gently curved surfaces. Zabow reports a method to do transfer printing on near arbitrary conformal surfaces using sugar (see the Perspective by Johnson). Corn syrup is added to the sugar to prevent it from crystallizing, and specific mixtures can be used to tailor the transfer substrate properties. Transfer is achieved using only gentle heating, and the sugar is readily dissolved away. Demonstrations include conformal coatings down vertical sidewalls, over sharp edges, and onto single strands of hair. —MSL

Science, add7023, this issue p. 894; see also ade6722, p. 826

VACCINES

A cornucopia of antigens

Vaccines serve as an indispensable tool for the control and prevention of influenza, but several challenges remain. Some populations, for example, the elderly, respond poorly to vaccination. Furthermore, the highly variable nature of influenza viruses can make targeting optimal antigens difficult. Broadly neutralizing antibodies have been proposed as a solution to such disadvantages, but they present their own pitfalls, including limited cross-reactivity to both influenza A and B strains and the need for repeated injections during flu season. Arevalo *et al*. developed a nucleoside-modified messenger RNA–lipid nanoparticle vaccine encoding hemagglutinin antigens from all 20 known influenza A and B virus subtypes (see the Perspective by Kelvin and Falzarano). Such vaccines may provide protection against antigenically variable viruses by simultaneously inducing antibodies against multiple antigens. —STS

Science, abm0271, this issue p. 899; see also adf0900, p. 827

ARTHROPOD EVOLUTION

Cambrian brain origin

Arthropods trace their evolutionary origins back to the Cambrian Period, and there has been continued debate about the origin of the brain in this speciose group. A prevailing view has been that the euarthropod brain was partly composed of ganglia originating from the ventral nervous system. However, Strausfield *et al*. describe the structure of the brain in a lobopodian from the Cambrian that is over 520 million years old, and found that instead the brain was already divided into three separate cerebral components even before the evolution of the head (see the Perspective by Briggs and Parry). These findings support the conclusion that the cerebral and caudal nervous system evolved differently in this group. —SNV

Science, abn6264, this issue p. 905; see also add7372, p. 831

GENE EDITING

Editing *RBM20* mutations

Gene therapies could potentially cure familial cardiomyopathies, but improvements in editing efficiency and avoidance of off-target gene editing are needed. Nishiyama *et al.* used highly precise adenine base editing (ABE) and prime editing (PE) approaches to correct pathogenic mutations in RNA-binding motif protein 20 (*RBM20*), which commonly cause familial dilated cardiomyopathy. In human induced pluripotent stem cell–derived cardiomyocytes, ABE corrected the *RMB20*^{R634Q} mutation with 92% efficiency of A-to-G editing, and PE corrected *RMB20*^{R636S} mutations with 40% efficiency of A-to-C editing. ABE correction of *Rbm20* in mice engineered to carry the R634Q mutation, which normally causes cardiac dysfunction, heart failure, and premature death, resulted in improved cardiac function and life span. These findings suggest that precise gene-editing approaches might be beneficial to treat familial dilated cardiomyopathies. —MN

Sci. Transl. Med. **14**, eade1633 (2022).

PLANETARY SCIENCE

Improving scientific inferences on Mars

Previous studies of Martian surface geology using mobile robotics have relied heavily on onboard analytical instruments that provide rock or mineral chemistry data alone. The Planetary Instrument for X-ray Lithochemistry (PIXL) on the Mars 2020 Perseverance rover enables the collection of both petrographic and chemical data for the same outcrops. In a study by Tice *et al.*, the PIXL team collected and analyzed an extensive dataset, finding that samples of the Sèìtah formation on the floor of Jezero crater consist of igneous crystalline minerals later altered by hydrothermal fluids. —KVH

Sci. Adv. 10.1126/sciadv.abp9084 (2022).

CORONAVIRUS

Prime and Spike passes the sniff test

Nearly 2 years after COVID-19 vaccines became widely available, a combination of waning vaccine-induced immunity and unabated viral mutations have resulted in reduced vaccine effectiveness. Mao *et al*. developed an alternative vaccine-boosting strategy they call "prime and spike" in animal models of COVID-19. After primary vaccination with a messenger RNA vaccine ("prime"), animals received an intranasal dose of unadjuvanted severe acute respiratory syndrome coronavirus 2 (SARS-CoV-2) spike protein ("spike"). This approach resulted in robust cellular and antibody-based immunity in the mucosa that protected animals as strongly and durably as a parenteral boost while also blocking viral transmission better. Spike could be administered in a variety of formulations and, if derived from SARS-CoV-1, could offer strong cross-protection against both viruses. —STS

Science, abo2523, this issue p. 872

NEURODEVELOPMENT

Synapse-specific translational control

Neurons, with their far-flung branches, cede some translational control to their periphery. In the adult brain, local protein synthesis occurs at synapses. Bernard *et al*. now show that decentralized control of protein synthesis also affects how developing neurons build synapses and circuits. Excitatory synapses forming on interneurons in the developing mouse cerebral cortex depend on messenger RNA translation that is responsive to which type of cell and which type of synapse is involved. —PJH

Science, abm7466, this issue p. 873

ATMOSPHERIC CHEMISTRY

Wildfires deplete the ozone layer

The Australian wildfires of late 2019 and early 2020 caused a substantial reduction in the thickness of the ozone layer. In a Perspective, Salawitch and McBride discuss the explanations for this reduction, including stratospheric wind patterns and wildfire-mediated chemical factors that drive photochemical loss of ozone. It is important to understand the effect of wildfires on stratospheric chemistry because wildfires are increasing in intensity and frequency. —GKA

Science, add2056, this issue p. 829

1848 SOCIETY
AAAS

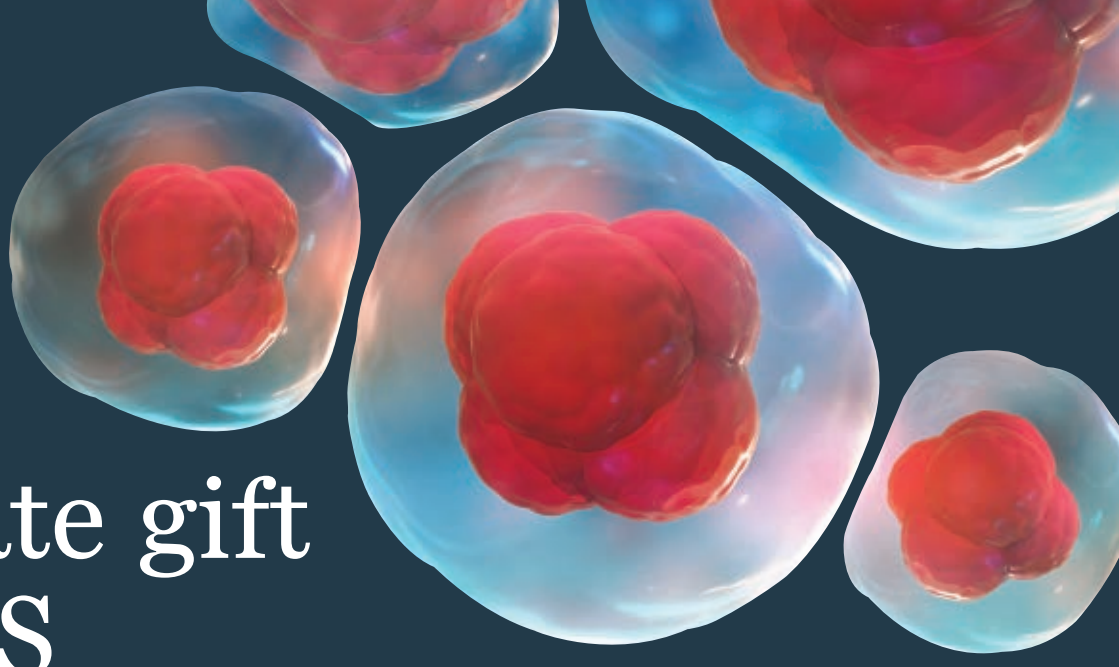

An estate gift to AAAS

Going all the way back to 1848, our founding year, the American Association for the Advancement of Science (AAAS) has been deeply committed to advancing science, engineering and innovation around the world for the benefit of all people.

Today, we are dedicated to advocating for science and scientific evidence to be fully and positively integrated into public policy and for the community to speak with one voice to advance science and engineering in the United States and around the world.

By making AAAS a beneficiary of your will, trust, retirement plan or life insurance policy, you will become a member of our 1848 Society and will help fuel our work on behalf of science and society – including publishing the world's most promising, innovative research in the *Science* family of journals and engaging in the issues that matter locally, nationally and around the world.

"As a teacher and instructor, I bear responsibility for the younger generations. If you have extra resources, concentrate them on organizations, like AAAS, that are doing work for all."

—Prof. Elisabeth Ervin-Blankenheim, 1848 Society member

If you intend to include AAAS in your estate plans, provide this information to your lawyer or financial adviser:

Legal Name: American Association for the Advancement of Science
Federal Tax ID Number: 53-0196568
Address: 1200 New York Avenue, NW, Washington, DC 20005

If you would like more information on making an estate gift to AAAS, cut out and return the form below or send an email to philanthropy@aaas.org. Additional details are also available online at **www.aaas.org/1848Society**.

AMERICAN ASSOCIATION FOR THE ADVANCEMENT OF SCIENCE

cut here

Yes, I would like more information about joining the AAAS 1848 Society.

1848 SOCIETY
AAAS

PLEASE CONTACT ME AT:

Name: _____

Address: _____

City: _____ State: _____ Zip code: _____ Country: _____

Email: _____ Phone: _____

RETURN THIS FORM TO:
AAAS Office of Philanthropy and Strategic Partnerships • 1200 New York Avenue, NW • Washington, DC 20005 USA

RESEARCH ARTICLE SUMMARY

CORONAVIRUS

Unadjuvanted intranasal spike vaccine elicits protective mucosal immunity against sarbecoviruses

Tianyang Mao†, Benjamin Israelow*†, Mario A. Peña-Hernández, Alexandra Suberi, Liqun Zhou, Sophia Luyten, Melanie Reschke, Huiping Dong, Robert J. Homer, W. Mark Saltzman, Akiko Iwasaki*

INTRODUCTION: During the first year of the severe acute respiratory syndrome coronavirus 2 (SARS-CoV-2) pandemic, multiple highly effective vaccines have been developed, using new technologies such as modified mRNA encapsulated in lipid nanoparticles and replication-deficient adenoviral vectors. Initial trials showed vaccine effectiveness >90% against symptomatic disease. Additional studies showed decreased infection rates of household contacts of vaccinated individuals, suggesting decreased rates of transmission. Unfortunately, waning immunity to vaccines and continued viral evolution with increasingly transmissible and immune-evasive variants have led to decreased vaccine effectiveness. Vaccines have also become much less effective at preventing transmission, which may be in part because of the poor induction of mucosal immunity within the respiratory tract.

RATIONALE: Although the goal of vaccination has been to prevent individual morbidity and mortality, the evolution of SARS-CoV-2 throughout the pandemic has highlighted the need for vaccines that better prevent transmission. Parenteral vaccines induce robust systemic immunity that is protective against disease. However, they induce poor immunity within the upper respiratory mucosa, where viral transmission occurs. Preclinical studies of both SARS-CoV-2 and influenza virus have demonstrated that intranasal vaccination decreases viral shedding and transmission relative to parenteral vaccines. Despite these studies, there is only one currently approved respiratory mucosal vaccine, FluMist, which is a live cold-adapted influenza virus. Most current clinical trials of mucosally administered SARS-CoV-2 vaccines rely on either replication-deficient or attenuated viral vectors, the safety and efficacy of which have yet to be established. All of these strategies become less effective with the development of antivector immunity. Here, we instead leverage preexisting immunity to boost mucosal immunity by intranasally administering unadjuvanted spike protein or mRNA. This consequently avoids the use of viral vectors or adjuvants in the respiratory tract.

RESULTS: We describe the preclinical development of an alternative vaccine strategy that we term "prime and spike" (P&S), which uses existing immunity generated by primary vaccination (prime) to elicit mucosal immune memory within the respiratory tract by using unadjuvanted intranasal spike booster. P&S elicits robust mucosal cellular and humoral memory responses, including the establishment of tissue-resident memory $CD8^+$ T cells, $CD4^+$ T cells, and B cells. Additionally, we found robust induction of mucosal immunoglobulin A (IgA) and IgG. Intranasal boosters can be delivered through distinct vaccine formulations, ranging from unadjuvanted trimeric recombinant spike proteins to spike-encoding mRNA encapsulated by immunosilent poly(amine-co-ester) (PACE) polymers. We found that an intranasal unadjuvanted spike booster can be administered months out from primary immunization and offers systemic neutralizing antibody responses comparable with that of mRNA–lipid nanoparticle (LNP) boost. P&S shows durability, leading to protection from lethal SCV2 challenge for as long as 118 days from vaccination. P&S is protective in hamsters and is superior to mRNA-LNP prime-boost at blocking transmission. Last, by using a divergent spike antigen from SARS-CoV-1, we demonstrate that P&S can generate mucosal immunity to SCV1 while also boosting systemic and mucosal neutralizing antibodies to SARS-CoV-2.

CONCLUSION: SARS-CoV-2 will continue to evolve and become more immune evasive and transmissible. We will require boosting in human populations for the foreseeable future. The respiratory mucosa provides a formidable barrier against viral pathogens after P&S administration. Therefore, strengthening mucosal immunity through vaccination holds substantial promise for enhancing protection and mitigating transmission. As new variants emerge, it will be a vital tool in combating other respiratory pathogens and the next pandemic. ■

The list of author affiliations is available in the full article online.
*Corresponding author. Email: benjamin.goldman-israelow@yale.edu (B.I.); akiko.iwasaki@yale.edu (A.I.)
†These authors contributed equally to ths work.

Cite this article as T. Mao *et al.*, *Science* 378, eabo2523 (2022). DOI: 10.1126/science.abo2523

READ THE FULL ARTICLE AT
https://doi.org/10.1126/science.abo2523

A parenteral prime-unadjuvanted mucosal boost vaccine that elicits mucosal immunity against sarbecoviruses. P&S converts systemic immunity generated by primary vaccination into local immunity in the respiratory mucosa. P&S affords protection against disease development, respiratory viral replication, and contact transmission after SARS-CoV-2 (SCV2) infection. Intranasal boosting by using a divergent spike protein from SARS-CoV-1 (SCV1) induces mucosal immunity against diverse sarbecovirus clades.

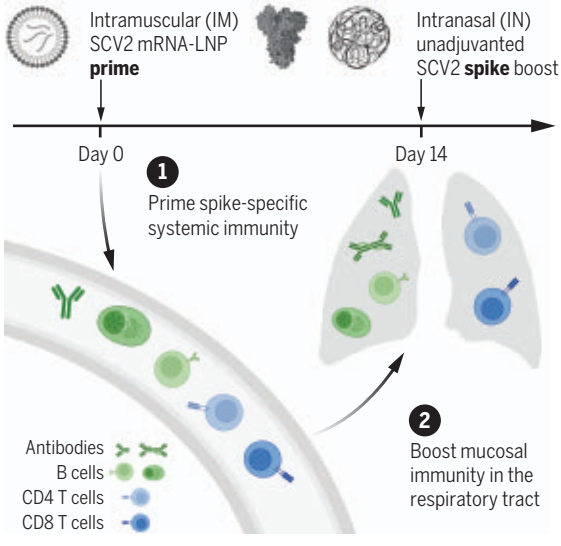

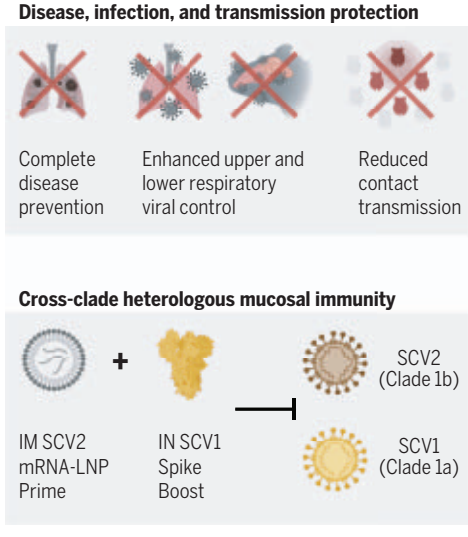

RESEARCH ARTICLE

CORONAVIRUS

Unadjuvanted intranasal spike vaccine elicits protective mucosal immunity against sarbecoviruses

Tianyang Mao[1]†, Benjamin Israelow[1,2]*†, Mario A. Peña-Hernández[1], Alexandra Suberi[3], Liqun Zhou[1], Sophia Luyten[1], Melanie Reschke[4], Huiping Dong[1], Robert J. Homer[5], W. Mark Saltzman[3,6,7,8], Akiko Iwasaki[1,9]*

The severe acute respiratory syndrome coronavirus 2 (SARS-CoV-2) pandemic has highlighted the need for vaccines that not only prevent disease but also prevent transmission. Parenteral vaccines induce robust systemic immunity but poor immunity at the respiratory mucosa. We developed a vaccine strategy that we call "prime and spike," which leverages existing immunity generated by primary vaccination (prime) to elicit mucosal immune memory within the respiratory tract by using unadjuvanted intranasal spike boosters (spike). We show that prime and spike induces robust resident memory B and T cell responses, induces immunoglobulin A at the respiratory mucosa, boosts systemic immunity, and completely protects mice with partial immunity from lethal SARS-CoV-2 infection. Using divergent spike proteins, prime and spike enables the induction of cross-reactive immunity against sarbecoviruses.

During the past 2 years of the severe acute respiratory syndrome coronavirus 2 (SARS-CoV-2) pandemic, there has been an unprecedented development of highly effective vaccines that use technologies including modified mRNA encapsulated in lipid nanoparticles (LNPs) and replication-deficient adenoviral vectors. Phase 3 clinical trials and subsequent postmarketing vaccine effectiveness studies initially showed >90% vaccine efficacy against symptomatic disease (*1*–*3*). Additionally, early transmission studies showed decreased rates of transmission in household members of vaccinated individuals (*4*, *5*). Unfortunately, recent studies have demonstrated decreasing vaccine effectiveness, starting 4 months after a second dose with mRNA-LNP–based regimens and earlier with other vaccines (*6*, *7*). Furthermore, continued viral evolution with increasing immune-evasive variants of concern (VOCs)—most recently, Omicron (B.1.529) and its sublineages—has also contributed to decreased vaccine effectiveness (*8*–*10*). With enhanced immune evasion and waning systemic immunity, current vaccines have become less effective at preventing viral transmission, which is likely worsened by increased viral transmissibility and their poor induction of mucosal immunity (*11*).

Currently approved SARS-CoV-2 vaccines rely on intramuscular (IM) administration, which induces high levels of circulating antibodies, memory B cells, and circulating effector $CD4^+$ and $CD8^+$ T cells in animal models and humans (*12*–*14*). However, parenteral vaccines do not induce high levels of potent antiviral immune memory at sites of infection, such as tissue-resident memory B cells (B_{RM} cells) and T cells (T_{RM} cells) as well as mucosal immunoglobulin G (IgG) and dimeric IgA (*15*–*17*). This contrasts with infection in humans and mice, in which $CD8^+$ T_{RM} cells and mucosal IgA are robustly induced (*15*, *18*). Vaccines that target the respiratory mucosa could address the shortcomings of parenteral vaccination; recent assessments of intranasally delivered SARS-CoV-2 spike encoding adenoviral vectors have shown mucosal immunogenicity as well as protection and reduced viral shedding in mice, hamsters, and nonhuman primates (*19*–*23*).

Although primary respiratory administration of vaccines induces mucosal immunity, systemic priming followed by intranasal (IN) boosting results in similar systemic immunity to systemic prime-boost regimens but with enhanced mucosal immunity (*24*–*26*). Most examples of recombinant subunit vaccines administered either systemically or IN are coformulated with adjuvants to enhance immunogenicity. However, administration of vaccines to the respiratory tract in humans has proven difficult. There have been cases of IN adjuvanted inactivated vaccine for seasonal influenza that have led to Bell's palsy, possibly caused by the specific toxin adjuvant mediating inflammation of neurons (*27*).

In the setting of nonprotective immunity from parenteral vaccination regimens, we assessed the immunogenicity and protection afforded by IN boosting with SARS-CoV-2 spike. We describe a vaccination strategy that uses systemic priming with mRNA-LNP followed by IN boosting with either unadjuvanted spike proteins or an immunosilent polyplex encapsulating spike mRNA.

Results

IN boosting with unadjuvanted SARS-CoV-2 spike induces mucosal humoral immunity

To assess the potential of IN unadjuvanted subunit vaccine boosting for the development of respiratory mucosal immunity, we decided to harness the strong systemic immunogenicity of mRNA-LNP. We additionally benefited from extensive SARS-CoV-2 spike engineering by using HexaPro, which has been shown to substantially enhance immunogenicity and increase protein stability (*28*).

We vaccinated K18-hACE2 (mice) with mRNA-LNP (Pfizer/BioNTech BNT162b2) by means of IM injection (prime), followed 14 days later with IN administration of recombinant unadjuvanted spike protein [prime and spike (P&S)]. Mice were euthanized at days 21 or 28 and assessed for mucosal humoral immunity (Fig. 1A).

First, we assessed anti–SARS-CoV-2 spike IgG and IgA in nasal wash (Fig. 1, B and C), bronchoalveolar lavage fluid (BALF) (Fig. 1, D and E), and serum (Fig. 1, F and G). Only mice that received P&S developed high levels of anti–SARS-CoV-2 IgA and IgG in the nasal wash and BALF. Neither IM prime nor IN spike alone was sufficient to develop mucosal antibodies. In the serum, prime alone was sufficient to induce low levels of IgA and IgG. By contrast, P&S led to significant systemic boosting of both anti-spike IgA and IgG. These increases in antibody levels correlated with increases in neutralization titers both in BALF (Fig. 1H) and serum (Fig. 1I). Thus, a single-dose unadjuvanted IN spike alone is not immunogenic, and the induction of a potent mucosal and systemic antibody response by unadjuvanted spike requires prior systemic priming, in this case with mRNA-LNP.

B_{RM} cells in the lungs assist in rapid recall response of antibody-secreting plasma cells upon secondary heterologous challenge in influenza models and may be an important local immune effector in protecting against SARS-CoV-2 (*29*). Using intravenous (IV) CD45 labeling to differentiate circulating immune cells within lung tissue combined with B cell tetramers specific for the receptor binding domain (RBD) of the spike protein, we found that P&S leads to increased antigen-specific B cells within lung tissue (IV-$CD45^-B220^+CD19^+$tetramer$^+$) (Fig. 1J). We also examined the polyclonal tissue response, which likely represents a more complete set of spike-specific B cells within the lungs. We found increases in class-switched antibody-secreting cells (ASCs) (IV-$CD45^-CD19^{+/-}CD138^+$)

[1]Department of Immunobiology, Yale University School of Medicine, New Haven, CT, USA. [2]Section of Infectious Diseases, Department of Medicine, Yale University School of Medicine, New Haven, CT, USA. [3]Department of Biomedical Engineering, Yale University, New Haven, CT, USA. [4]Department of Molecular Biophysics and Biochemistry, Yale University, New Haven, CT, USA. [5]Department of Pathology, Yale University School of Medicine, New Haven, CT, USA. [6]Department of Chemical and Environmental Engineering, Yale University, New Haven, CT, USA. [7]Department of Cellular and Molecular Physiology, Yale University, New Haven, CT, USA. [8]Department of Dermatology, Yale University, New Haven, CT, USA. [9]Howard Hughes Medical Institute, Chevy Chase, MD, USA.
*Corresponding author. Email: benjamin.goldman-israelow@yale.edu (B.I.); akiko.iwasaki@yale.edu (A.I.)
†These authors contributed equally to ths work.

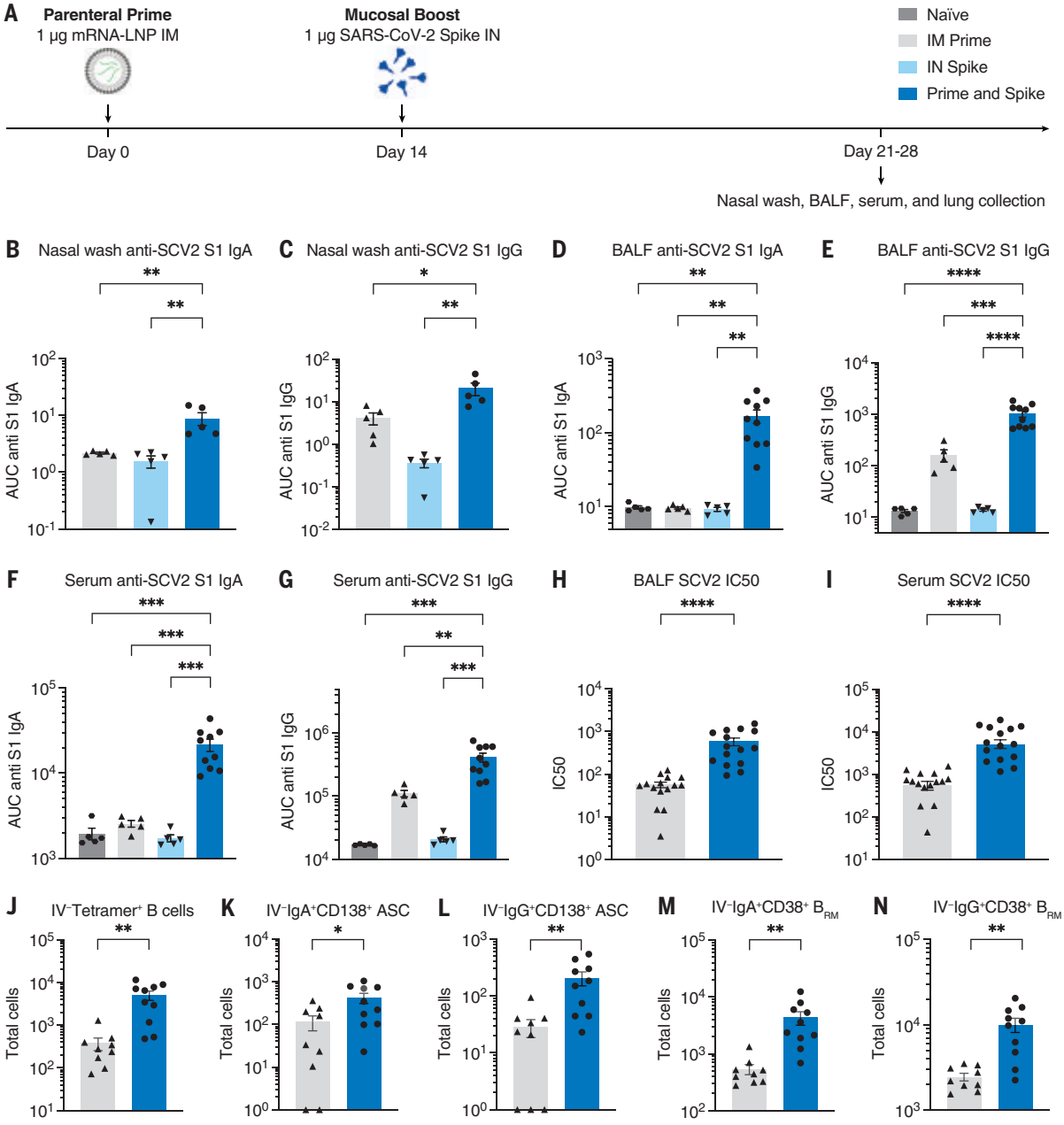

Fig. 1. IN boosting with stabilized SARS-CoV-2 spike induces mucosal humoral memory. (**A**) Experimental schema. Mice were intramuscularly immunized with 1 µg of mRNA-LNPs encoding full-length SARS-CoV-2 (SCV2) spike protein (Pfizer/BioNTech BNT162b2), followed by IN immunization with 1 µg of prefusion-stabilized (Hexapro), trimeric, recombinant SCV2 spike protein 14 days after mRNA-LNP immunization. Fourteen days after IN boost, serum, BALF, and nasal washes were collected to assess binding and neutralizing antibody responses. Lung tissues were collected for extravascular B cell analysis. (**B** to **G**) Measurement of SCV2 spike S1 subunit–specific (B) nasal wash IgA, (C) nasal wash IgG, (D) BALF IgA, (E) BALF IgG, (F) serum IgA, and (G) serum IgG in naïve mice, mice immunized with mRNA-LNP IM (IM Prime), mice immunized with the spike protein IN (IN Spike), or mice IM primed and IN boosted with spike (P&S). (**H** to **K**) Measurement of neutralization titer against SCV2 spike–pseudotyped vesicular stomatitis virus (VSV) in (H) BALF and (I) serum. (**J** to **N**) Using CD45 IV labeling, various extravascular (IV labeling antibody negative) B cell subsets were measured, including RBD tetramer-binding B cells, IgA^+ B_{RM} cells, IgG^+ B_{RM} cells, IgA^+ ASCs, and IgG^+ ASC in lung tissues from IM Prime or P&S mice. Mean ± SEM. Statistical significance was calculated by means of [(B) to (G)] one-way analysis of variance (ANOVA) or [(H) to (N)] Student's *t* test; $*P \le 0.05$, $**P \le 0.01$, $***P \le 0.001$, $****P \le 0.0001$. Individual data points are represented and are pooled from two or three independent experiments.

in lung tissue expressing IgA or IgG (Fig. 1, K and L), and we found increased class-switched B_{RM} cells (IV-$CD45^-B220^+CD19^+IgD^-IgM^-CD38^+$) expressing IgA or IgG (Fig. 1, M and N). Thus, P&S elicits local B cell responses in the lung.

Prime and spike induces mucosal T cell immunity

Given that P&S induced respiratory mucosal humoral memory, we next assessed the induction of lung T_{RM} cells. Although adjuvant-free subunit vaccines have not traditionally been potent inducers of antigen-specific T cell responses, we hypothesized that the immune memory generated by mRNA-LNP priming would enable subunit-mediated T cell–boosting responses. To identify spike-specific $CD8^+$ T cells,

we used major histocompatibility complex (MHC) class I tetramer $S_{539\text{-}546}$ (VNFNFNGL). There was a significant induction of IV-CD45$^-$tetramer$^+$ CD8$^+$ T cells, which expressed canonical markers of T_{RM} cells including CD69$^+$ and CD103$^+$, within lung tissue (Fig. 2, A to C), BALF (Fig. 2, D to F), and the nasal turbinate (Fig. 2, G to I). Moreover, there were significant increases in antigen-experienced CD4$^+$ T cells (IV-CD45$^-$CD44$^+$CD4$^+$), many of which also expressed CD69$^+$ and CD103$^+$ both within lung tissue (Fig. 2, J to L) and in the BALF (Fig. 2, M to O). Thus, P&S mediates expansion of lung parenchyma and airway CD8$^+$ T_{RM} and CD4$^+$ T_{RM} cells.

Host genotype, boosting interval, and IN volume have little effect on P&S

To assess whether mouse genotype, boosting interval, or boosting volume affected immunity induced by P&S, we compared mucosal CD8$^+$ T cell and antibody responses after P&S under varying conditions, including in K18-hACE2 versus C57B6/J (B6J) mice, 2-week versus 4-week boosting intervals, and 25- versus 50-μl IN inoculations (fig. S1A). Antigen-specific lung CD8$^+$ T_{RM} cells (fig. S1, B to D), BALF IgA and IgG (fig. S1, E and F), serum IgA and IgG (fig. S1, G and H), and serum neutralizing responses (fig. S1I) were similar among all groups and significantly higher than responses elicited by prime alone. These results support the robustness of P&S because multiple experimental variables can be modified without affecting overall immune responses.

Delayed-interval P&S induces mucosal immunity

We wondered whether boosting at an increased interval would affect P&S responses. To test this, mice received IM mRNA-LNP and were boosted with IN spike 84 days later. Humoral and cellular mucosal immune responses on days 91 and 140 were sampled (fig. S2A). Delayed P&S was sufficient to induce CD8$^+$ T_{RM} cells for at least 56 days (fig. S2, B to D). Polyclonal CD4$^+$ T_{RM} cells were induced early at 7 days after boost. However, their numbers appeared to wane by 56 days (fig. S2, E to G). Delayed P&S also resulted in enhanced mucosal IgA and IgG in BALF (fig. S2, H and I) and serum IgA and IgG (fig. S2, J and K) at 56 days after boost. Thus, P&S administered even up to 3 months after priming elicits durable mucosal humoral and cellular immune responses.

IN delivery of mRNA polyplexes also mediates mucosal boosting

Poly(amine-co-ester)s (PACEs) are biodegradable terpolymers that have been developed to encapsulate and deliver nucleic acids such as mRNA to specified tissues in vivo (*30*). Recent studies have shown that mRNA-LNP delivered to the respiratory tract is lethal in a dose-dependent manner in mice (*31*). By contrast, PACE materials have been developed to be

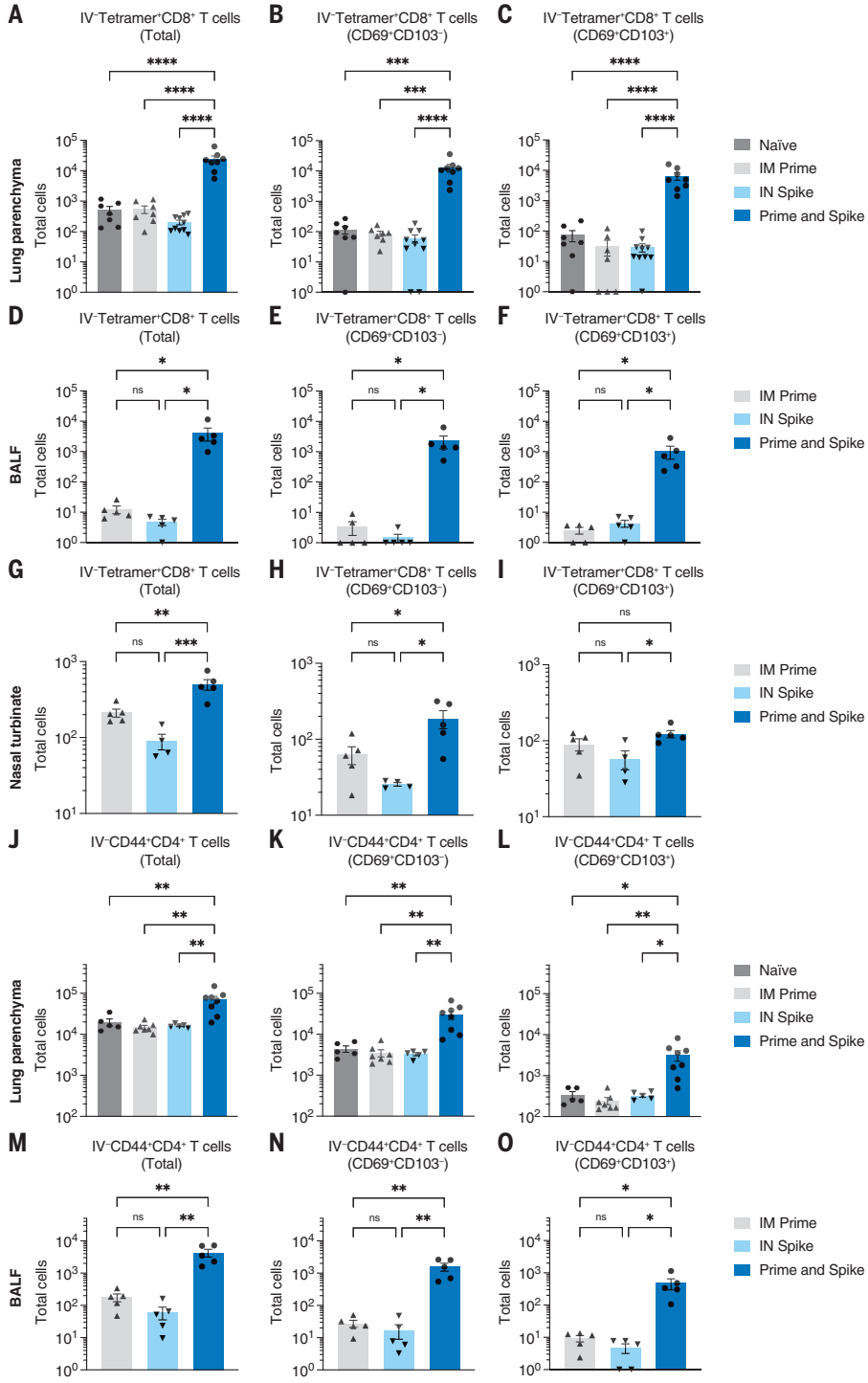

Fig. 2. IN boosting with stabilized SARS-CoV-2 spike induces mucosal T cell memory. K18-hACE2 mice were intramuscularly primed with 1 μg mRNA-LNP and 14 days later intranasally boosted with 1 μg SCV2 spike. Lung tissues, BALF, and nasal turbinates were collected for extravascular T cell analysis. Lung tissues were collected 14 days after boost, whereas BALF and nasal turbinates were obtained 7 days after boost. (**A** to **I**) Extravascular CD8 T cell responses. Shown are quantification of SCV2 spike–specific tetramer$^+$ CD8 T cells, CD69$^+$CD103$^-$tetramer$^+$ CD8 T cells, or CD69$^+$CD103$^+$tetramer$^+$ CD8 T cells in [(A) to (C)] lung tissues, [(D) to (F)] BALF, or [(G) to (I)] nasal turbinates from naïve, IM prime, IN spike, or P&S mice. (**J** to **O**) Extravascular CD4 T cell responses. Shown are quantification of activated polyclonal CD4 T cells, CD69$^+$CD103$^-$ CD4 T cells, or CD69$^+$CD103$^+$ CD4 T cells in [(J) to (L)] lung tissues or [(M) to (O)] BALF from naïve, IM prime, IN spike, or P&S mice. Mean ± SEM. Statistical significance was calculated by means of [(B) to (O)] one-way ANOVA followed by Tukey's correction; *$P \le 0.05$, **$P \le 0.01$, ***$P \le 0.001$, ****$P \le 0.0001$. Individual data points are represented and are pooled from two or three independent experiments.

relatively immunologically silent, enabling administration to locations more susceptible to immunopathology such as the respiratory tract. Chemically modifying PACE with polyethylene glycol dramatically improves in vivo lung delivery (*32*). To assess the utility of PACE encapsulating mRNA encoding spike protein as an IN booster, mRNA was extracted from BNT162b2 and encapsulated in PACE. Mice were primed intramuscularly with mRNA-LNP and boosted with IN spike mRNA encapsulated in PACE (PACE-spike). Additional control groups included PACE-spike only and IM prime + extracted mRNA (naked mRNA) (fig. S3A). Similar to what we found with P&S, prime and PACE-spike induced antigen-specific $CD8^+$ T_{RM} cells (IV-$CD45^-$tetramer$^+CD69^+CD103^+$) (fig. S3, B to D). Additionally, PACE-spike–boosted mice developed high levels of BALF IgA. Levels of BALF IgG and serum IgA and IgG were similar to IM prime alone (fig. S3, E to H). IM prime followed by IN naked mRNA was unable to induce mucosal or systemic immune responses above that of IM prime alone, indicating that mRNA encapsulation by PACE was required for mucosal boosting. Additionally, a single dose of IN PACE-spike alone was insufficient to elicit any detectable mucosal or systemic antibody response at this dose.

IN spike or IN PACE-spike boosts suboptimal prime to protect against lethal SARS-CoV-2 challenge

Although current vaccines were initially extremely effective at eliciting protective immunity, waning antibody levels and immune evasion will necessitate boosters for the foreseeable future. The best approach to boosting remains an open question. To test whether IN administration would provide an alternative protective boost, we used a low-dose (LD) 0.05 μg of mRNA-LNP vaccine to mimic nonprotective immunity. We have previously shown that this dose is insufficient to protect from SARS-CoV-2 challenge despite inducing systemic antibody responses (*15*). Mice intramuscularly primed with LD mRNA-LNP and boosted with IN spike developed antigen-specific lung $CD8^+$ T_{RM} cells and IgA and IgG in the BALF at 42 days after boost (fig. S4). Thus, low levels of immune memory allow for effective mucosal boosting of humoral and cellular responses by unadjuvanted IN spike.

Naïve, LD prime only, or LD P&S mice were challenged with SARS-CoV-2 and assessed for viral burden at 2 days after infection, assessed for lungs pathology at 5 days after infection, or monitored for weight loss and mortality for 14 days (Fig. 3A). All mice vaccinated with P&S were completely protected from weight loss or death, but neither naïve nor LD prime–only mice were protected (Fig. 3, B to D). This protection was accompanied by reduced viral burden in both the upper respiratory tract (nasal turbinates) and lower respiratory tract (lungs) (Fig. 3, E and F). Furthermore, P&S led to significant protection from lung pathology, with only one of six mice developing limited mononuclear infiltrates at 5 days after infection (Fig. 3, G and H). Next, to assess the protective capacity of PACE-spike IN boost, we again immunized mice with LD mRNA-LNP intramuscularly and boosted them intranasally with PACE-spike mRNA. Prime and PACE-spike resulted in significant protection from morbidity and mortality (Fig. 3, I to L). Thus, P&S represents a robust, versatile, and safe vaccine strategy because IN boosting by either IN unadjuvanted spike or PACE-spike is sufficient to induce mucosal immunity and to provide protection against lethal challenge and COVID-19–like pulmonary disease.

P&S achieves robust systemic booster responses similar to parenteral mRNA-LNP

IM mRNA-LNP–based boosts are the current standard. Thus, we compared systemic and mucosal immune responses in P&S-vaccinated and IM mRNA-LNP prime-boost–vaccinated mice (Fig. 4A). Only P&S-vaccinated animals developed lung IV-$CD45^-$tetramer$^+CD8^+$ T cells that express $CD69^+$ and $CD103^+$ (Fig. 4, B to D). The peptide sequence corresponding to spike 62-76 (S62-76) is an epitope recognized by $CD4^+$ T cells in convalescent C57BL/6 mice (*33*). We therefore developed an MHC class II tetramer S62-76 (VTWFHAIHVSGTNGT) that readily identified lung-resident $CD4^+$ T cells in both P&S and convalescent mice (fig. S5). Both infection and vaccination similarly led to increased IV-$CD45^-$tetramer$^+CD4^+CD69^+CD103^-$ T_{RM} cells. P&S induced significantly higher levels of lung-resident antigen-specific $CD4^+$ T cells that phenotypically resemble infection-induced $CD4^+$ T cells (IV-$CD45^-$tetramer$^+CD69^+CD4^+$) (Fig. 4, E and F). To further characterize the $CD4^+$ T_{RM} cell response, we used a peptide stimulation assay and found that P&S led to a higher number of tissue-resident $CD4^+$ T helper type 1 (T_H1) and T_H17 but not T_H2 $CD4^+$ T cells (Fig. 4, G to K). P&S also led to the induction of polyfunctional lung resident T_H1 cells (fig. S6, B to E).

P&S-vaccinated but not prime-boost–vaccinated animals developed increased levels of BALF IgA (Fig. 4L). Although BALF IgG levels were increased in prime-boost relative to naïve, P&S developed significantly higher BALF IgG than that of prime-boost (Fig. 4M). Serum IgA and IgG in prime-boost– and P&S-vaccinated mice were similar (Fig. 4, N and O), as were neutralizing antibody levels (Fig. 4P). Thus, P&S induces similar systemic binding and neutralizing antibody levels—a correlate of protection in humans—and elicits mucosal IgA, IgG, $CD4^+$ T_{RM} cells, and $CD8^+$ T_{RM} cells. Only P&S elicits T_H1 and T_H17 $CD4^+$ T_{RM} cells and not pathogenic T_H2 cell responses, which have been associated with vaccine-associated enhanced disease (VAED) (*34*).

To compare the protective efficacy of P&S to mRNA-LNP prime-boost, mice were primed with LD mRNA-LNP and boosted with either LD mRNA-LNP (intramuscularly) or unadjuvanted spike protein (intranasally). Mice were challenged 118 days after prime. Both vaccine strategies led to roughly equivalent protection from death, with two of nine prime-boost mice and zero of nine P&S mice succumbing to infection (Fig. 4, Q and R). P&S led to significantly enhanced disease-free survival indicated by only one of nine mice losing >5% of initial body weight, whereas six of nine mRNA-LNP prime-boost mice lost >5% of their starting body weight (Fig. 4S). P&S also led to enhanced upper-airway protection, indicated by decreased nasal turbinate viral load, and reduced although not statistically significant lower airway viral load (Fig. 4, T and U).

P&S reduces transmission in a hamster model of SARS-CoV-2

Next, we used Syrian hamsters to assess both the viability of P&S in an alternate SARS-CoV-2 model and its ability to reduce transmission. Hamsters were vaccinated by means of either IM mRNA-LNP prime-boost or P&S (Fig. 5A). Serum IgA and IgG levels at 67 days after prime were equivalent between the two groups (Fig. 5, B and C). Hamsters were infected with SARS-CoV-2 at 93 days after prime, and both groups were equivalently protected from disease, as indicated by minimal weight loss and reduced lung pathology relative to those of naïve animals (Fig. 5, D and E). P&S-vaccinated animals cleared viral shedding more quickly relative to naïve controls starting at 4 days after infection, with all oral swabs negative for infectious virus by 5 days after infection. Conversely, mRNA-LNP prime-boost animals did not have significantly lower titers at 4 or 5 days after infection and did not stop shedding virus until 6 days after infection. Cumulative viral shedding assessed with area under the curve (AUC) revealed that both mRNA-LNP prime-boost and P&S-vaccinated animals had significantly lower overall viral shedding than naïve animals. Although P&S AUC was less than mRNA-LNP prime-boost, the results were not statistically significant.

Although P&S reduced viral shedding after infection, whether P&S was able to reduce transmission to vaccinated animals was not yet determined. Vaccinated hamsters were therefore cohoused with naïve donor hamsters that had been infected 24 hours prior (Fig. 5J). P&S-vaccinated contact hamsters had significantly lower viral titers at days 2, 4, and 5 after exposure relative to naïve, whereas mRNA prime-boost–vaccinated animals did not have significantly reduced viral shedding at any single time point after exposure (Fig. 5, L to N). Both P&S and mRNA prime-boost were equally protected from lower respiratory tract pathology in the setting of transmission (Fig. 5K and fig. S7). Peak viral load (at 2 days after infection) and

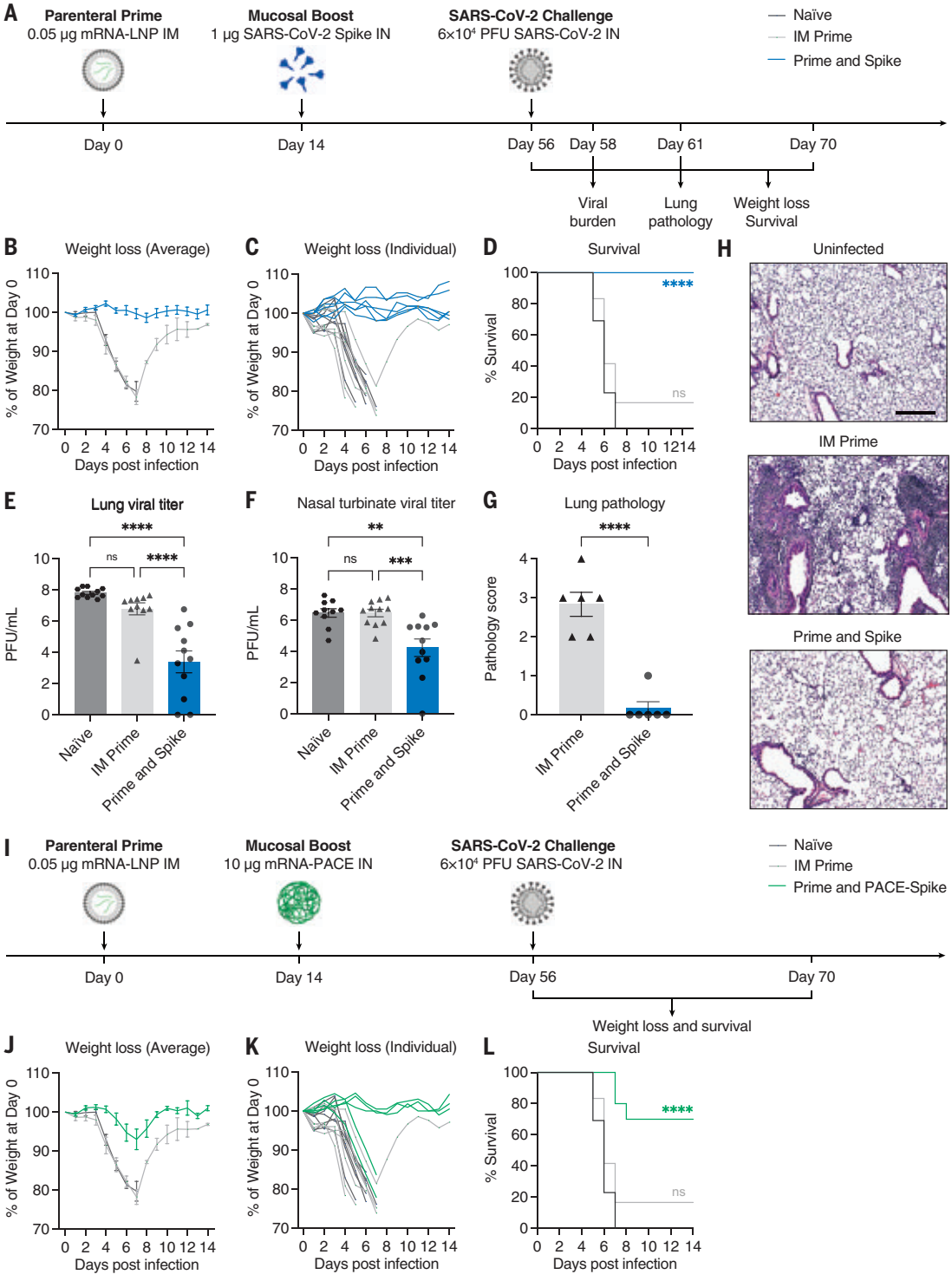

Fig. 3. IN SARS-CoV-2 spike boosting protects against COVID-19–like disease. (**A**) Experimental schema. K18-hACE2 mice were intramuscularly primed with 0.05 µg of mRNA-LNP and intranasally boosted with 1 µg of spike 14 days after IM prime. Six weeks after boost, mice were challenged with 6 × 10^4 PFU SCV2 (2019n-CoV/USA_WA1/2020). The first cohort was used to evaluate weight loss and survival up to 14 days after infection. The second cohort was used to collect lung and nasal turbinate tissues 2 days after infection for viral titer measurement. The third cohort was used to collect lung tissues 5 days after infection for histological assessment. (**B** to **D**) Weight loss and survival of naïve, IM prime, or P&S mice from 1 to 14 days after infection. (**E** to **F**) Measurement of infectious virus titer in lung and nasal turbinate tissues at 2 days after infection by means of plaque assay. (**G**) Pathology score of lung sections at 5 days after infection by means of H&E staining. (**H**) Representative H&E staining results from uninfected, IM prime, or P&S mice. Scale bar, 250 µm. Sections are representative of multiple sections from at least five mice per group. (**I**) Experimental schema. K18-hACE2 mice were intramuscularly primed with 0.05 µg of mRNA-LNP and intranasally boosted with 10 µg of mRNA encapsulated by PACE (IN PACE-Spike) 14 days after IM Prime. Six weeks after boost, mice were challenged with 6 × 10^4 PFU SCV2 (2019n-CoV/USA_WA1/2020). Weight loss and survival were monitored up to 14 days after infection. (**J** to **L**) Weight loss and survival of naïve, IM prime, or prime and PACE-spike K18-hACE2 mice from 1 to 14 days after infection. Mean ± SEM. Statistical significance was calculated by means of [(D) and (L)] log-rank Mantel-Cox test, [(E) and (F)] one-way ANOVA followed by Tukey's correction, or (G) Student's *t* test; *$P \leq 0.05$, **$P \leq 0.01$, ***$P \leq 0.001$, ****$P \leq 0.0001$. Individual data points are represented and are pooled from two independent experiments.

cumulative viral shedding were significantly reduced in P&S-vaccinated animals relative to both naïve and mRNA-LNP prime-boost contact hamsters (Fig. 5O). Thus, P&S appears to be an effective vaccine strategy in hamsters and reduces viral transmission.

Heterologous spike robustly elicits cross-reactive immunity

Boosting at a distinct anatomic location—in this case, the respiratory mucosa—by homologous unadjuvanted subunit spike enables the formation of new mucosal immune memory and enhances systemic immunity. However, VOCs such as current Omicron sublineages have substantial changes to the spike protein sequence, leading to evasion of preexisting humoral immunity. It is likely that future variants will diverge even more, which suggests that a

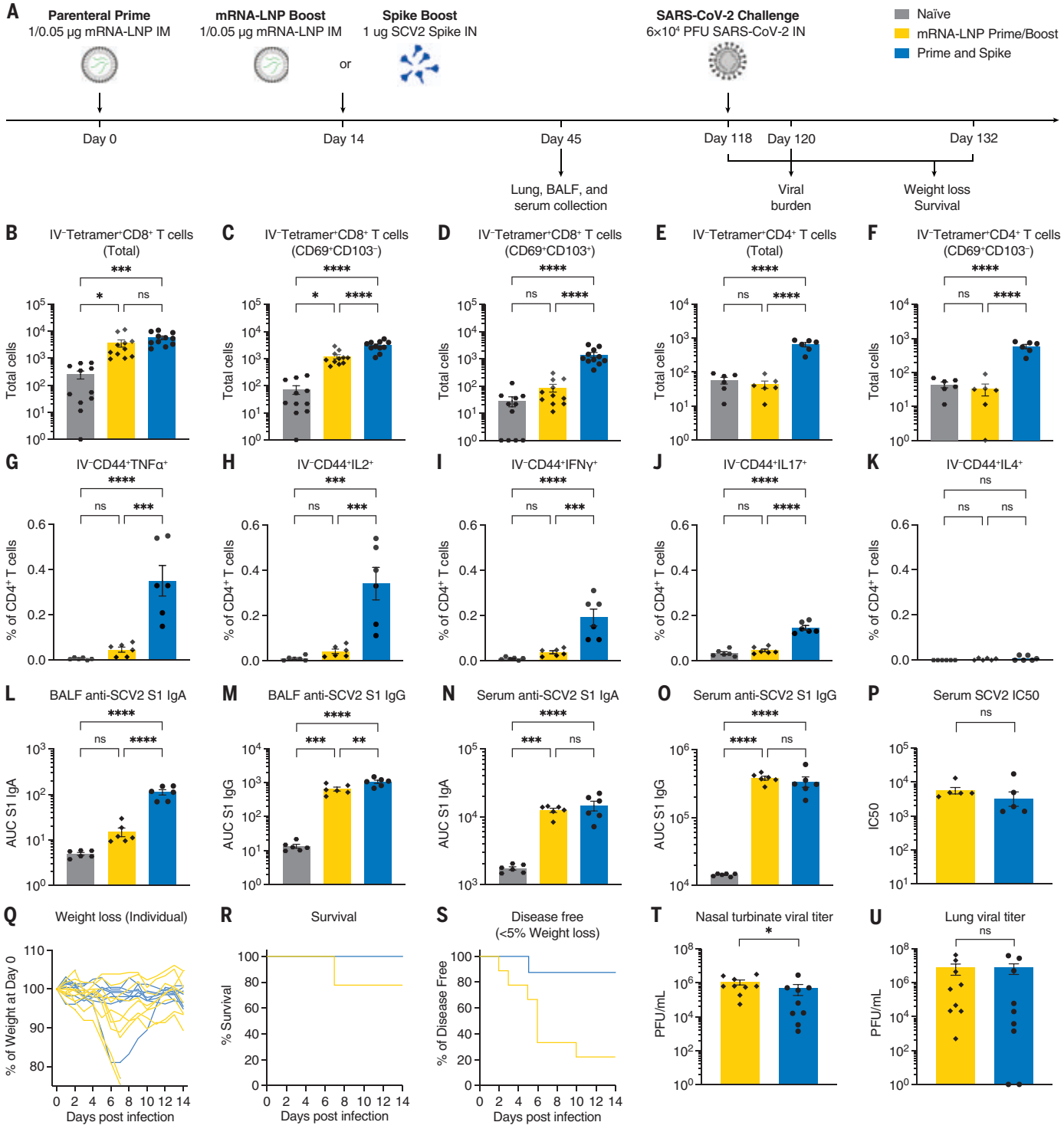

Fig. 4. IN spike boosting elicits enhanced mucosal immunity with similar systemic humoral responses to IM mRNA-LNP boosting. (**A**) Experimental schema. K18-hACE2 mice were IM primed with 1 μg of mRNA-LNP, followed 14 days later by boosting with 1 μg of mRNA-LNP IM or 1 μg of SCV2 spike IN. Forty-five days after prime, lung tissues were collected for T cell analysis by means of flow cytometry, and BALF and serum were collected for antibody measurement. K18-hACE2 mice were intramuscularly primed with 0.05 μg of mRNA-LNP, followed 14 days later by boosting with 0.05 μg of mRNA-LNP intramuscularly, or 1 μg of SCV2 spike intranasally and challenged with 6×10^4 PFU SCV2 at 118 days after prime. (**B** to **D**) Quantification of total tetramer$^+$ CD8 T cells, CD69$^+$CD103$^-$tetramer$^+$ CD8 T cells, or CD69$^+$CD103$^+$tetramer$^+$ CD8 T cells in lung tissues from naïve, mRNA-LNP prime-boost, or P&S mice. (**E** to **F**) Quantification of total tetramer$^+$ CD4 T cells or CD69$^+$CD103$^-$tetramer$^+$ CD4 T cells in lung tissues. (**G** to **K**) Lung lymphocytes were isolated by means of Percoll gradient and restimulated with spike peptide megapool from SCV2. Intracellular cytokine staining was performed to assess antigen-specific production of TNF-α, IL-2, IFN-γ, IL-17, and IL-4 by extravascular IV-CD45$^-$CD44$^+$ CD4 T cells. (**L** to **O**) Measurement of SCV2 spike S1 subunit–specific (L) BALF IgA, (M) BALF IgG, (N) serum IgA, and (O) serum IgG in naïve, mRNA-LNP prime-boost, or P&S mice. (**P**) Measurement of neutralization titer against

SCV2 spike–pseudotyped VSV. (**Q** to **S**) Weight loss, survival, and disease-free survival (<5% maximum weight loss) of mRNA-LNP prime-boost or P&S mice from 1 to 14 days after infection. (**T** and **U**) Measurement of infectious virus titer in lung and nasal turbinate tissues at 2 days after infection by means of plaque assay. To reduce overall number of experimental animals used, control data points from naïve and mRNA prime-boost are common to Figs. 4 and 6. Mean ± SEM. Statistical significance was calculated by means of [(B) to (O)] one-way ANOVA followed by Tukey's correction or [(P), (T), and (U)] Student's *t* test, and [(R) and (S)] log-rank Mantel-Cox test; $*P \le 0.05$, $**P \le 0.01$, $***P \le 0.001$, $****P \le 0.0001$. Individual data points are represented and are pooled from two independent experiments.

boosting strategy that elicits broadly reactive immunity will be necessary to neutralize future variants.

To test the ability of an unadjuvanted heterologous spike (Spike X) protein in P&S, mice were primed with SARS-CoV-2 mRNA-LNP followed by IN boosting with SARS-CoV-1 spike, which we refer to as P&Sx (Fig. 6A). Although SARS-CoV-1 is a related sarbecovirus, its spike protein only shares 76% homology with SARS-CoV-2 spike. At 45 days after prime, there were increased IV-CD45$^-$ tetramer$^+$ CD8$^+$ T_{RM} cells (Fig. 6, B to D). The MHC class I tetramer sequence was highly conserved within the sarbecovirus family (fig. S5A). We performed peptide stimulation assay using both SARS-CoV-1 and SARS-CoV-2 peptide pools to assess the development of antigen-specific lung CD4$^+$ T_{RM} cells. We found that P&Sx led to both the development of SARS-CoV-1–specific and to a lesser extent SARS-CoV-2–specific antigen-specific T_H1 and T_H17 CD4$^+$ T_{RM} cells and no induction of CD4$^+$ T_{RM} expressing the T_H2 cytokine interleukin-4 (IL-4) (Fig. 6, E to N, and fig. S8). There were also increased anti–SARS-CoV-1 IgA and IgG in both the BALF and serum in P&Sx relative to IM mRNA-LNP prime-boost (Fig. 6, O to R). P&Sx mice correspondingly developed higher neutralization titers against SARS-CoV-1 than those of mice vaccinated with SARS-CoV-2 mRNA-LNP prime-boost (Fig. 6S). P&Sx induced higher anti–SARS-CoV-2 BALF IgA than SARS-CoV-2 mRNA-LNP prime-boost and similar levels of anti–SARS-CoV-2 IgG in BALF (Fig. 6, T and U). Consistent with the elevated serum IgG levels, mRNA-LNP prime-boost mice had higher serum neutralization titers against SARS-CoV-2 than that of P&Sx mice (Fig. 6, V to X). Thus, IN boosting with unadjuvanted heterologous spike protein can induce potent mucosal cellular and humoral memory against a substantially divergent sarbecovirus.

Discussion

In this work, we describe the preclinical development of an alternative vaccine strategy, P&S, in which IN unadjuvanted spike subunit protein elicits robust protective mucosal immunity after mRNA-LNP parenteral immunization. These enhanced mucosal responses are characterized by the expansion of antigen-specific CD8$^+$ T_{RM}, CD4$^+$ T_{RM}, and B_{RM} cells as well as mucosal secretion of IgA and IgG. We found that an IN unadjuvanted spike booster can be administered months out from primary immunization and that it offers systemic neutralizing antibody booster responses comparable with that of IM mRNA-LNP boost. Similarly, prime and PACE-spike elicits increased antigen-specific CD8$^+$ T_{RM} cells and mucosal IgA. Both boosting methods result in protection from lethal SARS-CoV-2 challenge. We also found that P&S leads to durable responses with protective vaccine efficacy at 118 days from the initiation of vaccination. P&S is protective in hamsters and blocks viral transmission more effectively than does mRNA-LNP prime-boost. Last, by using a divergent spike antigen, we demonstrate that P&Sx can generate mucosal immunity to SARS-CoV-1 while also boosting the systemic and mucosal neutralizing antibodies to the original antigenic target, SARS-CoV-2. Although the goal of vaccination has been to prevent individual morbidity and mortality, the evolution of SARS-CoV-2 has highlighted the need for rapidly deployable mucosal vaccines that also prevent transmission. P&S shows promise in reducing both infection and transmission. Improving upon current vaccine platforms to provide mucosal immunity is vital to control this pandemic and will certainly be important for the next.

Preclinical studies of both SARS-CoV-2 and influenza have demonstrated that IN vaccination decreases viral shedding and transmission relative to those of parenteral vaccines (*19*–*23*). Despite these studies, there is only one currently approved respiratory mucosal vaccine, FluMist, which relies on a live attenuated influenza virus. FluMist is contraindicated in people with underlying respiratory conditions and is only approved for young people. Additionally, live attenuated vaccines are not amenable to rapid implementation because this technology requires extensive research and development. Accordingly, most current clinical trials of mucosally administered SARS-CoV-2 vaccines rely on either replication-deficient or attenuated viral vectors. However, the safety and efficacy of these approaches have not yet been established, especially given that preexisting immunity to these vectors can lead to reduced immunogenicity (*35*). Some vector-based mucosal vaccines—including two Merck candidates, V590 and V591—have already been abandoned after phase 1 clinical trials showed poor immunogenicity, whereas candidates by Bharat Biotech and CanSino have recently been approved (*36*).

P&S is likely broadly applicable as a booster against new SARS-CoV-2 VOCs in a previously vaccinated individual or as a de novo primary immunization strategy for newly emerging respiratory pathogens. Although it is possible that our results rely on specific characteristics of mRNA-LNP priming, we believe that this approach will likely work with other primary immunization regimens or in the case of previous infection. Although the above study assesses a single mRNA-LNP dose before IN boosting, we would expect unadjuvanted IN boosting to be as effective if not more so in individuals who have received multiple previous shots because P&S seems to leverage preexisting immunity rather than be inhibited by it. Additionally, it has been shown that the highly stabilized spike enhances its immunogenicity and that applying this vaccination strategy to other pathogens may require the addition of stabilizing mutations to enable unadjuvanted boosting. Our present study characterizes a method for the development of mucosal immunity to SARS-CoV-2 without the use of adjuvants or replicating viruses or vectors in two different well-validated preclinical vaccine models. These results are encouraging but require further validation and optimization for human use.

Vaccines that generate broadly neutralizing immunity against a wide variety of sarbecoviruses are a goal to combat both newly emerging SARS-CoV-2 variants and potential pandemic SARS-like coronaviruses. Using SARS-CoV-1 spike as a heterologous IN boost, P&Sx demonstrates that prior SARS-CoV-2 mRNA-LNP does not prevent the development of SARS-CoV-1–neutralizing antibodies but rather enables it. P&Sx simultaneously elicits broadly reactive neutralizing antibodies and mucosal immunity. Although some recent studies have successfully reported the development of systemic pan-sarbecovirus vaccines (*37*, *38*), P&Sx induces both systemic and mucosal immunity against both SARS-CoV-1 and SARS-CoV-2.

SARS-CoV-2 will continue to evolve and become more immune-evasive and transmissible. We will require boosting in human populations for the foreseeable future. Boosting that induces mucosal immunity may help enhance protection and slow transmission as these new variants emerge.

Materials and methods

All procedures were performed in a BSL-3 facility (for SARS-CoV-2–infected mice) with approval from the Yale Institutional Animal Care and Use Committee and Yale Environmental Health and Safety.

Cell and virus

As reported previously (*15*, *39*, *40*), Vero E6 cells overexpressing angiotensin-converting enzyme

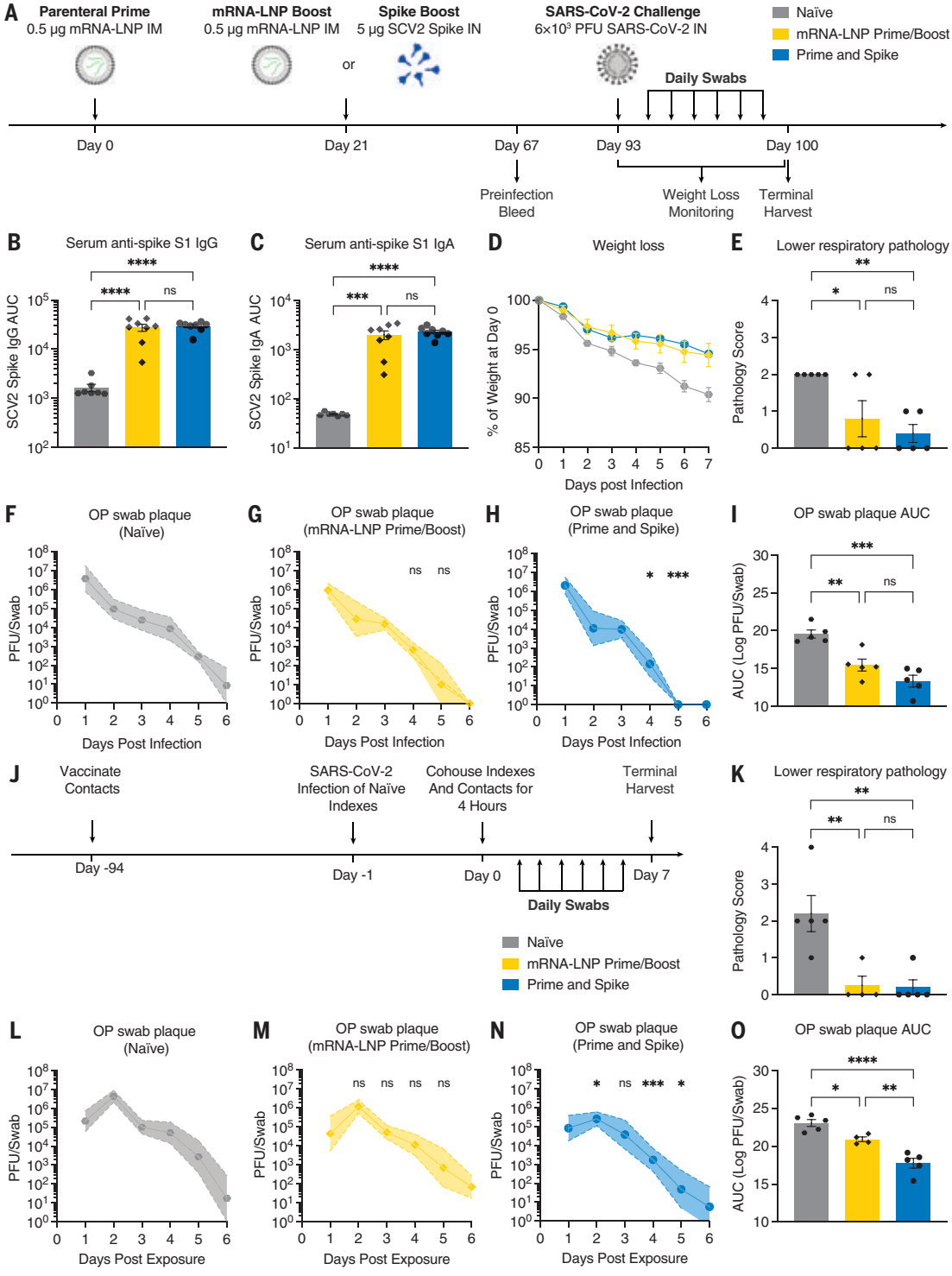

Fig. 5. IN spike boosting leads to reduced viral transmission in hamster model. (**A**) Experimental schema. Syrian hamsters were intramuscularly primed with 0.5 µg of mRNA-LNP, followed 21 days later by boosting with 0.5 µg of mRNA-LNP intramuscularly or 5 µg of SCV2 spike intranasally. (**B** and **C**) Sixty-seven days after prime, serum IgG and IgA were assessed by means of ELISA. At 93 days after prime, naïve, mRNA-LNP prime-boost, and P&S hamsters were infected with 6×10^3 PFU SCV2. (**D**) Weight loss as percent of starting. (**E**) Histopathologic analysis of lung samples at 7 days after infection. (**F** to **H**) Viral titer from oropharyngeal swabs are shown as mean (symbols) and standard deviation (shaded regions), *P* value relative to control at the same time point. (**I**) AUC analysis for viral titer over 6 days after infection. (**J**) Transmission experimental schema. Syrian hamsters vaccinated as above were cohoused for 4 hours with naïve donor hamsters that had been infected 24 hours earlier with 6×10^3 PFU SCV2. (**K**) Histopathologic analysis of lung samples at 7 days after exposure. (**L** to **N**) Viral titers from oropharyngeal swabs are shown as mean (symbols) and standard deviation (shade), *P* value relative to control at the same time point. (**O**) AUC analysis for viral titer over 6 days after infection. Mean ± SEM. Statistical significance was calculated by means of [(B), (C), (E), (I), (K), and (O)] one-way ANOVA followed by Tukey's correction, [(F) to (H)] mixed-effect analysis followed by Tukey's multiple comparison test, or [(L) to (N)] two-way ANOVA followed by Dunnett's multiple comparisons test; $*P \le 0.05$, $**P \le 0.01$, $***P \le 0.001$, $****P \le 0.0001$. Individual data points are represented from one independent experiment.

2 (ACE2) and TMPRSS2 [kindly provided by B. Graham at the National Institutes of Health Vaccine Research Center (NIH-VRC)] were cultured in Dulbecco's modified Eagle medium (DMEM) supplemented with 1% sodium pyruvate and 5% fetal bovine serum (FBS) at 37°C and 5% CO_2. SARS-CoV-2 isolate hCOV-19/USA-WA1/2020 (NR-52281) was obtained from BEI Resources and was amplified in VeroE6 cells overexpressing ACE2 and TMPRSS2. Cells were infected at a multiplicity of infection 0.01 for 2 to 3 days to generate a working stock, and after incubation, the supernatant was clarified by means of centrifugation (5 min, 500*g*) and filtered through a 0.45-µm filter and stored at −80°C. Viral titers were measured with standard plaque assay by using Vero E6 cells overexpressing hACE2 and TMPRSS2.

Animals

B6.Cg-Tg(K18-ACE2)2Prlmn/J (K18-hACE2) mice (stock no. 034860) were purchased from the Jackson Laboratory and subsequently bred and housed at Yale University. Eight- to

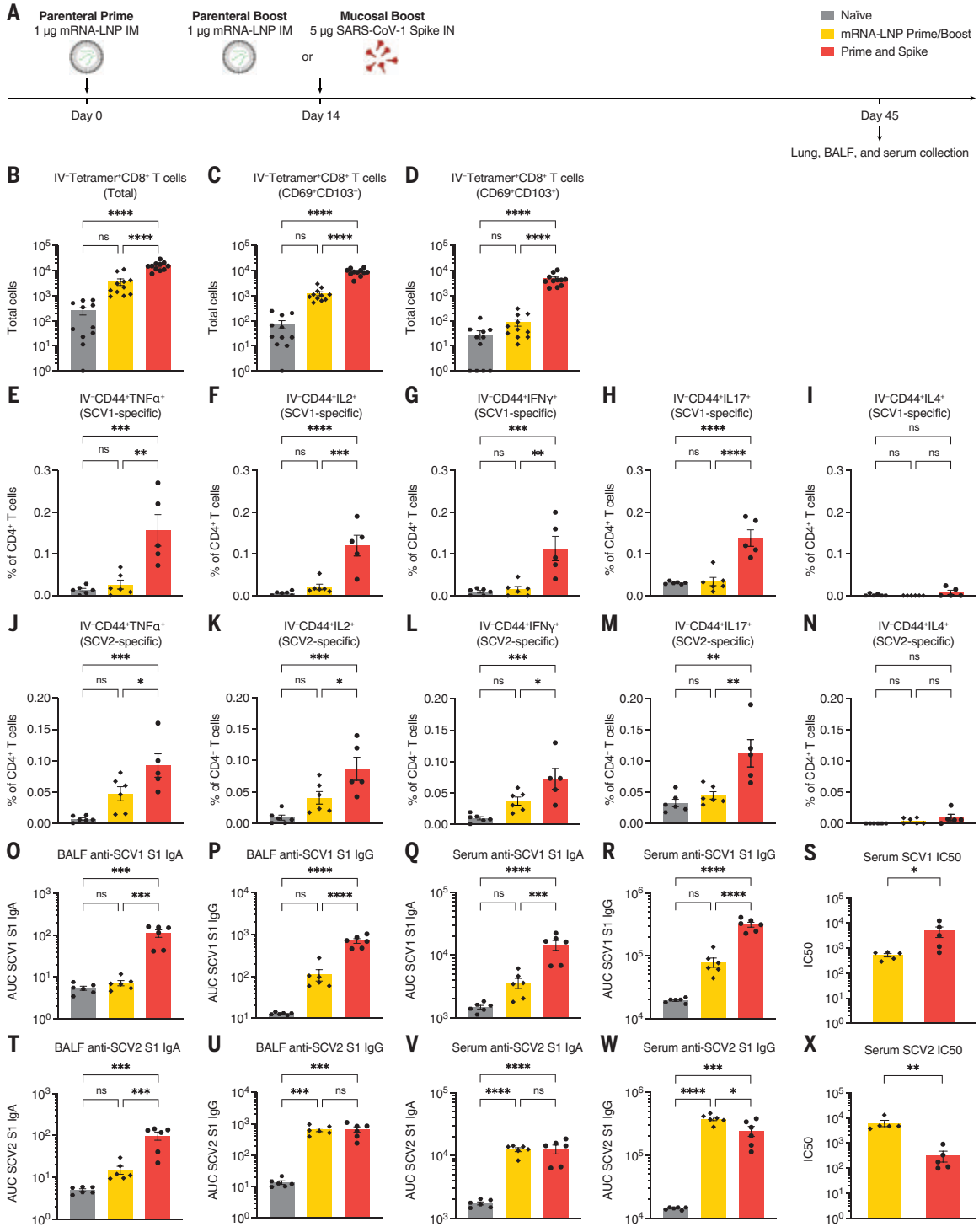

Fig. 6. Heterologous IN boosting with SARS-CoV-1 spike enhances preexisting SCV2-specific immunity and broadens reactivities to SCV1. (**A**) Experimental schema. K18-hACE2 mice were intramuscularly primed with 1 μg of mRNA-LNP, followed by boosting with 1 μg of mRNA-LNP intramuscularly, or 5 μg of prefusion-stabilized, trimeric, recombinant SARS-CoV-1 (SCV1) spike IN (IN SpikeX) 14 days after prime. (**B** to **D**) Quantification of total tetramer$^+$ CD8 T cells, CD69$^+$CD103$^-$tetramer$^+$ CD8 T cells, or CD69$^+$CD103$^+$tetramer$^+$ CD8 T cells in lung tissues from naïve, mRNA-LNP prime-boost, or P&Sx mice. (**E** to **N**) Percoll gradient purified lung lymphocytes were restimulated with spike peptide megapool from [(E) to (I)] SCV1 or [(J) to (N)] SCV2, and intracellular cytokine staining was performed to assess antigen-specific production of TNF-α, IL-2, IFN-γ, IL-17, and IL-4 by extravascular IV-CD45$^-$CD44$^+$ CD4 T cells. (**O** to **S**) Measurement of SCV1 spike S1 subunit–specific BALF IgA and IgG, and serum IgA and IgG. (S) Measurement of neutralization titer against SCV1 spike–pseudotyped VSV. (**T** to **W**) Measurement of SCV2 spike S1 subunit–specific BALF IgA and IgG, and serum IgA and IgG. (**X**) Measurement of neutralization titer against SCV2 spike–pseudotyped VSV. To reduce overall number of experimental animals used, control data points from naïve and mRNA prime-boost are common to Figs. 4 and 6. Mean ± SEM. Statistical significance was calculated by means of one-way ANOVA followed by Tukey's correction, except for [(S) and (X)] Student's *t* test; *$P \le 0.05$, **$P \le 0.01$, ***$P \le 0.001$, ****$P \le 0.0001$. Individual data points are represented and are pooled from two independent experiments.

twelve-week-old female mice were used for immunization experiments. Male Syrian hamsters (strain, HSdHan:AURA; stock no. 089) were purchased from Envigo, and vaccination began at 12 weeks of age. All procedures used in this study (such as sex matching and age matching) complied with federal guidelines and the institutional policies of the Yale School of Medicine Animal Care and Use Committee. To reduce the overall number of experimental animals used and to be consistent with our institutional animal use policy, control data points are shared among some figures when applicable and noted in figure legends. Sample sizes for animal experiments were determined empirically on the basis of previously published work in the field with similar experimental paradigms to provide sufficient statistical power for assessing biological effects of interest. No statistical methods were used to predetermine the sample size. Age- and sex-matched animals were randomly assigned to experimental groups at the beginning of the experiment. Investigators were not blinded, except for pathological analysis, because no subjective measurements were performed.

SARS-CoV-2 infection

Mice were anesthetized by using 30% v/v isoflurane diluted in propylene glycol. Using a pipette, 50 μl containing 6×10^4 plaque-forming units (PFU) SARS-CoV-2 was delivered intranasally. Hamsters were anesthetized by using 30% v/v isoflurane diluted in propylene glycol and administered 6×10^3 PFU SARS-CoV-2 intranasally in 100 μl.

mRNA extraction from Comirnaty (BNT162b2) mRNA-LNP

mRNA was extracted from the vaccine formulation with a TRIzol-chloroform separation method as previously described (*41*). Briefly, aliquots of vaccine were dissolved in TRIzol LS (Thermo Fisher Scientific) at 1:6.6 vaccine to TRIzol volume ratio. After a 15-min incubation (37°C, shaking), 0.2 ml of chloroform was added per 1 ml of TRIzol. The solution was shaken vigorously for 1 min and then incubated at room temperature for 3 min. The solution was centrifuged at 12,000*g* for 8 min at 4°C. The aqueous layer containing the isolated mRNA was further purified with a RNeasy Maxi Kit purchased from Qiagen (Germantown, MD, USA) following the manufacturers protocol. The RNA was eluted from the column on the final step with sodium acetate buffer (25 mM, pH 5.8) warmed to 37°C. Extracted mRNA was analyzed for concentration and purity with NanoDrop measurements of the absorbance at 260, 280, and 230 nm, with purity being assessed as A260/A280 > 2 and A260/A230 > 2. Agarose gel electrophoresis was used to determine the length and verify that the mRNA remained intact. Extracted mRNA containing 1:100 SYBR Safe stain (Thermo Fisher Scientific) was loaded onto a 1% agarose gel and run at 75 V with tris-acetate-EDTA buffer containing 1:5000 SYBR Safe stain (fig. S9).

PACE polyplex formulation and characterization

PACE polymers were synthesized and characterized as previously described (*42*). All polyplexes were formulated at a 50:1 weight ratio of polymer to mRNA. PACE polymers were dissolved at 100 mg/ml overnight in dimethyl sulfoxide (37°C, shaking). Before polyplex fabrication, an optimal PACE polymer blend was produced by mixing solutions of PACE polymers containing an end-group modification (*43*) and a polyethylene glycol tail (*30*). mRNA and polymer were diluted into equal volumes of sodium acetate buffer (25 mM, pH 5.8). The polymer dilution was then vortexed for 15 s, mixed with the mRNA dilution, and vortexed for an additional 25 s. Polyplexes were incubated at room temperature for 10 min before use.

Vaccination

Used vials of Comirnaty vaccine were acquired from Yale Health pharmacy within 24 hours of opening and stored at 4°C. Vials contained residual vaccine (diluted to 100 μg/ml per manufacturer's instructions), which was removed with spinal syringe and pooled. Pooled residual vaccine was aliquoted and stored at −80°C. Mice were anesthetized by using a mixture of ketamine (50 mg per kilogram of body weight) and xylazine (5 mg per kilogram of body weight) and injected intraperitoneally. Vaccine was diluted in sterile phosphate-buffered saline (PBS) and 10 or 20 μl was injected into the left quadriceps muscle with a 31G syringe for a final dose of 1 or 0.05 μg as indicated. Similarly, hamsters were administered 0.5 μg diluted in 20 μl by means of 31G syringe in the left quadriceps muscle. For IN vaccination, SARS-CoV-2–stabilized spike (ACRO biosystems, SPN-C52H9) or SARS-CoV-1 spike (ACRO biosystems, SPN-S52H6) was reconstituted in sterile endotoxin-free water according to the manufacturer's protocol and then diluted in sterile PBS and stored at −80°C. Mice or hamsters were anesthetized by using isoflurane and administered 1 or 5 μg (as indicated) in 50 μl (25 μl where indicated) through the IN route. For IN mRNA-PACE, 50 μl of polyplexes in solution was administered at the indicated dose.

Viral titer analysis

Viral titer analysis was performed as previously described (*15*, *39*, *40*), with modifications noted and summarized here. Mice were euthanized in 100% isoflurane at indicated time points. Approximately half of the total lung (right lobes) or nasal turbinate was homogenized in a bead homogenizer tube containing 1 ml of PBS supplemented with 2% FBS and 2% antibiotics/antimycotics (Gibco) and stored at −80°C. Nasal turbinate and lung homogenates were clarified of debris by centrifugation (10 min, 3100*g*). Daily oral swabs (Pruitan PurFlock Ultra 25-3206-U) were performed on hamsters and stored in 1 ml of DMEM with 2% FBS and 2% antibiotics/antimycotics (Gibco) and stored at −80°C. To determine infectious SARS-CoV-2 titers, plaque assay was performed by using ACE2- and TMPRSS2-overexpressing Vero E6 cells. Plaques were resolved by means of formalin fixation 40 to 42 hours after infection, followed by staining with crystal violet and rinsing with water for plaque visualization.

SARS-CoV-2–specific antibody measurements

Enzyme-linked immunosorbent assays (ELISAs) were performed as previously described (*39*, *44*), with modifications noted and summarized here. Ninety-six–well MaxiSorp plates (Thermo Scientific 442404) were coated with recombinant SARS-CoV-2 S1 protein (ACRO Biosystems S1N-C52H3) or SARS-CoV-1 S1 protein (ACRO Biosystems S1N-S52H5). After overnight incubation at 4°C, plates were replaced with blocking solution (PBS with 0.1% Tween-20, and 5% milk powder) and incubated for 1 to 2 hours at room temperature. Serum or BALF was diluted in dilution solution (PBS with 0.1% Tween-20 and 2% milk powder) and added to plates for 2 hours at room temperature. Plates were washed five times with PBS-T (PBS with 0.05% Tween-20) by using an automatic plate washer (250 μl per cycle), and 50 μl of horseradish peroxidase (HRP) anti-mouse IgG (Cell Signaling Technology 7076; 1:3000), HRP anti-mouse IgA (Southern Biotech 1040-05; 1:1000), HRP anti-hamster IgG (Southern Biotech 6060-05; 1:1000), or rabbit anti-hamster IgA HRP (Brookwood Biomedical, sab3003a, 1:250 100 μg/ml) diluted in dilution solution was added to each well. After 1 hour of incubation at room temperature (overnight at 4°C for hamster IgA), plates were washed three times with PBS-T by using an automatic plate washer. Fifty μl of TMB Substrate Reagent Set (BD Biosciences 555214) was added to plates. To terminate the reaction, another 50 μl of 2 N sulfuric acid was added after 15 min of substrate development. Plates were then recorded at wavelengths of 450 and 570 nm, and the difference was reported as AUC.

Immunohistochemistry and pathological analysis

Yale Pathology Tissue Services (YPTS) performed embedding, sectioning, and hematoxylin and eosin (H&E) staining of lung tissue. A pulmonary pathologist reviewed the slides blinded and identified immune cell infiltration and other related pathologies. Mouse lung scores of 1 to 4 were characterized as follows: 1, mild patchy mononuclear infiltrate, parenchymal and perivascular, with variably reactive pneumocytes and stromal rection; 2, moderate patchy mononuclear infiltrate, parenchymal and perivascular, with variably reactive pneumocytes

and stromal rection; 3, mild, dense mixed infiltrate, including mononuclear cells and granulocytes and neutrophils; and 4, moderate, dense mixed infiltrate, including mononuclear cells and granulocytes and neutrophils. Hamster lung scores of 0 to 4 were characterized as follows: 0, normal; 1, very focal injury, inflammation, and repair; 2, multifocal repair; and 4, multifocal repair with necrosis.

Intravascular labeling, cell isolation, and flow cytometry

To discriminate circulating from extravascular immune cells, mice were anesthetized with 30% isoflurane and injected intravenously with 2 μg of APC/Fire 750–labeled anti-CD45 Ab. After 3 min of labeling, mice were euthanized. Tissues were harvested and analyzed as previously described (*39*). Briefly, lungs and nasal turbinates were minced with scissors, incubated in a digestion cocktail containing collagenase A (Roche) and DNase I (Sigma-Aldrich) in RPMI at 37°C for 45 min, and dissociated through a 70-μm filter. Airway-resident immune cells were collected by centrifuging BALF at 600*g* for 5 min at 4°C, after which cell pellets were used for flow cytometry, and supernatants were used for antibody analysis. Cells were treated with ammonium-chloride-potassium (ACK) buffer to lyse red blood cells and then washed once with PBS. Single-cell suspensions were incubated with Fixable Aqua cell viability dye (Invitrogen L34957) and anti-mouse CD16/CD32 Fc Block (BD Biosciences 553141) for 30 min at 4°C. Cells were washed once with PBS before surface staining. For T cell analysis, cells were first stained with APC-labeled SARS-CoV-2 S 62-76 MHC class II tetramer [I-A(b)] for 60 min at RT. Cells were washed once with PBS and then stained with anti-CD103, anti-CD3, anti-CD44, anti-CD62L, anti-CD8a, anti-CD69, anti-CD183 (CXCR3), anti-CD4, and PE-SARS-CoV-2 S 539-546 MHC class I tetramer [H-2K(b)] for 30 min at 4°C. For B cell analysis, cells were stained with ant-GL7, anti-IgM, anti-CD138, anti-CD19, anti-IgA, anti-B220, PE-SARS-CoV-2 RBD tetramer, anti-CD38, APC-SARS-CoV-2 RBD tetramer, and anti-IgD for 30 min at 4°C. Cells were washed with PBS once, followed by 4% paraformaldehyde fixation for 45 min at 4°C. Flow cytometry data were acquired on an Attune NxT Flow Cytometer and analyzed by use of FlowJo Software (10.5.3; Tree Star). Gating strategy is provided in fig. S10, and detailed antibody information is provided in table S1.

Intracellular cytokine staining assay for detection of lung-resident spike-specific CD4 T cells

After intravascular labeling by using an anti-CD45 Ab at the dose of 2 μg per mouse, lung isolation, and processing, single cells from the lung tissue were first enriched by using a Percoll gradient before spike peptide stimulation. Briefly, total lung cells were first resuspended in 5 ml of 30% Percoll solution in a 15-ml conical tube, underlaid with 5 ml of 70% Percoll solution, and subject to centrifugation at 1000*g* for 20 min at room temperature. After centrifugation, lymphocytes located at the interphase between 30 and 70% Percoll solution were collected, washed once with PBS, and resuspended in complete RPMI. In a 96-well U-bottom plate, 10^6 lymphocytes enriched from each lung sample were added, together with spike peptide megapool from SARS-CoV-2 (JPT PM-WCPV-S-1) or SARS-CoV-1 (JPT PM-CVHSA-S-1) at a final working concentration of 1 μg/ml per peptide, 1X Protein Transport Inhibitor Cocktail (eBioscience 00-4980-03), and 10^6 freshly isolated splenocytes from CD45.1$^+$ mice, with complete RPMI for a final volume of 200 μl. Peptide stimulation was performed for 8 hours at 37°C. After peptide stimulation, cells were incubated at 4°C with Fc block (BioXCell BE0307) and Aqua cell viability dye (ThermoFisher L34957) for 20 min. Cells were washed once with PBS before surface staining with anti-CD3, anti-CD44, anti-CD4, and anti-CD45.1. After washing with PBS, cells were fixed by using 4% paraformaldehyde for 45 min at 4°C. Cells were then washed and permeabilized with 1X Permeabilization Buffer (eBioscience 00-8333-56) for 10 min at RT. After permeabilization, cells were stained with anti–IL-4, anti–IL-2, anti–tumor necrosis factor–α (TNF-α), anti–IL-17A, and anti–interferon-γ (IFN-γ). Cells were washed once with PBS before being acquired on Attune and analyzed by use of FlowJo. Gating strategy is provided in fig. S10, and detailed antibody information is provided in table S1.

SARS-CoV-2 RBD B cell tetramer production and staining

Recombinant SARS-CoV-2 spike RBD His Biotin Protein, CF (R&D BT10500-050) was incubated at a 4:1 molar ratio with either streptavidin-PE (Prozyme PJRS25) or streptavidin-APC (Prozyme PJ27S) for 30 min at 4°C. Mixture was then purified and concentrated in an Amicon Ultra (50 kDA MWCO) spin column and washed 1X with sterile cold PBS. The concentration was determined on a NanoDrop 8000 Spectrophotometer (ThermoFisher ND-8000-GL) by using fluorophore-specific absorbances. Tetramers were then diluted to 1.0 μM in PBS and stored at 4°C. For every 2×10^7 to 5×10^7 cells, 1 μl of stock 1.0 μM tetramer was used for staining.

Pseudovirus production and neutralization assay

Pseudoviruses were produced as previously described (*15*). Spike-encoding plasmid was kindly provided by V. Munster and previously described (*45*). To perform pseudovirus neutralization assays, Vero E6 overexpressing hACE2 and TMPRSS2 (Fig. 1) or Huh7.5 cell (Fig. 5 and fig. S3) were plated (3×10^4) in each well of a white 96-well plate the day before infection. On the day of infection, serum and BALF were heat-inactivated for 30 min at 56°C. Sera shown in Fig. 1 were tested at a starting dilution of 1:50, and BALF samples were tested at a starting dilution of 1:4, both with eight twofold serial dilutions. Sera shown in Fig. 5 and fig. S3 were tested at a starting dilution of 1:40 with eight threefold serial dilutions. Serial dilutions were mixed 1:1 with indicated pseudovirus and incubated for 1 hour at 37°C and 5% CO_2. Growth medium was then aspirated from the cells and replaced with 100 μl of serum-virus mixture. Twenty-four hours after infection, the infection-antibody mixture was removed, and plates were flash-frozen at −80°C. Thirty μl of passive lysis buffer (Promega) was added to each well, and plates were incubated for 15 min at room temperature. Thirty μl of Renilla-Glo Luciferase Assay System substrate (Promega) was then added to each well and incubated at room temperature for an additional 15 min. Luminescence was measured on a microplate reader (SpectraMax i3, Molecular Devices). Median inhibitory concentration was calculated with Prism 9 (GraphPad Software) nonlinear regression.

Sequence alignment

The following amino acid sequences of coronavirus Spike proteins used in alignment were obtained from Uniprot/Genebank: Wuhan (P0DTC2), B.1.1.7 (QWE88920.1), B.1.351 (QRN78347.1), B.1.617 (QUD52764.1), B.1.1.28.1 (QRX39425.1), BA.1 (UFO69279.1), BA.2 (UFO69279.1), BA.2.12.1 (UMZ92892.1), BA.4 (UPP14409.1), BA.5 (UOZ45804.1), Khosta (MZ190137.1), Khosta-2 (MZ190138.1), SARS-CoV (AY278489.2), WIV1 (KF367457), and BANAL236 (MZ937003.1). Sequence alignment was performed with MAFFT in JalView (v2.11.2.3).

Graphical illustrations

Graphical illustrations were made with Biorender.com.

REFERENCES AND NOTES

1. L. R. Baden *et al.*, Efficacy and safety of the mRNA-1273 SARS-CoV-2 vaccine. *N. Engl. J. Med.* **384**, 403–416 (2021). doi: 10.1056/NEJMoa2035389; pmid: 33378609
2. N. Dagan *et al.*, BNT162b2 mRNA COVID-19 vaccine in a nationwide mass vaccination setting. *N. Engl. J. Med.* **384**, 1412–1423 (2021). doi: 10.1056/NEJMoa2101765; pmid: 33626250
3. K. R. W. Emary *et al.*, Efficacy of ChAdOx1 nCoV-19 (AZD1222) vaccine against SARS-CoV-2 variant of concern 202012/01 (B.1.1.7): An exploratory analysis of a randomised controlled trial. *Lancet* **397**, 1351–1362 (2021). doi: 10.1016/S0140-6736(21)00628-0; pmid: 33798499
4. A. S. V. Shah *et al.*, Effect of vaccination on transmission of SARS-CoV-2. *N. Engl. J. Med.* **385**, 1718–1720 (2021). doi: 10.1056/NEJMc2106757; pmid: 34496200
5. R. J. Harris *et al.*, Effect of vaccination on household transmission of SARS-CoV-2 in England. *N. Engl. J. Med.* **385**, 759–760 (2021). doi: 10.1056/NEJMc2107717; pmid: 34161702
6. H. Chemaitelly *et al.*, Waning of BNT162b2 vaccine protection against SARS-CoV-2 infection in Qatar. *N. Engl. J. Med.* **385**, e83 (2021). doi: 10.1056/NEJMoa2114114; pmid: 34614327
7. B. A. Cohn, P. M. Cirillo, C. C. Murphy, N. Y. Krigbaum, A. W. Wallace, SARS-CoV-2 vaccine protection and deaths among US veterans during 2021. *Science* **375**, 331–336 (2022). doi: 10.1126/science.abm0620; pmid: 34735261

8. C. Lucas *et al*., Impact of circulating SARS-CoV-2 variants on mRNA vaccine-induced immunity. *Nature* **600**, 523–529 (2021). doi: 10.1038/s41586-021-04085-y; pmid: 34634791
9. F. Schmidt *et al*., Plasma neutralization of the SARS-CoV-2 Omicron variant. *N. Engl. J. Med.* **386**, 599–601 (2022). doi: 10.1056/NEJMc2119641; pmid: 35030645
10. S. Cele *et al*., SARS-CoV-2 Omicron has extensive but incomplete escape of Pfizer BNT162b2 elicited neutralization and requires ACE2 for infection. *Nature* **602**, 654–656 (2022). doi: 10.1038/s41586-021-04387-1; pmid: 35016196
11. A. Singanayagam *et al*., Community transmission and viral load kinetics of the SARS-CoV-2 delta (B.1.617.2) variant in vaccinated and unvaccinated individuals in the UK: A prospective, longitudinal, cohort study. *Lancet Infect. Dis.* **22**, 183–195 (2022). doi: 10.1016/S1473-3099(21)00648-4; pmid: 34756186
12. D. Laczkó *et al*., A single immunization with nucleoside-modified mRNA vaccines elicits strong cellular and humoral immune responses against SARS-CoV-2 in mice. *Immunity* **53**, 724–732.e7 (2020). doi: 10.1016/j.immuni.2020.07.019; pmid: 32783919
13. R. R. Goel *et al*., mRNA vaccines induce durable immune memory to SARS-CoV-2 and variants of concern. *Science* **374**, eabm0829 (2021). doi: 10.1126/science.abm0829; pmid: 34648302
14. J. S. Turner *et al*., SARS-CoV-2 mRNA vaccines induce persistent human germinal centre responses. *Nature* **596**, 109–113 (2021). doi: 10.1038/s41586-021-03738-2; pmid: 34182569
15. B. Israelow *et al*., Adaptive immune determinants of viral clearance and protection in mouse models of SARS-CoV-2. *Sci. Immunol.* **6**, eabl4509 (2021). doi: 10.1126/sciimmunol.abl4509; pmid: 34623900
16. S. Sheikh-Mohamed *et al*., Systemic and mucosal IgA responses are variably induced in response to SARS-CoV-2 mRNA vaccination and are associated with protection against subsequent infection. *Mucosal Immunol.* **15**, 799–808 (2022). doi: 10.1038/s41385-022-00511-0; pmid: 35468942
17. K. Sano *et al*., Efficient mucosal antibody response to SARS-CoV-2 vaccination is induced in previously infected individuals. medRxiv 2021.2012.2006.21267352 [Preprint] (2021). https://doi.org/10.1101/2021.12.06.21267352.
18. M. M. L. Poon *et al*., SARS-CoV-2 infection generates tissue-localized immunological memory in humans. *Sci. Immunol.* **6**, eabl9105 (2021). doi: 10.1126/sciimmunol.abl9105; pmid: 34618554
19. A. O. Hassan *et al*., A single-dose intranasal ChAd vaccine protects upper and lower respiratory tracts against SARS-CoV-2. *Cell* **183**, 169–184.e13 (2020). doi: 10.1016/j.cell.2020.08.026; pmid: 32931734
20. A. O. Hassan *et al*., A single intranasal dose of chimpanzee adenovirus-vectored vaccine protects against SARS-CoV-2 infection in rhesus macaques. *Cell Rep. Med.* **2**, 100230 (2021). doi: 10.1016/j.xcrm.2021.100230; pmid: 33754147
21. T. L. Bricker *et al*., A single intranasal or intramuscular immunization with chimpanzee adenovirus-vectored SARS-CoV-2 vaccine protects against pneumonia in hamsters. *Cell Rep.* **36**, 109400 (2021). doi: 10.1016/j.celrep.2021.109400; pmid: 34245672
22. R. J. Fischer *et al*., ChAdOx1 nCoV-19 (AZD1222) protects Syrian hamsters against SARS-CoV-2 B.1.351 and B.1.1.7. *Nat. Commun.* **12**, 5868 (2021). doi: 10.1038/s41467-021-26178-y; pmid: 34620866
23. N. van Doremalen *et al*., Intranasal ChAdOx1 nCoV-19/AZD1222 vaccination reduces viral shedding after SARS-CoV-2 D614G challenge in preclinical models. *Sci. Transl. Med.* **13**, eabh0755 (2021). doi: 10.1126/scitranslmed.abh0755; pmid: 34315826
24. J. Tang *et al*., Respiratory mucosal immunity against SARS-CoV-2 after mRNA vaccination. *Sci. Immunol.* **7**, eadd4853 (2022). doi: 10.1126/sciimmunol.add4853; pmid: 35857583
25. F. Fiorino, E. Pettini, G. Pozzi, D. Medaglini, A. Ciabattini, Prime-boost strategies in mucosal immunization affect local IgA production and the type of Th response. *Front. Immunol.* **4**, 128 (2013). doi: 10.3389/fimmu.2013.00128; pmid: 23755051
26. D. Lapuente *et al*., Protective mucosal immunity against SARS-CoV-2 after heterologous systemic prime-mucosal boost immunization. *Nat. Commun.* **12**, 6871 (2021). doi: 10.1038/s41467-021-27063-4; pmid: 34836955
27. M. Mutsch *et al*., Use of the inactivated intranasal influenza vaccine and the risk of Bell's palsy in Switzerland. *N. Engl. J. Med.* **350**, 896–903 (2004). doi: 10.1056/NEJMoa030595; pmid: 14985487
28. C.-L. Hsieh *et al*., Structure-based design of prefusion-stabilized SARS-CoV-2 spikes. *Science* **369**, 1501–1505 (2020). doi: 10.1126/science.abd0826; pmid: 32703906
29. S. R. Allie *et al*., The establishment of resident memory B cells in the lung requires local antigen encounter. *Nat. Immunol.* **20**, 97–108 (2019). doi: 10.1038/s41590-018-0260-6; pmid: 30510223
30. M. K. Grun *et al*., PEGylation of poly(amine-co-ester) polyplexes for tunable gene delivery. *Biomaterials* **272**, 120780 (2021). doi: 10.1016/j.biomaterials.2021.120780; pmid: 33813260
31. S. Ndeupen *et al*., The mRNA-LNP platform's lipid nanoparticle component used in preclinical vaccine studies is highly inflammatory. *iScience* **24**, 103479 (2021). doi: 10.1016/j.isci.2021.103479; pmid: 34841223
32. A. Suberi *et al*., Inhalable polymer nanoparticles for versatile mRNA delivery and mucosal vaccination. bioRxiv 485401 [Preprint] (2022). https://doi.org/10.1101/2022.03.22.485401
33. Z. Zhuang *et al*., Mapping and role of T cell response in SARS-CoV-2-infected mice. *J. Exp. Med.* **218**, e20202187 (2021). doi: 10.1084/jem.20202187; pmid: 33464307
34. C. Gartlan *et al*., Vaccine-associated enhanced disease and pathogenic human coronaviruses. *Front. Immunol.* **13**, 882972 (2022). doi: 10.3389/fimmu.2022.882972; pmid: 35444667
35. S. Sanchez, N. Palacio, T. Dangi, T. Ciucci, P. Penaloza-MacMaster, Fractionating a COVID-19 Ad5-vectored vaccine improves virus-specific immunity. *Sci. Immunol.* **6**, eabi8635 (2021). doi: 10.1126/sciimmunol.abi8635; pmid: 34648369
36. Merck, "Merck discontinues development of SARS-CoV-2/COVID-19 vaccine Candidates; Continues development of two investigational therapeutic candidates," press release (2021); https://www.merck.com/news/merck-discontinues-development-of-sars-cov-2-covid-19-vaccine-candidates-continues-development-of-two-investigational-therapeutic-candidates.
37. D. R. Martinez *et al*., Chimeric spike mRNA vaccines protect against Sarbecovirus challenge in mice. *Science* **373**, 991–998 (2021). doi: 10.1126/science.abi4506; pmid: 34214046
38. A. C. Walls *et al*., Elicitation of broadly protective sarbecovirus immunity by receptor-binding domain nanoparticle vaccines. *Cell* **184**, 5432–5447.e16 (2021). doi: 10.1016/j.cell.2021.09.015; pmid: 34619077
39. B. Israelow *et al*., Mouse model of SARS-CoV-2 reveals inflammatory role of type I interferon signaling. *J. Exp. Med.* **217**, e20201241 (2020). doi: 10.1084/jem.20201241; pmid: 32750141
40. T. Mao *et al*., A stem-loop RNA RIG-I agonist protects against acute and chronic SARS-CoV-2 infection in mice. *J. Exp. Med.* **219**, e20211818 (2022). doi: 10.1084/jem.20211818; pmid: 34757384
41. D. C. Rio, M. Ares Jr., G. J. Hannon, T. W. Nilsen, Purification of RNA using TRIzol (TRI reagent). *Cold Spring Harb. Protoc.* **2010**, prot5439 (2010). doi: 10.1101/pdb.prot5439; pmid: 20516177
42. A. C. Kauffman *et al*., Tunability of biodegradable poly(amine-co-ester) polymers for customized nucleic acid delivery and other biomedical applications. *Biomacromolecules* **19**, 3861–3873 (2018). doi: 10.1021/acs.biomac.8b00997; pmid: 30110158
43. Y. Jiang *et al*., Quantitating endosomal escape of a library of polymers for mRNA delivery. *Nano Lett.* **20**, 1117–1123 (2020). doi: 10.1021/acs.nanolett.9b04426; pmid: 32003222
44. F. Amanat *et al*., A serological assay to detect SARS-CoV-2 seroconversion in humans. *Nat. Med.* **26**, 1033–1036 (2020). doi: 10.1038/s41591-020-0913-5; pmid: 32398876
45. M. Letko, A. Marzi, V. Munster, Functional assessment of cell entry and receptor usage for SARS-CoV-2 and other lineage B betacoronaviruses. *Nat. Microbiol.* **5**, 562–569 (2020). doi: 10.1038/s41564-020-0688-y; pmid: 32094589

ACKNOWLEDGMENTS

We thank M. Linehan for her technical and logistical assistance. We thank B. Graham (NIH-VRC) for kindly providing Vero E6 cells overexpressing ACE2 and TMPRSS2. We thank the NIH tetramer Core Facility for providing PE-labeled SARS-CoV-2 S 539-546 tetramer [H-2K(b)] and APC-labeled SARS-CoV-2 S 62-76 MHC class II tetramer (I-A(b)). We thank H. Steach for providing the B cell tetramer production protocol. We thank C. Wilen and J. Wei for their technical expertise. We thank H. W. Suh for providing PACE polymers and A. S. Piotrowski-Daspit for her helpful discussions. We thank J. Frank for her technical assistance with coronavirus spike sequence alignment. We also give special recognition of the services of B. Fontes and the Yale Environmental Health and Safety Department for their continuing assistance in safely conducting biosafety level 3 research. **Funding:** This work was in part supported by the Howard Hughes Medical Institute, the Fast Grant from Emergent Ventures at the Mercatus Center, and 1R01AI157488. A.I. is an investigator of the Howard Hughes Medical Institute. B.I. is supported by NIAID T32AI007517 and K08AI163493. T.M. is supported by NIAID T32AI007019. W.M.S., A.S., and M.R. are supported by UG3 HL147352 from the NIH. **Author contributions:** B.I., T.M., and A.I. conceived and designed research, with contributions from A.S., M.R., R.J.H., and W.M.S.; T.M., B.I., A.S., M.R., L.Z., S.L., M.A.P.-H., R.J.H., and H.D. conducted experiments. T.M., B.I., and A.I. analyzed and interpreted results. B.I., T.M., and A.I. wrote the original manuscript, which was revised and edited by all authors. **Competing interests:** A.I., T.M., and B.I. are listed as inventors on patent applications relating to IN spike-based SARS-CoV-2 vaccines filed by the Yale University (US patent appplication no. 63/290,042 and 63/418,744). A.I., W.M.S., T.M, B.I., A.S., and M.R. are listed as inventors on patent applications relating to IN PACE nanoparticle delivery-based vaccines filed by the Yale University (US patent appplication no. 63/287,410 and 63/302,413). W.M.S. and A.I. are cofounders of Xanadu Bio, and T.M. and B.I. are consultants for Xanadu Bio. **Data and materials availability:** All data needed to evaluate this paper's conclusions are present in the main text or supplementary materials. The reagents used to conduct experiments in this manuscript are either publicly available as described under Materials and methods or are available with the appropriate materials transfer agreement. PACE polymer is available from W.M.S. under a materials transfer agreement with Yale University.

SUPPLEMENTARY MATERIALS

science.org/doi/10.1126/science.abo2523
Figs. S1 to S10
Table S1
MDAR Reproducibility Checklist

Submitted 23 January 2022; resubmitted 22 July 2022
Accepted 24 October 2022
Published online 27 October 2022
10.1126/science.abo2523

RESEARCH ARTICLE SUMMARY

NEURODEVELOPMENT

Cortical wiring by synapse type–specific control of local protein synthesis

Clémence Bernard, David Exposito-Alonso†, Martijn Selten†, Stella Sanalidou, Alicia Hanusz-Godoy, Alfonso Aguilera, Fursham Hamid, Fazal Oozeer, Patricia Maeso, Leanne Allison, Matthew Russell, Roland A. Fleck, Beatriz Rico*, Oscar Marín*

INTRODUCTION: The function of the cerebral cortex relies on the specificity of synaptic connections among dozens of different types of excitatory glutamatergic pyramidal cells and inhibitory γ-aminobutyric acid-containing (GABAergic) interneurons. Neurons use dedicated transcriptional programs to control synapse specificity during development. Still, it is presently unclear whether regulation of mRNA translation is also involved in promoting the formation of specific synapses. One of the main signaling pathways controlling protein synthesis involves the mechanistic target of rapamycin complex 1 (mTORC1), a molecular complex activated by growth factor signals and inhibited by the proteins Tsc1 and Tsc2 (TSC subunits 1 and 2, respectively). Multiple proteins of the mTORC1 pathway are present in developing axons, and local protein synthesis occurs at excitatory and inhibitory synapses in the adult cerebral cortex. Many genes whose variation has been linked to neurodevelopmental disorders code proteins found at synapses and altered protein synthesis is a plausible pathophysiological mechanism for several of these conditions. For example, mutations in *TSC1* and *TSC2* cause tuberous sclerosis, a syndrome whose clinical features include seizures and autism spectrum disorder (ASD).

RATIONALE: Local translation contributes to brain wiring during axon guidance but its direct contribution to synapse formation is unclear. Moreover, to what extent local translation is differentially regulated at the level of specific synaptic connections remains unknown. We used mouse genetics, RNA sequencing, biochemistry, and experimental manipulations in vivo to study local protein synthesis in the development of synaptic connections in the cerebral cortex. We investigated the formation of excitatory synaptic connections between cortical pyramidal cells and two of the main subclasses of cortical interneurons, parvalbumin (PV)- and somatostatin (SST)-expressing cells. These interneurons share similar developmental trajectories, occupy the same layers of the neocortex, and are reciprocally connected with pyramidal cells, but they play very different roles in cortical function.

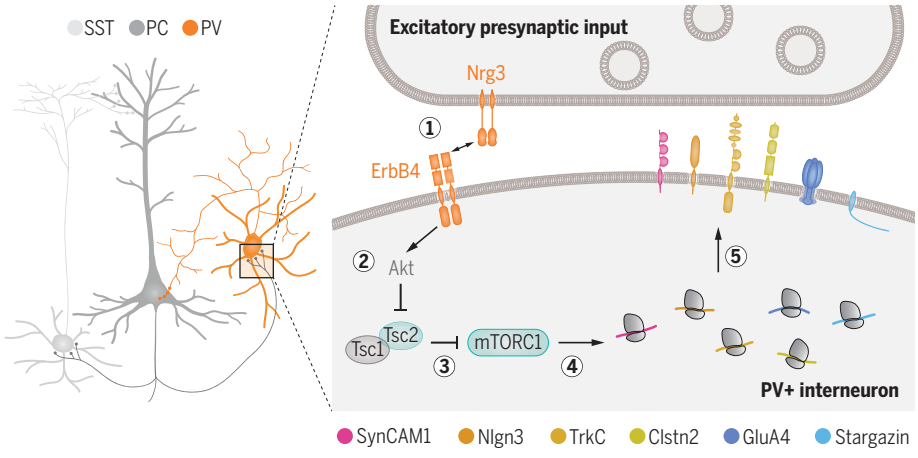

Local protein synthesis in synapse formation. Schematic of a pyramidal cell contacting parvalbumin-expressing (PV+) and somatostatin-expressing (SST+) interneurons in the cerebral cortex. The development of excitatory synapses on PV+ interneurons is mediated by (**1**) activation of ErbB4 through binding to neuregulin 3 (Nrg3) expressed by pyramidal cells, (**2**) inhibition of Tsc2 through Akt-dependent phosphorylation cascade, (**3**) inhibition of mTORC1 through Rheb-dependent phosphorylation cascade, (**4**) activation of protein synthesis of ErbB4 targets at the synapse, and (**5**) synapse formation through ErbB4 targets.

RESULTS: We found that loss of Tsc2 during development causes overactivation of mTORC1 in both PV^+ and SST^+ interneurons, leading to abnormal activation of mTORC1 effector protein S6rp and increased cell size. However, Tsc2 function seems required to establish a normal complement of excitatory synapses only onto PV^+ and not SST^+ interneurons. Tsc2 also seems dispensable for developing inhibitory PV^+ synapses onto pyramidal cells. Thus, although the loss of Tsc2 causes a global disruption of mTOR signaling in both PV^+ and SST^+ cells, it affects the wiring of interneurons in a cell type–specific and synapse type–specific manner. Our experiments indicate that this specificity is mediated by the Erb-B2 receptor tyrosine kinase 4 (ErbB4), which is specifically expressed by PV^+ interneurons and is present at postsynaptic densities contacted by excitatory axons. ErbB4 signaling inhibits Tsc2 function to enable mTOR activity at the postsynaptic densities of excitatory inputs contacting PV^+ interneurons. ErbB4 activation ultimately leads to the synaptic translation of mRNAs coding cell adhesion molecules (SynCAM1, Nlgn3, TrkC, and Clstn2) and AMPA receptor-related proteins (GluA4 and Stargazin). Loss of function experiments revealed that these molecules are required to develop a normal complement of excitatory synapses on PV^+ interneurons. Although a direct link between ErbB4 activation and local protein synthesis has only been established for a few mRNAs, analysis of the synaptic translatome of PV^+ interneurons lacking ErbB4 suggests that local translation of more transcripts—including many for which variation has been associated with ASD—might be under the control of this signaling pathway during synapse formation.

CONCLUSION: Our findings reveal that protein synthesis is regulated in a cell type–specific and synapse type–specific manner during synapse formation. Tsc2, a regulator of mTORC1 signaling in multiple cellular contexts, regulates the development of excitatory synapses onto PV^+ cells but not onto SST^+ interneurons. This specificity is mediated by activation of ErbB4, which controls excitatory synapse development through inhibition of Tsc2 and subsequent induction of a molecular program of local mRNA translation. Thus, local protein synthesis is regulated at the level of specific connections to control synapse formation in the nervous system. ■

The list of author affiliations is available in the full article online.
*Corresponding author. Email: beatriz.rico@kcl.ac.uk (B.R.); oscar.marin@kcl.ac.uk (O.M.)
†These authors contributed equally to this work.
Cite this article as C. Bernard *et al.*, *Science* 378, eabm7466 (2022). DOI: 10.1126/science.abm7466

READ THE FULL ARTICLE AT
https://doi.org/10.1126/science.abm7466

RESEARCH ARTICLE

NEURODEVELOPMENT

Cortical wiring by synapse type–specific control of local protein synthesis

Clémence Bernard[1,2], David Exposito-Alonso[1,2]†, Martijn Selten[1,2]†, Stella Sanalidou[1,2], Alicia Hanusz-Godoy[1,2], Alfonso Aguilera[1,2], Fursham Hamid[1,2], Fazal Oozeer[1,2], Patricia Maeso[1,2], Leanne Allison[3], Matthew Russell[3], Roland A. Fleck[3], Beatriz Rico[1,2]*, Oscar Marín[1,2]*

Neurons use local protein synthesis to support their morphological complexity, which requires independent control across multiple subcellular compartments up to the level of individual synapses. We identify a signaling pathway that regulates the local synthesis of proteins required to form excitatory synapses on parvalbumin-expressing (PV^+) interneurons in the mouse cerebral cortex. This process involves regulation of the TSC subunit 2 (Tsc2) by the Erb-B2 receptor tyrosine kinase 4 (ErbB4), which enables local control of messenger RNA {mRNA} translation in a cell type–specific and synapse type–specific manner. Ribosome-associated mRNA profiling reveals a molecular program of synaptic proteins downstream of ErbB4 signaling required to form excitatory inputs on PV^+ interneurons. Thus, specific connections use local protein synthesis to control synapse formation in the nervous system.

The diversity of animal behaviors relies on the precise assembly of neuronal circuits, a process in which synapse formation plays a role. In the cerebral cortex, dozens of different types of excitatory glutamatergic pyramidal cells and inhibitory γ-aminobutyric acid-containing (GABAergic) interneurons are wired through distinct connectivity motifs (*1*, *2*). For example, layer 4 excitatory neurons receive inputs from excitatory thalamic neurons and project to layer 2/3 excitatory neurons and feedforward interneurons (*3*). Synapse specificity is established during development by dedicated transcriptional programs (*4*–*10*), but whether regulation of mRNA translation is also involved in this process remains to be elucidated.

Several pathways control protein synthesis (*11*, *12*), including the mechanistic target of rapamycin complex 1 (mTORC1), a molecular complex composed of mTOR kinase and several other proteins, which is activated by nutrients and growth factor signals and inhibited by the proteins Tsc1 and Tsc2 (*13*, *14*). Multiple mTORC1 pathway proteins and the translation machinery have been identified in developing axons (*15*–*17*), and local protein synthesis occurs at excitatory and inhibitory synapses in the adult brain (*18*–*24*). To what extent local translation is differentially regulated in closely related cell types and at the level of specific synapses during the wiring of cortical circuits is unknown.

[1]Centre for Developmental Neurobiology, Institute of Psychiatry, Psychology and Neuroscience, King's College London, London SE1 1UL, UK. [2]MRC Centre for Neurodevelopmental Disorders, King's College London, London SE1 1UL, UK. [3]Centre for Ultrastructural Imaging, King's College London, London SE1 1UL, UK.
*Corresponding author. Email: beatriz.rico@kcl.ac.uk (BR); oscar.marin@kcl.ac.uk (OM)
†These authors contributed equally to this work.

Specific synaptic defects in interneurons lacking Tsc2

To explore the role of protein synthesis in the wiring of different cell types in the cerebral cortex, we generated mice in which we deleted *Tsc2* from the two largest groups of cortical GABAergic interneurons: parvalbumin (PV)- and somatostatin (SST)-expressing cells. To this end, we crossed *Lhx6-Cre* mice, which drives recombination in early postmitotic PV^+ and SST^+ interneurons, with mice carrying conditional (i.e., Cre-dependent) *Tsc2* alleles ($Tsc2^{F/F}$) and a reporter for the visualization of recombined cells (see Methods). We chose these two cell types because although they derive from common progenitors in the medial ganglionic eminence (MGE) and the preoptic area (POA), populate the same layers of the neocortex, and are both reciprocally connected with pyramidal cells (*25*), they play very different roles in cortical information processing (*26*). We first confirmed that loss of *Tsc2* (fig. S1, A and B) leads to overactivation of mTOR signaling in PV^+ and SST^+ interneurons by analyzing the levels of phosphorylated S6 ribosomal protein (P-S6rp), a critical downstream effector of mTORC1 (*12*). We observed increased levels of P-S6rp in conditional *Tsc2* mutants compared with controls (fig. S1, C and D). We also found that the cell size of PV^+ and SST^+ interneurons is larger in conditional *Tsc2* mutants than in controls (fig. S1, C and E), reinforcing the notion that mTOR signaling is indeed overactive in these cells (*27*, *28*). Consistent with a previous report (*29*), we also noticed an increased density in an infrequent population of cortical interneurons that coexpress PV^+ and SST^+ in conditional *Tsc2* mutants compared with controls (fig. S2). By contrast, *Tsc2* loss does not affect the density or laminar distribution of PV^+ and SST^+ interneurons (fig. S2).

We next investigated whether loss of Tsc2 affects synapse formation onto PV^+ and SST^+ interneurons in the neocortex. To this end, we assessed the number of excitatory synapses received by cortical PV^+ and SST^+ interneurons by quantifying puncta containing vesicular glutamate transporter 1 (VGluT1), a characteristic component of excitatory glutamatergic terminals, and PSD95, the primary scaffolding protein in the excitatory postsynaptic density, on the soma and dendrites of PV^+ and SST^+ interneurons (Fig. 1 and fig. S3). We found that the loss of one and, even more so, two *Tsc2* alleles in PV^+ interneurons led to an increase in the density of excitatory synapses received by these cells compared with control littermates (Fig. 1, A and B, and fig. S3, A and B). By contrast, conditional deletion of *Tsc2* caused no changes in the density of excitatory synapses received by SST^+ interneurons (Fig. 1, C and D, and fig. S3C). The size of $VGluT1^+$ boutons and $PSD95^+$ puncta was not altered by the loss of Tsc2 (fig. S4).

To explore whether the supernumerary excitatory synapses contacting PV^+ interneurons in conditional *Tsc2* mutants represent functional synapses, we analyzed synaptic function by whole-cell recordings. Analysis of miniature excitatory postsynaptic currents (mEPSCs) revealed no differences in the frequency or amplitude of these synaptic events between control and conditional *Tsc2* mutants (fig. S5, A to E), which indicated that the supernumerary excitatory synapses contacting PV^+ interneurons lacking Tsc2 could either have altered release properties or be functionally inactive. To distinguish between both possibilities, we assessed release probability by recording paired-pulse ratios in PV^+ interneurons and found no differences between both genotypes (fig. S5, F and G). These observations suggested that the supernumerary excitatory synapses decorating PV^+ interneurons in conditional *Tsc2* mutants might not be mature.

We also observed cell type–specific alterations in intrinsic properties following the conditional deletion of *Tsc2* (fig. S6A). These changes led to a reduction in the excitability of PV^+ interneurons in conditional *Tsc2* mutants compared with controls, whereas no difference was observed for SST^+ interneurons (fig. S6B). Finally, the differential impact of the loss of Tsc2 in the integration of PV^+ and SST^+ interneurons in cortical networks was examined by recording spontaneous excitatory postsynaptic currents (sEPSCs) in both cell types (Fig. 1E). *Tsc2*

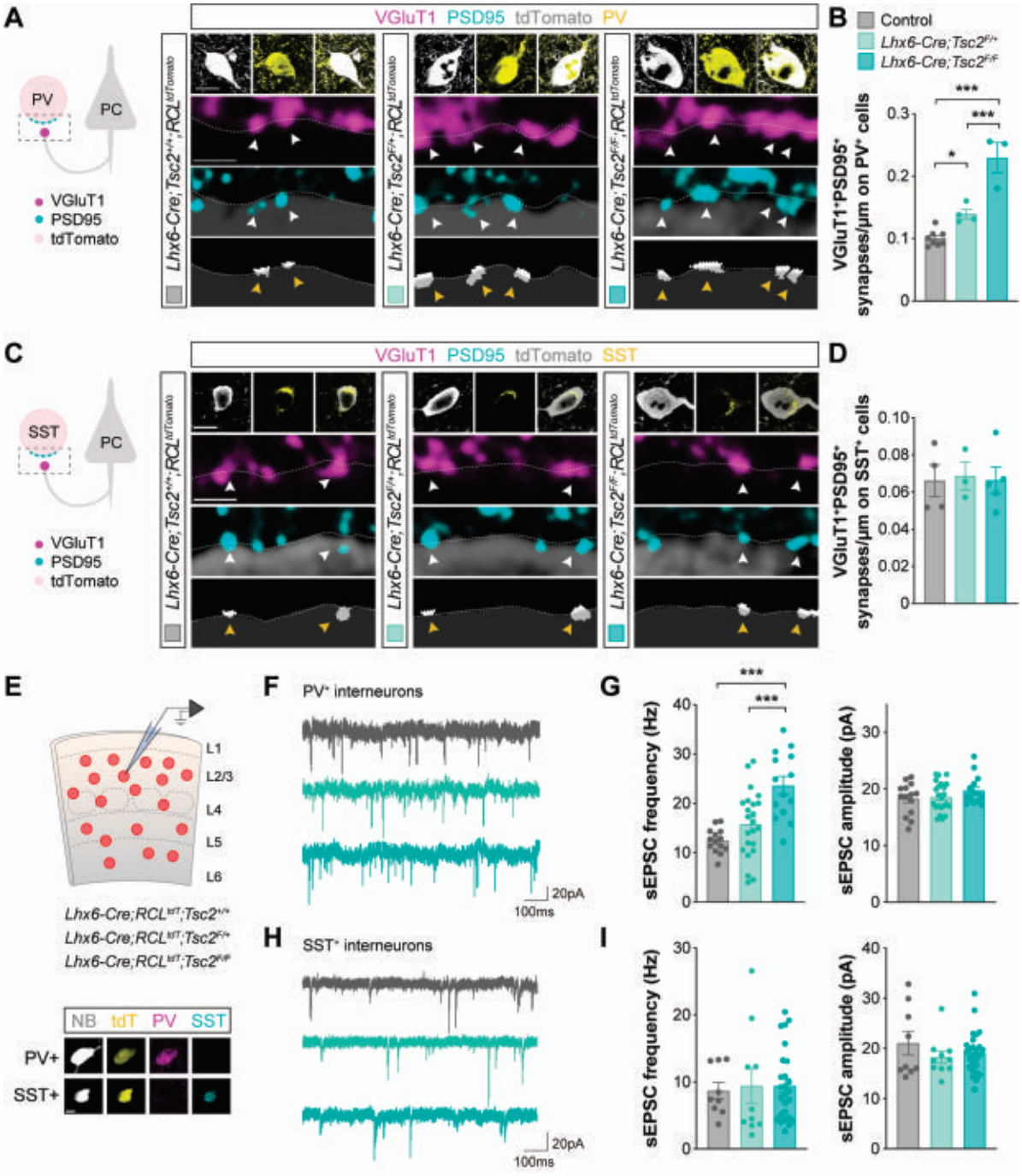

Fig. 1. Differential contribution of Tsc2 to synapse development.
(**A**) Schematic of synaptic markers analyzed (left). Confocal images (top) and binary images (bottom) illustrating presynaptic VGluT1$^+$ puncta (magenta) and postsynaptic PSD95$^+$ clusters (cyan) in PV$^+$ (yellow) tdTomato$^+$ (gray) interneurons from P18-21 control, heterozygous and homozygous conditional *Tsc2* mutants. (**B**) Quantification of the density of VGluT1$^+$PSD95$^+$ synapses contacting PV$^+$ interneurons (control, n = 111 cells from 8 mice; heterozygous, n = 70 cells from 4 mice; homozygous, n = 46 cells from 3 mice). (**C**) Schematic of synaptic markers analyzed (left). Confocal images (top) and binary images (bottom) illustrating presynaptic VGluT1$^+$ puncta (magenta) and postsynaptic PSD95$^+$ clusters (cyan) in SST$^+$ (yellow) tdTomato$^+$ (gray) interneurons from P18-21 control, heterozygous and homozygous conditional *Tsc2* mutants. (**D**) Quantification of the density of VGluT1$^+$PSD95$^+$ synapses contacting SST$^+$ interneurons (control, n = 67 cells from 4 mice; heterozygous, n = 41 cells from 3 mice; homozygous, n = 60 cells from 5 mice). (**E**) Schematic of experimental design (top) and post-recording labeling of neurobiotin (NB, gray)-filled tdTomato$^+$ (yellow) cells with PV (magenta) and SST (cyan) (bottom). (**F**) Example traces of sEPSCs recorded from PV$^+$ interneurons from P18-21 control, heterozygous and homozygous conditional *Tsc2* mutants. (**G**) Quantification of the frequency (left) and amplitude (right) of sEPSCs from PV$^+$ interneurons (control n = 14 cells from 5 mice, *Lhx6-Cre;Tsc2*$^{F/+}$ n = 23 cells from 8 mice, *Lhx6-Cre;Tsc2*$^{F/F}$ n = 14 cells from 6 mice). (**H**) Example traces of sEPSCs recorded from SST$^+$ interneurons from P18-21 control, heterozygous, and homozygous conditional *Tsc2* mutants. (**I**) Quantification of the frequency (left) and amplitude (right) of sEPSCs from SST$^+$ interneurons (control, n = 9 cells from 5 mice; heterozygous, n = 10 cells from 9 mice;

homozygous, n = 26 cells from 7 mice). One-way ANOVA followed by Tukey's multiple comparisons test or Kruskal-Wallis followed by Dunn's multiple comparisons test: *P < 0.05, **P < 0.01, ***P < 0.001. The dashed lines in the images shown in (A) and (C) outline the surface of the cells. Data are mean ± SEM. Scale bar, 10 μm and 1 μm (high magnification) (A and C), and 10 μm (E).

deletion in PV$^+$ interneurons led to a significant increase in the frequency of sEPSCs with no changes in amplitude (Fig. 1, F and G) whereas neither the frequency nor the amplitude of sEPSCs changed in SST$^+$ interneurons lacking *Tsc2* (Fig. 1, H and I). Altogether, these results revealed that loss of *Tsc2* differentially affects the wiring of PV$^+$ and SST$^+$ interneurons, suggesting a cell type–specific role for Tsc2 in synapse formation.

We next wondered whether the function of Tsc2 in synapse development might be synapse type-specific. We reasoned that if Tsc2 plays a role in synapse formation in PV$^+$ interneurons, loss of Tsc2 should also affect the development of the synapses made by these cells onto pyramidal cells. We focused on PV$^+$ basket cell synapses, which target the soma of pyramidal cells and can be identified by the presynaptic expression of synaptotagmin-2 (Syt2) and gephyrin (Geph), a postsynaptic scaffolding protein of GABAergic synapses (*30*). We found no differences in the density of Syt2$^+$Geph$^+$ synaptic puncta contacting the soma of pyramidal cells in conditional *Tsc2* mutants compared with control littermates (fig. S7). Thus, although the loss of Tsc2 causes a global disruption of mTOR signaling in PV$^+$ and SST$^+$ cells (e.g., increased cell size and P-S6rp), it seems to affect the wiring of interneurons in a cell type–specific and synapse type–specific manner.

Tsc2 functions downstream of ErbB4 in synapses

Because the loss of Tsc2 function leads only to changes in the excitatory synaptic input of PV$^+$ interneurons, we reasoned that Tsc2 activity could be regulated locally by a signaling pathway specific to these synapses and necessary for their formation. In other cellular contexts, Tsc2 activity is inhibited by factors that stimulate cell growth through the phosphorylation of Akt (*14*, *31*). The receptor tyrosine kinase ErbB4—which is enriched in PV$^+$ but not SST$^+$ interneurons and is required for the formation of excitatory synapses onto PV$^+$ interneurons (*32*–*34*)—activates Akt through PI3K phosphorylation (*35*), and associates with Tsc2 in synaptosome preparations obtained from the mouse neocortex during synaptogenesis (fig. S8). This led us to hypothesize that ErbB4 functions upstream of Tsc2 to regulate its activity during the development of these specific synapses (Fig. 2A). To begin testing this hypothesis, we analyzed Tsc2 phosphorylation in synaptosomes obtained from the neocortex of control and interneuron-specific *Erbb4* conditional mutants (Fig. 2B). These preparations are enriched in synaptosomes (fig. S9, A and B), which are predominantly bipartite (fig. S9, C and D, and fig. S10), have both the pre- and postsynaptic sides enclosed in a membrane (fig. S9, E and F, fig. S11) and contain synaptic proteins (fig. S9G). We found reduced Akt-mediated phosphorylation of Tsc2 in cortical synapses from *Erbb4* conditional mutants compared with controls (Fig. 2, C and D). We also found reduced phosphorylation of the mTORC1 effectors S6rp and eIF4E-binding protein 1 (4E-BP1) in synaptosomes from *Erbb4* conditional mutants (Fig. 2, C and D), which indicates that the loss of ErbB4 function decreases mTORC1 synaptic activity as a result of the overactivation of Tsc2. None of these changes were observed in cytosolic fractions (Fig. 2, E and F), suggesting that ErbB4 is required to modulate Tsc2 signaling specifically at the synapse.

We next investigated whether the mTORC1 inactivation observed in *Erbb4* conditional mutants occurs at specific cortical synapses. Because ErbB4 is only expressed by specific classes of interneurons in the cerebral cortex (*32*, *36*), we hypothesized that changes would be limited to synapses that contain ErbB4 receptors, such as the excitatory synapses received by PV$^+$ basket cells. To test this idea, we isolated and plated cortical synaptosomes and analyzed the phosphorylation of S6rp in postsynaptic structures identified with PSD95. We identified excitatory synapses onto inhibitory neurons using neuregulin 3 (Nrg3), a marker of presynaptic excitatory terminals contacting PV$^+$ interneurons (*37*, *38*). We found decreased P-S6rp specifically in Nrg3$^+$/PSD95$^+$ synaptosomes from *Erbb4* conditional mutants compared with controls, but no difference in ErbB4-independent glutamatergic synaptosomes (Fig. 2, G to I) or Syt2$^+$/Geph$^+$ synaptosomes (fig. S12), which correspond to the synapses made by PV$^+$ basket cells onto pyramidal cells. These results indicate that ErbB4 regulates mTOR signaling in excitatory synapses received by PV$^+$ interneurons.

To further support the idea that ErbB4 and Tsc2 function in the same signaling pathway controlling the formation of excitatory synapses onto PV$^+$ cells, we performed a genetic interaction experiment. We generated *Erbb4* conditional mutants carrying a conditional *Tsc2* allele to compromise the function of Tsc2 in PV$^+$ interneurons lacking ErbB4 and measured the density of excitatory synapses received by these cells. We found that deleting one *Tsc2* allele from PV$^+$ cells is sufficient to rescue the loss of excitatory synapses found in *Erbb4* conditional mutants (fig. S13). Altogether, these results demonstrate that Tsc2 functions downstream of ErbB4 in regulating the excitatory synaptic input of PV$^+$ interneurons.

Changes in the synaptic translatome of *Erbb4* mutants

To identify the specific targets of ErbB4 that are involved in the development of synapses in PV$^+$ interneurons, we first obtained the synaptic translatome of MGE/POA-derived interneurons from control and *Erbb4* conditional mutants. To this end, we bred into these mice alleles carrying a mutation in the locus encoding the ribosomal protein L22 (Rpl22) that allows the conditional tagging of ribosomes with a hemagglutinin epitope (HA) tag (*39*). We then prepared synaptosomes from the neocortex of P15 mice, pulled down ribosomes from this preparation using anti-HA beads to isolate ribosome-associated mRNA transcripts from MGE/POA-derived interneurons in control and *ErbB4* conditional mutants, and then analyzed them by RNA sequencing (Fig. 3A and fig. S14, A to D).

We found that 70% of the differentially expressed genes were down-regulated in *Erbb4* conditional mutants compared with controls (Fig. 3B and fig. S14D). Among the down-regulated genes, we observed a significant enrichment in genes associated with autism spectrum disorder (ASD) (fig. S15). Gene ontology (GO) analysis revealed an enrichment in genes involved in processes such as "synapse organization", "neurotransmitter receptor activity", and "glutamatergic synapse" (Fig. 3C and fig. S14E), highlighting synaptic alterations in *Erbb4* conditional mutants. We then identified genes coding for proteins with postsynaptic localization and/or function using synaptic GO annotations (*40*). This analysis revealed that within the postsynaptic category, the most enriched terms were postsynaptic specialization and postsynaptic membrane and, more specifically, genes encoding cell adhesion molecules and AMPA receptors (Fig. 3, D and E, and fig. S14F). Using a set of four additional criteria (see Methods), including their relative enrichment in PV$^+$ cells, we selected seven candidates for functional validation: five cell adhesion molecules, SynCAM1 (encoded by *Cadm1*), Nptn, Nlgn3, TrkC (encoded by *Ntrk3*), and Clstn2, and two AMPA receptor-related proteins, GluA4 (encoded by *GriA4*) and Stargazin (encoded by *Cacng2*) (Fig. 3E).

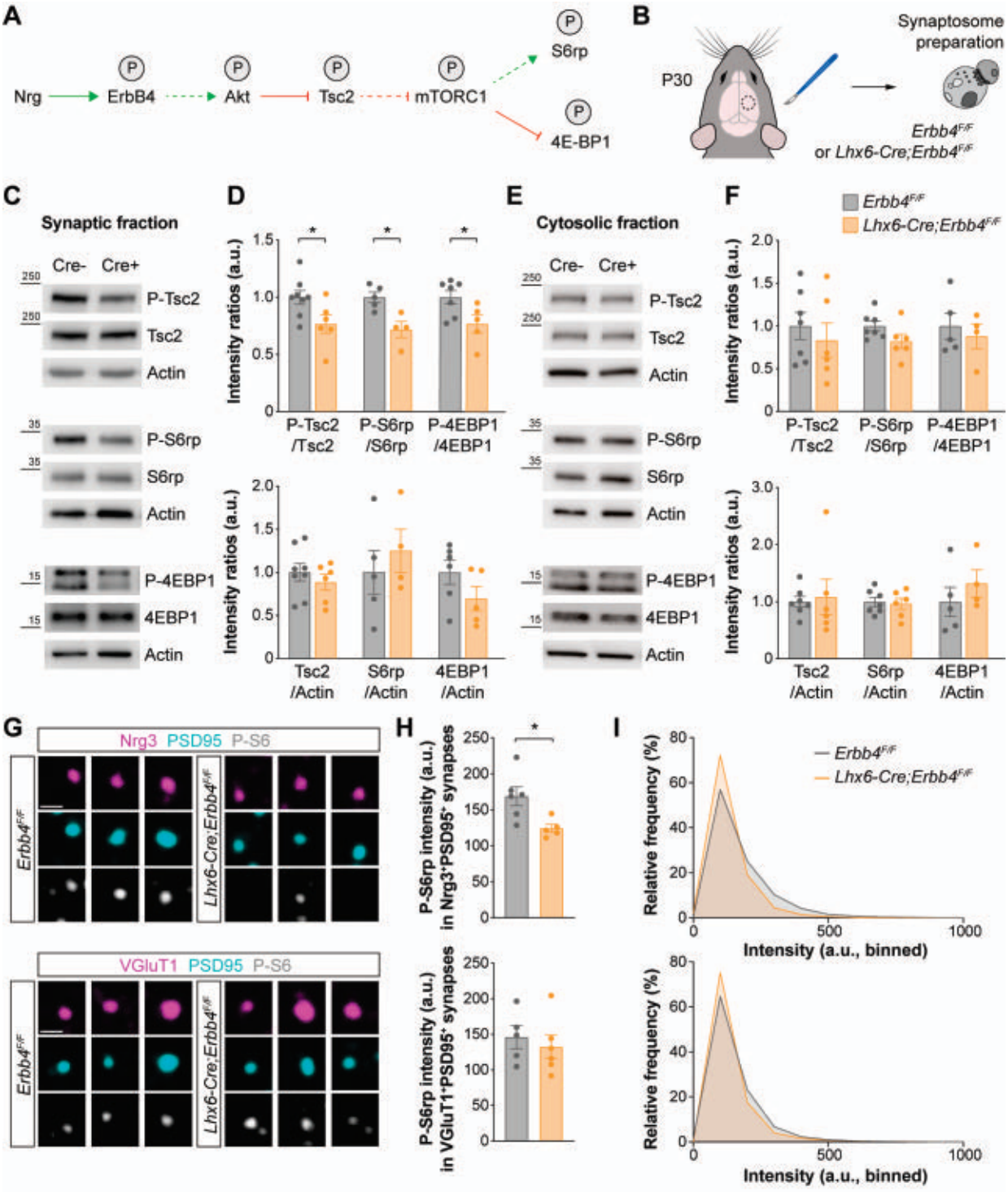

Fig. 2. ErbB4 regulates mTOR at excitatory synapses contacting PV$^+$ interneurons. (**A**) Hypothetical signaling pathway. P indicates phosphorylation; green arrow, activation; red arrow, inhibition; dotted arrows, indirect regulation. (**B**) Schematic of experimental design. (**C**) Phosphorylation and protein expression of Tsc2, S6rp, 4EBP1, and actin assessed by Western blot of cortical synaptic fractions from P30 homozygous conditional *Erbb4* mice and their control littermates. (**D**) Quantification of phosphorylation of Tsc2, S6rp, and 4EBP1 normalized to the total expression of the corresponding protein (top). Quantification of expression levels of Tsc2, S6rp, and 4EBP1 normalized to actin (bottom) (Tsc2: control, n = 8 mice, homozygous, n = 6 mice; S6rp: control, n = 5 mice, homozygous, n = 4 mice; 4EBP1: control, n = 7 mice, homozygous, n = 5 mice). (**E**) Phosphorylation and protein expression of Tsc2, S6rp, 4EBP1, and actin assessed by Western blot of cortical cytosolic fractions from P30 homozygous conditional *Erbb4* mice and their control littermates. (**F**) Quantification of phosphorylation of Tsc2, S6rp, and 4EBP1 normalized to the total expression of the corresponding protein (top). Quantification of expression levels of Tsc2, S6rp, and 4EBP1 normalized to actin (bottom) (Tsc2 and S6rp: control, n = 7 mice, homozygous, n = 6 mice; 4EBP1: control, n = 5 mice, homozygous, n = 4 mice). (**G**) Confocal images illustrating phosphorylation of S6rp (P-S6rp, gray) in Nrg3$^+$ (magenta) PSD95$^+$ (cyan)

synaptosomes (top) and in VGluT1$^+$ (magenta) PSD95$^+$ (cyan) synaptosomes (bottom) from P21 homozygous conditional *Erbb4* mice and their control littermates. (**H**) Quantification of P-S6rp staining intensity in Nrg3$^+$PSD95$^+$ (top) and VGluT1$^+$PSD95$^+$ synaptosomes (bottom). (**I**) Relative frequency distribution of P-S6rp staining intensity in Nrg3$^+$PSD95$^+$ synaptosomes (top) and in VGluT1$^+$PSD95$^+$ synaptosomes (bottom) (Nrg3$^+$PSD95$^+$: control, n = 22,063 synaptosomes from 6 mice, homozygous, n = 17,523 synaptosomes from 5 mice; VGluT1$^+$PSD95$^+$: control, n = 39,395 synaptosomes from 5 mice, homozygous, n = 48,057 synaptosomes from 6 mice). Two-tailed Student's unpaired t-tests: *P < 0.05. Data are mean ± SEM. Scale bar, 1 µm.

We confirmed that cortical PV$^+$ interneurons express these mRNAs during synaptogenesis (fig. S16, A and B) and that they are present in the dendrites of these cells (fig. S17; see also *24*). In addition, we found that these proteins cluster at the surface of PV$^+$ cells in close apposition to innervating axon terminals expressing the presynaptic ErbB4 ligand Nrg3 (fig. S16, C to E). Altogether, our data reveal dysregulation of postsynaptic molecular complexes in PV$^+$ cells lacking ErbB4.

ErbB4 regulates local protein synthesis at the synapse

Having identified ribosome-associated mRNAs that might be critical for the formation of excitatory synapses onto PV$^+$ cells, we next wondered whether ErbB4 might regulate this process by modulating the local translation of these transcripts. mTORC1 signaling is critical for the modulation of protein synthesis (*12*), and our previous results revealed that mTORC1 synaptic activity decreases in the absence of ErbB4 (Fig. 2). ErbB4 could therefore regulate synapse formation by controlling local protein synthesis at the synapse through the inhibition of Tsc2. To test this hypothesis, we assessed whether activation of ErbB4 signaling in cortical synaptosomes increases the translation of the ribosome-associated mRNAs we identified as down-regulated in *ErbB4* conditional mutants. To this end, we treated cortical synaptosomes with a soluble form of the epidermal growth factor (EGF)-like domain of neuregulin to activate ErbB4 receptors (*41*) (fig. S18, A to C) and examined candidate proteins by Western blot (Fig. 4A). We found increased protein levels for all but one of the downstream candidates of ErbB4 signaling (Fig. 4, B and C). We did not observe this increase when the samples were pretreated with the protein synthesis inhibitor cycloheximide (fig. S18, D and E), demonstrating that ErbB4 signaling induces the translation of these transcripts at the synapse. Altogether, these experiments revealed that ErbB4 regulates the local translation of synaptic proteins.

Mediators of excitatory synapse formation on PV$^+$ interneurons

To assess whether the proteins being synthesized downstream of ErbB4 are involved in the formation of excitatory synapses on cortical PV$^+$ interneurons, we performed interneuron-specific loss-of-function experiments in vivo using a conditional gene knockdown strategy (*42*). In brief, we designed conditional short-hairpin RNA vectors against the candidate genes (*shCadm1, shNptn, shNlgn3, shNtrk3, shClstn2, shGria4*, and *shCacng2*, with *shLacZ* as a control) and confirmed their effectiveness in vitro (fig. S19A). We generated adeno-associated viruses (AAVs) expressing

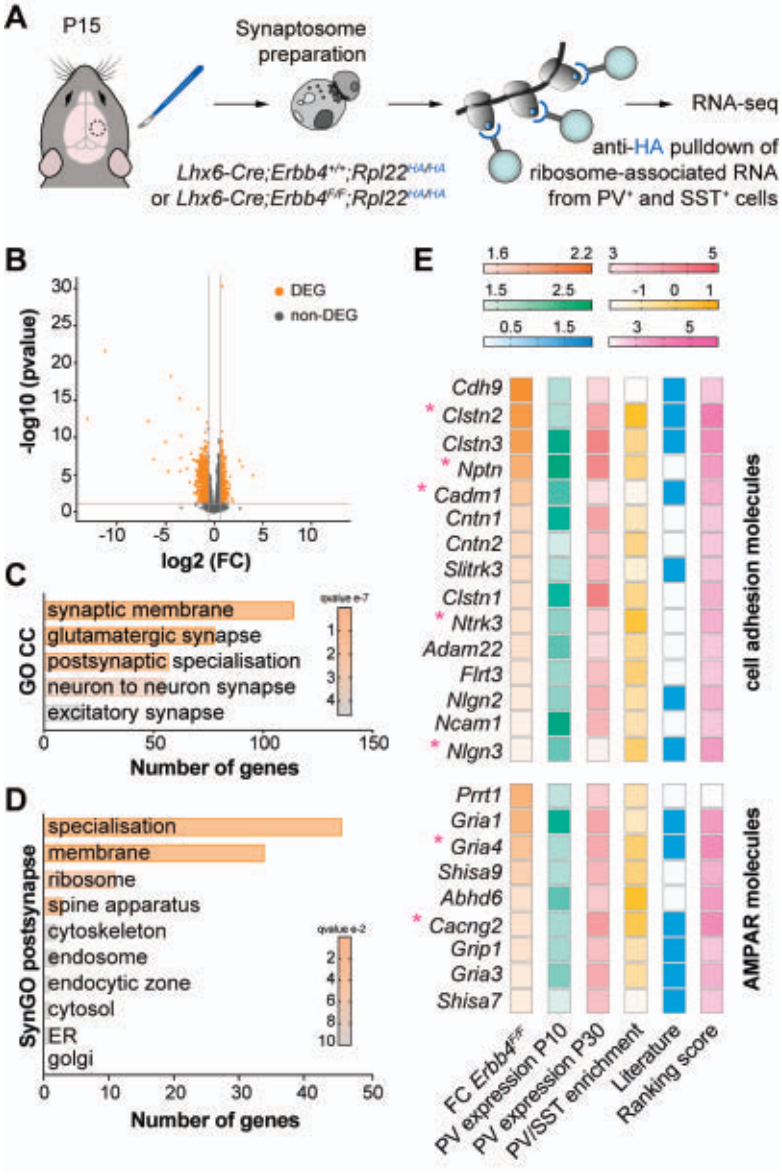

Fig. 3. Synaptic ribosome-associated mRNAs altered in *Erbb4* mutants. (**A**) Schematic of experimental design. (**B**) Volcano plot displaying significantly differentially expressed ribosome-associated RNAs (DEG, orange) in P15 cortical synaptosomes from homozygous conditional *Erbb4* mice compared with controls. Each dot represents one gene. FC, fold change (FC > 1.5, P < 0.05). (**C**) Selected gene ontology (GO) and cellular components (CC) terms significantly enriched in the dataset of downregulated genes in homozygous conditional *Erbb4* mutants compared with controls. (**D**) Synaptic gene ontology (SynGO) postsynaptic cellular component categories significantly enriched in the dataset of downregulated genes in homozygous conditional *Erbb4* mutants compared with controls. (**E**) Heatmaps showing the selection criteria for 15 "cell adhesion molecule" genes and 9 "AMPA receptor" genes. Asterisks indicate genes selected for validation.

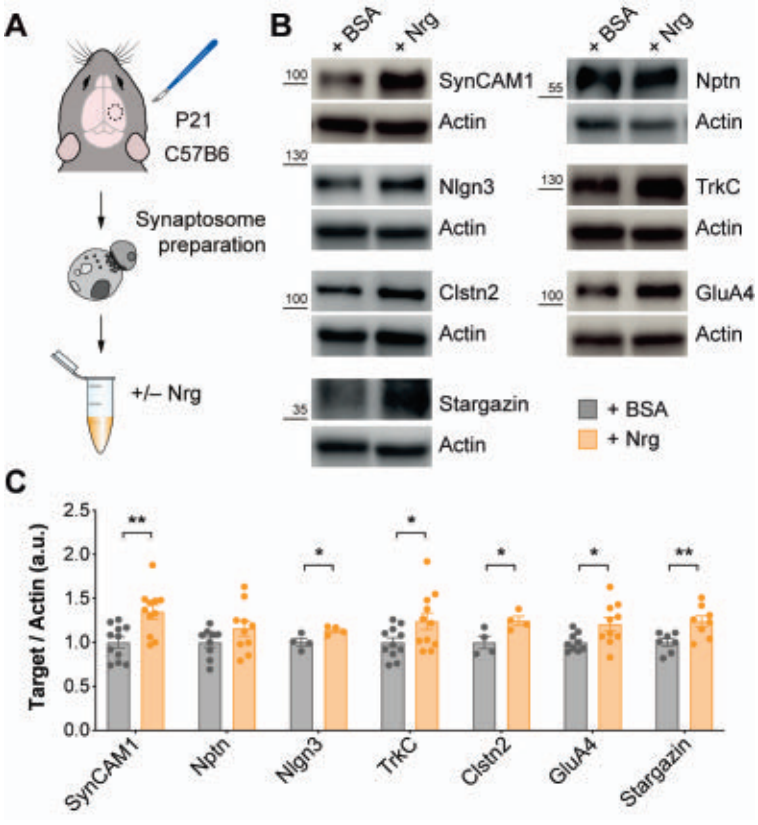

Fig. 4. ErbB4 regulates local translation of synaptic proteins. (**A**) Schematic of experimental design. (**B**) Protein expression of SynCAM1, Nptn, Nlgn3, TrkC, Clstn2, GluA4, Stargazin, and actin assessed by Western blot of cortical synaptic fractions treated with neuregulin (Nrg) from P21 C57B6 mice. (**C**) Quantification of expression levels of SynCAM1, Nptn, Nlgn3, TrkC, Clstn2, GluA4, and Stargazin normalized to actin. One-tailed Student's unpaired *t* tests: $*P < 0.05$, $**P < 0.01$ (SynCAM1 and TrkC: +BSA, n = 11 synaptosomes: +Nrg, n = 11 synaptosomes; Nptn and GluA4: +BSA, n = 9 synaptosomes, +Nrg, n = 10 synaptosomes; Nlgn3 and Clstn2: +BSA, n = 4 synaptosomes, +Nrg, n = 4 synaptosomes; Stargazin: +BSA, n = 7 synaptosomes, +Nrg, n = 8 synaptosomes). Data are mean ± SEM.

the most effective shRNA constructs, injected them into the neocortex of *Lhx6-Cre* neonates, and confirmed their ability to down-regulate the expression of the corresponding target genes in vivo (fig. S19B). We then assessed the number of excitatory synapses received by PV^+ interneurons expressing control and experimental *shRNAs* (Fig. 5A). We found that, compared with controls, reducing the expression of each of the seven targets in PV^+ interneurons led to a decrease in the density of excitatory synapses received by these cells (Fig. 5, B to D). These results revealed a complex molecular program regulated by ErbB4 that includes SynCAM1, Nlgn3, TrkC, Clstn2, GluA4, and Stargazin, and controls the formation of excitatory synapses onto PV^+ interneurons.

Discussion

Although local protein synthesis is common to synapses in the adult brain (*23*, *43*), the specificity of mRNA translation in different cell types and even in distinct connectivity motifs of the same neuron remains unexplored. Our work indicates that protein synthesis is regulated in a synapse type–specific manner during synapse formation. Tsc2, a regulator of mTORC1 signaling in multiple cellular contexts (*12*), regulates the development of excitatory synapses onto PV^+ cells but not onto SST^+ interneurons. This specificity is mediated by the activation of ErbB4, which controls excitatory synapse development through the inhibition of Tsc2 and the subsequent induction of a molecular program of mRNA translation involving the synthesis of several cell adhesion- and glutamate receptor-related proteins, including TrkC, Clstn2, GluA4, and Stargazin, as well as other molecules previously linked to glutamatergic synapses contacting interneurons (*44*–*46*). This synapse type–specific regulation could also involve a redistribution of the protein supply to neighboring maturing synapses, as described for synaptic plasticity (*47*).

Our results reveal that local translation is involved in synapse formation. Work in *Drosophila* suggested that the local action of the phosphatase Prl-1 (phosphatase of regenerating liver 1) in synapse formation might be achieved by local translation (*48*). Here, we found that translation occurs locally in developing synapses in the mammalian neocortex and that disrupting the machinery regulating protein synthesis deregulates synapse formation. Moreover, we demonstrate that many of the proteins identified as being synthesized at developing synapses are involved in synapse formation. Therefore, local translation contributes to brain wiring not only during axon guidance (*15*–*17*, *49*–*51*) but also in the final stages of neural circuit assembly.

Altered synthesis of synaptic proteins is a core pathophysiological mechanism in ASD (*52*–*57*). Although the evidence linking *ERBB4* with intellectual disability and ASD is scarce (*58*, *59*), the enrichment of autism-associated genes among the genes down-regulated in *ErbB4* conditional mutants and the identification of *NLGN3* as a target of ErbB4-Tsc2 signaling in the formation of excitatory synapses onto PV^+ interneurons is notable because mutations in *TSC2* and *NLGN3* are associated with ASD (*60*–*64*). The excitation received by PV^+ cells is modulated during experience (*42*, *65*, *66*), suggesting a prominent role in learning and memory. The synapse-specific molecular program unveiled in this study reinforces the idea that this connection is a sensitive hub for maladaptive network responses in neurodevelopmental disorders.

Materials and Methods summary

Conditional mouse mutants from MGE-derived interneurons were generated by crossing *Lhx6-Cre* mice with $Tsc2^{F/F}$ or $Erbb4^{F/F}$ mice. To generate cell type–specific knockdown in vivo, shRNAs against genes of interest were first tested for down-regulation in vitro. *Lhx6-Cre* neonates were then injected intracranially with Cre-dependent AAVs expressing the shRNAs with the highest knockdown efficiencies. For histological analyses, brains were fixed in 4% paraformaldehyde (PFA) and sectioned frozen on a sliding microtome (Leica). 40-μm thick sections were used for immunohistochemistry, whereas 30 μm thick sections were used to detect gene expression using the RNAscope Multiplex Fluorescent Assay protocol (ACDBio). Images were acquired with an inverted SP8 confocal microscope (Leica) or an ApoTome microscope (Zeiss) and analyzed with Imaris (Bitplane) and custom macros in FIJI (ImageJ). Synaptic function, paired-pulse ratio, and intrinsic properties of interneurons were analyzed by patch-clamp recordings on acute coronal slices using Mini Analysis (Synaptosoft) and Clampfit.

Synaptosomes were prepared with SynPER reagent (ThermoScientific) from cortical tissue and processed for several downstream

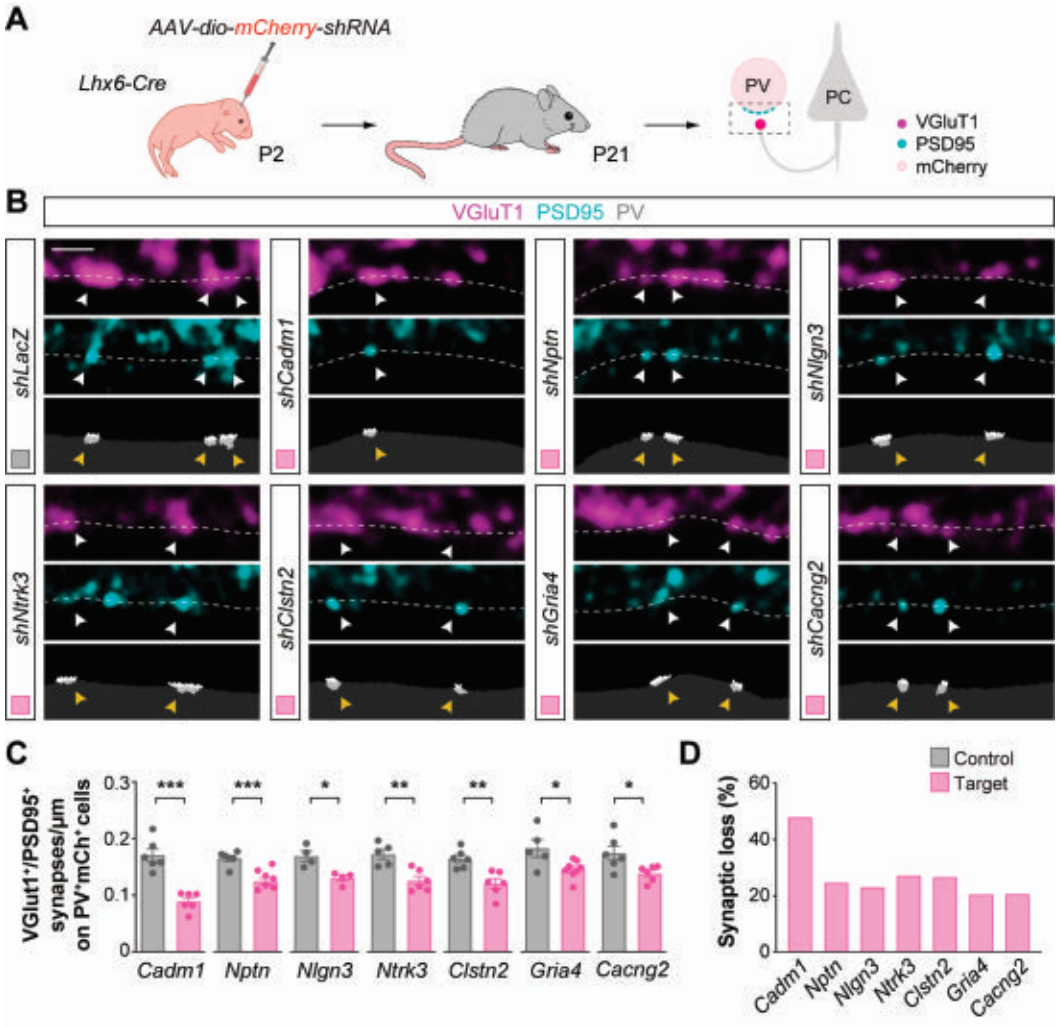

Fig. 5. ErbB4 targets control excitatory synapse formation on PV$^+$ interneurons. (**A**) Schematic of experimental design. (**B**) Confocal images (top) and binary images (bottom) illustrating presynaptic VGluT1$^+$ puncta (magenta) and postsynaptic PSD95$^+$ clusters (cyan) in PV$^+$ interneurons (gray) from P21 *Lhx6-Cre* mice injected with viruses expressing *shRNAs* targeting the genes of interest or with a control virus (*shLacZ*). (**C**) Quantification of the density of VGluT1$^+$PSD95$^+$ synapses contacting PV$^+$ interneurons in knockdown and control mice. Two-tailed Student's unpaired t-tests: $^*P < 0.05$, $^{**}P < 0.01$, $^{***}P < 0.001$; *shCadm1* (n = 122 cells from 6 mice) and control (n = 113 cells from 6 mice); *shNptn* (n = 131 cells from 6 mice) and control (n = 119 cells from 6 mice); *shNlgn3* (n = 86 cells from 4 mice) and control (n = 68 cells from 4 mice); *shNtrk3* (n = 126 cells from 6 mice) and control (n = 105 cells from 5 mice); *shClstn2* (n = 120 cells from 6 mice) and control (n = 112 cells from 6 mice); *shGria4* (n = 121 cells from 8 mice) and control (n = 93 cells from 5 mice); *shCacng2* (n = 115 cells from 6 mice) and control (n = 109 cells from 6 mice). (**D**) Proportion of synaptic loss in PV$^+$ interneurons upon knockdown of ErbB4 downstream targets. Data are mean ± SEM. Scale bar, 1 µm.

experiments, including coimmunoprecipitation, ErbB4 pathway activation and protein synthesis, Western blot, plating and immunofluorescence, and transmission electron microscopy. For coimmunoprecipitation, synaptosomes were incubated overnight with antibodies or isotype controls, added on Dynabeads (Invitrogen), and then extensively washed. For ErbB4 activation, synaptosomes were treated with Nrg-EGF or BSA for control, with or without pre-incubation with cycloheximide. For Western blot, denatured protein extracts were separated by SDS-PAGE and transferred onto PVDF membranes, blocked, and incubated with primary antibodies, HRP-conjugated secondary antibodies, and chemiluminescent substrates. Membranes were then imaged with an Odyssey FC (Li-Cor). Densitometry analyses were performed with Image Studio Lite. For immunofluorescence, synaptosomes were plated on 8-well chamber slides coated with poly-D-lysine and fixed with 4% PFA. Samples were then blocked and incubated overnight with primary antibodies, followed by washes and incubation with secondary antibodies for 2 hours at room temperature. For electron microscopy, synaptosomes were fixed in 2.5% glutaraldehyde. Following washes, postfixation, dehydration, and infiltration with Spurr epoxy resin-acetone mixture, samples were sectioned using an ultramicrotome (Leica) and examined on a JEM 1400 Flash transmission microscope (JEOL).

To isolate ribosome-associated RNAs of MGE-derived interneurons from cortical synaptic fractions, RiboTag (*Rpl22*$^{HA/HA}$) mice were crossed with *Lhx6-Cre;Erbb4*$^{F/F}$ mice. Following the preparation of synaptosomes and anti-HA pulldown using magnetic beads (Pierce), RNA samples were sequenced using a HiSeq 2500 platform (Illumina). Differential gene expression was performed using DESeq2 on R, and candidate targets were selected using the SynGO tool and ranked for validation using a set of criteria that included expression and enrichment in MGE-derived interneurons.

REFERENCES AND NOTES

1. T. Klausberger, P. Somogyi, Neuronal diversity and temporal dynamics: The unity of hippocampal circuit operations. *Science* **321**, 53–57 (2008). doi: 10.1126/science.1149381; pmid: 18599766
2. K. D. Harris, G. M. Shepherd, The neocortical circuit: Themes and variations. *Nat. Neurosci.* **18**, 170–181 (2015). doi: 10.1038/nn.3917; pmid: 25622573
3. R. J. Douglas, K. A. Martin, Neuronal circuits of the neocortex. *Annu. Rev. Neurosci.* **27**, 419–451 (2004). doi: 10.1146/annurev.neuro.27.070203.144152; pmid: 15217339
4. F. Ango *et al*., Ankyrin-based subcellular gradient of neurofascin, an immunoglobulin family protein, directs GABAergic innervation at purkinje axon initial segment. *Cell* **119**, 257–272 (2004). doi: 10.1016/j.cell.2004.10.004 pmid: 15479642
5. M. E. Williams *et al*., Cadherin-9 regulates synapse-specific differentiation in the developing hippocampus. *Neuron* **71**, 640–655 (2011). doi: 10.1016/j.neuron.2011.06.019 pmid: 21867881
6. X. Duan, A. Krishnaswamy, I. De la Huerta, J. R. Sanes, Type II cadherins guide assembly of a direction-selective retinal circuit. *Cell* **158**, 793–807 (2014). doi: 10.1016/j.cell.2014.06.047; pmid: 25126785
7. E. Favuzzi *et al*., Distinct molecular programs regulate synapse specificity in cortical inhibitory circuits. *Science* **363**, 413–417 (2019). doi: 10.1126/science.aau8977; pmid: 30679375
8. R. Sando, X. Jiang, T. C. Südhof, Latrophilin GPCRs direct synapse specificity by coincident binding of FLRTs and teneurins. *Science* **363**, eaav7969 (2019). doi: 10.1126/science.aav7969; pmid: 30792275
9. J. de Wit, A. Ghosh, Specification of synaptic connectivity by cell surface interactions. *Nat. Rev. Neurosci.* **17**, 22–35 (2016). doi: 10.1038/nrn.2015.3; pmid: 26656254
10. K. Shen, P. Scheiffele, Genetics and cell biology of building specific synaptic connectivity. *Annu. Rev. Neurosci.* **33**, 473–507 (2010). doi: 10.1146/annurev.neuro.051508.135302; pmid: 20367446
11. J. Pelletier, N. Sonenberg, The Organizing Principles of Eukaryotic Ribosome Recruitment. *Annu. Rev. Biochem.* **88**, 307–335 (2019). doi: 10.1146/annurev-biochem-013118-111042; pmid: 31220979
12. R. A. Saxton, D. M. Sabatini, mTOR signaling in growth, metabolism, and disease. *Cell* **168**, 960–976 (2017). doi: 10.1016/j.cell.2017.02.004; pmid: 28283069
13. X. Gao *et al*., Tsc tumour suppressor proteins antagonize amino-acid-TOR signalling. *Nat. Cell Biol.* **4**, 699–704 (2002). doi: 10.1038/ncb847; pmid: 12172555
14. K. Inoki, Y. Li, T. Zhu, J. Wu, K. L. Guan, TSC2 is phosphorylated and inhibited by Akt and suppresses mTOR signalling. *Nat. Cell Biol.* **4**, 648–657 (2002). doi: 10.1038/ncb839; pmid: 12172553
15. D. S. Campbell, C. E. Holt, Chemotropic responses of retinal growth cones mediated by rapid local protein synthesis and degradation. *Neuron* **32**, 1013–1026 (2001). doi: 10.1016/S0896-6273(01)00551-7; pmid: 11754834
16. P. A. Brittis, Q. Lu, J. G. Flanagan, Axonal protein synthesis provides a mechanism for localized regulation at an intermediate target. *Cell* **110**, 223–235 (2002). doi: 10.1016/S0092-8674(02)00813-9; pmid: 12150930
17. A. Poulopoulos *et al*., Subcellular transcriptomes and proteomes of developing axon projections in the cerebral cortex. *Nature* **565**, 356–360 (2019). doi: 10.1038/s41586-018-0847-y; pmid: 30626971
18. H. Kang, E. M. Schuman, A requirement for local protein synthesis in neurotrophin-induced hippocampal synaptic plasticity. *Science* **273**, 1402–1406 (1996). doi: 10.1126/science.273.5280.1402; pmid: 8703078
19. A. Gardiol, C. Racca, A. Triller, Dendritic and postsynaptic protein synthetic machinery. *J. Neurosci.* **19**, 168–179 (1999). doi: 10.1523/JNEUROSCI.19-01-00168.1999; pmid: 9870948
20. L. E. Ostroff, J. C. Fiala, B. Allwardt, K. M. Harris, Polyribosomes redistribute from dendritic shafts into spines with enlarged synapses during LTP in developing rat hippocampal slices. *Neuron* **35**, 535–545 (2002). doi: 10.1016/S0896-6273(02)00785-7; pmid: 12165474
21. S. J. Tang *et al*., A rapamycin-sensitive signaling pathway contributes to long-term synaptic plasticity in the hippocampus. *Proc. Natl. Acad. Sci. U.S.A.* **99**, 467–472 (2002). doi: 10.1073/pnas.012605299; pmid: 11756682
22. T. J. Younts *et al*., Presynaptic protein synthesis is required for long-term plasticity of GABA release. *Neuron* **92**, 479–492 (2016). doi: 10.1016/j.neuron.2016.09.040; pmid: 27764673
23. A. S. Hafner, P. G. Donlin-Asp, B. Leitch, E. Herzog, E. M. Schuman, Local protein synthesis is a ubiquitous feature of neuronal pre- and postsynaptic compartments. *Science* **364**, eaau3644 (2019). doi: 10.1126/science.aau3644; pmid: 31097639
24. J. D. Perez *et al*., Subcellular sequencing of single neurons reveals the dendritic transcriptome of GABAergic interneurons. *eLife* **10**, e63092 (2021). doi: 10.7554/eLife.63092; pmid: 33404500
25. L. Lim, D. Mi, A. Llorca, O. Marín, Development and functional diversification of cortical interneurons. *Neuron* **100**, 294–313 (2018). doi: 10.1016/j.neuron.2018.10.009; pmid: 30359598
26. A. Kepecs, G. Fishell, Interneuron cell types are fit to function. *Nature* **505**, 318–326 (2014). doi: 10.1038/nature12983 pmid: 24429630
27. D. C. Fingar, S. Salama, C. Tsou, E. Harlow, J. Blenis, Mammalian cell size is controlled by mTOR and its downstream targets S6K1 and 4EBP1/eIF4E. *Genes Dev.* **16**, 1472–1487 (2002). doi: 10.1101/gad.995802 pmid: 12080086
28. S. F. Tavazoie, V. A. Alvarez, D. A. Ridenour, D. J. Kwiatkowski, B. L. Sabatini, Regulation of neuronal morphology and function by the tumor suppressors Tsc1 and Tsc2. *Nat. Neurosci.* **8**, 1727–1734 (2005). doi: 10.1038/nn1566; pmid: 16286931
29. R. Malik *et al*., Tsc1 represses parvalbumin expression and fast-spiking properties in somatostatin lineage cortical interneurons. *Nat. Commun.* **10**, 4994 (2019). doi: 10.1038/s41467-019-12962-4; pmid: 31676823
30. J. P. Sommeijer, C. N. Levelt, Synaptotagmin-2 is a reliable marker for parvalbumin positive inhibitory boutons in the mouse visual cortex. *PLOS ONE* **7**, e35323 (2012). doi: 10.1371/journal.pone.0035323; pmid: 22539967
31. C. J. Potter, L. G. Pedraza, T. Xu, Akt regulates growth by directly phosphorylating Tsc2. *Nat. Cell Biol.* **4**, 658–665 (2002). doi: 10.1038/ncb840; pmid: 12172554
32. P. Fazzari *et al*., Control of cortical GABA circuitry development by Nrg1 and ErbB4 signalling. *Nature* **464**, 1376–1380 (2010). doi: 10.1038/nature08928; pmid: 20393464
33. A. K. Ting *et al*., Neuregulin 1 promotes excitatory synapse development and function in GABAergic interneurons. *J. Neurosci.* **31**, 15–25 (2011). doi: 10.1523/JNEUROSCI.2538-10.2011; pmid: 21209185
34. I. Del Pino *et al*., Erbb4 deletion from fast-spiking interneurons causes schizophrenia-like phenotypes. *Neuron* **79**, 1152–1168 (2013). doi: 10.1016/j.neuron.2013.07.010; pmid: 24050403
35. K. Elenius *et al*., Characterization of a naturally occurring ErbB4 isoform that does not bind or activate phosphatidyl inositol 3-kinase. *Oncogene* **18**, 2607–2615 (1999). doi: 10.1038/sj.onc.1202612; pmid: 10353604
36. D. Vullhorst *et al*., Selective expression of ErbB4 in interneurons, but not pyramidal cells, of the rodent hippocampus. *J. Neurosci.* **29**, 12255–12264 (2009). doi: 10.1523/JNEUROSCI.2454-09.2009; pmid: 19793984
37. T. Müller *et al*., Neuregulin 3 promotes excitatory synapse formation on hippocampal interneurons. *EMBO J.* **37**, 201798858 (2018). doi: 10.15252/embj.201798858 pmid: 30049711
38. D. Exposito-Alonso *et al*., Subcellular sorting of neuregulins controls the assembly of excitatory-inhibitory cortical circuits. *eLife* **9**, e57000 (2020). doi: 10.7554/eLife.57000 pmid: 33320083
39. E. Sanz *et al*., Cell-type-specific isolation of ribosome-associated mRNA from complex tissues. *Proc. Natl. Acad. Sci. U.S.A.* **106**, 13939–13944 (2009). doi: 10.1073/pnas.0907143106; pmid: 19666516
40. F. Koopmans *et al*., SynGO: An Evidence-Based, Expert-Curated Knowledge Base for the Synapse. *Neuron* **103**, 217–234.e4 (2019). doi: 10.1016/j.neuron.2019.05.002; pmid: 31171447
41. L. Mei, K. A. Nave, Neuregulin-ERBB signaling in the nervous system and neuropsychiatric diseases. *Neuron* **83**, 27–49 (2014). doi: 10.1016/j.neuron.2014.06.007; pmid: 24991953
42. E. Favuzzi *et al*., Activity-dependent gating of parvalbumin interneuron function by the perineuronal net protein Brevican. *Neuron* **95**, 639–655.e10 (2017). doi: 10.1016/j.neuron.2017.06.028; pmid: 28712654
43. J. D. Perez, C. M. Fusco, E. M. Schuman, A Functional Dissection of the mRNA and Locally Synthesized Protein Population in Neuronal Dendrites and Axons. *Annu. Rev. Genet.* **55**, 183–207 (2021). doi: 10.1146/annurev-genet-030321-054851; pmid: 34460296
44. J. S. Polepalli *et al*., Modulation of excitation on parvalbumin interneurons by neuroligin-3 regulates the hippocampal network. *Nat. Neurosci.* **20**, 219–229 (2017). doi: 10.1038/nn.4471; pmid: 28067903
45. K. A. Park *et al*., Excitatory Synaptic Drive and Feedforward Inhibition in the Hippocampal CA3 Circuit Are Regulated by SynCAM 1. *J. Neurosci.* **36**, 7464–7475 (2016). doi: 10.1523/JNEUROSCI.0189-16.2016; pmid: 27413156
46. A. Ribic, M. C. Crair, T. Biederer, Synapse-Selective Control of Cortical Maturation and Plasticity by Parvalbumin-Autonomous Action of SynCAM 1. *Cell Rep.* **26**, 381–393.e6 (2019). doi: 10.1016/j.celrep.2018.12.069 pmid: 30625321
47. C. Sun *et al*., The prevalence and specificity of local protein synthesis during neuronal synaptic plasticity. *Sci. Adv.* **7**, eabj0790 (2021). doi: 10.1126/sciadv.abj0790 pmid: 34533986
48. O. Urwyler *et al*., Branch-restricted localization of phosphatase Prl-1 specifies axonal synaptogenesis domains. *Science* **364**, eaau9952 (2019). doi: 10.1126/science.aau9952; pmid: 31048465
49. T. Shigeoka *et al*., Dynamic axonal translation in developing and mature visual circuits. *Cell* **166**, 181–192 (2016). doi: 10.1016/j.cell.2016.05.029; pmid: 27321671
50. T. Shigeoka *et al*., On-Site Ribosome Remodeling by Locally Synthesized Ribosomal Proteins in Axons. *Cell Rep.* **29**, 3605–3619.e10 (2019). doi: 10.1016/j.celrep.2019.11.025; pmid: 31825839
51. R. Cagnetta, C. K. Frese, T. Shigeoka, J. Krijgsveld, C. E. Holt, Rapid cue-specific remodeling of the nascent axonal proteome. *Neuron* **99**, 29–46.e4 (2018). doi: 10.1016/j.neuron.2018.06.004; pmid: 30008298
52. R. J. Kelleher 3rd, M. F. Bear, The autistic neuron: Troubled translation? *Cell* **135**, 401–406 (2008). doi: 10.1016/j.cell.2008.10.017; pmid: 18984149
53. M. Sahin, M. Sur, Genes, circuits, and precision therapies for autism and related neurodevelopmental disorders. *Science* **350**, aab3897 (2015). doi: 10.1126/science.aab3897; pmid: 26472761
54. C. Bagni, R. S. Zukin, A Synaptic Perspective of Fragile X Syndrome and Autism Spectrum Disorders. *Neuron* **101**, 1070–1088 (2019). doi: 10.1016/j.neuron.2019.02.041; pmid: 30897358
55. C. G. Gkogkas *et al*., Autism-related deficits via dysregulated eIF4E-dependent translational control. *Nature* **493**, 371–377 (2013). doi: 10.1038/nature11628; pmid: 23172145
56. E. Santini, E. Klann, Reciprocal signaling between translational control pathways and synaptic proteins in autism spectrum disorders. *Sci. Signal.* **7**, re10 (2014). doi: 10.1126/scisignal.2005832; pmid: 25351249
57. B. D. Auerbach, E. K. Osterweil, M. F. Bear, Mutations causing syndromic autism define an axis of synaptic pathophysiology. *Nature* **480**, 63–68 (2011). doi: 10.1038/nature10658; pmid: 22113615
58. J. Kasnauskiene *et al*., A new single gene deletion on 2q34: ERBB4 is associated with intellectual disability. *Am. J. Med. Genet. A.* **161A**, 1487–1490 (2013). doi: 10.1002/ajmg.a.35911; pmid: 23633123
59. A. B. Wilfert *et al*., Recent ultra-rare inherited variants implicate new autism candidate risk genes. *Nat. Genet.* **53**, 1125–1134 (2021). doi: 10.1038/s41588-021-00899-8 pmid: 34312540
60. P. J. de Vries *et al*., Tuberous sclerosis associated neuropsychiatric disorders (TAND) and the TAND Checklist. *Pediatr. Neurol.* **52**, 25–35 (2015). doi: 10.1016/j.pediatrneurol.2014.10.004; pmid: 25532776
61. C. L. Salussolia, K. Klonowska, D. J. Kwiatkowski, M. Sahin, Genetic Etiologies, Diagnosis, and Treatment of Tuberous Sclerosis Complex. *Annu. Rev. Genomics Hum. Genet.* **20**, 217–240 (2019). doi: 10.1146/annurev-genom-083118-015354; pmid: 31018109
62. K. D. Winden, D. Ebrahimi-Fakhari, M. Sahin, Abnormal mTOR Activation in Autism. *Annu. Rev. Neurosci.* **41**, 1–23 (2018). doi: 10.1146/annurev-neuro-080317-061747 pmid: 29490194
63. S. Jamain *et al*., Mutations of the X-linked genes encoding neuroligins NLGN3 and NLGN4 are associated with autism. *Nat. Genet.* **34**, 27–29 (2003). doi: 10.1038/ng1136 pmid: 12669065
64. S. J. Sanders *et al*., Insights into autism spectrum disorder genomic architecture and biology from 71 risk loci. *Neuron* **87**, 1215–1233 (2015). doi: 10.1016/j.neuron.2015.09.016; pmid: 26402605
65. F. Donato, S. B. Rompani, P. Caroni, Parvalbumin-expressing basket-cell network plasticity induced by experience regulates

adult learning. *Nature* **504**, 272–276 (2013). doi: 10.1038/nature12866; pmid: 24336286
66. N. Dehorter *et al*., Tuning of fast-spiking interneuron properties by an activity-dependent transcriptional switch. *Science* **349**, 1216–1220 (2015). doi: 10.1126/science.aab3415; pmid: 26359400

ACKNOWLEDGMENTS

We thank T. Garcés and E. Serafeimidou-Pouliou for general laboratory support, I. Andrew for managing mouse colonies, the Centre for Genomic Regulation (CRG) Genomics Unit for RNA-seq, P. de la Grange at GenoSplice for help with bioinformatic analyses, and P. Machado at the Centre for Ultrastructural Imaging for help with electron microscopy analysis. We are also grateful to J. Bateman, M.J. Conde-Dusman, G. Condomitti, N. Flames, and C. Houart for critical reading of the manuscript and members of the Marín and Rico laboratories for stimulating discussions and ideas. **Funding:** This work was supported by grants from the Innovative Medicines Initiative 2 Joint Undertaking grant agreement 777394 for the project AIMS-2-TRIALS and the Simons Foundation Autism Research Initiative (SFARI) grant 736666 to B.R. and O.M. The IMI2 Joint Undertaking receives support from the European Union's Horizon 2020 research and innovation program, EFPIA, Autism Speaks, Autistica, and SFARI. The funders had no role in the design of the study; in the collection, analyses, or interpretation of data; in the writing of the manuscript, or in the decision to publish the results. Any views expressed are those of the author(s) and not necessarily those of the funders. For the purpose of open access, the authors have applied a CC BY public copyright license to any Author Accepted Manuscript version arising from this submission. **Author contributions:** C.B., D.E-A., M.S., B.R., and O.M. designed experiments. C.B. carried out the biochemical experiments and the histological analysis of the *Tsc2* mutants. M.S. performed electrophysiological experiments. D.E-A. performed the functional analysis of target genes. A.A., A.H-G., and S.S. contributed to data collection and analysis. F.O. and P.M. produced the AAVs. F.H. performed the SFARI gene enrichment analysis. L.A., M.R., and R.F. prepared and imaged the electron microscopy samples. C.B., B.R., and O.M. wrote the manuscript with input from all authors. **Competing interests:** The authors declare no competing interests. **Data and materials availability:** Sequencing data have been deposited at the National Center for Biotechnology Information BioProjects Gene Expression Omnibus (GEO) and are accessible through GEO Series accession number GSE214258. All other data are available in the manuscript or the supplementary material.

SUPPLEMENTARY MATERIALS

science.org/doi/10.1126/science.abm7466
Materials and Methods
Figs. S1 to S19
Table S1
References (*67*–*75*)
MDAR Reproducibility Checklist

Submitted 15 June 2022; accepted 17 October 2022
10.1126/science.abm7466

RESEARCH ARTICLES

CRISPR

RNA-activated protein cleavage with a CRISPR-associated endopeptidase

Jonathan Strecker[1,2,3,4,5]*†, F. Esra Demircioglu[1,2,3,4,5]†, David Li[1,2,3,4,5,6], Guilhem Faure[1,2,3,4,5], Max E. Wilkinson[1,2,3,4,5], Jonathan S. Gootenberg[3], Omar O. Abudayyeh[3], Hiroshi Nishimasu[7,8,9,10], Rhiannon K. Macrae[1,2,3,4,5], Feng Zhang[1,2,3,4,5]*

In prokaryotes, CRISPR-Cas systems provide adaptive immune responses against foreign genetic elements through RNA-guided nuclease activity. Recently, additional genes with non-nuclease functions have been found in genetic association with CRISPR systems, suggesting that there may be other RNA-guided non-nucleolytic enzymes. One such gene from *Desulfonema ishimotonii* encodes the TPR-CHAT protease Csx29, which is associated with the CRISPR effector Cas7-11. Here, we demonstrate that this CRISPR-associated protease (CASP) exhibits programmable RNA-activated endopeptidase activity against a sigma factor inhibitor to regulate a transcriptional response. Cryo–electron microscopy of an active and substrate-bound CASP complex reveals an allosteric activation mechanism that reorganizes Csx29 catalytic residues upon target RNA binding. This work reveals an RNA-guided function in nature that can be leveraged for RNA-sensing applications in vitro and in human cells.

Prokaryotes possess a multitude of defense systems against foreign genetic elements, including CRISPR and CRISPR-associated proteins (Cas) systems (*1*–*3*). Although the predominant function of CRISPR-Cas systems is to provide adaptive immunity through RNA-guided DNA or RNA nuclease activity, additional proteins have been identified in genetic association with CRISPR loci (*3*–*5*). One example is the CRISPR-associated transposase (CAST) systems (*6*, *7*), which perform RNA-guided DNA insertion whereby nuclease-inactive CRISPR effectors guide Tn7-like mobile genetic elements to specific DNA sequences (*8*, *9*). CAST systems have evolved on at least three separate occasions (*10*), highlighting the ability of diverse CRISPR effectors to acquire, or be acquired by, other bacterial enzymes. Beyond CAST systems, additional functions genetically linked to CRISPR-Cas systems are beginning to emerge, and it is likely that more remain to be discovered and characterized.

Previous work has uncovered several RNA-targeting type III CRISPR-associated protease (CASP) systems (*3*, *4*), including a Lon protease that responds to cyclic oligoadenylate second messengers (cA_4) to cleave the CRISPR-T protein (*11*). A recently characterized subtype III-E effector Cas7-11 (*12*, *13*) (also referred to as gRAMP) is likewise associated with a protease, a CHAT family member containing tetratricopeptide repeats (TPR-CHAT, or Csx29). In contrast to prototypical type III CRISPR systems that consist of multisubunit Csm or Cmr complexes (*14*), Cas7-11 effectors contain naturally fused Cas7 and Cas11 domains (*3*). Members of the CHAT family of proteases harbor catalytic cysteine residues and include eukaryotic caspases that are involved in programmed cell death (*15*), and Cas7-11-Csx29 was previously hypothesized to act as a bacterial caspase and support viral immunity (*12*, *13*). Notably, Cas7-11 and Csx29 from *Candidatus Scalindua brodae* were shown to form a stable protein complex (*13*), but the substrate and function of the associated protease is unknown.

Here, we determined the protein substrate, structure, and mechanism of a type III-E CASP system from the marine anaerobe *Desulfonema ishimotonii*, which revealed insights into its natural function in coordinating a transcriptional response to foreign genetic material, and engineered it for new RNA sensing applications in vitro and in human cells.

A Cas7-11–Csx29 complex cleaves the Csx30 protein

The reported cleavage of CRISPR-T by the neighboring Lon protease (*11*) inspired us to look more closely at type III-E loci for potential substrates. In addition to the associated Csx29 protease, these loci frequently contain three additional genes [*csx30*, *csx31*, and a predicted sigma factor (*3*), hereafter CASP-σ] that we hypothesized were prime candidates (Fig. 1A and fig. S1). Starting from a system found in *D. ishimotonii* (DiCASP) (*12*), we purified a stable Cas7-11–Csx29–CRISPR RNA (crRNA) complex [as previously reported for *Candidatus S. brodae* (*13*)] (fig. S2A) and performed in vitro reactions by adding the proteins expressed from the three upstream genes in the presence or absence of a target RNA complementary to the crRNA. We identified that the largest protein, Csx30, is specifically cleaved in response to a target RNA (Fig. 1, B and C). Moreover, in vitro reactions yielded two precise protein products, indicating a single cleavage event within Csx30 as opposed to processive protein degradation.

We determined the requirements of Csx30 cleavage and found that whereas mutating the catalytic residues of the Csx29 protease [H615A/C658A (His^{615}→Ala/Cys^{658}→Ala)] abolished activity, disrupting the catalytic sites of the Cas7-11 endonuclease (dCas7-11:D429A/D654A; D, Asp) (*12*) did not (Fig. 1D and fig. S2B). This result indicates that target RNA binding alone is sufficient for Csx29 activation and that RNA cleavage is dispensable. In vitro characterization revealed that DiCASP is a highly active adenosine triphosphate (ATP)–independent protease that can cleave a 100-fold molar excess of Csx30 substrate in minutes, with an optimal activity between 37° and 45°C (fig. S2, C to F). Full Csx30 cleavage activity required 22 nucleotides of complementarity between the crRNA and target RNA, and we detected low tolerance to base-pair mismatches, particularly at the 5′ end of the target RNA (fig. S3).

Characterization of Csx30 proteolytic processing

Structural prediction of the Csx30 protein revealed two domains separated by a flexible linker (Fig. 1, E and F), which we hypothesized to be the site of cleavage. However, mass spectrometry analysis (and the estimated 48- and 16-kDa gel products) indicates that Csx30 is cleaved further downstream between residues 427 and 429 (fig. S4), placing the cleavage site within a small flexible loop (residues 423 to 437) in the C-terminal domain (CTD) of the structural model. By generating truncation mutations of Csx30, we determined that the N-terminal domain (NTD) is dispensable for processing by Cas7-11–Csx29 because Csx30 fragments containing residues 396 to 565 were efficiently cleaved in vitro (Fig. 1G and fig. S5). By contrast, we observed that Csx30 C-terminal residues are strictly required and that even a

[1]Howard Hughes Medical Institute, Massachusetts Institute of Technology, Cambridge, MA 02139, USA. [2]Broad Institute of MIT and Harvard, Cambridge, MA 02142, USA. [3]McGovern Institute for Brain Research, Massachusetts Institute of Technology, Cambridge, MA 02139, USA. [4]Department of Brain and Cognitive Sciences, Massachusetts Institute of Technology, Cambridge, MA 02139, USA. [5]Department of Biological Engineering, Massachusetts Institute of Technology, Cambridge, MA 02139, USA. [6]Department of Electrical Engineering and Computer Science, Massachusetts Institute of Technology, Cambridge, MA 02139, USA. [7]Structural Biology Division, Research Center for Advanced Science and Technology, The University of Tokyo, Tokyo 153-8904, Japan. [8]Department of Chemistry and Biotechnology, Graduate School of Engineering, The University of Tokyo, Tokyo 113-8656, Japan. [9]Department of Biological Sciences, Graduate School of Science, The University of Tokyo, Tokyo 113-0033, Japan. [10]Inamori Research Institute for Science, Kyoto 600-8411, Japan.
***Corresponding author. Email: zhang@broadinstitute.org (F.Z.); strecker@broadinstitute.org (J.S.)**
†These authors contributed equally to this work.

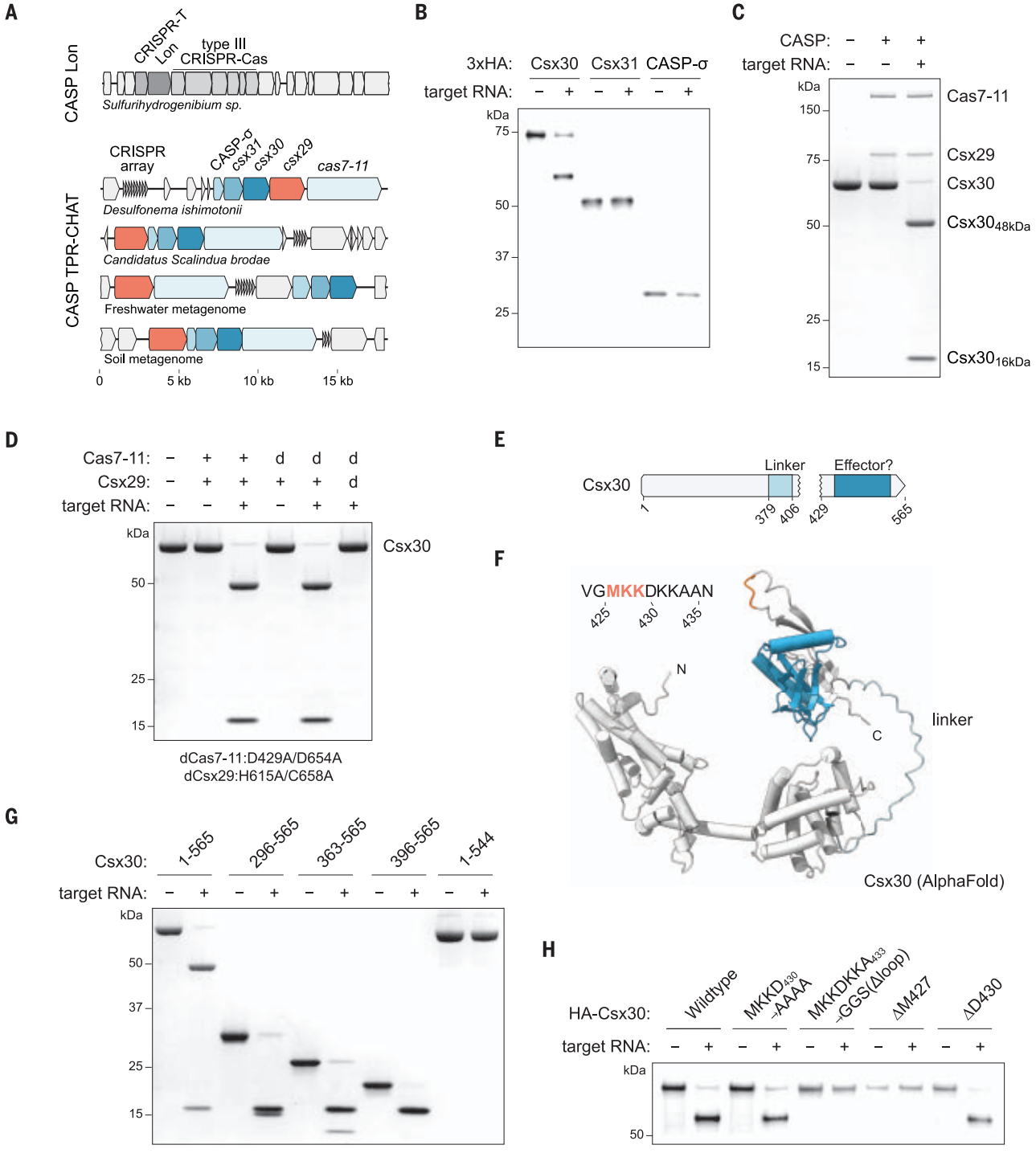

Fig. 1. The type III-E CASP Csx29 cleaves Csx30. (**A**) Schematic of selected CASP loci and three additional conserved genes in type III-E loci. (**B**) Immunoblot analysis of in vitro reactions with Cas7-11–Csx29 and HA-tagged Csx30, Csx31, and CASP-σ produced by cell-free transcription-translation. (**C**) A Cas7-11–Csx29–crRNA complex cleaves Csx30 protein in response to target RNA. (**D**) Csx30 cleavage requires target RNA and the Csx29 protease catalytic residues but not the catalytic residues of Cas7-11. (**E**) Schematic of Csx30 highlighting the cleavage site (amino acids 427 to 429), linker (amino acids 377 to 406), and a potential effector domain annotated from HHpred (amino acids 452 to 545). (**F**) AlphaFold2 prediction of Csx30. N, NTD; C, CTD. (**G**) Analysis of dCas7-11–Csx29 (Cas7-11: D429A/D654A) proteolytic activity on truncated Csx30 proteins. (**H**) Immunoblot analysis of HA-tagged Csx30 mutants produced by cell-free transcription-translation. G, Gly. (C), (D), and (G) are SDS–polyacrylamide gel electrophoresis (SDS-PAGE) gels stained with Coomassie brilliant blue.

20–amino acid truncation ($Csx30_{1\text{-}544}$) abolished cleavage activity (Fig. 1G).

Mutational analysis by alanine substitutions revealed no Csx30 residues that are essential for cleavage, although some reduced the efficiency (Fig. 1H and fig. S6). Instead, the size of the cleaved loop appears important for processing. We observed that truncating the loop by four residues, or deleting M427 (M, Met) alone, prevented Csx30 cleavage, whereas the deletion of D430 had no effect (Fig. 1H). Using an uncleavable $Csx30_{\Delta loop}$

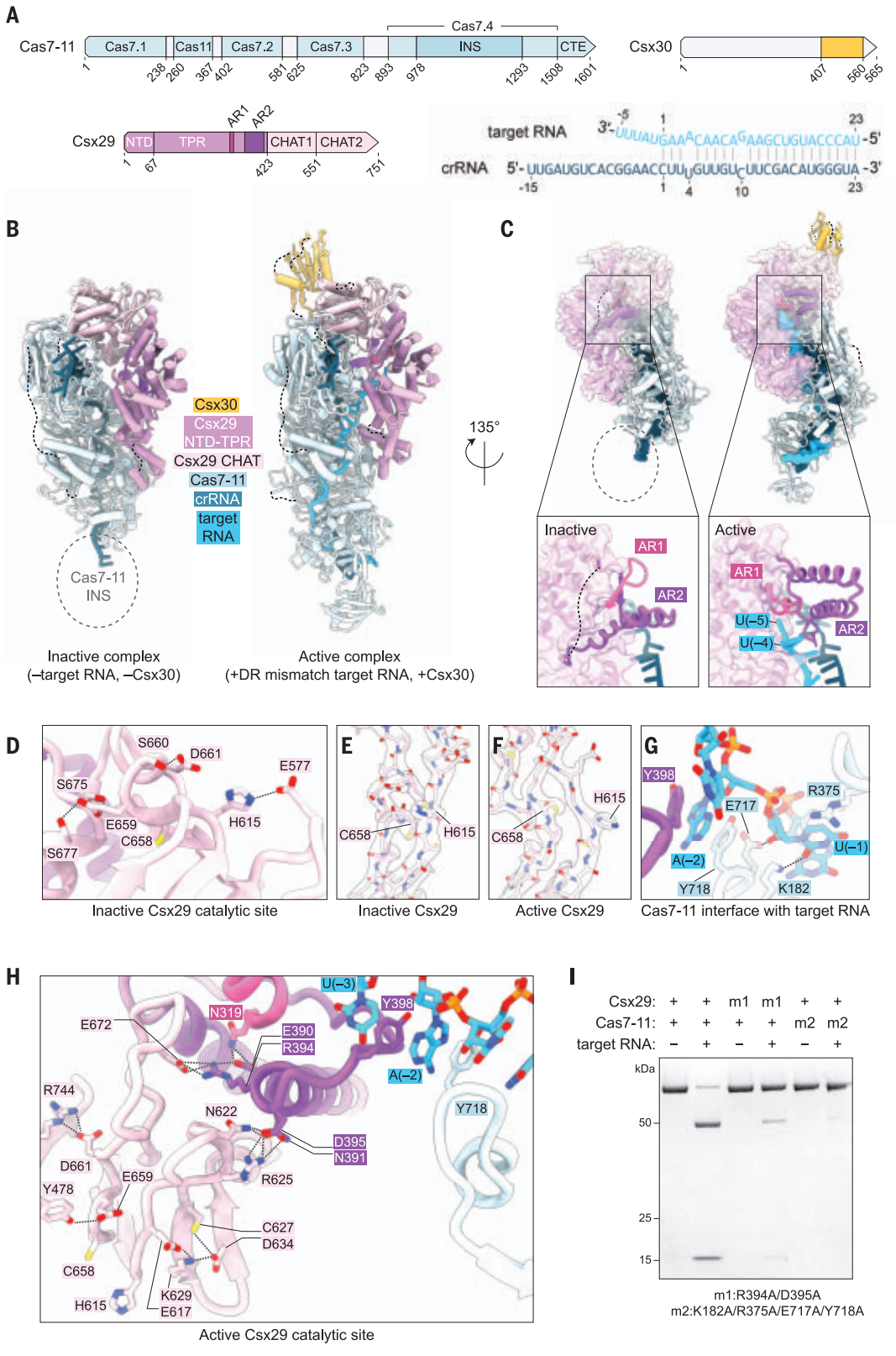

Fig. 2. Allosteric activation of Csx29 upon RNA binding. (**A**) Schematic of Cas7-11, Csx29, and Csx30 proteins domains and the crRNA and target RNA used in the structural studies. (**B**) Structures of the inactive (Cas7-11–Csx29–crRNA) and active (Cas7-11–Csx29–crRNA–target RNA–Csx30) CASP complexes. (**C**) Structural organization of the Csx29 AR in the inactive and active CASP complexes. The dashed circle indicates the Cas7-11 INS domain, which is also indicated in (B). (**D**) Electrostatic and hydrogen-bonded network within the Csx29 catalytic site in the inactive state. (**E** and **F**) Catalytic H615 and C658 residues in inactive and active Csx29 shown with EM density. (**G**) Contacts between Cas7-11 and the DR-mismatched portion of the target RNA in the active state. (**H**) Electrostatic and hydrogen-bonded network extending from the AR to the Csx29 catalytic site in the active state. (**I**) SDS-PAGE gel stained with Coomassie brilliant blue showing that mutations that disrupt allosteric activation residues impair Csx30 cleavage by Cas7-11–Csx29.

mutant as bait, we pulled down the Cas7-11–Csx29 complex both in the presence and absence of target RNA, suggesting that Csx30 binding to Cas7-11–Csx29 is not regulated by target RNA recognition or activation of the protease (fig. S7). By contrast, we did not detect Cas7-11–Csx29 binding using a truncated $Csx30_{1\text{-}544}$ mutant, revealing that an intact CTD is required for substrate binding (fig. S7).

Allosteric activation of Csx29 upon target RNA binding

To gain insight into the activation mechanism of Cas7-11–Csx29 and substrate recognition of Csx30, we solved single-particle cryo–electron

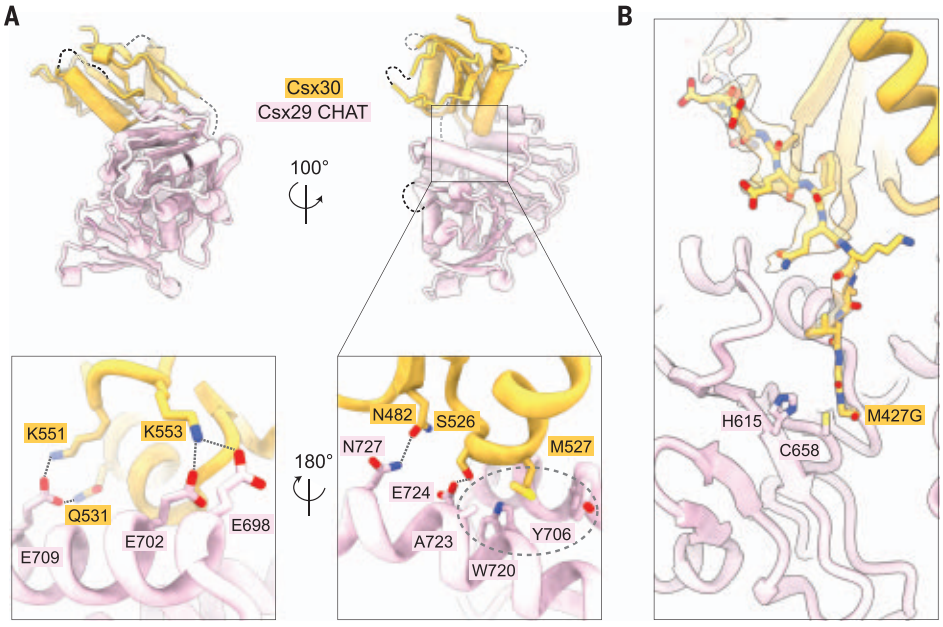

Fig. 3. Csx30 substrate recognition by Csx29. (**A**) Csx29-Csx30 interface in the active CASP structure. Electrostatic interactions and hydrogen bonds are drawn as dashed lines, and the hydrophobic pocket is drawn as a dashed oval. (**B**) Close-up of the Csx29-Csx30 interface near the catalytic H615 and C658 residues.

microscopy (cryo-EM) structures of $Csx30_{\Delta loop}$ bound to Cas7-11–Csx29 with target RNA and an inactive complex of Cas7-11–Csx29 alone at 2.5- and 3.0-Å resolution, respectively (Fig. 2, A to C; figs. S8 to S10; and table S1). The overall architecture of Cas7-11 in both complexes resembles the reported DiCas7-11 structure (*16*), in which the Cas7.1 to Cas7.4 domains organize into a filament around the crRNA core with Cas11 at the midpoint. The insertion (INS) domain within Cas7.4 was visible only in the active state (Fig. 2, B and C). Csx29 consists of a three-helix bundle NTD, a TPR domain with eight repeats, and a protease region containing a pseudo-caspase (CHAT1) and active-caspase (CHAT2) domain that resembles that of separases (*17*, *18*). In both complexes, Cas7.2 to Cas7.4 interface with the NTD, TPR, and CHAT1 domains of Csx29. Although the overall organization of Cas7-11 remains the same upon Csx29 binding, linker L2 and the Cas7.4 zinc-finger loop undergo structural changes that look similar in both the active and inactive states (fig. S11).

In the inactive state, the catalytic residues of CHAT2 are improperly positioned; C658 is turned downward away from the catalytic H615, and the catalytic histidine is instead positioned toward D661 (fig. S12). However, they are repositioned upon target RNA binding to resemble the geometry of active caspases (Fig. 2, D to F, and figs. S12 and S13). Because CHAT2 makes no direct contact with Cas7-11 or target RNA, we hypothesized that conformational changes likely occur in other regions of Csx29 and transduce an allosteric signal to the catalytic core. By comparing the inactive and active complexes we observed a major structural change within the eighth repeat of the TPR domain, which we term the activation region (AR). The AR is bipartite, composed of AR1 (amino acids 313 to 325) and AR2 (amino acids 356 to 411), which stack with each other in the inactive state (Fig. 2C). In the active complex, AR1 senses the 3′ end of target RNA (positions −4 and −5) through base-stacking interactions and pushes the AR2 helices away, preventing a steric clash (Fig. 2C).

The target RNA in our active complex is noncomplementary to the direct repeat (DR), and the structure reveals that this is an important feature. In this state, the 3′ portion of the target RNA is separated from the crRNA, and it makes a sharp kink at position −2, enabling it to traverse the TPR domain of Csx29 and reach AR1 (fig. S14A). This observation suggests that a DR-matched RNA might not activate Csx29 because it could stay hybridized with the crRNA at position −2 and beyond. Supporting this model, a target RNA that fully matched the DR strongly reduced Csx30 cleavage (fig. S14, B and C). Mismatches at positions −1 and −2 alone were only able to partially activate Csx29, and mismatches at positions −1 to −4 were required to restore full Csx30 cleavage (fig. S14C). Eliminating base pairing between the DR and the target RNA is therefore crucial for CASP activation and highlights the importance of the AR1–target RNA interaction. Of note, noncomplementarity between the DR and target RNA also plays an important role in type III-A and III-B CRISPR systems to suppress the response against host-derived transcripts (*19*, *20*) and thus is a generalized component of signal transduction in type III systems.

In addition to target RNA sensing by Csx29 AR1, we identified contacts between Cas7-11 and target RNA at the DR-mismatched site. In addition to Y718, which base-stacks with the nucleotide at position −2, we identified K182, R375, and E717 as contacting the nucleotide at position −1 (Y, Tyr; K, Lys; R, Arg; E, Glu) (Fig. 2G and fig. S13). To better understand CASP activation and the AR-induced signal transduction, we examined downstream allosteric events in Csx29. In the active complex, the kinked target RNA site at position −2 is stabilized by base-stacking interactions, provided by both Cas7-11–Y718 and Csx29-Y398 within AR2. Adjacent residues at the tip of the AR2 helix—E390, N391, R394, and D395—initiate a network of electrostatic and hydrogen-bonded contacts that extend all the way to the CHAT2 active site (N, Asn) (Fig. 2H and fig. S13). Prominent salt bridges formed between R394-E672 and D395-R625 help position the loop that contains the catalytic C658 and the strand that contains the catalytic H615, respectively. Further down, the active-site H615 is positioned by E617 contacts, whereas the active-site C658 is kept in place by E659-Y478 and D661-R744. In the inactive state, these same residues that position C658 in the active complex make entirely different contacts: E659 forms hydrogen bonds with S675 and S677, and D661 instead bonds with S660 (S, Ser) (Fig. 2, D and H, and fig. S13). We note the similarity of this mechanism to that in eukaryotic caspases, which are also thought to be regulated by the conformation of the L4 loop that contains their catalytic cysteine (*21*). Together, these structures reveal an allosteric cascade initiated by the 3′ end of DR-mismatched target RNA, which triggers the AR within the Csx29 TPR domain and transduces structural changes to the Csx29 CHAT2 domain to coordinate active-site residues.

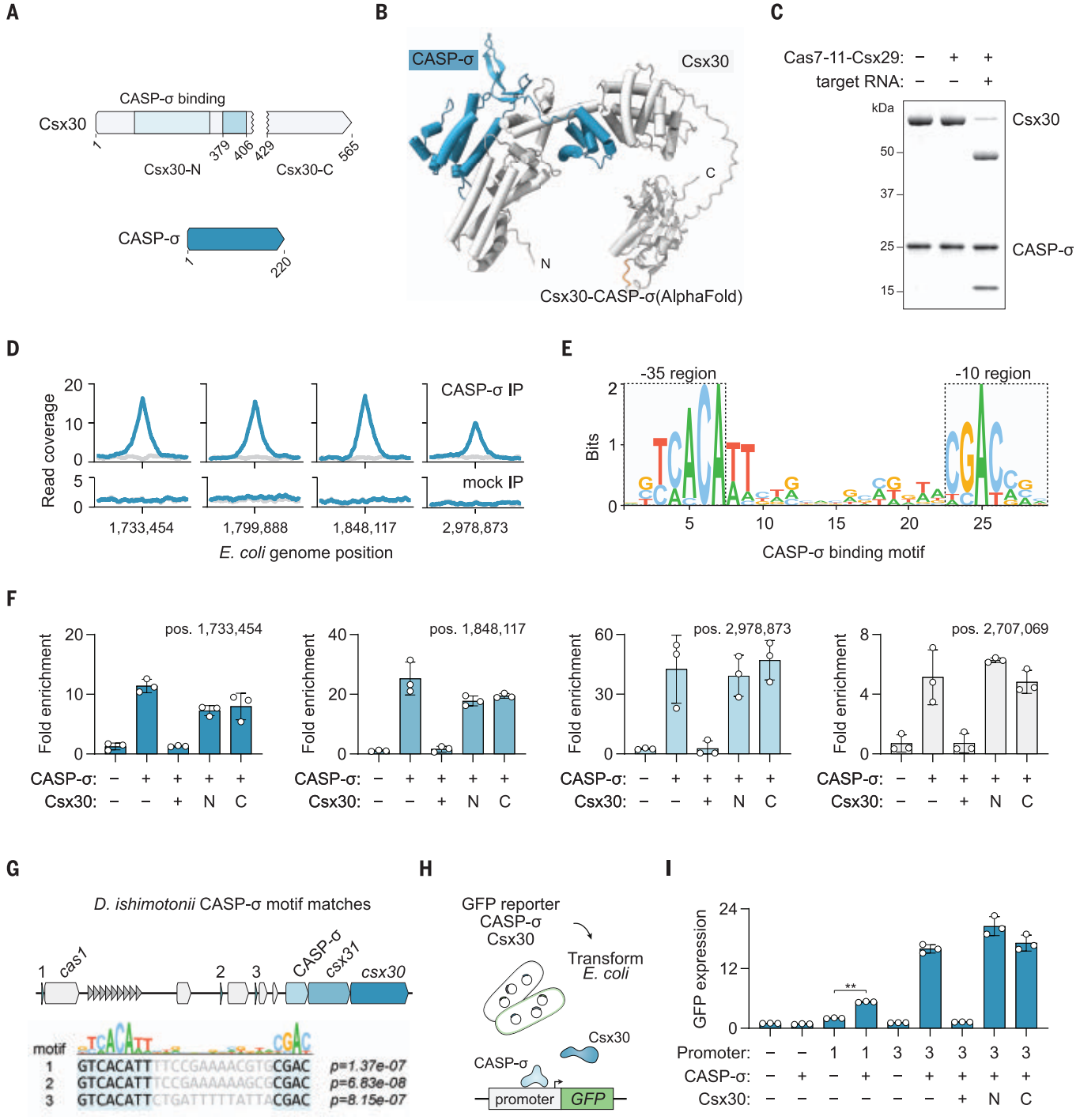

Fig. 4. Csx30 binds and inhibits the transcription factor CASP-σ. (**A**) Schematic of Csx30 and CASP-σ proteins. (**B**) AlphaFold2 prediction of a Csx30-CASP-σ interaction. (**C**) SDS-PAGE gel stained with Coomassie brilliant blue showing purification of a Csx30–CASP-σ complex that is cleaved by dCas7-11–Csx29. (**D**) Representative CASP-σ ChIP-seq peaks in *E. coli* with a 1-kb window; input coverage is shown in gray. (**E**) Identification of a CASP-σ binding motif from ChIP-seq peaks. (**F**) Enrichment of CASP-σ at four *E. coli* peaks by ChIP–quantitative polymerase chain reaction (qPCR). $n = 3$ replicates. pos., *E. coli* genome position. (**G**) Predicted CASP-σ targets in the *D. ishimotonii* CASP locus. (**H**) Schematic of the CASP-σ transcriptional reporter assay. (**I**) CASP-σ–mediated transcriptional activity in *E. coli*. GFP expression was normalized to cells with a scrambled promoter sequence. $n = 3$ replicates. $^{**}p < 0.01$ using Student's t test. In (F) and (I), error bars represent standard deviation from the mean.

To test this model, we made mutations in the allosteric network. A Csx29-R394A/D395A double mutant within AR2 formed a stable Cas7-11–Csx29 complex, but Csx30 cleavage was greatly impaired (Fig. 2I and fig. S14D). Further down the allosteric cascade, mutating Csx29 residues E659 and D661 in the vicinity of the catalytic C658 likely disrupted Csx29 folding, and we were unable to purify a Cas7-11–Csx29 complex. Finally, we tested the importance of contacts between Cas7-11 and target RNA at the DR-mismatched site. Mutating

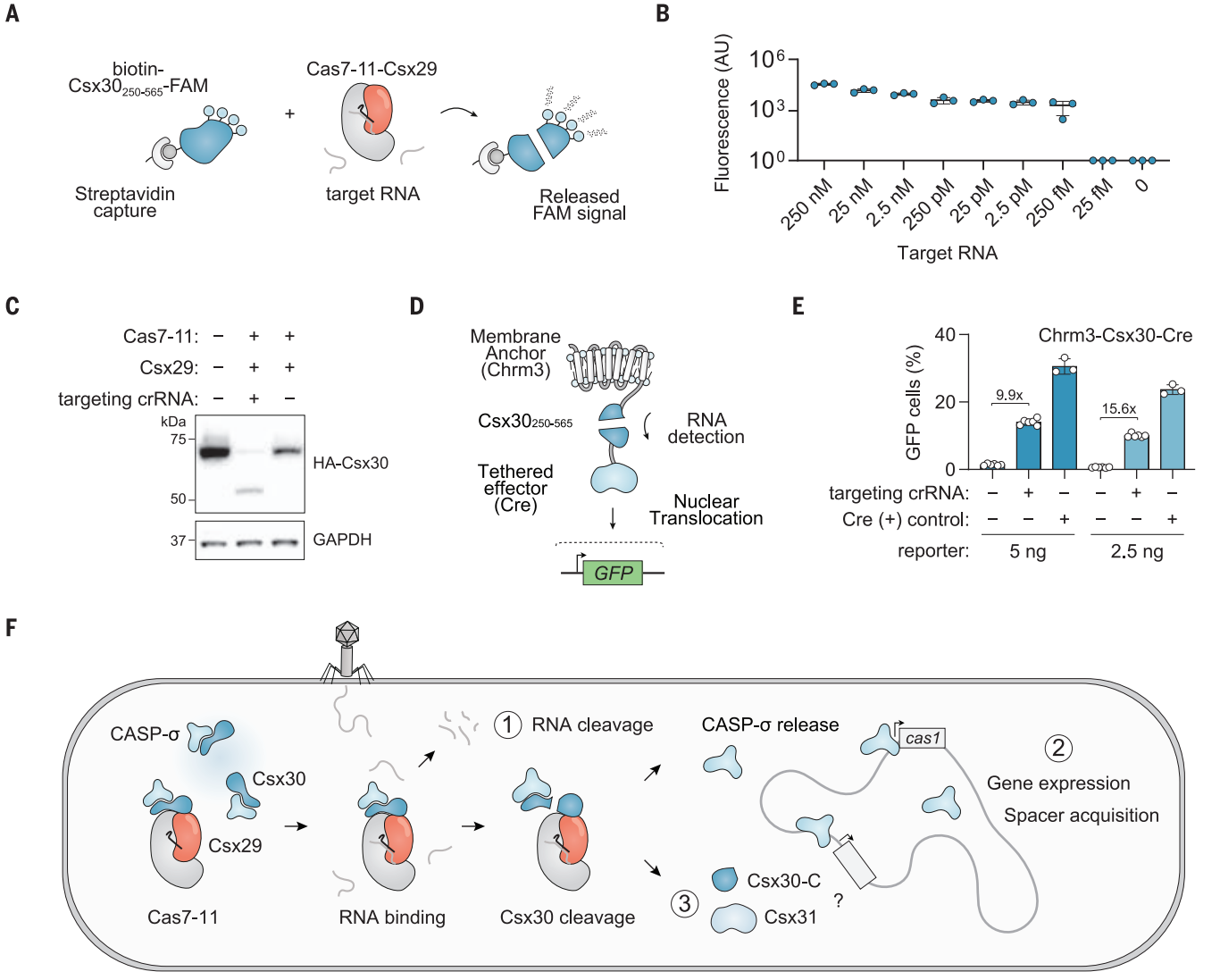

Fig. 5. RNA-sensing applications and a proposed model for CASP systems. (**A**) Schematic of in vitro RNA detection using CASP systems and fluorescent Csx30 reporters. FAM, 5′ 6-FAM (fluorescein). (**B**) In vitro detection of RNA as measured by released fluorescence. *n* = 3 replicates. AU, arbitrary units. (**C**) Immunoblot analysis of HA-tagged Csx30 in HEK293T human cells transfected with DiCASP components. GAPDH, glyceraldehyde phosphate dehydrogenase. (**D**) Schematic of engineered proteins containing a cell membrane tether, a Csx30 linker, and an effector domain. (**E**) Flow cytometry analysis of DiCASP activity in mouse Neuro2A loxP:GFP cells using a Chrm3-$Csx30_{250\text{-}565}$-Cre reporter. *n* = 3 to 6 replicates. (**F**) Model for a three-pronged strategy of CASP systems in the defense against foreign genetic elements, including Cas7-11–mediated RNA endonuclease activity, a Csx30-regulated CASP-σ transcriptional response, and a possible third arm involving Csx31. In (B) and (E), error bars represent standard deviation from the mean.

Cas7-11 residues K182, E717, R375, and Y718 into alanines did not impair Cas7-11–Csx29 complex assembly but strongly reduced CASP activation upon target RNA binding (Fig. 2I and fig. S14D). Thus, target RNA stabilization by Cas7-11 on the DR-mismatched end is also critical for protease activation.

Csx30 recognition by Cas7-11–Csx29

In addition to revealing insight into CASP activation, our active complex also provides structural details regarding the interaction with Csx30. Despite using a full-length $Csx30_{\Delta loop}$ mutant for complex assembly, only a small portion (amino acids 407 to 560) is visible in our structure (Fig. 3A and fig. S15A), and the remaining residues must therefore be flexible with respect to Cas7-11–Csx29. This region mirrors the minimal substrate we identified through truncation experiments and confirms that recognition of Csx30 is mediated through its CTD. In our structure, Csx30 is bound only to the Csx29 CHAT2 domain and does not interact with Cas7-11.

There is notable charge complementarity at the Csx29-Csx30 interface, and substrate recognition is likely electrostatically driven through the negatively charged surface of Csx29 and positively charged surface of Csx30 (fig. S15B). Detailed analysis of the interface reveals that Csx30 polar and positively charged residues (N482, S526, Q531, K551, and K553; Q, Gln) make contact with the Csx29 CHAT2 domain (Fig. 3A and fig. S16). In addition, Csx30-M527 is enclosed in a tight hydrophobic pocket lined with Csx29's Y706, W720, and A723 (W, Trp). The major determinant of Csx30 engagement is likely a cumulative effect of these interactions, because mutating individual regions of the Csx29-Csx30 interface did not affect Csx30 cleavage (fig. S15C). Consistent with our ability to pull

down a Cas7-11–Csx29–Csx30$_{\Delta loop}$ complex in the presence and absence of target RNA (fig. S7), the interfacing residues of Csx29 adopt a similar organization in both the active and inactive complexes, and therefore we conclude that Csx30 binding is not allosterically regulated.

We also examined the position of the Csx30 cleavage site within the active complex. One limitation of our structure is that the cleavage loop is mutated (and slightly shortened), and thus, we cannot observe substrate engagement in the active site in detail. Because the loop is also flexible, it is not well resolved, but its density places it near the active site of Csx29, positioning it for cleavage (Fig. 3B).

Csx30 binds and inhibits the transcription factor CASP-σ

We next sought to explore the biological function of Csx30 and understand how cleavage might regulate its activity. Because the Cas7-11 effector alone provides defense against phage (*12*), we reasoned that additional functions of DiCASP would similarly be involved in the immune response. One possibility is that processed Csx30 fragments, Csx30-N (residues 1 to 428) or Csx30-C (residues 429 to 565), promote cell death or an abortive infection response to prevent phage propagation. However, we did not observe defense against three tested phage (fig. S17A). Homology searches revealed a match of Csx30-C to a peptidoglycan *N*-acetylglucosamine deacetylase (HHpred probability: 92.85%; e-value: 0.56), but we did not detect modification of peptidoglycan or its components with cleaved Csx30 in vitro (fig. S17B). Overexpression of Csx30 fragments was not toxic in *Escherichia coli*, and we only observed a slight growth defect in cells expressing full-length Csx30, which was temperature dependent and suppressed by the addition of Csx31 and CASP-σ (fig. S18).

We next turned to the other proteins encoded in the locus to gain insight into Csx30 function. We predicted a strong binding interaction between the NTD of Csx30 and CASP-σ, which strongly resembles an extracytoplasmic function (ECF) sigma factor (*3*) (HHpred probability: 100%; e-value: 3.4×10^{-31}) (Fig. 4, A and B, and fig. S19). Sigma factors are transcription-initiation proteins that bind DNA and recruit the RNA polymerase catalytic core to specific promoters (*22*), hinting that Csx30 might be involved in regulating a transcriptional response. Consistent with our computational prediction, purification of CASP-σ in the presence of Csx30 yielded a Csx30–CASP-σ complex, in which Csx30 could still be cleaved by Cas7-11–Csx29 (Fig. 4C). Csx30-N was sufficient for the interaction with CASP-σ, although at considerably lower yield (fig. S20).

Although *D. ishimotonii* CASP-σ is unlikely to regulate its target genes heterologously in *E. coli*, we reasoned that the identification of putative CASP-σ binding sites might yield insight into its preferred sequence motif and function in the natural host. We performed chromatin immunoprecipitation sequencing (ChIP-seq) in *E. coli* with hemagglutinin (HA)–tagged CASP-σ and identified 13 high-confidence peaks compared with input and mock immunoprecipitation (IP) controls (Fig. 4D and fig. S21A). Motif analysis of ChIP-seq peaks yielded a clear hit (Fig. 4E and fig. S21B), which was similar to a de novo predicted motif (fig. S21C) (*23*).

Sigma factors are frequently regulated by inhibitors (anti-sigma factors), and there are examples in bacteria in which a protease cleaves an anti-sigma factor to activate a transcriptional stress response, including the anti-sigma factors RseA in *E. coli* (*24*) and RsiW in *Bacillus subtilis* (*25*). In *E. coli*, the DegS protease senses cell envelope stress and cleaves a transmembrane segment of RseA (*26*), resulting in the eventual release of the sequestered sigma factor RpoE. Based on our structural model, we predict that the Csx30–CASP-σ interaction would block CASP-σ DNA binding based on steric clashes to sigma factor–bound DNA in experimental structures (*27*) (fig. S22). To test whether Csx30 inhibits CASP-σ, we repeated ChIP experiments in *E. coli* coexpressing Csx30 and found that CASP-σ DNA binding was blocked at all four tested loci (Fig. 4F). This inhibition was dependent on full-length Csx30 because both Csx30-N and Csx30-C fragments were unable to antagonize CASP-σ binding (Fig. 4F). Together, our results suggest that Csx30 is an inhibitor of CASP-σ and that processing by Cas7-11–Csx29 alleviates this inhibition.

Csx30 processing regulates CASP-σ transcriptional activity

We next sought to identify potential CASP-σ targets in the natural host *D. ishimotonii*. Because many ECF sigma factors autoregulate their own expression (*28*), we first searched the DiCASP locus. We identified three strong matches in the promoters of *cas1* and two genes of unknown function (Fig. 4G and table S2), indicating that CASP-σ likely coordinates additional defense functions, including CRISPR spacer acquisition. Genome-wide searches for motifs in *D. ishimotonii* promoter regions yielded several candidates, although only one site, upstream of the *nhaA* gene, was below a *q* value of 0.6 (tables S3 and S4). To test these predictions, we constructed transcriptional reporters by placing putative CASP-σ promoters upstream of green fluorescent protein (GFP) and measured the resulting fluorescence in *E. coli* (Fig. 4H and fig. S23, A and B). We observed GFP expression with both tested promoters as compared with a random DNA control and found that fluorescence was fully dependent on CASP-σ expression (Fig. 4I). Consistent with our previous results, coexpression of full-length Csx30 was able to completely inhibit CASP-σ–mediated GFP expression, whereas processed Csx30 fragments had no effect (Fig. 4I). In support of a role for CASP-σ–mediated transcription in the immune response, we could computationally identify one of the two unknown open reading frames—a predicted membrane protein—in other CRISPR and defense loci (fig. S23C).

RNA-sensing applications with DiCASP

The high proteolytic activity of Cas7-11–Csx29 in response to a target RNA enables numerous biological applications. In addition, the ability to uncouple RNA cleavage from activation of the Csx29 protease allows for nondestructive sensing of RNA. Although the collateral nuclease activity of CRISPR effectors has been used to cleave nucleic acid–based reporters for diagnostic applications (*29*), CASP systems allow for a new modality of substrates using engineered Csx30 proteins. As a proof of concept, we generated a fluorescently labeled engineered variant of Csx30 and demonstrated its ability to detect RNA in vitro down to 250 fM without nucleic acid amplification (Fig. 5, A and B, and fig. S24).

We also sought to apply DiCASP for RNA-transcript sensing in live cells. To determine whether DiCASP can mediate RNA-activated proteolytic cleavage in human cells, we transfected plasmids expressing Cas7-11, Csx29, crRNA, a synthetic target RNA, and Csx30 fused to an HA epitope tag into human embryonic kidney (HEK) 293T cells. Immunoblots of cell lysate revealed processing of Csx30 that was dependent on a targeting crRNA and the catalytic residues of the Csx29 protease (Fig. 5C and fig. S25, A and B). Testing DiCASP activity across a panel of endogenous transcripts revealed Csx30 cleavage efficiencies ranging from 2 to 20% (fig. S25, C and D).

To convert RNA sensing with DiCASP into a discrete and readily detectable signal, we sought to design reporters containing effector domains that could be activated by Csx30 cleavage. We transfected plasmids encoding a fusion protein in which Cre recombinase is tethered to membrane anchors [e.g., the cholinergic receptor, muscarinic 3 (Chrm3) G protein–coupled receptor] by a Csx30-derived linker, sequestering Cre from the nucleus (Fig. 5D). Mouse Neuro-2A cells harboring an inactive loxP-GFP reporter cassette were transfected with DiCASP components and synthetic target RNA. Flow cytometry analysis revealed crRNA-dependent GFP expression in 10% of cells and a 15-fold increase over nontargeting crRNA controls under optimal conditions (Fig. 5E and fig. S25, E and F).

Discussion

Here, we demonstrate that the Csx29 protease associated with the type III-E effector Cas7-11 mediates RNA-activated endopeptidase activity and elucidate its substrate, structure, and mechanism. Although the full biological consequence of Csx30 processing in *D. ishimotonii* is unknown, our work supports a model in which Csx30 inhibits the sigma factor CASP-σ and proteolytic cleavage by the Csx29 protease acts to relieve this inhibition. The parallels between DiCASP and other protease-regulated anti-sigma factors, such as DegS and RseA (*26*), reveal convergent mechanisms for modulating gene expression in response to cellular threats. The NTD of Csx30 is sufficient for binding to CASP-σ, and it is therefore unclear how proteolytic cleavage within the Csx30 CTD would release CASP-σ or why expression of Csx30-N is unable to inhibit CASP-σ. One possibility is that the processed Csx30 fragments are unstable and that the exposed termini are subject to further degradation by host proteins. Consistent with this hypothesis, immunoblots of *E. coli* cell lysates that harbor HA-tagged isoforms of Csx30 revealed expression of full-length Csx30 and Csx30-C, but not Csx30-N, and blocking the "cleaved" termini with an epitope tag increased expression (fig. S26). We note potential similarities to other protease-regulated anti-sigma factor systems; DegS cleavage of RseA is insufficient to release the sigma factor RpoE, and the remaining RseA fragment is further processed by the RseP (*30*, *31*) and ClpXP proteases (*32*) to liberate RpoE.

Our identification of three CASP-σ binding motifs within the CASP locus points to the positive autoregulation of defense genes, including *cas1*, which may be a mechanism to acquire new spacers during active infection and to safeguard against the acquisition of self-targeting spacers during normal growth. This result is consistent with the reported up-regulation of *cas1* in *Pseudomonas aeruginosa* by the ECF sigma factor PvdS (*33*). The functions of the two other predicted up-regulated genes in the locus are unknown, although one has strong homology to a membrane transporter component EcsC (HHpred probability: 99.9; e-value: 3.1×10^{-22}). Interestingly, the top motif match outside of the CASP locus is upstream of *nhaA* (table S3), a Na^+-H^+ antiporter known to be up-regulated during phage infection (*34*), indicating that CASP-σ may also regulate targets elsewhere in the genome.

Together, our results suggest that the subtype III-E CASP systems use a three-pronged strategy to defend against foreign genetic material: (i) targeted RNA cleavage through the RNA endonuclease Cas7-11; (ii) a Csx30–CASP-σ regulated transcriptional response that leads to, among other possibilities, spacer acquisition; and (iii) a potential third arm mediated by Csx31 and possibly Csx30-C (Fig. 5F). The clear conservation of Csx31 (fig. S1) is a strong indication of its biological importance, and future work will be required to determine its role in the immune response.

We predict similar interactions between Csx30 and CASP-σ in other type III-E systems as well as putative CASP-σ binding motifs at *cas1* within the *Candidatus S. brodae* locus (fig. S27). There may also be parallels between DiCASP and the type III CRISPR-associated Lon protease (*11*). We note that CRISPR-T is also associated with a neighboring sigma factor and is predicted to physically interact (fig. S28). We hypothesize that cleavage of CRISPR-T could similarly trigger transcriptional changes and may reflect a common functional theme across diverse CASP families. This work reveals an example of CRISPR systems coordinating a wider cellular response beyond nuclease activity, and we expect that the continued investigation of CRISPR-associated enzymes will uncover many interesting, and potentially useful, RNA-activated biological processes.

REFERENCES AND NOTES

1. A. Bernheim, R. Sorek, *Nat. Rev. Microbiol.* **18**, 113–119 (2020).
2. L. Gao *et al*., *Science* **369**, 1077–1084 (2020).
3. K. S. Makarova *et al*., *Nat. Rev. Microbiol.* **18**, 67–83 (2020).
4. S. A. Shmakov, K. S. Makarova, Y. I. Wolf, K. V. Severinov, E. V. Koonin, *Proc. Natl. Acad. Sci. U.S.A.* **115**, E5307–E5316 (2018).
5. S. A. Shah *et al*., *RNA Biol.* **16**, 530–542 (2019).
6. J. E. Peters, K. S. Makarova, S. Shmakov, E. V. Koonin, *Proc. Natl. Acad. Sci. U.S.A.* **114**, E7358–E7366 (2017).
7. G. Faure *et al*., *Nat. Rev. Microbiol.* **17**, 513–525 (2019).
8. J. Strecker *et al*., *Science* **365**, 48–53 (2019).
9. S. E. Klompe, P. L. H. Vo, T. S. Halpin-Healy, S. H. Sternberg, *Nature* **571**, 219–225 (2019).
10. E. V. Koonin, K. S. Makarova, *PLOS Biol.* **20**, e3001481 (2022).
11. C. Rouillon *et al*., bioRxiv 2021.12.06.471393 [Preprint] (2021). https://doi.org/10.1101/2021.12.06.471393.
12. A. Özcan *et al*., *Nature* **597**, 720–725 (2021).
13. S. P. B. van Beljouw *et al*., *Science* **373**, 1349–1353 (2021).
14. J. van der Oost, E. R. Westra, R. N. Jackson, B. Wiedenheft, *Nat. Rev. Microbiol.* **12**, 479–492 (2014).
15. L. Aravind, E. V. Koonin, *Proteins* **46**, 355–367 (2002).
16. K. Kato *et al*., *Cell* **185**, 2324–2337.e16 (2022).
17. A. Boland *et al*., *Nat. Struct. Mol. Biol.* **24**, 414–418 (2017).
18. Z. Lin, X. Luo, H. Yu, *Nature* **532**, 131–134 (2016).
19. L. You *et al*., *Cell* **176**, 239–253.e16 (2019).
20. N. Sofos *et al*., *Mol. Cell* **79**, 741–757.e7 (2020).
21. K. McLuskey, J. C. Mottram, *Biochem. J.* **466**, 219–232 (2015).
22. A. Feklístov, B. D. Sharon, S. A. Darst, C. A. Gross, *Annu. Rev. Microbiol.* **68**, 357–376 (2014).
23. H. Todor *et al*., *Proc. Natl. Acad. Sci. U.S.A.* **117**, 33496–33506 (2020).
24. N. P. Walsh, B. M. Alba, B. Bose, C. A. Gross, R. T. Sauer, *Cell* **113**, 61–71 (2003).
25. S. Schöbel, S. Zellmeier, W. Schumann, T. Wiegert, *Mol. Microbiol.* **52**, 1091–1105 (2004).
26. S. E. Ades, L. E. Connolly, B. M. Alba, C. A. Gross, *Genes Dev.* **13**, 2449–2461 (1999).
27. W. J. Lane, S. A. Darst, *PLOS Biol.* **4**, e269 (2006).
28. D. Casas-Pastor *et al*., *Nucleic Acids Res.* **49**, 986–1005 (2021).
29. J. S. Gootenberg *et al*., *Science* **356**, 438–442 (2017).
30. B. M. Alba, J. A. Leeds, C. Onufryk, C. Z. Lu, C. A. Gross, *Genes Dev.* **16**, 2156–2168 (2002).
31. K. Kanehara, K. Ito, Y. Akiyama, *Genes Dev.* **16**, 2147–2155 (2002).
32. J. M. Flynn, I. Levchenko, R. T. Sauer, T. A. Baker, *Genes Dev.* **18**, 2292–2301 (2004).
33. S. D. Ahator, W. Jianhe, L.-H. Zhang, bioRxiv 2020.01.31.929752 [Preprint] (2020). https://doi.org/10.1101/2020.01.31.929752.
34. L. M. Malone, H. G. Hampton, X. C. Morgan, P. C. Fineran, *Nucleic Acids Res.* **50**, 160–174 (2022).
35. J. Strecker, D. Li, F. Zhang, Code and processed data for: RNA-activated protein cleavage with a CRISPR-associated endopeptidase, Version 1.0, Zenodo (2022). https://doi.org/10.5281/zenodo.7221526.

ACKNOWLEDGMENTS

We thank L. Gao, J. Schmid-Burgk, and D. Strebinger for valuable discussions; B. Lash for providing Neuro2A cells; E. Spooner and the Whitehead Institute Proteomics Core Facility for mass spectrometry analysis; E. Brignole and C. Borsa at the MIT.nano CryoEM Center; staff at the Arnold and Mabel Beckman Foundation for funding the MIT.nano CryoEM Center; and the entire Zhang lab for support and advice. **Funding:** F.Z. is supported by NIH grants 1DP1-HL141201 and 2R01HG009761-05; the Howard Hughes Medical Institute; the Yang-Tan Molecular Therapeutics Center at McGovern; and the Phillips family and J. and P. Poitras. J.S. is a Charles A. King Trust Postdoctoral Research Fellow. **Author contributions:** J.S. designed and performed experiments; F.E.D. solved cryo-EM structures with input from M.E.W.; J.S. and D.L. analyzed data; G.F. performed bioinformatic analysis and structural predictions; F.Z. supervised the research and experimental design with support from R.K.M.; J.S.G., O.O.A., and H.N. provided input and discussed unpublished work; and J.S., F.E.D., and D.L. wrote the manuscript with input from all authors. **Competing interests:** F.Z. is a scientific advisor for Editas Medicine, Beam Therapeutics, Pairwise Plants, Arbor Biotechnologies, Proof Diagnostics, and Octant. J.S., F.E.D., and F.Z. are inventors on US patent application 63/337,386 submitted by The Broad Institute, which covers programmable protease compositions. **Data and materials availability:** ChIP-seq data are available at the NCBI Sequence Read Archive (BioProject IDs PRJNA888197 and SAMN31210314-21). Code and processed data are available at Zenodo (*35*). Plasmids are available from Addgene. The cryo-EM maps have been deposited in the Electron Microscopy Data Bank with the following codes: EMD-28064 (inactive CASP, focused refinement of Cas7-11, crRNA, and Csx29 NTD), EMD-28070 (inactive CASP, focused refinement of Csx29 TPR-CHAT), EMD-28065 (active CASP, focused refinement of Cas7-11, except INS, crRNA, and target RNA), EMD-28071 (active CASP, focused refinement of Cas7-11 INS), EMD-28072 (active CASP, focused refinement of Csx29 NTD and TPR), and EMD-28073 (active CASP, focused refinement of Csx29 CHAT and Csx30). The coordinates for the composite atomic models have been deposited in the Protein Data Bank under accession codes 8EEX (inactive CASP) and 8EEY (active CASP).

SUPPLEMENTARY MATERIALS

science.org/doi/10.1126/science.add7450
Materials and Methods
Figs. S1 to S28
Tables S1 to S7
References (*36*–*56*)
MDAR Reproducibility Checklist

Submitted 30 June 2022; accepted 24 October 2022
10.1126/science.add7450

CRISPR

RNA-triggered protein cleavage and cell growth arrest by the type III-E CRISPR nuclease-protease

Kazuki Kato[1]†, Sae Okazaki[1]†, Cian Schmitt-Ulms[2]†, Kaiyi Jiang[2,3]†, Wenyuan Zhou[2], Junichiro Ishikawa[1], Yukari Isayama[1], Shungo Adachi[4], Tomohiro Nishizawa[5], Kira S. Makarova[6], Eugene V. Koonin[6], Omar O. Abudayyeh[2]*, Jonathan S. Gootenberg[2]*, Hiroshi Nishimasu[1,7,8,9]*

The type III-E CRISPR–Cas7-11 effector binds a CRISPR RNA (crRNA) and the putative protease Csx29 and catalyzes crRNA-guided RNA cleavage. We report cryo–electron microscopy structures of the Cas7-11–crRNA–Csx29 complex with and without target RNA (tgRNA), and demonstrate that tgRNA binding induces conformational changes in Csx29. Biochemical experiments revealed tgRNA-dependent cleavage of the accessory protein Csx30 by Csx29. Reconstitution of the system in bacteria showed that Csx30 cleavage yields toxic protein fragments that cause growth arrest, which is regulated by Csx31. Csx30 binds Csx31 and the associated sigma factor RpoE (RNA polymerase, extracytoplasmic E), suggesting that Csx30-mediated RpoE inhibition modulates the cellular response to infection. We engineered the Cas7-11–Csx29–Csx30 system for programmable RNA sensing in mammalian cells. Overall, the Cas7-11–Csx29 effector is an RNA-dependent nuclease-protease.

Prokaryotic CRISPR-Cas systems provide adaptive immunity against foreign nucleic acids, including phages and mobile genetic elements, through diverse mechanisms of programmed nucleic acid cleavage. CRISPR-Cas systems are divided into two classes based on the number of components in the effector complexes responsible for defense through the cleavage of invading nucleic acids programmed by a CRISPR RNA (crRNA) guide (*1*, *2*). In class 1 systems, which encompass types I, III, and IV, target nucleic acids are degraded by multiprotein effector complexes, whereas the effectors of class 2 systems (types II, V, and VI) are single-protein, multidomain Cas proteins (Cas9, Cas12, and Cas13, respectively). CRISPR-Cas systems also deploy a wide array of accessory proteins that enhance and modulate the antiviral activity of the primary effector nuclease (*3*–*7*).

Unlike typical class 1 effectors, the type III-E effector Cas7-11 (also known as gRAMP) is a single-protein, multidomain effector that consists of four Cas7 domains (Cas7.1 to Cas7.4) and a Cas11 domain (*8*, *9*). Cas7-11 associates with a crRNA and cleaves complementary single-stranded RNA (ssRNA) targets at two defined positions using the Cas7.2 and Cas7.3 domains. Whereas the type VI effector Cas13 displays promiscuous RNase activity (*10*, *11*), Cas7-11 exhibits precise, guide RNA–dependent tgRNA cleavage activity in human cells and has been used as a new RNA-targeting tool with high specificity and low cell toxicity (*8*, *9*). The type III-E locus encodes multiple conserved accessory proteins, including Csx29 (a caspase-like putative protease with fused TPR and CHAT domains), Csx30 and Csx31 (proteins with unknown functions), and RpoE (an alternative sigma factor). Cas7-11 forms a complex with Csx29 (*8*, *9*), suggesting a potential mechanism of RNA-guided protease activity for antiviral immunity. Recently, we reported the cryo–electron microscopy (cryo-EM) structure of *Desulfonema ishimotonii* Cas7-11 complexed with its cognate crRNA and tgRNA (*12*), providing mechanistic insights into pre-crRNA processing and tgRNA cleavage. Nonetheless, the means by which Cas7-11 cooperates with the other proteins encoded in the type III-E locus (Csx29, Csx30, Csx31, and RpoE) and binds Csx29 to potentially activate its protease activity remain unknown.

Results

Structures of Cas7-11 complexed with Csx29

We sought to solve the structure of the Cas7-11–Csx29 effector complex to gain insights into its action mechanism. We coexpressed the catalytically inactive *D. ishimotonii* Cas7-11 mutant (referred to as Cas7-11 for simplicity), with the D429A (Cas7.2) and D654A (Cas7.3) mutations introduced to prevent tgRNA cleavage by Cas7-11, together with Csx29 and a crRNA transcribed from a CRISPR array containing two repeat-spacer units and then purified the Cas7-11–crRNA–Csx29 complex. We determined cryo-EM structures of this Cas7-11–crRNA–Csx29 complex with and without a tgRNA at 2.5- and 2.8-Å resolutions, respectively (Fig. 1, A to D, figs. S1 to S3, table S1, and movie S1). In both structures, Cas7-11 adopts a modular architecture consisting of four Cas7 domains (Cas7.1 to Cas7.4) with a zinc finger (ZF) motif, a Cas11 domain, an insertion (INS) domain within the Cas7.4 domain, a C-terminal extension domain, and four interdomain linkers (L1 to L4) (Fig. 1, C and D), as in the Csx29-unbound Cas7-11–crRNA–tgRNA structure (*12*) (fig. S4).

The 15-nucleotide (nt) 5′ tag region [U(−15)–C(−1)] in the 38-nt crRNA [U(−15)–A23] is anchored by the Cas7.1 and Cas7.2 domains in both structures (Fig. 1, C and D, and figs. S4, B and C, and S5A), as in the Csx29-unbound Cas7-11–crRNA–tgRNA structure (*12*) (fig. S4A). The 23-nt crRNA spacer region is recognized by the Cas7.2 to Cas7.4 domains in the tgRNA-free structure (Fig. 1C and fig. S4B), whereas the crRNA spacer region (C1 to A23, except for U4 and C10) hybridizes with the tgRNA (G1 to U23, except for A4 and G10) to form a guide-target duplex in the tgRNA-bound structure (Fig. 1D and fig. S4C). A(−3) in the 5′ tag (6 nt downstream of the first flipped-out spacer nucleotide) is flipped out because of its interaction with the thumb-like β-hairpin in the Cas7.1 domain (fig. S5B), similar to the equivalent nucleotide C(−1) in the type III-A Csm effector complex (*13*, *14*) (fig. S5C). Nonetheless, unlike the Csm complex, A(−2) and C(−1), which are located upstream of A(−3), cannot base pair with the tgRNA in Cas7-11 because of the presence of the L2 linker (fig. S5B), explaining the distinct RNA cleavage patterns between the Cas7-11 and Csm effector complexes. In the present structures, the peripheral region (residues 1043 to 1124) of the INS domain was less resolved in the density map, probably because of its flexibility (fig. S3), and was excluded from the final models (fig. S4).

Csx29 structure

Csx29 consists of a tetratricopeptide repeat (TRP) domain (residues 1 to 422) and a Caspase HetF Associated with TPRs (CHAT) protease domain (residues 423 to 751) (Fig. 2A). The TRP domain can be divided into an N-terminal domain (NTD) (residues 1 to 64), seven TPR units (TPR1 to TPR7), and a central region referred to as the activation region (AR). The NTD adopts a three-helix bundle structure and interacts with the Cas7.4 domain of Cas7-11 (Fig. 2B). In Csx29, each TPR unit contains two α helices, similar to canonical TPR-containing proteins in which the TPRs interact with their protein targets (*15*). Correspondingly, TPR1 and TPR2 of Csx29 interact with the L2 linker of

[1]Structural Biology Division, Research Center for Advanced Science and Technology, The University of Tokyo, 4-6-1 Komaba, Meguro-ku, Tokyo 153-8904, Japan. [2]McGovern Institute for Brain Research at MIT, Massachusetts Institute of Technology, Cambridge, MA 02139, USA. [3]Department of Biological Engineering, Massachusetts Institute of Technology, Cambridge, MA 02139, USA. [4]Cellular and Molecular Biotechnology Research Institute, National Institute of Advanced Industrial Science and Technology, 2-4-7 Aomi, Koto-ku, Tokyo 135-0064, Japan. [5]Graduate School of Medical Life Science, Yokohama City University, 22-2 Seto, Kanazawa-ku, Yokohama, Kanagawa 236-0027, Japan. [6]National Center for Biotechnology Information, National Library of Medicine, National Institutes of Health, Bethesda, MD 20894, USA. [7]Department of Chemistry and Biotechnology, Graduate School of Engineering, The University of Tokyo, 7-3-1 Hongo, Bunkyo-ku, Tokyo 113-8656, Japan. [8]Department of Biological Sciences, Graduate School of Science, The University of Tokyo, 7-3-1 Hongo, Bunkyo-ku, Tokyo 113-0033, Japan. [9]Inamori Research Institute for Science, 620 Suiginya-cho, Shimogyo-ku, Kyoto 600-8411, Japan.
***Corresponding author. Email: omar@abudayyeh.science (O.O.A.); jgoot@mit.edu (J.S.G.); nisimasu@g.ecc.u-tokyo.ac.jp (H.N.)**
†These authors contributed equally to this work.

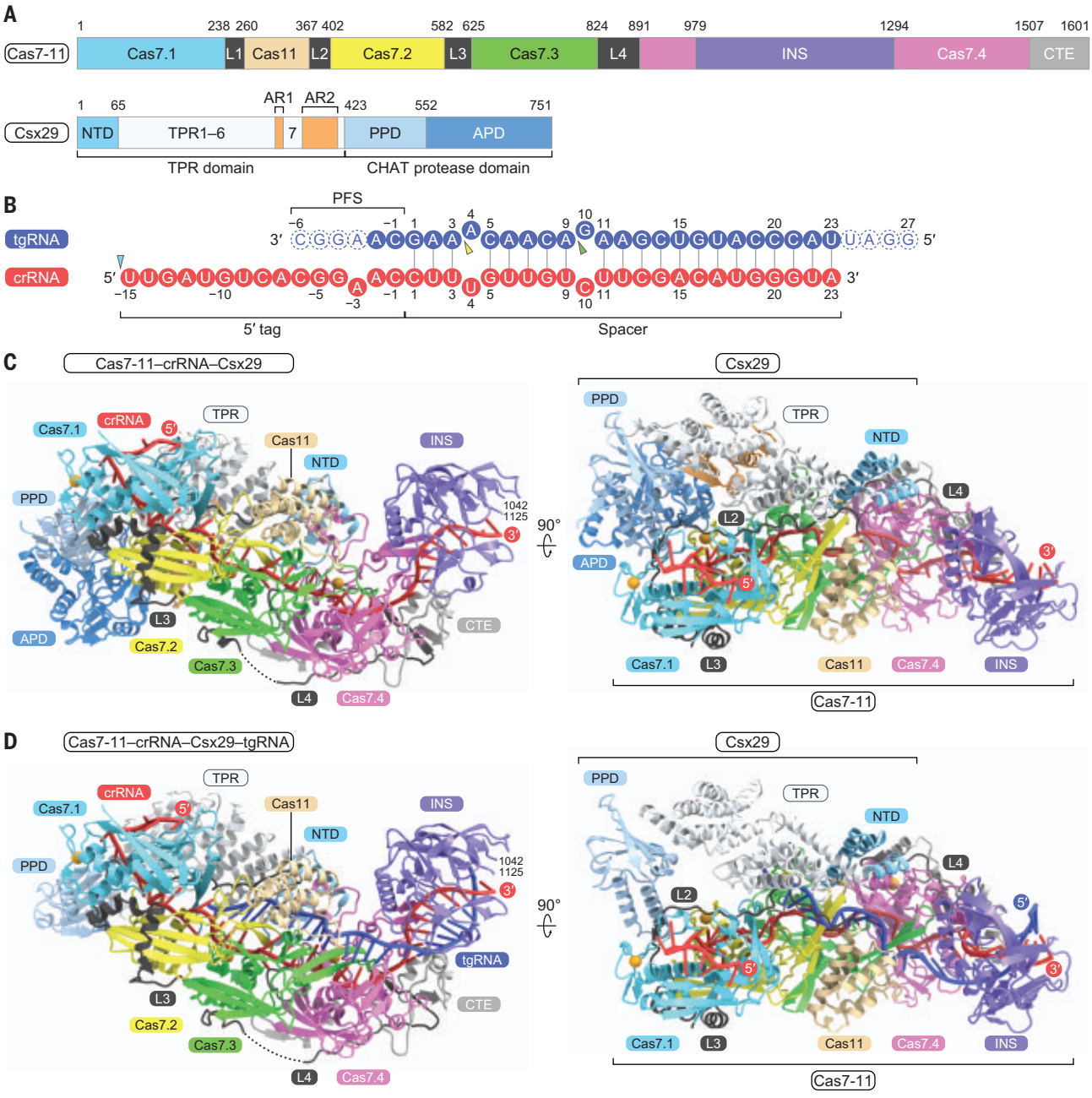

Fig. 1. Cryo-EM structures of the Cas7-11–crRNA–Csx29 complexes with and without the tgRNA. (**A**) Domain structures of Cas7-11 and Csx29. (**B**) Nucleotide sequences of the crRNA and its tgRNA. The pre-crRNA processing site and the tgRNA cleavage sites are indicated by cyan and yellow/green triangles, respectively. Disordered nucleotides are indicated by dotted lines. (**C** and **D**) Overall structures of Cas7-11–crRNA–Csx29 (C) and Cas7-11–crRNA–Csx29–tgRNA (D). The bound zinc ions are shown as orange spheres. The disordered L1 and L2 linkers are not shown for clarity. PPD, pseudo-protease domain.

Cas7-11 (Fig. 2B). The CHAT domain of Csx29 consists of a central 11-stranded mixed β-sheet and flanking α-helices, and can be divided into a pseudo-protease domain (residues 423 to 551) and an active-protease domain (APD) (residues 552 to 751) with the conserved putative catalytic residues H615 and C658 (Fig. 2A). A Dali search (*16*) confirmed that the CHAT domain of Csx29 structurally resembles caspase-like cysteine proteases such as human separase (*17*) (fig. S6). In the Cas7-11–crRNA–Csx29 structure, the AR consists of two regions, AR1 (a β-hairpin between TPR6 and TPR7) and AR2 (a β-strand and a helix-loop-helix after TPR7), and interacts with TPR1–TPR6 and the APD (Fig. 2A).

Interactions between Cas7-11 and Csx29

In the Cas7-11–crRNA–Csx29 structure, Csx29 interacts with multiple regions of Cas7-11 (Fig. 2B and fig. S7A). The L2 linker (residues 367 to 401) and α-helical insertion (residues 1313 to 1341) in the Cas7.4 ZF motif, which are disordered in the Csx29-unbound Cas7-11 structure (*12*) (fig. S7B), are ordered and form interactions with Csx29 in the Cas7-11–crRNA–Csx29 structure (Fig. 2B and fig. S7, C and D). This α-helical insertion in the ZF motif is unique to Cas7.4 (fig. S7C). The NTD of Csx29 mainly interacts with the Cas7.4 domain of Cas7-11 (Fig. 2B and figs. S7A and S8A). In addition, the Cas7.2 thumb-like β-hairpin and the L2/L4 linkers reinforce the binding to the Csx29 NTD (Fig. 2B and fig. S8, B and C).

TPR1 and TPR2 interact with Cas7.3 (ZF) and L2 of Cas7-11 (Fig. 2B and figs. S7A and S8D). TPR2 also interacts with Cas7.1 (thumb-like

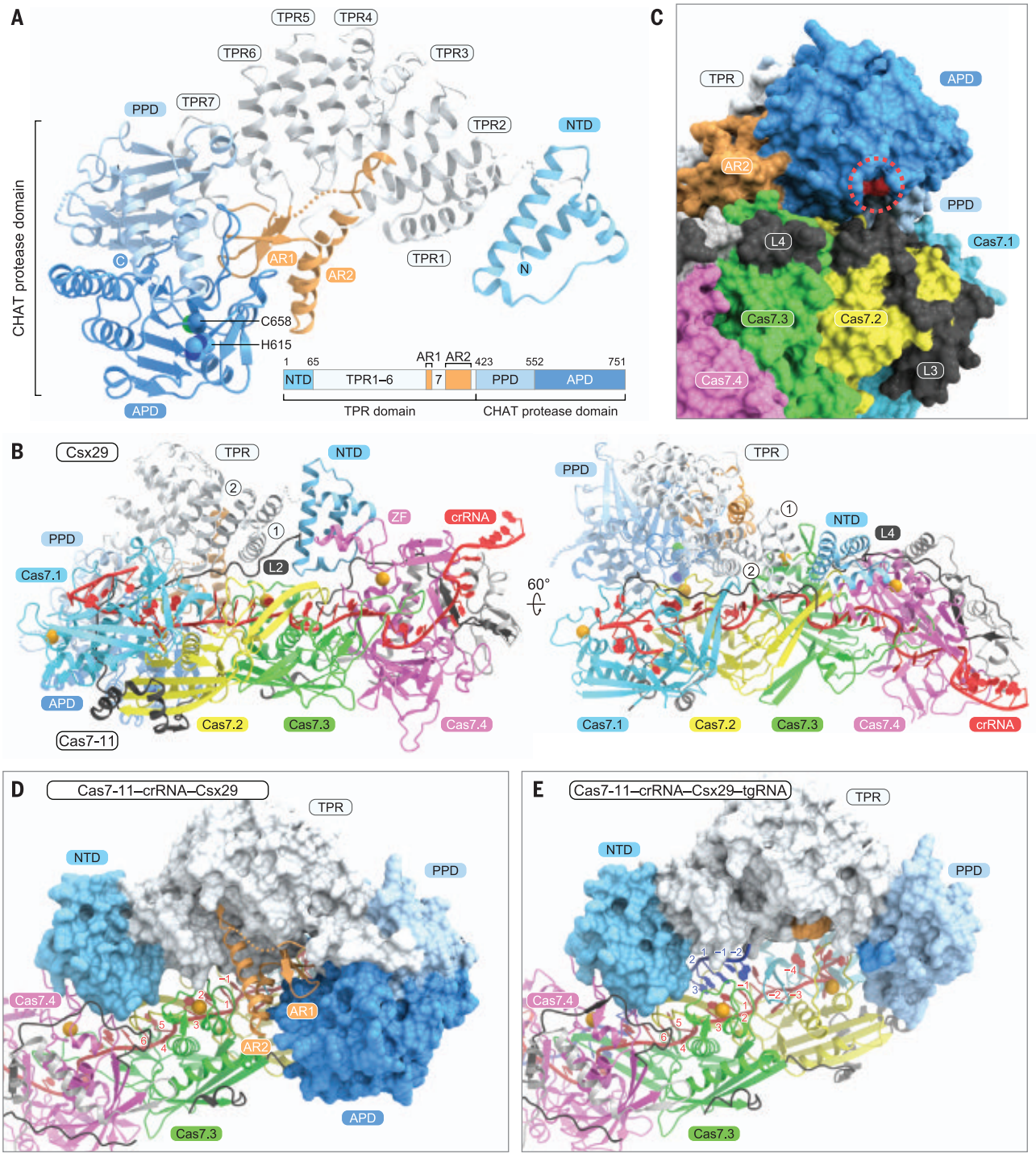

Fig. 2. Interaction between Cas7-11 and Csx29. (**A**) Structure of Csx29 in the Cas7-11–crRNA–Csx29 complex. (**B**) Interface between Cas7-11 and Csx29 in the Cas7-11–crRNA–Csx29 complex. The Cas11 and INS domains are omitted for clarity. (**C**) Location of the Csx29 active site. The catalytic residue H615 of the Csx29 protease is colored red. (**D** and **E**) Interfaces between Cas7-11 and Csx29 in Cas7-11–crRNA–Csx29 (D) and Cas7-11–crRNA–Csx29–tgRNA (E). Csx29 is shown as a surface representation, except for the AR, which is shown as a ribbon representation. The AR and APD are disordered in the Cas7-11–crRNA–Csx29–tgRNA structure in (E).

β-hairpin) and Cas7.2 (ZF) (Fig. 2B). TPR3 to TPR7 do not contact Cas7-11. The CHAT protease domain of Csx29 interacts with Cas7.1 (thumb-like β-hairpin), Cas7.2 (ZF), Cas7.3 (ZF), and L2 of Cas7-11 (Fig. 2B and fig. S7A). The protease active site of Csx29 is near the Cas7.2 domain of Cas7-11 (Fig. 2C), suggesting limited accessibility for the peptide substrate in this conformation. Furthermore, in contrast to the separase–securin structure (*17*), the side chain of the catalytic residue C658 is buried inside the CHAT domain in the present structure (fig. S6), indicating that a structural rearrangement of C658 would be required for the substrate cleavage. These observations suggest that the Cas7-11–crRNA–Csx29 structure represents the inactive state of the Csx29 putative protease.

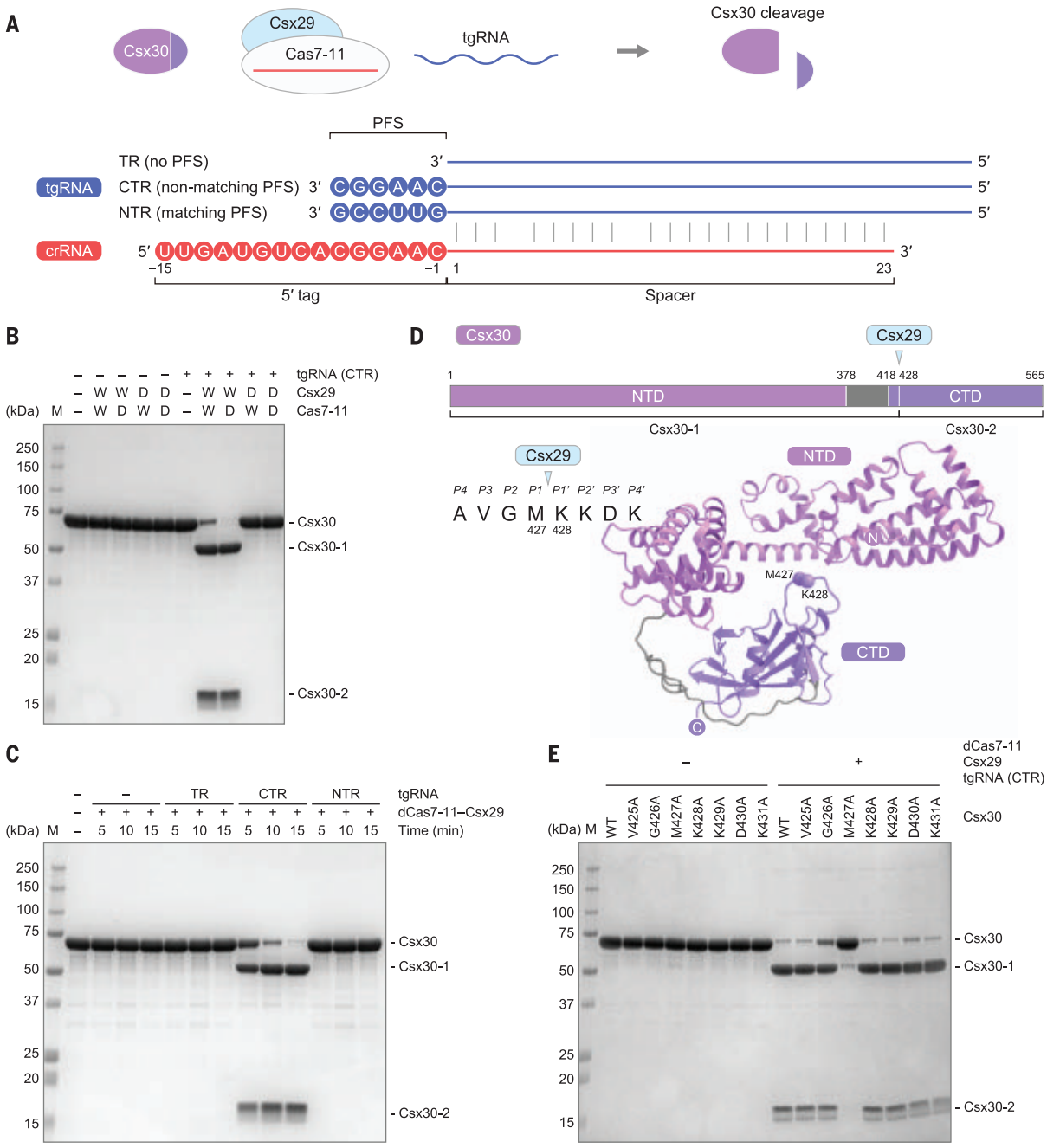

Fig. 3. tgRNA-triggered Csx30 cleavage by Csx29. (**A**) Schematic of the RNA-triggered Csx30 cleavage by the Cas7-11–crRNA–Csx29 complex. TR, tgRNA without a PFS; CTR, cognate tgRNA with a nonmatching PFS; NTR, noncognate tgRNA with a matching PFS. (**B**) RNA-triggered Csx30 cleavage by the Cas7-11–crRNA–Csx29 complex. The Cas7-11–crRNA–Csx29 complex was incubated with Csx30 at 37°C for 10 min in the presence or absence of the tgRNA (CTR). The wild-type (W) and catalytically deactivated (D) versions of Cas7-11 and Csx29 were used. (**C**) Effects of the complementarity between the crRNA 5′ tag and tgRNA PFS on the Csx30 cleavage. The dCas7-11–crRNA–Csx29 complex was incubated with Csx30 at 37°C for 5, 10, or 15 min in the presence of the tgRNA (TR, CTR, or NTR). (**D**) Proteolytic cleavage site in Csx30. The Csx30 site cleaved by Csx29 is indicated by a triangle. The Csx30 structure was predicted using AlphaFold2 (*18*), and the Cα atoms of M427 and K428 at the cleavage site are indicated by spheres. (**E**) Csx29-mediated cleavage of the Csx30 mutants. The dCas7-11–crRNA–Csx29 complex was incubated with the Csx30 mutants at 37°C for 10 min, in the presence or absence of the tgRNA (CTR). In (B), (C), and (E), the proteins were analyzed by SDS-polyacrylamide gel electrophoresis, and the gel was stained with Coomassie brilliant blue.

tgRNA binding–induced structural change in the Cas7-11–Csx29 complex

Comparison of the Cas7-11–crRNA–Csx29 structures with and without the tgRNA revealed different Csx29 conformations (Fig. 2, D and E, and movie S2). In the tgRNA-free structure, TPR1 and TPR2 of Csx29 interact with Cas7.3 and Cas7.1/Cas7.2 of Cas7-11, respectively (Fig. 2, B and D, and fig. S9A). By contrast, in the tgRNA-bound structure, TPR1 and TPR2 of Csx29 are farther away from Cas7-11 and do not interact with Cas7.1–Cas7.3 of Cas7-11 because of the binding of the tgRNA 3′ region between Cas7-11 and Csx29 (Fig. 2E and fig. S9B). In the 6-nt protospacer flanking sequence (PFS) of the tgRNA, only C(−1) and A(−2) are well resolved in the density map and interact with Cas7-11 (L2/Cas7.3) and Csx29 (TPR1/TPR2)

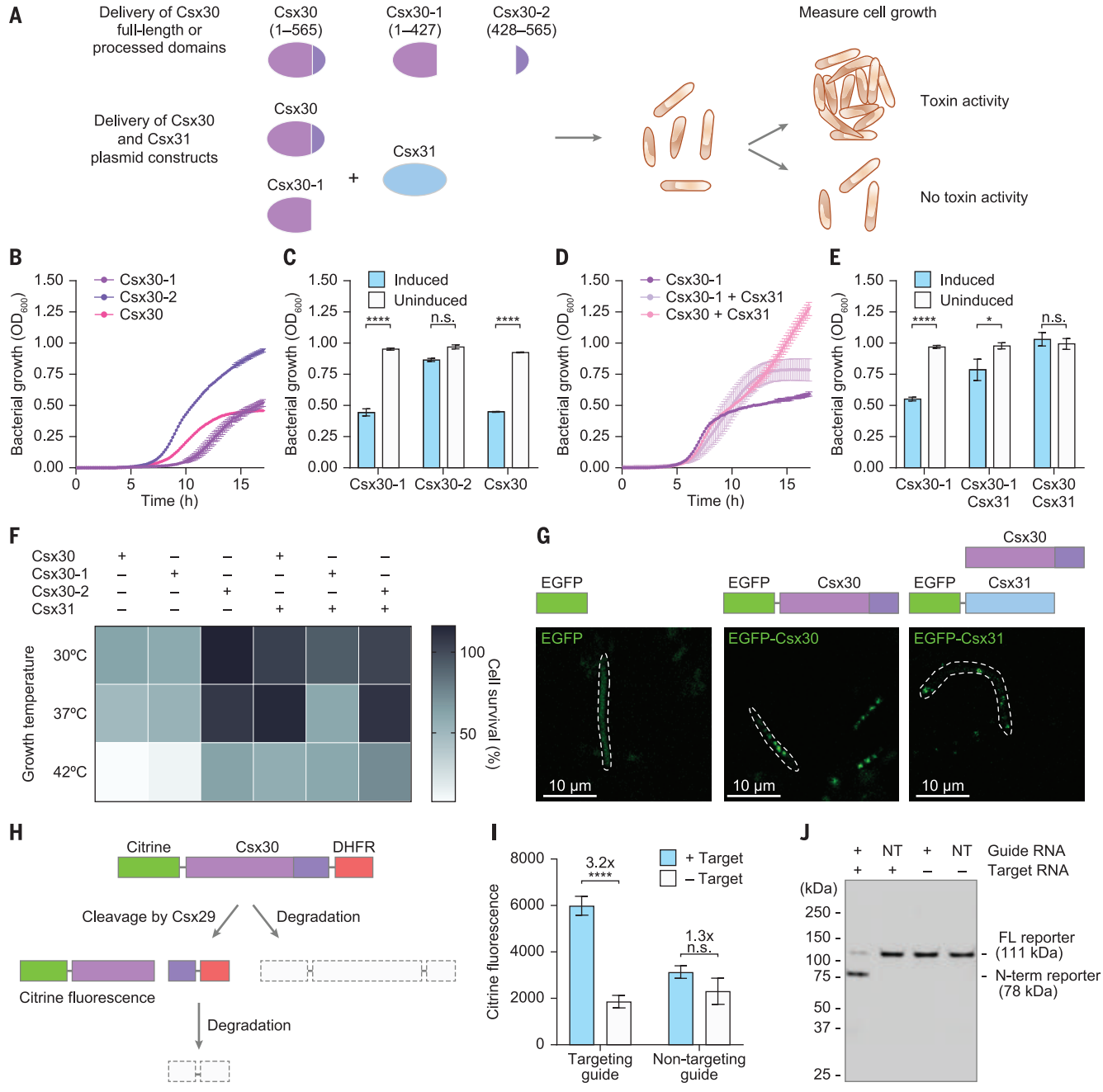

Fig. 4. Effects of Csx30 and Csx31 on bacterial cell growth. (**A**) Schematic of bacterial growth assays for studying the Csx30 and Csx31 functions. (**B** and **C**) Growth curves (B) and end-point analyses (C) of *E. coli* expressing full-length Csx30, the N-terminal fragment (residues 1 to 427) of Csx30 (Csx30-1), or the C-terminal fragment (residues 428 to 565) of Csx30 (Csx30-2). (**D** and **E**) Growth curves (D) and end-point analyses (E) of *E. coli* expressing Csx30-1, full-length Csx30 and Csx31, or Csx30-1 and Csx31. In (B) to (E), growth was compared between induced and uninduced expression conditions. In (C) and (E), significance was calculated by two-tailed Student's *t* test (****$P < 0.0001$; n.s., not significant). Data are shown as mean ± SEM ($n = 3$). (**F**) Heatmap comparing the survival percentages of bacteria expressing Csx30-1, Csx30-2, full-length Csx30 and Csx31, full-length Csx30 alone, Csx30-1 and Csx31, or Csx30-2 and Csx31, cultured at three different temperatures. Percent survival was calculated by the ratio of optical density at 600 nm (OD_{600}) of the bacterial culture under the induced conditions over the OD_{600} for the noninduced conditions. Color scale shows percent survival from 0 to 100%. (**G**) Confocal images of *E. coli* expressing EGFP alone, EGFP-Csx30, or EGFP-Csx31 and unlabeled Csx30. White outlines indicate the shapes of individual *E. coli* cells. (**H**) Schematic of the mammalian application of the Cas7-11–Csx29–Csx30 degron reporter system for RNA sensing in live cells. (**I**) Citrine fluorescence of HEK293FT cells transfected with either the Gluc target or pUC19 control target in the presence of the Cas7-11–Csx29–Csx30 degron reporter. Significance was calculated with two-tailed Student's *t* test (****$P < 0.0001$). Data are shown as mean ± SEM ($n = 3$). (**J**) RNA-triggered Csx30 reporter cleavage in HEK293FT cells. The N-terminally FLAG-tagged citrine–Csx30–degron reporter was transfected either with or without the Gluc target and with a targeting or nontargeting (NT) guide. Forty-eight hours after transfection, total protein was extracted from the transfected HEK293FT cells and analyzed by Western blot with an anti-FLAG antibody.

(fig. S9, B and C). The nucleobases C(−1) and A(−2) stack with R375 (L2) and Y718 (Cas7.3), respectively (fig. S9, B and C). In addition, the phosphate groups between A(−3) and A(−2) and between A(−2) and C(−1) interact with R131 (TPR2) and R145 (TPR2), respectively (fig. S9B). These interactions induce a kink turn between A(−2) and C(−1) in the PFS, thereby projecting the tgRNA nucleotides downstream of position −2 toward the AR of Csx29.

There are also structural differences in the AR–APD of Csx29 between the RNA-free and RNA-bound structures. Whereas the AR extensively interacts with TPR1 to TPR5 and APD in the tgRNA-free structure (Fig. 2D and fig. S9A), the AR-APD of Csx29 is not resolved in the density map in the tgRNA-bound structure (Fig. 2E and fig. S3B). In addition, the pseudoprotease domain of Csx29 in the tgRNA-bound structure exhibits weaker density compared with that in the tgRNA-free structure (fig. S3, A and B). These observations suggest that tgRNA binding increases the conformational flexibility of the CHAT protease domain of Csx29, and this conformational change releases the steric block of the Csx29 active site, allowing access to the substrate protein. Structural comparisons between the two Cas7-11–Csx29 complexes suggest steric clash between the tgRNA PFS and the Csx29 AR (fig. S9D), highlighting the importance of the PFS for the tgRNA-induced conformational change in Csx29. These structural observations indicate that Csx29 is a tgRNA-triggered protease.

tgRNA-triggered Csx30 cleavage by Csx29

Given that Csx30 and Csx31 are encoded together with Cas7-11 and Csx29 in the *D. ishimotonii* CRISPR locus and are highly conserved among the type III-E systems (*8*), we hypothesized that Csx29 could target either Csx30 or Csx31. To test this hypothesis, we attempted to prepare the recombinant Csx30 and Csx31 proteins and determine whether they are cleaved by Csx29 in a tgRNA-dependent manner. Csx30 was purified as a soluble protein, whereas Csx31 was expressed in an insoluble fraction. We examined the in vitro cleavage of Csx30 by Cas7-11–crRNA–Csx29 in the absence and presence of the tgRNA, and found that Cas7-11–crRNA–Csx29 cleaved Csx30 into two fragments, Csx30-1 (~50 kDa) and Csx30-2 (~15 kDa), only in the presence of the tgRNA (Fig. 3, A and B).

The H615A/C658A mutations in Csx29 abolished the Csx30 cleavage (Fig. 3B) but did not affect the tgRNA cleavage by Cas7-11 (fig. S10A), indicating the separable nuclease and protease activities. Furthermore, the D429A/D654A catalytic mutations in Cas7-11 abolished tgRNA cleavage (fig. S10A), as previously observed (*12*), and, unexpectedly, improved the Csx30 cleavage by Csx29 (Fig. 3B and fig. S10B). This improvement in the proteolytic activity suggests that the tgRNA dissociates from the effector complex after the Cas7-11–mediated cleavage, and that the Csx29 protease is only active when a tgRNA is bound to the Cas7-11–Csx29 complex. Thus, Csx30 is cleaved by the CHAT protease domain of Csx29 in a tgRNA-dependent manner.

The base complementarity between the crRNA 5′ tag and a tgRNA PFS regulates the activities of the type III-A Csm effector complex to avoid an autoimmune response in the type III-A system (*13*, *14*). Thus, we examined the effects of the PFS in the tgRNA on Csx30 cleavage using a tgRNA without a PFS, a cognate tgRNA with a nonmatching PFS, or a noncognate tgRNA with a matching PFS (Fig. 3A). Csx30 was cleaved by the Cas7-11–Csx29 complex efficiently in the presence of cognate tgRNA with a nonmatching PFS, but not the tgRNA without a PFS or the noncognate tgRNA with a matching PFS (Fig. 3C), consistent with our observation that a nonmatching PFS plays a role in the structural changes and protease activation of Csx29. These findings suggest a potential mechanism for self-targeting avoidance in the type III-E system, as in the type III-A system.

The N-terminal analysis of the Csx30-2 fragment showed that it begins with K428 (fig. S11), demonstrating that Csx30 is cleaved by Csx29 between M427 and K428 (Fig. 3D). Structure prediction using AlphaFold2 (*18*) indicated that Csx30 consists of an NTD and a C-terminal domain (CTD), which are connected by a linker region. The NTD (residues 1 to 377) contains two α-helical subdomains, whereas the CTD (residues 418 to 565) comprises a core β-barrel with flanking α helices (Fig. 3D). The cleavage site between M427 and K428 is located in a β-hairpin within the Csx30 CTD (Fig. 3D). We examined the in vitro Csx29-mediated cleavage of eight Csx30 mutants, in which residues V425 to K431 were individually replaced with alanine. The M427A and G416A substitutions substantially and slightly reduced the Csx30 cleavage, respectively, whereas the other substitutions had almost no effect (Fig. 3E). Accordingly, Csx29 seems to primarily recognize M427 at the P1 site within the AVGM|KKDK sequence in Csx30 and cleaves Csx30 between M427 (P1) and K428 (P1′). Thus, the Cas7-11–Csx29 complex catalyzes the tgRNA-triggered proteolysis of Csx30.

Effects of Csx30 and Csx31 on bacterial cell growth

To explore the physiological relevance of the Csx29-mediated Csx30 cleavage, we overexpressed the full-length Csx30 (referred to as Csx30 for simplicity), the N-terminal fragment of Csx30 (residues 1 to 427, Csx30-1), or the C-terminal fragment of Csx30 (residues 428 to 565, Csx30-2) in *Escherichia coli*, and monitored the cell growth (Fig. 4A). Overexpression of Csx30 substantially inhibited cell growth compared with uninduced controls (Fig. 4, B and C, and fig. S12, A and B). Overexpression of Csx30-1 similarly caused pronounced growth suppression, whereas Csx30-2 displayed only mild inhibition (Fig. 4, B and C, and fig. S12, A and B), indicating that Csx30-1 is necessary and sufficient for the observed growth effects of the full-length Csx30. Because the AlphaFold2 structural prediction (*18*) suggested that Csx30 and Csx31 have oppositely charged surfaces and could electrostatically interact with each other (fig. S12C), we also explored the effect of Csx31 on bacterial growth. Overexpression of Csx31 rescued the Csx30-mediated growth defect, but could not completely eliminate the Csx30-1–induced growth suppression (Fig. 4, D and E, and fig. S12, B and D). These data indicate that Csx31 interacts with Csx30 and regulates Csx30-induced growth suppression, whereas the generation of the Csx30-1 and Csx30-2 fragments by the Cas7-11–Csx29 protease interferes with this regulation.

Interactions among Csx30, Csx31, and RpoE

The common co-occurrence of Cas7-11, Csx30, Csx31, and the stress-associated sigma factor RpoE (*19*) in type III-E CRISPR loci (*2*, *8*) suggests interplay among these four proteins, such that the observed Csx30-induced growth suppression might be caused by interactions with endogenous *E. coli* RpoE (EcRpoE). Given the involvement of EcRpoE in cellular heat shock responses (*20*, *21*), we hypothesized that the growth defects might be more pronounced at higher temperatures because of the inhibition of EcRpoE by Csx30 and Csx31, and tested the effects of Csx30 and Csx31 in *E. coli* at temperatures ranging from 30° to 42°C. In agreement with our hypothesis, the growth suppression by Csx30 was stronger at higher temperatures across all tested combinations (Fig. 4F), implicating EcRpoE in the growth defects caused by the overexpression of Csx30 and Csx31.

To examine the direct interactions among Csx30, Csx31, and *D. ishimotonii* RpoE (DiRpoE), we coexpressed the three proteins in *E. coli* and analyzed complex formation by gel-filtration chromatography. Csx30, Csx31, and DiRpoE eluted as a single peak (fig. S13A), indicating that they form a stable complex. Like the isolated Csx30, Csx30 in the Csx30–Csx31–DiRpoE complex was cleaved by Cas7-11–Csx29, and Csx30-1, Csx31, and DiRpoE co-eluted from the column (fig. S13B), indicating that Csx30-1, Csx31, and RpoE remain complexed after Csx30 cleavage, whereas Csx30-2 dissociates from the complex. Consistently, structural prediction implied that Csx30, Csx31, and DiRpoE form a ternary complex in which the Csx30 NTD extensively interacts with DiRpoE (fig. S13C). DiRpoE is structurally similar to EcRpoE (fig. S13D), suggesting that the observed cell

growth inhibition could be mediated through Csx30–EcRpoE interactions, similar to the mechanism of the anti-sigma factor RseA (*22*). However, *D. ishimotonii* lacks RseA homologs (*23*), so DiRpoE probably mediates the transcriptional response through distinct mechanisms that remain to be characterized. A Dali search (*16*) revealed structural similarity between the Csx30 CTD and pore-forming proteins in type IV secretion systems, such as CagX (*24*) (fig. S13E). Given the reduced growth effects of full-length Csx30 in *E. coli* compared with Csx30-1, the Csx30 CTD might function as a membrane anchor rather than as a pore-forming protein, consistent with the role of the membrane-localized RseA (*19*, *23*). The CTD and NTD of Csx30 are connected through a flexible linker, suggesting that the Csx29-mediated cleavage releases the N-terminal fragment of Csx30 (Csx30-1) into the cytoplasm, thereby modulating gene expression through RpoE suppression. Csx30 NTDs are highly conserved (fig. S14), whereas Csx30 CTDs are divergent and can be divided into seven distinct groups (fig. S15), of which two are homologous protein domains found in other contexts. One is an uncharacterized DUF4384 family member that is often fused to different proteases (*25*). The other CTD is similar to the pilus assembly protein PilP, which forms a periplasmic ring of bacterial type IV pili (*26*). These observations highlight the mechanistic diversity of the Csx30-mediated RpoE interactions and programmed gene expression modulation.

Localization of Csx30 and Csx31 in bacterial cells

To explore the growth suppression associated with the expression of Csx30, the putative membrane localization of the Csx30 CTD, and the corresponding regulatory function of Csx31, we imaged Csx30 and Csx31 by fusing bacterial codon-optimized enhanced GFP (EGFP) to the N termini of both proteins. Protein localization in *E. coli* transformed with a plasmid expressing EGFP-Csx30, plasmids expressing EGFP-Csx31 and unlabeled Csx30, or a plasmid expressing EGFP alone was imaged. Both labeled Csx30 alone and labeled Csx31 co-expressed with Csx30 localized to individual foci, whereas EGFP diffused throughout the cells (Fig. 4G). These results suggest the direct interaction between Csx30 and Csx31 through colocalization at foci in bacterial cells before Csx29-mediated Csx30 cleavage.

Engineering Csx29 and Csx30 for programmable RNA sensing in mammalian cells

The programmable transcript-activated protease activity of the Cas7-11–Csx29–Csx30 system could enable multiple applications in mammalian cells, including transcript sensing. We codon-optimized Cas7-11, Csx29, and Csx30 for mammalian cells and placed the Csx30 protein sequence between a citrine protein and a dihydrofolate reductase (DHFR) degron (*27*), which would eliminate citrine fluorescence unless Csx30 was cleaved by Cas7-11–Csx29 because of the sequence-specific recognition of a target sequence (Fig. 4H). We transfected human embryonic kidney (HEK) 293FT cells with either a targeting or nontargeting guide RNA toward a Gaussia luciferase (Gluc) target to test the activation of the Cas7-11–Csx29–Csx30 system. In the presence of the Gluc mRNA target, we observed threefold higher citrine fluorescence with the targeting, but not nontargeting, guide RNA (Fig. 4I), indicating that Csx29 is activated and cleaves the DHFR degron from the citrine reporter. To validate that the increase in citrine fluorescence was caused by the cleavage of Csx30 in the reporter, we analyzed the total protein from the HEK293FT cells by Western blot using an anti-FLAG antibody and visualized the N-terminally FLAG-tagged reporter. The molecular mass of the reporter protein decreased from ~110 to 78 kDa only in the presence of the tgRNA and targeting guide, indicating the Csx29-mediated cleavage of Csx30 in the reporter (Fig. 4J and fig. S16). These results demonstrate that the Cas7-11–Csx29–Csx30 system is reprogrammable in mammalian cells and can be used as a protease-based RNA-guided posttranslational sensor.

Discussion

Our structural and functional analyses of the type III-E CRISPR-Cas systems revealed notable complexity and fine-tuned regulation. The effects of Csx30 and Csx31 on bacterial growth suggested that Csx29-mediated Csx30 cleavage releases the N-terminal fragment of Csx30 bound to Csx31, inhibiting host cell growth (fig. S17). Furthermore, our biochemical and structural analyses indicated that Csx30, Csx31, and RpoE can form a ternary complex in which Csx30 extensively interacts with RpoE, suggesting that RpoE inhibition by Csx30 contributes to the observed cell growth arrest, akin to the Cas13 collateral activity-based cell growth arrest (*28*). Csx30 cleavage by Csx29 could also facilitate the dissociation of RpoE from Csx30, allowing RpoE to engage in a transcriptional response to viral infection. By leveraging the programmable nature of this system, we developed a molecular RNA sensor for transcripts in mammalian cells, demonstrating the potential of this Cas7-11–Csx29–Csx30 system for sensing and therapeutic applications, analogous to recently developed mammalian RNA sensors (*29*, *30*).

Thus, in type III-E CRISPR-Cas systems, the Cas7-11–Csx29 effector complex likely degrades the ssRNA transcripts of phage genes and stimulates potentially toxic host cell stress responses through the Csx29-mediated Csx30 cleavage (fig. S17). This type of programmed growth suppression, through cell death or growth arrest, appears analogous to that caused by gasdermins, the bacterial membrane pore-forming toxins that are switched on by the release of auto-inhibitory peptides by associated proteases that become activated during phage infection (*31*, *32*). Moreover, given the high diversity of Csx30 CTDs (fig. S15), further explorations of other subtype III-E systems might reveal additional functions associated with Cas7-11–mediated tgRNA recognition.

Among the CRISPR-Cas systems, a biological, if not mechanistic, analogy can be found in the type VI systems, where the Cas13–crRNA effector complex recognizes complementary phage mRNAs and cleaves both phage (specifically and in *cis*) and host (indiscriminately and in *trans*) transcripts, thus stalling cell growth and with it the infectious cycle (*28*). Similarly, in some type III systems, the CRISPR-Lon protease is activated by cyclic oligoadenylates upon RNA recognition by the effector complexes and cleaves the associated CRISPR-T protein specifically, releasing a toxic fragment (*33*). Our characterization of the subtype III-E system highlights the remarkable diversity of CRISPR-associated functions activated by programmable nucleic acid recognition, motivating continued exploration of CRISPR-associated proteins and their programmable functions that could be useful for biological applications. Our findings that the type III-E Cas7-11–Csx29 effector complex is an RNA-triggered nuclease-protease establish a distinct paradigm of prokaryotic signal transduction in viral immunity and could pave the way for the development of new RNA/protein-targeting technologies, including in vitro diagnostics and cellular RNA sensing.

REFERENCES AND NOTES

1. F. Hille *et al.*, *Cell* **172**, 1239–1259 (2018).
2. K. S. Makarova *et al.*, *Nat. Rev. Microbiol.* **18**, 67–83 (2020).
3. M. Kazlauskiene, G. Kostiuk, Č. Venclovas, G. Tamulaitis, V. Siksnys, *Science* **357**, 605–609 (2017).
4. O. Niewoehner *et al.*, *Nature* **548**, 543–548 (2017).
5. C. Rouillon, J. S. Athukoralage, S. Graham, S. Grüschow, M. F. White, *eLife* **7**, e36734 (2018).
6. W. Han, S. Pan, B. López-Méndez, G. Montoya, Q. She, *Nucleic Acids Res.* **45**, 10740–10750 (2017).
7. A. R. VanderWal, J.-U. Park, B. Polevoda, E. H. Kellogg, M. R. O'Connell, CRISPR-Csx28 forms a Cas13b-activated membrane pore required for robust CRISPR-Cas adaptive immunity. bioRxiv 466367 [Preprint] (2021); https://doi.org/10.1101/2021.11.02.466367.
8. A. Özcan *et al.*, *Nature* **597**, 720–725 (2021).
9. S. P. B. van Beljouw *et al.*, *Science* **373**, 1349–1353 (2021).
10. O. O. Abudayyeh *et al.*, *Nature* **550**, 280–284 (2017).
11. J. S. Gootenberg *et al.*, *Science* **356**, 438–442 (2017).
12. K. Kato *et al.*, *Cell* **185**, 2324–2337.e16 (2022).
13. L. You *et al.*, *Cell* **176**, 239–253.e16 (2019).
14. N. Jia *et al.*, *Mol. Cell* **73**, 264–277.e5 (2019).
15. N. Zeytuni, R. Zarivach, *Structure* **20**, 397–405 (2012).
16. L. Holm, *Methods Mol. Biol.* **2112**, 29–42 (2020).
17. J. Yu *et al.*, *Nature* **596**, 138–142 (2021).
18. J. Jumper *et al.*, *Nature* **596**, 583–589 (2021).
19. L. Connolly, A. De Las Penas, B. M. Alba, C. A. Gross, *Genes Dev.* **11**, 2012–2021 (1997).

20. J. Mecsas, P. E. Rouviere, J. W. Erickson, T. J. Donohue, C. A. Gross, *Genes Dev.* **7** (12b), 2618–2628 (1993).
21. K. Hiratsu, M. Amemura, H. Nashimoto, H. Shinagawa, K. Makino, *J. Bacteriol.* **177**, 2918–2922 (1995).
22. E. A. Campbell *et al.*, *Mol. Cell* **11**, 1067–1078 (2003).
23. V. Schnaars *et al.*, *Microb. Physiol.* **31**, 1–20 (2021).
24. J. M. Chung *et al.*, *eLife* **8**, e47644 (2019).
25. S. Lu *et al.*, *Nucleic Acids Res.* **48**, D265–D268 (2020).
26. Y.-W. Chang *et al.*, *Science* **351**, aad2001 (2016).
27. X. J. Gao, L. S. Chong, M. S. Kim, M. B. Elowitz, *Science* **361**, 1252–1258 (2018).
28. A. J. Meeske, S. Nakandakari-Higa, L. A. Marraffini, *Nature* **570**, 241–245 (2019).
29. K. Jiang *et al.*, *Nat. Biotechnol.* 10.1038/s41587-022-01534-5 (2022).
30. E. M. Zhao *et al.*, *Nat. Biotechnol.* **40**, 539–545 (2022).
31. A. G. Johnson *et al.*, *Science* **375**, 221–225 (2022).
32. C. Clavé *et al.*, *Proc. Natl. Acad. Sci. U.S.A.* **119**, e2109418119 (2022).
33. C. Rouillon *et al.*, SAVED by a toxin: Structure and function of the CRISPR Lon protease. bioRxiv 471393 [Preprint] (2021); https://doi.org/10.1101/2021.12.06.471393.

ACKNOWLEDGMENTS

We thank M. Hiraizumi and the staff scientists at The University of Tokyo's cryo-EM facility, especially Y. Sakamaki, for help with cryo-EM data collection, and N. Okumura for help with the N-terminal analysis. **Funding:** S.A. is supported by the Japan Society for the Promotion of Science (JSPS) (KAKENHI grant 21H05736). K.S.M. and E.V.K are supported through the National Institutes of Health's (NIH's) Intramural Research Program (National Library of Medicine). H.N. is supported by the Platform Project for Supporting Drug Discovery and Life Science Research Basis for Supporting Innovative Drug Discovery and Life Science Research (BINDS) from the Japanese Agency for for Medical Research and Development (AMED) (grant JP21am0101115 support number 2792 and grant JP21wm0325048h0001), JSPS (KAKENHI grants 20K20579 and 21H05281), the Takeda Medical Research Foundation, and the Inamori Research Institute for Science. J.S.G. and O.O.A. are supported by the NIH (grants 1R21-AI149694, R01-EB031957, and R56-HG011857), the McGovern Institute Neurotechnology (MINT) program; the K. Lisa Yang and Hock E. Tan Center for Molecular Therapeutics in Neuroscience, the G. Harold & Leila Y. Mathers Charitable Foundation, the MIT John W. Jarve (1978) Seed Fund for Science Innovation, FastGrants, the Cystic Fibrosis Foundation, Google Ventures, by a Longevity Impetus Grant from the Norn Group, the NHGRI/TDCC Opportunity Fund, and the McGovern Institute. **Author contributions:** Conceptualization: K.K., O.O.A., J.S.G., H.N.; Funding acquisition: O.O.A., J.S.G., H.N.; Investigation: K.K., S.O., C.S., K.J., W.Z., J.I., Y.I., S.A., T.N., K.S.M., E.V.K., O.O.A., J.S.G., H.N.; Supervision: O.O.A., J.S.G., H.N.; Writing – original draft: K.K., C.S., K.J., O.O.A., J.S.G., H.N.; Writing – review and editing: E.V.K., O.O.A., J.S.G., H.N. **Competing interests:** The authors have filed a patent application related to this work. J.S.G. and O.O.A. are co-founders of Sherlock Biosciences, Proof Diagnostics, Moment Biosciences, and Tome Biosciences. H.N. is an adviser for Moment Biosciences. **Data and materials availability:** Relevant plasmids are available from the corresponding authors under a material transfer agreement with MIT or Addgene. The EM densities have been deposited in the Electron Microscopy Data Bank under the accession codes 33695 and 34218. The model coordinates have been deposited in the Protein Data Bank under the accession codes 7Y7X and 8GS2.

SUPPLEMENTARY MATERIALS

science.org/doi/10.1126/science.add7347
Materials and Methods
Figs. S1 to S17
Tables S1 to S2
References (*34*–*49*)
MDAR Reproducibility Checklist
Movies S1 and S2

Submitted 30 June 2022; accepted 24 October 2022
10.1126/science.add7347

REPORTS

PHOTOCATALYSIS

Earth-abundant photocatalyst for H_2 generation from NH_3 with light-emitting diode illumination

Yigao Yuan[1]†, Linan Zhou[1,2,3]†, Hossein Robatjazi[1,4]*, Junwei Lucas Bao[5], Jingyi Zhou[6], Aaron Bayles[1], Lin Yuan[1], Minghe Lou[1], Minhan Lou[2], Suman Khatiwada[4], Emily A. Carter[7]*, Peter Nordlander[2,8]*, Naomi J. Halas[1,2,8]*

Catalysts based on platinum group metals have been a major focus of the chemical industry for decades. We show that plasmonic photocatalysis can transform a thermally unreactive, earth-abundant transition metal into a catalytically active site under illumination. Fe active sites in a Cu-Fe antenna-reactor complex achieve efficiencies very similar to Ru for the photocatalytic decomposition of ammonia under ultrafast pulsed illumination. When illuminated with light-emitting diodes rather than lasers, the photocatalytic efficiencies remain comparable, even when the scale of reaction increases by nearly three orders of magnitude. This result demonstrates the potential for highly efficient, electrically driven production of hydrogen from an ammonia carrier with earth-abundant transition metals.

Surface plasmons excited by light in coinage metal nanoparticles (NPs) can generate both strong photothermal heating and nonequilibrium highly excited electrons or holes [hot carriers (HCs)] that can react with adsorbed molecules (*1*) and in turn provide an efficient way to transform light energy into chemical energy (*2*–*4*). Direct photocatalysis with metal NPs (*5*) has been demonstrated for numerous reactions, including H_2 dissociation on Au (*1*), O_2 dissociation on Ag (*6*), and propylene oxidation on Cu (*7*). However, despite their strong light-coupling properties (*8*), NPs composed solely of these metals do not provide active sites for the binding of adsorbates, which ultimately limits their catalytic properties.

Antenna-reactor (AR) complexes have been developed, typically consisting of a plasmonic NP (the antenna) decorated with reactor particles, such as islands, clusters, or single atoms of platinum group metals (PGMs) (*9*, *10*). For example, a Cu-Ru AR complex (Cu-Ru-AR) efficiently photocatalyzed ammonia decomposition (*11*). As suggested by the Sabatier principle (*12*), Ru is an ideal binding site for this reaction because it binds the nitrogen intermediate species neither too strongly nor too weakly (*13*). The Cu-Ru-AR has Ru reactors dispersed on Cu antennas, which generate HCs that enhance the reactivity of the photocatalyst and decrease reaction barriers by activating the Ru-N bond (*11*, *14*). Although incorporating PGM reactors substantially improves photocatalytic performance, their scarcity and cost (*15*) drive efforts to replace them with more earth-abundant transition metals, especially for an industrial-scale reaction such as the decomposition of ammonia, which enables its use as a hydrogen carrier (*16*, *17*). However, a metal such as Fe is far less reactive than Ru for this reaction when thermally driven because the Fe-N bond is so strong that the product fails to desorb (*18*).

We show that hot-carrier–facilitated activation on the surface of a plasmonic NP is as efficient for the Fe-N bond as for the Ru-N bond, resulting in a similarly large decrease in the activation barrier and notably similar photocatalytic reactivity under ultrafast pulsed laser illumination. Motivated by these findings, we investigate the feasibility of photocatalytically driving this reaction at room temperature using light-emitting diodes (LEDs) as the light source, scaling up the reaction by nearly three orders of magnitude in a custom photoreactor.

To compare photocatalytic Fe-N and Ru-N bond activation, we prepared Cu-Fe- and Cu-Ru-ARs through a coprecipitation method (*11*, *19*, *20*), which is described in the supplemental materials (SM). This approach resulted in similar metal concentrations (table S1), indistinguishable morphologies (fig. S1), and comparable size distributions (fig. S2). Optical properties were also similar because the absorption is dominated by the plasmonic Cu NP instead of the

[1]Department of Chemistry, Rice University; Houston, TX 77005, USA. [2]Department of Electrical and Computer Engineering, Rice University; Houston, TX 77005, USA. [3]School of Chemistry and Chemical Engineering, South China University of Technology, Guangzhou 510640, China. [4]Syzygy Plasmonics Inc., Houston, TX 77054, USA. [5]Department of Mechanical and Aerospace Engineering, Princeton University, Princeton, NJ 08544-5263; Present address: Department of Chemistry, Boston College; Chestnut Hill, MA 02467, USA. [6]Department of Materials Science and NanoEngineering, Rice University; Houston, TX 77005, USA. [7]Department of Chemical and Biomolecular Engineering, University of California, Los Angeles; Los Angeles, CA 90095-1405 and Department of Mechanical and Aerospace Engineering and the Andlinger Center for Energy and the Environment, Princeton University; Princeton, NJ 08544-5263, USA. [8]Department of Physics and Astronomy, Rice University, Houston, TX 77005, USA.
***Corresponding author. Email: hossein@plasmonics.tech (H.R.), eac@princeton.edu (E.A.C.), nordland@rice.edu (P.N.), halas@rice.edu (N.J.H.)**
†These authors contributed equally to this work.

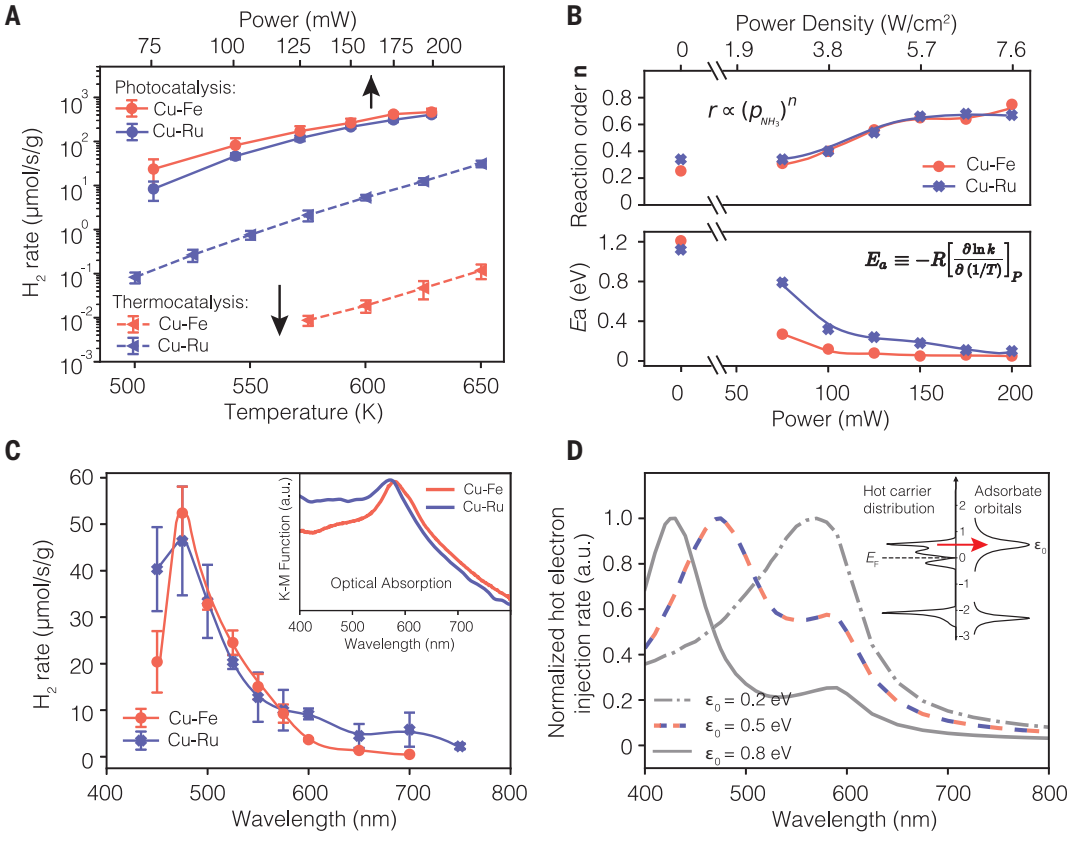

Fig. 1. The ammonia decomposition reaction on Cu-Fe- and Cu-Ru-ARs. (**A**) Comparison of photocatalysis and thermocatalysis for both ARs. Reactions were performed under differential reactor conditions (<2% reactant conversion), to avoid mass transfer limitations. Error bars represent standard deviations among three independent measurements. (**B**) Macroscopic kinetics studies: (top) the reaction orders of reactant, (bottom) the apparent activation barrier, E_a. A power of 0 mW refers to thermocatalysis. (**C**) Wavelength-dependent reaction rates. (Inset) Optical absorption spectra. (**D**) Calculated wavelength-dependent hot carrier injection rate with the antibonding orbital (ε_0) positioned at 0.2, 0.5, and 0.8 eV above Fermi level E_F. (Inset) Schematic of the HC injection model.

lossy Fe or Ru surface sites (fig. S3). We further characterized the catalysts as described in the SM. These similarities allowed us to compare the catalytic properties of Cu-Fe- and Cu-Ru-ARs directly.

The catalytic properties of Cu-Fe-AR were characterized both photocatalytically and thermocatalytically. Light-induced heating was monitored in operando with an infrared (IR) camera as a function of illumination power (SM). Because of the porous nature of the powder sample, the emissivity of the sample powder was set to be 0.95 (*21*). The Gaussian beam of the white-light laser (fig. S4) caused a similar distribution of light-induced heating on the catalyst surface. Taking into consideration that part of the incident laser power was absorbed and converted to heat, the temperature distribution in the catalyst was modeled (fig. S5B) using finite element analysis (see SM), which showed a trend similar to that of the experimental measurements. The power-dependent photocatalytic rates were correlated with temperature through T_{max} (power), the maximum surface temperature at a given power, which enabled a meaningful comparison with the thermocatalysis rate (Fig. 1A). Photocatalysis on Cu-Fe-AR showed an increase in reaction rate of about 10,000 times compared with thermocatalysis. The turnover frequency increased from 0.00017 s^{-1} at 625 K to 1.7 s^{-1} (0.466 mmol g^{-1} s^{-1}) at 200 mW (7.63 W/cm^2, fig. S4) illumination (T_{max} ~625 K) on Cu-Fe-AR and was comparable to the most efficient Ru-based thermocatalyst reported, which exhibited 0.435 mmol g^{-1} s^{-1} reactivity at 623 K (*22*). The Cu-Fe-AR was as efficient as the Cu-Ru-AR in photocatalysis despite its thermocatalytic reactivity being ~200 times lower (Fig. 1A). An H_2:N_2 stoichiometric ratio of 3:1 was observed, indicating the absence of side reactions (fig. S6). Both photocatalysts showed stable H_2 production after 6 hours of illumination (fig. S7).

The measurement of reaction orders of the reactant and the apparent activation barriers can provide an increased understanding of the effect of HCs and the differences between Fe and Ru. The reaction order of ammonia increased under illumination for both Cu-Fe- and Cu-Ru-ARs (Fig. 1B and fig. S8). Based on microkinetic analysis, an increase in reaction order implied a decrease in the coverage of surface N species (see SM, microkinetics analysis). This decrease suggested that HCs activated the metal-nitrogen bond and facilitated the desorption of surface species. Such a photochemical process is known as the desorption induced by electronic transition mechanism (*23*, *24*). The apparent activation barrier (E_a) is defined as the sum of the activation barrier of the rate-determining step (RDS), the net enthalpy of the steps that produce species involved in the RDS, and a coverage-dependent term related to the enthalpy required to desorb reaction intermediates from active sites (*25*). For photocatalysis, the aforementioned T_{max} were used in the Arrhenius equation to obtain the E_a. Cu-Fe-AR showed a higher E_a (1.21 eV) than Cu-Ru-AR (1.12 eV) in thermocatalysis, but this relationship was reversed in photocatalysis (Fig. 1B and fig. S9). The larger decrease of E_a on Cu-Fe-AR compared with Cu-Ru-AR was consistent with the greater enhancement in photocatalysis.

Wavelength dependence studies that correlate the incident wavelength with the output reaction rate also suggested that a contribution from HCs was essential. Photocatalytic reactivities of Cu-Fe- and Cu-Ru-ARs peaked at ~475 nm (Fig. 1C), which was far from the optical absorption peak at ~570 nm (Fig. 1C, inset). This difference further confirmed that photocatalytic reactivity was not a purely thermal effect. We used a simple HC injection model (see SM) to simulate the wavelength-dependent behavior. HC injection occurs when HCs scatter into metal-adsorbate orbitals (MAOs) (Fig. 1D, inset). For example, hot electrons can scatter into antibonding MAOs to form transient negative ion states (*6*). The normalized HC injection rate agreed with experiments for an MAO centered at 0.5 eV above the Fermi energy E_F (Fig. 1D). Our model suggests that the quantum efficiency of incident photons depended more on the generation of HCs at the MAO energy level, rather than on the optical absorption or the total HC generation rate predicted by near-field

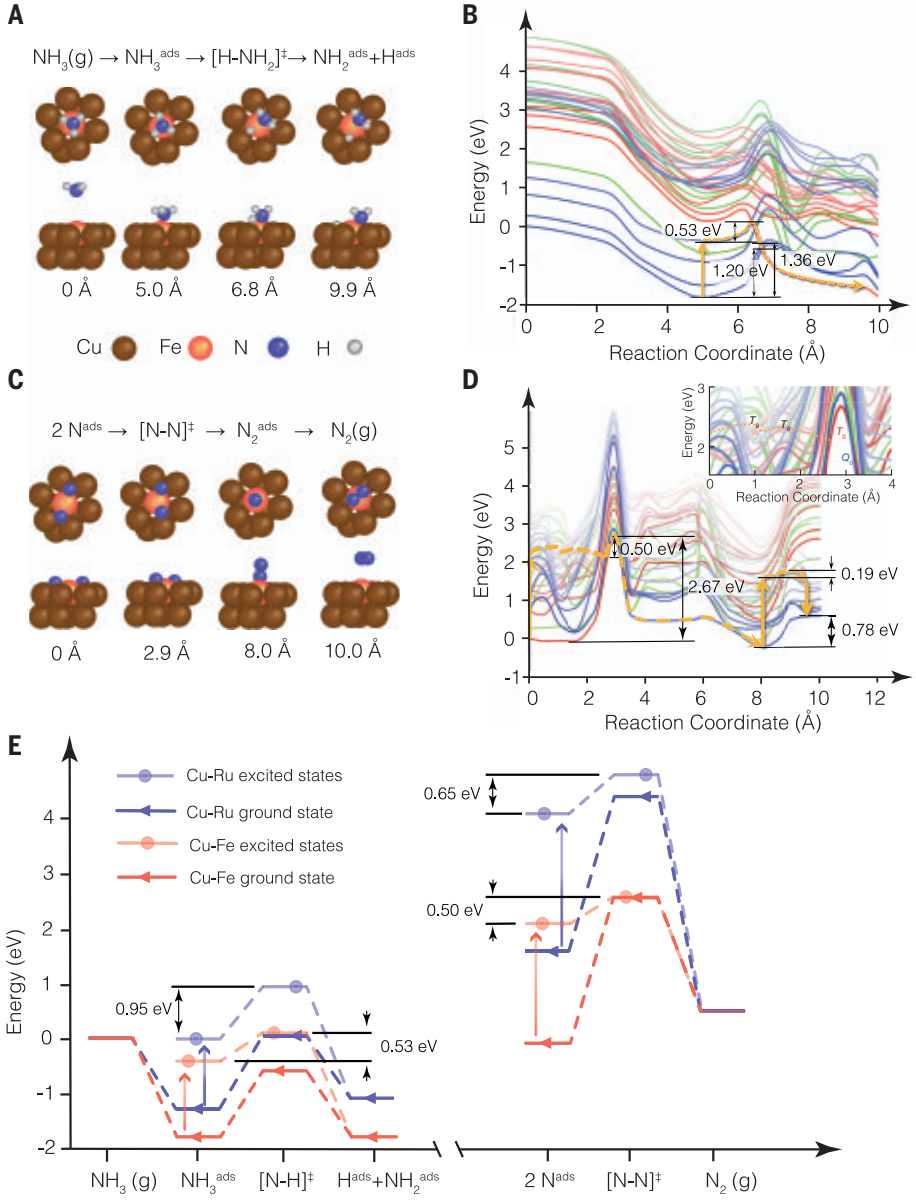

Fig. 2. First-principles quantum mechanical studies of photocatalytic ammonia decomposition. (**A**) Plane-wave density-functional theory with the Perdew-Burke-Ernzerhof exchange-correlation functional and D3 Becke-Johnson damping corrections (DFT-PBE-D3BJ) optimized structures along the MEP for NH_3 dissociative adsorption on a Cu-Fe-AR surface. (**B**) Ground- and excited-state emb-CASPT2 PESs along the MEP in (A) for the spin eigenstates: singlet (green), triplet (red), quintuplet (blue). Solid, straight, orange arrows represent vertical excitation and de-excitation, and dashed, curly, orange arrows represent productive (thermal) pathways. (**C**) The DFT-PBE-D3BJ optimized structures along the MEP for associative desorption of N_2. (**D**) Ground and excited-state emb-CASPT2 PESs along the MEP in (C) for the spin eigenstates, (inset) enlarged PESs at 0 to 4 Å. (**E**) Schematic comparison of the energy landscape for photocatalysis (excited states) and thermocatalysis (ground state) on Cu-Fe- and Cu-Ru-ARs. Red arrows refer to electronic excitation on Fe-N, and blue to Ru-N. Only the two possible RDSs are included for simplicity; migrations of nitrogen species are not considered for the same reason.

enhancement. The MAO energy level is defined by the electronic structure of the adsorbate, which is also influenced by the image potential at the metal NP surface (*26*) (fig. S10). For the previously reported Cu-Ru-AR—which had a lower Ru loading and smaller average NP size (*11*)—the electronic structure and the image potential were different, which resulted in a down-shift of the MAO energy and a red-shift of the reactivity peak.

To understand the microscopic reaction mechanism on Cu-Fe-AR, we used embedded correlated wave function (*27, 28*) theory to calculate potential energy surfaces (PESs) projected along minimum-energy paths (MEPs, characterized by their reaction coordinate *s*). Two possible RDSs were considered on Cu-Fe-AR, Cu-Ru-AR, and pure Cu surfaces: dissociative adsorption of NH_3 and associative desorption of N_2. NH_3 first binds molecularly to the catalytic sites with an adsorption energy of −1.81 eV on Cu-Fe-AR, −1.26 eV on Cu-Ru-AR, and −0.82 eV on Cu at the embedded complete-active-space second-order perturbation theory (emb-CASPT2) (*29*, *30*) level (Fig. 2A). The ground-state barrier for adsorbed NH_3 (NH_3^{ads}) dissociation to adsorbed NH_2 and H (NH_2^{ads} + H^{ads}) is 1.20 eV with a quintuplet-to-triplet crossing at *s* ~6.7 Å (Fig. 2B). The barrier would be 1.36 eV if it remained on the quintuplet PES (fig. S11). The same N-H bond dissociation in NH_3^{ads} has a barrier of 1.35 eV on Cu-Ru-AR and 2.06 eV on pure Cu, showing the power of alloying with Fe or Ru. Upon excitation, NH_3^{ads} (at *s* ~5 Å) reaches the third quintuplet excited state on Cu-Fe-AR (Fig. 2B, solid arrow). The resulting effective excited-state barrier for NH_3^{ads} dissociation to NH_2^{ads} + H^{ads} on Cu-Fe-AR is 0.53 eV with a quintuplet to triplet crossing at *s* ~6.4 Å, whereas it is 0.95 eV on Cu-Ru-AR (*14*) and 0.32 eV on pure Cu (note that the RDS on pure Cu becomes associative desorption of N_2 upon excitation, see below) (*31*).

The associative desorption of N_2 on Cu-Fe-AR (Fig. 2C) was experimentally observed to be the RDS. The ground-state barrier for this step was indeed rate limiting: 2.67 eV with a crossing from triplet to quintuplet at *s* ~3.2 Å (Fig. 2D and fig. S12). The corresponding barrier was 2.84 eV on Cu-Ru-AR but only 1.48 eV on pure Cu. Because of the lower barrier on pure Cu, N^{ads} potentially could migrate from Fe to Cu sites favored by entropy increase (fig. S13), then desorb with a smaller barrier. Upon excitation, the system could be promoted to the ninth excited state and then traverse a manifold of closely spaced spin states to reach the triplet ground state on Cu-Fe-AR (Fig. 2D, inset). The resulting excited-state barrier for associative desorption of N_2 is 0.50 eV whereas it is 0.65 eV on both Cu-Ru-AR (*14*) and pure Cu (*31*).

This model provides a qualitative description of both ground-state thermocatalysis and excited-state photocatalysis (Fig. 2E). The activation barriers of both steps on Cu-Fe-AR decreased considerably upon excitation, revealing why the reaction rate was greatly enhanced upon illumination. The resulting barriers were smaller (0.53 and 0.50 eV) than those on Cu-Ru-AR (0.95 and 0.65 eV) because the excited transition states had lower energies caused by extensive mixing of different spin manifolds. Note that the measured apparent E_as were coverage dependent and differed from calculated E_as of the elementary steps, which were calculated only for the low-coverage limit. Moreover, the actual Fe reactor NP could be in a

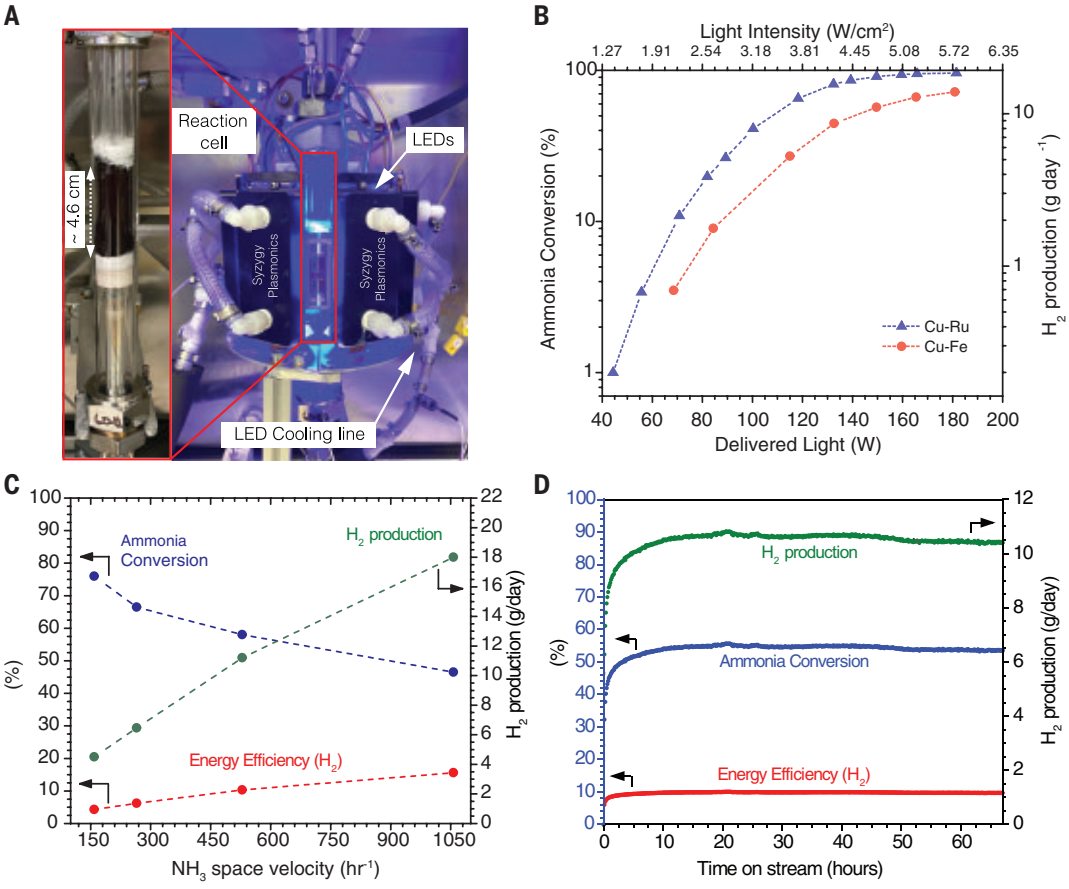

Fig. 3. Electrified photocatalysis of ammonia decomposition for gram-scale H_2 production. (**A**) Photograph of the reaction cell (left) and the photocatalytic platform (right) using LEDs at 470 nm for ammonia decomposition. The reaction cell consisted of two concentric tubes of different diameters, with the catalyst (~0.5 cm bed thickness) filled in between them. (**B**) Ammonia conversion and corresponding H_2 production rates on the Cu-Fe- and Cu-Ru-ARs as a function of delivered LED power at ammonia space velocity 487 hours^{-1}, which is defined as the volumetric flow rate of ammonia divided by the volume of the catalyst (11 cm^3). (**C**) Ammonia conversion, H_2 production, and energy efficiency as a function of the feed space velocity during ammonia decomposition on the Cu-Fe-AR under illumination power 140 W. (**D**) Long-term photocatalytic ammonia decomposition on the Cu-Fe-AR under illumination power 137 W (light on at time = 0). In each case, measurements were performed using ~3.7 g catalyst (60 to 120 mesh size and catalyst powder size 250 to 125 μm) and without supplying external heating.

more complex geometry than our single-atom catalyst model. Nevertheless, the matching theoretical and experimental qualitative trends in the nonthermal effects, both increasing reaction orders and decreasing E_a, clearly showed the distinct advantages of HC-based plasmonic photocatalysis over thermocatalysis.

Photocatalysis with antenna-reactor catalysts made by abundant materials, ideally fueled by renewable electricity, potentially represents a practical route for sustainable production of fuels and major commodity chemicals, replacing fossil fuel–based heat sources with low-cost photon sources such as LEDs. A continuous decline in the cost of renewable electricity (currently as low as 5¢ per kWh^{-1} in many parts of the world) (*32*) along with substantial and continuous improvements in the efficiency and cost of LEDs (*33*) could make renewable photons inexpensive and abundant (see SM). These innovations further motivate the development of plasmonic photocatalysis for industrially relevant reactions (*34*). The differences in the temporal structure of an ultrafast pulsed laser source and continuous-wave LEDs were also substantial and could provide valuable insight into the relative contributions of HCs and photothermal heating for different photocatalysts for the same chemical reaction.

To that end, we investigated visible-light–driven NH_3 decomposition using Cu-Fe- and Cu-Ru-ARs for gram-scale H_2 production in an LED-based, high-throughput photoreactor (Syzygy Plasmonics Inc.) (Fig. 3). The photoreactor included an annular reaction cell surrounded by a bank of customized 470-nm LEDs (Fig. 3A). The Cu-Fe-AR (3.7 g, 60 to 120 mesh size, that is, 250 to 125 μm) was packed into the space between the two concentric tubes (4.6 cm bed length and 0.5 cm bed depth) in the reaction cell. The gram-scale photoreactor design was fairly optimized for efficient light utilization and mass transfer based on the physical properties of the catalyst (mesh size), photon penetration depth (typically ~10 μm) (*35*), and photothermal heat diffusion to achieve optimum photocatalytic reaction rates and energy efficiency.

We performed photocatalytic measurements using this LED light source without external heating. Illumination resulted in efficient ammonia decomposition for both Cu-Fe- and Cu-Ru-ARs (Fig. 3B). Compared to the photocatalytic reactivity of the two catalysts under pulsed laser illumination (Fig. 1A), photocatalysis driven by LED irradiation also resulted in similar reactivities of the two photocatalysts, but with a slightly higher reactivity for the Cu-Ru-AR. A greater contribution from photothermal heating in the continuous wave LED case than under irradiation with ultrafast laser pulses would be expected, given that the latter is more efficient in the generation of HCs (*23*, *24*). The Cu-Fe-AR still exhibits a very high photocatalytic reactivity under LED illumination, up to 72% NH_3 conversion and 14 g H_2 per day under the delivered power of 180 W at a feed space velocity of 487 hours^{-1}.

We also investigated NH_3 conversion, H_2 production rates, and energy efficiency for the Cu-Fe-AR as a function of NH_3 space velocity under a constant LED power of 140 W (4.1 W cm^{-2}) (Fig. 3C). As shown, increasing the NH_3 feed hourly space velocity (SV) by more than six times (from 160 to 1060 hours^{-1}) only led to a ~40% feed conversion drop (from 77 to 47%). Accordingly, this resulted in a four-fold increase in H_2 production from ~4.5 g H_2/day to ~18 g/day, and thus a notable improvement in the photon-to-H_2 conversion efficiency from 4.3 to 15.6%. The energy efficiency here considered the efficiency of the absorbed photons being converted to chemical energy by comparing the

heat values of NH_3 and H_2 (see SM). However, when the losses associated with LED drivers, diode efficiency, and photons escaping the reactor were also considered, the input (wall plug) electricity-to-H_2 efficiency would be lower (from 1.5% to 5.6%) (fig. S14). Photocatalytic stability tests were also performed on the Cu-Fe-AR at 54% NH_3 feed conversion, showing excellent stability with no signs of decreased activity throughout an illumination period of 67 hours (Fig. 3D).

Currently, there are no commercial thermal ammonia decomposition plants for H_2 production in operation and industrial ammonia cracking has been primarily applied within the metallurgy industry using an electrically heated furnace with Ni catalysts operating at 900°C (*36*). Hence, achieving those reactivity metrics by using a relatively small volume (~11 cm^3) of an earth-abundant photocatalyst in a gram-scale photoreactor with commercially available LEDs demonstrates the potential scalability of electrified photocatalysis with LED illumination for producing low-temperature green H_2 from NH_3. Based on the H_2 production rates on the Cu-Fe-AR at SV 1060 $hours^{-1}$, we estimate an energy usage of 560 kWh/kg H_2. The input energy demand for chemical production, however, is strongly influenced by the size of the plant and other factors. Hence, we expect that photoreactor scaling with improved design, process optimization, and LED efficacy improvement could substantially reduce the required input electricity at large scale, that is, down to a few tens of kWh/kg H_2. This is critical to the economic viability and widespread adaptation of NH_3 as a green H_2 carrier in the future (see SM). It also requires technologies for producing green NH_3 such as electro- and photochemical approaches—which are currently in early stages of development—to become mature and economically viable with an energy demand at scale competitive to that of the energy consumption of state-of-the-art Haber-Bosch plants (9 to 15 kWh/kg NH_3) (*37*).

Alternatively, H_2 can be stored in materials, such as metal hydride and sorbent materials, with subsequent release at high temperature on demand. State of the art material-based H_2 storage is still under development, with the main target being small-scale applications in light-duty vehicles and opportunities for portable power generation. However, the projected cost of H_2 (US dollars per kilogram of H_2) produced in this way is very high as indicated by the US Department of Energy (DOE)'s ultimate target cost of $266 per kg of H_2 (*38*). The overarching goal of advancing H_2 storage materials is to reduce costs by discovering materials that can reduce the required storage pressure and temperature for H_2 release and increase gravimetric or volumetric storage capacity. The gravimetric H_2 storage capacity of NH_3 (17.6 wt %) already exceeds that of the H_2 storage materials currently investigated by the DOE Fuel Cell Technologies Office. Moreover, eliminating the need for external heating through photocatalysis of ammonia decomposition as shown here is consistent with the DOE's ultimate system target (fig. S15).

We have demonstrated that Cu-Fe-AR, an otherwise poor thermocatalyst, can serve as an excellent photocatalyst for NH_3 decomposition with an efficiency similar to that of Cu-Ru-AR under short-pulse laser illumination. The hot carriers, once created, stimulate the formation of adsorbate-metal excited states, activate the metal-adsorbate bond, decrease apparent and elementary step activation barriers, clean occupied active sites, and facilitate product desorption, thereby enhancing both the reactivity and stability of Cu-Fe-AR relative to the thermal case. Under continuous-wave LED illumination, Cu-Fe-AR showed a similarly high efficiency to Cu-Ru-AR, but the greater photothermal heating resulted in a slightly greater reactivity of Cu-Ru-AR. This study suggests that transition metals, traditionally regarded as unsuitable for conventional thermocatalysis, may be relevant substrates for plasmonic photocatalysis and also demonstrates that photocatalysis can be efficiently performed with inexpensive LED photon sources. These results strongly motivate the study of more abundant metals that can serve as highly efficient reactive sites for plasmonic antenna-reactor photocatalysis.

REFERENCES AND NOTES

1. M. L. Brongersma, N. J. Halas, P. Nordlander, *Nat. Nanotechnol.* **10**, 25–34 (2015).
2. X. Zhang *et al*., *Nat. Commun.* **8**, 14542 (2017).
3. J. L. Brooks, C. L. Warkentin, D. Saha, E. L. Keller, R. R. Frontiera, *Nanophotonics* **7**, 1697–1724 (2018).
4. S. Linic, P. Christopher, D. B. Ingram, *Nat. Mater.* **10**, 911–921 (2011).
5. M. J. Kale, T. Avanesian, P. Christopher, *ACS Catal.* **4**, 116–128 (2014).
6. P. Christopher, H. Xin, S. Linic, *Nat. Chem.* **3**, 467–472 (2011).
7. A. Marimuthu, J. Zhang, S. Linic, *Science* **339**, 1590–1593 (2013).
8. C. F. Bohren, *Am. J. Phys.* **51**, 323–327 (1983).
9. C. Zhang *et al*., *Nano Lett.* **16**, 6677–6682 (2016).
10. K. Sytwu *et al*., *Science* **371**, 280–283 (2021).
11. L. Zhou *et al*., *Science* **362**, 69–72 (2018).
12. G. Rothenberg, *Catalysis: Concepts and Green Applications* (Wiley, 2017).
13. M. C. Bradford, P. E. Fanning, M. A. Vannice, *J. Catal.* **172**, 479–484 (1997).
14. J. L. Bao, E. A. Carter, *J. Am. Chem. Soc.* **141**, 13320–13323 (2019).
15. D. L. Anderson, *Theory of the Earth* (Blackwell, 1989).
16. S. Yin, B. Xu, X. Zhou, C. Au, *Appl. Catal. A* **277**, 1–9 (2004).
17. F. Schüth, R. Palkovits, R. Schlögl, D. S. Su, *Energy Environ. Sci.* **5**, 6278–6289 (2012).
18. G. Ertl, M. Huber, *J. Catal.* **61**, 537–539 (1980).
19. M. Behrens *et al*., *Science* **336**, 893–897 (2012).
20. M. Behrens, *Catal. Today* **246**, 46–54 (2015).
21. H. Li, M. Rivallan, F. Thibault-Starzyk, A. Travert, F. C. Meunier, *Phys. Chem. Chem. Phys.* **15**, 7321–7327 (2013).
22. S. F. Yin, B. Q. Xu, S. J. Wang, C. F. Ng, C. T. Au, *Catal. Lett.* **96**, 113–116 (2004).
23. C. D. Lindstrom, X.-Y. Zhu, *Chem. Rev.* **106**, 4281–4300 (2006).
24. K. H. Kim, K. Watanabe, D. Mulugeta, H.-J. Freund, D. Menzel, *Phys. Rev. Lett.* **107**, 047401 (2011).
25. Y. Kim, D. Dumett Torres, P. K. Jain, *Nano Lett.* **16**, 3399–3407 (2016).
26. J.-P. Gauyacq, A. G. Borisov, *J. Phys. Condens. Matter* **10**, 6585–6619 (1998).
27. C. Huang, M. Pavone, E. A. Carter, *J. Chem. Phys.* **134**, 154110 (2011).
28. K. Yu, F. Libisch, E. A. Carter, *J. Chem. Phys.* **143**, 102806 (2015).
29. K. Andersson, P. Å. Malmqvist, B. O. Roos, *J. Chem. Phys.* **96**, 1218–1226 (1992).
30. K. Andersson, P. Å. Malmqvist, B. O. Roos, A. J. Sadlej, K. Wolinski, *J. Phys. Chem.* **94**, 5483–5488 (1990).
31. J. L. Bao, E. A. Carter, *ACS Nano* **13**, 9944–9957 (2019).
32. H. Apostoleris, S. Sgouridis, M. Stefancich, M. Chiesa, *Nat. Energy* **3**, 1109–1114 (2018).
33. K. Lee, "2022 Solid-State Lighting R&D Opportunities" (US Department of Energy, 2022).
34. E. Schroeder, P. Christopher, *ACS Energy Lett.* **7**, 880–884 (2022).
35. H. Robatjazi *et al*., *Nat. Commun.* **8**, 27 (2017).
36. I. Lucentini, X. Garcia, X. Vendrell, J. Llorca, *Ind. Eng. Chem. Res.* **60**, 18560–18611 (2021).
37. L. Hollevoet, M. De Ras, M. Roeffaers, J. Hofkens, J. A. Martens, *ACS Energy Lett.* **5**, 1124–1127 (2020).
38. Materials-Based Hydrogen Storage (US Department of Energy, 2022); https://www.energy.gov/eere/fuelcells/materials-based-hydrogen-storage.
39. Y. Yuan *et al*., Earth-abundant photocatalyst for H2 generation from NH3 with light-emitting diode illumination, Version 1, Zenodo (2022); https://doi.org/10.5281/zenodo.7240384.

ACKNOWLEDGMENTS

This article is based upon work supported by the Robert A. Welch foundation under grants C-1220 (N.J.H.) and C-1222 (P.N.) and by the Air Force Office of Scientific Research via the Department of Defense Multidisciplinary University Research Initiative under AFOSR Award FA9550-15-1-0022. Syzygy Plasmonics Inc. is acknowledged for providing the resources for the Gram-scale electrified photocatalysis studies. E.A.C. would like to thank the High-Performance Computing Modernization Program (HPCMP) of the US Department of Defense and Princeton University's Terascale Infrastructure for Groundbreaking Research in Engineering and Science (TIGRESS) for providing the computational resources. **Author contributions:** L.Z., Y.Y., and N.J.H. initiated the project. Y.Y. and L.Z. developed the photocatalysts, performed the characterizations (XRD, XPS, UV-Vis diffuse reflectance, Raman) and the micro-scale photocatalysis studies, and analyzed the data. H.R. performed gram-scale electrified photocatalysis studies with LEDs and analyzed the data. S.K. contributed to the gram-scale photoreactor design. J.L.B. carried out the quantum mechanical calculations. A.B. performed the HAADF-STEM. L.Y. performed the BET measurement. Ming.L. and L.Y. helped with interpreting the results. J. Z. and Minh.L. performed the electromagnetic calculations. Ming.L. performed the ICP-MS. H.R., E.A.C., P.N., and N.J.H. supervised the research. Y.Y., L.Z, H.R., J.L.B., J.Z., E.A.C., P.N., and N.J.H. contributed to the interpretation of the data and preparation of the manuscript. **Competing interests:** An international patent application for the antenna-reactor concept under the Patent Cooperation Treaty is pending (15977843). An international patent application filled by Syzygy Plasmonics for the photoreactor platform under the Patent Cooperation Treaty is pending (US20210339220A1). N.J.H., P.N., and S.K. are co-founders of Syzygy Plasmonics, and hold equity in the company. The remaining authors declare that the research was conducted in the absence of any commercial or financial relationships that could be construed as a potential conflict of interest. **Data and materials availability:** Additional data sets generated and/or analyzed during the current study that are not included in this published article (and its supplementary information files) are available at open-access repository (*39*).

SUPPLEMENTARY MATERIALS

science.org/doi/10.1126/science.abn5636
Materials and Methods
Figs. S1 to S23
Table S1
References (*40*–*94*)

Submitted 5 December 2021; resubmitted 24 May 2022
Accepted 31 October 2022
10.1126/science.abn5636

MICROFABRICATION

Reflow transfer for conformal three-dimensional microprinting

G. Zabow*

From microcircuits to metamaterials, the micropatterning of surfaces adds valuable functionality. For nonplanar surfaces, incompatibility with conventional microlithography requires the transfer of originally planar micropatterns onto those surfaces; however, existing approaches accommodate only limited curvatures. A microtransfer approach was developed using reflowable materials that transform between solid and liquid on demand, freely stretching to yield transfers that naturally conform down to nanoscale radii of curvature and arbitrarily complex topographies. Such reflow transfer helps generalize microprinting, extending the reach of precision planar microlithography to highly nonplanar substrates and microstructures. With gentle water-based processing, reflow transfer can be applied to a range of materials, with microprinting demonstrated onto metal, plastic, paper, glass, polystyrene, semiconductor, elastomer, hydrogel, and multiple biological surfaces.

Fueled by the semiconductor industry, microfabrication tools have evolved to pattern ever more precisely and efficiently, but only on rigid, planar substrates. Leveraging these lithographic technologies for advanced manufacturing on soft or nonplanar substrates requires the transfer of initially planar microfabricated designs onto these alternative materials. Although research over past decades has yielded multiple transfer printing techniques (*1*, *2*) able to transfer microstructures onto various soft or gently curved substrates common to fields such as flexible electronics and biointegrated sensing (*3*), accurate transfer onto more general surfaces of arbitrary curvature has remained elusive (*2*, *4*).

All transfer microprinting methods currently transport micropatterns or structures between substrates via either a solid or liquid transfer medium, or carrier. Solid carriers, commonly based on elastomers (*5*) or adhesive tapes (*6*), facilitate accurate placement and robust macroscopic handling of microscopic structures. However, even flexible solid carriers can deform only so far, impeding conformal transfer onto high curvature substrates or microstructures. Additionally, contact pressures needed to lift microstructures from their original substrates or to conform to receiving substrates can limit transfer of fragile structures, or transfer onto fragile substrates. Alternatively, liquids can gently float microstructures between substrates, improving conformability by supporting thinner, more flexible, carriers (*7*) or with the liquid itself as the carrier (*8*). However, wet transfers sacrifice placement accuracy and incur buoyancy and hydrophobicity limitations.

Applied Physics Division, National Institute of Standards and Technology; Boulder, CO 80305, USA.
*Corresponding author. Email: gary.zabow@nist.gov

Here, a printing process is described with thermally reflowable carriers that can controllably and locally transform between solid and liquid on demand. Combining advantages of both dry and wet transfer, the process overcomes drawbacks of each, enabling accurately positioned, ultraconformal printing over a wide array of surfaces, including those too topographically challenging to be patterned by existing methods. This reflow-driven flexible xfer (REFLEX) process is introduced with an unlikely material from a microfabrication viewpoint: regular table sugar (sucrose). Sugar is often dismissed because it crystallizes, yielding inhomogeneous surfaces incompatible with microfabrication (*9*). However, as known in food processing, adding corn syrup prevents crystallization, and caramelized sugar and corn syrup mixtures need not disturb micropattern geometries. Sugar mixtures also offer favorably low glass transition temperatures (T_g) near room temperature that can be tailored on the basis of composition (*10*) and degree of caramelization (*11*). Moreover, sugar mixtures fully dissolve in water, further broadening substrate compatibility by eliminating any carrier adhesion complications and enabling clean, physically and chemically gentle transfers free of any high temperatures, harsh solvents, or aggressive etchings needed to remove other common transfer intermediates or residues (*2*).

One simple composition comprises sugar and corn syrup heated with water until caramelized (*12*). Once cooled, the resulting solid can be melted or redissolved in water for pouring over micropatterns or structures that are to be transferred, with any remaining water subsequently removed via evaporative heating (Fig. 1A and fig. S1). Depending on substrate materials, the resulting sugar coating can be delaminated directly or released by dissolving an underlying sacrificial layer. Although water soluble, sugar resists dissolution in common solvents like acetone; therefore, using sugar allows selective release with widely available photoresists or other acetone-soluble materials (*12*). Being optically transparent, the released sugar layer with the transfer microstructures partially embedded in its underside can then be accurately positioned, with micrometer-level precision (fig. S2), on the receiving substrate and softened with gentle heating. The resulting viscous, creeping fluid carries the microstructures, ultra-conformally coating them over the receiving substrate before the sugar is finally dissolved away. Because the fluid can conform to the shape of its container or underlying surface, the surface curvature or feature sharpness that can be patterned is unlimited, in principle. Meanwhile, unlike free-flowing liquids, the high reflow viscosity of the resulting fluid helps maintain the relative positions of structures during transfer, largely suppressing disturbing liquid currents, translational forces between free-floating structures, and dislocations driven by surface tension, the latter frustrating traditional wet transfer enough to necessitate special-purpose floating microrobot aligners (*13*, *14*).

As an example of a simple substrate that is hard to pattern by any other technique, Fig. 1B shows an array of microfabricated disks, which double as microscale fiducial markers, transferred onto a surface with recessed holes. REFLEX microprinting patterns the whole surface, including down vertical sidewalls and over edges with nanoscale radii of curvature, for both rigid and flexible microstructures (fig. S3). Altered array spacings map the transfer material reflow as it locally stretches to cover new surfaces, which may differ in area from those on which the arrays were originally fabricated. For example, the extra sidewall forming the hole shown in Fig. 1B triples the local area to be accommodated. Such stretching would confound existing solid-based transfer schemes whereas surface tension effects at the abrupt feature edges would also disrupt liquid-based approaches (*14*). REFLEX microprints, however, remain ordered and reproducible (fig. S4), with orientational errors within 1° and pattern dilations consistent to within the order of one part in a hundred (fig. S5). Large surface area changes also accompany steep embossed reliefs (Fig. 1C.), which remain patternable by REFLEX printing but would similarly challenge other transfer techniques. With unlimited stretching, the reflow process can also pattern undercut structures with conventionally inaccessible overhangs (Fig. 1D), as well as adapt planar micropatterns to awkwardly shaped, macroscale objects. For example, Fig. 1E and movie S1 demonstrate REFLEX microprinting not onto the proverbial pinhead, but instead directly over the sharper tip. Similarly, fig. S6 shows transfer

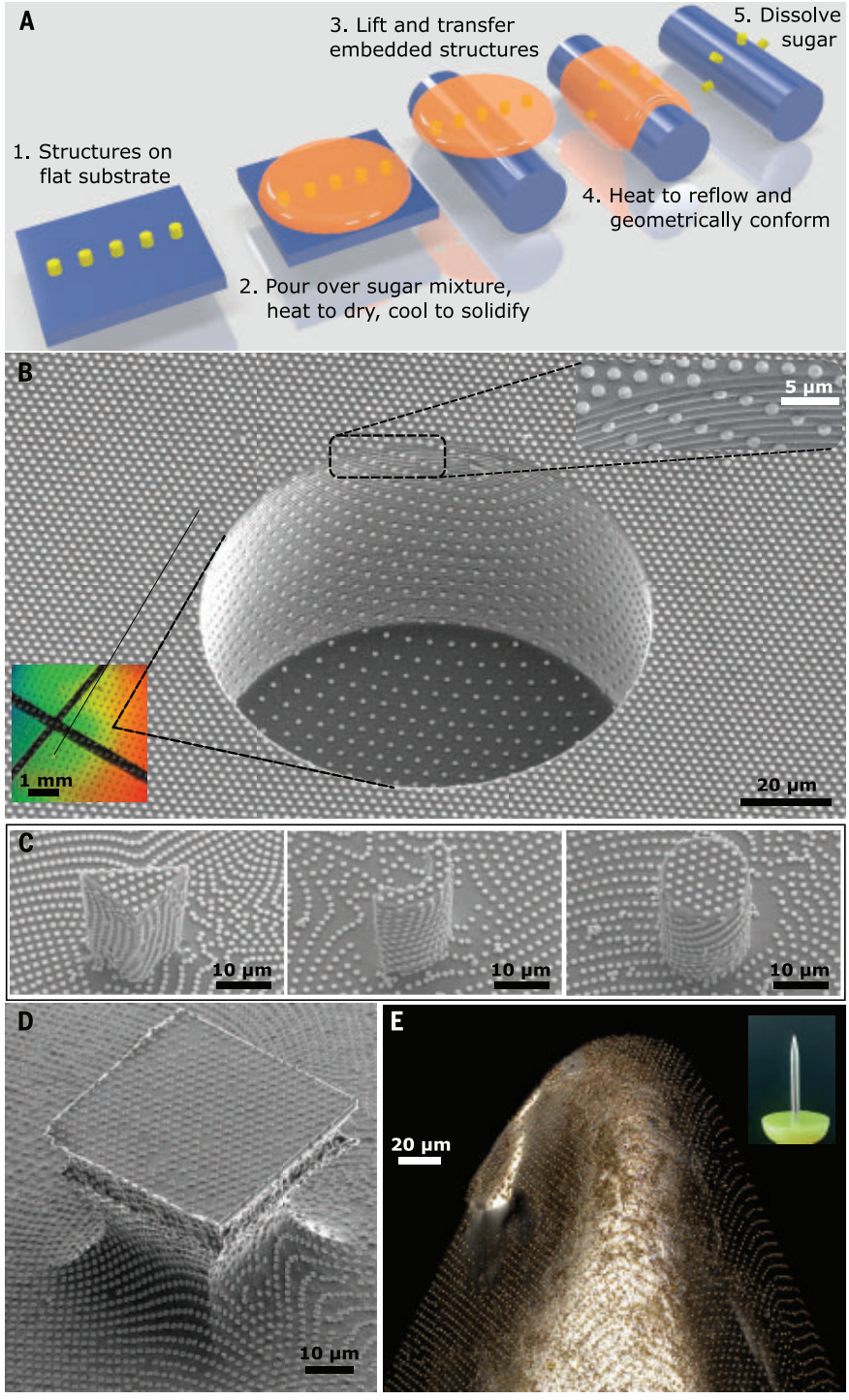

Fig. 1. Process schematic and example high-curvature conformal printing with reflowable materials. (**A**) Process steps, described in text, for structure transfer via reflowable materials that "melt" around the receiving substrate. (**B**) Scanning electron micrograph (SEM) of array of 1-μm disks transferred onto a surface with 100-μm-diameter, 50-μm-deep holes. Lower inset shows optical image of diffracted colors from transferred disk arrays; holes appear as dark spots. Upper inset shows magnification of pattern conformation over hole edge. (**C**) SEMs of disks transferred onto sharp, vertical, high-aspect ratio embossed features. (**D**) SEM showing transfer coverage of microstructure with multiple undercut regions. (**E**) Laser confocal optical micrograph of 1-μm disks transferred over the tip of a pin shown in the inset.

around a hypodermic needle point including within the lumen.

Conforming to nonplanar surfaces does not always require stretching or reflow. For example, a thin sheet can cover a cylinder or other developable surface of zero Gaussian curvature by bending alone. For suitable surface tension, γ, and bending modulus, B, the sheet may even spontaneously wrap the surface via capillary wetting, at least for radii of curvature exceeding the elastocapillary length scale, $\sqrt{B/\gamma}$ (*15*, *16*). Because B scales with thickness cubed, thinner sheets can wrap more tightly, but for the sheet wrapping to remain energetically favorable below microscale radii of curvature would require transfer carriers too thin to be mechanically practical (supplementary text). Even without microscale structure, however, many nonplanar surfaces have nonzero Gaussian curvature. As exemplified by the mapmaker's dilemma in projecting the spherical Earth onto a flat page, local area changes are mathematically unavoidable for many mappings. Therefore, truly conformal transfer requires that any solid carrier not only bend, but also stretch. Unlike bending stiffnesses, however, stretching stiffnesses

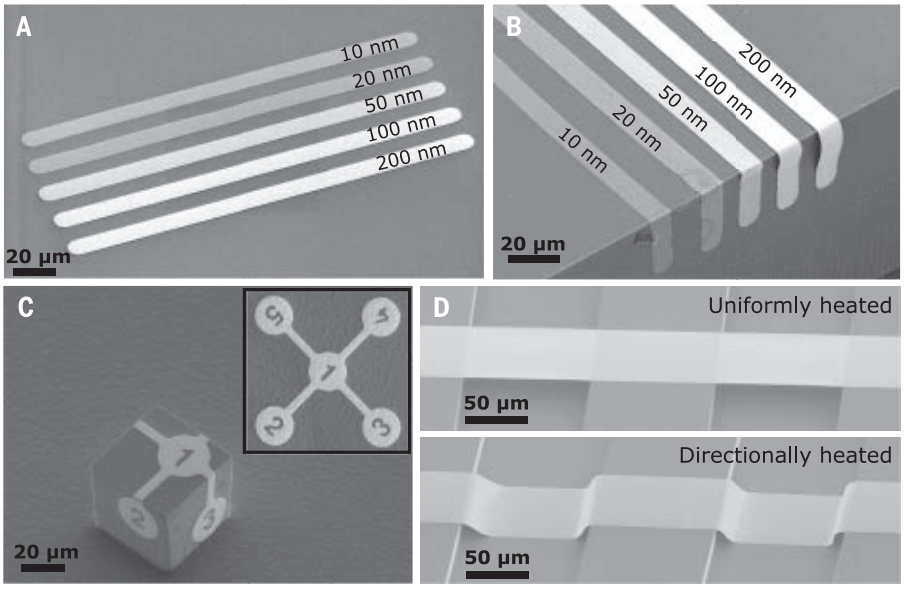

Fig. 2. Conformal transfer of extended structures. (**A**) SEM showing transfer of long, thin metal strips. Thicknesses as shown. (**B**) SEM of transferred structures of varying thicknesses (shown) wrapped around a sharp edge. (**C**) SEM of continuously connected printing around sides of a cube using 40-nm-thick transfer structure simultaneously bent around multiple axes. Inset shows reference structure transferred onto a flat substrate. (**D**) SEMs of 100-nm-thick metal strips printed across trenches, showing suspended (top) or conforming (bottom) placement, determined by controlling the reflow direction.

fall only linearly with reducing thicknesses (*15*), thwarting conformal transfers onto intrinsically curved surfaces. By contrast, reflowable materials eliminate resistance to both bending and stretching, accommodating sharp, tightly curved features as well as transfer between widely differing Gaussian curvatures.

Such flexibility also allows REFLEX printing to maintain long-range order while deforming locally to cover nonplanar features, as seen in the orderly array and diffracted colors of Fig. 1B. This preserved order suggests metamaterial or optical engineering of nontraditional surfaces (for example, Fig. 1B) or materials, as in fig. S7, fig. S8, movie S2, and fig. S9, which show bendable, stretchable, and stimuli-responsive diffraction gratings created by transferring microarrays onto plastics, soft elastomers, and smart hydrogels, respectively.

For sufficiently small transfer structures, mapping transformations due to varying curvatures can be accommodated by dilating the spacings between structures rather than those structures themselves. However, larger structures are also transferable (Fig. 2). Although such structures might not themselves be stretchable (*17*), if thin, reflow can still guide their bending. The resultant three-dimensional (3D) microprinting of continuously connected materials over edges (Fig. 2B) and around structures (Fig. 2C and movie S3) suggests possibilities for 3D microfabrication or for 3D integration in semiconductor manufacture. Locally transforming the carrier between solid and liquid via localized or directional heating (*12*) adds further control, enabling conforming or suspended constructions (Fig. 2D).

Because reflowing sugar gently envelops objects, naturally conforming without needing externally applied forces, REFLEX printing is also well suited for standalone microstructures, including those too fragile or tightly curved for other transfer methods. With reflow, microprinting over a self-standing strand of hair becomes comparatively undemanding for both small and relatively larger microstructures (Fig. 3, A and B, respectively) but serves to demonstrate both micropatterning and microtexturing [Fig. 3C (*12*)], as might be used to locally modify surface hydrophobicity. Or, scaling down in size, Fig. 3D and fig. S10 show printing onto more tightly curved fibers—namely, a milkweed seed floss fiber and cellulose fibers within a sheet of paper, respectively. The high curvature, yet gentle physicochemical attributes of the reflow process similarly support damage-free conformal printing over many other more complex biological surfaces. Examples include conformal transfer onto the corrugated surface of a poppy seed, into the subcellular-sized stomatal openings of a leaf, across increasingly tortuous, spiky surfaces of microscopic pollen grains and, for scale, over a red blood cell (Fig. 3, E to H).

Higher curvatures imply higher surface area to volume ratios. High-curvature patterning should thus afford efficient, tailored microstructure control through printable surface functionalizations. For example, patterning microfibers at previously inaccessible size scales and curvatures adds functionality while maintaining structural flexibility and surface accessibility. As a simple illustration, gold-coated iron microdisks transferred onto a milkweed floss fiber enable magnetic manipulation (Fig. 3D and movie S4).

At still smaller sizes, printing onto microparticles (Fig. 4) may influence biological responses to such particles (*18*), as well as advance subcellular-sized biomedical probes, drug delivery vehicles, and microrobots (*19*). Microrobot miniaturization increases in vivo access, but fabrication and functional integration at necessary sizes and scales have remained challenging (*20*). Direct-write lithographies promise highly functional micromachines (*21*) but are hard to parallelize. Meanwhile, more scalable approaches, such as surface functionalizing microbeads, are constrained by existing high-curvature surface patterning abilities. By harnessing planar lithographies, REFLEX printing extends options beyond conventional homogeneous, Janus, or colloidal shadow or cluster-based designs (*22*, *23*). As examples, Fig. 4, A to D, show high-curvature transfer of a range of functional materials, shapes, and 3D structures including (i) gold disks, nickel rings, and platinum ellipses integrated on the same microspheres for possible localized biochemical functionalization or plasmonic heating, magnetic orientation, and catalytic self-propulsion (*24*), respectively; (ii) thick gold-coated iron cylindrical pucks for magnetic manipulation or MRI-based tracking (*25*, *26*); and (iii) as illustrations of higher-aspect ratio transfers, cones and hollow cylinders incompatible with other transfer schemes because of fragility and/or the 3D reorientations needed for conformal mapping. In closely conforming to surfaces, the reflow process also increases contact areas between transferred patterns and receiving substrates, promoting clean physical adhesion of REFLEX prints without the need for externally applied placement pressure. For example, as shown in Fig. 4, E and F, microspheres removed from their patterning substrate, centrifuged, washed, and redispersed, at small size-scales, prints can adhere directly through van der Waals forces without substrate modification.

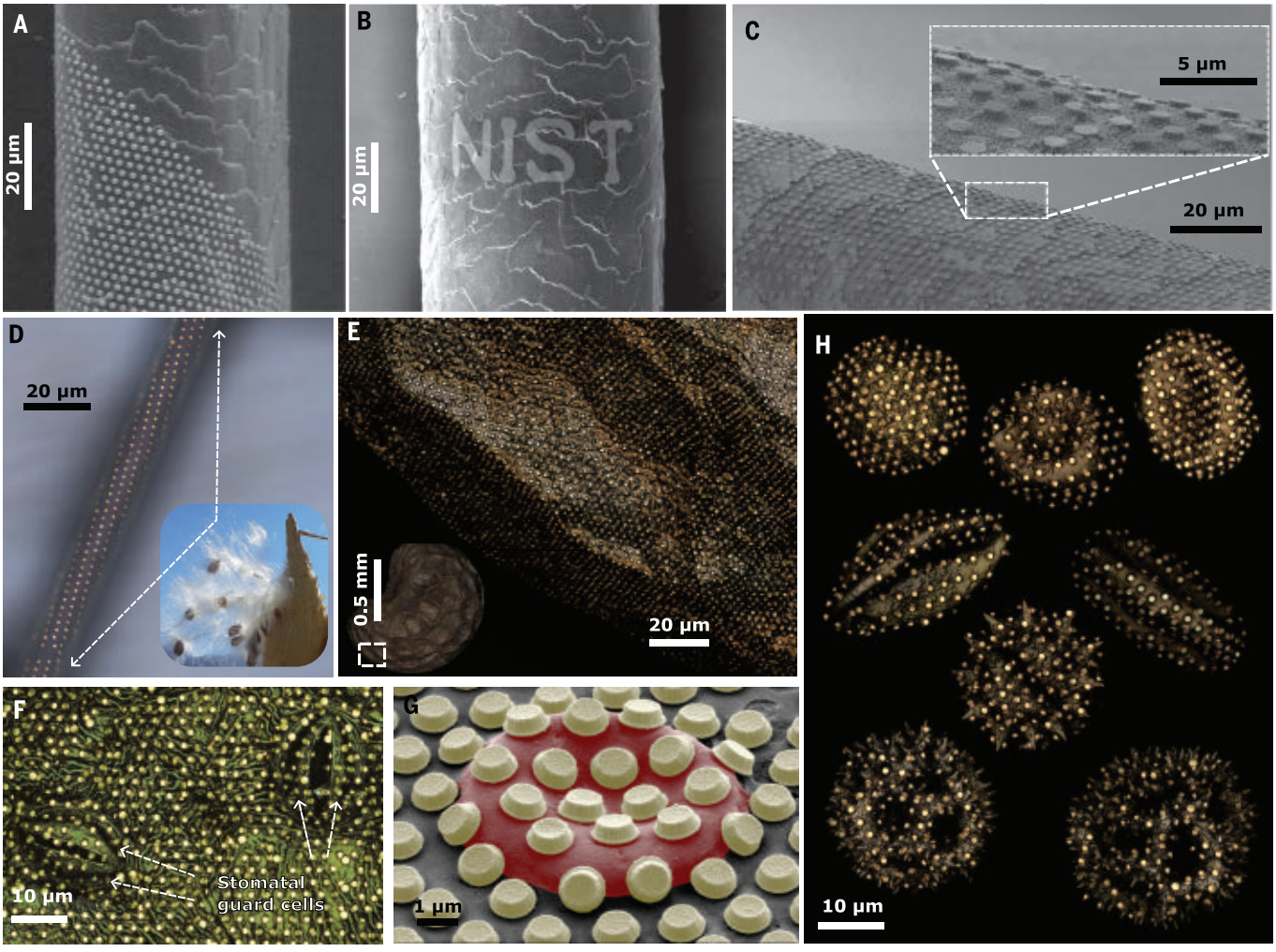

Fig. 3. Transfer patterning stand-alone microstructures. (**A**) and (**B**) show SEMs of 0.5-μm-thick, 1-μm-diameter Au disks and of 30-nm-thick Au lettering, respectively, transferred onto individual strands of hair. (**C**) SEM showing surface microtexturing of a strand of hair, after ultrasonicating off transferred disks used as temporary oxygen plasma etch masks. Inset magnifies view of resulting texture. (**D**) Optical micrograph of 1-μm disks transferred onto a milkweed seed floss fiber. Inset shows milkweed seed pod, with floss fibers attached to seeds. (**E**) Laser confocal micrographs of a micropatterned poppy seed, including magnified view of lower boxed region detailing transfer printed disk array. (**F**) Laser confocal micrograph of the underside of a leaf, showing conformal pattern transfer including into the stomatal pores. (**G**) False-colored SEM showing the same Au disks used in (A), (C) to (F), and (H) printed over a red blood cell for scale. (**H**) Collage of laser confocal micrographs of disk arrays conformally transferred onto various microscopic pollen grains of increasing surface complexity.

Moreover, for in vivo usage, biocompatible sugar-based manufacture adds no toxic solvents or transfer material residues.

The above transfers were randomly positioned but, as shaped hard candies attest, sugar can be molded, enabling surface-embossed transfer media that double as their own guiding templates for massively parallel, automatic alignment of receiving substrates. As shown in Fig. 4G and fig. S11, sugar is here cast over transfer motifs patterned atop sacrificial photoresist posts. Resist dissolution then leaves those motifs within recessed wells in the carrier, into which microbeads can self-assemble via capillary forces (*12, 27*). Reflowing and subsequently dissolving the carrier then conformally prints accurately registered transfers around potentially millions of separate substrates simultaneously (Fig. 4H). Removable stencils can also be similarly self-aligned for inverted etchings, functionalizations, or material depositions (Fig. 4, I and J), adding further possibilities for parallel printing of more arbitrarily designed colloidal "patchy" particles (*28*, *29*).

The same sugar formulation has been used throughout, but it is neither distinctive nor necessarily optimal. Even regular store-bought candy suffices (fig. S12), raising the prospect of multiple alternative material formulations offering modified chemical and thermophysical properties, and further increasing accessibility of an already facile, inexpensive process. Such simplicity does, however, belie certain complexities of the reflow printing process. First, although heating generally suffices for spontaneously conformal transfer, depending on surface energies, heated thin coatings can sometimes dewet rather than spread over a surface. If needed, wetting can be encouraged by pretreating the surface, applying gentle pressure, or using transfer layers a few millimeters thick to exceed any critical dewetting capillary length scales (*15*). Second, reflow over complex surfaces may trap air pockets, sealing off areas from pattern transfer. If necessary, directional heating (*12*) can help guide the reflow. Alternatively, provided the material vapor pressures are low enough to limit gas bubble formation within the transfer material (fig. S13), heating in a vacuum oven not only evacuates the air but, if any sealed off areas remain,

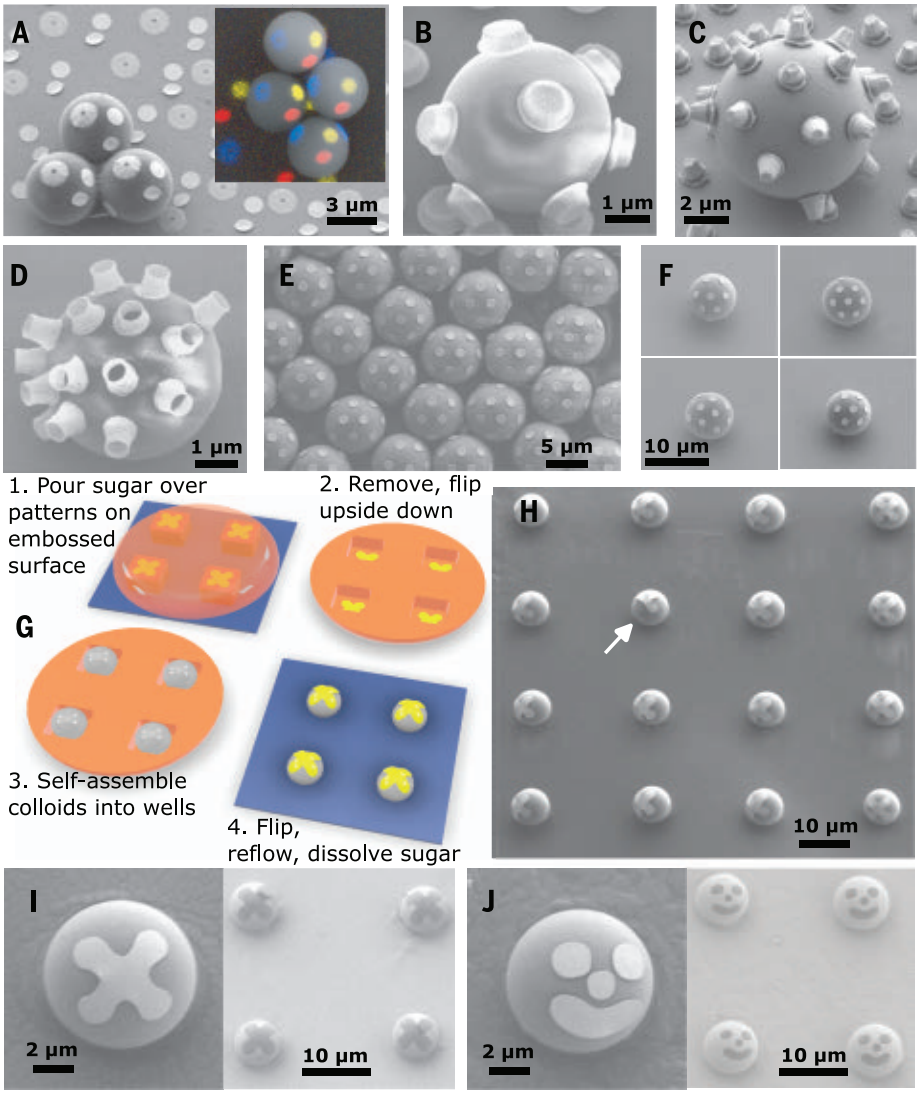

Fig. 4. Micropatterning colloids. (**A**) SEM of 4.5-μm polystyrene microspheres simultaneously transfer printed with multiple materials: Au disks, Pt ellipses, and Ni rings. Inset overlays color-coded energy dispersive x-ray spectroscopic scanned image on similar SEM to distinguish elements, revealing microsphere "faces" with red (platinum) "mouths," yellow (gold) "noses," and blue (nickel) "eyes." (**B**) SEM of 1-μm-diameter, 0.5-μm-thick, gold-coated magnetic iron disks transfer printed onto polystyrene microsphere. (**C**) SEM of gold cones (1-μm base diameter, 1-μm tall) transferred onto a 7.5-μm glass microsphere. (**D**) SEM of hollow 500-nm-diameter cylinders transferred onto polystyrene microsphere. (**E**) SEM of as-patterned and (**F**), subsequently redispersed microspheres showing robust print attachment. (**G**) Schematic for parallel, self-aligned transfer printing. (**H**) SEM of cross patterns transfer printed in parallel onto array of glass microspheres (arrow shows a folded-over defective transfer). (**I**) SEMs of patterned microsphere and its inverses created using original print as temporary mask for subsequent metal deposition. (**J**) As in (I), except with multipiece transfer design.

pressure differences on return to atmosphere help push the softened transfer material into these voids. Third, at least for hygroscopic sugar-based materials, water absorbed from background humidity acts as a plasticizer, reducing T_g's, sometimes to below room temperature. Although this enables ambient heat-free reflow, absorbed water can also increase material vapor pressures and distort embedded transfer patterns. Conversely, subsequent shrinkage from any evaporation from wet sugar layers can also distort transfers. Transfers not promptly redeposited onto receiving substrates may thus benefit from desiccator storage, which maintains dry sugar layers in a stable glassy state, preserving submicrometer pattern accuracy for months (fig. S14). Finally, despite broad compatibility across diverse substrate geometries and materials, work remains to ensure fully deterministic patterning over arbitrarily complex surfaces. Although this work has focused on overcoming challenging surface topographies, reflow paths and, hence, mapping transformations, may depend also on locally varying surface chemistries. Here, targeted surface pretreatments or heating profiles may offer further control. Additionally, not unlike with conventional photolithographic proximity corrections (*30*), initial pattern design modifications may compensate for anticipated mapping transformations.

REFERENCES AND NOTES

1. A. Carlson, A. M. Bowen, Y. Huang, R. G. Nuzzo, J. A. Rogers, *Adv. Mater.* **24**, 5284–5318 (2012).
2. C. Linghu, S. Zhang, C. Wang, J. Song, *Electron.* **2**, 26 (2018).
3. W.-H. Yeo *et al.*, *Adv. Mater.* **25**, 2773–2778 (2013).
4. J. Park, Y. Lee, H. Lee, H. Ko, *ACS Nano* **14**, 12–20 (2020).
5. M. A. Meitl *et al.*, *Nat. Mater.* **5**, 33–38 (2006).
6. Z. Yan *et al.*, *Adv. Sci. (Weinh.)* **4**, 1700251 (2017).
7. G. F. Schneider, V. E. Calado, H. Zandbergen, L. M. K. Vandersypen, C. Dekker, *Nano Lett.* **10**, 1912–1916 (2010).
8. M. Aghajamali, I. T. Cheong, J. G. C. Veinot, *Langmuir* **34**, 9418–9423 (2018).
9. V. Linder, B. D. Gates, D. Ryan, B. A. Parviz, G. M. Whitesides, *Small* **1**, 730–736 (2005).
10. J.-A. Seo *et al.*, *Carbohydr. Res.* **341**, 2516–2520 (2006).
11. B. Jiang, Y. Liu, B. Bhandari, W. Zhou, *J. Agric. Food Chem.* **56**, 5138–5147 (2008).
12. Materials and methods are available as supplementary materials.
13. D. Vella, L. Mahadevan, *Am. J. Phys.* **73**, 817–825 (2005).
14. A. Barbot, H. Tan, M. Power, F. Seichepine, G. Z. Yang, *Sci. Robot.* **4**, eaax8336 (2019).
15. J. Bico, E. Reyssat, B. Roman, *Annu. Rev. Fluid Mech.* **50**, 629–659 (2018).
16. D.-H. Kim *et al.*, *Nat. Mater.* **9**, 511–517 (2010).
17. J. A. Rogers, T. Someya, Y. Huang, *Science* **327**, 1603–1607 (2010).
18. S. Mitragotri, J. Lahann, *Nat. Mater.* **8**, 15–23 (2009).
19. B. J. Nelson, I. K. Kaliakatsos, J. J. Abbott, *Annu. Rev. Biomed. Eng.* **12**, 55–85 (2010).
20. S. Palagi, P. Fischer, *Nat. Rev. Mater.* **3**, 113–124 (2018).
21. C. C. J. Alcântara *et al.*, *Nat. Commun.* **11**, 5957 (2020).
22. S.-M. Yang, S. G. Jang, D.-G. Choi, S. Kim, H. K. Yu, *Small* **2**, 458–475 (2006).
23. Y. Wang *et al.*, *Nature* **491**, 51–55 (2012).
24. S. Sánchez, L. Soler, J. Katuri, *Angew. Chem. Int. Ed.* **54**, 1414–1444 (2015).
25. S. Martel *et al.*, *Appl. Phys. Lett.* **90**, 114105 (2007).
26. G. Zabow, S. J. Dodd, E. Shapiro, J. Moreland, A. P. Koretsky, *Magn. Reson. Med.* **65**, 645–655 (2011).
27. Y. Yin, Y. Lu, B. Gates, Y. Xia, *J. Am. Chem. Soc.* **123**, 8718–8729 (2001).
28. M. He *et al.*, *Nature* **585**, 524–529 (2020).
29. Z. Zhang, S. C. Glotzer, *Nano Lett.* **4**, 1407–1413 (2004).
30. A. Poonawala, P. Milanfar, *IEEE Trans. Image Process.* **16**, 774–788 (2007).

ACKNOWLEDGMENTS

The author acknowledges useful discussions with J. A. Liddle and S. Oberdick and thanks the anonymous reviewers for their comments and suggestions. **Funding:** This work was supported by National Institute of Standards and Technology (NIST) internal research funding. **Competing interests:** NIST has filed a provisional patent application on the reflow transfer print process. **Data and materials availability:** All data are available in the main text or the supplementary materials. This is a contribution of the National Institute of Standards and Technology, not subject to US copyright.

SUPPLEMENTARY MATERIALS

science.org/doi/10.1126/science.add7023
Materials and Methods
Supplementary Text
Figs. S1 to S14
Movies S1 to S4

Submitted 5 July 2022; accepted 6 October 2022
10.1126/science.add7023

VACCINES

A multivalent nucleoside-modified mRNA vaccine against all known influenza virus subtypes

Claudia P. Arevalo[1], Marcus J. Bolton[1], Valerie Le Sage[2], Naiqing Ye[1], Colleen Furey[1], Hiromi Muramatsu[1], Mohamad-Gabriel Alameh[3], Norbert Pardi[1], Elizabeth M. Drapeau[1], Kaela Parkhouse[1], Tyler Garretson[1], Jeffrey S. Morris[4], Louise H. Moncla[5], Ying K. Tam[6], Steven H. Y. Fan[6], Seema S. Lakdawala[2,7]†, Drew Weissman[3], Scott E. Hensley[1]*

Seasonal influenza vaccines offer little protection against pandemic influenza virus strains. It is difficult to create effective prepandemic vaccines because it is uncertain which influenza virus subtype will cause the next pandemic. In this work, we developed a nucleoside-modified messenger RNA (mRNA)–lipid nanoparticle vaccine encoding hemagglutinin antigens from all 20 known influenza A virus subtypes and influenza B virus lineages. This multivalent vaccine elicited high levels of cross-reactive and subtype-specific antibodies in mice and ferrets that reacted to all 20 encoded antigens. Vaccination protected mice and ferrets challenged with matched and mismatched viral strains, and this protection was at least partially dependent on antibodies. Our studies indicate that mRNA vaccines can provide protection against antigenically variable viruses by simultaneously inducing antibodies against multiple antigens.

There are at least 18 different influenza A virus (IAV) subtypes that circulate in animal reservoirs, and these viruses occasionally enter the human population and cause a pandemic (*1*). Currently, H1N1 and H3N2 IAVs, as well as one or two antigenically distinct lineages of influenza B viruses (IBVs), circulate seasonally in the human population. Although surveillance programs and modeling studies have increased our knowledge of pandemic risk (*2*, *3*), we cannot accurately predict which influenza subtype will cause the next pandemic. Several universal influenza vaccines are in development to provide protection against diverse influenza virus subtypes (*4*). Most universal influenza vaccines include a limited number of antigens that have epitopes that are conserved across different influenza virus subtypes (*5*–*7*). An alternative approach for inducing universal immunity is to design multivalent vaccines that encode antigens from every known influenza virus subtype. This approach may be impractical using conventional influenza vaccine technologies but is now feasible with nucleic acid–based vaccine platforms (*8*). We had previously developed nucleoside-modified mRNA–lipid nanoparticle (LNP) vaccines expressing hemagglutinin (HA) antigens from single influenza virus subtypes and had found that these vaccines elicit antibodies against both the HA head and stalk in mice and ferrets (*9*, *10*). In this study, we generated a nucleoside-modified mRNA-LNP vaccine expressing HA antigens from all known influenza virus subtypes and found that this multivalent vaccine elicits diverse antibodies that protect mice and ferrets against matched and mismatched viral strains.

We prepared 20 different HA-encoding nucleoside-modified mRNAs encapsulated in LNPs as previously described (*9*), ensuring that a representative HA from each IAV subtype and IBV lineage was included (fig. S1, A to C). We vaccinated groups of mice intramuscularly with a low dose (3 μg) of each individual HA mRNA vaccine to verify that each mRNA vaccine component was immunogenic. Each individual HA mRNA vaccine elicited antibodies that reacted more efficiently to the encoded HA compared with other HAs that we tested (fig. S1D). There was a low level of cross-reactivity among antibodies elicited by single-HA mRNA vaccinations, which is consistent with our previous work (*9*) that has demonstrated that higher doses of vaccines are required to elicit antibodies targeting conserved epitopes, such as the HA stalk.

We then vaccinated mice with all 20 HA mRNA-LNPs simultaneously with a combined dose of 50 μg of HA mRNA (2.5 μg of each individual HA mRNA-LNP). As controls, we vaccinated mice with a 50-μg dose of mRNA-LNPs encoding single HAs from H1N1, H3N2, IBV, or mRNA-LNPs expressing luciferase. Mice vaccinated with the 20-HA mRNA-LNPs produced antibodies that reacted to all 20 encoded HAs (Fig. 1A and fig. S2) [$P < 0.05$, comparing vaccinated versus phosphate-buffered saline (PBS) controls], whereas mice vaccinated with single-HA mRNA-LNPs (Fig. 1, B to D), PBS (Fig. 1E), or mRNA-LNPs expressing luciferase (fig. S3) did not. Antibody levels in mice immunized with the 20-HA mRNA-LNP vaccine remained largely unchanged 4 months post-vaccination (Fig. 1F). We created a vaccine containing 50 μg of 20 different recombinant HA proteins (2.5 μg per protein) so that we could compare the 20-HA mRNA-LNP vaccine with a more conventional protein vaccine platform. Mice immunized with the multivalent protein vaccine produced low levels of anti-HA antibodies (fig. S4). We also tested the 20-HA mRNA-LNP vaccine in mice that were previously infected with either antigenically matched or mismatched H1N1 viruses (fig. S5). Animals infected with H1N1 viruses had antibodies that reacted to H1 and other group 1 HAs before vaccination (fig. S5, A to C). H1 antibodies in preexposed animals were boosted by the 20-HA mRNA-LNP vaccine, but this did not come at the expense of generating de novo antibody responses against the other HA components (fig. S5, D to F). Thus, the 20-HA mRNA-LNP vaccine elicits high levels of antibodies against all 20 encoded HAs in mice with and without prior exposures to influenza virus.

We completed absorption assays to determine the level of cross-subtype reactivity of antibodies elicited by vaccination. mRNA-LNPs encoding single HAs elicited antibodies that were efficiently depleted by beads coupled with the corresponding encoded HA (Fig. 2, A to C). H1-coupled beads efficiently depleted H1-reactive antibodies, and H3-coupled beads efficiently depleted H3-reactive antibodies in the serum of mice vaccinated with the 20-HA mRNA-LNP vaccine, but these absorptions did not substantially decrease the binding of antibodies reactive to other HAs in our testing panel (Fig. 2D). Thus, the 20-HA mRNA-LNP vaccine elicits antibodies that are reactive to distinct HAs rather than purely cross-reactive antibodies capable of recognizing all HA subtypes. The 20-HA mRNA-LNP vaccine elicited group 1 (H1N1 and H5N1) and group 2 (H3N2 and H7N9) neutralizing antibodies (Fig. 2, E to H) as well as group 1 and 2 HA stalk–reactive antibodies (Fig. 2, I and J). As expected, H1 and H3 neutralizing antibodies were elicited at lower levels in mice receiving the 20-HA mRNA-LNP vaccine (which contained only 2.5 μg of H1 mRNA and 2.5 μg of H3 mRNA) compared with mice receiving 50 μg of H1 or H3 mRNA-LNPs (Fig. 2, E and F). Thus, mRNA vaccines can successfully deliver at least 20 distinct HA antigens that elicit antibodies targeting both variable and conserved epitopes.

We challenged mice 28 days after vaccination with an H1N1 virus (A/California/07/2009) that was similar (97.2% HA amino acid homology) to the H1 component of the vaccine

[1]Department of Microbiology, Perelman School of Medicine, University of Pennsylvania, Philadelphia, PA, USA. [2]Department of Microbiology and Molecular Genetics, University of Pittsburgh School of Medicine, Pittsburgh, PA, USA. [3]Department of Medicine, Perelman School of Medicine, University of Pennsylvania, Philadelphia, PA, USA. [4]Department of Biostatistics Epidemiology and Informatics, Perelman School of Medicine, University of Pennsylvania, Philadelphia, PA, USA. [5]Vaccine and Infectious Disease Division, Fred Hutchinson Cancer Center, Seattle, WA, USA. [6]Acuitas Therapeutics, Vancouver, BC V6T 1Z3, Canada. [7]Center for Vaccine Research, University of Pittsburgh School of Medicine, Pittsburgh, PA, USA.
*Corresponding author. Email: hensley@pennmedicine.upenn.edu
†Present address: Department of Microbiology and Immunology, Emory University, Atlanta, GA, USA.

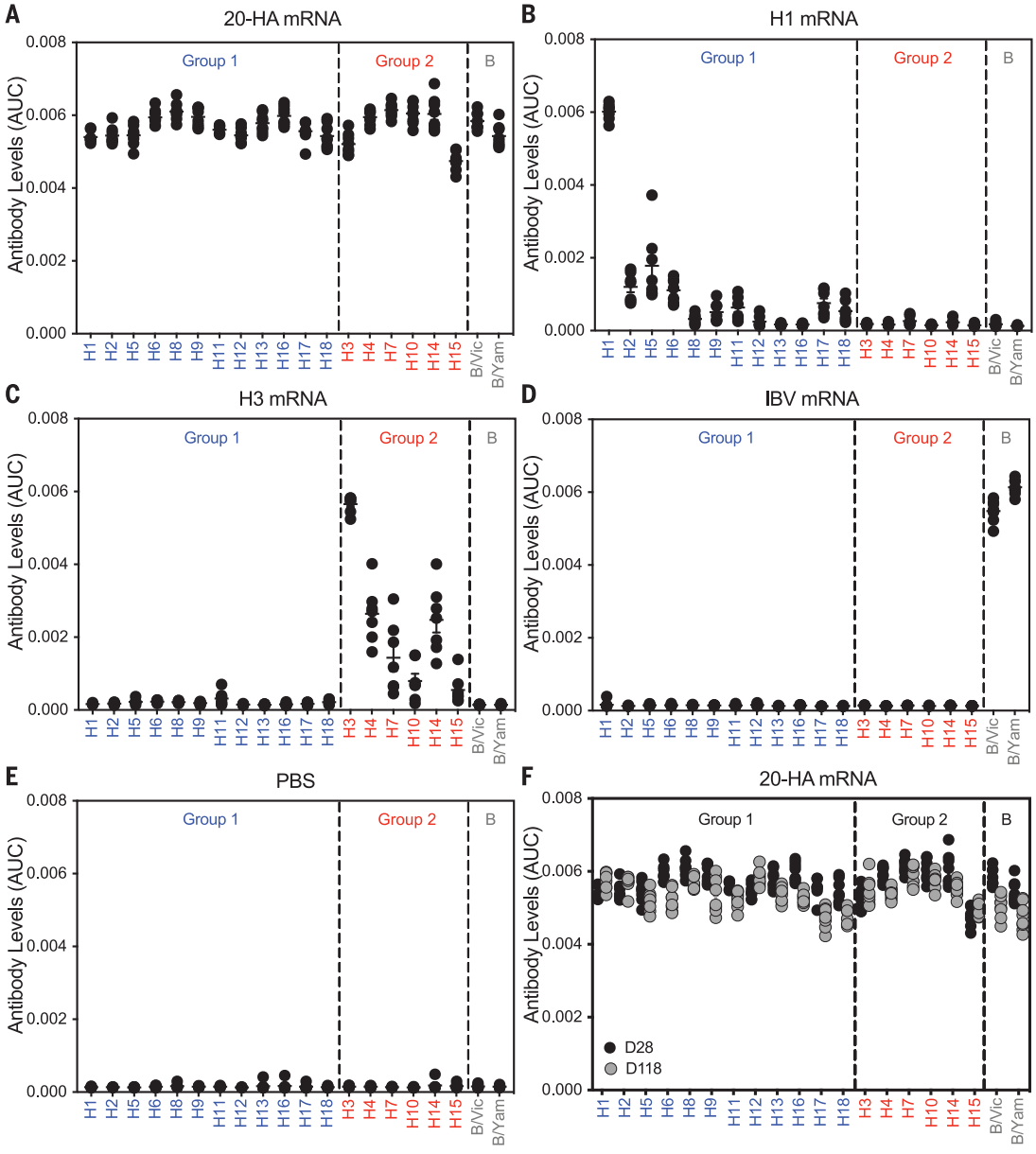

Fig. 1. The 20-HA mRNA-LNP vaccine elicits long-lived antibody responses that react to all 20 HAs. (**A**) Mice were simultaneously vaccinated intramuscularly (i.m.) with 20 different HA mRNA-LNPs (a combined total dose of 50 μg of mRNA-LNP, including 2.5 μg of each individual HA mRNA-LNP). AUC, area under the curve. (**B** to **E**) Other groups of mice were vaccinated i.m. with 50 μg of H1 mRNA-LNP (B), 50 μg of H3 mRNA-LNP (C), 50 μg of IBV HA mRNA-LNP (D), or PBS (E). Sera were collected 28 days (D28) [(A) to (E)] or 118 days (**F**) later, and antibody reactivities to different HAs were quantified using enzyme-linked immunosorbent assays (ELISAs) coated with recombinant proteins. Seven or eight mice were included for each experimental group, and in some instances, data points overlap. Group 1 HAs are shown in blue, and group 2 HAs are shown in red. Data are representative of two independent experiments and are shown as means ± SEMs. Raw ELISA data curves are shown in fig. S2.

(A/Michigan/45/2015) or an H1N1 virus (A/Puerto Rico/08/1934) that was antigenically distinct (81.8% HA amino acid homology) compared with the H1 component of the vaccine. Antibodies elicited by the 20-HA mRNA-LNP vaccine and the H1 mRNA-LNP vaccine bound to HAs from A/California/07/2009 and A/Puerto Rico/08/1934 (fig. S6, A and B) but only neutralized the A/California/07/2009 virus (fig. S6, C and D). Mice vaccinated with H3 mRNA-LNP, IBV mRNA-LNP, or an mRNA-LNP expressing luciferase rapidly lost weight, displayed severe clinical signs of disease, and died between 7 and 9 days after infection with either A/California/07/2009 (Fig. 3, A to C) or A/Puerto Rico/8/1934 (Fig. 3, F and G). Mice vaccinated with H1 mRNA-LNP or the 20-HA mRNA-LNP did not lose as much weight after infection with A/California/07/2009 (Fig. 3A), displayed few clinical signs of disease (Fig. 3B), and survived the viral challenge (Fig. 3C). A/California/07/2009 viral titers in the lungs of mice vaccinated with H1 mRNA-LNP or the 20-HA mRNA-LNP were undetectable 2 and 5 days after infection (Fig. 3, D and E). Mice vaccinated with H1 mRNA-LNP or the 20-HA mRNA-LNP initially lost weight after infection with the mismatched A/Puerto Rico/08/1934 virus (Fig. 3F), displayed clinical signs of disease (Fig. 3G), but then began recovering 7 to 8 days after infection (Fig. 3G), and most of these mice survived (Fig. 3H). A/Puerto Rico/08/1934 viral titers in the lungs were similar between the experimental groups 2 and 5 days after infection (Fig. 3, I and J). Thus, the 20-HA mRNA-LNP vaccine provided mice different degrees of protection against matched and mismatched viral strains.

To determine whether the 20-HA mRNA-LNP vaccine requires all 20 HA components, we vaccinated mice with a combination of every HA mRNA-LNP except H1 mRNA-LNP (19-HA mRNA-LNP vaccine) and then challenged these animals with A/California/07/2009 or A/Puerto Rico/08/1934 H1N1 viruses (fig. S7). Mice vaccinated with the multivalent 19-HA mRNA-LNP lacking the H1 mRNA-LNP rapidly lost weight (fig. S7A), displayed clinical signs of disease (fig. S7B), and frequently died (fig. S7C) after infection with A/California/07/2009 H1N1. This suggested that the H1 component of the 20-HA mRNA-LNP vaccine was critically important for eliciting protective responses against the A/California/07/2009 H1N1 strain. Mice vaccinated with the 19-HA mRNA-LNP lost weight (fig. S7A), displayed some clinical signs of disease (fig. S7B), but

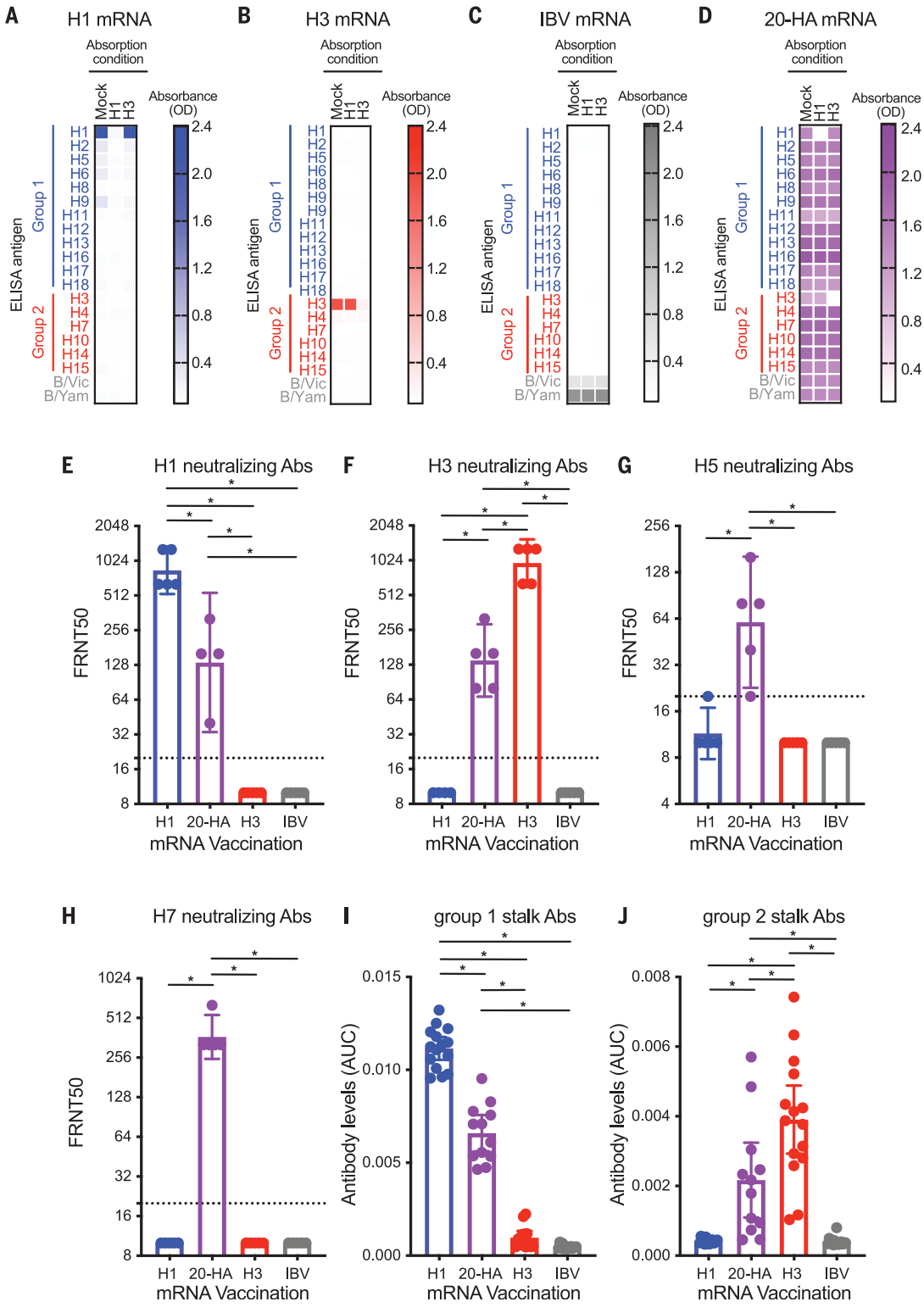

Fig. 2. The 20-HA mRNA-LNP vaccine elicits diverse antibodies targeting both conserved and variable epitopes. (**A** to **D**) Serum samples were collected from mice 28 days after H1 (A), H3 (B), IBV (C), or 20-HA (D) mRNA-LNP vaccination. Samples were absorbed with magnetic beads coupled to recombinant H1, H3, or no HA (mock), and antibody levels remaining in the unabsorbed fraction were quantified by ELISA (A to D). OD, optical density. (**E** to **H**) Focus reduction neutralization tests (FRNTs) were completed using A/Michigan/45/2015 H1 (E), A/Singapore/INFIMH-16-0019/2016 H3 (F), A/Vietnam/1203/2004 H5 (G), or A/Shanghai/02/1013 H7 (H). Titers are reported as the inverse of the highest dilutions of serum amount required to inhibit 50% of virus infections. Abs, antibodies. (**I** and **J**) HA stalk–reactive antibodies were quantified by ELISA using "headless" group 1 (H1) (I) and group 2 (H3) (J) recombinant proteins. (A to H) Six mice were included for each experimental group. (I and J) Twelve mice were included for each experimental group. Data are representative of two or three independent experiments. Data in (A) to (D) are shown as means. Data in (E) to (H) are shown as geometric means ± 95% confidence intervals (CIs), and values were log-transformed before statistical analysis. Data in (I) and (J) are shown as means ± 95% CIs. Data in (E) to (J) were compared using a one-way analysis of variance (ANOVA) with Tukey's post hoc test. *$P < 0.05$.

survived after A/Puerto Rico/08/1934 infection (fig. S7C). Although the immunological basis of this finding is unclear, the HA of A/Puerto Rico/08/1934—but not that of A/California/07/2009—likely shares a conserved epitope with a non-H1 immunogen in the 20-HA mRNA-LNP vaccine.

To further probe the mechanism(s) by which the 20-HA mRNA-LNP vaccine provides protection against different H1N1 virus strains, we depleted $CD4^+$ and $CD8^+$ T cells from mice vaccinated with the 20-HA mRNA-LNP vaccine and then challenged these animals with A/California/07/2009 or A/Puerto Rico/08/1934 (fig. S8, A to D). Vaccinated mice lacking $CD4^+$ and $CD8^+$ T cells had similar survival rates compared with vaccinated mice with intact T cells. Mice that received a passive transfer of serum from 20-HA mRNA-LNP–vaccinated mice survived A/California/07/2009 H1N1 infection but were not fully protected

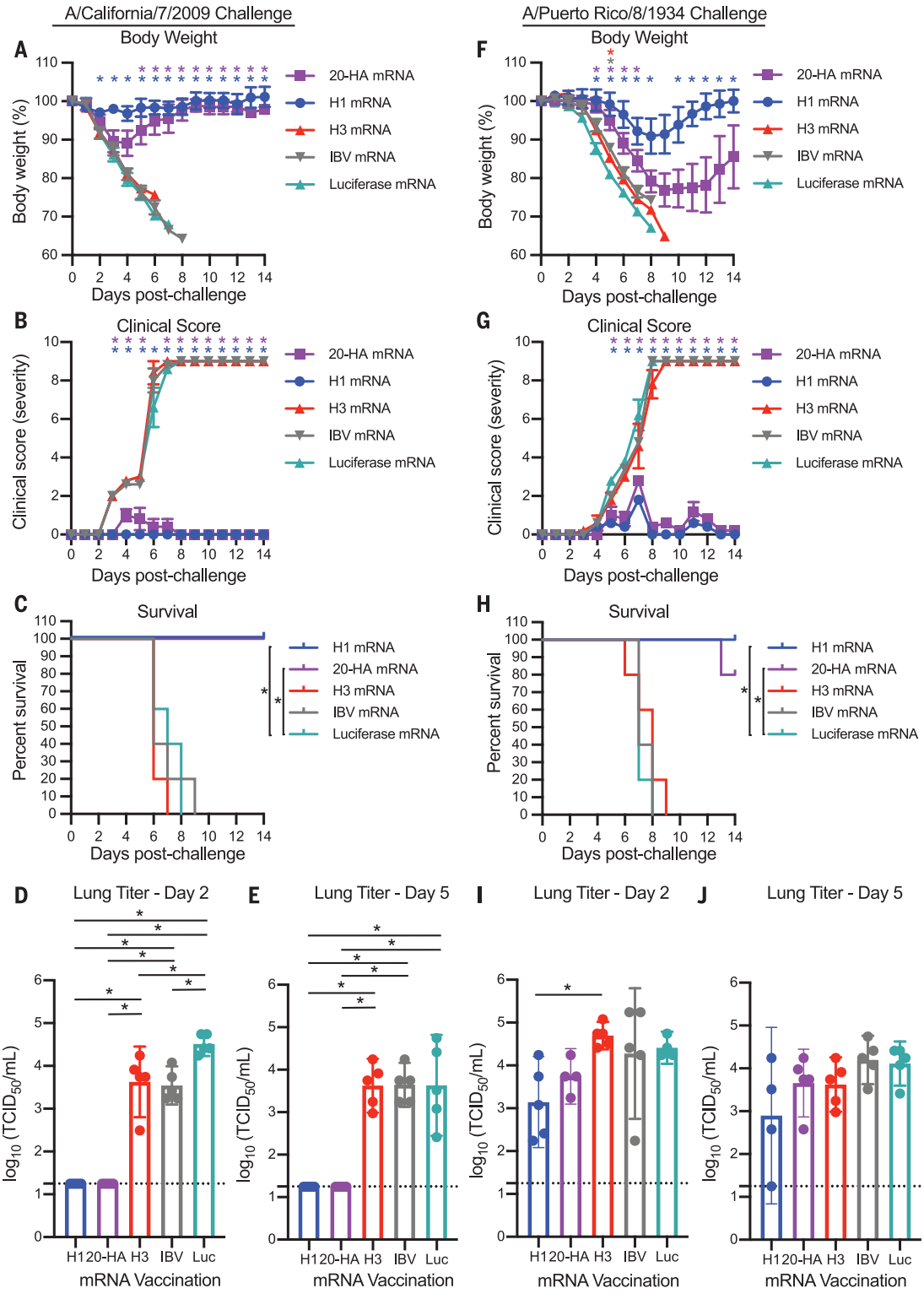

Fig. 3. The 20-HA mRNA-LNP vaccine protects mice from challenge with antigenically matched and mismatched distinct H1N1 strains. Mice were vaccinated with mRNA-LNPs encoding H1 (blue), H3 (red), IBV (gray), luciferase (Luc) (green), or 20 HAs (purple). Twenty-eight days later, they were infected intranasally (i.n.) with A/California/7/2009 [5 median lethal doses (LD_{50})] or A/Puerto Rico/8/1934 H1N1 (2 LD_{50}) influenza virus. (**A** to **C**) Weight loss (A), clinical scores (B), and survival (C) were monitored for 14 days after A/California/7/2009 infection. (**D** and **E**) Virus levels in lung homogenate samples isolated 2 days (D) and 5 days (E) after infection were quantified using median tissue culture infectious dose ($TCID_{50}$) assays. (**F** to **H**) Weight loss (F), clinical scores (G), and survival (H) were monitored for 14 days after A/Puerto Rico/8/1934 H1N1 infection. (**I** and **J**) Virus levels in lung homogenate samples isolated 2 days (I) and 5 days (J) after infection were quantified using $TCID_{50}$ assays. Horizontal dotted lines in (D), (E), (I), and (J) denote limit of detection of the assay, and samples with no detectable titers were assigned a titer at this limit of detection. Five mice were included per group. Data in (A), (B), (F), and (G) are shown as means ± SEMs and were analyzed by mixed-model ANOVA with Greenhouse-Geisser correction and Sidak's multiple comparisons test. The homologous viral challenge [(A) to (E)] was performed once. The heterologous viral challenge [(F) to (J)] was repeated at 3 months post-vaccination (instead of 28 days postvaccination) with similar results. The viral titers shown in (D), (E), (I), and (J) are from one experiment. For animals that died, their weight on the day before death was carried forward for statistical analyses. Differences compared with luciferase mRNA vaccination are indicated in (A), (B), (F), and (G); *$P < 0.05$. Data in (C) and (H) were analyzed using a log rank test; *$P < 0.05$. Data in (D), (E), (I), and (J) are shown as means ± 95% CIs, and titers were compared using a one-way ANOVA with Tukey's post hoc test; *$P < 0.05$.

against A/Puerto Rico/08/1934 H1N1 infection (fig. S8, E and F). We hypothesized that antibodies elicited by the 20-HA mRNA-LNP vaccine contribute to protection against mismatched viral strains through nonneutralizing mechanisms, such as antibody-dependent cellular cytotoxicity (ADCC) (*11*). Antibodies elicited by the 20-HA mRNA-LNP vaccine efficiently mediated ADCC with cells expressing either matched or mismatched HAs (fig. S9). Antibodies elicited by the H1 mRNA-LNP vaccine were able to mediate ADCC with cells expressing a mismatched H1 antigen but not with a matched H1 antigen (fig. S9). This was likely because the H1 mRNA-LNP

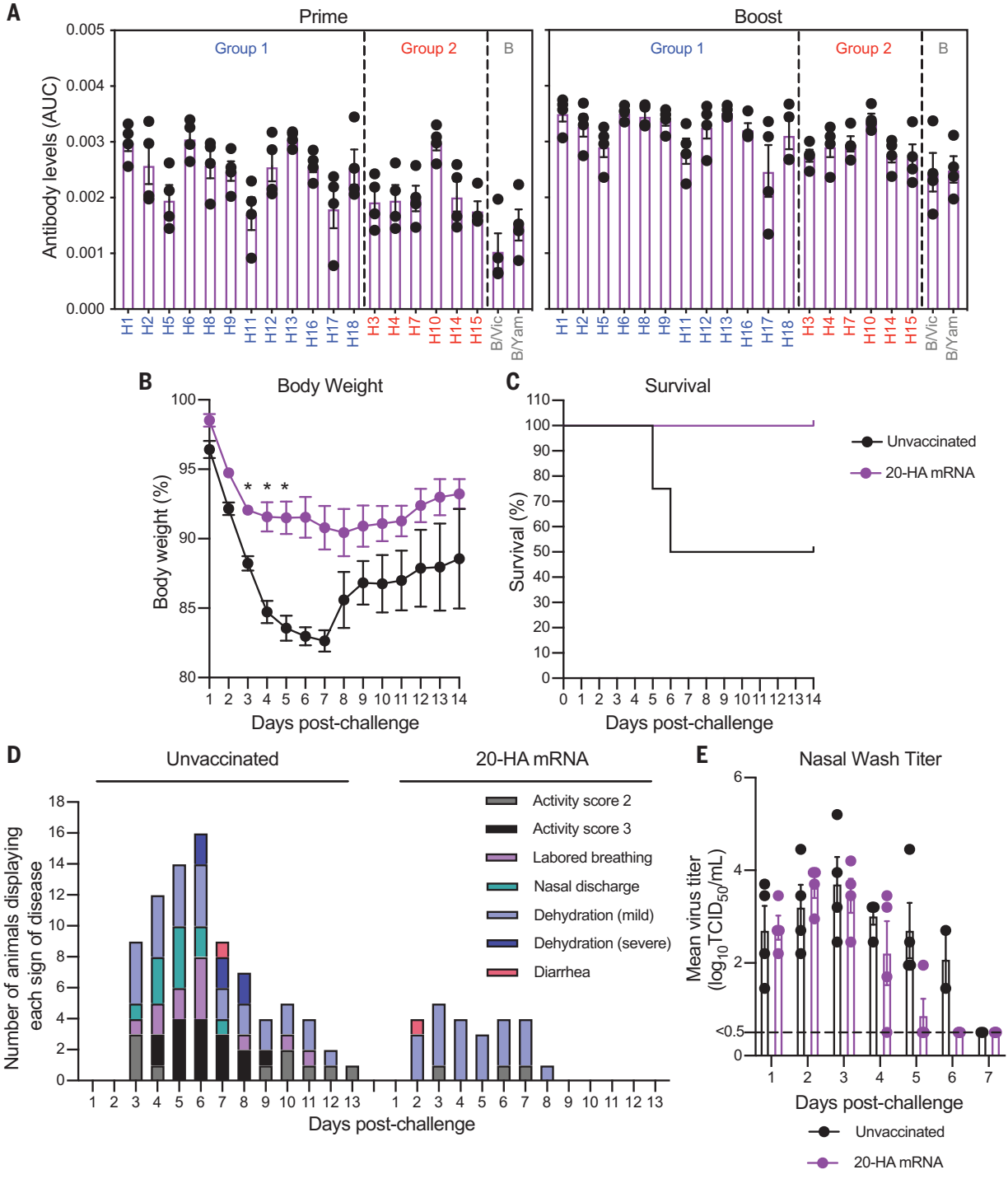

Fig. 4. Twenty-HA mRNA-LNP vaccination protects ferrets from challenge with an antigenically distinct H1N1 strain. Ferrets were primed with 60 μg of the 20-HA mRNA-LNP vaccine (3 μg of each HA mRNA-LNP) and were then boosted with the same vaccine dose 28 days later. (**A**) Sera were collected 28 days after the first and second vaccinations, and antibody reactivities to different HAs were quantified using ELISAs coated with recombinant proteins. Twenty-eight days after the second vaccination, ferrets were infected i.n. with 10^6 $TCID_{50}$ of A/Ruddy turnstone/Delaware/300/2009 H1N1 influenza virus. As a control, unvaccinated animals were also infected with the virus. (**B** to **D**) Weight loss (B), survival (C), and signs of disease (D) were monitored for 14 days after infection. The same animal could make multiple contributions to the graph in (D). (**E**) Virus levels in nasal wash samples isolated 1 to 7 days after infection were quantified using $TCID_{50}$ assays. The horizontal dashed line indicates limit of detection. Four ferrets were included for each experimental group, and the experiment was performed once. Data shown are means ± SEMs [(A), (B), and (E)]. Data in (B) and (E) are shown as means ± SEMs and were analyzed by mixed-model ANOVA with Greenhouse-Geisser correction and Sidak's multiple comparisons test; $*P < 0.05$. For animals that died, their weight on the day before death was carried forward for statistical analyses. Data in (C) were analyzed using a Mantel-Cox log rank test.

vaccine elicited high levels of H1N1 neutralizing antibodies (fig. S6), which have previously been found to inhibit ADCC activity mediated by nonneutralizing antibodies (*12*, *13*).

Finally, we completed a prime-boost vaccination experiment in ferrets to mimic the dosing schedule initially used for severe acute respiratory syndrome coronavirus 2 (SARS-CoV-2) mRNA vaccines (*14*, *15*). Each ferret produced antibodies reactive to all 20 HAs after a single vaccination, and antibody levels increased after a booster vaccination delivered 28 days later (Fig. 4A). We challenged vaccinated and unvaccinated ferrets with an avian H1N1 virus (A/Ruddy turnstone/Delaware/300/2009) that was distinct from the H1 HA that was included in the vaccine (81.8% HA amino acid homology with vaccine H1 component) to mimic a pandemic featuring an unknown viral strain. Unvaccinated animals lost >16% of their initial weight by 5 days after infection and two out of four animals died, whereas vaccinated ferrets lost only ~8.5% of their initial weight by 5 days after infection and all animals survived (Fig. 4, B and C). Unvaccinated animals displayed more clinical signs of disease relative to vaccinated animals after infection (Fig. 4D). Viral titers in nasal washes were similar in unvaccinated and vaccinated animals at days 1 to 4 after infection, but the virus was cleared more efficiently in vaccinated animals at days 5 and 6 after infection (Fig. 4E). Thus, the 20-HA mRNA-LNP vaccine protected ferrets against an antigenically mismatched avian H1N1 virus.

In this Report, we present an alternative strategy for inducing universal immunity against distinct influenza virus strains. We had previously demonstrated that nucleoside-modified mRNA-LNP vaccines expressing HA and conserved influenza virus antigens are immunogenic in mice (*9*, *14*). Instead of focusing on immunogens to elicit antibodies against epitopes that are conserved among many different influenza virus strains, we designed a vaccine that encodes separate immunogens from all known IAV subtypes and IBV lineages. Previous studies have shown that cocktails of virus-like particles encoding antigens from four different influenza virus subtypes are immunogenic in mice when delivered intranasally (*16*). We found that antigens from at least 20 distinct influenza viruses can be simultaneously delivered through mRNA-LNPs. The production and standardization of different antigens expressed by mRNA-LNP vaccines is simpler compared with other vaccine approaches (*17*, *18*) and there may be specific properties of mRNA vaccines that allow for the induction of immune responses to multiple antigens without noticeable immunodominance biases, even in the context of preexisting immune responses. For example, we had previously reported that mRNA-LNP vaccines induce long-lived germinal center reactions in mice (*19*), a finding that has recently been found to occur in SARS-CoV-2 mRNA–vaccinated humans as well (*20*, *21*). Long-lived germinal centers may facilitate the simultaneous induction of immune responses against multiple epitopes, including epitopes that are usually subdominant.

Further studies will be required to fully elucidate the mechanisms by which the 20-HA mRNA vaccine provides protection. Our present findings suggest that protection against antigenically matched strains is mediated by neutralizing antibodies, whereas protection against mismatched viral strains may occur through nonneutralizing mechanisms, such as ADCC. Over the course of our studies, we used antigenically matched as well as antigenically mismatched challenge strains to mimic the emergence of a novel pandemic influenza virus strain. It is likely that mRNA influenza vaccines that are imperfectly matched to novel pandemic influenza virus strains will not provide sterilizing immunity but will instead limit disease severity and protect against death through nonneutralizing mechanisms. A similar phenomenon may be occurring with SARS-CoV-2 variant infections in humans immunized with SARS-CoV-2 mRNA vaccines that were developed using spike sequences obtained from viral strains isolated early in the pandemic. In most cases, symptoms and severity are greatly reduced and virus is cleared faster in vaccinated individuals infected with antigenically drifted SARS-CoV-2 variants (*22*, *23*).

Our overall approach will likely be useful for infectious diseases other than influenza viruses. Multivalent mRNA-LNP vaccines may be applied against other variable pathogens, such as coronaviruses and rhinoviruses. For example, SARS-CoV-2 mRNA vaccines are being updated to include multiple spike components to combat antigenically distinct strains (*24*). Additional studies will be required to determine the maximum number of antigens that can be simultaneously delivered through mRNA-LNP vaccines and the underlying immunological mechanisms that allow for the induction of responses against multiple antigens.

REFERENCES AND NOTES

1. F. Krammer *et al*., *Nat. Rev. Dis. Primers* **4**, 3 (2018).
2. M. I. Nelson *et al*., *Epidemics* **26**, 116–127 (2019).
3. W. N. Harrington, C. M. Kackos, R. J. Webby, *Exp. Mol. Med.* **53**, 737–749 (2021).
4. E. J. Erbelding *et al*., *J. Infect. Dis.* **218**, 347–354 (2018).
5. H. M. Yassine *et al*., *Nat. Med.* **21**, 1065–1070 (2015).
6. K. S. Corbett *et al*., *mBio* **10**, e02810-18 (2019).
7. R. Nachbagauer *et al*., *Nat. Med.* **27**, 106–114 (2021).
8. B. S. Graham, J. R. Mascola, A. S. Fauci, *JAMA* **319**, 1431–1432 (2018).
9. N. Pardi *et al*., *Nat. Commun.* **9**, 3361 (2018).
10. E. Willis *et al*., *Sci. Transl. Med.* **12**, eaav5701 (2020).
11. D. J. DiLillo, G. S. Tan, P. Palese, J. V. Ravetch, *Nat. Med.* **20**, 143–151 (2014).
12. W. He *et al*., *Proc. Natl. Acad. Sci. U.S.A.* **113**, 11931–11936 (2016).
13. P. E. Leon *et al*., *Proc. Natl. Acad. Sci. U.S.A.* **113**, E5944–E5951 (2016).
14. A. W. Freyn *et al*., *Mol. Ther.* **28**, 1569–1584 (2020).
15. E. J. Topol, *Cell* **184**, 1401 (2021).
16. L. M. Schwartzman *et al*., *mBio* **6**, e01044-15 (2015).
17. N. Pardi, M. J. Hogan, D. Weissman, *Curr. Opin. Immunol.* **65**, 14–20 (2020).
18. N. Pardi, M. J. Hogan, F. W. Porter, D. Weissman, *Nat. Rev. Drug Discov.* **17**, 261–279 (2018).
19. N. Pardi *et al*., *J. Exp. Med.* **215**, 1571–1588 (2018).
20. J. S. Turner *et al*., *Nature* **595**, 421–425 (2021).
21. K. Lederer *et al*., *Cell* **185**, 1008–1024.e15 (2022).
22. A. Sheikh, J. McMenamin, B. Taylor, C. Robertson, Public Health Scotland and the EAVE II Collaborators, *Lancet* **397**, 2461–2462 (2021).
23. J. Lopez Bernal *et al*., *N. Engl. J. Med.* **385**, 585–594 (2021).
24. G. McLean *et al*., *mBio* **13**, e02979-21 (2022).

ACKNOWLEDGMENTS

We thank all members of the Hensley laboratory for helpful discussions related to this project. We thank A. McDermott and B. Graham (Vaccine Research Center at the National Institutes of Health) for providing plasmids to express headless H1 and H3 proteins and J. Bloom (Fred Hutchinson Cancer Center) for providing plasmids to generate viruses expressing green fluorescent protein (GFP). **Funding:** This project has been funded in part with federal funds from the National Institute of Allergy and Infectious Diseases, the National Institutes of Health, and the Department of Health and Human Services under contract nos. 75N93021C00015 (S.E.H.), 75N93019C00050 (S.E.H.), 1R01AI108686 (S.E.H.), and R56AI150677 (S.E.H.). C.P.A. was supported by the Training in Emerging Infectious Diseases grant T32AI055400. S.E.H. holds an Investigators in the Pathogenesis of Infectious Disease Award from the Burroughs Wellcome Fund. **Author contributions:** C.P.A. and S.E.H. designed the experiments, analyzed and interpreted the data, and wrote the manuscript. C.P.A., M.J.B., V.L.S., N.Y., C.F., H.M., M.-G.A., N.P., E.M.D., K.P., and T.G. performed experiments. J.S.M. provided advice on statistical analyses of data. L.H.M. completed phylogenetic analyses of vaccine antigens. Y.K.T. and S.H.Y.F. encapsulated RNAs in LNPs. S.S.L. supervised ferret experiments, D.W. supervised mRNA-LNP production, and S.E.H. supervised all other activities. **Competing interests:** S.E.H. reports receiving consulting fees from Sanofi Pasteur, Lumen, Novavax, and Merck for work unrelated to this manuscript. S.H.Y.F. and Y.K.T. are employees and Y.K.T. is an officer of Acuitas Therapeutics, a company focused on the development of lipid nanoparticulate nucleic acid delivery systems for therapeutic applications. Y.K.T. is named on patents describing the use of modified mRNA LNPs. D.W. is a coinventor on patents that describe the use of nucleoside-modified mRNA as a platform to deliver therapeutic proteins. D.W. and N.P. are coinventors on patents describing the use of modified mRNA in LNPs as a vaccine platform. S.E.H. and D.W. are named inventors on a University of Pennsylvania–owned patent application on this work. T.G. is now an employee at GSK but was working as a postdoctoral fellow at the University of Pennsylvania while completing experiments for this manuscript. C.P.A. and M.J.B. are now employees of Pfizer but were working as graduate students at the University of Pennsylvania while completing experiments for this manuscript. The authors declare no other competing interests. **Data and materials availability:** The data that support the findings of this study are included in the manuscript. All materials used in this manuscript are available from the authors upon reasonable request.

SUPPLEMENTARY MATERIALS

science.org/doi/10.1126/science.abm0271
Materials and Methods
Figs. S1 to S9
References (*25*–*39*)
MDAR Reproducibility Checklist
Data S1

Submitted 20 August 2021; resubmitted 24 May 2022
Accepted 29 September 2022
10.1126/science.abm0271

ARTHROPOD EVOLUTION

The lower Cambrian lobopodian *Cardiodictyon* resolves the origin of euarthropod brains

Nicholas J. Strausfeld[1]*, Xianguang Hou[2], Marcel E. Sayre[3,4], Frank Hirth[5]*

For more than a century, the origin and evolution of the arthropod head and brain have eluded a unifying rationale reconciling divergent morphologies and phylogenetic relationships. Here, clarification is provided by the fossilized nervous system of the lower Cambrian lobopodian *Cardiodictyon catenulum*, which reveals an unsegmented head and brain comprising three cephalic domains, distinct from the metameric ventral nervous system serving its appendicular trunk. Each domain aligns with one of three components of the foregut and with a pair of head appendages. Morphological correspondences with stem group arthropods and alignments of homologous gene expression patterns with those of extant panarthropods demonstrate that cephalic domains of *C. catenulum* predate the evolution of the euarthropod head yet correspond to neuromeres defining brains of living chelicerates and mandibulates.

During the past decade, the discovery of fossilized brains and nervous systems in exceptionally preserved middle and lower Cambrian fossils has reopened the historic and sometimes contentious debate (*1*) about the composition and evolution of the arthropod head and brain and hence the early evolution of this phylum (*2*, *3*). Two major questions arise: What comprises the head of an arthropod, and does its composition illuminate the organization of the brain (*4*)? A persistent assumption (*5*, *6*) has been that exoskeletal organization of the head is an indicator of a segmental brain. Developmental and genetic studies have not supported this view.

Already in 1901, Heymons (*7*), in his meticulous embryological analysis of the centipede brain, showed that the rostral germ band gives rise to three nonmetameric cephalic domains. The anteriormost domain is associated with the labra, the most anterior appendages of the head. The next domain is a pair of lobes associated with the optic areas. Together, these two domains constitute the forebrain. The third pair of lobes constitutes the midbrain, which includes the antennal lobes. Heymons also documented the forward displacement of the trunk's incipient first true segment from the segmented ventral cord (*7*). The three cephalic domains, now identifiable by their unique gene expression patterns, are the proso-, proto-, and deutocerebrum. The rostrally displaced first trunk ganglion is the tritocerebrum. The ubiquity of these developmental events across arthropods (*8*, *9*) suggests an ancient origin of the developmental program patterning the brain. Nevertheless, data from developmental genetics that might clarify ambiguities of interpretation (*10*) have generally been absent from studies of fossils. This is made possible in this study by the fossilized remains of the nervous system in the lobopodian *Cardiodictyon catenulum*, whose cerebral domains align with expression patterns of gene homologs in extant panarthropods.

Lobopodians are an extinct group of worm-like animals that were once abundant in the lower Cambrian and were mainly constrained to the seafloor, along which they moved using tubelike, unjointed legs (*11*). The present species was retrieved in the late 1980s from Cambrian deposits belonging to the 518-million-year-old Chiungchussu (Yu'anshan) Formation near Kunming, China (*12*, *13*). Lobopodians are distantly related to today's Onychophora (velvet worms), recognized by genomics and developmental genetics as belonging to the clade Panarthropoda and the superphylum Ecdysozoa, or molting animals (*3*), which also includes nematode worms and priapulids. *Cardiodictyon* belongs to the "armored" lobopodians, thus named because of the sclerites and spikelike cuticular adornments on their trunks, isolated examples of which are ascribed to the oldest series of the Cambrian ~525 million years ago (*14*). Figure 1 provides a comprehensive description of the preserved features of *Cardiodictyon* (see also figs. S1 to S3). Central to our understanding of early nervous system evolution is the identification of neural traces, many at the micrometer scale, that resolve an expansive ventral nervous system and a brain occupying a capsule-like head.

Fossilization of nervous tissues has been ascertained for numerous Cambrian taxa, including gilled lobopodians, stem euarthropods, and annelids (*15*). Most traces are recognized as ventral nerve cord or brain because of their likeness to features of extant euarthropod nervous systems. Illustrative are the optic tracts and brain of the lower Cambrian anomalocarid *Lyrarapax unguispinus*, which was imaged using digital filtering of chromatic channels to distinguish carbonaceous traces identically resolved by energy-dispersive x-ray spectroscopy (*16*). Chromatic filtering of high-resolution digitized images of the *Cardiodictyon* trunk and head resolves preserved neuropils and nerve cords (specimens YKLP11434 and YKLP11422; Figs. 1 and 2 and figs. S4 and S5). Unlike dark carbonaceous compressions familiar as preserved neuropil (*16*, *17*), structures interpreted here as neural are resolved as magenta to rust-brown deposits. A recent hypothesis by Saleh *et al.* (*18*) explaining preservation of neural tissue proposes that authigenic tissue pyritization may be initiated by breakdown of the neuropil's native ferritin (*18*, *19*). The absence of dark deposits indicative of overlying carbon (*17*) could be explained by partial decay of the carcass or recent weathering (*20*). In specimen YKLP11434, ganglion-like varicosities connected by ventral nerve cords beneath or lateral to the gut (Fig. 2, A to D) provide abundant collaterals extending dorsally in the trunk (Figs. 1, K and L, and 2, C and D). The head of specimen YKLP11422 is embedded in matrix showing its left half (Fig. 2, F to H). Exposed are parts of the mouth and the rostral digestive tract and its expansion into a funnel-like stomodeum at the junction of the head and trunk (Fig. 2F and fig. S6). These arrangements correspond to pharyngeal systems in the lobopodian *Onychodictyon ferox* (*21*) and in extant tardigrades (*22*) (Fig. 2, E and I). Three domains of fossilized neural tissue in the head (ce1, ce2, and ce3) reflect the sequential organization of the foregut components and the origins of the three pairs of head appendages (Figs. 1L and 2, F to H, and fig. S3). Neural traces in the head are interpreted as lying above, beneath, or lateral to pharyngeal structures. The anteriormost cephalic domain (ce1) is interpreted as lying above and partially encircling the buccal tube, as is the second domain's (ce2) reach beneath the pharyngeal bulb (Figs. 1L and 2, G and H). The third domain (ce3) is confluent with the first ventral ganglion-like varicosity (va1) at the interface of the gut and stomodeum (Figs. 1L and 2, G and H, and fig. S6).

Considerations of the early organization of the panarthropod central nervous system usually refer to extant Onychophora and Tardigrada (*11*, *23*, *24*). Both possess unarthrodized lobopodian appendages. In Onychophora, segmental ganglia are absent (*24*). Paired lateral nerve cords comprising continuous synaptic neuropil provide an orthogonal arrangement of collaterals (*25*) extending dorsally within the trunk's musculature (fig. S7). This contrasts with tardigrades (*24*), wherein nerves extending

[1]Department of Neuroscience, University of Arizona, Tucson, AZ, USA. [2]Yunnan Key Laboratory for Palaeobiology, Institute of Palaeontology, Yunnan University, Kunming, China. [3]Lund Vision Group, Department of Biology, Lund University, Lund, Sweden. [4]Department of Biological Sciences, Macquarie University, Sydney, NSW, Australia. [5]Department of Basic and Clinical Neuroscience, Institute of Psychiatry, Psychology and Neuroscience, King's College London, London, UK.
*Corresponding author. Email: flybrain@arizona.edu (N.J.S.); frank.hirth@kcl.ac.uk (F.H.)

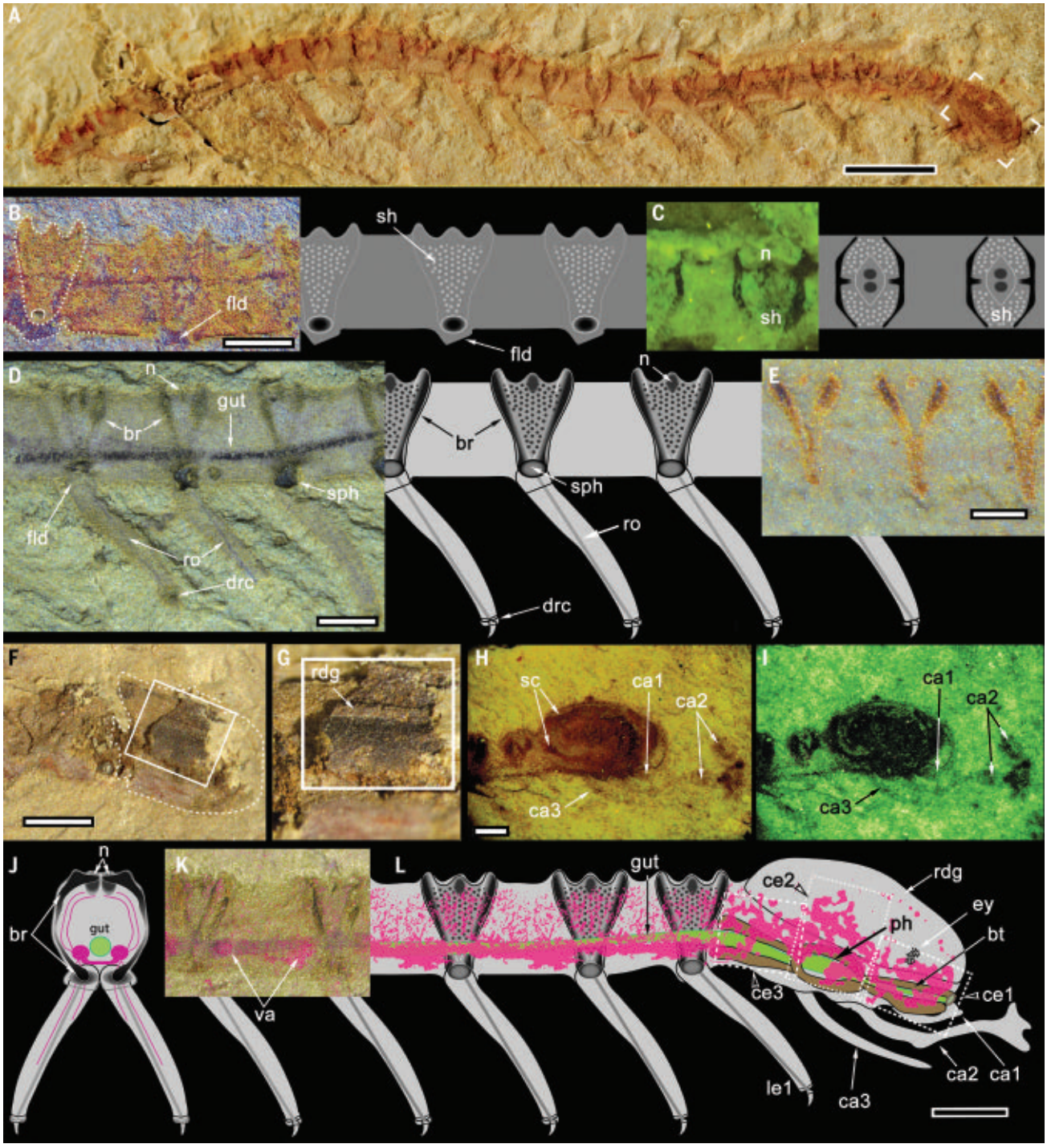

Fig. 1. External and internal organization of *C. catenulum*. (**A**) YKLP11426: Behind an oval head (bracketed), the trunk has 25 identical segments. (**B**) YKLP11425: Each segment bears bilateral shield-like sclerites (sh, outline) with punctate thickenings (fig. S2). (**C**) YKLP11426: Oblique top view of sclerites, following the trunk curvature, their dorsal nodules (n) meeting at the midline. (**D**) YKLP11423 and (**E**) YKLP11415: Sclerite side braces (br) converge ventrally to a spherical density (sph) at the base of each leg. A rodlike element (ro) extends from a cuticular fold (fld) beneath the density into the annulated leg and terminates at a distal ring and claw (drc; fig. S1). (**F** and **G**) YKLP11421 and (**H** and **I**) YKLP11464: An oval carapace with a sculpted midline ridge [rdg, boxed in (F) and (G)] covers the head, laterally reinforced by paired sclerites [sc, (H)]. Three pairs of appendages [ca1 to ca3; (H) and (I)] extend ventrally. The short ca1 pair projects forward from the mouth; the middle pair (ca2) each comprise three podomere-like articles terminating as a spatula-like element (fig. S3, A to C); the ca3 pair are long and curved, tapering to a blunt end (see also fig. S3, D to F). (**J**) Schematic cross section of trunk: magenta, ventral cords and orthogon collaterals; green, gut. (**K**) YKLP11434: Segment with ganglion-like varicosities (va) and ventral nerve cord. (**L**) Schematic based on YKLP11422, YKLP11423, and YKLP11434: Segmentally arranged ganglion-like varicosities and connecting nerve cords project alongside the gut; collaterals extend dorsally. Three cerebral domains (ce1 to ce3), each associated with a distinct part of the foregut and an appendage pair: ce1 to buccal tube (bt) and ca1; ce2 to the pharyngeal bulb (ph) and ca2; ce3 to the stomodeum and ca3 (also fig. S6). Simple eyes (ey) comprising reflective puncta are associated with ce1. Scale bars: (A) 1 mm; (F) 500 μm; (all others) 250 μm.

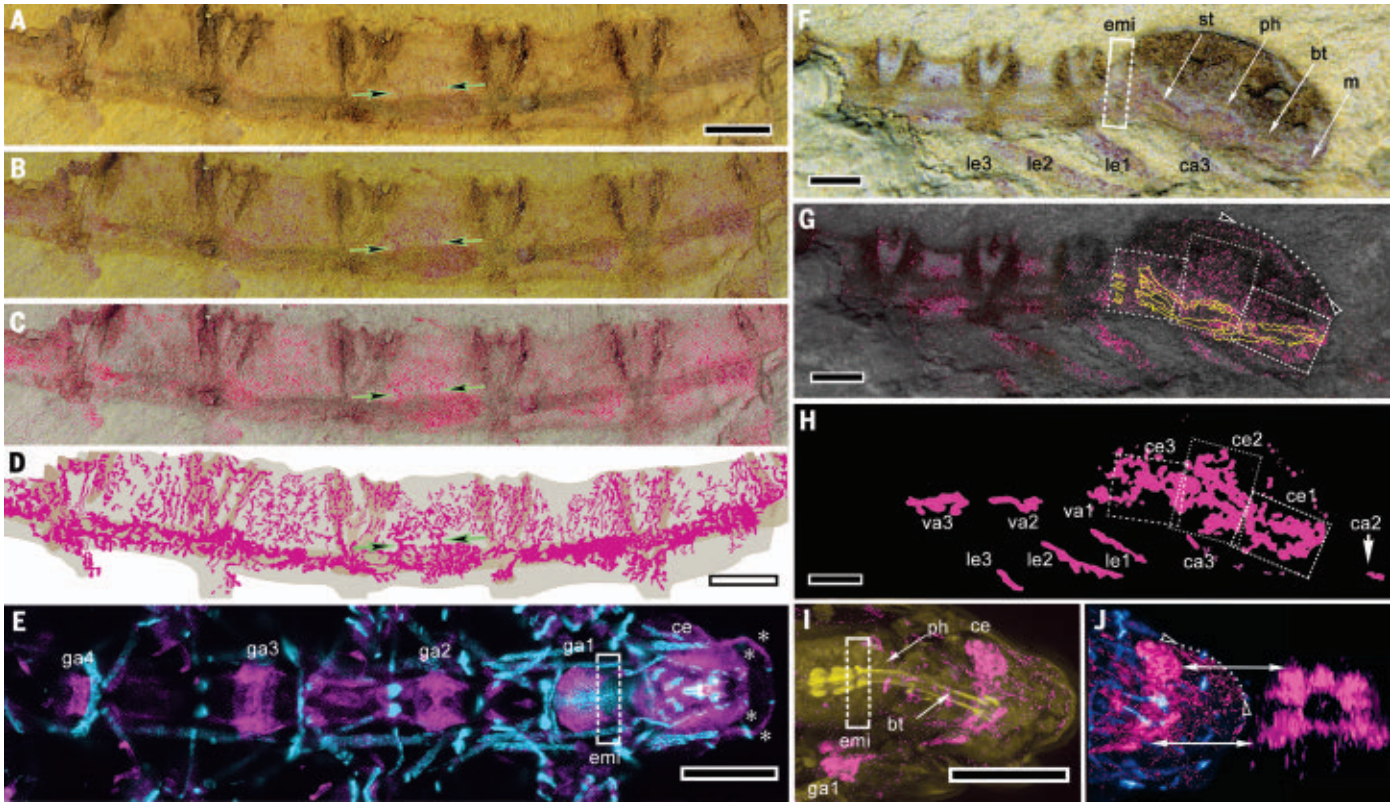

Fig. 2. Segmental nervous system and asegmental brain of *C. catenulum* and *Hypsibius exemplaris*. (**A** to **D**) YKLP11434, lateral view, white-light illumination. Arrows denote identical locations throughout chromatic filtering that resolves nerve cord and varicosities, with branches ascending within each trunk segment (fig. S4). (**E**) Anti-synapsin (magenta) and F-actin (cyan) immunostaining of the tardigrade *H. exemplaris* (dorsal view) resolving synaptic neuropils of the four trunk ganglia (ga1 to ga4). Boxed area rostral to ga1 indicates the endomesodermal interface (emi), the origin of the gut. (**F**) YKLP11422: white-light illumination of left half of split head of *Cardiodictyon*. Mouth (m) and buccal tube (bt) lead to the pharyngeal bulb (ph) connecting to the stomodeum (st); emi is boxed (fig. S6); le1 to le3 indicate the first three leg pairs of the segmented trunk. (**G**) Fossilized neural tissue (magenta) and structures outlined in yellow (buccal tube, pharyngeal bulb, and stomodeum) provide comparison with arrangements in *Hypsibius* (I). (**H**) Maximum density rendition (fig. S5) of neural tissue resolves cerebral domains ce1, ce2, and ce3 (boxed) associated with cephalic appendages ca2 and ca3. Segmental varicosities (va1 to va3) of the ventral nerve cord relate to legs le1 to le3. (**I**) Lateral view of *Hypsibius* stained with anti-synapsin and F-actin, showing relationship of cerebrum (ce) and ganglion (ga1) to the autofluorescent (yellow) buccal tube (bt) and pharyngeal bulb (ph); boxed area, emi. (**J**) (Left) Brain [as in (I)] showing dorsal field of small dense synaptic boutons (beneath dotted line) corresponding to dorsal puncta in *Cardiodictyon* [dotted line in (G)]. (Right) Frontal view of circumesophageal brain neuropil. Scale bars: [(A) to (D) and (F) to (H)] 250 μm; [(E) and (I)] 20 μm.

to muscle fibers originate from discrete ganglia (Fig. 2E). In *Cardiodictyon*, numerous collaterals extend dorsally from ganglion-like varicosities and their connecting nerve cords (Fig. 2, C and D). Collaterals also ascend the sclerite braces, whose grooves and pits may suggest muscle attachment sites (fig. S2), as in crustaceans (*26*).

The organization in *C. catenulum* of collateral nerves from segmental varicosities and nerve cord corresponds to the fossilized trunk nervous system of the fuxianhuiid *Chengjiangocaris kunmingensis*, in which bilaterally extending nerves originate from the segmental ganglia as well as from their connecting nerve cords. This arrangement of lateral nerves looping around the inside of the trunk has been proposed as an ecdysozoan plesiomorphy owing to its occurrence in crown priapulids, nematodes, and onychophorans (*27*). An evolved reduction and loss of the ganglionic varicosities of *C. catenulum* would provide onychophoran-like ventral cords linked heterolaterally by looped collaterals. Alternatively, an evolved segmental condensation of collaterals restricted to ganglion-like varicosities would provide an organization comparable to that of tardigrades, where metameric ganglia express the segmental marker Engrailed at their caudal margins. Notably, the absence of Engrailed expression at the caudal margin of the tardigrade brain suggests its asegmental organization (*28*). The disposition of *Cardiodictyon* neuropil at its buccal tract aligns ce1 with the most anterior part of the tardigrade brain (Fig. 2J). The absence of head appendages in tardigrades, however, obliges comparison of *C. catenulum* with Euarthropoda, which offers neuroanatomical as well as molecular and developmental genetic correspondences (Fig. 3).

All taxa, including fossils considered in this study, can be compared by aligning their specific non-neural indicator: the origin of the gut from the stomodeum (Fig. 3 and fig. S6), which denotes the endomesodermal interface (emi). In *C. catenulum*, this occurs immediately posterior to domain ce3, at its confluence with va1, which lies beneath the gut and is associated with the first pair of trunk appendages (Fig. 2, F and H, and fig. S6). The ce3 domain and corresponding ca3 appendages align with the deutocerebrum and its appendages (the jaws) in Onychophora. They also align with the deutocerebral ganglion in stem leanchoiliids (*10*), which receives nerves from the grasping appendages (Fig. 3B). In extant panarthropods, this is characterized by Empty spiracles (*Emx*) and the exclusion of Homeotic (*Hox*) gene expression (Fig. 3A).

The ce2 domain and appendage pair of *C. catenulum* align with the radiodontan protocerebrum and eyestalks and the protocerebrum and lateral eyes of Leanchoiliidae (Fig. 3B). In extant panarthropods, it is characterized

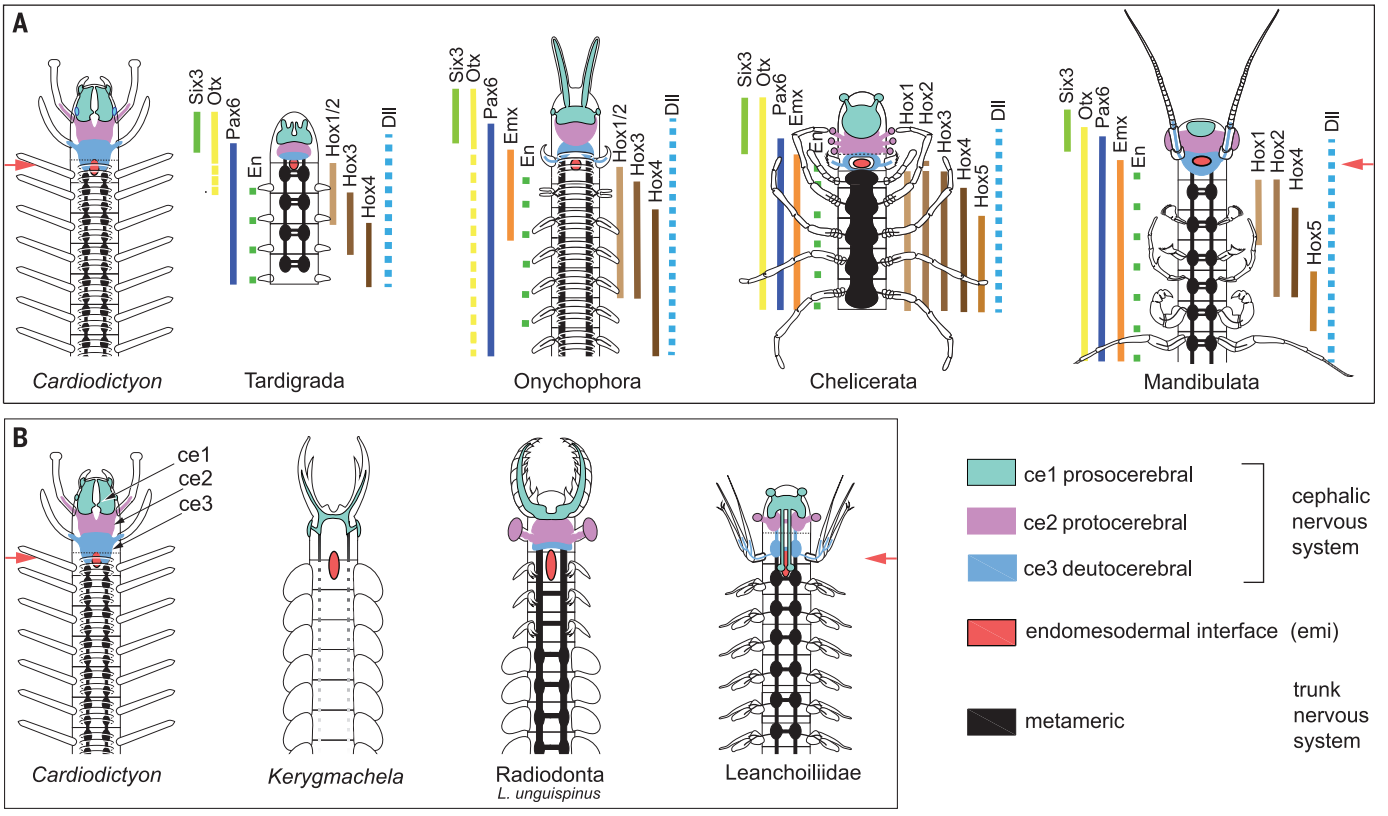

Fig. 3. Correspondence of nervous systems. Cerebral domains ce1 to ce3 in *C. catenulum* and corresponding neuromeres in fossil and extant taxa aligned (red arrows) by endomesodermal interface (emi; red ellipses). (**A**) *Cardiodictyon* aligned with tardigrade (*Hypsibius*), Onychophora, and crown euarthropods. Trunk nervous systems defined by orthogon collaterals and ganglia in *Cardiodictyon*, orthogon only in Onychophora, and ganglia in all other taxa. Expression domains of gene homologs (see table S1): *Six3* demarcating the prosocerebrum and protocerebrum (Proso +Proto); *Pax6*, the entire nervous system except the prosocerebrum; *Hox* expression patterns align with the mesodermal domain; *Dll* expression extends rostrally to the prosocerebral labrum aligning with *Dll* expression in the tardigrade head. These relationships expressed in set theory: Anterior brain = (*Six3*) ∩ (*Pax6*) | (anterior to endomesodermal interface) ⊄ (*Hox*-mesoderm) ∴ {Proso+Proto+Deutocerebrum}. (**B**) Alignment of *Cardiodictyon* with extinct taxa shows the diminutive cerebral volume of the gilled lobopodian *Kerygmachela* as extreme rostral to the emi, indicating a prosocerebral identity contrasting with the radiodontan *L. unguispinus* (*16*) and upper stem Leanchoiliidae (*10*) that reveal ce1, ce2, and ce3.

by Orthodenticle (*Otx*) and Paired box 6 (*Pax6*) gene expression (Fig. 3A). The ce1 domain and the minute frontal appendage pair of *C. catenulum* align with the preoral raptorial appendages and their neuropil in Radiodonta (*16*, *29*) and with the prosocerebrum and its labral neuropil in Leanchoiliidae (Fig. 3B) (*10*), characterized by *Six3* gene expression in extant panarthropods (Fig. 3A) (*8*). In the gilled lobopodian *Kerygmachela*, nerve cords extend from a rostral bridge of neuropil distant from the pharyngeal/buccal apparatus (*30*), thus aligning the brain with the ce1 domain of *C. catenulum* (Fig. 3B). The fact that benthic lobopodians possess a single pair of rostral appendages (*31*, *32*), as does nektonic *Kerygmachela*, predicts a comparable neural organization; their phylogenetic position suggests an evolved loss of ce2 and ce3 (fig. S8).

In the tardigrade, the resolution of Distal-less (*Dll*) rostral to the endomesodermal interface (*33*, *34*) is a cryptic correspondence with appendicular attributes of the prosocerebrum (labra) and protocerebrum [stalked eyes or their derivatives (*35*)] of stem and crown euarthropods, and thereby the two anterior pairs of cephalic appendages in *C. catenulum* (Fig. 3). Although the three cephalic domains of *C. catenulum* are not morphologically identical, and thus lack the segmental attributes denoted by trunk segmentation (*36*, *37*), they correspond to the rostral neuromeres of the brains of crown euarthropods (Fig. 3). Evidence from spiders, the beetle *Tribolium*, and *Drosophila* demonstrates that mutation of any of the several genes required for formation of the anterior gut and the cephalic appendages affects not only their development but also that of the corresponding neuromere (*38*–*43*). Hence their formation and alignment are genetically determined.

For well over a century, the euarthropod brain has been viewed as a composite of metameric neuromeres in a segmented head (*44*, *45*). Here, the lower Cambrian lobopodian *C. catenulum* resolves the brain's ancient origin as asegmental domains, the alignments of which reflect their transformation into neuromeres, as seen in upper stem euarthropods (Fig. 3 and fig. S8). Evidence that the brain evolved independently of the caudal nervous system is validated by observations that different mechanisms underlie their formation in insects (*42*, *46*). Only in crown Euarthropoda is there an embryonic contribution to the brain from the first metameric trunk ganglion, which migrates forward to become the tritocerebrum, contiguous with the deutocerebrum. The deuto- and tritocerebral interface defines the boundary between the mid- and hindbrain (*47*), thus marking the point of coalescence of two connected but genetically and evolutionarily distinct components of the nervous system.

REFERENCES AND NOTES

1. J. G. Rempel, *Quaest. Entomol.* **11**, 7–25 (1975).
2. G. D. Edgecombe, *Integr. Comp. Biol.* **57**, 467–476 (2017).
3. G. D. Edgecombe, *Annu. Rev. Ecol. Evol. Syst.* **51**, 1–25 (2020).
4. G. Scholtz, G. D. Edgecombe, *Dev. Genes Evol.* **216**, 395–415 (2006).
5. J. Vinther, *Curr. Biol.* **32**, R833–R836 (2022).
6. G. E. Budd, *Arthropod Struct. Dev.* **62**, 101048 (2021).
7. R. Heymons, *Zoologica (Stuttg.)* **33**, 1–244 (1901).
8. P. R. Steinmetz *et al.*, *EvoDevo* **1**, 14 (2010).
9. E. Clark, A. D. Peel, M. Akam, *Development* **146**, dev170480 (2019).
10. T. Lan *et al.*, *Curr. Biol.* **31**, 4397–4404.e2 (2021).
11. J. Ortega-Hernández, *Curr. Biol.* **25**, R873–R875 (2015).
12. X.-G. Hou, J. Bergström, *Zool. J. Linn. Soc.* **114**, 3–19 (1995).
13. L. Ramsköld, *Lethaia* **25**, 443–460 (1992).
14. M. J. Betts *et al.*, *Gondwana Res.* **36**, 176–208 (2016).

15. L. A. Parry *et al*., *BioEssays* **40**, 1700167 (2018).
16. P. Cong, X. Ma, X. Hou, G. D. Edgecombe, N. J. Strausfeld, *Nature* **513**, 538–542 (2014).
17. X. Ma, G. D. Edgecombe, X. Hou, T. Goral, N. J. Strausfeld, *Curr. Biol.* **25**, 2969–2975 (2015).
18. F. Saleh, A. C. Daley, B. Lefebvre, B. Pittet, J. P. Perrillat, *BioEssays* **42**, e1900243 (2020).
19. R. P. Anderson, *BioEssays* **42**, 2000070 (2020).
20. J.-P. Lin, D. E. G. Briggs, *Palaios* **25**, 463–467 (2010).
21. Q. Ou, D. Shu, G. Mayer, *Nat. Commun.* **3**, 1261 (2012).
22. R. Guidetti *et al*., *Zoomorphology* **131**, 127–148 (2012).
23. L. I. Campbell *et al*., *Proc. Natl. Acad. Sci. U.S.A.* **108**, 15920–15924 (2011).
24. G. Mayer *et al*., *BMC Evol. Biol.* **13**, 230 (2013).
25. G. Mayer, P. M. Whitington, *Dev. Biol.* **335**, 263–275 (2009).
26. R. E. Snodgrass, *Smithson. Misc. Collect.* **142**, 1–7 (1960).
27. J. Yang *et al*., *Proc. Natl. Acad. Sci. U.S.A.* **113**, 2988–2993 (2016).
28. W. N. Gabriel, B. Goldstein, *Dev. Genes Evol.* **217**, 421–433 (2007).
29. P. Cong, A. C. Daley, G. D. Edgecombe, X. Hou, *BMC Evol. Biol.* **17**, 208 (2017).
30. T. S. Park *et al*., *Nat. Commun.* **9**, 1019 (2018).
31. H. B. Whittington, *Philos. Trans. R. Soc. London Ser. B* **284**, 165–197 (1978).
32. J. Liu, D. Shu, J. Han, Z. Zhang, X. Zhang, *Acta Palaeontol. Pol.* **51**, 215–222 (2006).
33. F. W. Smith, M. Cumming, B. Goldstein, *EvoDevo* **9**, 19 (2018).
34. M. Game, F. W. Smith, *Proc. Biol. Sci.* **287**, 20201135 (2020).
35. D. M. Maynard, *J. Exp. Biol.* **43**, 79–106 (1965).
36. G. E. Budd, *Evol. Dev.* **3**, 332–342 (2001).
37. R. L. Hannibal, N. H. Patel, *EvoDevo* **4**, 35 (2013).
38. M. Kanayama *et al*., *Nat. Commun.* **2**, 500 (2011).
39. M. I. Schacht, C. Schomburg, G. Bucher, *Dev. Genes Evol.* **230**, 95–104 (2020).
40. J. B. Schinko *et al*., *Dev. Biol.* **317**, 600–613 (2008).
41. P. Kitzmann, M. Weißkopf, M. I. Schacht, G. Bucher, *Development* **144**, 2969–2981 (2017).
42. S. M. Cohen, G. Jürgens, *Nature* **346**, 482–485 (1990).
43. J. Zhu, S. Palliyil, C. Ran, J. P. Kumar, *Proc. Natl. Acad. Sci. U.S.A.* **114**, 5846–5853 (2017).
44. E. S. Goodrich, *Q. J. Microsc. Sci.* **40**, 247–268 (1898).
45. O. Lev, G. D. Edgecombe, A. D. Chipman, *Integr. Org. Biol.* **4**, obac015 (2022).
46. O. Lev, A. D. Chipman, *Front. Cell Dev. Biol.* **9**, 695135 (2021).
47. J. C. Bridi *et al*., *Proc. Natl. Acad. Sci. U.S.A.* **117**, 19544–19555 (2020).

ACKNOWLEDGMENTS

We thank J. Liu, Shaanxi Key Laboratory of Early Life and Environments, Xian, China, for permission to reproduce the image in fig. S2B. We also thank G. D. Edgecombe, UK Natural History Museum, for valued advice, and X. Ma, University of Exeter, UK, for suggestions pertaining to lobopodian anatomy. W. Gronenberg, University of Arizona, provided comments. We are indebted to C. Strausfeld for refining the text and editing the work in its entirety. **Funding:** This work was supported by the National Science Foundation under grant 1754798 awarded to N.J.S., and by the University of Arizona Regents Fund. F.H. acknowledges support from the UK Biotechnology and Biological Sciences Research Council (BB/N001230/1). **Author contributions:** N.J.S. and F.H. originated the project. N.J.S. analyzed and documented the specimens. F.H. ascribed published gene expression data to described panarthropodans. X.H. collected, provided, and advised on specimens. M.E.S. prepared and documented immunocytological data. N.J.S. and F.H. prepared the manuscript, with input from X.H. and M.E.S. **Competing interests:** The authors declare that they have no competing interests. **Data and materials availability:** All data are available in the main text or the supplementary materials.

SUPPLEMENTARY MATERIALS

science.org/doi/10.1126/science.abn6264
Provenance Statement
Materials and Methods
Figs. S1 to S8
Table S1
References (*48*–*84*)
MDAR Reproducibility Checklist

Submitted 9 December 2021; accepted 7 October 2022
10.1126/science.abn6264

PHYSIOLOGY

Variation in human water turnover associated with environmental and lifestyle factors

Yosuke Yamada[1,2]*†, Xueying Zhang[3,4]†, Mary E. T. Henderson[5]†, Hiroyuki Sagayama[6]*, Herman Pontzer[7,8]*, Daiki Watanabe[1,2,9], Tsukasa Yoshida[1,2], Misaka Kimura[2], Philip N. Ainslie[10], Lene F. Andersen[11], Liam J. Anderson[12,13], Lenore Arab[14], Issad Baddou[15], Kweku Bedu-Addo[16], Ellen E. Blaak[17], Stephane Blanc[18,19], Alberto G. Bonomi[20], Carlijn V. C. Bouten[21], Pascal Bovet[22], Maciej S. Buchowski[23], Nancy F. Butte[24], Stefan G. Camps[21,25], Graeme L. Close[12], Jamie A. Cooper[26], Richard Cooper[27], Sai Krupa Das[28], Lara R. Dugas[29,30], Simon Eaton[31], Ulf Ekelund[32,33], Sonja Entringer[34,35], Terrence Forrester[36], Barry W. Fudge[37], Annelies H. Goris[21], Michael Gurven[38], Lewis G. Halsey[5], Catherine Hambly[4], Asmaa El Hamdouchi[15], Marije B. Hoos[21], Sumei Hu[39], Noorjehan Joonas[40], Annemiek M. Joosen[21], Peter Katzmarzyk[41], Kitty P. Kempen[21], William E. Kraus[42], Wantanee Kriengsinyos[43], Robert F. Kushner[44], Estelle V. Lambert[45], William R. Leonard[46], Nader Lessan[47,48], Corby K. Martin[41], Anine C. Medin[11,49], Erwin P. Meijer[21], James C. Morehen[50,12], James P. Morton[12], Marian L. Neuhouser[51], Theresa A. Nicklas[24], Robert M. Ojiambo[52,53], Kirsi H. Pietiläinen[54], Yannis P. Pitsiladis[55], Jacob Plange-Rhule[16]‡, Guy Plasqui[56], Ross L. Prentice[51], Roberto A. Rabinovich[57], Susan B. Racette[58], David A. Raichlen[59], Eric Ravussin[41], Leanne M. Redman[41], John J. Reilly[60], Rebecca M. Reynolds[61], Susan B. Roberts[28], Albertine J. Schuit[62], Luis B. Sardinha[63], Analiza M. Silva[63], Anders M. Sjödin[64], Eric Stice[65], Samuel S. Urlacher[66,67], Giulio Valenti[21,20], Ludo M. Van Etten[21], Edgar A. Van Mil[68], Jonathan C. K. Wells[69], George Wilson[12], Brian M. Wood[70,71], Jack A. Yanovski[72], Alexia J. Murphy-Alford[73], Cornelia U. Loechl[73], Amy H. Luke[74]*, Jennifer Rood[41]*, Klaas R. Westerterp[75]*, William W. Wong[24]*, Motohiko Miyachi[1,9]*, Dale A. Schoeller[76]*, John R. Speakman[3,4,77,78]*†; International Atomic Energy Agency (IAEA) Doubly Labeled Water (DLW) Database Consortium§

Water is essential for survival, but one in three individuals worldwide (2.2 billion people) lacks access to safe drinking water. Water intake requirements largely reflect water turnover (WT), the water used by the body each day. We investigated the determinants of human WT in 5604 people from the ages of 8 days to 96 years from 23 countries using isotope-tracking (^{2}H) methods. Age, body size, and composition were significantly associated with WT, as were physical activity, athletic status, pregnancy, socioeconomic status, and environmental characteristics (latitude, altitude, air temperature, and humidity). People who lived in countries with a low human development index (HDI) had higher WT than people in high-HDI countries. On the basis of this extensive dataset, we provide equations to predict human WT in relation to anthropometric, economic, and environmental factors.

Water is essential for life (*1*), and daily water intake is necessary to prevent dehydration (i.e., net loss of body water) in most terrestrial animals, including humans (*2*). Total body water (TBW, measured in liters) is homeostatically controlled (*3*) and tightly regulated day to day by thirst and hunger drives that lead to the intake of fluids and food to offset water losses (*4*). Body water is lost as urine, insensible transcutaneous evaporation and sweat loss, respiratory water vapor, and water in feces (Fig. 1A). To maintain water balance, these losses must be matched by intake of water from liquids (drinking water and other beverages) and foods (*5*, *6*), water vapor in respiratory air intake, transcutaneous water uptake, and water formed during aerobic respiration and metabolism (Fig. 1A) (*2*, *7*). The total movement of water through the body, both intake and loss, is called water turnover (WT, measured in liters per day).

Despite adaptations to minimize dehydration, humans can survive for only ~3 days without consuming water (*1*). The risk of dehydration is greater under conditions requiring increased respiration, blood circulation, and sweating, such as during vigorous physical activity or in hot and humid environments (*3*). Insufficient water intake is a risk factor for heat stroke, urinary and kidney diseases, and cardiovascular failure (*8*, *9*). An understanding of WT and its determinants is critical for global public health decision-making regarding the provision of drinking water and water-enriched food (*10*).

Public health officals need to be able to anticipate future daily water intake demands of their populations, especially during periods of impending crisis. Ideally, this would be based on scientific evidence regarding the levels of normal water intake. The current recommended intakes for water (*8*, *9*, *11*), however, rely on epidemiologic self-reported surveys or laboratory-based physiological studies with rather small sample sizes. Results obtained from self-reported intake surveys show large variations linked to imprecision in the assessment method. It is thus difficult to establish clear guidelines for worldwide public health actions from these sources of information. Most people who lack access to safely managed drinking water live

in countries with a low human development index (HDI), but few studies have examined WT in those populations (*2*). To develop global guidelines for daily water intake, empirical measurements of WT under free-living conditions are required across a broad range of economic and environmental conditions.

We report WT and TBW for 5604 human subjects (3729 females and 1875 males) ranging in age from 8 days to 96 years from 23 countries around the globe and across a wide range of environments and living conditions (fig. S1 and table S1). We used the hydrogen isotope dilution and elimination technique, which provides an objective, accurate, reliable, and precise measurement of both TBW and WT under free-living conditions (Fig. 1B) (*7*). This method involves the subject drinking ~100 ml of water enriched with ~5% deuterated water. The deuterium floods into the body water pool, providing an estimate of TBW using the dilution principle (*12*). The excess deuterium isotope is then eliminated from the body by the elimination routes detailed in Fig. 1A. Because there is no enriched isotope tracer entering the system, the isotope enrichment declines exponentionally back to the baseline level. The rate constant of this exponential return to baseline multiplied by the body water pool is equal to the WT.

Data were obtained from the International Atomic Energy Agency Doubly Labelled Water (DLW) Database (*13*, *14*). The current study aimed to examine (i) the dependence of WT and TBW on age, body size, body composition, total energy expenditure (TEE, in megajoules per day), and physical activity level (PAL, which is the TEE/basal energy expenditure) through the human life course; (ii) the effects of climate, including latitude, altitude, outside air temperature, and humidity; and (iii) the potential influence of economic development as measured by the HDI.

WT was greatest in men 20 to 30 years of age and in women 25 to 60 years of age (Fig. 2A and table S2) and was lower in men >40 and women >65 years. TBW was also highest for adults 20 to 60 years of age (Fig. 2B). As a fraction of TBW, WT was highest in neonates (28.3 ± 7.2% per day) and decreased with age to 9.9 ± 3.0% per day in adults aged 18 to 40 years (Fig. 2C). TBW as a proportion of body weight also decreased with age, from 60.0 ± 6.4% of body weight from birth to 6 months to 50.4 ± 5.3% (males) and 42.0 ± 4.8% (females) at 60 years (Fig. 2D). Sex differences and the relationship with age and TBW in adults largely reflected variations in the percentage of body fat, which contains less water than muscle and other organs. The ratio of WT to TEE was 0.33 ± 0.09 liters/MJ (1.4 ± 0.4 ml/kcal) for adults, comparable to previous isotope-based measures (*15*) (Fig. 2, E and F).

Body size and composition, TEE, PAL, and climate variables were all correlated with WT. After limiting our analysis to adults aged 18 to 60 years to avoid strong age effects (as shown in Fig. 2), bivariate analyses showed that WT was positively correlated with fat-free mass (FFM), TEE, and PAL and negatively correlated with percent body fat ($P < 0.001$) (Fig. 3, A to D). We found a significant curve-linear relationship between outdoor mean air temperature and WT and between latitude and WT ($P < 0.001$) (Fig. 3, E and F). Air temperature was positively correlated with WT when it was higher than 10°C ($P < 0.001$). Daily water intake was highest at ~0° effective latitude and lowest at –50° or +50° latitude. People living above the Arctic Circle had higher WT than those living at –50° or +50° latitude.

Linear regression analysis showed that age, FFM, PAL, air temperature, relative humidity, HDI, and altitude were significant predictors of WT in adults aged 18 years and older (table S3). We conducted multiple regression analysis (including first- and second-order polynomial terms) to examine potential nonlinear relationships between WT and the above variables in adults aged 18 years and older (table S4). The

[1]National Institute of Health and Nutrition, National Institutes of Biomedical Innovation, Health and Nutrition, Osaka, Japan. [2]Institute for Active Health, Kyoto University of Advanced Science, Kyoto, Japan. [3]Shenzhen Key Laboratory of Metabolic Health, Center for Energy Metabolism and Reproduction, Shenzhen Institutes of Advanced Technology, Chinese Academy of Sciences, Shenzhen, China. [4]Institute of Biological and Environmental Sciences, University of Aberdeen, Aberdeen, UK. [5]School of Life and Health Sciences, University of Roehampton, London, UK. [6]Faculty of Health and Sport Sciences, University of Tsukuba, Ibaraki, Japan. [7]Department of Evolutionary Anthropology, Duke University, Durham, NC, USA. [8]Duke Global Health Institute, Duke University, Durham, NC, USA. [9]Faculty of Sport Sciences, Waseda University, Saitama, Japan. [10]Centre for Heart, Lung and Vascular Health, School of Health and Exercise Sciences, Faculty of Health and Social Development, University of British Columbia Okanagan, Kelowna, British Columbia, Canada. [11]Department of Nutrition, Institute of Basic Medical Sciences, University of Oslo, Oslo, Norway. [12]Research Institute for Sport and Exercise Sciences, Liverpool John Moores University, Liverpool, UK. [13]School of Sport, Exercise and Rehabilitation Sciences, University of Birmingham, Birmingham, UK. [14]David Geffen School of Medicine, University of California, Los Angeles, CA, USA. [15]Unité Mixte de Recherche en Nutrition et Alimentation, CNESTEN-Université Ibn Tofail URAC39, Regional Designated Center of Nutrition Associated with AFRA/IAEA, Rabat, Morocco. [16]Department of Physiology, Kwame Nkrumah University of Science and Technology, Kumasi, Ghana. [17]Department of Human Biology, Maastricht University, Maastricht, Netherlands. [18]Nutritional Sciences, University of Wisconsin, Madison, WI, USA. [19]Institut Pluridisciplinaire Hubert Curien, CNRS Université de Strasbourg, UMR7178, France. [20]Phillips Research, Eindoven, Netherlands. [21]Maastricht University, Maastricht, Netherlands. [22]University Center for Primary Care and Public Health (Unisanté), Lausanne, Switzerland. [23]Division of Gastroenterology, Hepatology and Nutrition, Department of Medicine, Vanderbilt University, Nashville, TN, USA. [24]Department of Pediatrics, Baylor College of Medicine, US Department of Agriculture (USDA)/Agricultural Research Service (ARS) Children's Nutrition Research Center, Houston, TX, USA. [25]Clinical Nutrition Research Centre (CNRC), Singapore Institute of Food and Biotechnology Innovation (SIFBI), Agency of Science, Technology and Research (A*STAR), Singapore. [26]Nutritional Sciences, University of Georgia, Athens, GA, USA. [27]Department of Public Health Sciences, Parkinson School of Health Sciences and Public Health, Loyola University, Maywood, IL, USA. [28]USDA Human Nutrition Research Center on Aging at Tufts University, Boston, MA, USA. [29]Public Health Sciences, Loyola University of Chicago, Maywood, IL, USA. [30]Division of Epidemiology and Biostatistics, School of Public Health & Family Medicine, University of Cape Town, Cape Town, South Africa. [31]Developmental Biology and Cancer Department, UCL Great Ormond Street Institute of Child Health, London, UK. [32]Department of Sport Medicine, Norwegian School of Sport Sciences, Oslo, Norway. [33]Department of Chronic Diseases, Norwegian Institute of Public Health, Oslo, Norway. [34]Charité – Universitätsmedizin Berlin, corporate member of Freie Universität Berlin and Humboldt-Universität zu Berlin, Institute of Medical Psychology, Berlin, Germany. [35]Department of Pediatrics, University of California Irvine, Irvine, CA, USA. [36]Solutions for Developing Countries, University of the West Indies, Mona, Kingston, Jamaica. [37]Aspire Academy, Doha, Qatar. [38]Department of Anthropology, University of California Santa Barbara, Santa Barbara, CA, USA. [39]Beijing Technology and Business University, Beijing, China. [40]Central Health Laboratory, Ministry of Health and Wellness, Mauritius. [41]Pennington Biomedical Research Center, Baton Rouge, LA, USA. [42]Department of Medicine, Duke University, Durham, NC, USA. [43]Institute of Nutrition, Mahidol University, Salaya, Phutthamonthon, Nakon-Pathom, Thailand. [44]Feinberg School of Medicine, Northwestern University, Chicago, IL, USA. [45]Health Through Physical Activity, Lifestyle and Sport Research Centre (HPALS) Division of Exercise Science and Sports Medicine (ESSM), FIMS International Collaborating Centre of Sports Medicine, Department of Human Biology, Faculty of Health Sciences, University of Cape Town, Cape Town, South Africa. [46]Department of Anthropology, Northwestern University, Evanston, IL, USA. [47]Imperial College London Diabetes Centre, Abu Dhabi, United Arab Emirates. [48]Imperial College London, London, UK. [49]Department of Nutrition and Public Health, Faculty of Health and Sport Sciences, University of Agder, Kristiansand, Norway. [50]The FA Group, Burton-Upon-Trent, Staffordshire, UK. [51]Division of Public Health Sciences, Fred Hutchinson Cancer Center and School of Public Health, University of Washington, Seattle, WA, USA. [52]Kenya School of Medicine, Moi University, Eldoret, Kenya. [53]Rwanda Division of Basic Sciences, University of Global Health Equity, Rwanda. [54]Obesity Research Unit, Research Program for Clinical and Molecular Metabolism, Faculty of Medicine, University of Helsinki, and Abdominal Center, Obesity Center, HealthyWeightHub, Helsinki University Hospital and University of Helsinki, Helsinki, Finland. [55]School of Sport and Service Management, University of Brighton, Eastbourne, UK. [56]Department of Nutrition and Movement Sciences, Maastricht University, Maastricht, Netherlands. [57]The Queen's Medical Research Institute, University of Edinburgh, Edinburgh, UK. [58]Program in Physical Therapy and Department of Medicine, Washington University School of Medicine, St. Louis, MO, USA, and College of Health Solutions, Arizona State University, Phoenix, AZ, USA. [59]Biological Sciences and Anthropology, University of Southern California, Los Angeles, CA, USA. [60]University of Starthclyde, Glasgow, Scotland. [61]Centre for Cardiovascular Sciences, Queen's Medical Research Institute, University of Edinburgh, Edinburgh, UK. [62]School of Social and Behavioral Sciences, University of Tilburg, Tilburg, Netherlands. [63]Department of Sport and Health of the Faculty of Human Kinetics, University of Lisbon, Lisbon, Portugal. [64]Department of Nutrition, Exercise and Sports, Copenhagen University, Copenhagen, Denmark. [65]Department of Psychiatry and Behavioral Sciences, Stanford University, Stanford, CA, USA. [66]Department of Anthropology, Baylor University, Waco, TX, USA. [67]Child and Brain Development Program, Canadian Institute for Advanced Research (CIFAR), Toronto, Ontario, Canada. [68]Maastricht University, Brightlands Campus Greenport Venlo and Lifestyle Medicine Center for Children, Jeroen Bosch Hospital, Hertogenbosch, Netherlands. [69]Population, Policy and Practice Research and Teaching Department, UCL Great Ormond Street Institute of Child Health, London, UK. [70]Department of Anthropology, University of California Los Angeles, Los Angeles, CA, USA. [71]Max Planck Institute for Evolutionary Anthropology, Department of Human Behavior, Ecology, and Culture, Leipzig, Germany. [72]Section on Growth and Obesity, Division of Intramural Research, *Eunice Kennedy Shriver* National Institute of Child Health and Human Development, National Institutes of Health, Bethesda, MD, USA. [73]Nutritional and Health-Related Environmental Studies Section, Division of Human Health, International Atomic Energy Agency, Vienna, Austria. [74]Department of Public Health Sciences, Parkinson School of Health Sciences and Public Health, Loyola University Chicago, Chicago, IL, USA. [75]NUTRIM, Maastricht University, Maastricht, Netherlands. [76]Biotechnology Center and Department of Nutritional Sciences, University of Wisconsin, Madison, WI, USA. [77]State Key Laboratory of Molecular Developmental Biology, Institute of Genetics and Developmental Biology, Chinese Academy of Sciences, Beijing, China. [78]CAS Center of Excellence in Animal Evolution and Genetics, Kunming, China.
***Corresponding author. Email: yyamada831@gmail.com (Y.Y.); sagayama.hiroyuki.ka@u.tsukuba.ac.jp (H.S.); herman.pontzer@duke.edu (H.P.); Aluke@luc.edu (A.H.L.); jennifer.rood@pbrc.edu (J.R.); k.westerterp@maastrichtuniversity.nl (K.R.W.); wwong@bcm.edu (W.W.W.); miyachim@waseda.jp (M.M.); dschoell@nutrisci.wisc.edu (D.A.S.); j.speakman@abdn.ac.uk (J.R.S.)**
†These authors contributed equally to this work. ‡Deceased. §IAEA DLW Database Consortium members are listed in the supplementary materials.

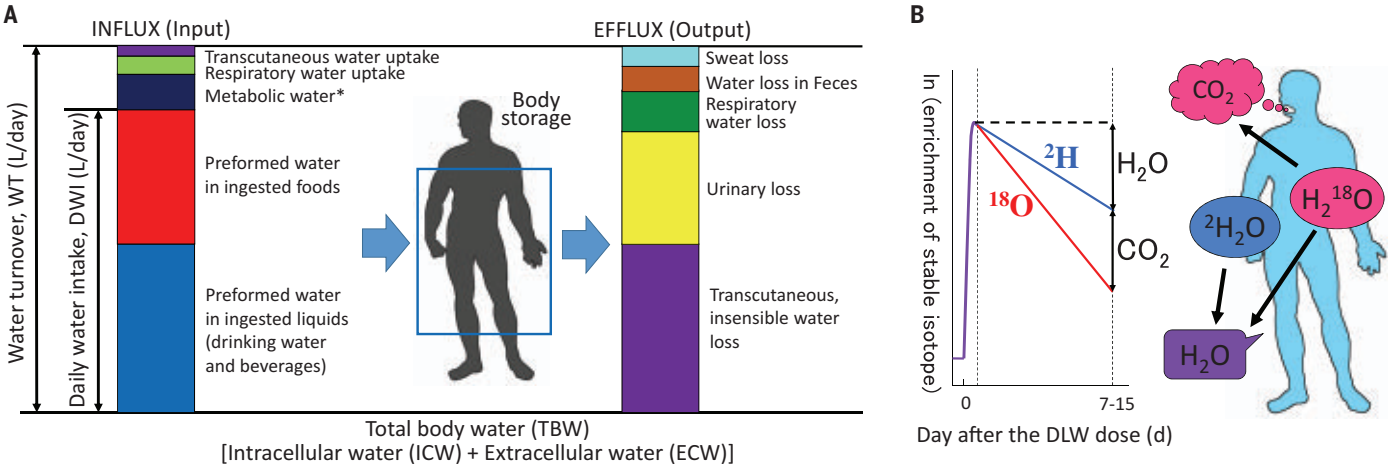

Fig. 1. Conceptual diagram of human WT and its measurement. (**A**) Conceptual diagram showing sources of water influx and efflux on human body. *Metabolic water produced inside a living organism as an end product of the oxidation of energy-containing substances in their food. (**B**) Hydrogen isotope dilution and elimination provides an objective measure of TBW and WT.

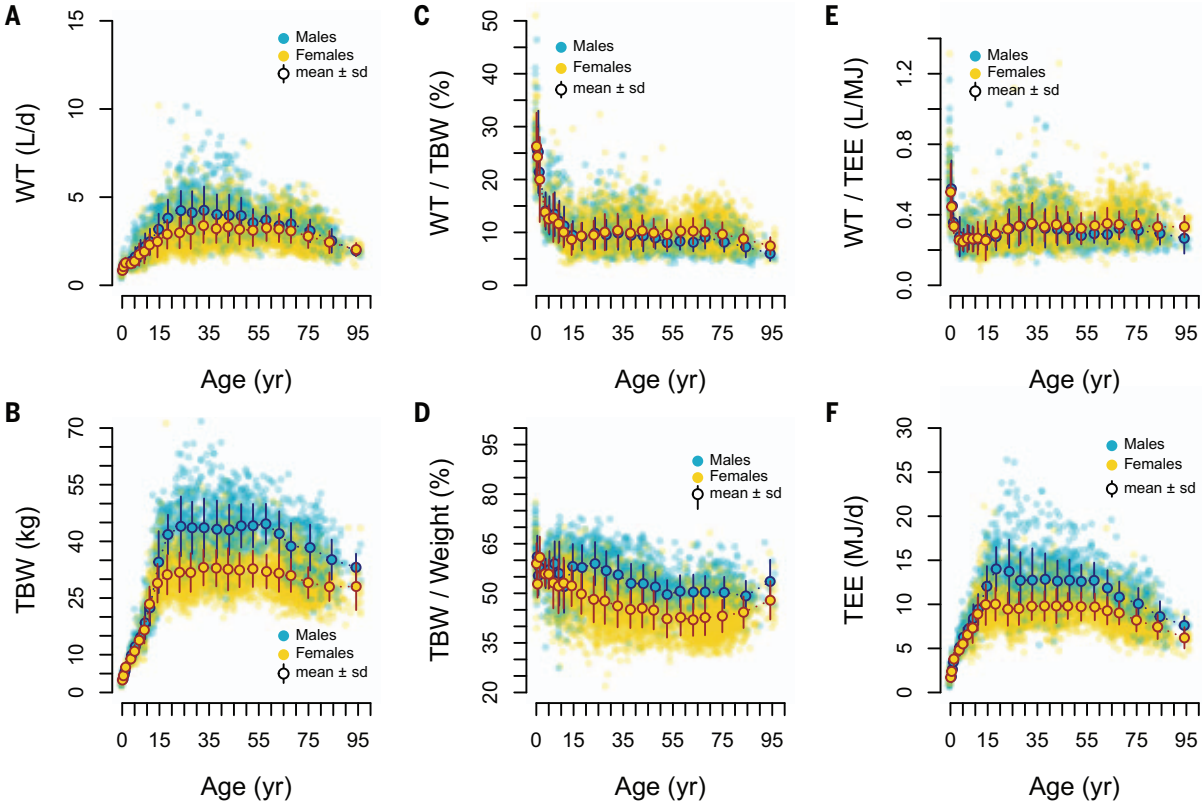

Fig. 2. Relationships between age and TBW or WT. Shown are relationships between age and TBW or WT in 3729 females (orange) and 1875 males (blue) aged 0 to 96 years with mean and SD. (**A**) WT (liters/d). (**B**) TBW (kg). (**C**) WT per TBW (%). (**D**) TBW per body weight (%). (**E**) WT per TEE (liters/MJ). (**F**) TEE (MJ/d). WT increases with age until ~30 years and is higher in men (4.3 liters/d) than in women (3.4 liters/d). WT significantly decreases after 40 years in men and 65 years in women, reaching an average WT of 3.1 and 2.8 liters/d in men and women >70 years of age, respectively. The average WT rate as a percentage of TBW is a maximum of ~25% in neonates, decreases with development, and is ~15% in 5-year-old children. At puberty, WT falls to ~10% and remains constant until age 40 in men and age 65 in women, after which it decreases. The average WT per TEE is about 0.33 liters/MJ (~1.4 ml/kcal) in adults. Note that the variation in WT is incredibly large: The low end for men and women is ~1 to 1.5 liters/day and the upper end is ~6 liters/day; outliers lie in the 10 liters/d range. On average, water accounts for 60% of the body weight in infants, 50% in older adults, and only 42% in women at 60 years of age, reflecting a larger percent body fat.

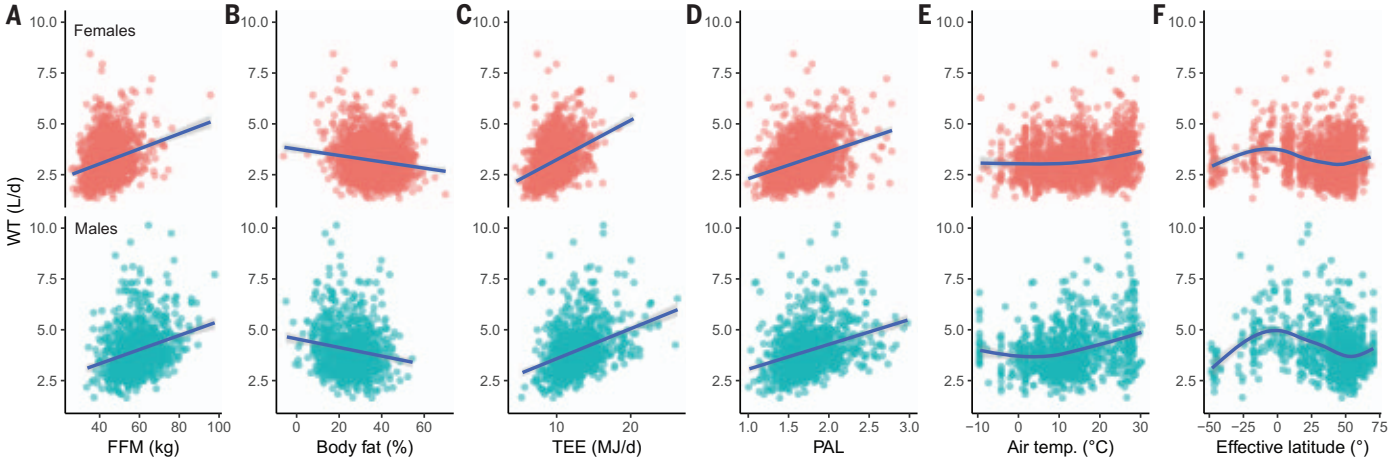

Fig. 3. Relationships between WT and body composition, TEE, physical activity, and environmental factors. Relationships between WT against FFM (**A**), percent body fat (**B**), TEE (**C**), PAL (**D**), air temperature (**E**), and effective latitude (**F**) in 1657 females (top panels; red) and 1013 males (bottom panels; blue) aged 20 to 60 years. The blue line represents generalized additive models with integrated smoothness. Pearson correlation analysis shows a positive correlations between WT and FFM (r = 0.442, P < 0.001), TEE (r = 0.488, P < 0.001), PAL (r = 0.388, P < 0.001), and altitude (r = 0.100, P < 0.001). WT was negatively correlated with percent body fat (−0.311, P < 0.001). Outdoor air temperature was only weakly correlated with WT in the whole sample (r = 0.160, P < 0.001). A significant curvilinear relationship between WT and the air temperature and between WT and effective latitude were observed (see text for details). Average WT reached the highest values at ~0° and the lowest values at ~−50° or +50° of effective latitude. People who lived near the Arctic Circle had higher average WT than those who lived around −50° or +50° of effective latitude.

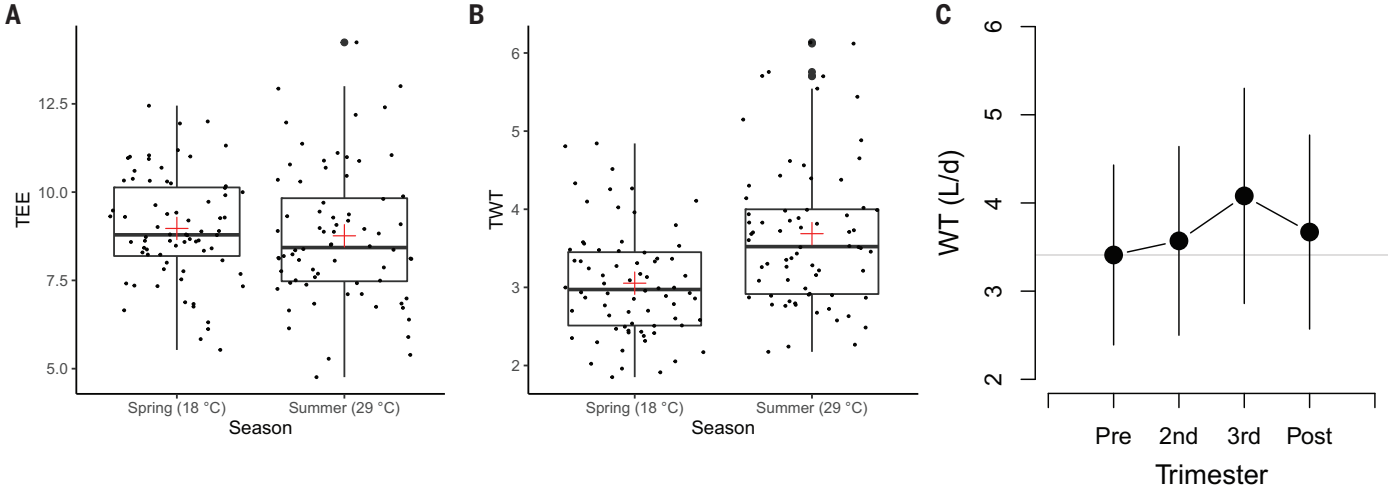

Fig. 4. Effect of season or pregnancy on WT. (**A**) Repeated-measures analysis of 72 people (31 females and 41 males) showing that WT was significantly higher in the summer (3.7 ± 1.0 liters/d), with an average temperature of 29°C, than in the spring (3.0 ± 0.7 liters/d), with an average temperature of 18°C (P < 0.001). (**B**) By contrast, TEE was not significantly different between summer and spring (P = 0.233). (**C**) Repeated-measures analysis of 63 pregnant women showing that the total WT was significantly higher during late pregnancy and lactation [data are from (*17*)]. Pre, pre-pregnancy; Post, 27 weeks postpartum.

positive coefficient of the second-order term of air temperature indicated a curvilinear relationship between WT and air temperature. The negative coefficient of the second-order term of age also indicated a curvilinear relationship between WT and age. A nonlinear increase of WT with increase of air temperature is predicted from the standard Scholander curve (*16*) for the impact of ambient temperature on metabolic rate and evaporative water loss. In an additional test of these relationships, repeated-measures analysis for 72 people in spring and summer indicated higher WT in the summer (mean air temperature of 29°C) than in the spring (mean air temperature of 18°C) (P < 0.001), whereas TEE did not differ seasonally (Fig. 4, A and B).

WT of pregnant and lactating women is of interest because pregnant women have higher TBW and FFM than do nonpregnant women (*17*), and lactating women also lose water through milk production (*11*). Repeated-measures analysis of 63 women indicated that WT increases in the third trimester of pregnancy (+670 ml/d) and during lactation (+260 ml/d) compared with prepregnancy (Fig. 4C) (*17*). The increase of WT during pregnancy is consistent with the increase in TBW.

The highest WTs in our sample are consistent with the effects of temperature, climate, physical activity, and body size. Nine of the 1875 males had WT >10 liters/d; of these, four were athletes, four were adult Shuar forager-horticulturalists of Amazonian Ecuador (*18*), and one was a Caucasian with a normal BMI but was measured in the summer with a maximal air temperature of 31.7°C. Thirteen of 3729 females had WT >7 liters/d; of these, five were athletes, two were pregnant women who had extremely high BMI (>45 kg/m^2) and were measured in the summer; three had high BMI (>30 kg/m^2) and two were measured in the summer; and three were measured in the summer with a maximal air temperature of >30°C.

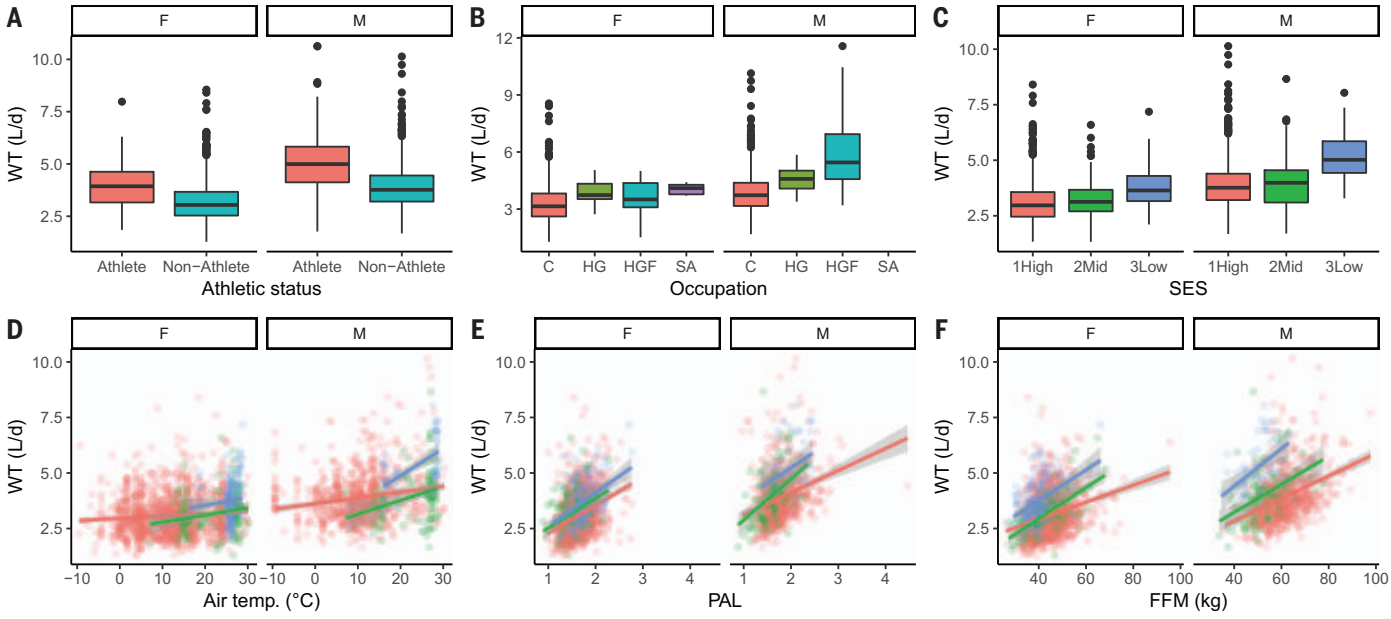

Fig. 5. Effect of lifestyle factors on WT. (**A**) Athletes had higher WT than nonathletes, even after adjusting for physiological and environmental variables ($P < 0.001$). (**B**) Hunter-gatherers (HG), mixed farmer and hunter-gatherers (HGF), and subsistence agriculturalists (SA) had higher WT than other people (C), even after adjusting for physiological and environmental variables ($P < 0.001$). Note that there are no males in the database who fell into the SA category. (**C**) People who lived in low-HDI countries had higher WT than people in high- or middle-HDI countries, even after adjusting for physiological and environmental variables ($P < 0.001$). (**D** to **F**) Relationship between WT and outdoor air temperature, PAL, and FFM. The countries were categorized as high-HDI (red), middle-HDI (green), and low-HDI (blue). (D) A significant interaction ($P < 0.001$) was observed between outdoor air temperature and HDI in WT. The association between outdoor air temperature and WT was weak in high-HDI countries ($r = 0.086$, $P < 0.001$) but strong in men in low-HDI countries ($r = 0.604$, $P < 0.001$). (E and F) A significant interaction ($P < 0.001$) was observed between HDI and PAL or FFM in WT. Correlation coefficients were significantly higher ($P < 0.001$) in low-HDI countries ($r = 0.484$ to 0.670, $P < 0.001$) than in high-HDI countries ($r = 0.367$ to 0.510, $P < 0.001$).

Fig. 6. Determinants of human WT. Objective measures of WT from a large global dataset indicate that WT is strongly related to anthropometric, lifestyle, and environmental factors.

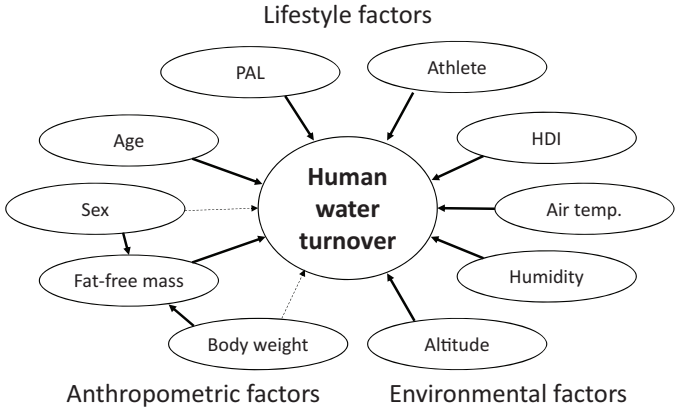

Lifestyle had clear effects on WT. Athletes had higher WT than nonathletes ($P < 0.001$; Fig. 5A and table S5). Hunter-gatherers, mixed farmers, and subsistence agriculturalists all had higher WT than those in industrialized economies ($P < 0.001$; Fig. 5B and table S6). People living in low-HDI countries had higher WT than those in middle- and high-HDI countries, even after adjustment for physiological and environmental variables ($P < 0.001$; Fig. 5C and table S7). The effects of body size, PAL, and air temperature were greater for people in low-HDI countries (Fig. 5, D to F). The smaller effects for these variables in high-HDI populations suggests that water needs are buffered against environmental influences through effective indoor climate control (e.g., air-conditioning). In high-HDI countries with access to air-conditioning and heating, people are exposed primarily to a narrow range of indoor temperatures (18 to 25°C) (*19*). By comparison, people living in low-HDI countries are more likely to be exposed to ambient environmental temperatures without climate control. This view is consistent with the greater size-adjusted WT for hunter-gatherers and manual laborers compared with sedentary adults in industrialized countries (*2*). Similarly, a previous comparison of regional water use (*20*) noted that it is relatively high in Africa and relatively low in Europe, and results from our analysis may help to explain why.

We developed the following equation to predict WT (Fig. 6):

$$\text{WT (ml/d)} = [1076 \times \text{PAL}] + [14.34 \times \text{body weight (kg)}] + [374.9 \times \text{sex}] + [5.823 \times \text{humidity (\%)}] + [1070 \times \text{athlete status}] + [104.6 \times \text{HDI}] + [0.4726 \times \text{altitude (m)}] - [0.3529 \times \text{age (years)}^2] + [24.78 \times \text{age (years)}] + [1.865 \times \text{temperature (°C)}^2] - [19.66 \times \text{temperature (°C)}] - 713.1 \quad (1)$$

where sex is 0 for female and 1 for male; athlete status is 0 for nonathlete and 1 for athlete; and HDI is 0 for high-HDI countries, 1 for middle-HDI countries, and 2 for low-HDI countries. This equation explains 47.1% of the variation in WT: An increase in PAL of 1.0 induces an ~1000-ml increase in WT; a 50-kg increase in body weight induces an ~700-ml increase in WT; a 50% increase in relative humidity induces an ~300-ml increase in WT; and a 1000-m increase in altitude induces an ~500-ml increase in WT. Males exhibit ~400 ml more WT than do females of the same weight because males have greater FFM and a lower percent body fat. People who live in low-HDI

countries exhibit ~200 ml more WT than people who live in high-HDI countries after controlling for the other measured variables. Athletes have ~1000 ml more WT than do nonathletes with everything else being equal. A U-shaped relationship between WT and air temperature shows ~1000 ml more WT at +30°C air temperature than the nadir between ±0 and +10°C air temperature, and also ~400 ml more WT at −10°C air temperature than that nadir. A curvilinear relationship between WT and age shows that the peak WT is between the 20s and 40s and decreases after the 50s; there is ~700 ml less WT at age 80 than at age 30.

A 20-year-old male weighing 70 kg who is not athletic, has a PAL of 1.75, and lives in a high-HDI country at 0-m altitude where the mean air temperature is 10°C and relative humidity is 50% has a predicted WT of 3.2 liters/d. A nonathletic 20-year-old female weighing 60 kg living at the same location will have a WT of 2.7 liters/d. By contrast, a 20-year-old male weighing 70 kg who is athletic, has a PAL of 2.5, and lives in a high-HDI country at 2000-m altitude where the mean air temperature is 30°C and relative humidity is 90% has a WT of 7.3 liters/d. An athletic 20-year-old female weighing 60 kg living at the same location will have a WT of 6.8 liters/d. In this equation, we used weight and sex as a proxy for FFM because body composition is not easily measured in the daily life. If body composition can be assessed, then the following equation can be used to predict WT (Fig. 6):

$$\begin{aligned}\text{WT (ml/d)} = {} & [861.9 \times \text{PAL}] + [37.34 \times \text{fat-free mass (kg)}] + [4.288 \times \text{humidity (\%)}] + \\ & [699.7 \times \text{athlete status}] + [105.0 \times \text{HDI}] + \\ & [0.5140 \times \text{altitude (m)}] - [0.3625 \times \text{age (years)}^2] + [29.42 \times \text{age (years)}] + \\ & [1.937 \times \text{temperature (°C)}^2] - \\ & [23.15 \times \text{temperature (°C)}] - 984.8 \quad (2)\end{aligned}$$

TEE was not included in the equations because sex, body weight, and PAL capture the variance explained by TEE. When FFM was included in the model, the effect of sex was not significant. The sex difference of WT can be explained by the sex difference of the FFM/body weight ratio.

Values of WT in this study represented average values under normal conditions. Many health conditions, including parasitic infections and diarrhea, affect water loss and intake (*21*). Additionally, the current study did not assess any indicators of hydration status and did not determine whether the participants were adequately hydrated. Older adults or vulnerable individuals have a higher risk of both acute and chronic dehydration (*22*, *23*) because they have a decreased thirst response. Medications, anorexia, or frailty and low TBW (storage) are associated with a lower skeletal muscle mass (i.e., sarcopenia). Skeletal muscle tissues contain a large volume of water, particularly in the intracellular space (*24*). Mean WT values presented here are not necessarily representative of all people or conditions (*21*) but do provide a comparative framework for investigating water intakes in populations with greater needs.

Objective measures of WT from a large global dataset indicate that it is strongly related to anthropometric, lifestyle, and environmental factors. We found significant correlations between WT and several known markers of health, wellness, and disease risks. WT is positively correlated with FFM, TEE, PAL, and athletic status and negatively correlated with percent body fat and age in adults. WT may therefore provide a useful integrative biomarker of metabolic health. Biomarkers that capture global metabolic health are generally lacking and of potentially enormous value for public health and medical management.

As shown in Fig. 1, we need to be aware that WT obtained by the hydrogen isotope dilution and elimination technique is not equal to daily water intake from liquids and foods. Metabolic water accounts for ~10% of WT, and respiratory water uptake and transcutaneous water uptake each account for 2 to 3% of WT. Therefore, daily water intake from liquids and foods is equivalent to ~85% of WT (*7*). An unsolved question is what percentage of water intake comes from food? Self-reported surveys around the world have suggested that 20 to 50% of daily water intake is from food (*5*, *6*, *11*). These estimates, however, are questionable because many studies using self-reported surveys underestimate energy, protein, and salt intake. Therefore, dietary survey methods probably also underestimate the water intake in food and overestimate that from drinking water and other beverages. Conversely, if people consume a higher-energy-density diet with lower water content (*25*, *26*), then they may need more water from drinks and beverages. Without measured water intakes from food, it was not possible to assess the relative contributions of food and drinking water or beverages to WT in this study, and indeed no studies to date have adequately addressed this issue. Nonetheless, the current study clearly indicates that one size does not fit all for drinking water guidelines, and the common suggestion that we should drink eight 8-ounce glasses of water per day (~2 liters) is not backed up by objective evidence.

We provide equations to predict human WT using environmental, lifestyle, and anthropometric factors guided by a large dataset. Improved guidelines are of increasing importance because of the explosive population growth and climate change the world currently faces, which will affect the availability of water for human consumption (*27*, *28*) and noningestive uses such as irrigation, cooling, and manufacturing (*29*). Presently, 2.2 billion people lack access to safe drinking water (*30*). The WT measures provided here can help to shape strategies for drinking water and water-enriched food management as the global population increases and the climate changes.

REFERENCES AND NOTES

1. B. M. Popkin, K. E. D'Anci, I. H. Rosenberg, *Nutr. Rev.* **68**, 439–458 (2010).
2. H. Pontzer *et al.*, *Curr. Biol.* **31**, 1804–1810.e5 (2021).
3. T. Morimoto, T. Itoh, *J. Basic Clin. Physiol. Pharmacol.* **9**, 51–72 (1998).
4. C. A. Zimmerman *et al.*, *Nature* **537**, 680–684 (2016).
5. A. Rosinger, S. Tanner, *Public Health Nutr.* **18**, 1098–1108 (2015).
6. Y. Tani *et al.*, *Eur. J. Clin. Nutr.* **69**, 907–913 (2015).
7. A. Raman *et al.*, *Am. J. Physiol. Renal Physiol.* **286**, F394–F401 (2004).
8. R. J. Johnson *et al.*, *J. Am. Soc. Nephrol.* **27**, 2247–2256 (2016).
9. J. Glaser *et al.*, *Clin. J. Am. Soc. Nephrol.* **11**, 1472–1483 (2016).
10. P. H. Gleick, *Science* **354**, 555–556 (2016).
11. Food and Nutrition Board, Institute of Medicine, "Dietary reference intakes for water, potassium, sodium, chloride, and sulfate" (National Academies Press, 2005); https://nap.nationalacademies.org/read/10925/chapter/1.
12. International Atomic Energy Agency, "Assessment of body composition and total energy expenditure in humans using stable isotope techniques, IAEA human health series no. 3" (IAEA, 2009); https://www.iaea.org/publications/7982/assessment-of-body-composition-and-total-energy-expenditure-in-humans-using-stable-isotope-techniques.
13. J. R. Speakman *et al.*, *Cell Rep. Med.* **2**, 100203 (2021).
14. H. Pontzer *et al.*, *Science* **373**, 808–812 (2021).
15. K. R. Westerterp, G. Plasqui, A. H. Goris, *Br. J. Nutr.* **93**, 199–203 (2005).
16. P. F. Scholander, R. Hock, V. Walters, F. Johnson, L. Irving, *Biol. Bull.* **99**, 237–258 (1950).
17. N. F. Butte, W. W. Wong, M. S. Treuth, K. J. Ellis, E. O'Brian Smith, *Am. J. Clin. Nutr.* **79**, 1078–1087 (2004).
18. L. Christopher *et al*, *Am. J. Hum. Biol.*e23223 (2019).
19. X. Zhang *et al.*, *iScience* **25**, 104682 (2022).
20. S. Pande, A. Pandit, *Palgrave Commun.* **4**, 85 (2018).
21. A. Y. Rosinger, *Am. J. Hum. Biol.* **32**, e23338 (2020).
22. A. M. El-Sharkawy *et al.*, *Age Ageing* **44**, 943–947 (2015).
23. R. J. Maughan, *Nutr. Rev.* **70** (Suppl 2), S152–S155 (2012).
24. Y. Yamada *et al.*, *J. Gerontol. A Biol. Sci. Med. Sci.* **65**, 510–516 (2010).
25. A. Drewnowski, *Nutr. Rev.* **56**, 347–353 (1998).
26. J. H. Ledikwe *et al.*, *Am. J. Clin. Nutr.* **83**, 1362–1368 (2006).
27. UNESCO World Water Assessment Programme, "United Nations world water development report 2020: Water and climate change" (UNESCO, 2020); https://en.unesco.org/themes/water-security/wwap/wwdr/2020.
28. G. Woodward, D. M. Perkins, L. E. Brown, *Philos. Trans. R. Soc. Lond. B Biol. Sci.* **365**, 2093–2106 (2010).
29. F. Jaramillo, G. Destouni, *Science* **350**, 1248–1251 (2015).
30. Department of Economic and Social Affairs, United Nations, "Sustainable development goals report 2019" (United Nations, 2019); https://www.un.org/en/desa/sustainable-development-goals-report-2019.

ACKNOWLEDGMENTS

We thank the International Atomic Energy Agency (IAEA), Taiyo Nippon Sanso, and SERCON for their support and T. Oono for his tremendous efforts at fundraising on our behalf. Y.Y., T.Y., and M.M. thank K. Abe for his support. Y.Y. and M.K. would like to pay gratitude and respect to their mentor, T. Morimoto, an emeritus professor of the Department of Physiology, Kyoto Prefectural University of Medicine, who passed away in July 2019. **Funding:** The IAEA DLW Database is generously supported by the IAEA, Taiyo Nippon Sanso, and SERCON. The authors also gratefully acknowledge funding support for the database from the US National Science Foundation (grant BCS-1824466 to H.P.) and the Chinese Academy of Sciences (CAS grant 153E11KYSB20190045 to J.R.S.). The funders played no role in the content of this manuscript. **Conflict of interest:** Y.Y. has a patent pending that is partly related to this study. The remaining authors declare no competing interests. **Data availability:** All data used in these analyses are freely available on the IAEA DLW Database, which can be found at https://doubly-labelled-water-database.iaea.org/home or www.dlwdatabase.org. **Author contributions:** Y.Y., X.Y.Z., M.E.T.H., and J.R.S. compiled

and analyzed data. Y.Y., X.Y.Z., H.S., H.P., L.G.H., A.H.L., J.R., K.R.W., W.W.W., M.Y., and D.A.S. wrote and edited the manuscript. Y.Y., H.S., H.P., D.W., T.Y., M.K., P.A.N., L.F.A., L.J.S., L.A., I.B., K.B.A., E.E.B., S.B., A.G.B., C.V.C.B., P.B., M.S.B., N.F.B., S.G.C., G.L.C., J.A.C., R.C., S.K.D., L.R.D., S.E., U.E., S.E., T.F., B.W.F., A.H.G., M.G., C.H., A.E.H., M.B.H., S.M.H., N.J., A.M.J., P.K., K.P.K., W.E.K., W.K., R.F.K., E.V.L., W.R.L., N.L., C.K.M., A.C.M., E.P.M., J.C.M., J.P.M., M.L.N., T.A.N., R.M.O., K.H.P., Y.P.P., J.P.R., G.P., R.L.P., R.A.R., S.B.R., D.A.R., E.R., L.M.R., J.J.R., R.M.R., S.B.R., X.Y.Z., A.J.S., L.B.S., A.M.Si., A.M.Sj., E.S., S.S.U., G.V., L.M.V.E., E.A.V.M., J.C.K.W., G.W., J.A.Y., J.R., K.R.W., W.W.W., M.Y., D.A.S., and J.R.S. contributed DLW data to the database. H.P. and J.R.S. fundraised for the database. Y.Y., H.S., H.P., C.H., A.J.M.-A., C.U., A.M.L., J.R., M.M., K.R.W., W.W.W., M.Y., D.A.S., and J.R.S. provided database administration work.

SUPPLEMENTARY MATERIALS

science.org/doi/10.1126/science.abm8668

Submitted 18 October 2021; accepted 31 October 2022
10.1126/science.abm8668

DRYLAND ECOLOGY

Grazing and ecosystem service delivery in global drylands

Fernando T. Maestre[1,2]*, Yoann Le Bagousse-Pinguet[3], Manuel Delgado-Baquerizo[4,5], David J. Eldridge[6], Hugo Saiz[7,8], Miguel Berdugo[9,10], Beatriz Gozalo[1], Victoria Ochoa[1,11], Emilio Guirado[1], Miguel García-Gómez[12], Enrique Valencia[13,14], Juan J. Gaitán[15,16,17], Sergio Asensio[1], Betty J. Mendoza[13], César Plaza[11], Paloma Díaz-Martínez[11], Ana Rey[18], Hang-Wei Hu[19,20], Ji-Zheng He[19,20], Jun-Tao Wang[21,22,23], Anika Lehmann[24,25], Matthias C. Rillig[24,25], Simone Cesarz[26,27], Nico Eisenhauer[26,27], Jaime Martínez-Valderrama[1], Eduardo Moreno-Jiménez[28], Osvaldo Sala[29,30,31], Mehdi Abedi[32], Negar Ahmadian[32], Concepción L. Alados[33], Valeria Aramayo[34], Fateh Amghar[35], Tulio Arredondo[36], Rodrigo J. Ahumada[37], Khadijeh Bahalkeh[32], Farah Ben Salem[38], Niels Blaum[39], Bazartseren Boldgiv[40], Matthew A. Bowker[41,42], Donaldo Bran[34], Chongfeng Bu[43,44], Rafaella Canessa[45,46], Andrea P. Castillo-Monroy[47], Helena Castro[48], Ignacio Castro[49], Patricio Castro-Quezada[50], Roukaya Chibani[38], Abel A. Conceição[51], Courtney M. Currier[29,31], Anthony Darrouzet-Nardi[52], Balázs Deák[53], David A. Donoso[47,54], Andrew J. Dougill[55], Jorge Durán[48,56], Batdelger Erdenetsetseg[40], Carlos I. Espinosa[57], Alex Fajardo[58], Mohammad Farzam[59], Daniela Ferrante[60,61], Anke S. K. Frank[62,63,64], Lauchlan H. Fraser[65], Laureano A. Gherardi[66], Aaron C. Greenville[63], Carlos A. Guerra[26,67], Elizabeth Gusmán-Montalvan[57], Rosa M. Hernández-Hernández[49], Norbert Hölzel[68], Elisabeth Huber-Sannwald[36], Frederic M. Hughes[51,69], Oswaldo Jadán-Maza[50], Florian Jeltsch[25,39], Anke Jentsch[70], Kudzai F. Kaseke[71], Melanie Köbel[72], Jessica E. Koopman[73], Cintia V. Leder[17,74], Anja Linstädter[64,75], Peter C. le Roux[76], Xinkai Li[43,44], Pierre Liancourt[46,77,78], Jushan Liu[79], Michelle A. Louw[76], Gillian Maggs-Kölling[80], Thulani P. Makhalanyane[73], Oumarou Malam Issa[81], Antonio J. Manzaneda[82,83], Eugene Marais[80], Juan P. Mora[58], Gerardo Moreno[84], Seth M. Munson[85], Alice Nunes[72], Gabriel Oliva[60,61], Gastón R. Oñatibia[86], Guadalupe Peter[17,74], Marco O. D. Pivari[87], Yolanda Pueyo[33], R. Emiliano Quiroga[37,88], Soroor Rahmanian[59,89], Sasha C. Reed[90], Pedro J. Rey[82,83], Benoit Richard[91], Alexandra Rodríguez[48], Víctor Rolo[84], Juan G. Rubalcaba[92], Jan C. Ruppert[46], Ayman Salah[93], Max A. Schuchardt[70], Sedona Spann[41], Ilan Stavi[94], Colton R. A. Stephens[65], Anthony M. Swemmer[95], Alberto L. Teixido[96], Andrew D. Thomas[97], Heather L. Throop[98,99], Katja Tielbörger[46], Samantha Travers[100], James Val[101], Orsolya Valkó[53], Liesbeth van den Brink[46], Sergio Velasco Ayuso[86], Frederike Velbert[68], Wanyoike Wamiti[102], Deli Wang[79], Lixin Wang[103], Glenda M. Wardle[63], Laura Yahdjian[86], Eli Zaady[104], Yuanming Zhang[105], Xiaobing Zhou[105], Brajesh K. Singh[21,22], Nicolas Gross[106]

Grazing represents the most extensive use of land worldwide. Yet its impacts on ecosystem services remain uncertain because pervasive interactions between grazing pressure, climate, soil properties, and biodiversity may occur but have never been addressed simultaneously. Using a standardized survey at 98 sites across six continents, we show that interactions between grazing pressure, climate, soil, and biodiversity are critical to explain the delivery of fundamental ecosystem services across drylands worldwide. Increasing grazing pressure reduced ecosystem service delivery in warmer and species-poor drylands, whereas positive effects of grazing were observed in colder and species-rich areas. Considering interactions between grazing and local abiotic and biotic factors is key for understanding the fate of dryland ecosystems under climate change and increasing human pressure.

Grazing accounts for 77% of global agricultural land (*1*), sustains billions of people worldwide, and is closely linked to 10 of 17 United Nations (UN) Sustainable Development Goals (*2*). Despite its importance, there is no consensus on how grazing affects ecosystem services (*3*–*6*), which may depend on the coevolutionary history between vegetation and herbivores (*3*), grazing pressure (*4*), and local climatic, edaphic, and biodiversity conditions (*7*, *8*). Most field assessments have focused on local to regional scales (*3*, *4*, *6*, *8*), have studied a limited number of taxa—mostly plants—and single ecosystem services (*3*, *4*, *9*), and have not considered domestic and wild herbivores simultaneously. Another major source of uncertainty relates to interactions between grazing pressure and abiotic and biotic features, which results in strong context-dependent ecological impacts of grazing (*3*, *4*, *10*, *11*). Large-scale, standardized field surveys that explore how such impacts depend on above- and belowground biodiversity, soils, and climate to drive multiple ecosystem services across contrasting regions and environmental contexts are lacking at present but are sorely needed to evaluate whether general patterns emerge beyond these context dependencies (*12*).

Investigating the effects of grazing pressure across global abiotic and biotic gradients is particularly important in drylands [areas with an aridity index (precipitation divided by potential evapotranspiration) <0.65 (*13*)] because they constitute 78% of rangelands worldwide (*14*) and support ~1 billion people who rely on grazing by livestock as a critical source of protein and income (*15*). Although grazing may have beneficial effects by reducing fuel loads and enhancing primary production and plant diversity under certain conditions (*3*, *16*), increasing grazing pressure is also considered a major driver of rangeland degradation and desertification across drylands worldwide (*17*). These contrasting effects of grazing likely depend on local climate, soil conditions, and both plant and soil diversity, which largely influence dryland functioning (*18*, *19*). However, the interactions of these factors with grazing pressure have never, to our knowledge, been assessed. Identifying environmental conditions and biodiversity levels under which increasing grazing pressure will favor or detract ecosystem service delivery is a crucial step toward achieving multiple UN Sustainable Development Goals (*2*) and other international initiatives related to dryland desertification and restoration (*20*).

Here, we used a standardized field survey (*13*) carried out at 98 sites across 25 countries and six continents (Fig. 1 and movie S1) to assess how the effects of grazing pressure on nine essential ecosystem services depend on biodiversity, climate, and soil conditions across global drylands. Each site included a collection

of three or four 45-m–by–45-m plots representing local gradients of grazing pressure [from ungrazed or low grazing pressure to high grazing pressure (*13*)], resulting in a total of 326 plots. These gradients were mostly driven by livestock (fig. S1), although wild herbivores were also present in each site and taken into account. In each plot, we assessed vascular plant, mammalian herbivore (accounting for domestic and wild herbivores), and belowground (soil bacteria, fungi, protists, and invertebrates) diversity as well as multiple regulating (water regulation, soil carbon storage, organic matter decomposition, and erosion control), supporting (soil fertility and aboveground plant biomass and its temporal stability), and provisioning (wood quantity, forage quantity, and quality) ecosystem services (table S1). Our survey captured most climatic conditions supporting livestock grazing in drylands, as well as a wide range of ecosystem types; soil properties; plant, soil, and mammalian diversities; and grazing pressure levels (figs. S2 to S9 and table S2). These distinctive features of our global study rendered grazing pressure largely independent of climate, soil, and biodiversity attributes [table S3 and (*13*)] and allowed us to (i) evaluate the main and interactive effects of grazing pressure, climate, soil properties, and biodiversity on ecosystem service delivery across global drylands; (ii) identify the environmental and biodiversity conditions under which the effects of grazing pressure on ecosystem services are positive or negative; and (iii) simultaneously assess relationships between plant, soil, and mammalian herbivore diversity and multiple ecosystem services.

We fitted linear mixed models to data from all sites and grazing pressure levels and applied a multimodel inference procedure based on Akaike information criterion (AIC) to select the set of best-fitting models [i.e., those with a ΔAIC <2 (*13*)]. We also considered potential indirect effects of grazing through the modification

[1]Instituto Multidisciplinar para el Estudio del Medio "Ramón Margalef," Universidad de Alicante, Alicante, Spain. [2]Departamento de Ecología, Universidad de Alicante, Alicante, Spain. [3]Aix Marseille Univ, CNRS, Avignon Université, IRD, IMBE, Aix-en-Provence, France. [4]Laboratorio de Biodiversidad y Funcionamiento Ecosistémico, Instituto de Recursos Naturales y Agrobiología de Sevilla (IRNAS), CSIC, Sevilla, Spain. [5]Unidad Asociada CSIC-UPO (BioFun), Universidad Pablo de Olavide, Sevilla, Spain. [6]Department of Planning and Environment, c/o Centre for Ecosystem Science, School of Biological, Earth and Environmental Sciences, University of New South Wales, Sydney, New South Wales, Australia. [7]Departamento de Ciencias Agrarias y Medio Natural, Escuela Politécnica Superior, Instituto Universitario de Investigación en Ciencias Ambientales de Aragón (IUCA), Universidad de Zaragoza, Huesca, Spain. [8]Institute of Plant Sciences, University of Bern, Bern, Switzerland. [9]Institut de Biología Evolutiva (UPF-CSIC), Barcelona, Spain. [10]Department of Environmental Systems Science, ETH Zurich, Zurich, Switzerland. [11]Instituto de Ciencias Agrarias, Consejo Superior de Investigaciones Científicas, Madrid, Spain. [12]Departamento de Ingeniería y Morfología del Terreno, Escuela Técnica Superior de Ingenieros de Caminos, Canales y Puertos, Universidad Politécnica de Madrid, Madrid, Spain. [13]Departamento de Biología y Geología, Física y Química Inorgánica, Universidad Rey Juan Carlos, Móstoles, Spain. [14]Departamento de Biodiversidad, Ecología y Evolución, Facultad de Ciencias Biológicas, Universidad Complutense de Madrid, Madrid, Spain. [15]Instituto Nacional de Tecnología Agropecuaria (INTA), Instituto de Suelos-CNIA, Buenos Aires, Argentina. [16]Universidad Nacional de Luján, Departamento de Tecnología, Luján, Argentina. [17]Consejo Nacional de Investigaciones Científicas y Técnicas de Argentina (CONICET), Buenos Aires, Argentina. [18]Museo Nacional de Ciencias Naturales, Consejo Superior de Investigaciones Científicas, Madrid, Spain. [19]Key Laboratory for Humid Subtropical Eco-geographical Processes of the Ministry of Education, School of Geographical Science, Fujian Normal University, Fuzhou, China. [20]Faculty of Veterinary and Agricultural Sciences, The University of Melbourne, Melbourne, Victoria, Australia. [21]Global Centre for Land-Based Innovation, Western Sydney University, Sydney, New South Wales, Australia. [22]Hawkesbury Institute for the Environment, Western Sydney University, Sydney, New South Wales, Australia. [23]State Key Laboratory of Urban and Regional Ecology, Research Center for Eco-Environmental Sciences, Chinese Academy of Sciences, Beijing, China. [24]Freie Universität Berlin, Institute of Biology, Berlin, Germany. [25]Berlin-Brandenburg Institute of Advanced Biodiversity Research (BBIB), Berlin, Germany. [26]German Centre for Integrative Biodiversity Research (iDiv) Halle-Jena-Leipzig, Leipzig, Germany. [27]Leipzig University, Institute of Biology, Leipzig, Germany. [28]Department of Agricultural and Food Chemistry, Faculty of Sciences, Universidad Autónoma de Madrid, Madrid, Spain. [29]School of Life Sciences, Arizona State University, Tempe, AZ, USA. [30]School of Sustainability, Arizona State University, Tempe, AZ, USA. [31]Global Drylands Center, Arizona State University, Tempe, AZ, USA. [32]Department of Range Management, Faculty of Natural Resources and Marine Sciences, Tarbiat Modares University, Noor, Mazandaran Province, Iran. [33]Instituto Pirenaico de Ecología (IPE, CSIC), Zaragoza, Spain. [34]Instituto Nacional de Tecnología Agropecuaria (INTA), Estación Experimental Agropecuaria Bariloche, Bariloche, Río Negro, Argentina. [35]Laboratoire de Recherche: Biodiversité, Biotechnologie, Environnement et Développement Durable (BioDev), Faculté des Sciences, Université M'hamed Bougara de Boumerdès, Boumerdès, Algérie. [36]Instituto Potosino de Investigación Científica y Tecnológica, A.C., San Luis Potosí, Mexico. [37]Instituto Nacional de Tecnología Agropecuaria, Estación Experimental Agropecuaria Catamarca, Catamarca, Argentina. [38]Laboratory of Range Ecology, Institut des Régions Arides (IRA), Médenine, Tunisia. [39]University of Potsdam, Plant Ecology and Conservation Biology, Potsdam, Germany. [40]Laboratory of Ecological and Evolutionary Synthesis, Department of Biology, School of Arts and Sciences, National University of Mongolia, Ulaanbaatar, Mongolia. [41]School of Forestry, Northern Arizona University, Flagstaff, AZ, USA. [42]Center for Ecosystem Science and Society, Northern Arizona University, Flagstaff, AZ, USA. [43]Institute of Soil and Water Conservation, Northwest A&F University, Yangling, Shaanxi, China. [44]Institute of Soil and Water Conservation, Chinese Academy of Sciences and Ministry of Water Resources, Yangling, Shaanxi, China. [45]Ecological Plant Geography, Faculty of Geography, University of Marburg, Marburg, Germany. [46]Plant Ecology Group, University of Tübingen, Tübingen, Germany. [47]Departamento de Biología, Escuela Politécnica Nacional, Quito, Ecuador. [48]Centre for Functional Ecology, Department of Life Sciences, University of Coimbra, Coimbra, Portugal. [49]Universidad Nacional Experimental Simón Rodríguez (UNESR), Instituto de Estudios Científicos y Tecnológicos (IDECYT), Centro de Estudios de Agroecología Tropical (CEDAT), Miranda, Venezuela. [50]Universidad de Cuenca, Facultad de Ciencias Agropecuarias, Carrera de Ingeniería Agronómica, Grupo de Agroforestería, Manejo y Conservación del paisaje, Cuenca, Ecuador. [51]Universidade Estadual de Feira de Santana (UEFS), Departamento de Ciências Biológicas, Bahia, Brazil. [52]Department of Biological Sciences, University of Texas at El Paso, El Paso, TX, USA. [53]Lendület Seed Ecology Research Group, Institute of Ecology and Botany, Centre for Ecological Research, Vácrátót, Hungary. [54]Centro de Investigación de la Biodiversidad y Cambio Climático, Universidad Tecnológica Indoamérica, Quito, Ecuador. [55]Department of Environment and Geography, University of York, York, UK. [56]Misión Biológica de Galicia, CSIC, Pontevedra, Spain. [57]Departamento de Ciencias Biológicas, Universidad Técnica Particular de Loja, Loja, Ecuador. [58]Instituto de Investigación Interdisciplinaria (I^3), Vicerrectoría Académica, Universidad de Talca, Talca, Chile. [59]Department of Range and Watershed Management, Ferdowsi University of Mashhad, Mashhad, Iran. [60]Instituto Nacional de Tecnología Agropecuaria EEA Santa Cruz, Río Gallegos, Santa Cruz, Argentina. [61]Universidad Nacional de la Patagonia Austral, Río Gallegos, Santa Cruz, Argentina. [62]School of Agriculture, Environmental and Veterinary Sciences, Charles Sturt University, Port Macquarie, New South Wales, Australia. [63]Desert Ecology Research Group, School of Life and Environmental Sciences, The University of Sydney, Sydney, New South Wales, Australia. [64]Institute of Crop Science and Resource Conservation, University of Bonn, Bonn, Germany. [65]Department of Natural Resource Science, Thompson Rivers University, Kamloops, British Columbia, Canada. [66]Department of Environmental Science, Policy and Management, University of California, Berkeley, Berkeley, CA, USA. [67]Institute of Biology, Martin-Luther University Halle Wittenberg, Halle (Saale), Germany. [68]Institute of Landscape Ecology, University of Münster, Münster, Germany. [69]Instituto Nacional da Mata Atlântica (INMA), Espírito Santo, Brazil. [70]Department of Disturbance Ecology, Bayreuth Center of Ecology and Environmental Research BayCEER, University of Bayreuth, Bayreuth, Germany. [71]Earth Research Institute, University of California, Santa Barbara, Santa Barbara, CA, USA. [72]Centre for Ecology, Evolution and Environmental Changes, Faculdade de Ciências, Universidade de Lisboa, Lisboa, Portugal. [73]Microbiome@UP, Department of Biochemistry, Genetics and Microbiology, University of Pretoria, Pretoria, South Africa. [74]Universidad Nacional de Río Negro, Sede Atlántica, CEANPa, Río Negro, Argentina. [75]Biodiversity Research/Systematic Botany Group, Institute of Biochemistry and Biology, University of Potsdam, Potsdam, Germany. [76]Department of Plant and Soil Sciences, University of Pretoria, Pretoria, South Africa. [77]Institute of Botany, Czech Academy of Sciences, Pruhonice, Czech Republic. [78]Botany Department, State Museum of Natural History Stuttgart, Stuttgart, Germany. [79]Key Laboratory of Vegetation Ecology of the Ministry of Education, Jilin Songnen Grassland Ecosystem National Observation and Research Station, Institute of Grassland Science, Northeast Normal University, Changchun, China. [80]Gobabeb-Namib Research Institute, Walvis Bay, Namibia. [81]Institut d'Écologie et des Sciences de l'Environnement de Paris (iEES-Paris), Sorbonne Université, IRD, CNRS, INRAE, Université Paris Est Creteil, Université de Paris, Centre IRD de France Nord, Bondy, France. [82]Instituto Interuniversitario de Investigación del Sistema Tierra en Andalucía, Universidad de Jaén, Jaén, Spain. [83]Departamento de Biología Animal, Biología Vegetal y Ecología, Universidad de Jaén, Jaén, Spain. [84]Forestry School, INDEHESA, Universidad de Extremadura, Plasencia, Spain. [85]US Geological Survey, Southwest Biological Science Center, Flagstaff, AZ, USA. [86]Cátedra de Ecología, Facultad de Agronomía, Universidad de Buenos Aires, Instituto de Investigaciones Fisiológicas y Ecológicas Vinculadas a la Agricultura (IFEVA-CONICET), Ciudad Autónoma de Buenos Aires, Argentina. [87]Departamento de Botânica, Universidade Federal de Minas Gerais, Minas Gerais, Brazil. [88]Cátedra de Manejo de Pastizales Naturales, Facultad de Ciencias Agrarias, Universidad Nacional de Catamarca, Catamarca, Argentina. [89]Department of Forest Engineering, Forest Management Planning and Terrestrial Measurements, Faculty of Silviculture and Forest Engineering, Transilvania University of Brasov, Brasov, Romania [90]US Geological Survey, Southwest Biological Science Center, Moab, UT, USA. [91]Normandie Univ, UNIROUEN, INRAE, ECODIV, Rouen, France. [92]Deparment of Biology, McGill University, Montreal, Quebec, Canada. [93]Al Quds University, Abu Dis, Palestine. [94]Dead Sea and Arava Science Center, Yotvata, Israel. [95]South African Environmental Observation Network (SAEON), Phalaborwa, Kruger National Park, South Africa. [96]Departamento de Botânica e Ecologia, Instituto de Biociências, Universidade Federal de Mato Grosso, Mato Grosso, Brazil. [97]Department of Geography and Earth Sciences, Aberystwyth University, Wales, UK. [98]School of Earth and Space Exploration, Arizona State University, Tempe, AZ, USA. [99]School of Life Sciences, Arizona State University, Tempe, AZ, USA. [100]Centre for Ecosystem Science, School of Biological, Earth and Environmental Sciences, University of New South Wales, Sydney, New South Wales, Australia. [101]Science Division, Department of Planning, Industry and Environment, New South Wales Government, Buronga, New South Wales, Australia. [102]Zoology Department, National Museums of Kenya, Nairobi, Kenya. [103]Department of Earth Sciences, Indiana University–Purdue University Indianapolis (IUPUI), Indianapolis, IN, USA. [104]Department of Natural Resources, Agricultural Research Organization, Institute of Plant Sciences, Gilat Research Center, Mobile Post Negev, Israel. [105]State Key Laboratory of Desert and Oasis Ecology, Xinjiang Institute of Ecology and Geography, Chinese Academy of Sciences, Urumqi, China. [106]Université Clermont Auvergne, INRAE, VetAgro Sup, Unité Mixte de Recherche Ecosystème Prairial, Clermont-Ferrand, France.
***Corresponding author. Email: ft.maestre@ua.es**

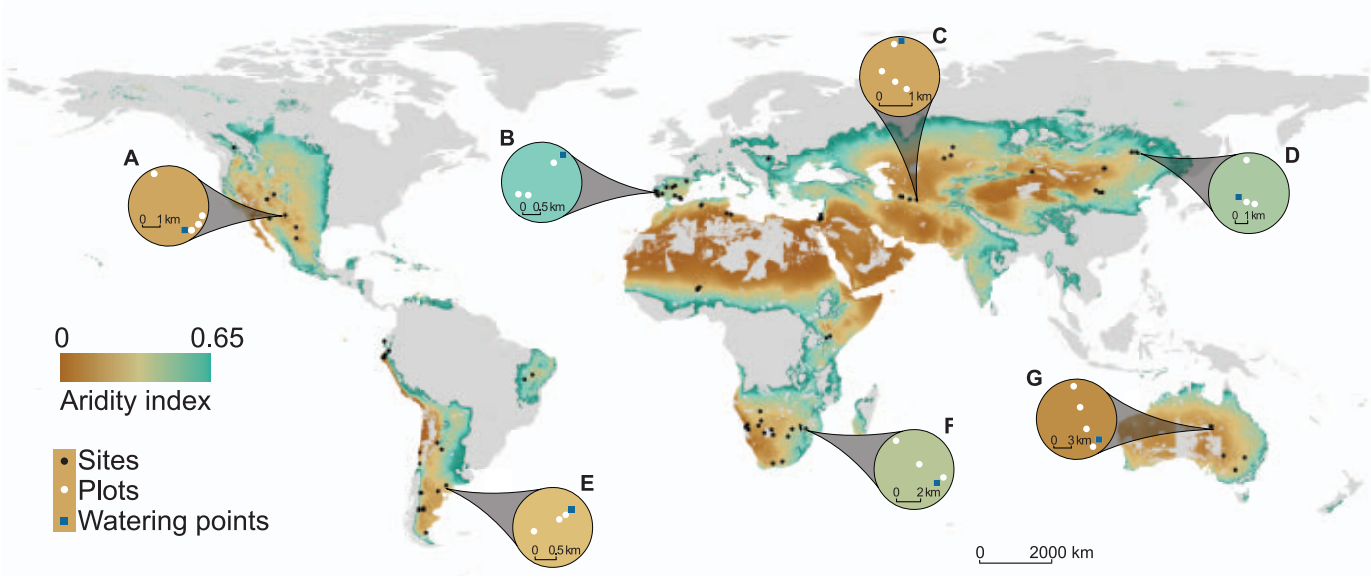

Fig. 1. Locations of the 98 study sites with examples of the local grazing gradients surveyed at each site. Each black dot represents a site with multiple 45-m–by–45-m plots (white dots) surveyed in situ; a total of 326 plots were surveyed across the 98 study sites. The inset graphics [(**A**) to (**G**)] highlight examples of the local gradients surveyed at each site. Watering points are ponds, impoundments, or drinking troughs that provide permanent sources of water for livestock in drylands; they were used in this study to create local grazing gradients (*13*). The background of the map indicates the extent of dryland rangeland areas. The aridity index is calculated as precipitation divided by potential evapotranspiration and is strongly related to mean annual precipitation in our dataset [coefficient of determination (R^2) = 0.82]. See (*13*) for the aridity index and rangeland area data sources that were used.

of local biodiversity and soil parameters using confirmatory path analyses (*13*). We found that increasing grazing pressure affects ecosystem services through direct effects (no significant indirect effects through changes in soil properties or biodiversity were found; figs. S10 and S11 and tables S4 to S12) and interactive effects (interactions between grazing and climate, grazing and soil properties, or grazing and biodiversity were selected in 86% of the best-fitting models; Fig. 2 and tables S13 to S28).

Interactions between grazing and climate were selected in 48% of the best-fitting models (fig. S12), with grazing primarily interacting with mean annual temperature (40% of the best-fitting models) and rainfall seasonality (20% of the best-fitting models) and, to a lesser extent, with mean annual precipitation (9% of the best-fitting models). A negative relationship between mean annual temperature and soil carbon storage, organic matter decomposition, and erosion control was found under high, but not under low, grazing pressure (Fig. 3, A to C). Our results provide an empirical validation of the importance of interactions between climate change drivers, grazing, and soil carbon storage that are predicted by global modeling studies (*21*). They also indicate that considering grazing pressure can improve our capacity to assess soil carbon–temperature feedbacks, a key process involved in climate warming (*22*).

Soil texture also regulated grazing pressure effects on multiple ecosystem services, which

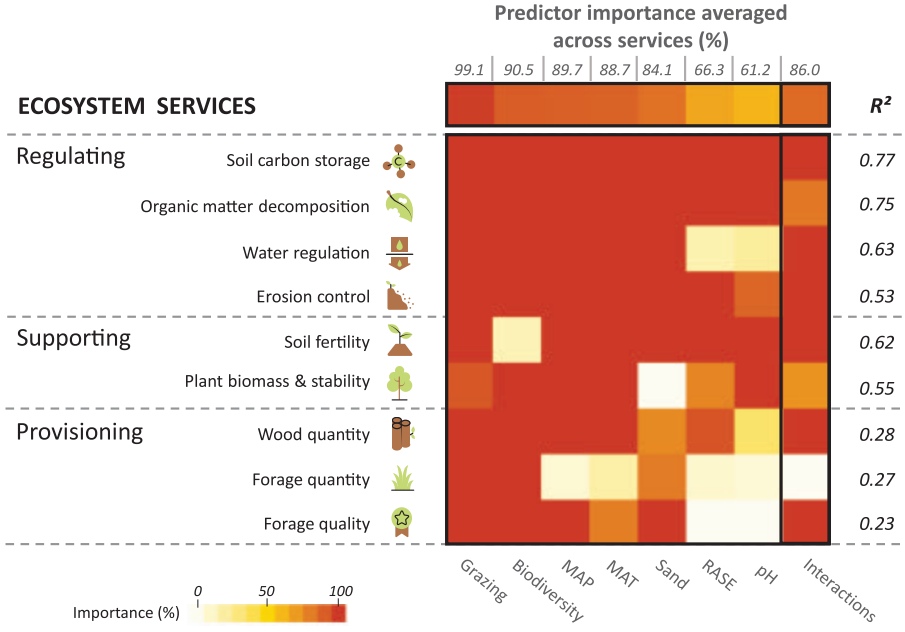

Fig. 2. Relative importance of predictors of ecosystem services selected in the best-fitting models. Importance is quantified as the sum of the Akaike weights of all models that included the predictor (grazing pressure, climate, biodiversity, and soil variables, and their interactions) of interest, considering the number of models in which each predictor appears. It is proportional to the number of times that a given predictor (and its interactions with other predictors) was selected in the final set of best-fitting models (*13*). Interactions include all interactions between grazing pressure and climate, biodiversity, and soil variables; the importance of each interaction type is shown in fig. S12. In the case of biodiversity, predictor importance considers the number of models that include at least one biodiversity proxy (plant species richness, mammalian herbivore richness, or belowground diversity). Separate results for each biodiversity proxy are shown in fig. S12. Full details on model results, including the number of best-fitting models, are available in tables S13 to S15. "Plant biomass and stability" represents aboveground plant biomass and its temporal stability, and "grazing" represents grazing pressure. MAT, mean annual temperature; RASE, rainfall seasonality; MAP, mean annual precipitation.

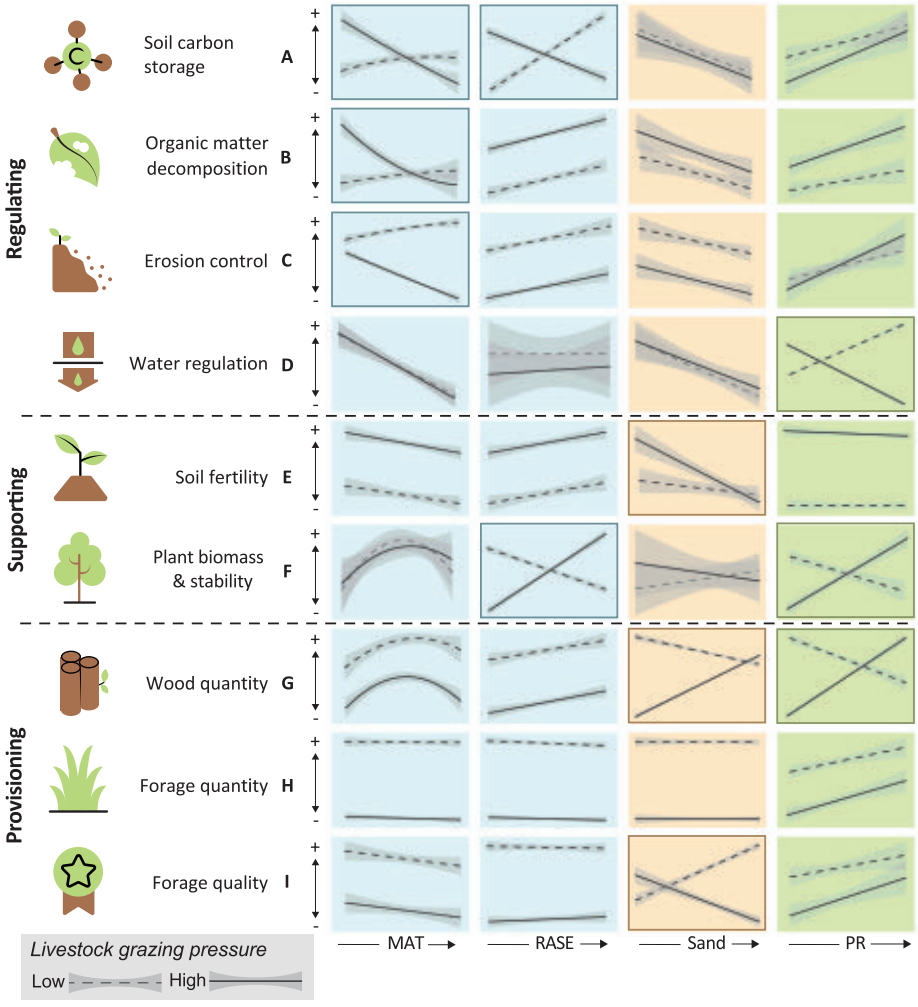

Fig. 3. Predicted responses of ecosystem services to changes in climate, sand content, and plant species richness at low and high grazing pressure levels. (**A** to **I**) Predicted responses of regulating [(A) to (D)], supporting [(E) and (F)], and provisioning [(G) to (I)] ecosystem services. The lines in each panel show model fits (using partial residuals) for each predictor selected in the final best-fitting models at low (dashed lines) and high (solid lines) grazing pressures for each service. Shading around each line represents the 95% confidence interval. Panels surrounded by a border denote significant interactions between grazing and other predictors. Predicted responses of ecosystem services to all grazing pressure levels (ungrazed, low, medium, and high) and to other model predictors are presented in figs. S13 to S15. The complete set of statistical results and model fits are available in tables S13 to S15. "Sand" represents sand content. PR, plant species richness.

include soil fertility, wood quantity, and forage quality (interactions between grazing and sand content were selected in 37% of the best-fitting models; fig. S12). As sand content increased, soil fertility declined more steeply under high grazing pressure (Fig. 3E), wood quantity increased under high but declined under low grazing pressure (Fig. 3G), and forage quality declined under high but increased under low grazing pressure (Fig. 3I). These findings illustrate how increases in grazing pressure interact with soil properties to either increase or reduce the delivery of multiple ecosystem services.

Biodiversity impacts on ecosystem functioning and services are typically examined in isolation from other drivers in experimental and observational studies (*23*). However, we found interactions between grazing and biodiversity in 44% of the best-fitting models (fig. S12). For instance, increasing grazing pressure shifted the relationships between plant species richness and water regulation from positive to negative (Fig. 3D) and those between plant species richness and both wood quantity and aboveground plant biomass and its temporal stability from negative to positive (Fig. 3, F and G). We also found positive relationships between plant species richness and soil carbon storage, organic matter decomposition, erosion control, and both forage quality and quantity (Fig. 3, A to C, H, and I) and between belowground diversity and organic matter decomposition (fig. S13), irrespective of grazing pressure. These results broaden and validate previous findings on the relationship between biodiversity and ecosystem functioning (*18*, *19*) and support arguments for conserving and restoring diverse plant communities to prevent land degradation, increase forage production, and mitigate climate change in grazed drylands (*20*).

Mammalian herbivore richness, which was selected in 33% of the best-fitting models (fig. S12), was positively related to multiple ecosystem services. Greater herbivore richness positively correlated with soil carbon storage regardless of grazing pressure (fig. S13), with aboveground plant biomass and its temporal stability under high grazing pressure (fig. S14), and with forage quality under low grazing pressure (fig. S15). Both domestic and wild herbivore species can exhibit strong feeding niche differences (*24*, *25*); thus, increasing their diversity can enhance ecosystem functioning (*25*). Despite a renewed interest in mixed-species grazing, studies have been conducted at only a handful of sites or with a limited suite of herbivores (*25*–*27*). Our findings provide empirical evidence of the potential benefits of increasing herbivore richness to enhance the delivery of key ecosystem services across contrasting environmental and biodiversity conditions. They also suggest that efforts to promote diverse grazing systems may enhance soil carbon storage and reduce negative impacts of increased grazing pressure. To date, such results have only been modeled or observed locally (*26*, *27*).

The multiple interactions we observed highlight that the effect of grazing pressure on ecosystem services can be positive or negative depending on local climate, soil, and biodiversity conditions (Fig. 4). On average, increasing grazing pressure had positive effects on ecosystem services in colder sites with high plant species richness but negative effects in warmer sites with high rainfall seasonality and low plant species richness (Fig. 4, E and I). When sets of ecosystem services were considered separately, responses to grazing pressure ranged from mostly neutral to positive (regulating and supporting services; Fig. 4, B and C) and from negative to neutral (provisioning services; Fig. 4D). These results allow us to identify ecological conditions under which ecosystem services are positively or negatively associated with changes in grazing pressure (Fig. 4 and figs. S16 to S18) and to frame new hypotheses that explore the local context dependencies of grazing impacts. For instance, we observed negative effects of increasing grazing pressure on ecosystem services in plant species–poor drylands, as reported in recent local-scale studies [e.g., (*11*)], whereas positive effects of grazing were mostly observed

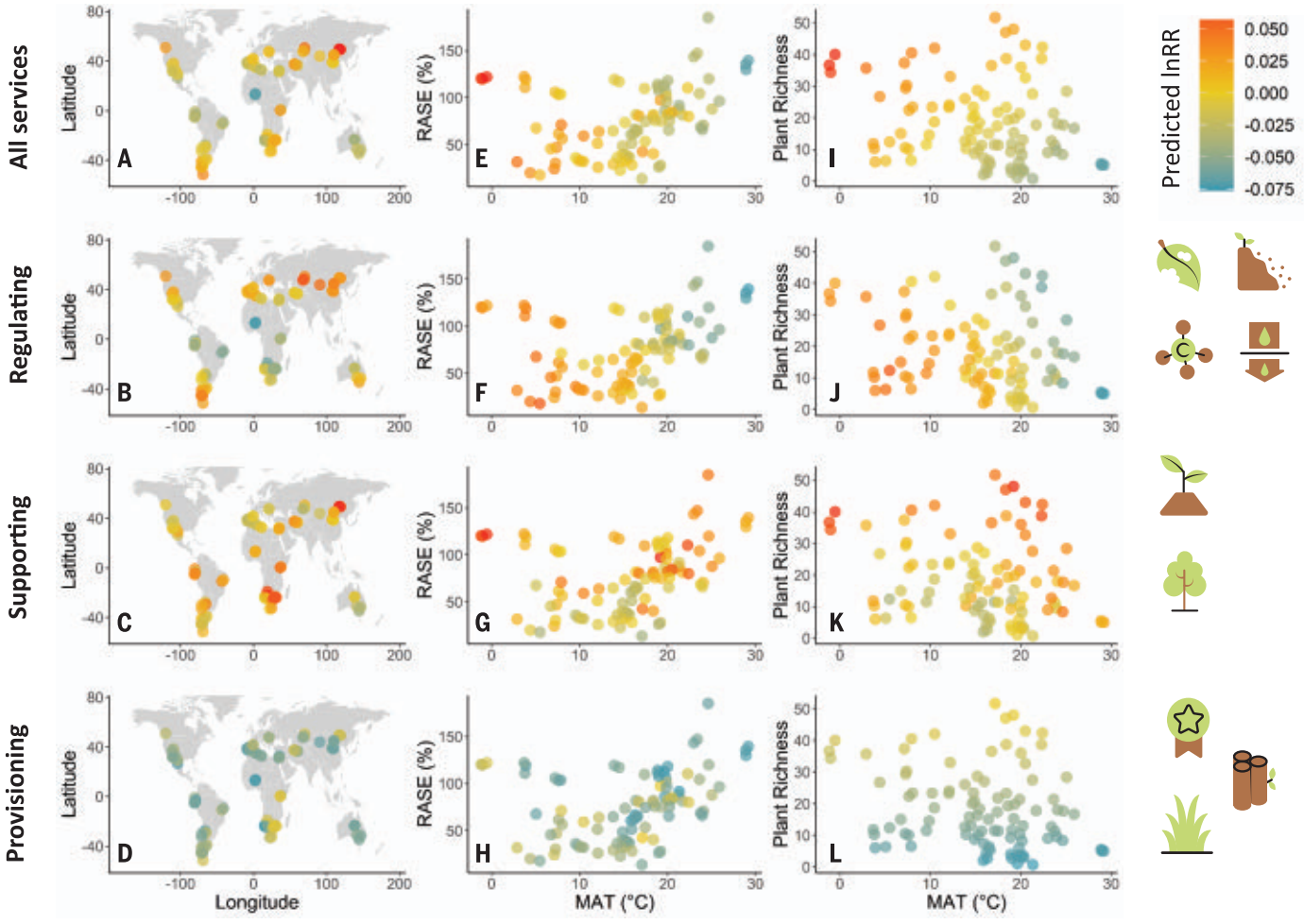

Fig. 4. Geographical variation in the effect of grazing pressure on ecosystem services across global drylands. (**A** to **L**) For each of the 98 sites surveyed, the effect of grazing pressure on ecosystem services predicted by model parameters is plotted along the wide climatic and plant species richness gradients that were evaluated. To do this, each ecosystem service at low and high grazing pressures was first predicted using predictor estimates of the best-fitting models (see tables S13 to S15). Then, the predicted effect of grazing at each site was calculated as the difference between high and low grazing pressure levels using a log response ratio (lnRR) (*13*). Predictions were made using plant species richness, mean annual temperature, and rainfall seasonality; all other parameters were fixed at their mean value (*13*). For simplicity, grazing effects were averaged across all ecosystem services [(A), (E), and (I)] and across regulating [(B), (F), and (J)], supporting [(C), (G), and (K)], and provisioning [(D), (H), and (L)] services. Blue and red dots indicate the most-negative and most-positive effects of grazing, respectively. See figs. S16 and S17 for detailed results on each service and Fig. 2 for the meaning of the symbols depicting each ecosystem service.

in species-rich drylands. Thus, protecting biodiversity in species-rich areas or restoring it in species-poor areas could minimize some of the negative effects of increasing grazing pressure on ecosystem service delivery (fig. S19).

The effects of increasing grazing pressure on ecosystem services were mostly negative in warmer drylands (Fig. 4 and fig. S17), where a large proportion of the human population relies heavily on livestock for subsistence (*15*). Limiting grazing pressure through livestock removal is neither socially nor economically feasible in these areas (*2*), yet they are expected to experience high warming rates and water shortages under most climate change scenarios (*17*). Our results thus suggest that grazing pressure may interact with climate change to reduce ecosystem service delivery in warmer drylands, with potentially devastating implications for the fate of these ecosystems [e.g., increased land degradation and desertification (*17*)] and their inhabitants [e.g., greater poverty, migration, and/or social unrest (*28*)]. Although dryland pastoralists have historically adopted strategies to cope with environmental uncertainty (e.g., nomadism, transhumance), benefits of these strategies will wane if livestock concentrates in particular areas as a result of resource scarcity or droughts (*29*).

Our findings underscore the importance of accounting for interactions between grazing and local abiotic and biotic factors when assessing ecosystem service delivery in drylands. They also illustrate those climate change and biodiversity loss drivers that are the most likely to interact with increases in grazing pressure. Understanding these drivers is critical to predict the fate of dryland ecosystems under increasing temperature, biodiversity loss, and demand for animal products. Our study also allowed us to overcome uncertainties in grazing assessments that arise from the use of unstandardized data (*30*) and provides abundant ground data to validate remote-sensing products that are used when mapping and modeling grazing impacts at the global scale (*5*). Finally, we deliver empirical evidence of the positive links between mammalian herbivore richness and the provision of multiple ecosystem services across contrasting environmental conditions, plant and soil diversities, and grazing pressure levels. Our work addresses a key knowledge gap that can lead to better management of drylands, the largest rangeland area on Earth.

REFERENCES AND NOTES

1. H. Ritchie, M. Roser, "Land use" (2013); https://ourworldindata.org/land-use.
2. Z. Mehrabi, M. Gill, M. van Wijk, M. Herrero, N. Ramankutty, *Nat. Food* **1**, 160–165 (2020).
3. D. G. Milchunas, W. K. Lauenroth, *Ecol. Monogr.* **63**, 327–366 (1993).
4. D. J. Eldridge, A. G. B. Poore, M. Ruiz-Colmenero, M. Letnic, S. Soliveres, *Ecol. Appl.* **26**, 1273–1283 (2016).
5. K. Petz *et al*., *Glob. Environ. Change* **29**, 223–234 (2014).
6. D. J. Eldridge, M. Delgado-Baquerizo, *Land Degrad. Dev.* **28**, 1473–1481 (2017).
7. J. A. Mavromihalis, J. Dorrough, S. G. Clark, V. Turner, C. Moxham, *Rangeland J.* **35**, 95–108 (2013).
8. J. J. Gaitán *et al*., *Land Degrad. Dev.* **29**, 210–218 (2018).
9. P. D'Ottavio *et al*., *Grass Forage Sci.* **73**, 15–25 (2018).
10. A. Linstädter *et al*., *PLOS ONE* **9**, e104672 (2014).
11. M. Liang, C. Liang, Y. Hautier, K. R. Wilcox, S. Wang, *Ecol. Lett.* **24**, 2054–2064 (2021).
12. P. Manzano *et al*., *One Earth* **4**, 651–665 (2021).
13. See materials and methods.
14. International Livestock Research Institute (ILRI) *et al*., *Rangelands Atlas* (ILRI, 2021).
15. United Nations Environment Management Group, *Global Drylands: A UN System-Wide Response* (United Nations, 2011).
16. S. E. Koerner *et al*., *Nat. Ecol. Evol.* **2**, 1925–1932 (2018).
17. A. Mirzabaev *et al*., in *Climate Change and Land: An IPCC Special Report on Climate Change, Desertification, Land Degradation, Sustainable Land Management, Food Security, and Greenhouse Gas Fluxes in Terrestrial Ecosystems*, *et al*., Eds. (Intergovernmental Panel on Climate Change, 2019), pp. 249–344.
18. F. T. Maestre *et al*., *Science* **335**, 214–218 (2012).
19. M. Delgado-Baquerizo *et al*., *Nat. Commun.* **7**, 10541 (2016).
20. N. M. Gadzama, *World J. Sci. Technol. Sustain. Dev.* **14**, 279–289 (2017).
21. J. Chang *et al*., *Nat. Commun.* **12**, 118 (2021).
22. P. García-Palacios *et al*., *Nat. Rev. Earth Environ.* **2**, 507–517 (2021).
23. J. E. Duffy, C. M. Godwin, B. J. Cardinale, *Nature* **549**, 261–264 (2017).
24. E. S. Forbes *et al*., *Funct. Ecol.* **33**, 1597–1610 (2019).
25. L. Wang *et al*., *Proc. Natl. Acad. Sci. U.S.A.* **116**, 6187–6192 (2019).
26. J. P. G. M. Cromsigt *et al*., *Philos. Trans. R. Soc. London Ser. B* **373**, 20170440 (2018).
27. N. Pettorelli, S. M. Durant, J. T. du Toit, Eds., *Rewilding* (Cambridge Univ. Press, 2019).
28. C. Almer, J. Laurent-Lucchetti, M. Oechslin, *J. Environ. Econ. Manage.* **86**, 193–209 (2017).
29. S. A. Mousavi, M. Sarshad Ghahfarokhi, S. Soltani Koupaei, *Ecol. Indic.* **110**, 105946 (2020).
30. T. Fetzel *et al*., *Global Biogeochem. Cycles* **31**, 1089–1102 (2017).
31. F. T. Maestre *et al*., Data and R code from "Grazing and ecosystem service delivery in global drylands," figshare (2022); https://doi.org/10.6084/m9.figshare.20131355.v1.
32. B. K. Singh, J.-T. Wang, M. Delgado-Baquerizo, F. T. Maestre, 16S and 18S data from "Grazing and ecosystem service delivery in global drylands," figshare (2022); https://doi.org/10.6084/m9.figshare.20131355.v1.

ACKNOWLEDGMENTS

We acknowledge S. Undrakhbold, M. Uuganbayar, B. Byambatsogt, S. Khaliun, S. Solongo, B. Batchuluun, M. Sloan, J. Spence, E. Geiger, I. Souza, R. Onoo, T. Araújo, M. Mabaso, P. M. Lunga, L. Eloff, P. Eloff, J. Sebei, J. Joordan, E. Mudongo, V. Mokoka, B. Mokhou, T. Maphanga, F. Hoffmann, R. Peters, A. Lozada, E. Vidal, F. Perrona, R. Ledezma, R. Matjea, L. Kindermann, C. Goebel, B. Semple, and B. Tamayo for assistance with field work. We thank Bush Heritage Australia; the University of Limpopo; the Ministry of Environment and Tourism (Namibia); the Ministry of Agriculture, Water and Land Reform (Namibia); Corporación Nacional Forestal (CONAF) and the agricultural community Quebrada de Talca (Chile); and the South African military for granting research permissions and/or granting access to their research farms and properties. We also thank B. Benito for his revisions to the R code, and C. Abel for her comments on the manuscript. Any use of trade, product, or firm names in this paper is for descriptive purposes only and does not imply endorsement by the US government. **Funding:** This research was funded by the European Research Council [ERC grant agreement 647038 (BIODESERT)] and Generalitat Valenciana (CIDEGENT/2018/041). F.T.M. acknowledges support from a Rei Jaume I Award, the Alexander von Humboldt Foundation, and the Synthesis Center (sDiv) of the German Centre for Integrative Biodiversity Research Halle–Jena–Leipzig (iDiv). C.A.G., S.C., and N.E. acknowledge support from iDiv and the Deutsche Forschungsgemeinschaft (DFG– FZT 118, 202548816; Flexpool proposal 34600850). Y.L.B.-P. was supported by a Marie Sklodowska-Curie Actions Individual Fellowship (MSCA-IF) within the European Program Horizon 2020 (DRYFUN Project 656035). N.G. was supported by CAP 20-25 (16-IDEX-0001) and the AgreenSkills+ fellowship program, which has received funding from the EU's Seventh Framework Programme under grant agreement N° FP7-609398 (AgreenSkills+ contract). B.B. and B.E. were supported by the Taylor Family–Asia Foundation Endowed Chair in Ecology and Conservation Biology. J.D., A.Ro., and H.C. acknowledge support from the Fundação para a Ciência e a Tecnologia (IF/00950/2014 and 2020.03670.CEECIND, SFRH/BDP/108913/2015, and in the scope of the framework contract foreseen in the numbers 4-6 of the article 23, of the Decree-Law 57/2016, August 29, changed by Law 57/2017, July 19, respectively), as well as from the MCTES, FSE, UE, and the CFE (UIDB/04004/2020) research unit financed by Fundação para a Ciência e a Tecnologia/MCTES through national funds (PIDDAC). C.P. acknowledges support from the Spanish Ministry of Science and Innovation (ref. AGL201675762-R, AEI/FEDER, UE, and PID2020-116578RB-I00, MCIN/AEI/10.13039/501100011033) and the European Union's Horizon 2020 Research and Innovation Programme under grant agreement no. 101000224. E.V. was funded by the 2017 program for attracting and retaining talent of Comunidad de Madrid (no. 2017-T2/ AMB-5406). M.A.B. acknowledges support from the School of Forestry and College of the Environment, Forestry and Natural Sciences of Northern Arizona University. E.H.-S. acknowledges support from the Consejo Nacional de Ciencia y Tecnología (SEP-CB-2015-01-251388, PN 2017-5036 and PRONAII 319059). F.M.H. acknowledges support from the National Council for Scientific and Technological Development (CNPq - PCI/INMA) of the Brazilian Ministry of Science, Technology and Innovation (MCTI, processes number 302381/2020-1). H.L.T. acknowledges support from the US National Science Foundation (NSF) (DEB 0953864). A.N. and M.K. acknowledge support from the Fundação para a Ciência e a Tecnologia (SFRH/BD/130274/2017, CEECIND/02453/2018/CP1534/CT0001, PTDC/ASP-SIL/7743/2020 and UIDB/00329/2020). A.A.C. acknowledges support from the Coordenação de Aperfeiçoamento de Pessoal de Nível Superior - Brasil (CAPES) - Finance Code 001. J.E.K. and T.P.M. acknowledge the National Research Foundation of South Africa (grant no. 114412). F.J. and N.B. acknowledge support from the German Federal Ministry of Education and Research (BMBF) in the framework of the SPACES projects OPTIMASS (FKZ: 01LL1302A) and ORYCS (FKZ: 01LL1804A). A.Li. and A.S.K.F. acknowledge support from the German Federal Ministry of Education and Research (BMBF) in the framework of the SPACES projects Limpopo Living Landscapes (FKZ: 01LL1304D) and SALLnet (FKZ: 01LL1802C). L.W. acknowledges support from the US NSF (EAR 1554894). L.H.F. acknowledges support from the Natural Sciences and Engineering Research Council of Canada Industrial Research Chair Program in Ecosystem Reclamation. S.C.R. acknowledges support from the US Geological Survey Ecosystems Mission Area and the US Bureau of Land Management. G.M.W. acknowledges support from the Australian Research Council. L.v.d.B. and K.T. acknowledge support from the German Research Foundation (DFG) priority research program SPP-1803 "EarthShape: Earth Surface Shaping by Biota" (TI 338/14-1). M.D.-B. acknowledges support from the Spanish Ministry of Science and Innovation for the I+D+i project PID2020-115813RA-I00 funded by MCIN/AEI/10.13039/501100011033. M.D.-B. is also supported by a project of the Fondo Europeo de Desarrollo Regional (FEDER) and the Consejería de Transformación Económica, Industria, Conocimiento y Universidades of the Junta de Andalucía (FEDER Andalucía 2014-2020 Objetivo temático "01 - Refuerzo de la investigación, el desarrollo tecnológico y la innovación") associated with the research project P20_00879 (ANDABIOMA). P.J.R. and A.J.M. acknowledge support from Fondo Europeo de Desarrollo Regional through the FEDER Andalucía operative program, FEDER-UJA 1261180 project. A.F. thanks ANID PIA/BASAL FB210006 and Millennium Science Initiative Program NCN2021-050. A.J. acknowledges support from the Bavarian Research Alliance Germany (BayIntAn_UBT_2017_61). C.B. acknowledges the National Natural Science Foundation of China (grant no. 41971131). Biodiversity and ecosystem function research in the B.K.S. laboratory is funded by the Australian Research Council (DP210102081). Any use of trade, product, or firm names in this paper is for descriptive purposes only and does not imply endorsement by the US government. H.S. is supported by a María Zambrano fellowship funded by the Ministry of Universities and European Union-Next Generation plan. G.P. and C.V.L. acknowledge support from Universidad Nacional de Río Negro (PI 40-C-873 and 654). V.R. acknowledges support from the Regional Government of Extremadura (Spain) through a "Talento" fellowship (TA18022). M.F. acknowledges support from the Department of Range and Watershed Management, Ferdowsi University of Mashhad, Mashhad, Iran. Participation of recent graduates in collecting field data at four sites in Namibia was supported by a capacity building grant to Gobabeb–Namib Research Institute by the Environmental Investment Fund in Namibia. **Author contributions:** Conceptualization: F.T.M., N.G., Y.L.B.-P.; Methodology: F.T.M., N.G., Y.L.B.-P., D.J.E., H.S.; Investigation: Y.L.B.-P., D.J.E., H.S., M.B., B.G., V.O., M.G.-G., E.V., J.J.G., S.A., B.J.M., C.P., P.D.-M., A.Re., A.Le., M.C.R., S.C., N.E., E.M.-J., O.S., M.A., N.A., C.L.A., V.A., F.A., T.A., R.J.A., K.B., F.B.S., N.B., B.B., M.A.B., D.B., C.B., R.Ca., A.P.C.-M., H.C., I.C., P.C.-Q., R.Ch., A.A.C., C.M.C., A.D.-N., B.D., D.A.D., A.J.D., J.D., B.E., C.I.E., A.F., M.F., D.F., A.S.K.F., L.H.F., L.A.G., A.C.G., E.G.-M., R.M.H.-H., N.H., E.H.-S., F.M.H., O.J.-M., F.J., A.J., K.F.K., M.K., J.E.K., C.V.L., A.Li., P.C.I.R., X.L., P.L., J.L., M.A.L., G.M.-K., T.P.M., O.M.I., A.J.M., E.M., J.P.M., G.M., S.M.M., A.N., G.O., G.R.O., G.P., M.O.D.P., Y.P., R.E.Q., S.R., S.C.R., P.J.R., B.R., A.Ro., V.R., J.G.R., J.C.R., A.S., M.A.S., S.S., I.S., C.R.A.S., A.M.S., A.L.T., A.D.T., H.L.T., K.T., S.T., J.V., O.V., L.v.d.B., S.V.A., F.V., W.W., D.W., L.W., G.M.W., L.Y., E.Z., Y.Z., X.Z., B.K.S. **Competing interests:** The authors declare that they have no competing interests. **Data and materials availability:** All the data used in this article and the R scripts used to generate the main results of the study are available through figshare (*31*). The raw sequence data generated in this study are also available through figshare (*32*).

SUPPLEMENTARY MATERIALS

science.org/doi/10.1126/science.abq4062
Materials and Methods
Figs. S1 to S19
Tables S1 to S28
References (*33*–*269*)
MDAR Reproducibility Checklist
Movie S1

Submitted 6 April 2022; accepted 6 October 2022
10.1126/science.abq4062

EPFL

Faculty Position in Cancer Bioengineering

at the Ecole polytechnique fédérale de Lausanne (EPFL)

The School of Life Sciences of EPFL (Ecole polytechnique fédérale de Lausanne) invites applications for a tenure track assistant professor position in the field of **Cancer Bioengineering**.

This search is part of major initiatives in the Lake Geneva region to promote cancer research, which is increasingly driven by integrating research from different fields ranging from basic sciences (life sciences, physics, chemistry, computing and engineering) to clinical research and treatment.

The successful candidate will join the faculty of the Swiss Institute for Experimental Cancer Research (ISREC); develop an independent internationally prominent research program in the broad domain of cancer research; commit to excellence in teaching at the undergraduate and graduate levels, and supervise Ph.D. students and postdoctoral fellows. We are looking for candidates with core expertise and experience in any bioengineering-related area, including but not limited to tissue engineering, synthetic biology, chemical biology, materials science, drug design, computational biology, and instrumentation development. Their future research proposal must have a strong cancer research focus.

The successful candidate will be a part of EPFL's cancer research institute (ISREC), and is expected to perform and coordinate highly interactive biomedical research, reaching out and taking advantage of EPFL's interdisciplinary campus (Schools of Basic Sciences, Engineering, and Information and Communication Technologies) and its involvement in the multi-institutional Swiss Cancer Center Leman, which brings together EPFL, the Universities of Lausanne and Geneva, and clinical and translational research components of the University Hospitals of Lausanne and Geneva.

Applications should include a cover letter, a curriculum vitae, a list of publications (annotated to indicate the candidate's contributions) a synopsis of major accomplishments, and a concise statement of future research agenda and teaching interests, along with the contacts of 3-5 referees who are ready to supply their letter upon request. Applications should be uploaded as PDF files to the recruitment web site:

https://facultyrecruiting.epfl.ch/position/42303490

Formal evaluation of candidates will begin on **January 9, 2023,** and continue until the position is filled.

Enquiries may be sent to:
Prof. Elisa Oricchio
Search Committee Chair
E-mail: cancer.research@epfl.ch

For additional information on EPFL and the Institute of Bioengineering, please consult: www.epfl.ch, sv.epfl.ch

EPFL is an equal opportunity employer and family friendly university. It is committed to increasing the diversity of its faculty. It strongly encourages women to apply.

EPFL

Faculty position in Geotechnical & Geosystems Engineering

at the Ecole polytechnique fédérale de Lausanne (EPFL)

The EPFL School of Architecture, Civil and Environmental Engineering (ENAC) invites applications for an Assistant Professor (tenure-track) of **Geotechnical & Geosystems Engineering** in the Institute of Civil Engineering.

The Institute of Civil Engineering in ENAC carries out basic and translational research spanning fundamental understanding in Geosystems and Geomechanics, Structures and Materials, Transportation and Networks, and Hydraulic Engineering. It covers a diverse portfolio in research, teaching, and innovative technology development across transversal themes: understanding and adapting to climate change, natural hazards, infrastructure resilience and sustainability, design for re-use, geo-energy and geosystems.

Topics of interest cover fundamental research in mechanics of geomaterials and applications to sustainable design of geosystems and geotechnical structures. The use and development of novel experimental and/or theoretical methods is expected to advance understanding of the behaviour of soil-structure interactions, granular systems as well as vulnerability assessment of slope instabilities, among others.

The successful candidate will have a strong research background in Geotechnical Engineering and Soil Mechanics as well as the potential to develop an innovative and internationally recognized research program leading to an outstanding record of scientific accomplishments.

As a faculty member of the Civil Engineering Section, he/she will excel in undergraduate and graduate teaching, and supervision of research students.

EPFL, with its main campus located in Lausanne, on the shores of Lake Geneva, is a dynamically growing and well-funded institution fostering excellence and diversity. It is well equipped with experimental and computational infrastructure and offers a fertile environment for research collaboration between various disciplines. The EPFL environment is multilingual and multicultural, with English serving as a common interface. EPFL offers significant start-up resources and internationally competitive salaries and benefits, as well as excellent experimental and computational facilities.

The following documents are requested in PDF format: cover letter including a statement of motivation, curriculum vitae, publication list, concise statements of research vision and teaching interests (up to 5 pages for each) and the names and addresses (including e-mail) of at least three referees who are ready to supply their letter of reference upon request. Applications should be uploaded to the EPFL recruitment web site:

https://facultyrecruiting.epfl.ch/position/40599572

Formal evaluation of the applications will begin on **February 1st, 2023**.

Further enquiries should be made to:
Prof. Brice Lecampion
Chair of the Search Committee
e-mail: SearchGeoTechnical@epfl.ch

For additional information on EPFL, please consult the websites: www.epfl.ch, enac.epfl.ch, iic.epfl.ch, sgc.epfl.ch

EPFL is an equal opportunity employer and a family-friendly university that is committed to increasing the diversity of its faculty. It strongly encourages women to apply.

By **Omid V. Ebrahimi**

Sidelined by bureaucracy

I hung up the phone and tried to come to terms with the news. I had been hoping to present my work at an upcoming international conference, in the country that hosts nearly all major global scientific meetings. I had spent the past year working feverishly to obtain a visa. The process had been so drawn out that I had already missed two other conferences there. But I had been holding onto hope I would be able to attend this third one—until the phone call with the embassy. After being transferred between operators in various countries, I was informed there was essentially no way I would get a visa in time. (I won't name the country, because I still hope to travel there.) I was going to miss another opportunity to connect with my academic peers because of my birthplace.

Having experienced the isolation of the pandemic as a Ph.D. student, I was thrilled when my proposals were accepted at three in-person conferences. I could hardly wait to begin the "typical" academic journey, filled with face-to-face interactions. As the first conference approached, my colleague and I—both Norwegian citizens, affiliated with Norwegian institutions—started our visa applications. My colleague, a native Norwegian, finished the portal rapidly and paid a $20 fee, and their visa requirement was waived. After booking travel and accommodation, they were ready to go.

I was born in Iran, and my experience couldn't have been more different. I spent hours responding to strange questions in the same portal and paid an eightfold larger fee, after which I was informed I needed to book an in-person interview. The first available appointment in the Netherlands, where I was working as a visiting researcher, was 9 months away—6 months after the first conference was to take place.

I heard from a friend that the interview queue was shorter at home in Norway, but the application I had filed was not transferable. Frustrated but committed, I sat down in the same portal to answer the exact same questions and paid another $160, which activated the appointment scheduling page—only to learn it would still be 3 months too late. But I reminded myself the next conferences were a few months after my newly scheduled interview, so I remained hopeful.

About half a year later, I was at the embassy for the interview. After I waited in line for hours, the interview was over in minutes. My visa was temporarily denied, and I was sent home to provide "additional necessary information."

The documents I was being asked for would be difficult, time-consuming, and costly to obtain and translate, but I was determined. A month after resubmitting, my visa was redenied for a new round of information. I was now being asked to provide every single place I had lived or visited; dates and reason for each stay, and how I funded them; phone numbers, email addresses, and social media accounts I had used; jobs I had held; and more—for the past 15 years. The task seemed insurmountable. Still, I plowed forward and did as I was asked, spending weeks (re)collecting this information and paying a price in time, energy, and sleep.

"I was going to miss another opportunity to connect with my academic peers."

As weeks passed without an update and the second conference came and went, I reached out to the embassy—resulting in that deflating phone call. By that point I had lost countless hours and a substantial sum of money, including nonrefundable conference registration fees, and was emotionally drained—all in the hope of attending a conference lasting just a few days.

Many scholars born in ostracized countries face these drawn-out, oftentimes years-spanning processes when we need to travel. The obstacles take a toll on our professional development, our future opportunities, and our mental health. Conference organizers have a responsibility to address this. To truly foster inclusivity, meetings must be hosted in more open countries. As for me, I am still holding out hope that eventually my visa will come through, and that my career won't unduly suffer from the opportunities already missed. ■

Omid V. Ebrahimi is a double-degree Ph.D. candidate at the University of Oslo and Modum Bad Psychiatric Hospital. Send your career story to SciCareerEditor@aaas.org.

ILLUSTRATION: ROBERT NEUBECKER

AAAS.ORG/COMMUNITY

AAAS' Member Community is a one-stop destination for scientists and STEM enthusiasts alike. It's "Where Science Gets Social": a community where facts matter, ideas are big and there's always a reason to come hang out, share, discuss and explore.

Member COMMUNITY
AAAS

AMERICAN ASSOCIATION FOR THE ADVANCEMENT OF SCIENCE

CAR-T Animal Studies

Testing *In Vivo* Efficacy & More for Cell Therapy Research

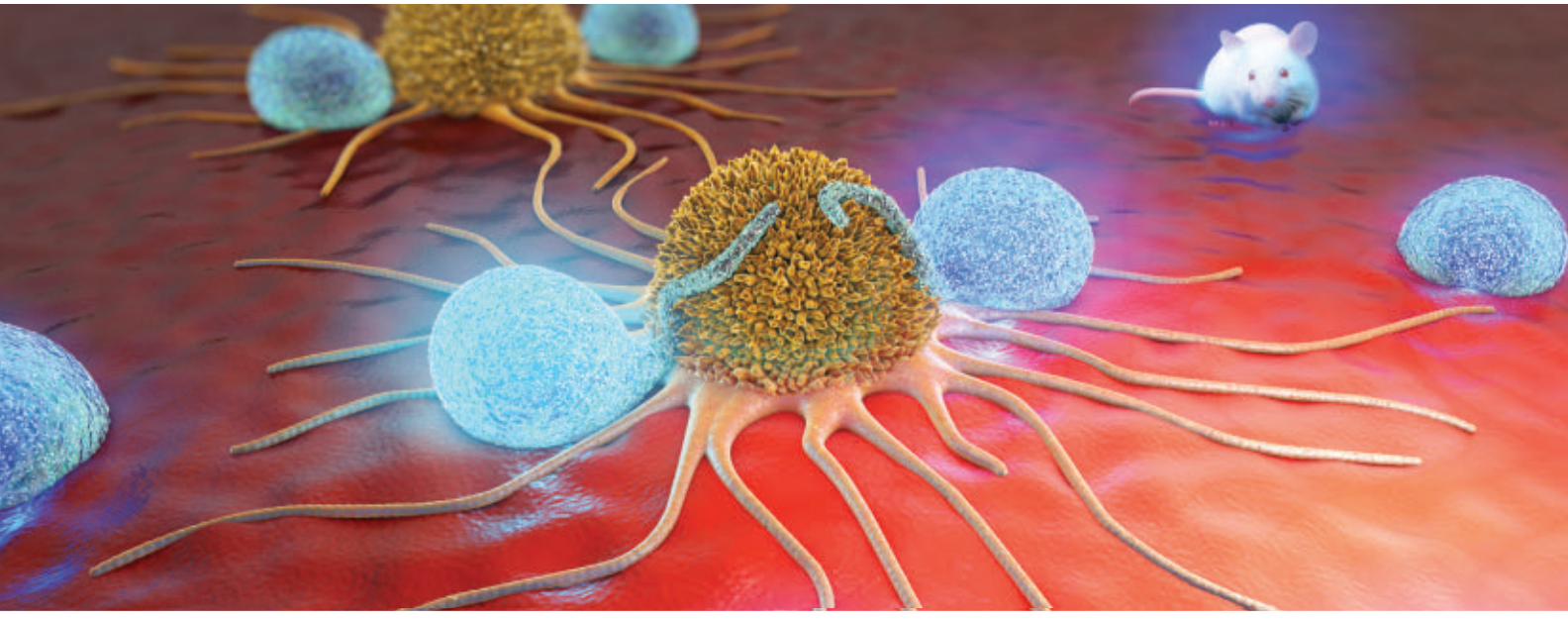

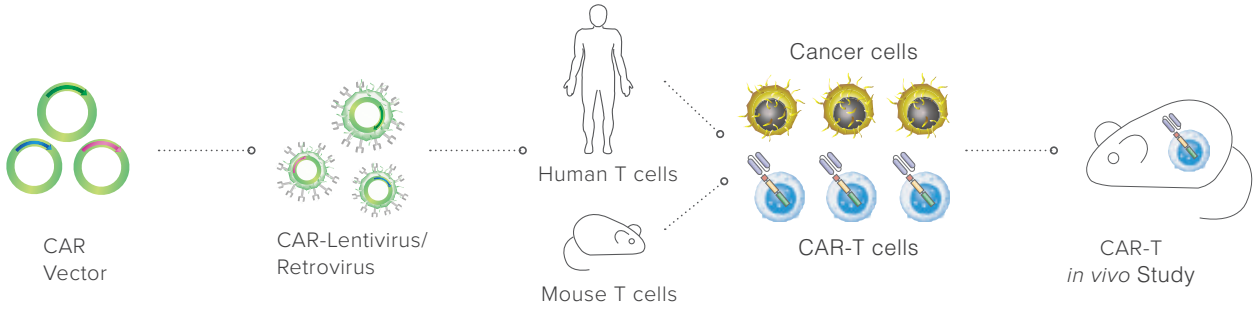

Animal Research Custom Services

Custom services available.

- IVIS imaging
- Toxicology
- PK/PD models
- Immunohistochemistry (IHC)
- Cytokine panels
- Tumor volume and weight
- Histopathology
- Genomic parameters
- Cell phenotyping

ProMab Biotechnologies offers a fully comprehensive in vivo functionality service to analyze your cell therapy product using xenograft NSG mice models. CAR-T cells can be made to expedite preclinical research studies in xenogeneic or syngeneic mouse models. ProMab has developed patient-derived xenograft models of different types of cancers to study and validate the efficacy of cell therapy products against solid and hematological tumors and its microenvironment.

All products are for research use only

Discover more | www.promab.com

ProMab Biotechnologies, Inc.
2600 Hilltop Dr, Building B, Richmond, CA 94806
1.866.339.0871 | info@promab.com
SCAN ME

A Sponsored Supplement to *Science*

Frontiers of Medical Research: Cancer

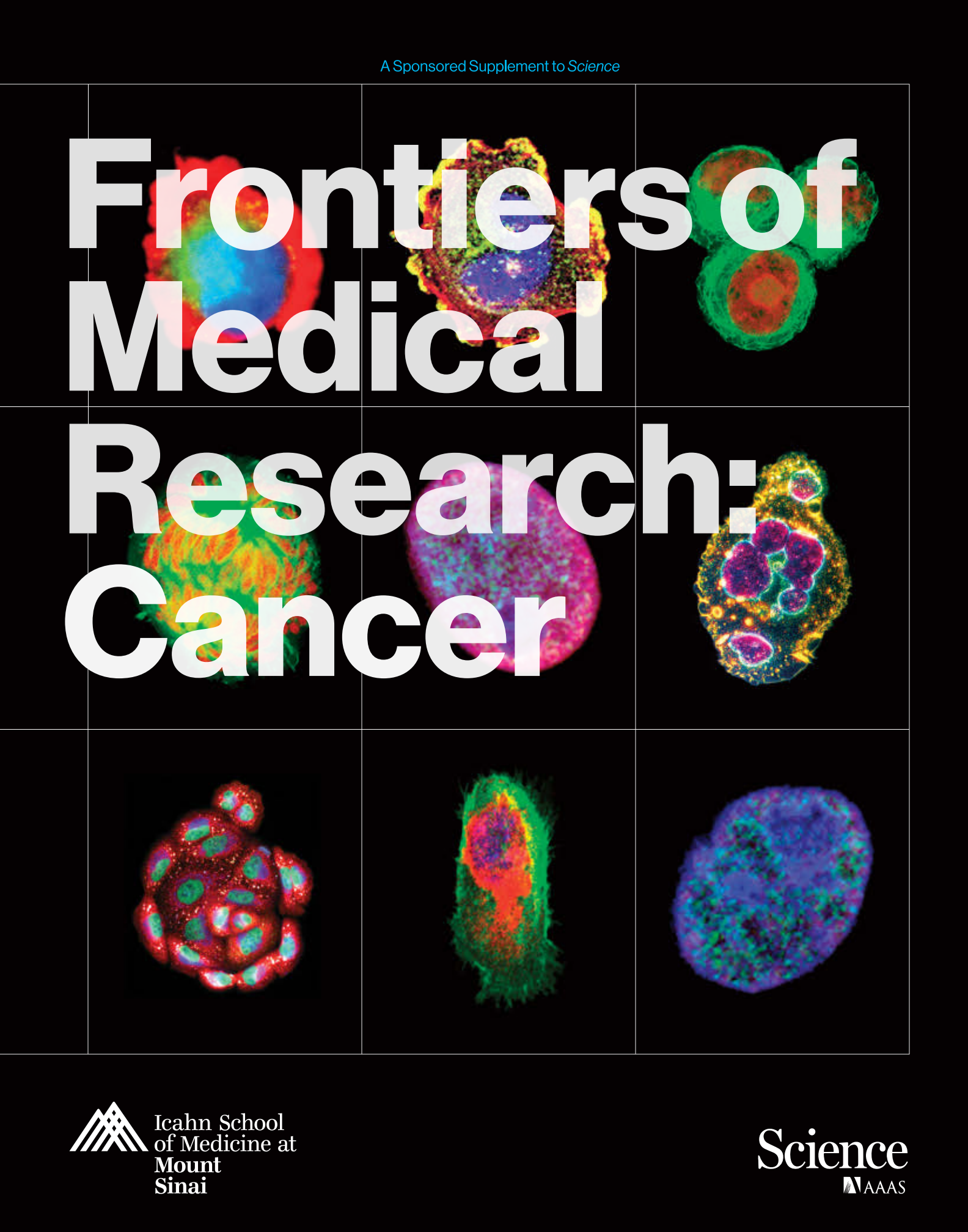

Icahn School of Medicine at Mount Sinai

Science
AAAS

Table of Contents

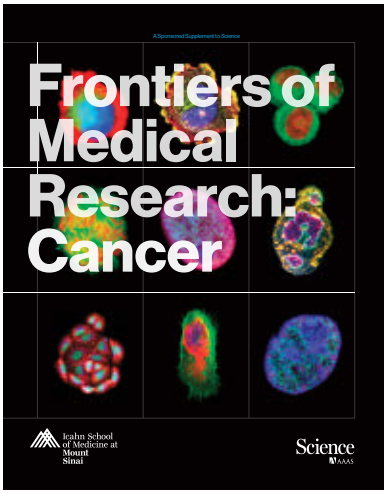

This supplement was produced by the *Science*/AAAS Custom Publishing Office and sponsored by Icahn School of Medicine at Mount Sinai.

Materials that appear in this supplement have not been peer reviewed nor have they been assessed by *Science*. Articles can be cited using the following format: [AUTHOR NAME(S)] [CHAPTER TITLE] in The Frontiers of Medical Research: Cancer (*Science*/AAAS, Washington, DC, 2022), p. [xx-xx].

Editor: Sean Sanders, Ph.D.
Proofreader/Copyeditor: Bob French
Designer: JD Huntsinger

Chris Hoag
Sales Manager
choag@aaas.org
+1 (202) 590-8176

Introductions

Articles

Untying cancer's Gordian knot

Cancer is not a monolithic disease. Even the same class of cancer can manifest in many different ways and be driven by a multitude of genetic and epigenetic changes. Finding common causative pathways in cancers can provide the opportunity for the creation of broad and potentially effective treatments, but to truly give clinicians a chance to cure individual patients will require an understanding of the molecular basis of each cancer and the range of alterations that lead to tumor initiation and progression. Add to these additional environmental factors and the unique genetic and physiological background of each patient, and the complexity of unraveling any particular cancer feels daunting.

But researchers are not giving up. And despite significant hurdles, progress is being made. This supplement is the second in a series being published in cooperation with the Icahn School of Medicine at Mount Sinai. In the first, entitled "The Frontiers of Medical Research," physicians and scientists from the Icahn School of Medicine summarized for readers major new developments across 16 fields of medicine. In this second supplement, we focus on breakthroughs in cancer research and care through a collection of articles by researchers and clinicians at The Tisch Cancer Institute at Mount Sinai.

These researchers and their collaborators around the world are building a fundamental knowledge base covering all aspects of cancer, attempting to find vulnerabilities that might be targets for as-yet undiscovered therapies. Their work includes better defining the tumor immune microenvironment, using synthetic biology and immunotherapy to make tumors more vulnerable to current therapies, improving our understanding of how cancers metastasize and gain drug resistance, and deploying cutting-edge processes like targeted protein degradation to home in on and dispatch pro-oncogenic proteins.

The challenges ahead for those attempting to uncover cancer's complex secrets are significant. But what is clear from the articles presented here is that there is progress, excitement, and hope among those tackling this puzzle. The work performed at The Tisch Cancer Institute promises not only to provide insights into the pathways that lead to tumor formation, but also to pinpoint ways to interrupt those pathways earlier in the tumorigenesis process than was previously possible, or at the very least, to identify the causative agents and offer clues as to how they might be targeted through novel treatments in the future.

Sean Sanders, Ph.D.
Science/AAAS

Dennis S. Charney, M.D., is the Anne and Joel Ehrenkranz Dean of the Icahn School of Medicine at Mount Sinai and president for academic affairs for the Mount Sinai Health System.

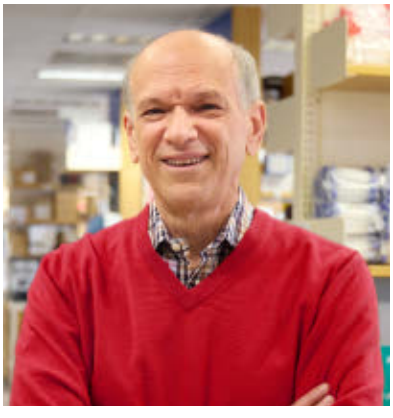

Eric J. Nestler, M.D., Ph.D., is dean for academic and scientific affairs for the Icahn School of Medicine at Mount Sinai and chief scientific officer of the Mount Sinai Health System, director of the Friedman Brain Institute, and the Nash Family Professor of Neuroscience.

Ramon E. Parsons, M.D., Ph.D., is director of The Tisch Cancer Institute at the Icahn School of Medicine at Mount Sinai; director of Mount Sinai Cancer, Mount Sinai Health System; Ward-Coleman chair in cancer research; and chair of the Department of Oncological Sciences at the Icahn School of Medicine.

On the frontiers of cancer research

In November 2021, we were pleased to develop, in partnership with *Science*/AAAS, a supplement to *Science* entitled "The Frontiers of Medical Research." In that publication, physicians and scientists at the Icahn School of Medicine at Mount Sinai highlighted exciting new developments in 16 different fields of medicine. Now in this new supplement, our authors—all associated with The Tisch Cancer Institute at Mount Sinai—focus specifically on important advances in cancer research and treatment.

Cancer is a wily opponent. It hides before unleashing lethal assaults. It repels attackers. It suppresses immune defenses. It stealthily metastasizes and then mutates to gain new powers of resistance. These offensive and defensive moves can be tracked today as never before, thanks to advances in genetics and molecular and cell biology. The more we learn about cancer, the more we recognize the need to expand our arsenal of weapons that can effectively target, attack, and destroy or neutralize neoplasms.

Fortunately, scientists are making exciting progress at the frontiers of cancer research. Striking methodological innovations have made it possible to better dissect and understand the pathogenic mechanisms of cancer. Advances in next-generation sequencing and flow cytometry have enabled identification of the underlying mutations that drive tumor growth, immune evasion, and ability to metastasize. This new information is empowering scientists to identify pathways of tumor development and proliferation and target them to control and defeat cancer.

In this supplement you will read about:

- new cutting-edge approaches to target previously undruggable cancer-promoting proteins
- advances in understanding and better treating multiple myeloma
- the effort to develop new therapies that can prevent metastatic outbreaks
- pioneering approaches to fight the rising epidemic of liver cancer, and
- progress in understanding how tumor cells evade immune detection and reprogram the immune system to promote tumor growth.

Scientists are starting to understand how tumors escape immune surveillance by modeling the highly complex interactions between cancers and the immune system. Through improved analysis of the tumor microenvironment, scientists are developing novel approaches to overcoming immune system suppression; this is a critical objective within cancer research—because immunotherapy today is effective for only one of every five patients. In this publication, we discuss exciting and innovative methods to overcome immune system suppression, including in-situ vaccination, the application of messenger RNA (mRNA)-nanoparticle technology to create vaccines that promote antitumor immunity, and the use of viruses to initiate an antitumor response.

Researchers are building a fundamentally new biology of cancer that is leading to a better understanding of the molecular and cellular underpinnings of the many forms of this disease. Our challenge is to be clever enough to quickly and efficiently leverage these discoveries to develop new approaches that target specific features of tumor cells. Ultimately, the new biology must translate to better medicine that will save the lives of more cancer patients.

Insights into chromatin dependencies and therapeutic opportunities in cancer

Ernesto Guccione[1,2], Emily Bernstein[1,2]

Recent large-scale cancer genome sequencing efforts have revealed a plethora of high-frequency mutations in posttranscriptional and epigenetic machinery across cancers. While RNA and chromatin biologists have long appreciated that such mechanisms play an important role in tumorigenesis (e.g., RNA splicing, DNA methylation, and histone acetylation, among others), the findings derived from these sequencing efforts have propelled and fostered cross-disciplinary collaborations toward understanding the role of such mutations. Investigators at The Tisch Cancer Institute (TCI) at Mount Sinai are actively engaged in such research from the unique perspective of modeling how these mutations/alterations drive cancer initiation and progression as well as guiding the development of novel therapeutic strategies and modalities to combat them.

Epigenetic vulnerabilities in cancer

Histone posttranslational modifications (PTMs) are tightly regulated by families of enzymes that either place ("writers") or remove ("erasers") their respective modifications, while chromatin binding proteins ("readers") dock on cognate PTMs to facilitate downstream effects on chromatin structure and gene expression (Figure 1). Some of the first evidence for malfunction of these processes via mutation was the identification of hyperactivating mutations in the H3K27 lysine methyltransferase EZH2 in B cell non-Hodgkin lymphomas (e.g., follicular lymphoma, FL), which block B cell differentiation (*1*). Studies further validated EZH2 as a dependency in FL, and the U.S. Food and Drug Administration approved the use of tazemetostat (an EZH2 inhibitor, EZH2i) in FL patients in 2020. This was a significant advancement for the field, as it represents a new class of epigenetic inhibitors for cancer therapy and is currently in clinical trials for a variety of liquid and solid cancers. EZH2 is also mutated or aberrantly overexpressed in many other tumors including prostate and breast cancer, where it can serve as a cancer dependency. TCI investigators have developed first-in-class EZH2 degraders that act cytotoxically in triple-negative breast cancer cells that are resistant to EZH2i, suggesting enzymatic-independent functions of EZH2 (*2*) (see article by Jin et al. on p. 10). Moreover, cancers that are not genetically altered for EZH2 can still display dependency on this factor, for example, in tumors with mutations in subunits of switch/sucrose-non-fermentable (SWI/SNF) chromatin remodeling complexes that normally function to counteract EZH2 activity (*3*). ATRX is an SWI/SNF-like chromatin remodeler that is altered in a rare but aggressive subtype of neuroblastoma, and TCI investigators showed that this cancer displays sensitivity to EZH2i (*4*), which is now being investigated in preclinical trials for this disease. As opposed to the above oncogenic functions, EZH2 acts as a tumor suppressor in myelodysplastic syndrome (MDS) and acute myeloid leukemia (AML), where in addition to missense/frameshift mutations or deletions, mutations in the splicing factor SRSF2 lead to inclusion of a "poison exon" in EZH2, causing transcript degradation and a block in myeloid differentiation. TCI scientists discovered that either administration of antisense oligonucleotides (ASOs) to repair the splicing defect or inhibition of protein arginine methyltransferases (PRMTs) restores EZH2 function and preferentially reduces cell viability in SRSF2-mutant cells (*5*).

[1]Tisch Cancer Institute, [2]Department of Oncological Sciences, Icahn School of Medicine at Mount Sinai, New York, NY

Incorporation of histone variants into chromatin has distinct and profound consequences within the cell. The discovery of high-frequency histone H3.3 mutations (coined "oncohistones"; Figure 1) in pediatric diffuse midline glioma has led to international collaborations that have defined the consequences of H3K27M mutations on the epigenome and uncovered therapeutic opportunities. Our investigators and others have developed representative mouse and human cellular models of these mutations, and found that H3K27M opposes the catalytic function of EZH2, allowing cells to adopt a neural progenitor-like state (*6*). While H3.3 mutations are largely restricted to the pediatric setting, linker histone H1 mutations have recently been reported in a subset of lymphomas. Through large-scale chromatin reorganization, these mutations induce a more stem-like state (*7*), an emerging theme in epigenetically altered cancers.

Transcriptional and posttranscriptional aberrations in cancer

Beyond epigenetic alterations, splicing dysregulation has emerged as a key feature of cancer and can be caused by genetic mutations that directly disrupt splicing in *cis*, or via mutation or altered expression of components of the splicing machinery, affecting multiple downstream targets in *trans*. Regarding the latter, somatic mutation of splicing factors is a recurrent theme across multiple tumor types including *SF3B1*, *U2AF1*, and *SRSF2* mutations in MDS/AML (*8*), and *SF3B1* in uveal melanoma (*9*) (Figure 1). While the community is actively characterizing the downstream splicing defects causative of disease, convergence on transcriptional and chromatin networks has been identified, such as missplicing of EZH2 (as noted above) and BRD9, a component of the noncanonical Brm/Brg-associated factor (ncBAF) SWI/SNF chromatin remodeling complex (*8*). TCI scientists have utilized human induced pluripotent stem cell (iPSC) models to identify mutant splicing signatures and altered transcription factor (TF) activity in MDS, including the TEAD family in *SF3B1* mutant cells (*8*).

TFs are critical in integrating signaling cascades and dictating gene expression programs and therefore cellular states. Often these altered TF programs are associated with dedifferentiation or even transdifferentiation in cancer (Figure 1). For example, in melanoma, the levels of the master lineage TF microphthalmia-associated transcription factor (MITF) determine a proliferative versus invasive phenotype that has now been borne out in human patient samples through single-cell sequencing approaches (*10*). Through epigenomic analyses, our scientists have revealed AP-1 and TEAD TFs as critical components of the invasive state (*11*), but given the extent of tumor heterogeneity, other TFs are also likely to be involved. Other interesting examples are the integration of signaling cascades, such as PI3K/AKT/mTOR in B cell lymphomas, which are regulated by a network of TFs including PRDM15. This TF is normally involved in maintenance of naïve stem cell functions, but is reactivated in B cell lymphomas to fuel their enhanced metabolic requirement (*12*). Another example is FOXO1, mutation of which is associated with hyperactivation of PI3K and stress-activated kinases, and enables B cells to access germinal-center positive selection programs to confer a competitive advantage (*13*).

The pursuit of drugging TFs in cancer represents an outstanding opportunity due to their critical downstream functions in signaling cascades and control of adaptive drug resistance mechanisms. However, targeting TFs has been a longstanding challenge due to their lack of enzymatic activity or druggable pockets. A notable example is the oncogenic TF MYC, whose deregulation is a hallmark of multiple malignancies. Transient inhibition of MYC is well tolerated in vivo and results in blockage of tumor growth. Importantly from a therapeutic standpoint, inhibition of chromatin factors involved in RNA polymerase II control, such as the histone acetylation reader BRD4 or the transcription regulatory kinase CDK7, preferentially downregulates the expression of inducible genes such as *c-MYC*, while sparing housekeeping genes due to their regulation by superenhancers and

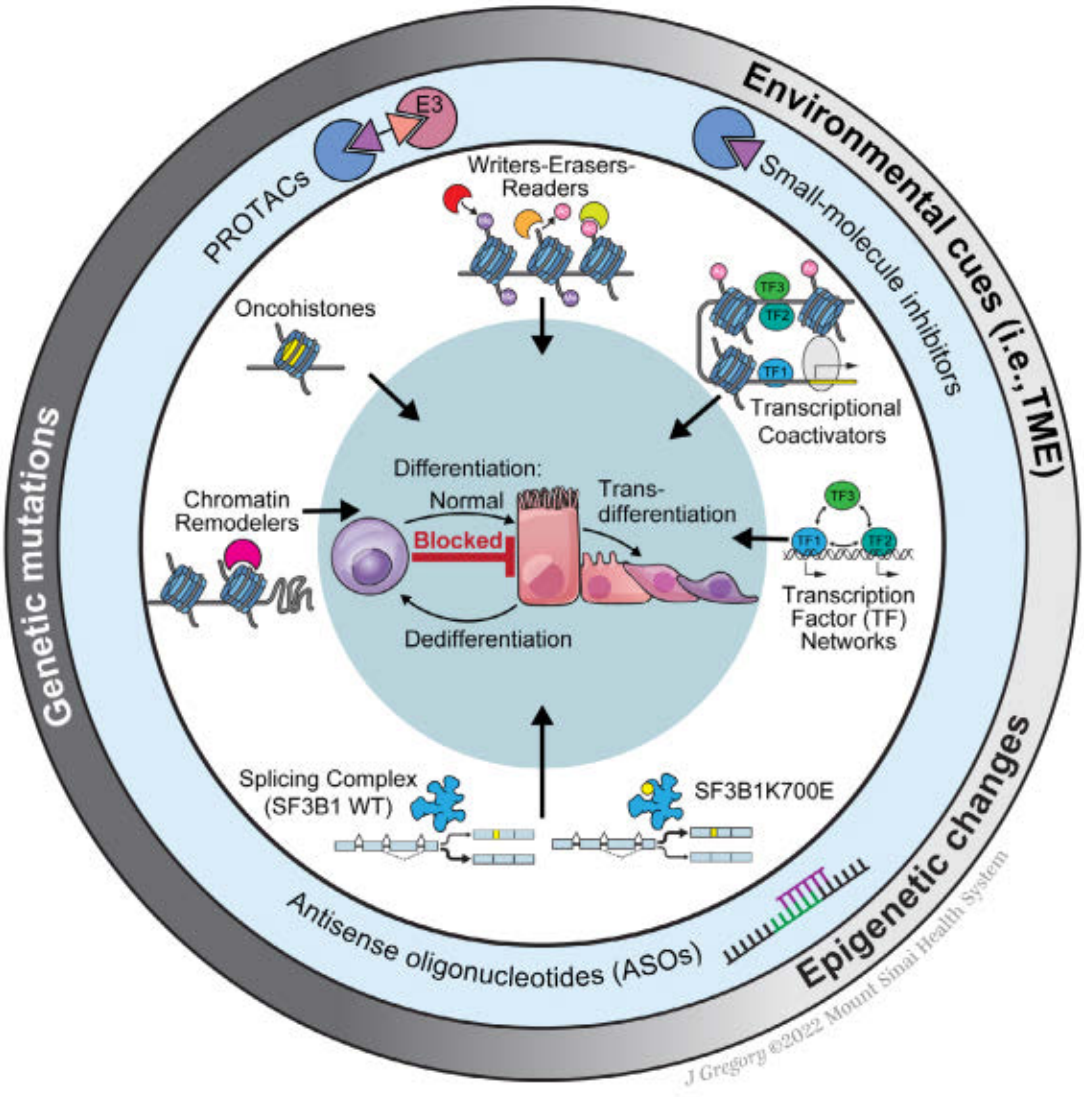

FIGURE 1. Therapeutic opportunities to target chromatin and transcriptional dependencies in cancer to restore cell identity.

their unique chromatin environment (*14*). Clinical success in directly targeting TFs has nonetheless been achieved in unique cases. For example, proteasome-mediated degradation of promyelocytic leukemia/retinoic acid receptor alpha (PML-RARA) can be induced by prodifferentiation compounds in acute PML, and phthalimide-based analogs (e.g., lenalidomide) induce degradation of Ikaros family TFs in multiple myeloma, resulting in reduced cell survival (*15*). In addition, proteolysis-targeting chimera (PROTAC)-based small molecules, which are actively being developed and tested by researchers at TCI, can also be designed to directly degrade TFs, in addition to other chromatin regulators that function as cancer dependencies (see article by Jin et al. on p. 10).

While precision therapies currently on the market often target upstream regulators of signaling cascades (e.g., kinase inhibitors or antibody-based biologics), the subsequent rewiring in cell signaling or epigenetic switching of cell identity limits therapeutic success. If we understand the transcriptional networks and chromatin dependencies underlying different types of cellular plasticity (e.g., tumor cell dormancy, dedifferentiation, inflammation- or drug-induced transdifferentiation) and their microenvironmental cues (Figure 1), we can devise new therapeutic strategies to target metastasis and resistance to therapy. Thus, we look forward to clinical studies combining epigenetic inhibition with cytotoxic therapies and/or checkpoint inhibitors targeting the immune compartment. In sum, while cancer genome sequencing projects have provided researchers with exciting new targets, future efforts will revolve around the identification of those (or their critical downstream targets) that are directly druggable, those that spare nontransformed cells, and importantly, those that constitute unique vulnerabilities for combination therapies.

References

1. M. T. McCabe *et al.*, *Nature* **492**, 108–112 (2012).
2. A. Ma *et al.*, *Nat. Chem. Biol.* **16**, 214–222 (2020).
3. C. Kadoch, R. A. Copeland, H. Keilhack, *Biochemistry* **55**, 1600–1614 (2016).
4. Z. A. Qadeer *et al.*, *Cancer Cell* **36**, 512–527.e9 (2019).
5. J. Y. Fong *et al.*, *Cancer Cell* **36**, 194–209.e9 (2019).
6. F. M. Mendez *et al.*, *Neuro. Oncol.* **22**, 195–206 (2020).
7. N. Yusufova *et al.*, *Nature* **589**, 299–305 (2021).
8. G. Asimomitis *et al.*, *Blood Adv.* **6**, 2992–3005 (2022).
9. J. W. Harbour *et al.*, *Nat. Genet.* **45**, 133–135 (2013).
10. F. Rambow *et al.*, *Cell* **174**, 843–855.e19 (2018).
11. S. Carcamo *et al.*, *Cell Rep.* **39**, 110637 (2022).
12. S. Mzoughi *et al.*, *Nat. Commun.* **11**, 3520 (2020).
13. M. P. Roberto *et al.*, *Immunity* **54**, 1807–1824.e14 (2021).
14. I. Marazzi, B. D. Greenbaum, D. H. P. Low, E. Guccione, *Nat. Rev. Mol. Cell. Biol.* **19**, 245–261 (2018).
15. R. J. Stubbins, A. Karsan, *Blood Cancer J.* **11**, 193 (2021).

Turning remission into cures: Novel therapies to outpace drug resistance and metastasis

Jose Javier Bravo-Cordero[1]*, Thomas U. Marron[1], Maria Sosa[2], Juan Arriaga[3], Andrew L. Ji[4], Poulikos I. Poulikakos[5]*

Cancer patients can remain in remission for many years and in some cases for decades after removal of the primary tumor. Unfortunately, some of these patients are not truly cured, and their cancer recurs and eventually becomes untreatable. The biology behind these recurrences is beginning to be uncovered and represents a unique opportunity to prevent metastatic relapse and prolong life.

As tumors grow, cells escaping through the bloodstream spread to distant organs from the tissue of origin, a process known as metastasis, ultimately accounting for over 90% of cancer deaths (*1*). Intrinsic properties of metastatic tumors include (a) unique signaling pathways that allow them to disseminate and colonize distant organs; (b) capacity to survive in a dormant, nonproliferative, and treatment-refractory state for years if not decades; and (c) intricate interactions with specific microenvironmental niches. These factors shape if, how, and where the tumors spread, and present us with unique challenges in early detection and effective treatment that, if surmounted, could have a dramatic impact on the survival and well-being of cancer patients.

Before or after a tumor is surgically removed, patients often receive cytotoxic chemotherapy to help kill off any remaining cancer cells in the body that may have already spread but have not yet formed tumors that are detectable with standard imaging. While dormant disseminated tumor cells (DTCs) are generally thought to be resistant to chemotherapy, which only kills rapidly dividing cells, our evolving understanding of the biology of DTCs—the seed of metastasis—present an exceptional opportunity to develop treatments targeting this unique subset of cancer cells. The efficacy of most cancer therapy is inversely correlated with the amount of cancer in the body, and as such in this setting where only microscopic disease is present, this new window of opportunity can lead to early interventions to prevent metastatic outbreaks. Novel therapeutic approaches for prevention of a relapse could potentially be developed by understanding how DTCs remain dormant and survive in their niche and by delineating the pathways that drive their awakening into metastatic tumors. There are reasons for optimism based on exciting new discoveries in the metastasis field. This excitement is reflected in new initiatives by funding agencies such as the National Cancer Institute's programs focused on metastatic and tumor microenvironment research. Several researchers at The Tisch Cancer Institute (TCI) at Mount Sinai are using state-of-the-art imaging techniques, model systems, spatial profiling, and therapeutic approaches to understand metastasis in multiple tumor types, raising hope that these studies can lead to major improvements in patient survival.

[1]Department of Medicine, Division of Hematology and Medical Oncology, Tisch Cancer Institute; [2]Department of Pharmacological Sciences, Department of Oncological Sciences, Tisch Cancer Institute; [3]Department of Oncological Sciences, Department of Urology; [4]Department of Dermatology, Department of Oncological Sciences, Black Family Stem Cell Institute, Tisch Cancer Institute; [5]Department of Oncological Sciences, Precision Immunology Institute, Tisch Cancer Institute, Icahn School of Medicine at Mount Sinai Hospital, New York, NY

*Corresponding authors: josejavier.bravo-cordero@mssm.edu (J.J.B.), poulikos.poulikakos@mssm.edu (P.I.P.)

Understanding early dissemination to prioritize prevention strategies

Clinical data have revealed that DTCs are detected in organs such as the bone marrow and lymph nodes, but those cells do not form a tumor right after landing in those organs. Rather, they reside in special niches where they activate a molecular program that allows them to remain in a hibernation state, also called dormancy, not proliferating and evading therapies.

In the last 20 years, clinical and experimental evidence suggests that dissemination of cancer cells may occur very early during tumor progression, even before clinically detectable tumors are found, as shown in melanoma, breast, colorectal and pancreatic cancers (*2*, *3*). This means that tumor cells that disseminate before the tumor is considered invasive can also reach distant sites, becoming early DTCs, and that they can also enter a hibernation state. Thus, these DTCs will remain silent for several years until the right signals allow them to reawaken and form metastases.

Moreover, molecular signatures present in primary tumors before metastasis is observed can be used to predict which tumors have a higher propensity to metastasize and will therefore be more receptive to earlier treatment. In a recent example, researchers have developed novel mouse models of prostate cancer that help elucidate how metastasis initiates and develops in vivo, accounting for the multiple benign cells and tissues, including those in the immune system, that shape metastatic progression (*4*).

Technology-driven approaches to profile DTCs and metastasis

Because some dormant early and late DTCs will eventually "turn on" and become metastases, efforts to develop new technologies to identify early and late DTCs in patients will open the possibility of new treatments that could increase survival rates. The complex interplay between DTCs and distant target organs, which is affected by the cellular composition and spatial organization of the distant organ microenvironment, ultimately determines DTC state and metastatic competency. Recent advances in high-throughput spatial multiomic profiling techniques, including spatial transcriptomics and proteomics, provide anatomical precision and single-cell and even subcellular resolution of DTC-neighboring cells and potential interactions that facilitate colonization, dormancy, or outgrowth (*5*). At TCI, investigators are leveraging the latest spatial profiling technologies to assess which cell–cell interactions within metastases are most relevant to tumor-cell behavior and can therapeutically target these interactions.

The art of disguise: Adapting and surviving in the new home

Targeted cancer therapies are directed toward suppressing signaling pathways necessary for tumor growth. However, mechanisms that prevent complete inhibition of the target pathway result in survival of a small number of drug-tolerant or "persister" tumor cells that may eventually become DTCs and drive future recurrences. Through complex homeostatic and feedback mechanisms, these drug-tolerant cells are capable of rewiring the specific pathways that therapies such as chemotherapy and targeted therapies aim to disrupt. Recent findings highlight the need for development of new drugs or drug combinations to overcome resistance and to eliminate persister cells before they have a chance to restore tumor growth (*6*). TCI is pioneering the development of therapies to overcome resistance through the design of drug combinations that would effectively target both the main driver of the oncogenic pathway as well as mediators of resistance (*7*).

Along with developing mechanisms to resist therapy, how do drug-tolerant DTCs survive in other distant organs after treatment? High-resolution imaging has revealed that dormant DTCs can self-assemble a dormancy-supportive niche by depositing specific extracellular matrix molecules that help sustain their dormant state (*8*). Moreover, the interplay

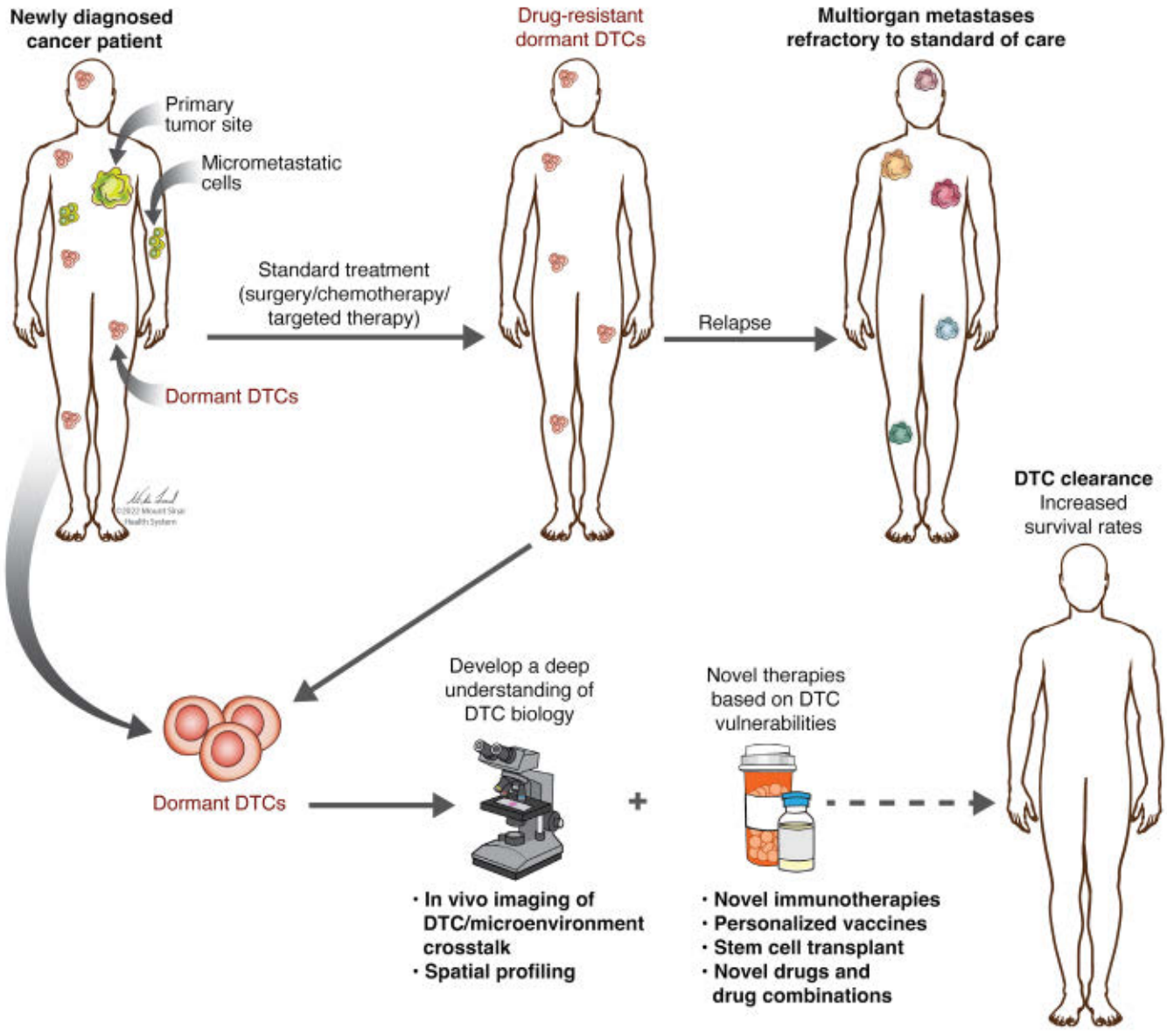

FIGURE 1. (Top) Standard of care of newly diagnosed patients and progression. At the time of diagnosis, disseminated tumor cells (DTCs) have already spread to distant organs and will survive systemic treatments while remaining in a dormant state. Eventually, these residual DTCs will reawaken and form metastases. (**Bottom**) Alternative path to target metastasis outbreaks based on an increased understanding of the biology of DTCs and development of new DTC-based therapies. This new path may lead to the clearance of dormant DTCs and to more patient cures.

of cancer cells and their microenvironment can also determine their cellular state, meaning that certain environments are capable of encouraging cancer cells that have shed from the primary tumor and landed in a distant site to achieve this self-preserving dormant state (*9*).

Looking into future therapies

The immune system may play a role in establishing and maintaining DTCs and potentially in awakening these dormant cells. However, as opposed to targeted and cytotoxic chemotherapies, novel immunotherapies don't require cell division to work, and these new treatment modalities that modulate and/or educate the immune system can be employed to target DTCs. TCI has led the development of novel cancer immunotherapies, and recently launched The neoAdjuvant Research Group to Evaluate Therapeutics (TARGET), a program geared to using novel immunotherapies around the time of surgery to help decrease the likelihood that cancer will come back (*10*). While surgery and/or radiation are often used to kill the tumor that we see using imaging, it is the microscopic DTCs that will lead to metastatic recurrence in many patients, and our early data suggest that using immunotherapies around the time of surgery may in effect "vaccinate" the patient against their cancer before removal of the primary tumor, thereby increase the likelihood of complete and permanent remission. TCI has also led efforts to develop personalized vaccine approaches that can be administered after a patient has had curative-intent surgery or radiation (or stem cell transplant in the case of hematologic malignancies) and can enable the immune system to search out and eliminate hidden DTCs in patients who are in remission but in whom the risk of relapse remains high (*11*).

While novel therapeutic approaches have revolutionized the treatment of cancer in the past decade, the majority of patients diagnosed with advanced cancer will still die from their disease, often due to metastatic recurrence after they achieve remission with up-front therapy. Only through

better understanding of how cancer metastasizes, and how dormancy of residual disease enables resistance to the therapies we are using today, will we improve cure rates. Close collaborations between experts in dormancy and metastasis, experts in cancer biology and immunology, and the clinicians treating our cancer patients will ensure better therapies to extend remission and achieve a cure for cancer patients (Figure 1).

References

1. K. Ganesh, J. Massagué, *Nat. Med.* **27**, 34–44 (2021).
2. C. Rodriguez-Tirado *et al.*, *Cancer Res.* (2022), https://doi/10.1158/0008-5472.CAN-21-4145.
3. H. Hosseini *et al.*, *Nature* **540**, 552–558 (2016).
4. J. M. Arriaga *et al.*, *Nat. Cancer* **1**, 1082–1096 (2020).
5. S. M. Lewis *et al.*, *Nat. Methods* **18**, 997–1012 (2021).
6. X. Wu *et al.*, *Nat. Cancer* **2**, 429–443 (2021).
7. C. Adamopoulos *et al.*, *Cancer Discov.* **11**, 1716–1735 (2021).
8. J. S. Di Martino *et al.*, *Nat. Cancer* **3**, 90–107 (2022).
9. D. F. Quail, J. A. Joyce, *Nat. Med.* **19**, 1423–1437 (2013).
10. T. U. Marron *et al.*, *Nat. Med.* **28**, 626–629 (2022).
11. T. U. Marron *et al.*, *Cancer Res.* **81**, LB048 (2021).

Obesity and cancer: Of molecules, societies, and other conundrums

Emily J. Gallagher[1,2*], Benjamin D. Hopkins[2,3,4], Dara J. Lundon[2,5], Nina A. Bickell[2,6]

Obesity is a major risk factor for cancer. Excess adiposity results in the coercion of numerous systemic and local metabolic, endocrine, inflammatory, immune, mechanical, genetic, and molecular factors that promote cancer development and progression. While obesity is not an infectious disease, it is socially communicable (*1*). Environmental exposures and social conditions and networks play a significant role in its development. No longer a disease of the wealthy and high-income countries, today obesity is linked with social deprivation in high-income countries and increasingly affects low-income countries that simultaneously and somewhat paradoxically struggle with the burdens of malnutrition and infectious diseases (*2*). Obesity impacts every aspect of cancer's evolution, from tumor initiation through diagnosis, therapeutic response, and survivorship.

Obesity-related cancers

In 2016, the International Agency for Research on Cancer (IARC) identified 13 cancers associated with being overweight or obese (Figure 1) (*3*). Weight loss through bariatric surgery decreases the risk (*4*). Body mass index (BMI) has been used in many epidemiological studies to define people who are overweight or obese. In European populations, increasing BMI is associated with worsening of metabolic disease; however, globally, and across diverse racial and ethnic groups, BMI poorly predicts metabolic health. Additional anthropometric measures, such as body composition assessment and metabolic biomarkers, are needed to better understand the complex relationships among systemic metabolism, body mass, and cancer.

How does obesity increase cancer risk? Many of the social and environmental factors that contribute to the development of obesity or metabolic unhealthiness are similarly linked with increased cancer incidence. Poverty, unemployment, food environment, neighborhood walkability, psychosocial stress, lack of access to high-quality medical care, and exposure to toxins or metabolic disruptors all potentially contribute to both obesity and cancer (*5*, *6*). Biological and molecular mechanisms also explain part of the complex link between these conditions (Figure 2) (*7*). Metabolic unhealthiness (as defined by insulin resistance) is associated with a greater risk of certain cancers, independent of BMI, suggesting that it is in part the metabolic dysfunction frequently coexisting with obesity that increases cancer risk (*8*).

Effects of obesity on tumor initiation and progression

The impact of obesity on tumor initiation and progression is multifaceted, as a myriad of systemic and local tissue changes occur in association with obesity. While cells frequently acquire mutations, cells with mutations are often suppressed from forming tumors by cells without mutations through a process known as competitive inhibition. Insulin or insulin-like growth factors enhance the ability of the mutation-carrying cells to survive and increase the chances of tumor initiation (*8*). Importantly, the systemic and local changes that often occur with obesity may also functionally act like many oncogenic mutations, thereby reducing the mutational requirements and provoking tumor initiation (*7*).

The relationship between obesity and cancer recurrence and mortality is even more complex. Early studies reported that obesity was associated with decreased overall survival in individuals with cancer (*9*). For certain cancers, obesity or obesity-associated factors such as hyperinsulinemia are associated with increased rates of cancer recurrence and mortality. Mechanistically, hyperinsulinemia may directly activate the phosphatidylinositol 3-kinase (PI3K)-AKT signaling pathway in cancer cells that affects cell metabolism; it also increases the expression of genes and proteins that promote cancer metastasis (*8*).

Complexities of treating cancer in the setting of obesity

Therapeutic responses to medical interventions may be worse in individuals with obesity, due to potentially receiving subtherapeutic doses of chemotherapy because of body size. Additionally, drug pharmacokinetics may be altered in obese patients, with potentially decreased tissue blood flow affecting absorption, reduced hepatic conversion of prodrugs to active drugs, and changes in hepatic and renal drug clearance (*10*). Interestingly, some recent retrospective analyses of individuals with cancers reported that those with obesity had better survival when treated with chemotherapy or immune checkpoint inhibitors than did normal-weight individuals (*11*, *12*). These reports are intriguing and worthy of further investigation. Were the people with lower BMIs in these studies individuals who had lost weight due to cancer cachexia? Alternatively, could obesity-related tumor

[1]Division of Endocrinology, Diabetes and Bone Diseases; [2]Tisch Cancer Institute; [3]Department of Genetics and Genomic Sciences; [4]Department of Oncological Sciences; [5]Department of Urology; and [6]Institute for Health Equity Research, Departments of Population Health Science and Policy, and Medicine, Icahn School of Medicine at Mount Sinai, New York, NY

*Corresponding author: emily.gallagher@mssm.edu

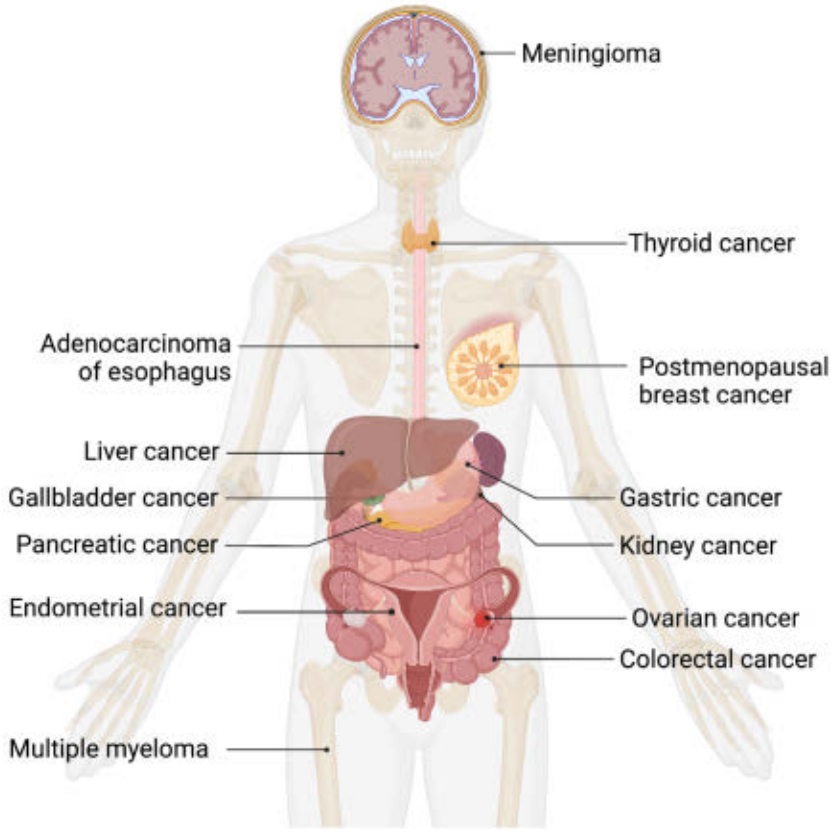

FIGURE 1. Cancers associated with obesity. The 13 obesity-associated cancers as described by the International Agency for Research on Cancer (IARC) in 2016. Created with BioRender.com.

mutational burden, inflammation, immune cell infiltration, or fibrosis in the tumor microenvironment affect responses to treatments?

For patients with cancer, surgery offers a potential cure. Being overweight or obese impacts the risk–benefit profile of this intervention, where the surgery may be more technically challenging, and peri- and postoperative complications are increased. To address these issues, it is necessary to enhance surgical techniques.

Another complexity in the obesity and cancer relationship is that cancer treatments can worsen metabolic diseases. Many individuals with breast and prostate cancer are treated with hormonal therapy; in cases of multiple myeloma, glucocorticoids are given for therapeutic benefit. For individuals with these cancers, weight gain and metabolic dysfunction are well-recognized side effects of the treatment and are associated with worse outcomes. Novel small-molecule inhibitors target specific pathways that are mutated in cancers; for example, PI3K inhibitors have been approved for breast cancer and lymphoma, and mammalian target of rapamycin (mTOR) inhibitors are used in the treatment of several solid cancers. While these agents target the pathways that may be activated in cancers in the setting of obesity, inhibiting them also impairs metabolic signaling pathways, leading to insulin resistance and hyperglycemia, particularly in those with obesity (*8*). These effects can cause treatment interruptions and morbidity and may also result in drug resistance by reactivating the target-

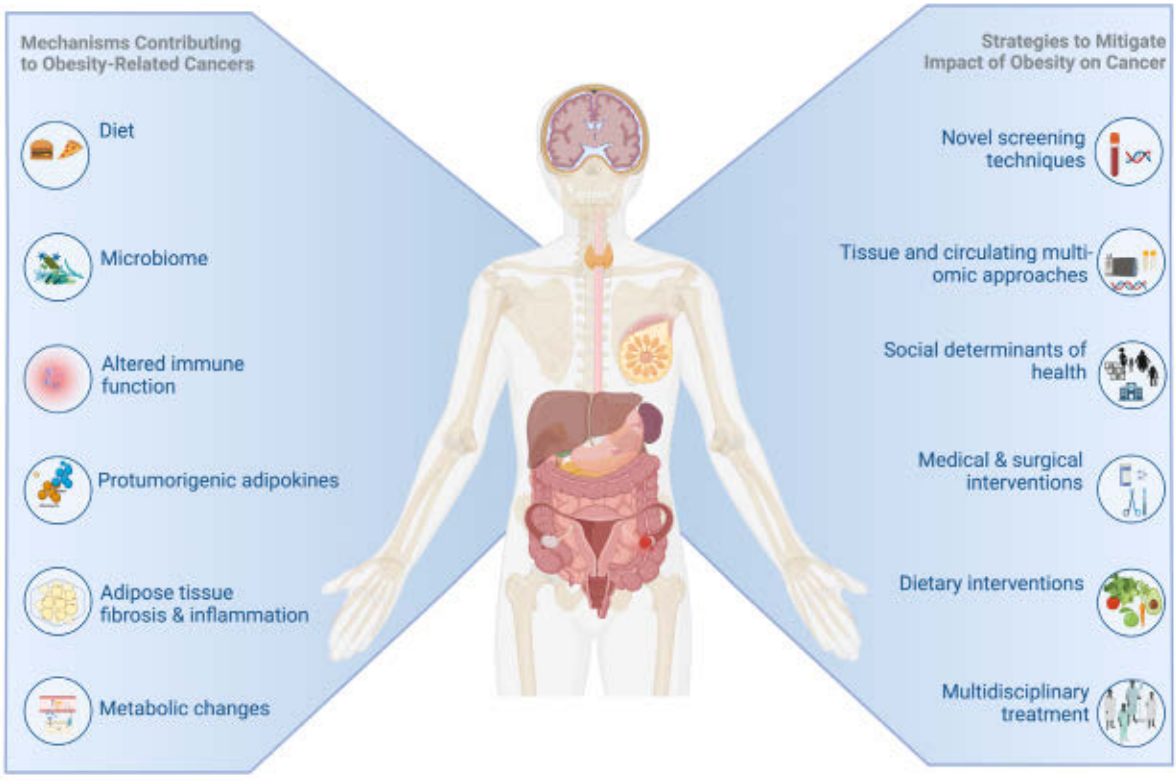

FIGURE 2. Mechanisms linking obesity and cancer, and strategies to mitigate the impact of obesity on cancer. A nutrient-dense diet of processed food can lead to changes in the microbiome, directly interacting with the cells of the gastrointestinal tract and impacting circulating nutrients. Increased adiposity can cause chronic inflammation, with changes in immune-cell tissue infiltration and function, increased cytokine production, and changes in circulating adipokines (e.g., leptin, adiponectin). Adipose tissue fibrosis occurs in obesity, leading to changes in the mechanical properties of those tissues and cell-signal transduction. Metabolically unhealthy obesity is associated with hyperinsulinemia, dyslipidemia, and hyperglycemia as well as changes in sterol hormone levels. A number of approaches are needed to reduce the impact of obesity on cancer risk and outcomes. Created with BioRender.com.

ed pathway. Identifying molecular targets that can inhibit cancer growth without worsening systemic metabolism is essential (*13*).

Future strategies to address obesity-related cancer

While epidemic and challenging, obesity is treatable. However, managing obesity requires active redress of obesity-related stigmas and perceptions. In some cultures, it represents abundance and comfort, in others, laziness and weak self-control. Addressing these stigmas is necessary to motivate behavior change from underutilizing cancer screening to detect precancerous lesions to losing weight to reduce the risk of cancer recurrence. Gaining a greater understanding of the impact of social and environmental factors and developing transdisciplinary, medical, community, and governmental engagement strategies to address behavior change is crucial. Studying the risks of individual cancers associated with obesity and determining what changes to screening and treatment recommendations would alter outcomes in obesity-associated cancers will require careful investigation across diverse racial and ethnic groups. Understanding how obesity impacts cancer risk in transgender individuals is also critical (*14*).

Employing multiple emerging technological approaches will expand our knowledge of the mechanisms leading to obesity-associated cancers and uncover novel therapeutic targets. Dietary interventions, such as intermittent fasting and low-carbohydrate, fasting-mimicking, and ketogenic diets are being investigated as strategies to improve treatment responses in individuals with cancers that rely on signaling through pathways such as the PI3K-AKT pathway. Dietary strategies are also being explored to reduce adverse metabolic effects of pharmacological therapies (*13*). While these approaches may provide therapeutic benefits, it will be essential to address societal food insecurity before they can be universally adopted. Understanding whether cancer risk reduction from bariatric surgery is simply attributable to weight loss, or other mechanisms, will be important in developing future therapeutic strategies (*4*). The widespread availability of bariatric surgery is limited relative to the number of individuals with obesity, due to its cost, invasiveness, and requirement for advanced expertise, so less invasive or nonsurgical interventions that achieve similar results are being explored (*15*). The repurposing of weight loss treatments, such as glucose-dependent insulinotropic peptide and glucagon-like peptide-1 receptor agonists that lead to dramatic weight loss in individuals with obesity, warrants investigation as a means of preventing cancer and reducing recurrence or mortality.

Given the global obesity pandemic and the growth of obesity-related cancers, elucidating the mechanisms that give rise to these cancers, from molecular to societal, is essential if we are to develop novel strategies to prevent and treat them.

References

1. N. A. Christakis, J. H. Fowler, *N. Engl. J. Med.* **357**, 370–379 (2007).
2. M. Bluher, *Nat. Rev. Endocrinol.* **15**, 288–298 (2019).
3. B. Lauby-Secretan *et al.*, *N. Engl. J. Med.* **375**, 794–798 (2016).
4. A. Aminian *et al.*, *JAMA* **327**, 2423–2433 (2022).
5. G. R. Kamath *et al.*, *Front. Oncol.* **8**, 220 (2018).
6. G. R. Kamath *et al.*, *Ann. Epidemiol.* **48**, 43–50.e4 (2020).
7. B. D. Hopkins, M. D. Goncalves, L. C. Cantley, *J. Clin. Oncol.* **34**, 4277–4283 (2016).
8. E. J. Gallagher, D. LeRoith, *Nat. Rev. Cancer* **20**, 629–644 (2020).
9. E. E. Calle, C. Rodriguez, K. Walker-Thurmond, M. J. Thun, *N. Engl. J. Med.* **348**, 1625–1638 (2003).
10. J. J. Griggs *et al.*, *J. Clin. Oncol.* **39**, 2037–2048 (2021).
11. A. Martini *et al.*, *Prostate Cancer Prostatic Dis.* **25**, 472–478 (2022).
12. J. L. McQuade *et al.*, *Lancet Oncol.* **19**, 310–322 (2018).
13. B. D. Hopkins *et al.*, *Nature* **560**, 499–503 (2018).
14. S. Gaglani, R. S. Purohit, A. K. Tewari, N. Kyprianou, D. J. Lundon, *Am. J. Clin. Exp. Urol.* **10**, 63–72 (2022).
15. S. Chablaney, N. A. Kumta, *J. Diabetes* **11**, 351–358 (2019).

Advancing cancer precision medicine by creating a better toolbox for cancer therapy

Jian Jin[1,2,3,4,5]*, Arvin C. Dar[1,2,3,4], Deborah Doroshow[1]

Among approximately 20,000 proteins in the human proteome, 627 have been identified by cancer-dependency studies as priority cancer targets, which are functionally important for various cancers. Of these 600-plus priority targets, 232 are enzymes and 395 are nonenzyme proteins (*1*). Tremendous progress has been made over the past several decades in targeting enzymes, in particular kinases, which have suitable binding pockets that can be occupied by small-molecule inhibitors, leading to U.S. Food and Drug Administration (FDA) approvals of many small-molecule drugs as targeted anticancer therapies. However, most of the 395 nonenzyme protein targets, including transcription factors (TFs), do not have suitable binding pockets that can be effectively targeted by small molecules. These targets have consequently been considered undruggable; however, new cutting-edge approaches and technologies have recently been developed to target some of these "undruggable" proteins in order to advance precision oncology.

[1]Tisch Cancer Institute; [2]Department of Oncological Sciences; [3]Department of Pharmacological Sciences; [4]Mount Sinai Center for Therapeutics Discovery; [5]Department of Neuroscience, Icahn School of Medicine at Mount Sinai, New York, NY

*Corresponding author: jian.jin@mssm.edu

TPD, a promising approach to precision cancer therapeutics

Targeted protein degradation (TPD) refers to the process of chemically eliminating proteins of interest (POIs) by utilizing small molecules, which are broadly divided into two types of modalities: PROteolysis Targeting Chimeras (PROTACs) and molecular glues (*2*). PROTACs are heterobifunctional small molecules that contain two moieties: one binding the POI, linked to another binding an ubiquitin E3 ligase. The induced proximity between the POI and ubiquitination machinery leads to selective polyubiquitylation of the POI and its subsequent degradation by the ubiquitin–proteasome system (UPS). Molecular glues are monovalent small molecules, which, when built for TPD, directly induce interactions between the POI and an E3 ligase, also resulting in polyubiquitylation and subsequent degradation of the POI by the UPS. One of the biggest potential advantages of these therapeutic modalities over traditional inhibitors

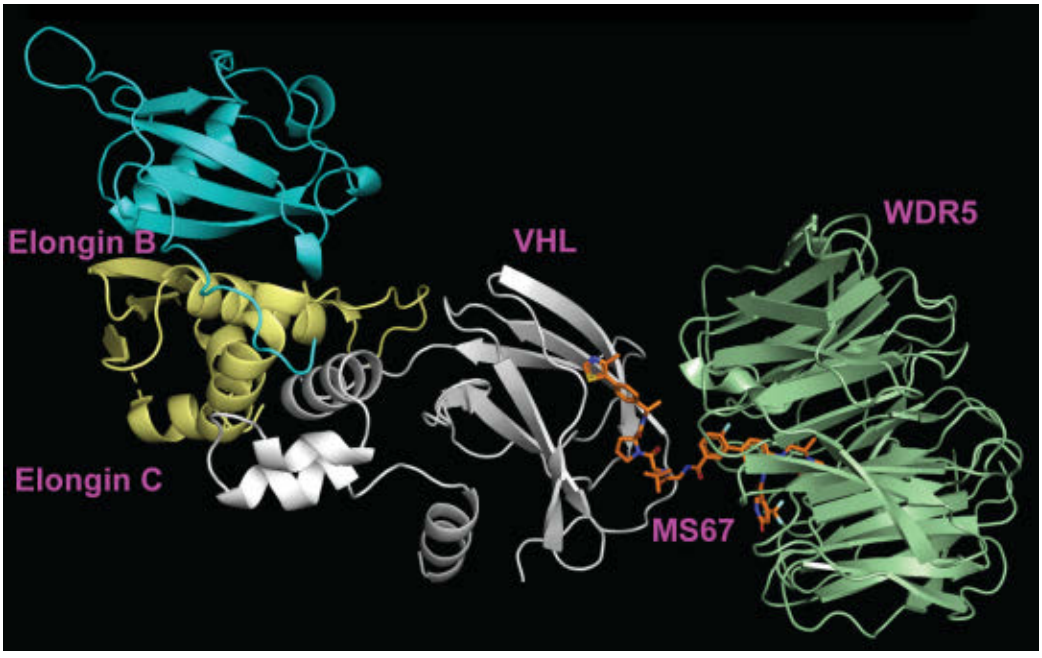

FIGURE 1. A high-resolution (2.1 Å) crystal structure of the WDR5–MS67–VCB ternary complex (Protein Data Bank ID: 7JTP), which is the first crystal structure of any WDR5-PROTAC-E3 ligase ternary complexes. MS67 induced extensive protein–protein interactions and enhanced binding cooperativity between WDR5 and the E3 ligase VHL, resulting in highly effective WDR5 degradation and cancer cell–killing effects.

is that PROTACs and molecular glues can target undruggable proteins. Explosive growth has been seen in the TPD field over recent years (*2*, *3*). Here, we highlight several recent advancements.

TF-PROTAC, a novel platform for targeting undruggable tumorigenic TFs

Many undruggable TFs are tumorigenic. To target them, TF-PROTAC was developed (*4*), which exploits the fact that TFs bind DNA in a sequence-specific manner. TF-PROTAC was created to selectively bind a TF and E3 ligase simultaneously, by conjugating a DNA oligonucleotide specific for the TF of interest to a selective E3 ligase ligand. As stated earlier, this simultaneous binding and induced proximity leads to selective polyubiquitination of the TF and its subsequent degradation by the UPS. TF-PROTAC is a cutting-edge technology that could potentially provide a universal strategy for targeting most undruggable tumorigenic TFs.

Development of novel PROTAC degraders

WDR5, an important scaffolding protein, not an enzyme, is essential for sustaining tumorigenesis in multiple cancers, including MLL-rearranged (*MLL*-r) leukemia. However, small-molecule inhibitors that block the protein–protein interaction (PPI) between WDR5 and its binding partners exhibit very modest cancer cell–killing effects, likely due to the confounding fact that these PPI inhibitors target only some—but not all—of WDR5's oncogenic functions. To address this shortcoming, a novel WDR5 PROTAC, MS67, was recently created using a powerful approach that effectively eliminates the protein and thereby all WDR5 functions via ternary complex structure-based design (Figure 1) (*5*). MS67 is a highly effective WDR5 degrader that potently and selectively degrades WDR5 and effectively suppresses the proliferation of tumor cells both in vitro and in vivo. This study provides strong evidence that pharmacological degradation of WDR5 as a novel therapeutic strategy is superior to WDR5 PPI inhibition for treating WDR5-dependent cancers.

EZH2 is an oncogenic methyltransferase that catalyzes histone H3 lysine 27 trimethylation, mediating gene repression. In addition to this canonical function, EZH2 has numerous noncanonical tumorigenic functions. EZH2 enzymatic inhibitors, however, are generally ineffective in suppressing tumor growth in triple-negative breast cancer (TNBC) and *MLL*-r leukemia models and fail to phenocopy antitumor effects induced by EZH2 knockdown strategies. To target both canonical and noncanonical oncogenic functions of EZH2, several novel EZH2 degraders were recently developed, including MS1943, a hydrophobic tag–based EZH2 degrader (*6*), and MS177, an EZH2 PROTAC (*7*). MS1943 and MS177 effectively degrade EZH2 and suppress in vitro and in vivo growth in TNBC and *MLL*-r leukemia, respectively, suggesting that EZH2 degraders could provide a novel and effective therapeutic strategy for EZH2-dependent tumors.

MS21, a novel AKT PROTAC degrader, was developed to target activated AKT, the central node of the PI3K–AKT–mTOR signaling pathway (*8*). MS21 effectively suppresses the proliferation of PI3K–PTEN pathway-mutant cancers with wild-type KRAS and BRAF, which represent a large percentage of all human cancers. Another recent technology that expands the bifunctional toolbox for TPD is the demonstration that the E3 ligase KEAP1 can be leveraged for PROTAC development using a selective KEAP1 ligand (*9*). Overall, tremendous progress has been made in discovering novel degraders, some of which have advanced to clinical development as targeted therapies (*2*, *3*).

Novel approaches to selective TPD in cancer cells

To minimize uncontrolled protein degradation in normal tissues, which may cause potential toxicity, a new technology was developed that incorporates a light-inducible switch, termed "opto-PROTAC" (*10*). This switch serves as a caging group that renders opto-PROTAC inactive in all cells in the absence of ultraviolet (UV) light. Upon UV irradiation, however, the caging group is removed, resulting in the release of the active degrader and spatiotemporal control of TPD in cancer cells. Another strategy to achieve selective TPD in cancer over normal cells is to cage degraders with a folate group (*11*, *12*). Folate-caged degraders are inert and selectively concentrated within cancer cells, which overexpress folate receptors compared to normal cells. The caging group is subsequently removed inside tumor cells, releasing active degraders and achieving selective TPD in these cells. These novel approaches potentially enable degraders to be precision cancer medicines.

Trametiglue, a novel and atypical molecular glue

The RAS–RAF–MEK–ERK signaling pathway, one of the most frequently mutated pathways in cancer, has been intensively targeted. Several drugs, such as the KRAS G12C inhibitor sotorasib and the MEK inhibitor trametinib, have been approved by the FDA. A significant advancement in this area is the discovery that trametinib unexpectedly binds a pseudokinase scaffold termed "KSR" in addition to MEK through interfacial contacts (*13*). Based on this structural and mechanistic insight, trametiglue, an analog of trametinib, was created as a novel molecular glue to limit adaptive resistance to MEK inhibition by enhancing interfacial binding between MEK, KSR, and the related homolog RAF. This study provides a strong foundation for developing next-generation drugs that target the RAS pathway.

TF-DUBTAC, a novel technology to stabilize undruggable tumor-suppressive TFs

Complementary to degrading tumorigenic TFs, stabilizing tumor-suppressive TFs could provide another effective approach for treating cancer. While most tumor-suppressive TFs are undruggable, TF-DUBTAC was recently developed as a generalizable platform to stabilize tumor-suppressive TFs (*14*). Deubiquitinase-targeting chimeras (DUBTACs) are heterobifunctional small molecules with a deubiquitinase (DUB) ligand linked to a POI ligand, which stabilize POIs by harnessing the deubiquitination machinery (*15*). Similar to TF-PROTAC, TF-DUBTAC exploits the fact that most TFs bind specific DNA sequences. TF-DUBTAC links a DNA oligonucleotide specific to a tumor-suppressive TF with a selective DUB ligand, resulting in simultaneous binding of the TF and DUB. The induced proximity between the TF and DUB leads to selective deubiquitination of the TF and its stabilization. As an exciting new technology, TF-DUBTAC provides a potential general strategy to stabilize most undruggable tumor-suppressive TFs for treating cancer.

Future outlook

The breathtaking pace we are seeing in the development of innovative approaches and technologies for advancing cancer therapies is only expected to accelerate. The promising clinical results achieved by PROTACs with established targets are particularly encouraging and pave the way for development of PROTACs for newer and more innovative targets. These groundbreaking discoveries have now put opportunities to fully realize cancer precision medicine within our reach.

References

1. F. M. Behan *et al., Nature* **568**, 511–516 (2019).
2. B. Dale *et al., Nat. Rev. Cancer* **21**, 638–654 (2021).
3. A. Mullard, *Nat. Rev. Drug Discov.* **20**, 247–250 (2021).
4. J. Liu *et al., J. Am. Chem. Soc.* **143**, 8902–8910 (2021).
5. X. Yu *et al., Sci. Transl. Med.* **13**, eabj1578 (2021).
6. A. Ma *et al., Nat. Chem. Biol.* **16**, 214–222 (2020).
7. J. Wang *et al., Nat. Cell Biol.* **24**, 384–399 (2022).
8. J. Xu *et al., Cancer Discov.* **11**, 3064–3089 (2021).
9. J. Wei *et al., J. Am. Chem. Soc.* **143**, 15073–15083 (2021).
10. J. Liu *et al., Sci. Adv.* **6**, eaay5154 (2020).
11. J. Liu *et al., J. Am. Chem. Soc.* **143**, 7380–7387 (2021).
12. H. Chen *et al., J. Med. Chem.* **64**, 12273–12285 (2021).
13. Z. M. Khan *et al., Nature* **588**, 509–514 (2020).
14. J. Liu *et al., J. Am. Chem. Soc.* **144**, 12934–12941 (2022).
15. N. J. Henning *et al., Nat. Chem. Biol.* **18**, 412–421 (2022).

Putting a bull's-eye on cancer's back

Scientists are aiming the immune system's "troops" directly at tumors to better treat cancer

Joshua D. Brody, Brian D. Brown

Immunotherapy has transformed the treatment of several types of cancers. In particular, immune checkpoint blockade (ICB), which reinvigorates killer T cells, has helped extend the lives of many patients with advanced-stage lung, bladder, kidney, or skin cancers. Unfortunately, ~80% of patients do not respond to current immunotherapies or eventually relapse. Emerging data indicate that one of the most profound ways cancers resist immunotherapy is by keeping killer T cells out of the tumor and putting other immune cells in a suppressed state (*1*). This understanding is giving rise to a new frontier in immunotherapy that is using synthetic biology and other approaches to reprogram the tumor from immune "cold" to immune "hot," so T cells can be recruited to the tumor, and enter, target, and destroy the cancer cells (*2*) (Figure 1).

Cancers protect themselves by keeping out immune cells

Cancers grow in tissues like foreign invaders. Though they start from healthy cells, mutations turn cells malignant and allow them to grow unchecked. T cells can kill malignant cells that express mutated proteins, but cancers employ strategies to fend off the T cells. One way they do this is by upregulating a molecule called programmed death ligand 1 (PD-L1), which binds to the immune checkpoint PD-1 on T cells and suppresses the T cells' ability to kill cancer cells. Immunotherapy drugs that block PD-1 or PD-L1, such as pembrolizumab or atezolizumab, reactivate T cells in the tumor and enable them to eliminate cancer cells.

As noted, most patients do not respond to current immunotherapies; this is because cancers use additional mechanisms to evade T cells. These mechanisms are now being revealed by extensive profiling of patient tumors at cancer centers such as The Tisch Cancer Institute at Mount Sinai, using state-of-the-art techniques, including single-cell and spatial 'omics and multiplex imaging (*3*, *4*). Converging evidence indicates that one of the most profound ways that tumors evade the immune system is by keeping themselves "cold." This is a state in which there are either few T cells in the tumor or the T cells are kept out of reach of cancer cells completely. Cold tumors also have few dendritic cells (DCs)—a type of immune cell that turns on T cells. Cold tumors generally respond poorly to immunotherapy (*5*). In contrast, "hot" tumors have a high content of T cells and DCs, have better outcomes, and are more responsive to immunotherapy (*1*). Studies from the lab of Miriam Merad and others have refined this understanding even further by showing that a particular subtype of DC, called DC1, needs to be in the tumor for immunotherapy to achieve an effective antitumor T-cell response (*6*), and that even when DC1s are present, the tumor often puts them in a suppressed state (*7*).

Icahn Genomics Institute, Precision Immunology Institute, and Tisch Cancer Institute, Icahn School of Medicine at Mount Sinai, New York, NY

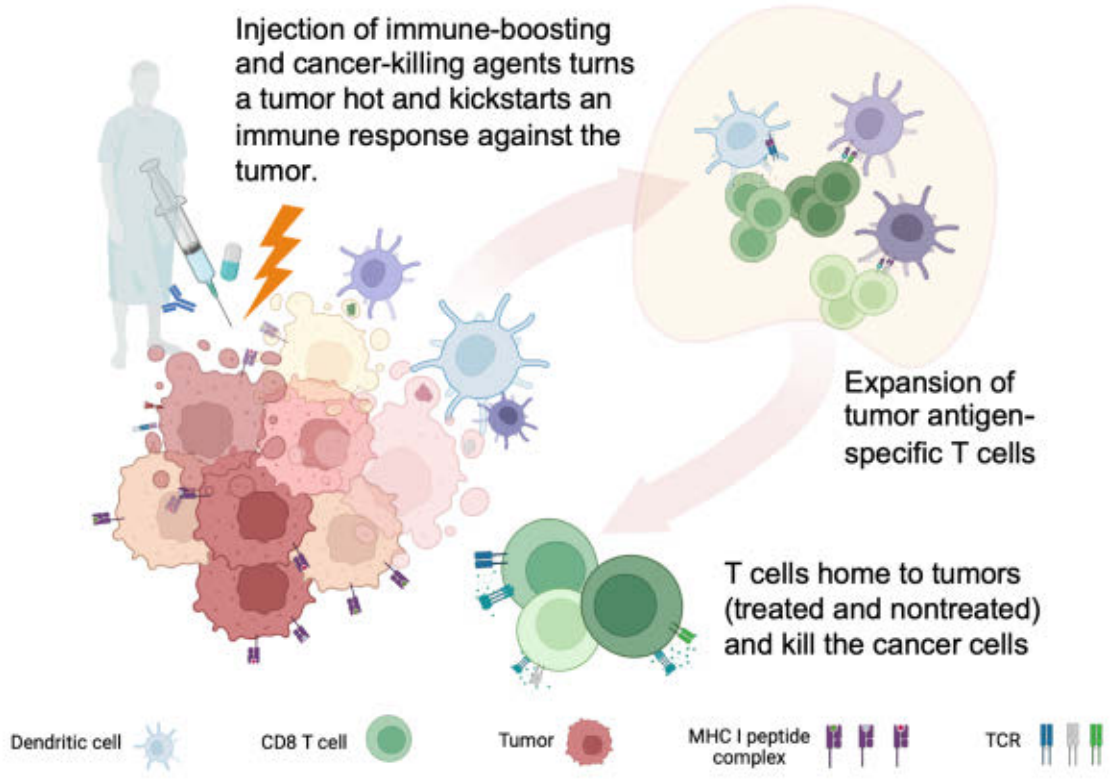

FIGURE 1. In situ vaccine (ISV) turns up the heat in a patient's tumor and kickstarts an immune response against metastatic cancer. A tumor region is locally treated with: (1) a cancer cell–killing agent, such as an oncolytic virus or radiation, to release antigens from the cancer cells; (2) a proinflammatory agent, such as a toll-like receptor (TLR) agonist or a cytokine-encoding messenger RNA (mRNA), to activate the immune system and recruit T cells; and (3) dendritic cell (DC) growth factors, such as FLT3L or GM-CSF, to expand DCs, which take up and present tumor antigens to T cells and direct the T cells to kill cancer cells. CD8, cluster of differentiation 8; MHC I, major histocompatibility complex class I; TCR, T cell receptor.

In situ vaccination: Turning up the heat in the tumor

The insights being uncovered from studies of tumor immunology are leading to the development of more comprehensive immunotherapy strategies that engage multiple arms of the immune system. One very promising example is in situ vaccination (ISV), which is designed to remodel the tumor from cold to hot while boosting antitumor T cells (*2*). Early iterations of ISV relied primarily on the injection of inflammatory agents, such as toll-like receptor (TLR) or stimulator of interferon genes (STING) agonists, into the tumor, but more sophisticated approaches are now being employed to induce robust antitumor responses (*8*). Our team at Mount Sinai developed a novel ISV cocktail that combines the cytokine FLT3L with a TLR3 agonist, the former to recruit and expand DC1s and the latter to activate the DC1s and induce an inflamed tumor state (*9*). Additionally, the tumor injected with FLT3L/TLR3 agonist is treated with local radiation, which kills cancer cells and releases tumor antigens that are picked up by the DC1s, which then activate T cells. In preclinical studies, we showed that ISV very effectively induces antitumor T cells. When patients with advanced-stage lymphoma were treated by ISV, many had complete and durable tumor regressions not only of the treated tumor, but also of distal tumors that had not received the ISV treatment, an indicator that the treatment had induced systemic tumor immunity (*9*). Immune monitoring of the trial suggested that T cells in the tumors had been turned off by PD1; this has prompted follow-up clinical trials combining ISV and anti-PD1 immunotherapy. Recent data from this trial found that the combination approach achieved partial and sometimes complete cancer remissions not only for lymphoma but also advanced-stage breast cancer that had failed numerous prior chemotherapies.

Attacking tumors with synthetic bioarmaments

Scientists are also turning to synthetic biology in their effort to turn the tumors hot and induce antitumor immunity. One promising strategy is the use of oncolytic viruses. As their name implies, oncolytic viruses lyse (break down) cancer cells. The general principle in the design of these viruses is to engineer them to infect or replicate only in cancer cells. The initial hypothesis was that the virus would spread throughout the body killing cancer cells and sparing healthy cells until the cancer was eliminated. However, it is now understood that these viruses are most effective when they are used as an ISV to provoke an antitumor immune response. This rethinking led to the development of the FDA-approved oncolytic virus talimogene laherparepvec (T-VEC), which is a herpes virus designed not only to replicate in melanoma cells but also to express the cytokine GM-CSF, which attracts DCs to the tumor (*10*). Newer iterations of viral oncolytics are being designed to express additional immune-stimulating molecules, including PD1 antagonists (*11*), and using even more inflammatory viruses, such as Newcastle disease virus (*12*), which all serve to render the tumor hot and improve therapeutic efficacy.

The technology used for the COVID messenger RNA (mRNA) vaccines is also being used to promote antitumor immunity. One way this is being done is through an approach similar to that used for other cancer vaccines, in which tumor antigens are encoded in the mRNA and injected into patients to provoke an immune response against the tumor (*13*). An even newer concept in the application of mRNA technology involves applying it to reprogram the tumor from cold to hot. Virtually any gene can be encoded with mRNA technology, so scientists took advantage of this fact to develop an mRNA cocktail that encoded four different proinflammatory

cytokines (*14*). Intratumoral injection of the mRNA cocktail in mice led to immune infiltration of different tumors and antitumor immunity even against distal tumors. Achieving efficient, targeted delivery of mRNA to tumors is still a challenge, as it is critical for enough cells in the tumor to express the mRNA-encoded proteins and to ensure the inflammatory mRNAs are not expressed in healthy tissue. To achieve this goal, researchers are making advances in mRNA design to enhance tumor targeting of the payload, including the use of microRNA-based targeting (*15*, *16*).

Genetic engineering of T cells is another strategy being employed to turn tumors from suppressed to stimulatory states. T cells can be engineered to express a chimeric antigen receptor (CAR) specific for molecules on the surface of cancer cells (*17*). When injected, CAR T cells home to tumors and kill cancer cells. Though CAR T cells can be effective in treating hematopoietic cancers, they have been less successful against solid tumors, and this is partly because the CAR T cells are kept out of the tumors or get suppressed once they enter. To counter this defense, CAR T cells are being "armed" to express molecules, such as IL-12 or other factors, that make the tumor susceptible to killing by the patient's other T cells (*18*). A novel advance in CAR T cell therapy is to design them to home to and kill immunosuppressive cells in the tumor, including macrophages and fibroblasts (*19*). This method has been effective in animal models in promoting tumor immunity and reducing tumor growth of several solid tumors, but its effectiveness in humans still requires clinical testing.

The array of different strategies being developed to change the tumor's immune composition from cold to hot and from suppressed to stimulatory is removing key mechanisms used by tumors to evade the immune system. In doing so, this powerful new arsenal of therapeutics is enabling even more effective immunotherapies for the treatment of cancer.

References

1. H. Salmon, R. Remark, S. Gnjatic, M. Merad, *Nat. Rev. Cancer* **19**, 215–227 (2019).
2. M. J. Lin *et al.*, *Nat. Cancer* **3**, 911–926 (2022).
3. Y. Lavin *et al.*, *Cell* **169**, 750–765.e17 (2017).
4. A. M. Leader *et al.*, *Cancer Cell* **39**, 1594–1609.e12 (2021).
5. R. Cristescu *et al.*, *Science* **362**, eaar3593 (2018).
6. H. Salmon *et al.*, *Immunity* **44**, 924–938 (2016).
7. B. Maier *et al.*, *Nature* **580**, 257–262 (2020).
8. A. Pavlick *et al.*, *Cancer Immunol. Res.* **8**, 70–80 (2020).
9. L. Hammerich *et al.*, *Nat. Med.* **25**, 814–824 (2019), doi: 10.1038/s41591-019-0410-x.
10. R. H. I. Andtbacka *et al.*, *J. Clin. Oncol.* **33**, 2780–2788 (2015).
11. B. B. Haines *et al.*, *Cancer Immunol. Res.* **9**, 291–308 (2021).
12. A. Javaheri *et al.*, *Cancer Res. Commun.* **2**, (2022), doi: 10.1158/2767-9764.crc-22-0025.
13. U. Sahin *et al.*, *Nature* **585**, 107–112 (2020).
14. C. Hotz *et al.*, *Sci. Transl. Med.* **13**, eabc7804 (2021), doi: 10.1126/scitranslmed.abc7804.
15. R. Jain *et al.*, *Nucleic Acid Ther.* **28**, 285–296 (2018).
16. B. D. Brown, L. Naldini, *Nat. Rev. Genet.* **10**, 578–585 (2009).
17. C. H. June, M. Sadelain, *N. Engl. J. Med.* **379**, 64–73 (2018).
18. S. Rafiq, C. S. Hackett, R. J. Brentjens, *Nat. Rev. Clin. Oncol.* **17**, 147–167 (2020).
19. A. R. Sánchez-Paulete *et al.*, *Cancer Immunol. Res.* **12**, CIR-21-1075 (2022), doi: 10.1158/2326-6066.CIR-21-1075.

Decoding the tumor immune microenvironment for cancer therapy

Lucas Ferrari de Andrade[1,2,3], Marta Łuksza[1,2,3,4], Robert M. Samstein[1,3,5], Miriam Merad[1,2,3], Nina Bhardwaj[1,3,6]*

Immunotherapy has revolutionized cancer care with unprecedented responses and long-term survival rates, but lack of response and acquired resistance in certain cancer types remain as major challenges. Here we discuss the biology of immune cells in the tumor microenvironment and their effect on tumor evolution, as well as efforts to harness innate immunity for therapy. The use of neoantigens in immune activation and mechanisms of immunotherapy resistance are also discussed.

Immunotherapy response and resistance

Immune checkpoint inhibitors (ICIs) targeting CTLA-4 and PD1/PDL-1 have offered a new therapeutic pillar that harnesses host immunity, with dramatic and durable benefit for some patients (Figure 1). However, only a minority of cancer patients ultimately benefit from ICI therapy, which emphasizes the importance of identifying predictors of response and understanding both intrinsic and acquired resistance. While tumor expression of PDL-1 has remained the primary biomarker utilized in prospective clinical studies, next-generation sequencing has revealed other associations with improved response and less resistance (*1*). An improved understanding of tumor features that predicts response or resistance to therapy will facilitate development of novel strategies to broaden the number of patients who benefit from immunotherapy. DNA damage repair deficiencies and associated high tumor mutational burden with presumed increased tumor neoantigens have been associated with improved outcomes (*2*). Germline associations with ICI response have also been implicated, including human leukocyte antigen (HLA) heterozygosity and diversity (*3*). Furthermore, tumor-infiltrating T cells and the presence of B cells in tertiary lymphoid structures within the tumor have been implicated in ICI response, along with increased type-1 conventional dendritic cells (cDC1s) and natural killer (NK) cells, and decreased suppressive macrophage and neutrophil infiltrations within the tumor (*4*). The complex integration of multiple clinical and genomic datapoints can be further leveraged using high-dimensional mapping and machine learning to improve ICI response prediction. Additional mechanistic studies are required in order to understand why only some patients respond to ICIs and to develop rational immunotherapy combination strategies.

High-dimensional mapping to identify mechanisms of resistance

The cancer immunology field is rapidly expanding, with nearly 5,000 novel agents in clinical trials. However, progress is impaired in part by an incomplete understanding of the mechanisms underlying the antitumor activity of and resistance to immunotherapeutic agents in vivo in humans. While clinical outcomes are ultimately the most important metrics to support regulatory approvals, it is only through smaller focused trials that enable the characterization of molecular responses to drug candidates that we can transform our understanding and advance the cancer immunity field.

Due to their ability to profile tissue in the context of active treatment, neoadjuvant clinical trials in which patients receive brief presurgical therapeutic interventions—often termed "window-of-opportunity" trials—provide an invaluable opportunity to elucidate how agents work in humans using high-dimensional mapping of cancer lesions during exposure to novel or established agents.

[1]Precision Immunology Institute, [2]Department of Oncological Sciences, [3]Tisch Cancer Institute, Icahn School of Medicine at Mount Sinai, [4]Department of Genetics and Genomics, and [5]Department of Radiation Oncology, Icahn School of Medicine at Mount Sinai, New York, NY; [6]Extramural member, Parker Institute for Cancer Immunotherapy, San Francisco, CA

*Corresponding author: nina.bhardwaj@mssm.edu

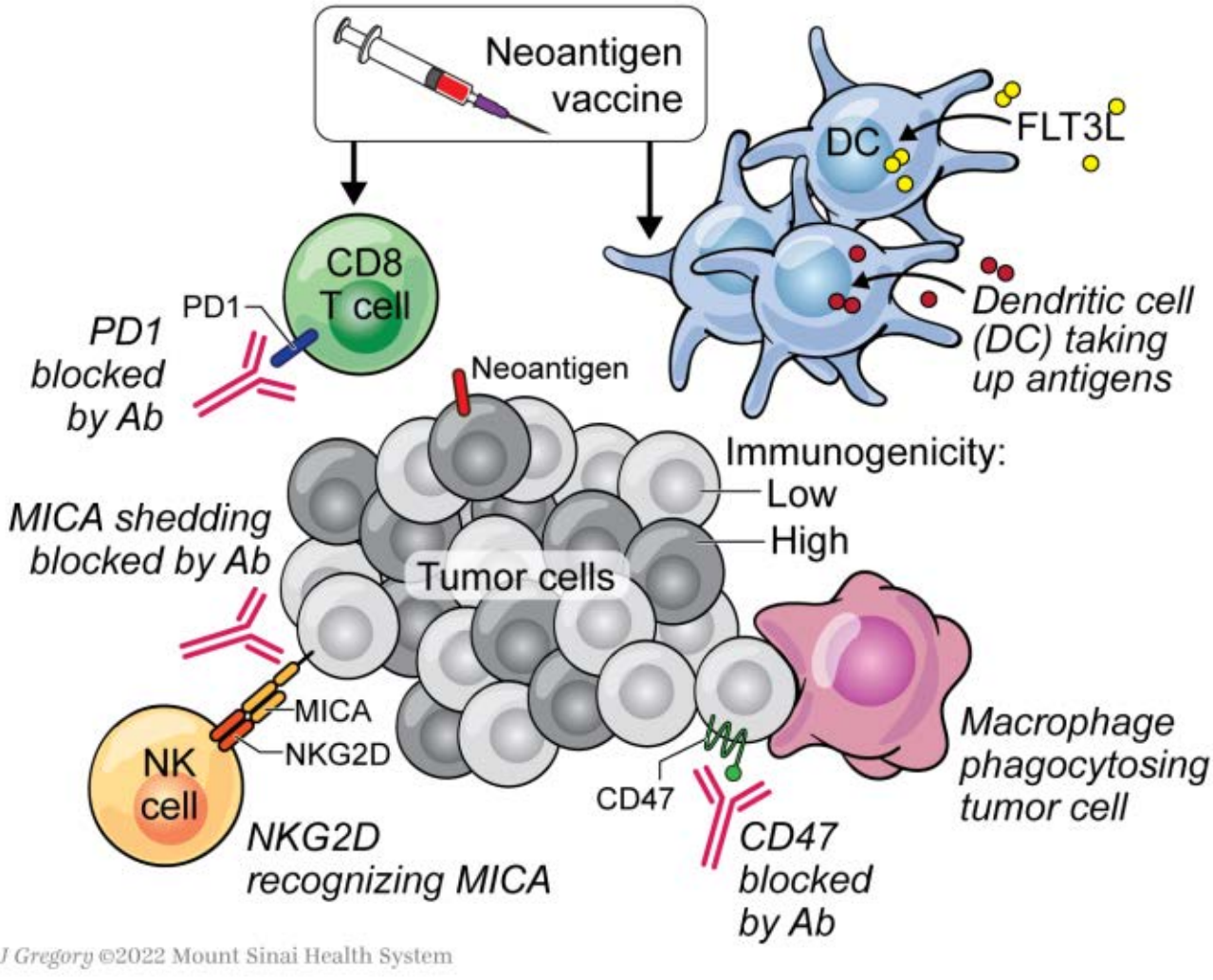

FIGURE 1. Immunotherapeutic approaches for solid tumors. CD8⁺ T cells recognize tumor-associated antigens, such as neoantigens expressed by tumor cells, as a consequence of tumor evolution. Neoantigens can be highly immunogenic and can be used in vaccines that further enhance the antitumor activity of CD8⁺ T cells via antigen presentation by dendritic cells. Antibody (Ab)-mediated blockade of PD-1, an inhibitory receptor, helps unleash CD8⁺ T cell functions. However, tumor cells can display low immunogenicity through low tumor mutation burden or loss of immunogenic antigens and can escape adaptive immunity through "immune resistance." The antibody-mediated blockades of MHC class I polypeptide–related sequence A (MICA) and CD47 are examples of how cytotoxic functions of natural killer cells and macrophages can be restored to improve antitumor immunity, respectively, enabling treatment for tumors that otherwise would be resistant to immunotherapy.

However, these trials require centralized multidisciplinary teams such as the one established at The Tisch Cancer Institute of Mount Sinai under the cooperative program The neoAdjuvant Research Group to Evaluate Therapeutics (TARGET). Programs such as this support trials that will yield relevant multidimensional datasets, inform future clinical development, and identify mechanisms of resistance, thus creating a virtuous cycle of bedside-to-bench-to-bedside-to-bench research (*5*). The Mount Sinai Human Immune Monitoring Center is an essential partner of TARGET, as it provides expertise as well as access to new technological platforms. This approach helps generate tissue "atlases" with unprecedented detail and reveals specific molecular alterations in cancer tissues. Among the many findings, these studies have discovered unique molecular programs within skewed innate immune populations of macrophages and dendritic cells that dampen tumor immunity and cause resistance to checkpoint immunotherapy (*6*). More work is needed to enhance these atlases, particularly through incorporation of spatial resolution and longitudinal measurements connected to cancer outcomes (*7*).

Novel approaches to overcome immune resistance in tumors

Besides using checkpoint inhibitors to target CTLA-4 and PD-1/PDL-1, researchers are deploying new approaches involving vaccines to target cancer cells, such as neoantigen vaccines. Cancers can generate neoantigens, which can be recognized by T cells (Figure 1). Neoantigens are mostly unique to an individual's tumor but can be shared among tumors and may be highly immunogenic if they evade central tolerance mechanisms. Advances in computational biology have enabled rapid identification of neoantigens from the cancer genome, resulting in the development of individualized vaccines for several cancers, including melanoma, glioblastoma, breast, bladder, lung, and liver cancers (*8*). The first neoantigen vaccines, regardless of vaccine platform (RNA or DNA vaccines, peptide–adjuvant formulations, dendritic cells, viral vectors), have proven to be safe and immunogenic, and include examples from our institution, with some studies showing reduced recurrence rates or prolonged survival, in some cases in combination with PD1 and PDL1 blockade (*9*). These early results have shown neoantigen vaccines to be a promising means to overcome poorly immunogenic tumors or those invaded by terminally exhausted T cells.

Many challenges remain in this emerging field, however, which include choosing computational platforms to select and validate neoantigens through mutation calling, ensuring priming of quality T cells with strong antitumor potential, developing potent vaccine formulations, determining the clinical settings most likely to benefit from vaccination, and discovering optimal combinatorial approaches with immune oncology or other agents. Acquired resistance to neoantigen vaccination is an emerging concern that may be partly ameliorated with ICI through reinvigoration of exhausted T cells. Other resistance mechanisms, such as loss of antigen clonality, HLA heterogeneity, defective interferon signaling, paucity of antigen-presenting cells, and infiltration with immune suppressive myeloid cells, can impact the effectiveness of vaccination as well as other immunotherapies. In this regard, vaccination may require combination not only with ICI but other modalities such as adoptive T cell therapies or intratumoral interventions (*9*).

Interrogation of tumor evolution, fitness, and neoantigen qualities to improve immune responses to cancer and overcome resistance

Tumors consist of genetically heterogeneous cell populations that, by laws of natural selection, evolve to adapt to the tumor microenvironment. While certain mutations (e.g., in tumor oncogenes) will provide a fitness advantage to cancer cells, many mutations come with a certain fitness cost due to their effect on intrinsic protein functions, and notably, on generation of immunogenic neoantigens. It is still not fully understood which of the multiple neoantigens in a tumor generate successful immune responses, and neoantigen quality scores have been proposed to characterize the immunogenicity of evolving tumors (*10*–*12*). These measures account for computationally predicted neoantigens' HLA presentation probability, which depends on protein expression levels and the MHC–peptide affinity; the probability of T cell recognition of presented neoantigens, including evasion of central tolerance mechanisms; and tumor clonal fraction. To evade central tolerance, neoantigens—which often differ from self peptides only by single amino acids—must appear sufficiently foreign to the immune system. Proposed scores of foreignness account for sequence similarity of neoantigens to viral and microbial epitopes as well as their dissimilarity from the self-proteome (*10*, *12*). Evolutionary modeling approaches and characterization of "selective pressures"—for example, immune pressure—are at the core of predictive methods used to understand therapy response, resistance, and optimal therapy design. These include reconstruction of tumor clonal structures and quantification of neoantigen qualities, respectively, for uses such as personalized vaccine composition.

Role of innate immunity in response and resistance to cancer

In addition to activating T cells through vaccines or ICI, NK cells, antigen-presenting dendritic cells, and macrophages contribute to tumor immunity by direct cytotoxicity and by assisting the mounting of adaptive immunity responses, respectively (Figure 1). NK cells use diverse surface receptors to recognize "danger signals" expressed on the surface of tumor cells in response to stress pathways. Antibodies can further increase the innate immunogenicity of tumors by inhibiting downregulation of ligands for NK cell receptors or mediating NK cell–tumor cell engagement. For example, tumor cells downregulate MICA and MICB (MHC class I polypeptide–related sequences A and B) by cleavage that otherwise would be recognized by the NKG2D-activating receptor in NK cells; antibodies inhibitory of MICA and MICB cleavage restore NK cell–driven surveillance for cancers and have transitioned to clinical trials in patients with solid tumors (e.g., NCT05117476) (*13*). Cellular therapies have also been developed to bypass the limitation of decreased NK cell tumor infiltration compared to T cells by inoculation of in vitro-expanded allogeneic or induced pluripotent stem cell–derived NK cells. Dendritic cells, particularly the critical cDC1 subset, are recruited to tumor sites through NK cell–derived chemokines and cytokines and are required for the cross presentation of tumor-associated antigens to prime cytolytic $CD8^+$ T cells (*9*). In the absence of DCs, the response to anti-PD-1/PDL-1 is also suboptimal. Efforts to increase DC numbers through systemic or intratumor delivery of FLT3L can heighten antitumor immunity (*14*). On the other hand, macrophage infiltration is not an issue, because solid tumors, such as non–small cell lung cancer, are often highly infiltrated by monocyte-derived macrophages. However, the phagocytic function of intratumor macrophages can be turned off by tumor cell expression of CD47, a "don't eat me" signal (*15*). Antibody-mediated blockade of CD47 promotes macrophage-driven immunity and is being tested in a range of clinical trials (e.g., NCT04827576) (*15*). The clinical outcomes of those trials are enthusiastically awaited and are sure to reveal the promising therapeutic potential of targeting innate immunity for cancer.

Summary

Decoding the tumor microenvironment through the development of novel methodologies and technologies has enabled the development of new approaches to overcome tumor microenvironment–mediated immune suppression. Future challenges to overcome acquired immune resistance will require combination therapies that target T cells, the innate immune system, and the tumor along with its associated stroma.

References

1. D. B. Doroshow *et al.*, *Nat. Rev. Clin. Oncol.* **18**, 345–362 (2021).
2. R. M. Samstein *et al.*, *Nat. Cancer* **1**, 1188–1203 (2021).
3. D. Chowell *et al.*, *Nat. Med.* **25**, 1715–1720 (2019).
4. W. H. Fridman *et al.*, *Nat. Rev. Clin. Oncol.* **19**, 441–457 (2022).
5. T. U. Marron *et al.*, *Nat. Med.* **28**, 626–629 (2022).
6. B. Maier *et al.*, *Nature* **580**, 257–262 (2020).
7. A. Magen *et al.*, *bioRxiv* (2022), https://doi.org/10.1101/2022.06.22.497216.
8. F. Lang, B. Schrors, M. Lower, O. Tureci, U. Sahin, *Nat. Rev. Drug Discov.* **21**, 261–282 (2022).
9. M. Saxena, S. H. van der Burg, C. J. M. Melief, N. Bhardwaj, *Nat. Rev. Cancer* **21**, 360–378 (2021).
10. M. Łuksza *et al.*, *Nature* **606**, 389–395 (2022).
11. D. K. Wells *et al.*, *Cell* **183**, 818–834.e13 (2020).
12. L. P. Richman, R. H. Vonderheide, A. J. Rech, *Cell Syst.* **9**, 375–382.e4 (2019).
13. L. F. de Andrade *et al.*, *Science* **359**, 1537–1542 (2018).
14. N. Bhardwaj *et al.*, *Nat. Cancer* **1**, 1204–1217 (2020).
15. S. B. Willingham *et al.*, *Proc. Natl. Acad. Sci. U.S.A.* **109**, 6662–6667 (2012).

The complexity of multiple myeloma: From pathogenesis to therapeutic alternatives

Alessandro Laganà, Ajai Chari, Luis Isola, Hearn Jay Cho, Sundar Jaganath, Samir Parekh*

Introduction

Multiple myeloma (MM) affects ~30,000 new individuals every year in the United States and is the most common hematologic malignancy in African Americans (*1*). Most patients are diagnosed during routine health checkups while asymptomatic or minimally symptomatic with anemia. More advanced presentations with bone disease, fracture, and renal failure have become rarer (*2*). Active MM is preceded by precancerous states: monoclonal gammopathy of undetermined significance (MGUS) and smoldering MM (SMM). Ongoing trials are exploring treatment of these precursor forms to prevent their progression to active disease.

Great strides have been made in understanding the genomic architecture and subclonal heterogeneity of MM and in drug development for treating MM, developments that have increased the complexity of pathogenesis and treatment choices (Figure 1). Furthermore, studies carried out during the COVID-19 pandemic have led to novel insights into the MM tumor microenvironment and therapy (*3*, *4*), paving the way for continued efforts to define and understand what makes immunocompromised MM patients different from healthy individuals and to guide management and treatment recommendations.

Complexity in pathogenesis

MM is caused by a neoplastic proliferation of plasma cells, characterized by chromosomal translocations and copy number alterations in the early phase, with increased DNA instability and accumulation of point muta-

Tisch Cancer Institute, Icahn School of Medicine at Mount Sinai, New York, NY

*Corresponding author: samir.parekh@mssm.edu

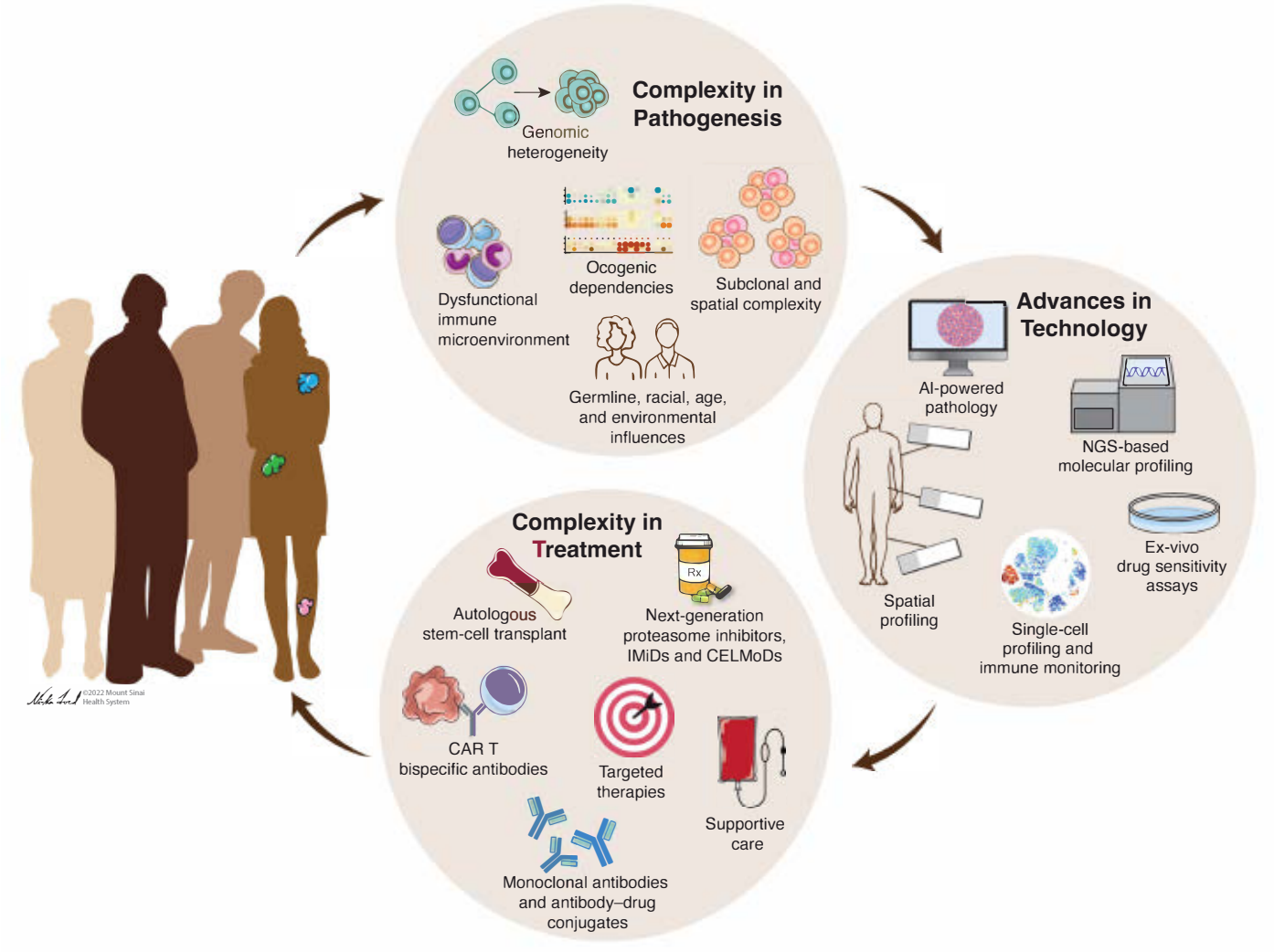

FIGURE 1. The complexity of multiple myeloma. Inter- and intrapatient heterogeneity driven by diversity in tumor clonality and immune microenvironment composition is being addressed by cutting-edge advances in technology and therapeutic advances. IMiDs, immunomodulatory imide drugs; CELMoDs, cereblon E3 ligase-modulating drugs; NGS, next-generation sequencing.

tions arising in later stages. Data generated from thousands of patients indicates a possible germline predisposition to myeloma, which is currently being explored at Mount Sinai's Tisch Cancer Institute (*5*).

Inter- and intrapatient heterogeneity are key features of MM, with different patients harboring different genetic drivers and spatial and subclonal heterogeneity observed within each patient. Multiomics integrative analysis of genomic and transcriptomic data has improved patient classification and identified patterns of co-occurring alterations associated with therapy outcome and survival (*6*). Molecular profiling and modeling in individual patients have revealed a complex clonal landscape, where multiple tumor subclones evolve over time with or without therapy pressure, ultimately leading to treatment resistance.

Furthermore, MM cells critically depend on microenvironmental support from surrounding stromal cells, immune cells, and cytokines to establish their niche, and later modify their environment to achieve a growth advantage.

Complexity in treatment options

Treatment of newly diagnosed MM has been revolutionized by proteasome inhibitors, immunomodulatory drugs, autologous transplantation, and antibody therapies. Initial therapy consists of combinations of these agents, which induce remission in over 90% of cases, with an overall survival greater than 7–8 years in most patients (*7*). With the advent of newer generations of drugs, ~20% of patients are enjoying long-term cures. This has created a need for improving our understanding and definition of cure, so that new treatment trials can have rapid readouts instead of waiting for years to collect outcomes. An additional aim is to limit the duration of treatment, as current therapy designs continue maintenance therapy indefinitely.

With more than a dozen U.S. Food and Drug Administration (FDA)-approved treatments that can be given in sequential combinations, treatment selection in relapsed MM patients is an art. Prior therapies, patient comorbidities, preferences, and disease characteristics are taken into account to plan out non-cross-resistant salvage regimens incorporating monoclonal antibodies (*8*) and new small molecules (*9*) to produce long-term remissions even in patients whose disease may have relapsed multiple times.

The development of potent novel immunotherapeutics calls for early identification of drug-resistant clones, as this may help improve the timing and sequencing of these therapies. Bispecific antibodies and genetically engineered chimeric antigen receptor T (CAR T) cells targeting B cell surface antigens (*10*, *11*) can induce deep and durable remissions even in patients with very refractory disease. Judicious incorporation of these novel T cell redirecting treatments earlier in the treatment will attack chemotherapy resistant clones and significantly improve long-term outcomes. Widespread application of these new immune therapies would require understanding and successful mitigation of unique adverse events such as cytokine storms, neurological side effects [e.g., ICANS (immune effector cell-associated neurotoxicity syndrome) and Parkinsonism] (*12*), infections, and long-term cytopenias. The high cost of these therapies and the difficulty of gaining access to them means they are currently limited to major medical centers—a disparity that needs to be addressed by the medical, pharmaceutical, and regulatory community.

Resolving complexity and aiming for a cure in myeloma

High-resolution technologies, including single-cell DNA and RNA sequencing, mass cytometry (or cytometry by time-of-flight, CyTOF), and spectral flow cytometry, can now reveal both the genomic and tumor microenvironment complexity of individual MM patients and aid in development of the next generation of therapeutics (*13*). Recent studies have uncovered a complex interplay between tumors and surrounding cells, as well as stochastic differences in tumor subclones and immune compartments within individual patients. Precision medicine approaches based on sequencing and ex vivo drug-sensitivity assays are attempting to tailor treatment to each patient's genetic makeup and can be effective even in the post-CAR T setting (*14*, *15*). However, these approaches are in their infancy. Differences in the tumor microenvironment that govern response to the new therapies still need to be defined and profiled in a standardized manner, using high-resolution technologies to further investigate individual MM cells and their spatial relationships with the microenvironment in the next generation of trials.

Disparities in health care should be vigorously addressed by centers that are geographically positioned and staffed to ensure equity in level of care and clinical trial access, as well as delivery of complex new antibody and cellular therapies.

References

1. R. L. Siegel, K. D. Miller, H. E. Fuchs, A. Jemal, *CA Cancer J. Clin.* **72**, 7–33 (2022).
2. N. C. Munshi, S. Jagannath, in *Hematology* (Elsevier, Philadelphia, PA, 2018), pp. 1381–1418.e1.
3. O. Van Oekelen *et al.*, *Cancer Cell* **39**, 1028–1030 (2021).
4. A. Aleman *et al.*, *Cancer Cell* **40**, 441–443 (2022).
5. S. Thibaud *et al.*, *Blood* **138**, 399 (2021).
6. S. Bhalla *et al.*, *Sci. Adv.* **7**, eabg9551 (2021).
7. P. G. Richardson *et al.*, *N. Engl. J. Med.* **387**, 132–147 (2022).
8. A. Chari *et al.*, *Blood* **134**, 421–431 (2019).
9. A. Chari *et al.*, *N. Engl. J. Med.* **381**, 727–738 (2019).
10. P. Moreau *et al.*, *N. Engl. J. Med.* **387**, 495–505 (2022).
11. N. C. Munshi *et al.*, *N. Engl. J. Med.* **384**, 705–716 (2021).
12. O. Van Oekelen *et al.*, *Nat. Med.* **27**, 2099–2103 (2021).
13. Y. C. Cohen *et al.*, *Nat. Med.* **27**, 491–503 (2021).
14. A. Laganà *et al.*, *JCO Precis. Oncol.* **2018**, (2018), doi:10.1200/PO.18.00019.
15. M. Elnaggar *et al.*, *J. Hematol. Oncol.* **15**, 109 (2022).

Meeting the challenges of the liver cancer epidemic

Scott L. Friedman[1,2]*, Bachir Taouli[1,3], Augusto Villanueva[1,2], Amaia Lujambio[1,4], Ernesto Guccione[1,4], Daniela Sia[1,2], Josep M. Llovet[1,2], Myron Schwartz[1,5]

A high worldwide prevalence of chronic viral hepatitis B, C, and D, combined with rising numbers of patients with fatty liver- and alcohol-associated hepatic diseases, has wrought an epidemic of chronic liver disease that can give rise to primary cancer of hepatocytes (hepatocellular carcinoma, or HCC) and bile duct cells (intrahepatic cholangiocarcinoma, or ICC). These neoplasms have the fastest-rising incidence of any cancer in the Western world and are the fourth-leading cause of cancer deaths worldwide (*1*). Their detection and management present unique challenges, since these neoplasms typically arise within livers that are already damaged, are often asymptomatic until no longer curable, and are highly heterogeneous, making personalized therapies especially daunting.

These challenges are being surmounted by multidisciplinary teams of epidemiologists, cancer biologists, and physicians who are advancing methods for early detection, clarifying concepts of immunopathogenesis by leveraging creative new animal models, and pioneering novel medical, radiotherapeutic, and surgical approaches (Figure 1).

Prevention/surveillance

There are no drugs that can prevent HCC in patients with ongoing liver disease, although effective prevention or treatment of underlying viral infections can attenuate its development. For instance, national vaccination campaigns against hepatitis B virus have dramatically decreased HCC incidence due to this virus, while long-term cures of chronic hepatitis C virus (HCV) can reduce, but not eliminate, HCC risk.

Early detection of liver cancer saves lives by finding tumors when they are small and curable. Current practice guidelines recommend HCC surveillance in high-risk patients (e.g., those with cirrhosis or advanced fibrosis) using abdominal ultrasound, with or without serum alpha-fetoprotein assessment every 6 months (*2*). Despite the ease of this approach, HCC surveillance programs are still significantly underutilized in the United States and must be improved, as abdominal ultrasound identifies only ~63% of tumors at early stages. In the Liver Cancer Program at The Tisch Cancer Institute (TCI) at Mount Sinai, more sensitive HCC screening methods are being evaluated to improve early detection, which include an abbreviated magnetic resonance imaging (MRI) exam (less than 15 minutes) and liquid biopsy technologies (*3*). For example, genomic analysis of circulating tumor DNA or of nucleotides present in extracellular vesicles significantly increases detection rates and outperforms imaging for HCC surveillance, highlighting its paradigm-changing potential (*3*).

Pathogenesis and experimental models

Implementation of effective, personalized treatments for liver cancer requires a clearer understanding of its pathogenesis. The disease arises from persistent liver damage leading to fibrosis, cirrhosis, and eventually liver cancer, whose genetic composition is especially heterogeneous due to the accumulation of genetic alterations in specific driver genes (e.g., mutations in *CTNNB1* and *TERT* promoter in HCC or *IDH* mutations and *FGFR2* fusions in ICC); aberrant signaling orchestrated by mutant p53, chromatin remodelers, and tyrosine kinases; and dynamic cross-talk between cancer cells and the surrounding stroma.

To yield progress, preclinical testing must be built upon experimental systems that accurately predict drug efficacy. While current models, including liver cancer cell lines and toxin- or diet-induced mouse models of HCC, have been informative, they do not fully capture the complexity of liver tumors, which limits the discovery of biomarkers that can predict or monitor response to therapies. To address this gap, more precise experimental models are emerging, such as expanded collections of liver cancer cell lines and patient-derived organoids (PDOs) or patient-derived xenografts (PDXs). Still, these approaches do not capture the immune component of tumors and their stroma, which are now recognized as critical determinants of cancer pathogenesis and its response to treatment.

The multidisciplinary Liver Cancer Program within TCI is at the forefront of developing novel models of HCC and ICC. The worldwide obesity epidemic has made nonalcoholic fatty liver disease (NAFLD) the fastest rising etiology of HCC, a challenge further compounded by the relative resistance to immunotherapy of tumors in this disease (*4*, *5*). The "FAT-NASH" (fibrosis and tumors, nonalcoholic steatohepatitis) model addresses this unmet need (*4*). Furthermore, versatile mouse models that reproduce the key genetic alterations in ICC (*6*) and HCC (*7*) can be leveraged in preclinical studies to identify biomarkers of response to immunotherapies (*8*).

Advances in management and therapies

A revolution in liver cancer management is unfolding. More effective treatments of viral hepatitis are leading to better responses to cancer treatments, reduced tumor recurrences, and less need for liver transplantation (*9*). When surgery is necessary to resect a liver cancer, it can often be performed without big incisions, instead using laparoscopy or a robot. Early-stage tumors can increasingly be destroyed without surgery using microwaves, internal radiation (*10*), or focused external radiation, combined with cutting off blood flow to the tumor (*11*). For patients with more advanced cancer that remains confined within the liver, these nonsurgical treatments can often shrink the tumors sufficiently to make a liver transplant possible (*12*). With this enlarging array of options to treat liver cancer, deciding how best to treat each patient requires the input of many specialists working together in a multidisciplinary team.

Complementing the exciting developments in the treatment of early-stage disease are even greater breakthroughs in the treatment of advanced HCC, where systemic therapies—which are indicated in up to 50% of patients—have improved the survival of advanced cases from 6–8 months to up to ~20 months using the current standard-of-care drug atezolizumab (a checkpoint inhibitor) plus bevacizumab (an anti-angiogenic agent). In a milestone achievement in 2008, sorafenib was the first approved oral drug for HCC based upon the Mount Sinai–led Phase 3 investigation demonstrating its efficacy against placebo in patients with advanced disease (*13*). Subsequent therapies (lenvatinib, regorafenib, cabozantinib, and ramucirumab) and immune-based combinations (atezolizumab plus bevacizumab and tremelimumab plus durvalumab) have further extended the survival of HCC patients (*14*). The unprecedented expansion of treatment options has accelerated both the earlier use of systemic therapies complemented by locoregional therapies as well as emerging efforts to prescribe immuno-oncology agents at earlier stages of the disease, either prior to or after surgical resection or local ablation. In one such pioneering study at TCI, immune-based neoadjuvant therapy, was administered prior to surgery with promising results (*15*). These advances, coupled with the prospect of deeper DNA sequencing of tumors

[1]Tisch Cancer Institute Liver Cancer Program; [2]Division of Liver Diseases, Department of Medicine; [3]Department of Radiology; [4]Department of Oncological Sciences; [5]Department of Surgery, Icahn School of Medicine at Mount Sinai, New York, NY

*Corresponding author: scott.friedman@mssm.edu

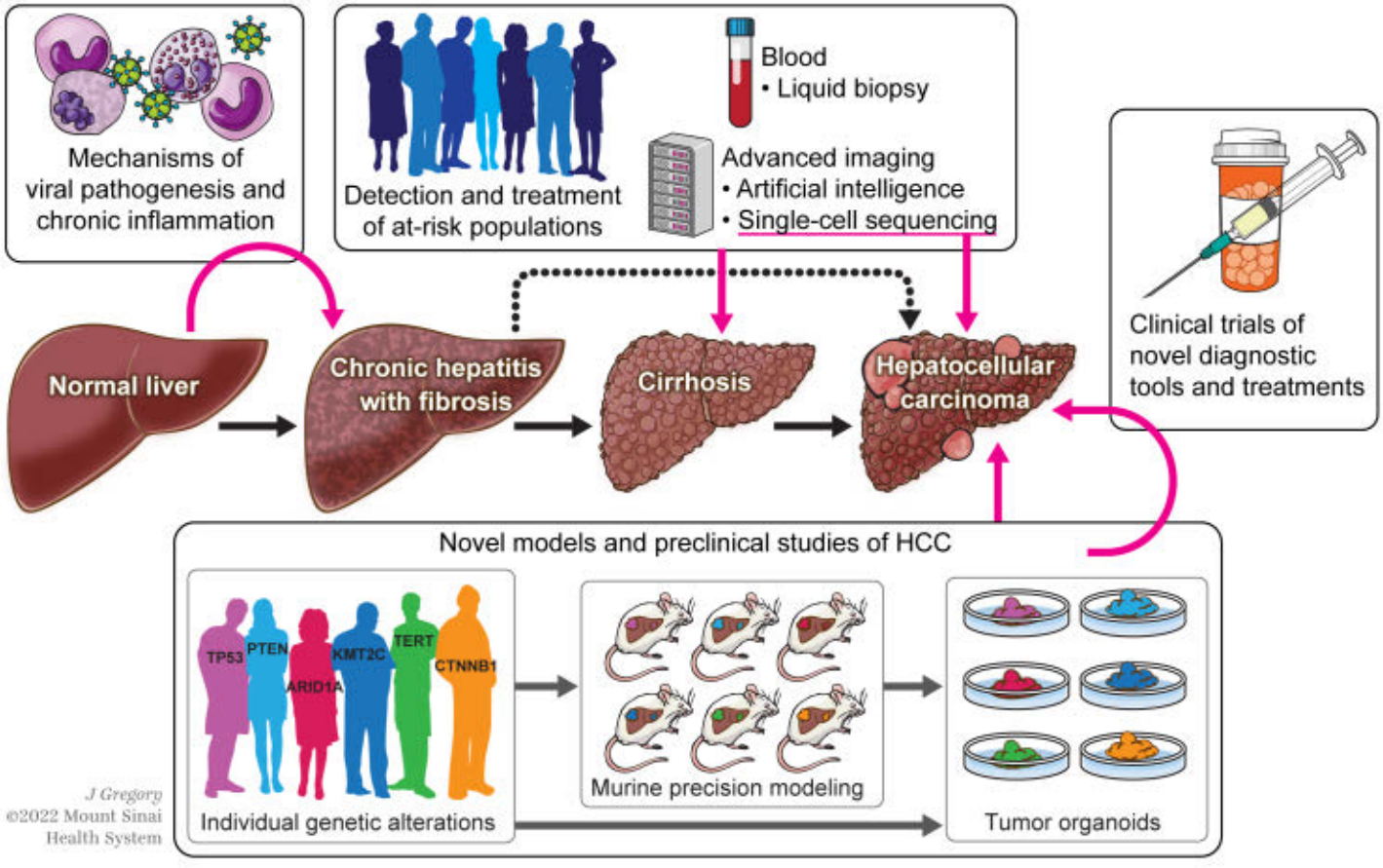

FIGURE 1. Strategies for meeting the challenges of the liver cancer epidemic. A multipronged attack on the pathogenesis, detection, and treatment of liver cancer is underway to improve outcomes for patients. Basic laboratory studies seek to define the pathways of liver injury and inflammation that drive the development of chronic hepatitis from viral infection, fatty liver disease (alcohol-associated and nonalcoholic), drug toxicity, and other insults. Efforts to increase detection and characterization of tumors require clarification of at-risk populations as well as determination of molecular markers in tissue and blood through single-cell sequencing and other technologies, combined with advanced imaging technologies. Novel models built upon genetic risks and mutational profiles of individuals and tumors can support preclinical studies using precision modeling in rodents and organoids. These efforts collectively will yield more refined, precision diagnostics and therapies tailored to specific abnormalities in the tumor and the surrounding stromal cells. HCC, hepatocellular carcinoma.

using single-cell technologies to uncover abnormalities that can inform personalized therapies, will likely further improve outcomes.

Future prospects

Several challenges remain. Although improved treatment of underlying liver disease can reduce the incidence of liver cancer, we must further refine noninvasive screening methods and improve their implementation in at-risk populations. Indeed, we are far from our ultimate goal of curing liver cancer in most patients, particularly in advanced stages. Going forward, the accuracy and utility of experimental models in mimicking the complexity of liver cancer will be progressively refined to enable more seamless recapitulation of complex phenotypes that support improved screening as we hunt for more effective therapies. An ongoing challenge is the development of patient-derived models that include both systemic and tissue-specific immune components of the disease. Models that better recapitulate these features within the tumor microenvironment, combined with the use of humanized mice, will significantly strengthen their value. In addition, complementing mouse models harboring liver damage with strategies to introduce specific genetic alterations (e.g., using gene editing with CRISPR/Cas9) will significantly refine precision mouse modeling.

Finally, more precise, cost-effective medical therapies are needed, based on identifying tissue- and/or blood-based biomarkers that can predict disease behavior and responses to systemic treatments. The accelerating pace of progress in understanding, detecting, and treating liver cancer augurs well for the future.

References

1. J. M. Llovet *et al., Nat. Rev. Dis. Primers* **7**, 6 (2021).
2. J. A. Marrero *et al., Hepatology* **68**, 723–750 (2018).
3. J. von Felden *et al., Gut* (2021).
4. T. Tsuchida *et al., J. Hepatol.* **69**, 385–395 (2018).
5. D. Pfister *et al., Nature* **592**, 450–456 (2021).
6. M. A. Martin-Serrano *et al., Gut* (2022), doi: 10.1136/gutjnl-2022-327782.
7. P. Molina-Sanchez *et al., Gastroenterology* **159**, 2203–2220.e14 (2020).
8. M. Ruiz de Galarreta *et al., Cancer Discov.* **9**, 1124–1141 (2019).
9. P. Tabrizian *et al., HPB (Oxford)* **24**, 1082–1090 (2022).
10. E. Kim *et al., Lancet Gastroenterol. Hepatol.* **7**, 843–850 (2022).
11. M. Buckstein *et al., Int. J. Radiat. Oncol. Biol. Phys.* **14**, 221–230 (2022).
12. P. Tabrizian *et al., JAMA Surg.* **157**, 779–788 (2022).
13. J. M. Llovet *et al., N. Engl. J. Med.* **359**, 378–390 (2008).
14. L. Broutier *et al., Nat. Med.* **23**, 1424–1435 (2017).
15. T. U. Marron *et al., Lancet Gastroenterol. Hepatol.* **7**, 219–229 (2022).

Ramon Parsons, MD, PhD
Director, The Tisch Cancer Institute

Joseph A. Sparano, MD
Deputy Director, The Tisch Cancer Institute

Connecting Breakthrough Research and First-Rate Patient Care

The Tisch Cancer Institute at Mount Sinai brings together a team of internationally renowned researchers and superb clinicians to take on cancer's most complex challenges. The Tisch Cancer Institute is our National Cancer Institute-designated cancer center.

To find out what our team of Tisch Cancer Institute researchers are working on to improve medical care and prolong lives, we invite you to listen to a recent interview of the Institute's director, Ramon Parsons, MD, PhD, on the *Science* magazine podcast. **Visit the podcast's website at www.science.org/podcasts to download the October 6 episode.**

WE FIND A WAY

NCI Designated Comprehensive Cancer Center

Mount Sinai *The Tisch Cancer Institute*

Read more about The Tisch Cancer Institute

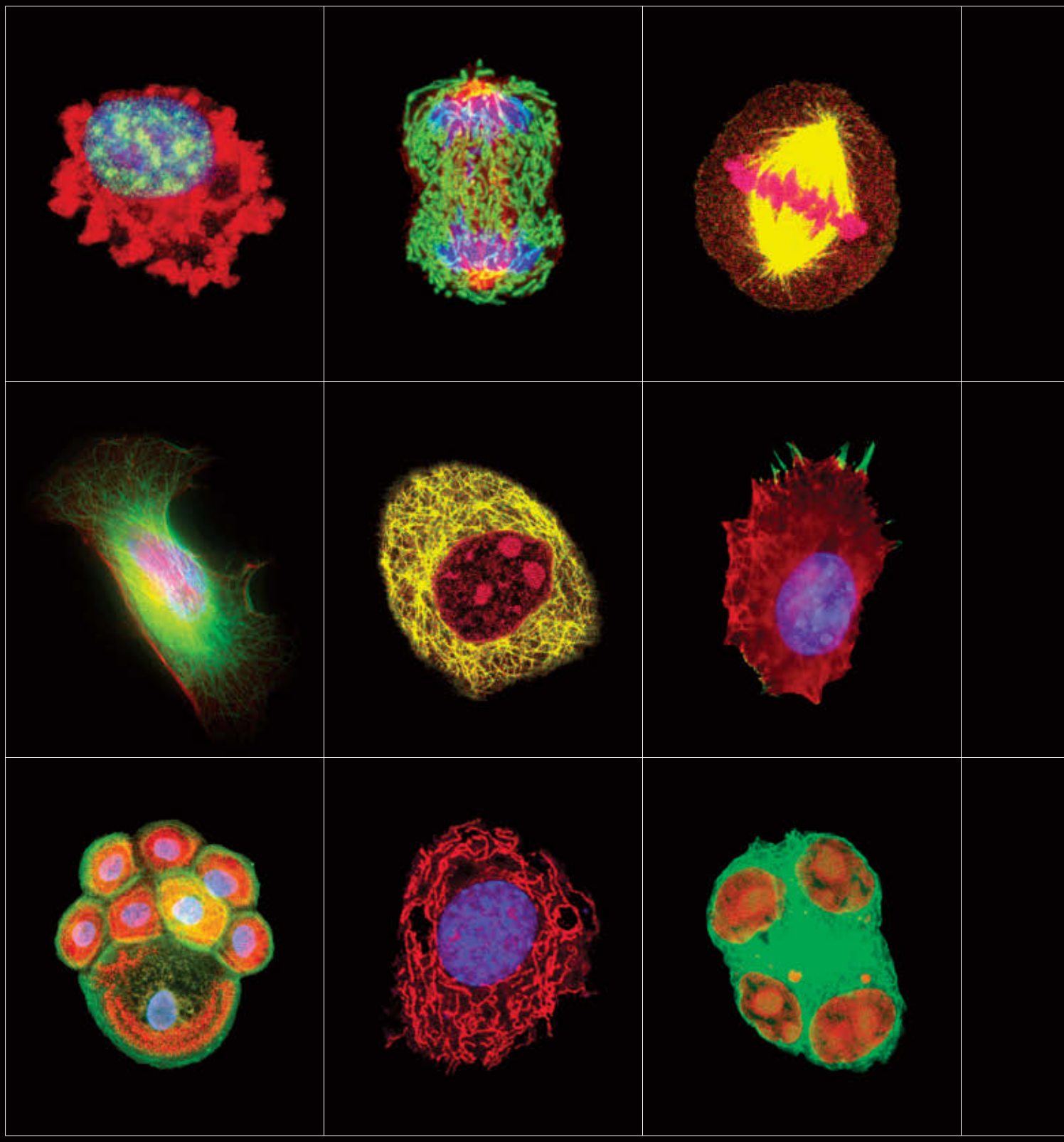

Icahn School of Medicine
at Mount Sinai
One Gustave L. Levy Place
New York, NY 10029-6574

icahn.mssm.edu